frontiers | Research Topics

# The potential role of gut microbiome in animal gut-linked diseases

**Edited by**
Tang Zhaoxin, Yung-Fu Chang, Mujeeb Ur Rehman and Hui Zhang

**Published in**
Frontiers in Microbiology

ISSN 1664-8714
ISBN 978-2-83252-153-3
DOI 10.3389/978-2-83252-153-3

## About Frontiers

Frontiers is more than just an open access publisher of scholarly articles: it is a pioneering approach to the world of academia, radically improving the way scholarly research is managed. The grand vision of Frontiers is a world where all people have an equal opportunity to seek, share and generate knowledge. Frontiers provides immediate and permanent online open access to all its publications, but this alone is not enough to realize our grand goals.

## Frontiers journal series

The Frontiers journal series is a multi-tier and interdisciplinary set of open-access, online journals, promising a paradigm shift from the current review, selection and dissemination processes in academic publishing. All Frontiers journals are driven by researchers for researchers; therefore, they constitute a service to the scholarly community. At the same time, the *Frontiers journal series* operates on a revolutionary invention, the tiered publishing system, initially addressing specific communities of scholars, and gradually climbing up to broader public understanding, thus serving the interests of the lay society, too.

## Dedication to quality

Each Frontiers article is a landmark of the highest quality, thanks to genuinely collaborative interactions between authors and review editors, who include some of the world's best academicians. Research must be certified by peers before entering a stream of knowledge that may eventually reach the public - and shape society; therefore, Frontiers only applies the most rigorous and unbiased reviews. Frontiers revolutionizes research publishing by freely delivering the most outstanding research, evaluated with no bias from both the academic and social point of view. By applying the most advanced information technologies, Frontiers is catapulting scholarly publishing into a new generation.

## What are Frontiers Research Topics?

Frontiers Research Topics are very popular trademarks of the *Frontiers journals series*: they are collections of at least ten articles, all centered on a particular subject. With their unique mix of varied contributions from Original Research to Review Articles, Frontiers Research Topics unify the most influential researchers, the latest key findings and historical advances in a hot research area.

Find out more on how to host your own Frontiers Research Topic or contribute to one as an author by contacting the Frontiers editorial office: frontiersin.org/about/contact

# The potential role of gut microbiome in animal gut-linked diseases

**Topic editors**

Tang Zhaoxin — South China Agricultural University, China
Yung-Fu Chang — Cornell University, United States
Mujeeb Ur Rehman — Directorate Planning and Development, Livestock & Dairy Development Department, Balochistan, Pakistan
Hui Zhang — South China Agricultural University, China

**Citation**

Zhaoxin, T., Chang, Y.-F., Rehman, M. U., Zhang, H., eds. (2023). *The potential role of gut microbiome in animal gut-linked diseases*. Lausanne: Frontiers Media SA. doi: 10.3389/978-2-83252-153-3

# Table of contents

frontiers | Frontiers in Microbiology

TYPE Editorial
PUBLISHED 28 March 2023
DOI 10.3389/fmicb.2023.1179481



OPEN ACCESS

EDITED AND REVIEWED BY
Knut Rudi,
Norwegian University of Life Sciences, Norway

*CORRESPONDENCE
Hui Zhang
✉ hz236@scau.edu.cn
Mujeeb Ur Rehman
✉ mujeebnasar@yahoo.com

SPECIALTY SECTION
This article was submitted to Microorganisms in Vertebrate Digestive Systems, a section of the journal Frontiers in Microbiology

RECEIVED 04 March 2023
ACCEPTED 20 March 2023
PUBLISHED 28 March 2023

CITATION
Zhang H, Rehman MU, Chang Y-F and Zhaoxin T (2023) Editorial: The potential role of gut microbiome in animal gut-linked diseases. *Front. Microbiol.* 14:1179481. doi: 10.3389/fmicb.2023.1179481



# Editorial: The potential role of gut microbiome in animal gut-linked diseases

Hui Zhang[1]*, Mujeeb Ur Rehman[2,3]*, Yung-Fu Chang[4] and Tang Zhaoxin[1]

[1]College of Veterinary Medicine, South China Agricultural University, Guangzhou, China, [2]Directorate Planning and Development, Livestock and Dairy Development Department Balochistan, Quetta, Pakistan, [3]State Key Laboratory of Marine Resource Utilization in South China Sea, College of Oceanology, Hainan University, Haikou, Hainan, China, [4]Cornell University Ithaca, Ithaca, NY, United States

KEYWORDS

**gut microbiota, intestinal immunity, gastrointestinal diseases, metagenomics, probiotics**

Editorial on the Research Topic
The potential role of gut microbiome in animal gut-linked diseases

The animal gastrointestinal tracts contain trillions of microorganisms, which play critical roles in immune system maturation, intestinal epithelium differentiation and nutrient absorption and metabolism (Belkaid and Hand, 2014). The gut contains more than $10^{14}$ microorganisms, including bacteria, fungi, and viruses, which interact in a synergistic or antagonistic relationship to maintain a stable intestinal environment and function (Zheng et al., 2020). Stabilized gut microbiota has been demonstrated to be a prerequisite for the intestine to perform various complicated physiological processes, but gut microbial dysbiosis may cause multiple gastrointestinal diseases, including diarrhea, stomachache, and colitis. Moreover, the effects of the gut microbial community extend beyond the gastrointestinal system and can cause other systemic diseases. Similarly, several studies have reported the associations between diseases status and gut microbiota, in order to improve our knowledge on microbiome and host interactions and to develop an effective approach to rehabilitate perturbed animal and human microbial ecosystems.

The gut microbial alternations in animal gastrointestinal system or the differences in gut microbiome composition and function have been associated with a variety of diseases ranging from metabolic conditions and gastrointestinal inflammatory to colitis, and respiratory illnesses. In this area of research, Zhang et al. have conducted a bibliometric analysis of publications in the field of intestinal flora and ulcerative colitis research in the past 10 years, which summarizes current knowledge regarding the global research trends in intestinal flora and ulcerative colitis. On the other hands, to understand the microbial composition of the entire gut and to provide insights on how to improve the overall health and productivity of the animals. Chang et al. have updated our knowledge on the structure and function of the intestinal microbiota at different growth and developmental stages of Tibetan pigs, which plays an important role in their immune performance.

Currently, metagenomic analysis and high-throughput sequencing have been used for investigating gut microbial alterations in several diseases that are considered to be linked with gut microbes. Gut microbial comparison and analysis have the potential to benefit the understanding of the pathogenesis of various animal gut-linked diseases and the development of corresponding strategies to decrease the collateral damages. Hang et al. have briefly analyzed the influence of Shugan Decoction (SGD) on intestinal microbiota and fecal metabolites in diarrhea predominant irritable bowel syndrome (IBS-D) rats by multiple omics techniques, including metagenomic sequencing and metabolomics. The authors have shown that how SGD can regulate specific intestinal microbiota and some metabolic pathways, which may explain its effect of alleviating visceral hypersensitivity and abnormal intestinal motility in WAS-induced IBS-D rats. Similarly, Wang L. et al. have updated our knowledge by utilizing high-throughput sequencing to analyze the intestinal flora of Weining cattle, Angus cattle, and diarrheal Angus cattle. The authors have revealed the potential bacteria associated with diarrhea for the subsequent treatment of diarrhea in Angus cattle. In order to better understand the relationship between intestinal flora and health, the significant changes in the type and proportion of bacteria have been explored and explained that how diarrhea not only directly modifies the diversity and abundance of gut microbiota but also indirectly affects some functional bacteria.

The role of gut microbial regulation in the prevention and treatment of animal diseases, such as by fecal bacteria transplantation, probiotic supplementation and other means is one of the hot Research Topic these days. In the same direction, Lin et al. have conducted a study on Echinacea exert to confirm its influence of intestinal flora in immunosuppressed ducks. The authors concluded that Echinacea extract can improve the development of immunosuppressed ducks by modulating the intestinal immune function and by increasing the abundance of beneficial bacterial genera in the intestine in birds. Similarly, prenatal and early postnatal development are known to influence future health, in the same area of research, Wang H. et al. have performed a surrogate fostering experiment in mice to examine the relationship between the metabolic markers associated to insulin resistance and the composition of the gut microbiota. The authors findings revealed that alterations in the early growth environment may prevent fetal-programmed glucose metabolic disorder *via* modulation of the microbiota-gut-brain axis.

In conclusion, this Research Topic provided diverse knowledge on the role of gut microbiota and animal intestinal diseases occurrence using multidisciplinary approaches combining multi-omics techniques. However, there is still a lot of research gap to understand the importance and role of gut microbial regulation in the prevention and treatment of animal diseases. Thus, future research should be emphasized on the factors contributing to prevent or occur gut microbiota inked diseases in animals.

## Author contributions

All authors listed have made a substantial, direct, and intellectual contribution to the work and approved it for publication.

## Funding

This work was supported by the National Key Research and Development Program (2022YFD1600904).

## Acknowledgments

The authors wish to thank the editor for proofreading the manuscript.

## Conflict of interest

The authors declare that the research was conducted in the absence of any commercial or financial relationships that could be construed as a potential conflict of interest.

## Publisher's note



## References

Belkaid, Y., and Hand, T. W. (2014). Role of the microbiota in immunity and inflammation. *Cell* 157, 121–141. doi: 10.1016/j.cell.2014.03.011

Zheng, D., Liwinski, T., and Elinav, E. (2020). Interaction between microbiota and immunity in health and disease. *Cell Res*. 30, 492–506. doi: 10.1038/s41422-020-0332-7

frontiers | Frontiers in Microbiology

ORIGINAL RESEARCH
published: 12 July 2022
doi: 10.3389/fmicb.2022.944416

# Gut Commensal Fungi Protect Against Acetaminophen-Induced Hepatotoxicity by Reducing *Cyp2a5* Expression in Mice

*Zhuoen He[1,2†], Yunong Zeng[2†], Shuyu Li[2†], Lizhen Lin[2†], Ruisi Zhou[2], Fangzhao Wang[2], Wenjiao Yang[3], Yuhao Wu[2], Junhao Yang[4], Ali Chen[5], Zhang Wang[4], Hong Yang[1], Xiaoshan Zhao[2], Wei Xiao[2,6]*, Lei Li[7]* and Shenhai Gong[1,2]**

[1]Department of Critical Care Medicine, The Third Affiliated Hospital of Southern Medical University, Guangzhou, China, [2]School of Traditional Chinese Medicine, Southern Medical University, Guangzhou, China, [3]Department of Simulation Center, Zhujiang Hospital of Southern Medical University, Guangzhou, China, [4]School of Life Science, South China Normal University, Guangzhou, China, [5]School of Chemistry and Chemical Engineering, Guangdong Pharmaceutical University, Guangzhou, China, [6]Key Laboratory of Glucolipid Metabolic Disorder, Ministry of Education, Guangdong Pharmaceutical University, Guangzhou, China, [7]Department of Respiratory and Critical Care Medicine, Affiliated Dongguan Hospital, Southern Medical University, Dongguan, China

**Background and Aims:** Drug-induced liver injury (DILI) is a common cause of acute liver failure and represents a significant global public health problem. When discussing the gut-liver axis, although a great deal of research has focused on the role of gut microbiota in regulating the progression of DILI, the gut commensal fungal component has not yet been functionally identified.

**Methods:** Mice were pretreated with fluconazole (FC) to deplete the gut commensal fungi and were then subject to acetaminophen (APAP) gavage. In addition, transcriptome sequencing was performed to identify differentially expressed genes (DEGs) between control and fluconazole-pretreated groups of the mice challenged with APAP.

**Results:** Gut commensal fungi ablation through fluconazole pretreatment predisposed mice to APAP-induced hepatotoxicity, characterized by elevated serum liver enzyme levels and more severe centrilobular necrosis, which appears to be caused by robust inflammation and oxidative stress. The 16S rDNA sequencing results indicated that *Akkermansia muciniphila* abundance had significantly decreased in gut fungi-depleted mice, whereas increased abundance of *Helicobacter rodentium* was observed. The gene interaction network between DEGs identified by the transcriptome sequencing highlighted a significant enrichment of *Cyp2a5* in the liver of APAP-treated mice that were preadministrated with fluconazole. Pharmacological inhibition of *Cyp2a5* by 8-methoxypsoralen (8-MOP) could significantly attenuate hepatic inflammation and oxidative stress in mice, thereby conferring resistance to acute liver injury caused by APAP administration.

**Conclusion:** Our data highlighted the significance of gut commensal fungi in hepatic inflammation and oxidative stress of APAP mice, shedding light on promising therapeutic strategies targeting *Cyp2a5* for DILI treatment.

**Keywords: acetaminophen, gut fungi, *Cyp2a5*, acute liver injury, inflammation, oxidative stress**

OPEN ACCESS

***Edited by:***
*Hui Zhang,*
*South China Agricultural University, China*

***Reviewed by:***
*Dayou Shi,*
*South China Agricultural University, China*
*Jiang Congqing,*
*Wuhan University, China*

***Correspondence:**
*Shenhai Gong*
*gsh0526@smu.edu.cn*
*Lei Li*
*2697363714@qq.com*
*Wei Xiao*
*xw7688@smu.edu.cn*

*†These authors have contributed equally to this work and share first authorship*

***Specialty section:***
*This article was submitted to Microorganisms in Vertebrate Digestive Systems, a section of the journal Frontiers in Microbiology*

***Received:*** *15 May 2022*
***Accepted:*** *09 June 2022*
***Published:*** *12 July 2022*

***Citation:***
*He Z, Zeng Y, Li S, Lin L, Zhou R, Wang F, Yang W, Wu Y, Yang J, Chen A, Wang Z, Yang H, Zhao X, Xiao W, Li L and Gong S (2022) Gut Commensal Fungi Protect Against Acetaminophen-Induced Hepatotoxicity by Reducing Cyp2a5 Expression in Mice. Front. Microbiol. 13:944416. doi: 10.3389/fmicb.2022.944416*

## INTRODUCTION

Drug-induced liver injury (DILI) is becoming an increasingly severe public health problem worldwide as it is one of the leading causes of acute liver failure (ALF; Bernal and Wendon, 2013). A large body of evidence has revealed that acetaminophen (APAP) is extensively used to treat pain and fever, although hepatotoxicity caused by an APAP overdose is the major cause of DILI in many European and North American countries (Larson et al., 2005; Bernal et al., 2013; Stravitz and Lee, 2019). APAP-induced ALF is a progressive disease that is characterized by extensive hepatocellular necrosis and has unacceptably high levels of mortality (Larson et al., 2005; Fernandez-Checa et al., 2021). Although substantial efforts have been made to improve medical management of the condition, APAP-induced liver failure nevertheless causes more than 500 deaths annually in the US (Li et al., 2020). The pathogenesis of APAP hepatotoxicity is linked to the intracellular depletion of hepatic reduced glutathione (GSH), with the consequence of predisposing hepatocytes to mitochondrial reactive oxygen species (ROS; Yuan and Kaplowitz, 2013). A normal dose of APAP can be mostly metabolized in the liver by glucuronidation and sulfation into non-toxic substances, thereby promoting the excretion of APAP *via* the kidneys (Watkins and Seeff, 2006). However, APAP is metabolized to a large number of N-acetyl-p-benzoquinoneimine (NAPQI) through cytochrome P450 enzymes when both glucuronidation and sulfation pathways become saturated following an APAP overdose (Krenkel et al., 2014). After hepatic GSH exhaustion, the excessive NAPQI bonds covalently with hepatocellular macromolecules to form APAP-protein adducts, which leads to hepatocyte necrosis or ferroptosis through mitochondrial dysfunction (Jaeschke et al., 2019; Shojaie et al., 2020).

The gut microbiota is an enormous microscopic community consisting of bacteria, fungi, viruses, and microeukaryotes (Norman et al., 2014). During the dynamic development of the gut microbiome in early life, bacteria-fungi crosstalk is important in maintaining microecological homeostasis and can define the trajectory of the health of the host (Iliev and Leonardi, 2017; Schei et al., 2017). In recent years, the ecological balance in the gut has been shown to regulate the pathogenesis of liver disease *via* the gut-liver axis (Albillos et al., 2020). Prior studies from our laboratory have revealed that the oscillation of gut microbiota mediated the diurnal variation of acetaminophen-induced acute liver injury through the generation of the gut microbial metabolite 1-phenyl-1,2-propanedione (PPD) in mice (Gong et al., 2018). With the increased understanding of intestinal microecology, research is gradually focusing on the potential of the gut fungal component in treating liver disease. For example, the yeast *Saccharomyces boulardii* seems to hinder the growth of pathogenic bacteria, revealing the potential therapeutic implications of certain fungi against infectious disease (Chen et al., 2020). In addition, gut commensal fungal dysbiosis induced by fluconazole (FC) could aggravate allergic airway disease in a house dust mite challenge mode by increasing the infiltration of gut-resident mononuclear phagocytes (MNPs) that express the fractalkine receptor CX3CR1 (Li et al., 2018). However, exactly what role the gut commensal fungi play in preventing the development and progression of drug-induced ALF remains unknown. In the present study, we revealed that gut commensal fungi ablation by fluconazole resulted in hepatic *Cyp2a5* overexpression, thereby increasing susceptibility to APAP hepatotoxicity due to enhanced inflammatory responses and oxidative stress.

**Abbreviations:** DILI, drug-induced liver injury; ALF, acute liver failure; APAP, acetaminophen; GSH, glutathione; ROS, reactive oxygen species; NAPQI, n-acetyl-p-benzoquinoneimine; PPD, 1-phenyl-1,2-propanedione; MNPs, mononuclear phagocytes; FC, fluconazole; PBS, phosphate-buffered saline; 8-MOP, 8-methoxypsoralen; ALT, alanine transaminase; AST, aspartate transaminase; MDA, malondialdehyde; SOD, superoxide dismutase; PFA, paraformaldehyde; HE, hematoxylin and eosin; HRP, horseradish peroxidase; TUNEL, terminal-deoxynucleotidyl transferase-mediated nick end labeling; DHE, dihydroethidium; MFI, mean fluorescence intensity; PCR, polymerase chain reaction; qRT-PCR, quantitative real-time polymerase chain reaction; TBST, tris-buffered saline tween; ECL, enhanced chemiluminescence; DEGs, differentially expressed genes; SEM, standard error of the mean; PD, phylogenetic distance; LDA, linear discriminant analysis; LEfSe, linear discriminant analysis effect size; *A. muciniphila*, *Akkermansia muciniphila*; *H. rodentium*, *Helicobacter rodentium*; IHC, immunohistochemical; PCoA, principal coordinate analysis; PCA, principal component analysis.

## MATERIALS AND METHODS

### Animal Models

A number of 6–8-week-old male specific-pathogen-free C57BL/6J mice were housed in standard laboratory conditions under a cycle of 12 h light/12 h dark at room temperature, with food and water *ad libitum*.

The mice were initially treated with fluconazole dissolved in distilled drinking water at a concentration of 0.5 g/l for 14 days (with the solution replaced every 2 days) in order to deplete the gut commensal fungi (Iliev et al., 2012). The mice in the control group were given distilled water. After fluconazole pretreatment, mice were given a single oral dose of 300 mg/kg APAP dissolved in phosphate-buffered saline (PBS) before being sacrificed for tissues collection 24 h later. In addition, mice were treated with a dose of 20 mg/kg 8-methoxypsoralen (8-MOP) dissolved in corn oil to investigate the role of *Cyp2a5* expression toward inhibiting inflammatory responses and oxidative stress in hepatotoxicity caused by APAP.

All experimental procedures were performed in accordance with the National Institutes of Health guidelines and were approved by the local Animal Care and Use Committee of Southern Medical University, Guangzhou, China.

### Biochemical Analysis

The levels of alanine transaminase (ALT) and aspartate transaminase (AST) in the serum were quantitated using commercial assay kits (Jiancheng, Nanjing, China) according to the manufacturer's instructions. Malondialdehyde (MDA), superoxide dismutase (SOD), and glutathione (GSH) activity in the liver tissues were determined using a corresponding

commercial assay kit (Jiancheng, Nanjing, China). TNF-α, IL-6, and MCP-1 concentrations in the plasma were measured by the ELISA assay kits (Neobioscience, Shenzhen, China), and the serum MCP-3 level was detected with an ELISA assay kit (CUSABIO, Wuhan, China).

## Histopathological Analysis

Liver tissues were fixed in 4% paraformaldehyde (PFA) for 24 h at room temperature, before being embedded in paraffin and sectioned. Hematoxylin and eosin (HE) staining were performed to assess pathological changes in the liver. At least 6–8 randomly selected fields per sample were used to calculate the area of liver necrosis over the whole field using ImageJ software (National Institute of Health).

## Immunohistochemical Staining

The paraffin-embedded slides were dewaxed, rehydrated, and incubated in 3% $H_2O_2$ for 20 min and calf serum for 15 min, respectively. Next, the slides were incubated with anti-CD11b antibody (Servicebio, Wuhan, China) at 4°C overnight, before being incubated with horseradish peroxidase (HRP)-labeled secondary antibody (Gene Tech, Shanghai, China). After washing with PBS, the slides were stained with DAB and hematoxylin, respectively. Finally, eight fields per slide were randomly photographed in order to assess and quantify CD11b-positive cells using ImageJ software.

## Fluorescence Staining

The paraffin-embedded liver sections were subjected to terminal-deoxynucleotidyl transferase-mediated nick end labeling (TUNEL) staining using a commercial assay kit (KeyGEN BioTECH, Nanjing, China) according to the manufacturer's instructions. At least 6–7 fields per slide were randomly selected in order to determine the number of TUNEL-positive cells.

To detect the hepatic ROS levels, the frozen liver sections were incubated with dihydroethidium (DHE, Thermo Scientific, MA, United States) at a final concentration of 2 μM at 37°C for 30 min. Between four and eight fields per slide were then selected at random and the mean fluorescence intensity (MFI) was analyzed using ImageJ software.

## Microbial Analysis

Feces from mice were collected on day 14 after fluconazole treatment and were immediately stored at-80°C. The fecal samples were mashed in PBS containing 0.5% Tween20 solution and were then subjected to repeated freezing at-80°C for 10 min and thawing at 60°C for 5 min. The next steps involved extracting and purifying the DNA using the phenol-chloroform isoamyl alcohol method and a commercial reagent (Solarbio, Beijing, China). Next, the concentration and purity of total DNA were determined by using a NanoDrop spectrophotometer (Thermo Scientific, MA, United States). The hypervariable region 4 (V4) of the bacterial 16S rRNA was amplified by a polymerase chain reaction (PCR) using primers V4-F (5′-GTGTGYCAGCMGCCGCGGTAA-3′) and V4-R (5′-CCG GACTACNVGGGTWTCTAAT-3′). DNA sequencing was performed on an Illumina Hiseq PE250, and the raw data of 16S rRNA gene sequencing were analyzed with the QIIME2 platform (v2020.2).

## Quantitative Real-Time PCR Analysis

RNA was extracted from the liver tissues using TRIzol reagent (Thermo Scientific, MA, United States) and separated by chloroform. cDNA was obtained by reverse transcription with ReverTra Ace qPCR RT Kit (Toyobo, Shanghai, China). Quantitative real-time PCR (qRT-PCR) analysis were performed on a 7,500 Real-Time PCR System (Applied Biosystems, CA, United States) and 18S ribosomal RNA was used for normalization and quantification of the target gene expression levels using the comparative CT method. All primers for qRT-PCR analysis were listed in **Table 1**.

## Western Blot

Liver tissues were homogenized in RIPA lysis buffer (Beyotime, Shanghai, China) on ice to prepare for total protein extraction. Total protein extractions were denatured with SDS loading buffer by heating at 95°C for 5 min. After blocking with 5% non-fat milk in tris-buffered saline tween (TBST), the membranes were incubated separately with total JNK (Cell Signaling Technology, MA, United States), p-JNK (Cell Signaling Technology, MA, United States), total p65 (Cell Signaling Technology, MA, United States), p-p65 (Cell Signaling Technology, MA, United States), total p38 (Cell Signaling Technology, MA, United States), p-p38 (Cell Signaling Technology, MA, United States), total ERK (Cell Signaling Technology, MA, United States), and p-ERK (Cell Signaling Technology, MA, United States) antibodies overnight at 4°C. Finally, the protein bands were incubated with secondary antibodies (Proteintech, Wuhan, China) for 1 h at room temperature and were then visualized using an enhanced chemiluminescence (ECL) detection kit (Vazyme, Wuhan, China).

## Transcriptomic Sequencing Analysis

To conduct the transcriptomic sequencing analysis, the total RNA from the livers of the APAP-treated mice with or without fluconazole pretreatment was extracted using TRIzol reagent (Thermo Scientific, MA, United States). Purified total RNA was performed to construct libraries, followed by subjection to sequence through Illumina NovaSeq 6,000 (Novogene Co., Ltd., Beijing, China). Statistical analysis was performed with the DESeq2 R package. The genes with $|\log2 \text{ (fold change)}| > 1$ and adjusted $p < 0.05$ were identified as differentially expressed genes (DEGs).

## Data Availability Statement

The transcriptome and 16S rDNA data have been uploaded to the China Nucleotide Sequence Archive (CNSA, https://db.cngb.org/cnsa/) under accession codes CNP0002810 and CNP0002825, respectively.

**TABLE 1** | Primers for qPCR.

| | Forward primer | Reverse primer |
|---|---|---|
| *18S* | AGTCCCTGCCCTTTGTACACA | CGATCCGAGGGCCTCACTA |
| *16S* | TGATGCACTTGCAGAAAACA | ACCAGAGGAAATTTTCAATAGGC |
| *Ccl2* | TAAAAACCTGGATCGGAACCAAA | GCATTAGCTTCAGATTTACGGGT |
| *Ccl3* | TGTACCATGACACTCTGCAAC | CAACGATGAATTGGCGTGGAA |
| *Ccl7* | CCACATGCTGCTATGTCAAGA | ACACCGACTACTGGTGATCCT |
| *Ptges* | GGATGCGCTGAAACGTGGA | CAGGAATGAGTACACGAAGCC |
| *Cbr3* | CATCGGCTTTGCGATCACG | GACCAGCACGTTAAGTCCCC |
| *Firmicutes* | GGAGYATGTGGTTTAATTCGA | AGCTGACGACAACCATGCAC |
| *Bacteroidetes* | GGCGACCGGCGCACGGG | GRCCTTCCTCTCAGAACCC |
| *A. muciniphila*[a] | CAGCACGTGAAGGTGGGGAC | CCTTGCGGTTGGCTTCAGAT |
| *H. rodentium*[b] | GTGGAGTGCTAGCTTGCTAGAA | ACCGTAGCATAGCTGATCTA |
| *FungiQuant* | GGRAAACTCACCAGGTCCAG | GSWCTATCCCCAKCACGA |
| *Cyp2a5* | TGGTCCTGTATTCACCATCTACC | ACTACGCCATAGCCTTTGAAAA |

[a]*Akkermansia muciniphila.*
[b]*Helicobacter rodentium.*

## Statistical Analysis

All data were expressed as mean ± standard error of the mean (SEM) and were evaluated by an unpaired two-tailed Student's *t*-test. A value of $p$ lower than 0.05 was considered significant ($^*p < 0.05$).

# RESULTS

## Gut Commensal Fungi Protect Mice Against APAP-Induced Acute Liver Failure

To explore the role of gut commensal fungi in APAP-induced hepatotoxicity, the mice were orally pretreated with fluconazole (FC) for 14 days to deplete the gut commensal fungi, followed by subjection to APAP administration (**Figure 1A**). First, we determined whether the gut commensal fungi depletion through fluconazole administration affected energy intake. As shown in **Figures 1B,C**, we found that food consumption and body weight were not altered by the presence of fluconazole in mice. Serum biochemistry results showed that ALT levels were comparable in control and fluconazole-treated mice (**Figure 1D**), which was further confirmed by the hepatic expression of inflammatory chemokine including *Ccl2*, *Ccl3* and *Ccl7* (**Figure 1E**). The above data suggested that the dose of fluconazole used in our study did not directly cause hepatotoxicity. Consistent with previous study (Qiu et al., 2015), the qRT-PCR result showed that the fluconazole-treated mice had a lesser abundance of gut fungi in comparison with the control group (**Figure 1F**). Interestingly, gut fungi ablation caused by the fluconazole pretreatment resulted in a significant increase in plasma ALT and AST levels in response to APAP administration (**Figure 1G**). Histopathological examination displayed that gut commensal fungi depletion significantly elevated the area of necrosis in the liver tissues of APAP-treated mice (**Figure 1H**). This result was further supported by the TUNEL staining, which measured the level of cell death including necrosis, apoptosis and necroptosis (**Figure 1I**; Grasl-Kraupp et al., 1995). All of the above-mentioned results indicated that gut commensal fungi depletion predisposed mice to APAP-induced hepatotoxicity.

## Gut Commensal Fungi Depletion Alters Bacterial Community Structure in Mice

A previous study had shown that the interactions between gut commensal fungi and bacteria are important for maintaining intestinal health and improving disease resistance (Sam et al., 2017). For this reason, we next performed 16S rDNA sequencing to determine the alterations in gut bacterial community structure in response to fluconazole treatment. The qRT-PCR result indicated a significant decrease in the *Firmicutes*/*Bacteroidetes* ratio, reflecting the composition of gut microbes in mice subjected to fluconazole treatment for 14 days (**Figure 2A**). There were significant changes in the alpha diversity of gut bacteria as shown by Faith's Phylogenetic Distance (PD) and Observed OTUs, although not in the Shannon diversity index (**Figure 2B**). Consistently, significant intergroup differences among control and fluconazole-treated mice were assessed using the Bray-Curtis metric distance according to the principal coordinates analysis (**Figure 2C**). Moreover, gut fungi ablation through fluconazole treatment induced a distinct clustering of microbiota composition at the phylum level in mice (**Figure 2D**).

Specially, the linear discriminant analysis (LDA) effect size (LEfSe) statistical analysis indicated that mice subjected to fluconazole treatment were enriched for members of genus *Helicobacter* and *Dorea*, whereas genus *Akkermansia* and *Allobaculum* were enriched in control group (**Figure 2E**). To validate these results, we performed qRT-PCR to determine the changes in gut microbiota in response to fluconazole treatment and found that the abundance of *Akkermansia muciniphila* (*A. muciniphila*) was decreased, however, *Helicobacter rodentium* (*H. rodentium*) abundance exhibited an opposite trend in fluconazole-treated mice compared with the control group (**Figure 2F**). PICRUSt analysis on the OTU derived from the 16S rDNA sequence was also conducted to predict potential metabolic functions of gut microbiota in fluconazole-treated mice. In company with

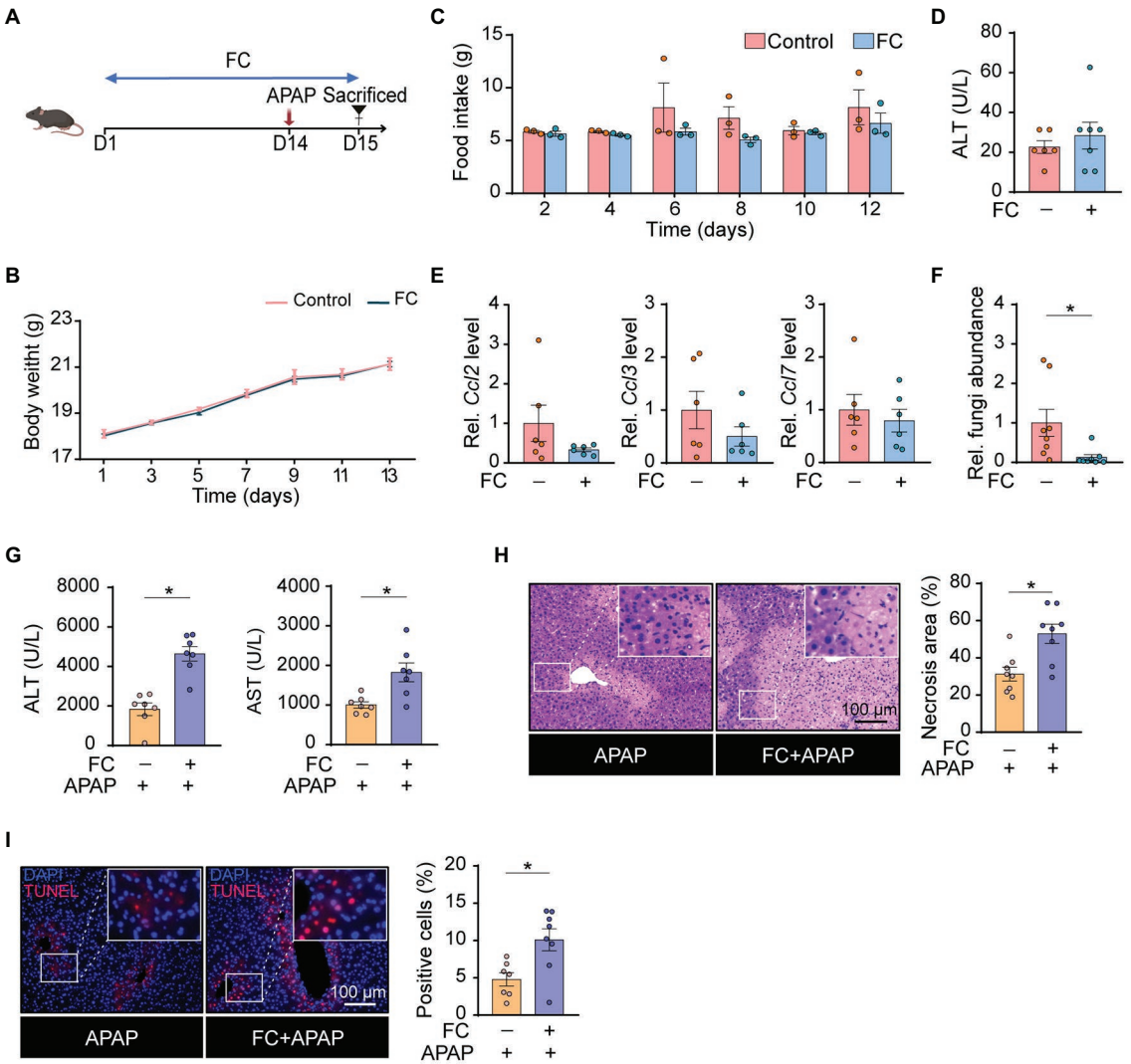


**FIGURE 1** | Gut commensal fungi protect mice against APAP-induced acute liver failure. **(A)** Study design. C57BL/6 mice were pretreated with fluconazole for 14 days to deplete the gut commensal fungi, followed by subjection to APAP administration for 24 h. Tissues were collected after mice were euthanized. **(B)** Body weight change in the control and fluconazole-only group. **(C)** Food intake of the control and fluconazole-only group. **(D)** Effect of fluconazole administration alone on serum ALT levels. **(E)** Relative mRNA levels of *Ccl2, Ccl3,* and *Ccl7* in the liver of control and fluconazole-only group were detected by qRT-PCR. **(F)** Relative abundance of fungi in the gut of the control and fluconazole-only group. **(G)** Plasma ALT and AST levels in APAP-treated mice with or without preadministration of fluconazole. **(H)** Representative H&E staining images and quantification of necrotic areas in the livers of APAP-treated mice with or without preadministration of fluconazole. **(I)** TUNEL staining of the liver from APAP-treated mice with or without preadministration of fluconazole and quantification of dead cells. $^*p < 0.05$. Data were expressed as mean ± SEM and were evaluated by a two-tailed unpaired Student's *t*-test. $n = 3$–8. Scale bar = 100 μm. FC, fluconazole; APAP, acetaminophen; ALT, alanine aminotransferase; AST, aspartate aminotransferase; Rel, Relative; H&E, hematoxylin and eosin; and TUNEL, terminal-deoxynucleotidyl transferase-mediated nick end labeling.

increased abundance of *Helicobacter*, which is defined as pathogens associated with generation of lipopolysaccharides (Hynes et al., 2004), the genomic abundance of some pathways, which included lipopolysaccharide biosynthesis and NOD-like receptor signaling pathway were significantly enhanced in fluconazole-treated mice compared with the control group (**Figure 2G**). In contrast, we also found that some pathways including sulfur metabolism and steroid biosynthesis were enriched in the control group (**Figure 2G**). All of the above data demonstrated that the crosstalk of bacteria and fungi is important in maintaining microecological homeostasis.

## Gut Commensal Fungi Ablation Promotes the Inflammatory Response Associated With Aberrant Arachidonic Acid Metabolism in APAP-Treated Mice

To explore how gut commensal fungi protected mice against APAP-induced acute liver injury, we performed transcriptome

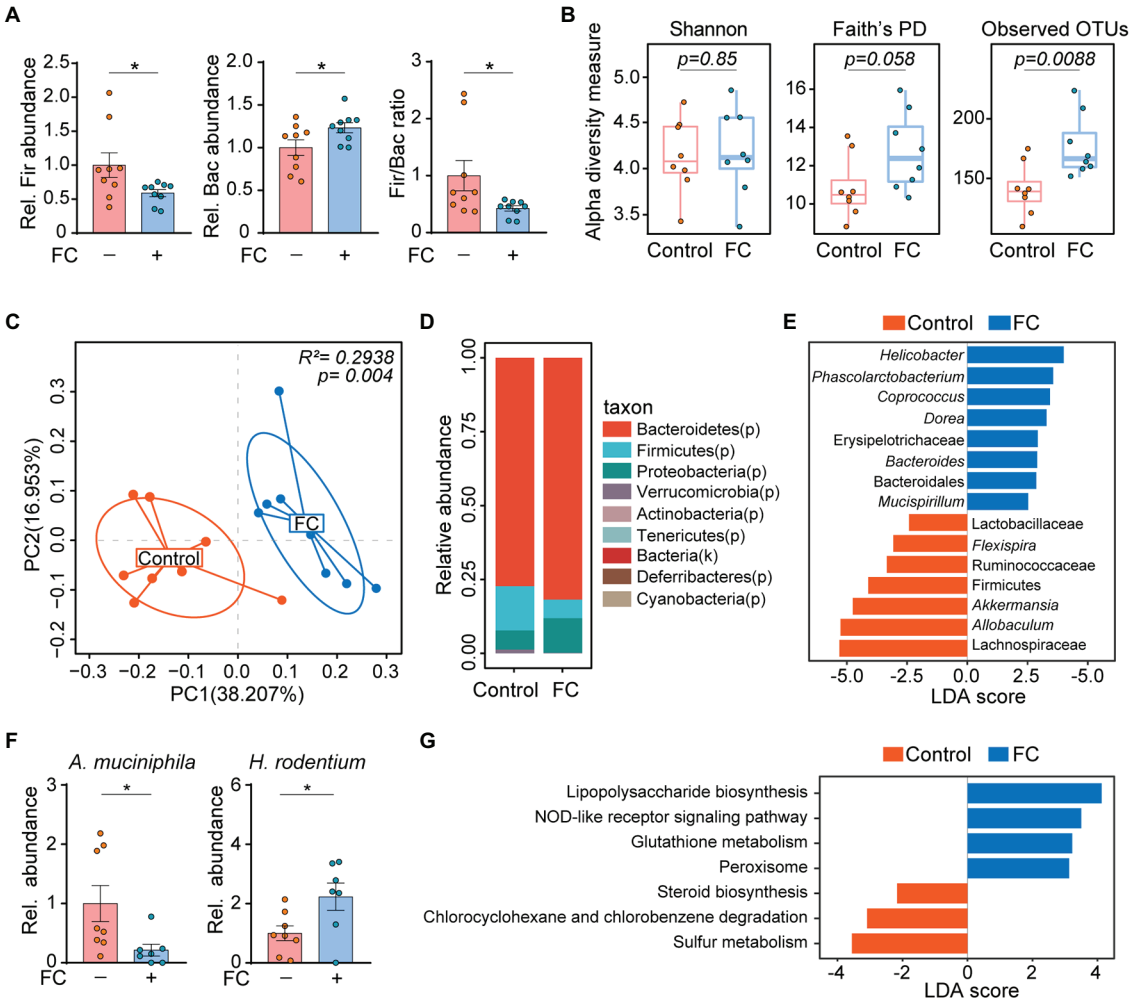


**FIGURE 2 |** Gut commensal fungi depletion alters bacterial community structure in mice. **(A)** C57BL/6 mice were treated with fluconazole to deplete the gut commensal fungi. Feces were collected after 14 days of fluconazole treatment. Relative abundance of *Firmicutes* and *Bacteroidetes* as well as the ratio of *Firmicutes*/*Bacteroidetes* in the feces of control and fluconazole-only group. **(B)** Alpha diversity based on Shannon Index, Faith's PD, and Observed OTUs of gut microbiota in the control and fluconazole-only group. These data were evaluated by Wilcoxon rank-sum test. **(C)** Principal coordinate analysis (PCoA) using Bray–Curtis distance of microbial composition in control and fluconazole-treated mice. These data were evaluated by the Adonis test. **(D)** Relative abundance of gut microbiota at phylum level from control and fluconazole-treated mice. **(E)** The differences in specific microbiota taxa between the control and fluconazole-treated mice were identified by linear discriminant analysis effect size (LEfSe) analysis. **(F)** Relative abundance of *Akkermansia muciniphila* and *Helicobacter rodentium* in control and fluconazole-treated mice. **(G)** Predicated functional KEGG pathways were inferred from OTUs by PICRUSt analysis in control and fluconazole-treated mice. *$p < 0.05$. All bar graph data were expressed as mean ± SEM and were evaluated by a two-tailed unpaired Student's *t*-test. $n = 7$–9. Rel, Relative; FC, fluconazole; Fir, *Firmicutes*; Bac, *Bacteroidetes*; *A. muciniphila*, *Akkermansia muciniphila*; *H. rodentium*, *Helicobacter rodentium*; LEfSe, linear discriminant analysis effect size; and LDA, linear discriminant analysis.

analysis of the liver tissues collected from the APAP-treated mice subjected to fluconazole preadministration. Notably, the KEGG pathway enrichment analysis of DEGs showed that the pathway of arachidonic acid metabolism was enhanced in fluconazole-pretreated mice compared with the control group in the presence APAP administration (**Figure 3A**), which was also confirmed by PCA analysis (**Figure 3B**). Concomitantly, volcano plots displayed that mice subjected to fluconazole pretreatment exhibited an increase in the hepatic mRNA levels of the *Ptges* and *Cbr3* genes responsible for inflammatory mediator prostaglandin E2 biosynthesis and metabolism in the presence of APAP (**Figure 3C**). The DEGs identified by the transcriptome analysis were also convincingly supported by real-time quantitative PCR analysis (**Figure 3D**).

Emerging evidence indicated that the aberrant metabolism of arachidonic acid profoundly triggers an inflammatory response in the host, thus resulting in an acceleration of the disease process (Harizi et al., 2008). Therefore, it was reasonable to speculate that gut commensal fungi ablation through fluconazole treatment predisposed mice to hepatotoxicity caused by APAP overdose, which appeared to be due to vigorous proinflammatory cytokine production. Indeed, compared with control mice, fluconazole pretreatment resulted in a larger increase in the concentrations of cytokine and chemokine including TNF-α, IL-6, MCP-1 and MCP-3 in the blood of APAP-treated mice (**Figure 3E**). In addition, we also observed that gut commensal fungi depletion exacerbated hepatic inflammatory responses

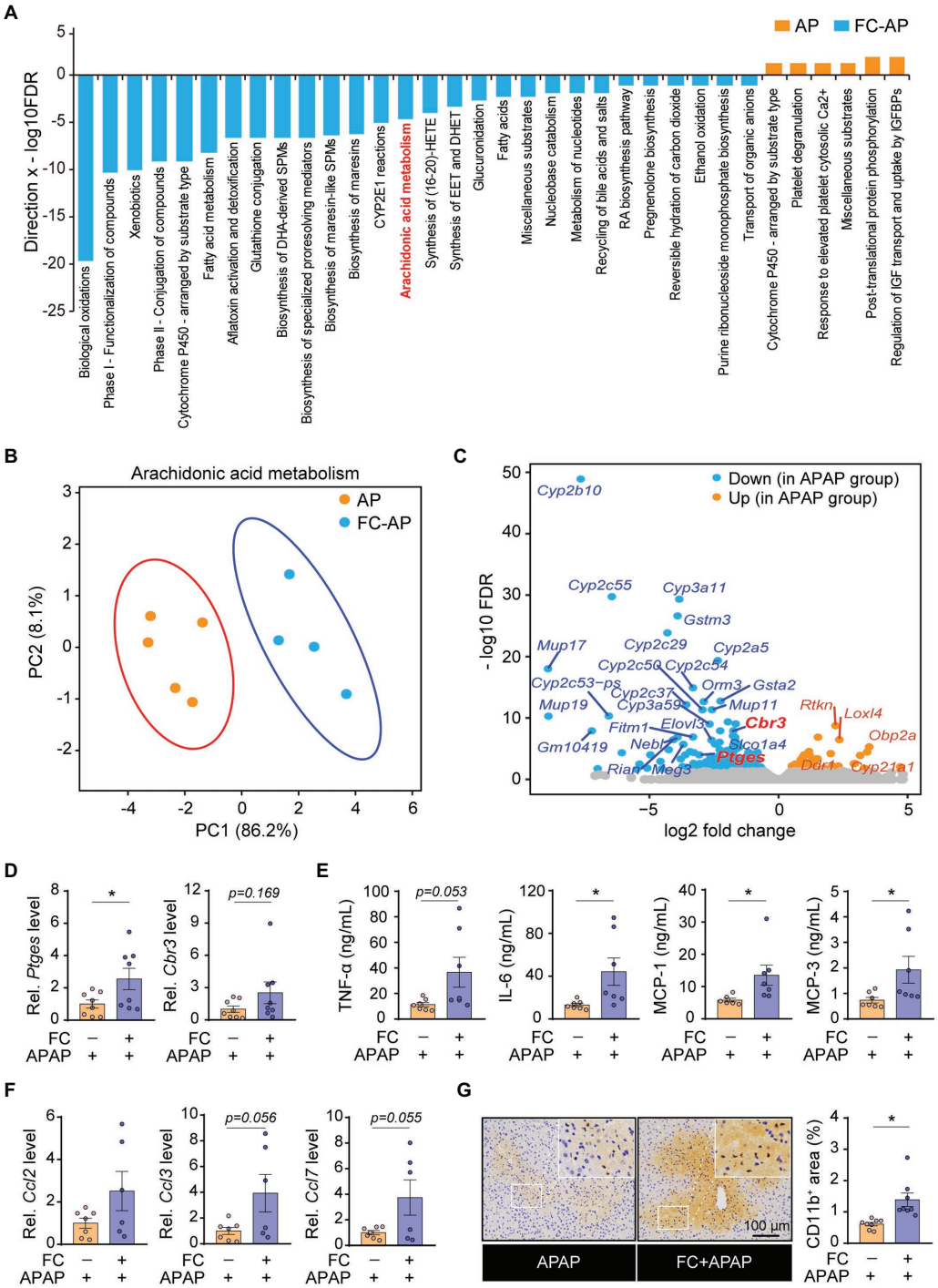


**FIGURE 3 |** Gut commensal fungi ablation promotes the inflammatory response associated with aberrant arachidonic acid metabolism in APAP-treated mice. **(A)** Hypergeometric analysis showing pathway enrichment analysis of the liver tissues from APAP-treated mice with or without preadministration of fluconazole. **(B)** The principal component analysis (PCA) of arachidonic acid metabolism is based on transcriptomic analysis in APAP-treated mice with or without preadministration of fluconazole. **(C)** Volcano plot of DEGs in the control group compared with fluconazole-pretreated mice in presence of APAP administration. **(D)** Relative mRNA levels of *Ptges* and *Cbr3* in liver tissues of APAP-treated mice with or without preadministration of fluconazole. **(E)** Quantification of pro-inflammatory cytokines including TNF-α, IL-6, MCP-1 and MCP-3 in the blood from APAP-treated mice with or without preadministration of fluconazole. **(F)** Relative mRNA levels of *Ccl2, Ccl3,* and *Ccl7* in the liver of APAP-treated mice with or without preadministration of fluconazole were detected by qRT-PCR. **(G)** Immunohistochemical staining of CD11b and quantification of positive cells in the liver tissues of APAP-treated mice with or without preadministration of fluconazole. *$p < 0.05$. All bar graph data were expressed as mean ± SEM and were evaluated by a two-tailed unpaired Student's *t*-test. $n = 4–8$. Scale bar = 100 μm. APAP, acetaminophen; FC, fluconazole; and Rel, Relative.

in response to APAP administration, as indicated by the increase in the mRNA levels of chemokines (**Figure 3F**). Furthermore, immunohistochemical (IHC) staining displayed that the number of infiltrating CD11b-positive cells, defined as inflammatory cells (Solovjov et al., 2005), increased in the liver tissues of APAP-treated mice who had been pretreated with fluconazole (**Figure 3G**). In all, the above results suggested that the gut fungi ablation by fluconazole pretreatment have enhanced hepatic inflammation in mice upon APAP exposure.

## Gut Commensal Fungi Ablation Exacerbates Hepatic Oxidative Stress in APAP-Treated Mice

A previous study demonstrated that the depletion of hepatic reduced glutathione and the subsequent oxidative stress is involved in the pathogenesis of APAP-induced acute liver injury (Goldring et al., 2004). In order to further understand the underlying mechanism by which gut fungi ablation enhanced hepatotoxicity induced by APAP in mice, we thus determined the level of oxidative stress in the liver from APAP-treated mice subjected to fluconazole pretreatment. We first found that hepatic malondialdehyde (MDA) levels in APAP-treated mice subjected to fluconazole preadministration were significantly higher than in the APAP-only group (**Figure 4A**). Correspondingly, the markers of antioxidant capacity, SOD activity and GSH levels were significantly repressed in the livers of APAP-treated mice subjected to fluconazole preadministration (**Figures 4B,C**). In addition, DHE staining showed that fluconazole preadministration significantly increased ROS accumulation in the liver of APAP-treated mice (**Figure 4D**). We next focused on the down signaling pathway which was affected by fluconazole preadministration in APAP-treated mice. As shown in **Figure 4E**, the phosphorylation level of JNK was significantly increased in the livers of APAP-treated mice subjected to fluconazole preadministration compared with the APAP-only group, whereas other MAPK and NF-κB signaling pathways remained comparable in the two groups. All of these data indicated that fluconazole-induced oxidative stress and sustained JNK activation predisposed mice to APAP-induced hepatotoxicity.

## Gut Commensal Fungi Ablation Enhances the Susceptibility to APAP-Induced Hepatotoxicity by Upregulation of Hepatic *Cyp2a5* Level

To further illustrate the underlying molecular mechanism of fluconazole pretreatment responsible for excessive inflammatory response and oxidative stress in APAP-treated mice, we performed transcriptome analysis and selected the top twenty DEGs ranked by value of $p$ for interaction network analysis. **Figures 5A,B** show that the expression of *Cyp2a5*, identified as the hub gene and highlighted in red, was increased in liver tissues of APAP-treated mice subjected to fluconazole pretreatment. On the basis of these observations, we considered that gut commensal fungi ablation through fluconazole treatment could promote hepatic *Cyp2a5* overexpression, thereby resulting in increasing the susceptibility to APAP-induced hepatotoxicity in mice.

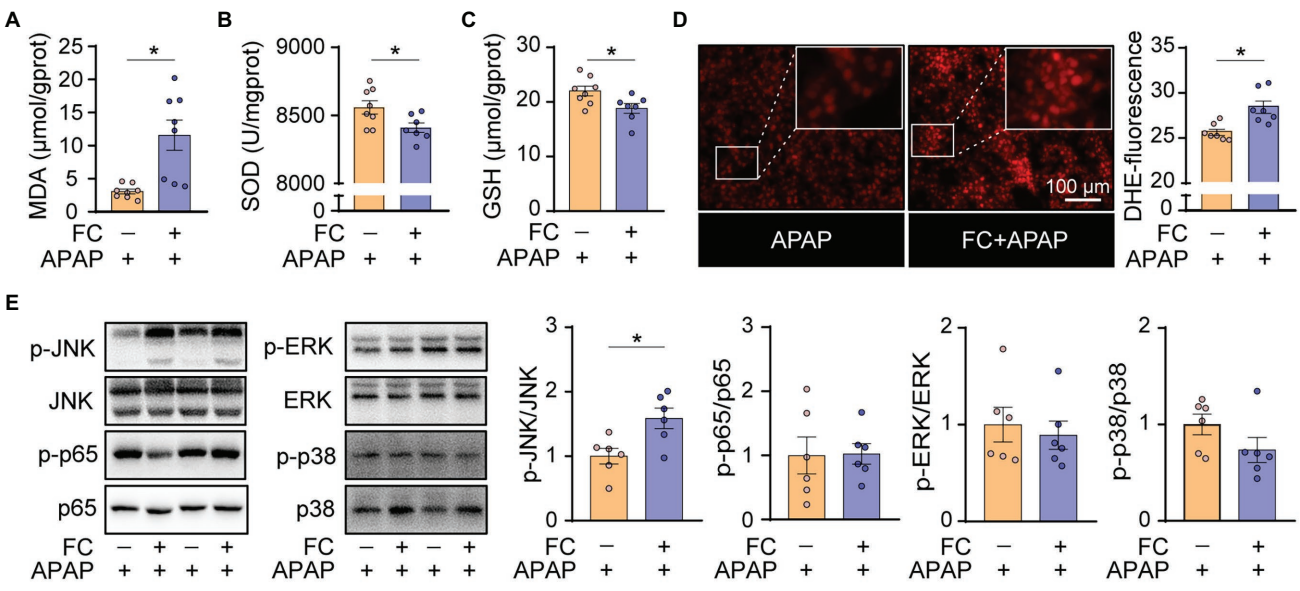


**FIGURE 4 |** Gut commensal fungi ablation exacerbates hepatic oxidative stress in APAP-treated mice. **(A–C)** C57BL/6 mice were pretreated with fluconazole for 14 days to deplete the gut commensal fungi and were then subjected to APAP administration for 1 h. Hepatic MDA **(A)**, SOD **(B)** and total GSH **(C)** levels in APAP-treated mice with or without preadministration of fluconazole. **(D)** Representative images of DHE immunofluorescence staining and quantification of hepatic ROS production in APAP-treated mice with or without preadministration of fluconazole. **(E)** Western blot was performed with specific antibodies to quantify the phosphorylated JNK, ERK, p38 and p65 in the liver tissues from APAP-treated mice with or without preadministration of fluconazole. *$p < 0.05$. Data were expressed as mean ± SEM and were evaluated by a two-tailed unpaired Student's $t$-test. $n = 6–8$. Scale bar = 100 μm. APAP, acetaminophen; FC, fluconazole; MDA, malonaldehyde; SOD, superoxide dismutase; GSH, glutathione; and DHE, dihydroethidium.

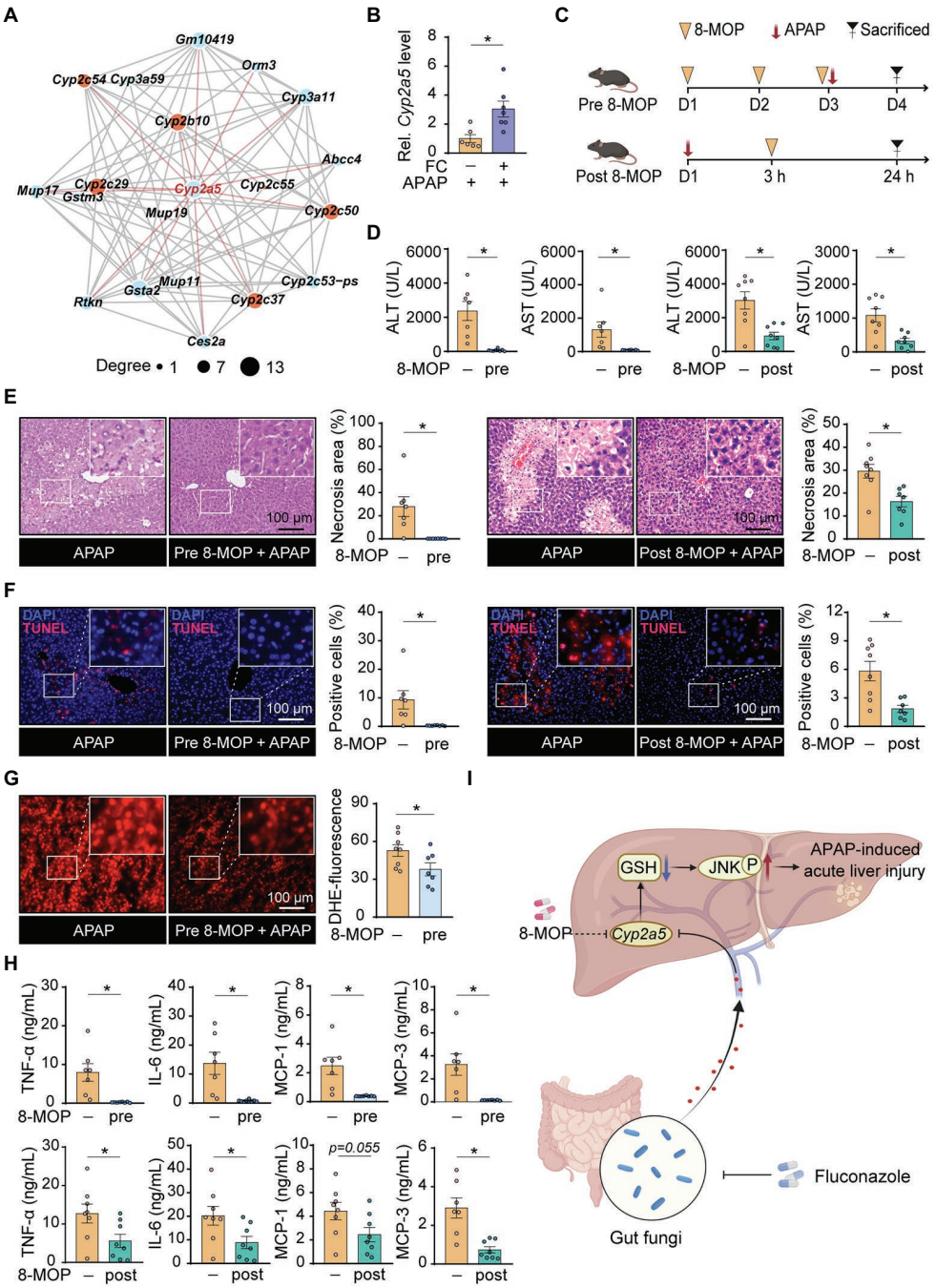


**FIGURE 5 |** Gut commensal fungi ablation enhances the susceptibility to APAP-induced hepatotoxicity by upregulation of hepatic *Cyp2a5* level. **(A)** The interaction network of the top twenty DEGs in the control group compared with fluconazole-pretreated mice in presence of APAP administration. C57BL/6 mice were pretreated with fluconazole for 14 days to deplete the gut commensal fungi, followed by subjection to APAP administration for 24 h. Liver tissues were collected for transcriptome sequencing analysis. **(B)** Relative mRNA levels of *Cyp2a5* in the liver tissues from APAP-treated mice with or without preadministration of fluconazole. **(C)** Study design. Mice were pre- and post-treated with the *Cyp2a5* inhibitor, 8-MOP, in presence of APAP administration. After 24 h of APAP treatment, the mice were sacrificed, and tissues were collected for further analysis. **(D)** Effect of 8-MOP on ALT and AST levels in the blood of APAP-treated mice. **(E)** Representative H&E staining images and quantification of necrotic areas in the liver from APAP-treated mice with or without administration of 8-MOP. **(F)** TUNEL staining of the liver from APAP-treated mice with or without administration of 8-MOP and quantification of dead cells. **(G)** Representative images of DHE immunofluorescence staining and quantification of hepatic ROS production in APAP-treated mice with or without preadministration of 8-MOP. **(H)** Quantification of pro-inflammatory cytokines including TNF-α, IL-6, MCP-1 and MCP-3 in the blood of APAP-treated mice with or without 8-MOP administration. **(I)** Working model: Mice with gut fungi depletion by fluconazole treatment showed more sensitivity to APAP-induced acute liver injury through the promotion of hepatic *Cyp2a5* overexpression (Created with BioRender.com). *$p < 0.05$. Data were expressed as mean ± SEM and were evaluated by a two-tailed unpaired Student's *t*-test. $n = 6$–8. Scale bar = 100 μm. APAP, acetaminophen; FC, fluconazole; Rel, Relative; 8-MOP, 8-methoxypsoralen; ALT, alanine aminotransferase; AST, aspartate aminotransferase; H&E, hematoxylin and eosin; TUNEL, terminal-deoxynucleotidyl transferase-mediated nick end labeling; and DHE, dihydroethidium.

To verify this hypothesis, mice were pre- and post-treated with 8-methoxypsoralen (8-MOP, known as a *Cyp2a5* inhibitor) in the presence of APAP administration, respectively (**Figure 5C**). Interestingly, pharmacologic inhibition of *Cyp2a5*, by administration of 8-MOP to control mice, fully reversed the hepatotoxicity induced by APAP administration, as indicated by the result of serum biochemistry (**Figure 5D**). Furthermore, histopathological examination displayed that the percentage of cell death apparently decreased in the liver tissues of APAP-treated mice subjected to 8-MOP treatment compared with the APAP-only group (**Figures 5E,F**). In line with the above results, pharmacologic inhibition of *Cyp2a5* significantly suppressed the accumulation of hepatic ROS as well as cytokine and chemokine release in APAP-treated mice (**Figures 5G,H**). Taken together, these discoveries suggested that inhibiting hepatic *Cyp2a5* overexpression may hold promise as a novel pharmacological strategy for treating APAP-induced acute liver injury.

## DISCUSSION

DILI is a common acute liver disease characterized by high mortality and is mainly caused by an overdose of APAP in Western countries (Andrade et al., 2019). The pathogenesis of APAP-induced hepatotoxicity is associated with the persistent depletion of hepatic reduced glutathione (GSH), leading to predispose hepatocytes to sustained oxidative stress-induced necroptosis and ferroptosis (Matsumaru et al., 2003; Yamada et al., 2020). The incidence of DILI was progressively increased worldwide that accompany with the action of abuse drugs (Haque et al., 2016). Therefore, novel targeted strategies for the treatment of drug-induced hepatotoxicity are essential.

Although maintaining the ecological homeostasis in the gut has recently been shown to increase resistance to ALF, the biological functions of gut commensal fungi in regulation of the sustained oxidative stress during acute liver injury induced by APAP overdose remain largely undefined (Chopyk and Grakoui, 2020). Our data clearly revealed that fluconazole pretreatment predisposed mice to accelerated hepatotoxicity induced by APAP. We next explored whether the effects of fluconazole in the progression of APAP-induced liver injury were in gut fungi-dependent manner. It is well known that glutathione biosynthesis is dependent on the uptake of amino acids during food processing and digestion (Minich and Brown, 2019). We first monitored food consumption and body weight periodically until the end of the fluconazole treatment period to exclude the possibility that any difference in energy metabolism between the fluconazole-treated mice and the control group influenced the process of glutathione biosynthesis in the liver. Additionally, we also found that fluconazole treatment alone did not cause liver injury in our study, as confirmed by the serum level of ALT, and the expression of chemokines in control and fluconazole-treated mice, whereas we found that the gut fungi load was significantly reduced in fluconazole-treated mice compared with the control group, a result consistent with previous literature (Li et al., 2018). These above results indicated that gut commensal fungi could protect mice against APAP-induced liver injury, which suggested that maintaining the gut commensal fungi balance could be a promising therapeutic strategy for preventing DILI. Further preclinical and clinical research will be necessary to identify the specific intestinal-resident fungi responsible for protecting against drug-induced hepatotoxicity.

Since commensal bacteria coexist with fungi in the intestine, maintaining microecological homeostasis can increase resistance to disease through the modulation of host immunity (Clemente et al., 2012). This notion is supported by the other observation that antibiotic-mediated depletion of intestinal-resident bacteria may shift the organizational structure of gut commensal fungi, leading to result in an overabundance of *Saccharomycetes* fungi in particular (Jiang et al., 2017). However, less is known about whether fluconazole-induced fungi depletion leads to persistent changes in the composition of gut bacteria. In the present study, we noted that gut commensal fungi ablation through fluconazole treatment could increase the diversity of intestinal bacteria communities, as shown by Faith's Phylogenetic Distance (PD) and the Observed OTUs, which appears to be due to a strong competition between enteric bacterial and fungal components for commonly available nutrients in a shared environment. In addition, our data showed that the relative ratio of *Firmicutes* and *Bacteroidetes* was decreased in fluconazole-treated mice compared with the control group, indicating the occurrence of a gut microbiota disorder. In particular, we found that gut fungi ablation leads to an overabundance of the enteric bacterial pathogen *H. rodentium*, while the level of probiotic *A. muciniphila* was decreased. Therefore, our study has provided new insight into the significance of enteric bacteria-fungi interactions, although the functions of the bacteria or its derived metabolites modulated by fungal components in the gut need further clarification.

A key finding of the current study was the highlighting of inhibition of hepatic *Cyp2a5* expression as a novel therapeutic strategy for treating drug-induced liver failure. As a member of the CYP2A subfamily, murine *Cyp2a5*, and its human ortholog, *Cyp2a6*, have been identified as important xenobiotic-metabolizing enzymes in the liver (Kim et al., 2005; Kirby et al., 2011). Recent research indicated that exposure to chemicals including ethanol, thioacetamide, and cadmium could promote upregulations of hepatic *Cyp2a5* expression in mice, thereby modulating disease susceptibility by affecting oxidative stress (Lu et al., 2011; Hong et al., 2016). However, the pathogenic role of *Cyp2a5* in regulating acute liver injury induced by APAP overdose remains unclear. In the present study, we found that the expression of *Cyp2a5* was increased in APAP-treated mice subjected to fluconazole pretreatment, suggesting that *Cyp2a5* appears to be a dominant-positive regulator of APAP hepatotoxicity. To verify this hypothesis, we applied a known *Cyp2a5* inhibitor, 8-methoxypsoralen (8-MOP), to APAP-treated mice and found that the pharmacologic inhibition of *Cyp2a5* fully reversed the hepatotoxicity induced by APAP administration.

Given the possibility that the protective role of 8-MOP on APAP-induced hepatotoxicity was mediated through the blocking of APAP metabolic bioactivation, mice were treated with 8-MOP after 3 h of APAP administration, by which time the processes of intrahepatic APAP metabolic is end (Souza et al., 2022).

Serum biochemical analysis showed that administering 8-MOP post-treatment also reduced APAP-induced hepatotoxicity in mice, a conclusion which was further confirmed by histopathological examination. The pharmacologic inhibition of *Cyp2a5*, therefore, could play a role in preventing drug-induced liver failure, although the potential therapeutic effects of 8-MOP will require further clinical study.

In summary, our findings identified the protective role of gut commensal fungi against acute APAP-induced liver injury through an attenuated inflammatory response and oxidative stress in mice and have shed light on the significance of downregulating *Cyp2a5* by 8-MOP as a novel pharmacological strategy for treating DILI.

## DATA AVAILABILITY STATEMENT

The datasets presented in this study can be found in online repositories. The names of the repository/repositories and accession number(s) can be found in the article/**Supplementary Material**.

## ETHICS STATEMENT

The animal study was reviewed and approved by the Institutional Animal Care and Use Committee of Southern Medical University, Guangzhou, China.

## AUTHOR CONTRIBUTIONS

SG, LL, WX, XZ, and HY were responsible for the study design, supervision, and manuscript preparation. ZH, YZ, SL, LL, RZ, FW, WY, and YW were responsible for the experiment. JY, AC, and ZW were responsible for sequencing analysis. All authors contributed to the article and approved the submitted version.

## FUNDING

This work was financially supported by the National Natural Science Foundation of China (81973804), Shenzhen Science and Technology Program (RCBS20210706092252059), the Key Project of National Natural Science Foundation of China (81830117), and the National Natural Science Foundation of China (82104382).

## ACKNOWLEDGMENTS

We thank Jiaqi Li for the excellent technical assistance.

## SUPPLEMENTARY MATERIAL

The Supplementary Material for this article can be found online at: https://www.frontiersin.org/articles/10.3389/fmicb.2022.944416/full#supplementary-material

## REFERENCES

Albillos, A., De Gottardi, A., and Rescigno, M. (2020). The gut-liver axis in liver disease: pathophysiological basis for therapy. *J. Hepatol.* 72, 558–577. doi: 10.1016/j.jhep.2019.10.003

Andrade, R. J., Chalasani, N., Björnsson, E. S., Suzuki, A., Kullak-Ublick, G. A., Watkins, P. B., et al. (2019). Drug-induced liver injury. *Nat. Rev. Dis. Primers.* 5:58. doi: 10.1038/s41572-019-0105-0

Bernal, W., Hyyrylainen, A., Gera, A., Audimoolam, V. K., McPhail, M. J., Auzinger, G., et al. (2013). Lessons from look-back in acute liver failure? A single Centre experience of 3300 patients. *J. Hepatol.* 59, 74–80. doi: 10.1016/j.jhep.2013.02.010

Bernal, W., and Wendon, J. (2013). Acute liver failure. *N. Engl. J. Med.* 369, 2525–2534. doi: 10.1056/NEJMra1208937

Chen, K., Zhu, Y., Zhang, Y., Hamza, T., Yu, H., Saint Fleur, A., et al. (2020). A probiotic yeast-based immunotherapy against Clostridioides difficile infection. *Sci. Transl. Med.* 12:eaax4905. doi: 10.1126/scitranslmed.aax4905

Chopyk, D. M., and Grakoui, A. (2020). Contribution of the intestinal microbiome and gut barrier to hepatic disorders. *Gastroenterology* 159, 849–863. doi: 10.1053/j.gastro.2020.04.077

Clemente, J. C., Ursell, L. K., Parfrey, L. W., and Knight, R. (2012). The impact of the gut microbiota on human health: an integrative view. *Cell* 148, 1258–1270. doi: 10.1016/j.cell.2012.01.035

Fernandez-Checa, J. C., Bagnaninchi, P., Ye, H., Sancho-Bru, P., Falcon-Perez, J. M., Royo, F., et al. (2021). Advanced preclinical models for evaluation of drug-induced liver injury–consensus statement by the European drug-induced liver injury network [PRO-EURO-DILI-NET]. *J. Hepatol.* 75, 935–959. doi: 10.1016/j.jhep.2021.06.021

Goldring, C. E., Kitteringham, N. R., Elsby, R., Randle, L. E., Clement, Y. N., Williams, D. P., et al. (2004). Activation of hepatic Nrf2 in vivo by acetaminophen in CD-1 mice. *Hepatology* 39, 1267–1276. doi: 10.1002/hep.20183

Gong, S., Lan, T., Zeng, L., Luo, H., Yang, X., Li, N., et al. (2018). Gut microbiota mediates diurnal variation of acetaminophen induced acute liver injury in mice. *J. Hepatol.* 69, 51–59. doi: 10.1016/j.jhep.2018.02.024

Grasl-Kraupp, B., Ruttkay-Nedecky, B., Koudelka, H., Bukowska, K., Bursch, W., and Schulte-Hermann, R. (1995). In situ detection of fragmented DNA (TUNEL assay) fails to discriminate among apoptosis, necrosis, and autolytic cell death: a cautionary note. *Hepatology* 21, 1465–1468. doi: 10.1002/hep.1840210534

Haque, T., Sasatomi, E., and Hayashi, P. H. (2016). Drug-induced liver injury: pattern recognition and future directions. *Gut. Liver* 10, 27–36. doi: 10.5009/gnl15114

Harizi, H., Corcuff, J.-B., and Gualde, N. (2008). Arachidonic-acid-derived eicosanoids: roles in biology and immunopathology. *Trends Mol. Med.* 14, 461–469. doi: 10.1016/j.molmed.2008.08.005

Hong, F., Si, C., Gao, P., Cederbaum, A. I., Xiong, H., and Lu, Y. (2016). The role of CYP2A5 in liver injury and fibrosis: chemical-specific difference. *Naunyn. Schmiedebergs Arch. Pharmacol.* 389, 33–43. doi: 10.1007/s00210-015-1172-8

Hynes, S. O., Ferris, J. A., Szponar, B., Wadström, T., Fox, J. G., O'Rourke, J., et al. (2004). Comparative chemical and biological characterization of the lipopolysaccharides of gastric and enterohepatic helicobacters. *Helicobacter* 9, 313–323. doi: 10.1111/j.1083-4389.2004.00237.x

Iliev, I. D., Funari, V. A., Taylor, K. D., Nguyen, Q., Reyes, C. N., Strom, S. P., et al. (2012). Interactions between commensal fungi and the C-type lectin receptor Dectin-1 influence colitis. *Science* 336, 1314–1317. doi: 10.1126/science.1221789

Iliev, I. D., and Leonardi, I. (2017). Fungal dysbiosis: immunity and interactions at mucosal barriers. *Nat. Rev. Immunol.* 17, 635–646. doi: 10.1038/nri.2017.55

Jaeschke, H., Ramachandran, A., Chao, X., and Ding, W.-X. (2019). Emerging and established modes of cell death during acetaminophen-induced liver injury. *Arch. Toxicol.* 93, 3491–3502. doi: 10.1007/s00204-019-02597-1

Jiang, T. T., Shao, T.-Y., Ang, W. G., Kinder, J. M., Turner, L. H., Pham, G., et al. (2017). Commensal fungi recapitulate the protective benefits of intestinal bacteria. *Cell Host Microbe* 22, 809.e4–816.e4. doi: 10.1016/j.chom.2017.10.013

Kim, D., Wu, Z.-L., and Guengerich, F. P. (2005). Analysis of coumarin 7-hydroxylation activity of cytochrome P450 2A6 using random mutagenesis. *J. Biol. Chem.* 280, 40319–40327. doi: 10.1074/jbc.M508171200

Kirby, G. M., Nichols, K. D., and Antenos, M. (2011). CYP2A5 induction and hepatocellular stress: an adaptive response to perturbations of heme homeostasis. *Curr. Drug Metab.* 12, 186–197. doi: 10.2174/138920011795016845

Krenkel, O., Mossanen, J. C., and Tacke, F. (2014). Immune mechanisms in acetaminophen-induced acute liver failure. *Hepatobiliary Surg. Nutr.* 3, 331–343. doi: 10.3978/j.issn.2304-3881.2014.11.01

Larson, A. M., Polson, J., Fontana, R. J., Davern, T. J., Lalani, E., Hynan, L. S., et al. (2005). Acetaminophen-induced acute liver failure: results of a United States multicenter, prospective study. *Hepatology* 42, 1364–1372. doi: 10.1002/hep.20948

Li, X., Leonardi, I., Semon, A., Doron, I., Gao, I. H., Putzel, G. G., et al. (2018). Response to fungal dysbiosis by gut-resident CX3CR1$^{+}$ mononuclear phagocytes aggravates allergic airway disease. *Cell Host Microbe* 24, 847–856.e4. doi: 10.1016/j.chom.2018.11.003

Li, L., Wang, H., Zhang, J., Sha, Y., Wu, F., Wen, S., et al. (2020). SPHK1 deficiency protects mice from acetaminophen-induced ER stress and mitochondrial permeability transition. *Cell Death Differ.* 27, 1924–1937. doi: 10.1038/s41418-019-0471-x

Lu, Y., Zhuge, J., Wu, D., and Cederbaum, A. I. (2011). Ethanol induction of CYP2A5: permissive role for CYP2E1. *Drug Metab. Dispos.* 39, 330–336. doi: 10.1124/dmd.110.035691

Matsumaru, K., Ji, C., and Kaplowitz, N. (2003). Mechanisms for sensitization to TNF-induced apoptosis by acute glutathione depletion in murine hepatocytes. *Hepatology* 37, 1425–1434. doi: 10.1053/jhep.2003.50230

Minich, D. M., and Brown, B. I. (2019). A review of dietary (phyto) nutrients for glutathione support. *Nutrients* 11:2073. doi: 10.3390/nu11092073

Norman, J. M., Handley, S. A., and Virgin, H. W. (2014). Kingdom-agnostic metagenomics and the importance of complete characterization of enteric microbial communities. *Gastroenterology* 146, 1459–1469. doi: 10.1053/j.gastro.2014.02.001

Qiu, X., Zhang, F., Yang, X., Wu, N., Jiang, W., Li, X., et al. (2015). Changes in the composition of intestinal fungi and their role in mice with dextran sulfate sodium-induced colitis. *Sci. Rep.* 5:10416. doi: 10.1038/srep10416

Sam, Q. H., Chang, M. W., and Chai, L. Y. A. (2017). The fungal mycobiome and its interaction with gut bacteria in the host. *Int. J. Mol. Sci.* 18:330. doi: 10.3390/ijms18020330

Schei, K., Avershina, E., Øien, T., Rudi, K., Follestad, T., Salamati, S., et al. (2017). Early gut mycobiota and mother-offspring transfer. *Microbiome* 5:107. doi: 10.1186/s40168-017-0319-x

Shojaie, L., Iorga, A., and Dara, L. (2020). Cell Death in Liver Diseases: A Review. *Int. J. Mol. Sci.* 21:9682. doi: 10.3390/ijms21249682

Solovjov, D. A., Pluskota, E., and Plow, E. F. (2005). Distinct roles for the α and β subunits in the functions of integrin αMβ2. *J. Biol. Chem.* 280, 1336–1345. doi: 10.1074/jbc.M406968200

Souza, V. D., Shetty, M., Badanthadka, M., Mamatha, B., and Vijayanarayana, K. (2022). The effect of nutritional status on the pharmacokinetic profile of acetaminophen. *Toxicol. Appl. Pharmacol.* 438:115888. doi: 10.1016/j.taap.2022.115888

Stravitz, R. T., and Lee, W. M. (2019). Acute liver failure. *Lancet* 394, 869–881. doi: 10.1016/s0140-6736(19)31894-x

Watkins, P. B., and Seeff, L. B. (2006). Drug-induced liver injury: summary of a single topic clinical research conference. *Hepatology* 43, 618–631. doi: 10.1002/hep.21095

Yamada, N., Karasawa, T., Kimura, H., Watanabe, S., Komada, T., Kamata, R., et al. (2020). Ferroptosis driven by radical oxidation of n-6 polyunsaturated fatty acids mediates acetaminophen-induced acute liver failure. *Cell Death Dis.* 11:144. doi: 10.1038/s41419-020-2334-2

Yuan, L., and Kaplowitz, N. (2013). Mechanisms of drug-induced liver injury. *Clin. Liver Dis.* 17, 507–518. doi: 10.1016/j.cld.2013.07.002

**Conflict of Interest:** The authors declare that the research was conducted in the absence of any commercial or financial relationships that could be construed as a potential conflict of interest.

**Publisher's Note:** All claims expressed in this article are solely those of the authors and do not necessarily represent those of their affiliated organizations, or those of the publisher, the editors and the reviewers. Any product that may be evaluated in this article, or claim that may be made by its manufacturer, is not guaranteed or endorsed by the publisher.

frontiers | Frontiers in Microbiology

ORIGINAL RESEARCH
published: 19 July 2022
doi: 10.3389/fmicb.2022.965292

# Healthy Gut Microbiome Composition Enhances Disease Resistance and Fat Deposition in Tibetan Pigs

*Peng Shang[1,2†], Mingbang Wei[1,2†], Mengqi Duan[1,2], Feifei Yan[1,2] and Yangzom Chamba[1,2*]*

[1] College of Animal Science, Tibet Agriculture and Animal Husbandry University, Linzhi, China, [2] The Provincial and Ministerial Co-founded Collaborative Innovation Center for R&D in Tibet Characteristic Agricultural and Animal Husbandry Resources, Linzhi, China

OPEN ACCESS

**Edited by:**
Tang Zhaoxin,
South China Agricultural University, China

**Reviewed by:**
Yanfen Cheng,
Nanjing Agricultural University, China
Wenyu Gou,
Medical University of South Carolina, United States

***Correspondence:**
Yangzom Chamba
qbyz628@126.com

[†] These authors have contributed equally to this work

**Specialty section:**
This article was submitted to Microorganisms in Vertebrate Digestive Systems, a section of the journal Frontiers in Microbiology

**Received:** 09 June 2022
**Accepted:** 24 June 2022
**Published:** 19 July 2022

**Citation:**
Shang P, Wei M, Duan M, Yan F and Chamba Y (2022) Healthy Gut Microbiome Composition Enhances Disease Resistance and Fat Deposition in Tibetan Pigs. Front. Microbiol. 13:965292. doi: 10.3389/fmicb.2022.965292

The gut microbiota is involved in a range of physiological processes in animals, and modulating the microbiome composition is considered a novel target for identifying animal traits. Tibetan pigs show better fat deposition and disease resistance compared to Yorkshire pigs. However, studies investigating the correlation between favorable characteristics in Tibetan pigs and the gut microbial community remain scarce. In the current study, 1,249,822 high-quality sequences were obtained by amplicon sequencing of the colon contents of Tibetan and Yorkshire pigs. We found that at the boundary level, the abundance and relative abundance of colon bacterial community in Tibetan pigs were higher than that in Yorkshire pigs ($P > 0.05$). Phylum level, Firmicutes were the dominant colonic microflora of Tibetan and Yorkshire pigs, and the ratio of Firmicutes to Bacteroides in Tibetan pigs was slightly higher than in Yorkshire pigs. Actinobacteria and Spirobacteria were significantly higher in Tibetan pigs than in Yorkshire pigs ($P < 0.05$). At the genus level, the relative abundance of Bifidobacterium, *Lactobacillus*, and Bacteriologist, which are related to disease resistance, was significantly higher than that in Yorkshire pigs in Yorkshire pigs. In conclusion, the composition and abundance of colonic intestinal microflora in Tibetan pigs were closely related to their superior traits. Bifidobacteria, Ruminococcaceae, and Family-XIII-AD3011-Group are conducive to improving disease resistance in Tibetan pigs. *Lactobacillus* and *Solobacterium* were observed to be the main bacterial communities involved in fat deposition in Tibetan pigs. This study will provide a new reference for the development and utilization of Tibetan pigs in future.

**Keywords: Tibetan pig, Yorkshire pig, gut microbiota, 16SrRNA gene, disease resistance, fat deposition, microbiome composition**

**Abbreviations:** OUT, operational taxa.

## INTRODUCTION

The Tibetan pig is an indigenous fatty pig breed in China, mainly found in Tibet and the Sichuan, Gansu, and Yunnan provinces, where the altitude is approximately 3,000 m above sea level or higher (Ma et al., 2019). Tibetan pigs are the only high-altitude pasture pig breed in China, and live in high-altitude and cold areas; these pigs are characterized by strong fat deposition ability, disease and stress resistance, resistance to low oxygen conditions, and tolerance to rough feeding (Ai et al., 2014; Zhang et al., 2017; Shang et al., 2019). The Yorkshire pig is a typical lean pig breed that originated in the United Kingdom. It is widely distributed and is currently one of the most commonly raised pig breeds worldwide. Yorkshire pigs have excellent characteristics such as fast weight gain, high feed conversion rate, and high lean meat rate of carcasses (Gong et al., 2022). At present, Tibetan pigs on the Tibetan plateau are raised mainly through stabling and half-stabling feeding, often grazing in the sports arena, and their feed, comprising grass, leaves, fruits, roots, and insects, is rich in fiber. Therefore, the special living environment and half-barn feeding method make the Tibetan pig disease-resistant and they show excellent characteristics of fatty deposits.

The intestinal tract is the main site of nutrient digestion and absorption. Intestinal microbes are dense bioactive communities that serve as the junction between animals and their nutritional environment (Anand and Mande, 2018). Thus, their activity profoundly affects many aspects of host animal physiology and metabolism (Judkins et al., 2020). Intestinal microbiota is essential for nutrient digestion and absorption, and plays an important role in the physiological, nutritional, and immune functions of the host (Park et al., 2014; Chen et al., 2017). The intestinal mucosa and microbial community together promote the development of the host immune system. Symbiotic microorganisms affect disease resistance in animals by competing for receptors and intestinal nutrients, producing antibacterial compounds, creating a disease-resistant microenvironment, and stimulating the innate immune system (Fernandez et al., 2003; Liang et al., 2014).

The gastrointestinal tract of pigs contains numerous species of bacteria, the composition and relative proportions of which vary with animal species, age, nutrition, and environmental factors (Lu et al., 2014; Yang et al., 2014). To date, a series of intestinal microbial structural components and metabolites have been found to interact directly with host intestinal cells and tissues, often by consuming, storing, and redistributing energy to maintain the dynamic balance of the body (Hillman et al., 2017). It affects nutrient absorption and host health (Ghosh et al., 2021; Gill et al., 2021). The mechanisms of microbial influence are mainly derived from microbial activity in the gut, and then projected into the body through a variety of integrated pathways. The complexity of these interactions means that different microbial community compositions can lead to different results, which may be related to the host diet or a specific system. It has also been shown to be closely related to the host species, genetic background, and intestinal microbial taxa and characteristics of the host (Kim and Isaacson, 2015).

The colon is the main site of microbial fermentation and the core flora in the gut directly affects intestinal function (Luo et al., 2021). Recently, the intestinal microbiota of Tibetan pigs has been extensively studied; however, the relationship between the composition of colon microbiota and lipid deposition and the host resistance to disease requires worth further exploration. In this study, 16SrRNA high-throughput sequencing technology was used to compare the specificity of the colon microbial structure and composition of Tibetan pigs and Yorkshire pigs and to explore the effects of the colon microbial community on disease resistance and fat deposition traits of Tibetan pigs. This will be conducive to further development and utilization of Tibetan pig germplasm resources.

## MATERIALS AND METHODS

### Sample Collection

The samples in this study were randomly collected from the practice pasture of the Tibet Agriculture and Animal Husbandry University, Linzhi, Tibet (average altitude 2,980 m above sea level, longitude 94.34°E, latitude 29.67°N). Six adult Tibetan pigs (T1, T2, T3, T4, T5, and T6) and six Yorkshire pigs (Y1, Y2, Y3, Y4, Y5, and Y6) were used, both male and female. Yorkshire and Tibetan pigs were fed using the traditional and half-house feeding methods, respectively. In addition to the feed, which was the same as that provided to the Yorkshire pigs, Tibetan pigs also ate fruit, grass, leaves, roots, and other food. The pigs were sacrificed by bloodletting the anterior vena cava. The abdominal cavity was cut open, the intestine was removed, and the 20 cm intestine was ligated in the middle part of the colon. Under aseptic conditions, a small opening was made in the middle of the ligated intestine with ophthalmic scissors, squeezed into an aseptic frozen tube, placed into liquid nitrogen for quick freezing, and the sample was stored at −80°C until subsequent use and further 16SrRNA analysis. Colon samples were collected and immediately placed in formalin for histopathological analyses.

### Histological Analysis

The collected colon samples were placed at room temperature and fixed for 24 h. After the fixed colon was dehydrated in increasing ethanol concentration and cleared in xylene, paraffin was embedded to prepare histological sections of 5 mm thickness. Sections of 5 mm were stained with hematoxylin for 3 min, and then stained with eosin at room temperature for 20 s. Sections were examined by inverted microscope (OlympusBX51, Japan), the morphology of colon was observed.

### DNA Extraction and 16SrDNA Amplicon Sequencing

A Hi Pure Stool DNA Kit (model D3141, Guangzhou Meiji Biotechnology Co., Ltd., Guangzhou, China) was used to extract microbial DNA. The purity and concentration of DNA were determined using Namedrop 2000 (Mother). The integrity of the DNA was detected using 1.0% agarose gel electrophoresis. To investigate the gut microbial composition,

the V3–V4 region of 16SrDNA was amplified by PCR with primers 341F (CCTACGGGNGGCWGCAG) and 806R (GGACTACHVGGGTATCTAAT). As mentioned earlier, triple polymerase chain reaction was carried out (procedure: 95°C, 2 min; 98°C, 10 s; 62°C, 30 s; 68°C, 30 s; 27 cycles, 68°C, 10 min; system: 5 μL 10 × KOD buffer, 5 μL 2.5 mM dNTPs, upstream and downstream primers 1.5 μL, 1 μL KOD polymerase, and 100 ng template DNA). According to the manufacturer's instructions, the amplification products were extracted on a 2% agarose gel, and amplification products obtained on the second round were purified using AMPure XP Beads. All amplification products were quantified using an ABI Step One Plus Real-Time PCR System (Life Technologies, CA, United States), and the pooling was sequenced according to the PE250 mode of Novaseq 6000.

## Bioinformatics and Statistical Analysis

Adapters and low-quality raw data may influence the assembly and analysis of data. To obtain high-quality clean readings, the original readings were further filtered according to the guidelines of FASTP[1] to remove reads containing 10% unknown nucleotides and to remove less than 80% of the bases with mass (Q) > 20. Subsequently, FLASH (version 1.2.11) (Magoč and Salzberg, 2011) was used to merge the paired-end clean readout into the original label, with a minimum overlap of 10 bp and a mismatch error rate of 2%. The interference sequences of the original tags were filtered through the QIIME (version 1.9.1) (Caporaso et al., 2010) pipeline under specific filtering conditions (Bokulich et al., 2013) to obtain high-quality, clean tags. The cleaning tags were searched against the reference database[2]. Reference-based chimera examination was performed using the UCHIME algorithm[3]. Following this, all chimeric tags were removed, and valid tags were obtained and employed for further analysis. UPARSE (Edgar, 2013) pipes were used to aggregate valid labels into ≥97% operational taxa (OTU). The tag sequence with the highest abundance was selected as the representative sequence in each cluster. Based on the SILA database[4] (Pruesse et al., 2007), the RDP classifier (version 2.2) (Wang et al., 2007) was used to classify the representative sequences using a naive Bayesian model. The confidence threshold was 0.8–1.0.

The abundance statistics for each category were visualized using Krona (version 2.6) (Ondov et al., 2011). The stacked bar chart of community composition was visualized using the R Project ggplot2 package (version 2.2.1). The diversity indexes of Chao1, Simpson, and Alpha were calculated using QIIME. The ecological function spectrum of the bacteria was generated using the Functional Annotation of Prokaryotic Taxa (FAPROTAX) and related software (version 1.0) (Louca et al., 2016). Tax4 Fun (version 1.0) or PICRUSt (version 2.1.4) were used to analyze the KEGG path of OTUs (version 1.0) (Aßhauer et al., 2015).

[1]https://github.com/OpenGene/fastp

[2]http://drive5.com/uchime/uchime_download.html

[3]http://www.drive5.com/usearch/manual/uchime_algo.html

[4]https://www.arb-silva.de/

## Statistical Analysis

The abundance statistics for each classification were visualized using Krona. The diversity indices of Chao1, Simpson, and Alpha were calculated using QIIME. Welch's *t*-test and Wilcoxon rank test were used for alpha diversity analysis. The ecological function map of the bacteria was generated using the FAPROTAX database and related software (version 1.0). The functional differences between groups were tested using Welch's *t*-test, Wilcoxon rank test, Kruskal-Wallis *h* test, and Tukey's honest significant difference (HSD) test.

# RESULTS

## Differences in Colonic Morphology Between Tibetan and Yorkshire Pigs

The results of HE staining showed that the intestinal structure of Tibetan pig and Yorkshire pig was intact, the boundary was clear, and the goblet cells were evenly distributed in the intestinal mucosa. As can be seen from **Figures 1A1,B1**, the colonic intestines of Tibetan pigs and Yorkshire pigs of the same age are generally smaller than those of Yorkshire pigs, and the intestinal structure is more compact. Under the same magnification, the colon morphology of Tibetan pig and Yorkshire pig showed that compared with Yorkshire pig, the thickness of colon mucosal layer, intestinal villus density, intestinal villus length and muscle layer thickness of Tibetan pig were larger than those of Yorkshire pig (**Figure 1**).

## Sequence Analysis

The results of this study showed that a total of 1,249,822 high quality sequences were available from 12 fecal samples, and the average effective combination sequence of each sample was 104,151. The length distribution of each sample was 200∼474 bp (**Table 1**). All the optimized sequences were compared with the OTU representative sequences using the UPARSE software, and sequences with more than 97% similarity to the representative sequences were selected to generate OTUs. After classification and matching, a total of 16,070 OTUs were obtained.

## Analysis of Microbial Composition and Structure

The relative abundance of taxa at the phylum and genus levels was evaluated based on the distribution of microbial taxa in the two groups (**Figure 2**). The abundant microflora in the intestinal tract of Tibetan pigs and Yorkshire pigs show great diversity at both the gate and genus levels. At the gate level, Firmicutes, Bacteroidetes, Euryarchaeota, Actinobacteria, Fusobacteria, Spirochetes, Proteobacteria, Synergistetes, Patescibacteria, and Kiritimatiellaeota were the ten most abundant phyla (**Figure 2A**). At the genus level, *Clostridium sensu stricto 1*, *Lactobacillus*, *Terrisporobacter*, *Christensenellaceae* R-7 group, *Streptococcus*, *Romboutsia*, *Eubacterium coprostanoligenes*_group, *Methanobrevibacter*, *Turicibacter*, and *Ruminococcaceae* UCG-005 were the ten most abundant genera (**Figure 2B**). The horizontal cluster analysis

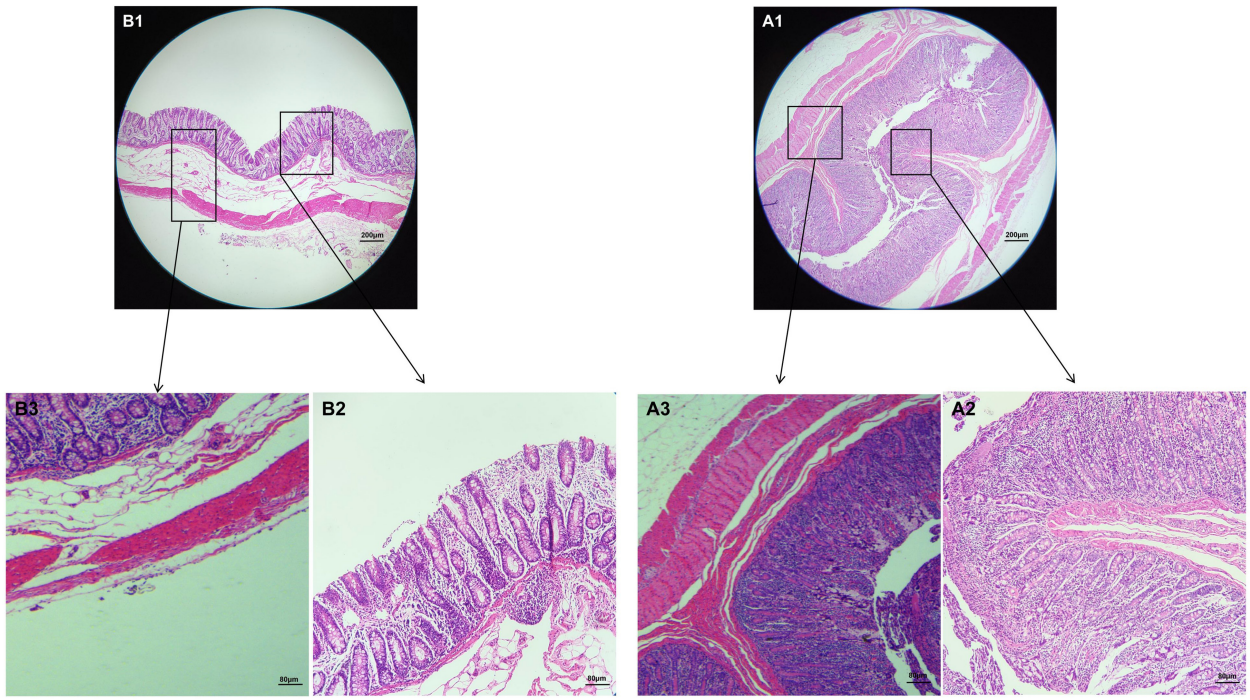


**FIGURE 1 |** Morphological observation of colon in Tibetan pigs and Yorkshire pigs under different magnifications. **(A1–A3)** Colon and intestinal sections of Tibetan pigs; **(B1–B3)** Colon and intestinal sections of Yorkshire pigs.

**TABLE 1 |** Quantitative statistics of Tags and OTUs.

| Samples name | Raw reads | Clean reads | Raw tags | Clean tags | Chimera | Effective tags | Effective ratio (%) | OTUs |
|---|---|---|---|---|---|---|---|---|
| T1 | 114113 | 114020 | 112733 | 112027 | 14456 | 97571 | 85.5 | 642 |
| T2 | 130597 | 130468 | 129126 | 128134 | 16688 | 111446 | 85.34 | 1075 |
| T3 | 129466 | 129353 | 127884 | 126912 | 18900 | 108012 | 83.43 | 1182 |
| T4 | 121107 | 120999 | 119507 | 118919 | 14279 | 104640 | 86.4 | 1142 |
| T5 | 133281 | 133178 | 131648 | 130686 | 20262 | 110424 | 82.85 | 1694 |
| T6 | 126212 | 126107 | 124344 | 123082 | 16141 | 106941 | 84.73 | 1532 |
| Y1 | 130924 | 130834 | 129459 | 127823 | 19308 | 108515 | 82.88 | 1578 |
| Y2 | 133586 | 133461 | 131642 | 129998 | 18054 | 111944 | 83.8 | 1451 |
| Y3 | 120997 | 120894 | 119640 | 118413 | 17412 | 101001 | 83.47 | 1547 |
| Y4 | 130559 | 130456 | 128942 | 127444 | 17529 | 109915 | 84.19 | 1197 |
| Y5 | 121377 | 121280 | 119809 | 118613 | 15490 | 103123 | 84.96 | 1042 |
| Y6 | 88623 | 88546 | 87511 | 87022 | 10732 | 76290 | 86.08 | 752 |

of phyla and genera using a heat map showed that 17 phyla were co-clustered at the gate level, 97 different genera were co-clustered at the genus level, and the distribution of bacterial phyla and genera in different individuals was consistent with the relative abundance stack map. The similarity of intra-group samples was also shown to be higher than that of inter-group samples (**Figures 2C–E**).

Upon studying the classification and distribution of the microbial communities in the two groups, the relative percentages of the dominant taxa at the boundaries, phyla, classes, orders, families, and genera were evaluated (**Figure 3**). More than 94.5% of the colonic microorganisms in Tibetan and Yorkshire pigs belong to the bacterial kingdom, and the proportion of colonic microorganisms in Tibetan pigs (97.44%) was larger than that in Yorkshire pigs (94.54%) (**Figure 3A**). At the gate level, the thick-walled bacteria in the colons of Tibetan pigs and Yorkshire pigs were the dominant communities, accounting for 81.15 and 76.26%, respectively (**Figure 3B**). The 10 most prevalent colonic microorganisms in Tibetan and Yorkshire pigs were *Clostridia* (60.70 and 65.74%), *Bacilli* (17.17 and 4.79%), *Bacteroidia* (6.80 and 6.44%), *Methanobacteria* (3.06 and 5.43%), *Erysipelotrichia* (2.78 and 5.27%), *Fusobacteria* (2.54 and 4.16%), *Spirochaetia* (2.54 and 1.03%), *Actinobacteria* (2.10 and 0.92%), *Coriobacteriia*

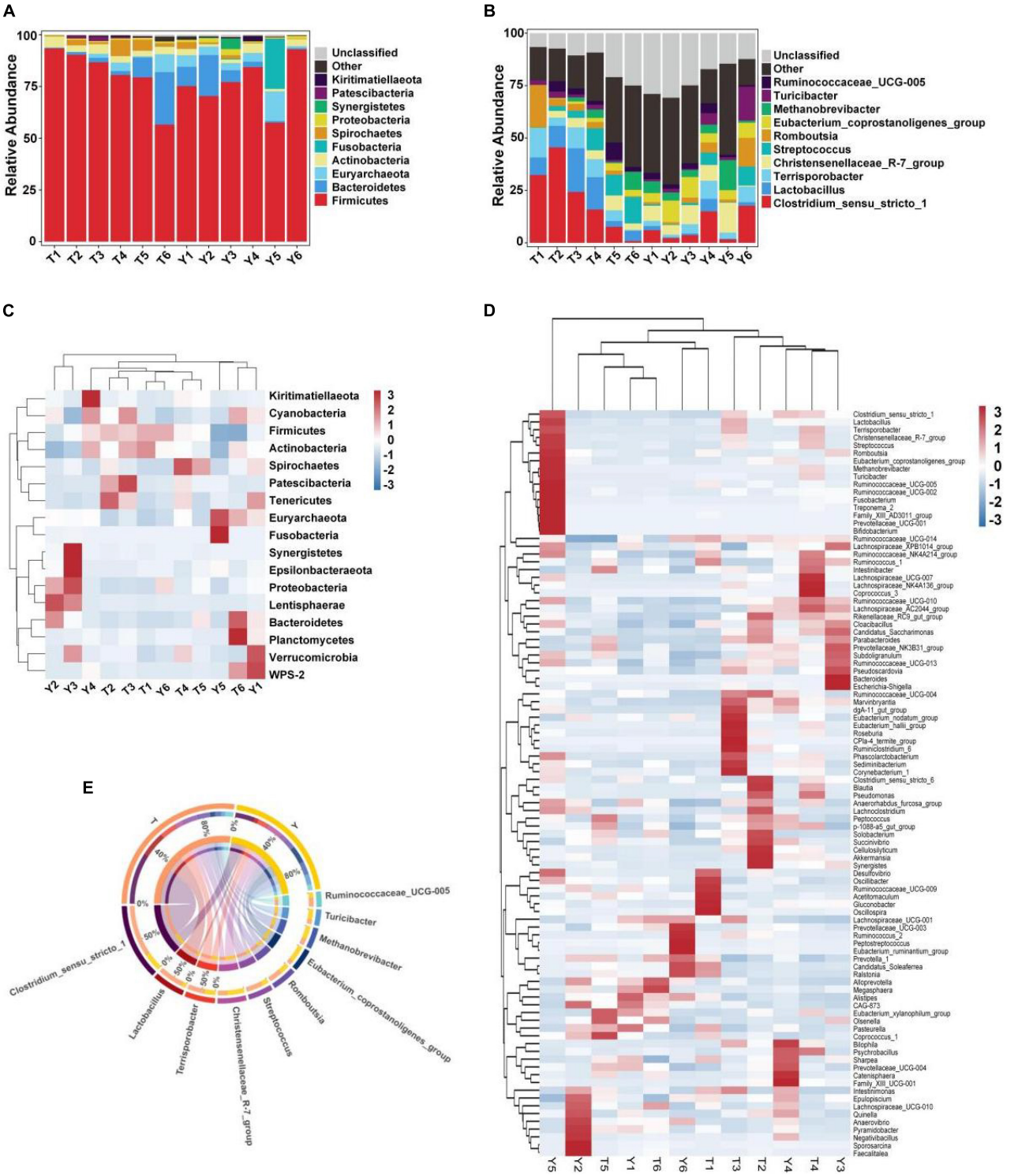


**FIGURE 2 |** Heat map showing the relative abundance of intestinal microflora in Tibetan and Yorkshire pigs at phylum and genus level. **(A,B)** Represent the distribution at the phylum and genus level, respectively. **(C)** Heat maps of the 17 most common gates in different communities. **(D)** Heat maps of the 96 most common genera in different communities. Each color block in the heat map represents the relative abundance of a genus in the sample. Clustering can distinguish taxon with different abundance, and color gradient and similarity can reflect the similarities and differences of multiple samples at different classification levels. The blue-red gradient shows the change of abundance from low to high. **(E)** Composition of microorganisms among horizontal species.

(0.92 and 1.55%), and *Gammaproteobacteria* (0.91 and 0.98%) (**Figure 3C**). The relative abundance of colonic *Bacilli* and *Spirochaetia* in Tibetan pigs was significantly higher than that in Yorkshire pigs. *Clostridiales* were dominant in the colons of Tibetan and Yorkshire pigs, accounting for more than 60% of the total community composition (**Figure 3D**). The relative abundances of *Lactobacillus* (17.01%), *Spirulina* (3.06%), and *Bifidobacterium* (2.43%) in the colonic microbiota of Tibetan pigs were significantly higher than those of Yorkshire pigs (4.76%, 1.03%, and 0.79%) ($P < 0.05$). The composition of microflora at the family level is shown in **Figure 3E**. The relative abundances of *Clostridium*-1 (21.26%), *Enterostreptococcus* (14.67%), *Lactobacillus* (10.44%), and *Streptococcus* (6.50%) in the colonic microbiota of Tibetan pigs were higher than those of Yorkshire pigs (*Clostridium*-17.94%, digestive *Streptococcaceae* 9.75%, *Lactobacillaceae* 1.83%, and *Streptococcus* 2.90%). **Figure 3F** shows the composition of the microflora at the genus level. Predominantly, *Clostridium sensu stricto 1*, *Lactobacillus*, *Terrisporobacter*, *Christensenellaceae* R-7 group, *Streptococcus*, *Romboutsia*, *Eubacterium coprostanoligenes* group, *Methanobrevibacter*, *Turicibacter*, and *Ruminococcaceae*_UCG-005 were observed. The predominant groups in the Tibetan and Yorkshire pigs were substantially different.

## Analysis of Colonic Microbial Diversity in Tibetan and Yorkshire Pigs

The sequence numbers were confirmed by the store line in the sequencing abundance curve, the evenness of microbial species, and the platform period of the sob and Shannon curves to meet the requirements of sequencing and analysis. The Simpson index of Yorkshire pig (0.96) was higher than that of the Tibetan pigs (0.92); however, this difference was not significant. The Shannon indices of the two groups were 5.68 and 6.33, respectively, and the difference was not significant. The Chao1 and Sob indices of the Tibetan and Yorkshire pig groups were 1,349.83, 1,396.12, 1,211.17, and 1,261.17, respectively. However, there were no significant differences in the two indices between the groups ($P > 0.05$). The Chao1 and Sob indices showed no significant difference in fungal microbial evenness among the different groups (**Figure 4**).

## Analysis of Representative Microbial Species of Tibetan and Yorkshire Pigs

The previous analysis showed that the Tibetan and Yorkshire pigs showed varied colon microbiota at the gate and genus levels; therefore, the microbial community composition of the two levels was analyzed, and the results are shown in **Figure 5**. The ten most dominant phyla were Firmicutes, Bacteroidetes, Euryarchaeota, Actinobacteria, Fusobacteria, Spirochetes, Proteobacteria, Synergistetes, Patescibacteria, and Kiritimatiellaeota (**Figure 5A**). Actinomycetes and Spirochetes were the dominant communities in the colons of Tibetan and Yorkshire pigs, accounting for 81.15 and 76.26%, respectively. The relative abundances of Actinomycetes and Spirochetes in Tibetan pigs were significantly higher than those in Yorkshire pigs ($P < 0.05$). There were no significant differences in the relative abundance of other bacteria between Tibetan and Yorkshire pigs ($P > 0.05$). **Figure 5B** shows great differences in the composition of microflora at the genus level between Tibetan and Yorkshire pigs, and the relative abundance of most microflora in the Tibetan pig colon was higher than that in the Yorkshire pig group. The relative abundance of *Clostridium sensu stricto 1* (21.08%), *Lactobacillus* (10.44%), *Sporobacillus* (6.98%), *Streptococcus* (6.50%), and *Ruminococcaceae*_UCG-005 (3.36%) in the colon microbiota of Tibetan pigs was significantly higher than that in Yorkshire pigs (*Clostridium sensu stricto* 1 7.73%, *Lactobacillus* 1.83%, *Bacillus* 4.53%, *Streptococcus* 2.90%, and *Ruminococcaceae* UCG-005 2.36%) ($P < 0.05$).

In this study, the Venn diagram of intestinal microorganisms in Tibetan and Yorkshire pigs was intersected at the genus level (**Figure 6A**). There were 152 genera in these two groups, and 33 species of endemic fungi were found in the colonic secretions of Tibetan pigs. To determine the specific bacterial species in the intestinal microorganisms of Tibetan and Yorkshire pigs, we further analyzed the communities using Linear discriminant analysis Effect Size (LEfSe) with Linear Discriminant Analysis (LDA) > 2, and further determined the differences in species composition between Tibetan and Yorkshire pigs (**Figures 6B,C**). In the Yorkshire pig group, 29 colons were higher, and 24 were lower in the Tibetan pig group. The 14 OTUs representing bacilli were more abundant in Tibetan pigs. Tibetan pigs contained 10 kinds of OTUs representing *Lactobacillus* (Lactobacillales) and three kinds of OTUs representing Bacillales, both of which belong to the Bacilli class. In addition, Tibetan pigs were enriched in six and two OTUs representing actinomycetes (Actinobacteria) and actinomycetes (Acidimicrobiia), respectively. As shown in **Figure 6D**, the relative abundance of colonic microbiota in Tibetan pigs in the Bacilli and Actinobacteria classes was significantly higher than that in the Yorkshire pigs ($P < 0.01$ or $P < 0.05$). As shown in **Figure 6E**, there were extremely significant differences in the compositions of *Solobacterium*, *Lactobacillus*, Family-XIII-AD3011-group, *Eubacterium xylanophilum*-group, *Eubacterium coprostanoligenes*-group, and Bifidobacterium between Tibetan and Yorkshire pigs. The relative abundances of *Solobacterium*, *Lactobacillus*, and *Bifidobacterium* in the colonic microflora of the Tibetan pig group were significantly higher than those of the Yorkshire pig group. As shown in **Figure 6F**, the relative abundance of *Lactobacillus mucosae* and *Lactobacillus delbrueckii* subsp. *bulgaricus* in the Tibetan pig colonic microbiome was considerably higher than that in the Yorkshire group at the species level, and both *Lactobacillus mucosae* and *Lactobacillus delbrueckii* subsp. *bulgaricus* belonged to the *Lactobacillus* genus.

## Prediction of Ecological Function of Microbiota in Tibetan and Yorkshire Pigs

Through principal component analysis, significant differences were observed in fungal structure among the different groups, which was consistent with the previous analysis, especially at the family and genus levels of the Tibetan pig and Yorkshire pig groups (**Figures 7A,B**). In this study, the abscissa of the stacked chart represents different individuals, and the histogram

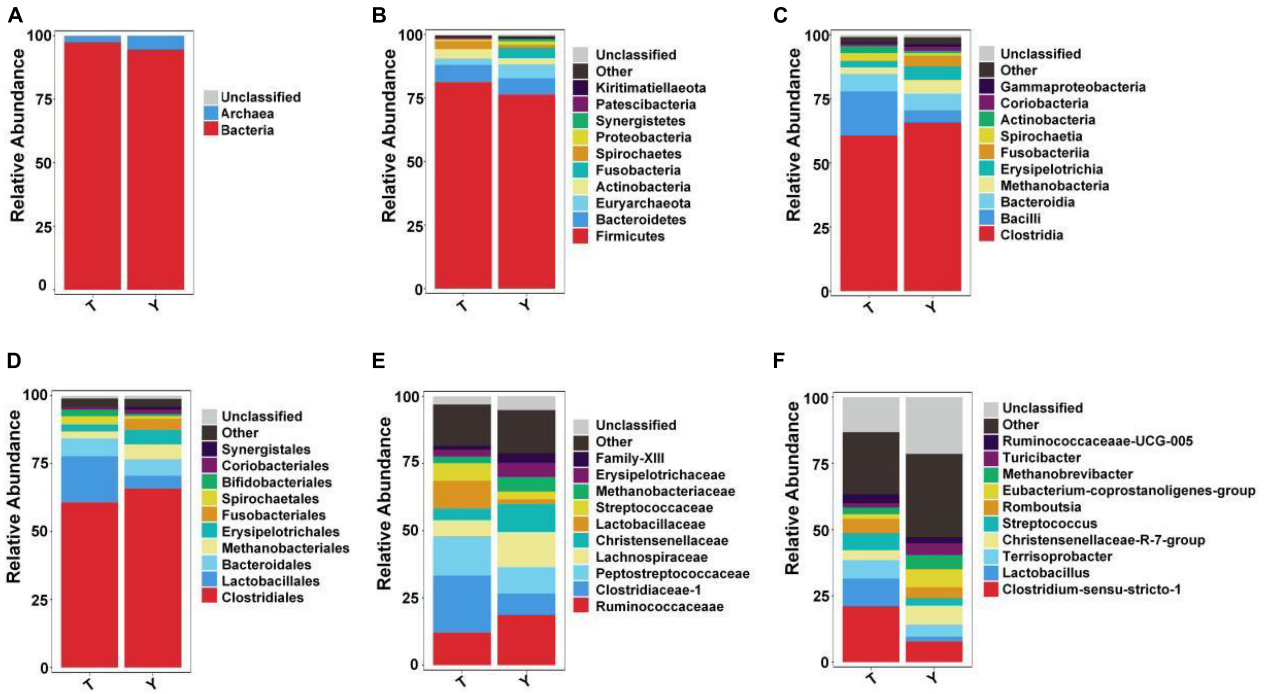


**FIGURE 3 |** Ten most abundant taxa of intestinal microflora in Tibetan (T) and Yorkshire (Y) pigs at boundary. Relative abundance at the kingdom **(A)**, phylum **(B)**, class **(C)**, order **(D)**, family **(E)**, and genus **(F)** levels.

of different colors in the chart shows the relative abundance of different ecological functions. The microbial communities in groups T and Y were mainly related to metabolism, genetic information processing, cell processes, environmental information processing, organic systems, and human diseases. Its main functions are concentrated in the metabolism of amino acids, cofactors, vitamins, terpenes, holystones, amino acids, and lipids. The comparative abundance of colonic microbial communities in the Tibetan pig group was higher than that in the Yorkshire pig group (**Table 2**). According to **Figures 7C–E**, the colonic microbial community of the Tibetan pig group was significantly more active than that of the Yorkshire pigs in the functions of transmembrane transport, potential pathogenicity, and aerobic function ($P < 0.05$) functions. Functional predictions of the top 11 genes are shown in **Figure 7F**.

## DISCUSSION

The pig is commercially important in animal husbandry, and an important biomedical model of human beings. The number of pigs in the world is estimated to be approximately 1 billion. Intestinal microbes can regulate the growth characteristics and health status of the host, such as fat deposition traits (Lei et al., 2021), chronic diseases (cancer and metabolic disorders) (Coleman et al., 2018; Just et al., 2018; Zitvogel et al., 2018), and disease resistance (resistance to intestinal infection) (Kumar et al., 2018). The Tibetan pig is a unique and valuable pig breed from the Tibetan Plateau that shows strong fat deposition ability, strong disease resistance, adaptability to high altitude hypoxia, and resistance to the cold and rough feeding.

Intestinal morphology is very important for nutrient digestion and absorption, and intestinal villus length, goblet cell characteristics, mucosal thickness, and muscle thickness are integral for this function. In general, dietary fiber intake leads to an increase in the size and length of the digestive organs, such as the cecum and colon of pigs, chicken, and rats. These effects are usually associated with changes in the morphology of intestinal epithelial cells, thus affecting the hydrolysis and absorption function of epithelial cells (Hedemann et al., 2006). The intestinal mucosa, muscle thickness, and intestinal microorganisms are closely related to the disease resistance of animals, and they interact to maintain the health of animals (Candela et al., 2008). The results showed that the mucosal and muscle layer thicknesses of Tibetan pigs were higher than those of Yorkshire pigs. This may be because Tibetan pigs eat more crude fiber food and show outstanding disease resistance, which are consistent with previous studies.

The pig intestine is a microenvironment composed of numerous microflora, which is generally regarded as a large metabolic spectrum that maintains its basic life and has a considerable impact on the growth and health of the host by participating in energy, metabolism, the intestinal barrier, and immune function (Langille et al., 2013; Lo et al., 2021). Among them, the relationship between microorganisms and microorganisms, between microorganisms and the intestinal environment, and between microbial communities and hosts constitutes an extremely complex ecosystem in which the main

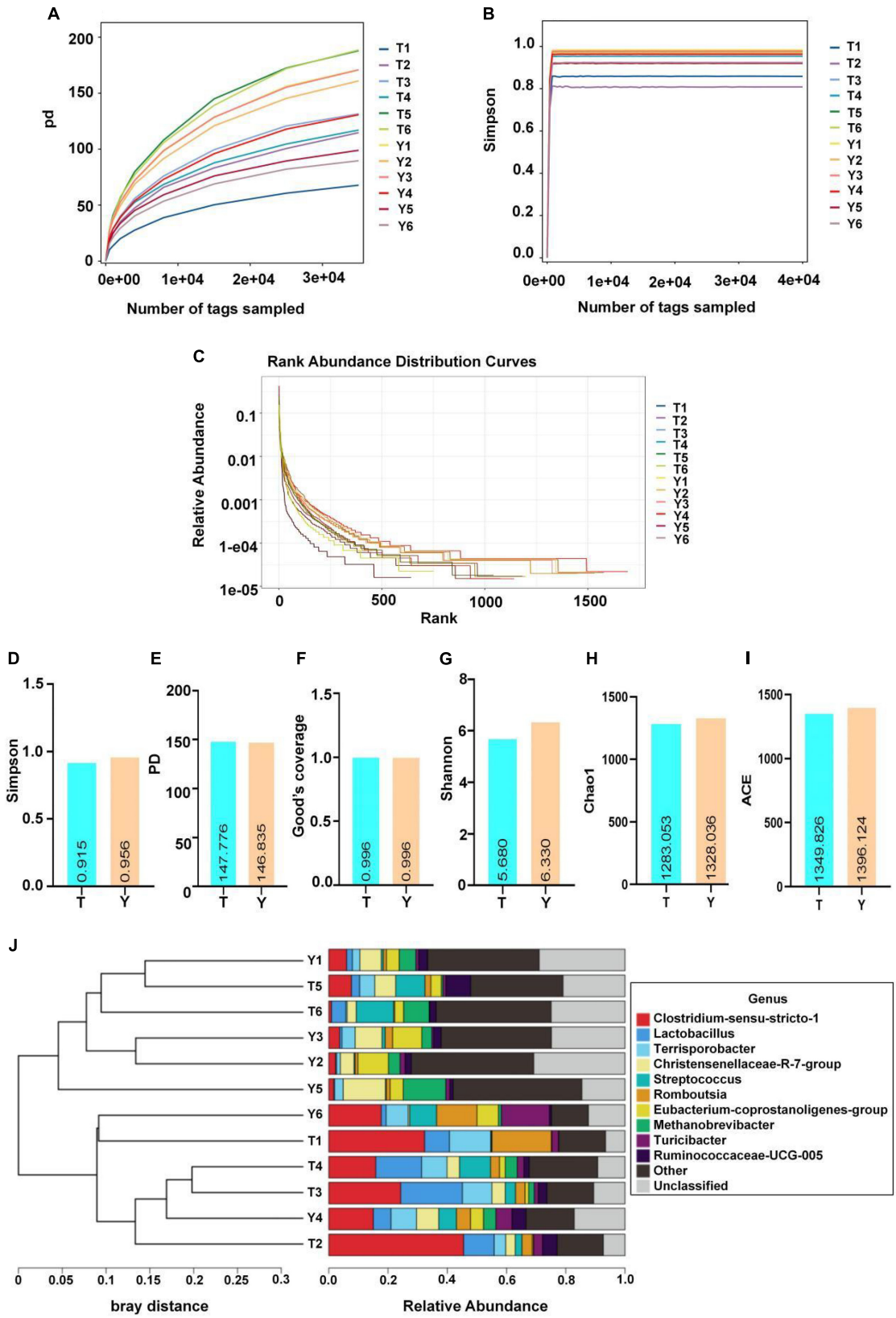


**FIGURE 4 |** Microbial diversity in colon of Tibetan (T) and Yorkshire (Y) pigs. **(A)** PD diversity index curve. **(B)** Simpson diversity index curve. **(C)** Rank abundance curve. **(D–I)** Alpha diversity index (Simpson, PD, Good's coverage, Shannon, Chao1, and ACE). **(J)** UPGMA cluster tree. Each curve represents a sample.

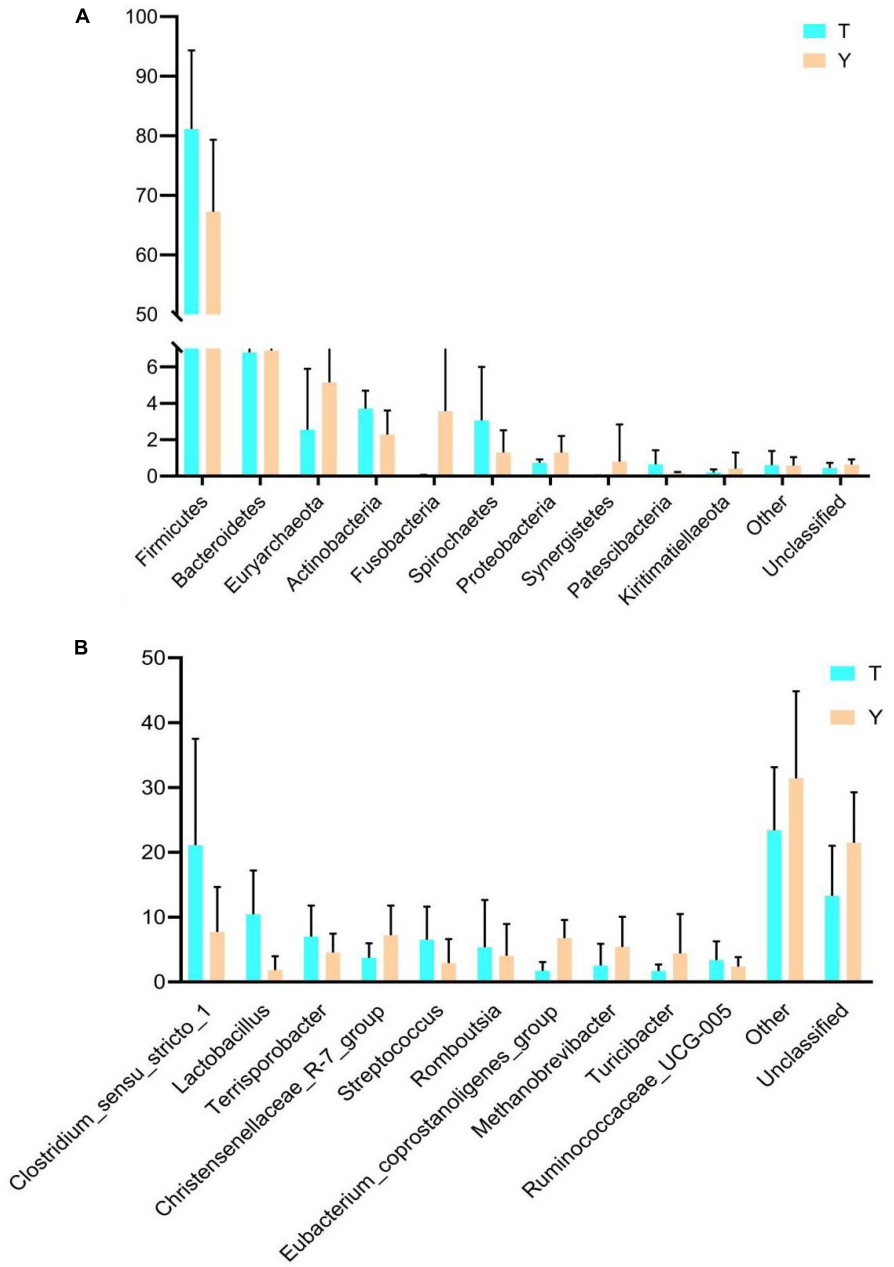


**FIGURE 5 |** Comparison of community differences in intestinal microbial composition between Tibetan pigs and Yorkshire pigs at the phylum **(A)** and genus **(B)** levels. All data represent average values.

composition of the microbial community is a thick-walled phylum and Bacteroides (Tan et al., 2017; Lu et al., 2018). The results showed a relative abundance of actinomycetes. *Clostridium* and *Spirochetes* were higher in the colonic microorganisms of Tibetan and Yorkshire pigs, which is consistent with the results of previous studies.

The composition of the intestinal microbial community greatly influences health. The intestinal microbiota is very important for nutrition, energy, inflammatory immunity, and physiological status of pigs. Simultaneously, the breed, age, body weight, diet, heredity, environment, and other factors cause changes in the intestinal microflora (Yang et al., 2017; Crespo-Piazuelo et al., 2019; Wang et al., 2019). The relative abundance of colonic microbial communities in the Tibetan pig group was higher than that in the Yorkshire pig group. This may be explained by the fact that Yorkshire pigs were raised in houses, whereas Tibetan pigs are fed in semi-houses. Additionally, Tibetan pigs also ate grass, tree roots, grass roots, and insects. Studies have demonstrated that a high-fiber diet can promote the diversity of the intestinal flora; therefore, intestinal

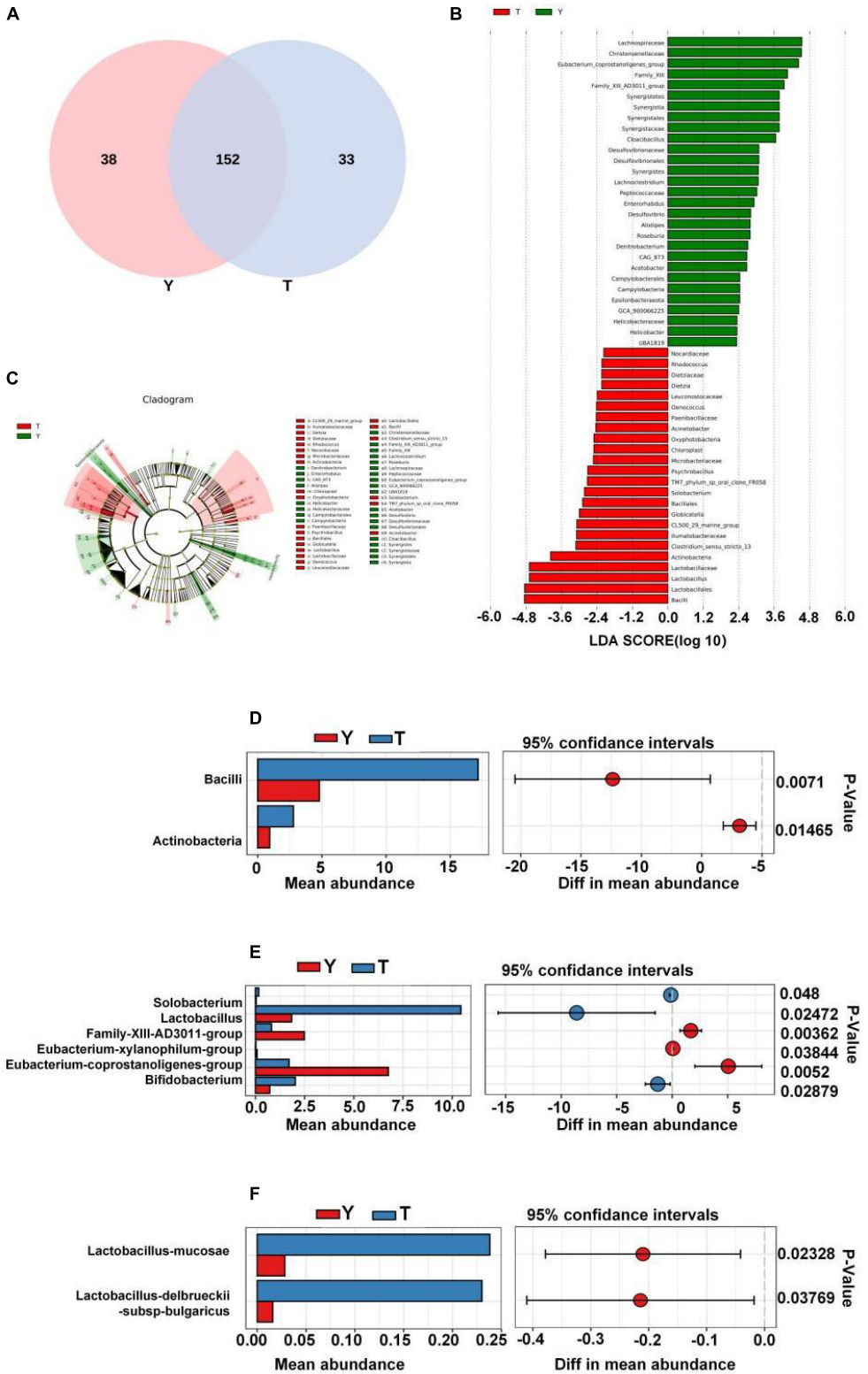


**FIGURE 6 |** Differences in intestinal microbial composition between Tibetan (T) and Yorkshire (Y) pigs. **(A)** Venn diagram analysis of colonic intestinal microflora in T and Y groups at genus level. **(B)** Variation in abundances of different species between T and Y groups (Linear Discriminant Analysis, LDA > 2). **(C)** Phylogenetic distribution map of microbial communities related to T and Y groups. In the evolutionary tree, the circles from inside to outside represent different levels, and the yellow circles represent taxa with obvious differences. There were significant differences in the class **(D)**, genus **(E)**, and species **(F)** levels of colonic microflora between groups T and Y.

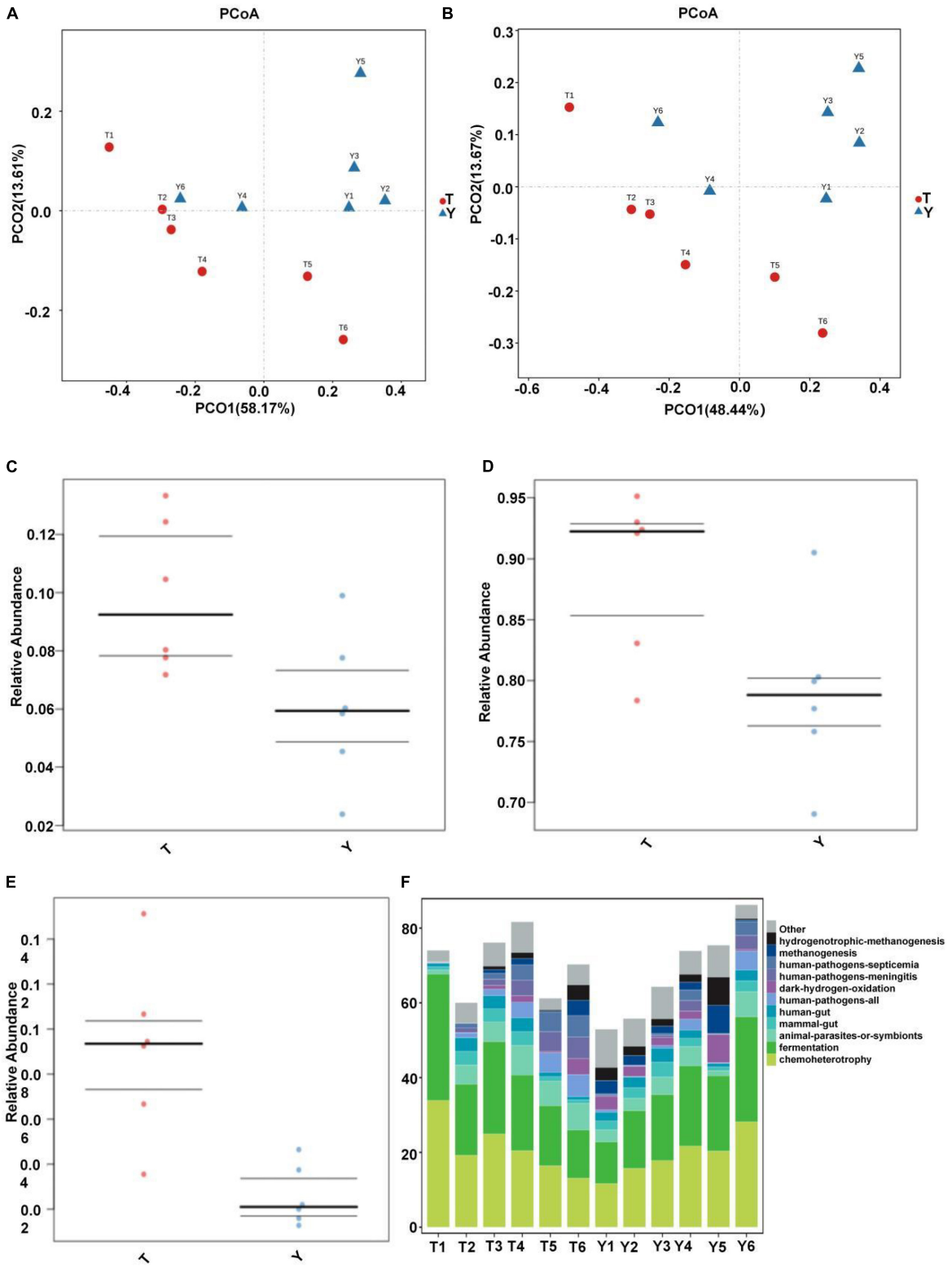


**FIGURE 7 |** Prediction of ecological functions performed by intestinal microbiota of Tibetan (T) and Yorkshire (Y) pigs. Principal component analysis of group T and group Y at family **(A)** and genus **(B)** levels. Each point represents a sample. Distance between the two points indicates difference in fecal microbiota. Transmembrane transport **(C)**, potential pathogenicity **(D)**, and aerobic activity **(E)** are some of the predicted ecological functions of the intestinal microbiota in both groups **(F)**.

**TABLE 2 |** Functional prediction of colonic microbiota in Tibetan and Yorkshire pigs.

| Level_1 | Level_2 | *T* | *Y* |
|---|---|---|---|
| Metabolism | Carbohydrate metabolism | 305267.04 | 256121.47 |
| Metabolism | Amino acid metabolism | 273214.46 | 239735.41 |
| Metabolism | Metabolism of cofactors and vitamins | 254228.24 | 227617.69 |
| Metabolism | Metabolism of terpenoids and polyketides | 215782.42 | 182950.76 |
| Metabolism | Metabolism of other amino acids | 162799.46 | 133328.51 |
| Metabolism | Lipid metabolism | 156651.76 | 110977.63 |
| Metabolism | Energy metabolism | 116304.73 | 102474.17 |
| Metabolism | Xenobiotics biodegradation and metabolism | 98826.78 | 74501.90 |
| Metabolism | Glycan biosynthesis and metabolism | 58828.02 | 54900.18 |
| Metabolism | Nucleotide metabolism | 48393.17 | 41063.84 |
| Metabolism | Biosynthesis of other secondary metabolites | 43840.67 | 38691.30 |
| Genetic information processing | Replication and repair | 144037.25 | 120813.52 |
| Genetic information processing | Translation | 77198.95 | 70203.12 |
| Genetic information processing | Folding, sorting and degradation | 71196.89 | 63858.14 |
| Genetic information processing | Transcription | 22587.97 | 24442.64 |
| Cellular processes | Cell motility | 47364.51 | 54467.32 |
| Cellular processes | Cell growth and death | 34557.93 | 28240.98 |
| Cellular processes | Transport and catabolism | 4270.04 | 3029.48 |
| Cellular processes | Cellular community - prokaryotes | 3505.88 | 3274.08 |
| Environmental information processing | Membrane transport | 50752.30 | 36982.53 |
| Environmental information processing | Signal transduction | 8003.29 | 7446.62 |
| Environmental information processing | Signaling molecules and interaction | 0.62 | 0.64 |
| Organismal systems | Environmental adaptation | 4677.55 | 4643.96 |
| Organismal systems | Endocrine system | 2051.06 | 1907.85 |
| Organismal systems | Immune system | 1372.58 | 1426.66 |
| Organismal systems | Digestive system | 257.11 | 204.33 |
| Organismal systems | Excretory system | 0.01 | 0.01 |
| Human diseases | Infectious diseases | 7123.71 | 4664.47 |
| Human diseases | Neurodegenerative diseases | 380.00 | 250.24 |
| Human diseases | Cardiovascular diseases | 0.43 | 0.81 |
| Human diseases | Immune diseases | 0.01 | 0.00 |

microorganisms were more diverse in Tibetan pigs than that in Yorkshire pigs. This is in agreement with the study by Ngoc et al. (2021), which showed that dietary fiber has significant effects on the intestinal environment and microflora of pigs. Pig breeds and different diets can cause significant changes in the ideal colonic microflora. The Tibetan pig is a fat pig breed, while the Yorkshire pig is a typical lean pig breed. Intestinal microorganisms not only provide energy for life-sustaining activities, but are also involved in regulating lipid storage (Backhed et al., 2004). Additionally, the abundance of intestinal microflora is significantly correlated with obesity parameters (Bergamaschi et al., 2020; Hao et al., 2021). Colonic microbes and complex traits such as obesity have been shown to be closely related (Backhed et al., 2004; Camarinha-Silva et al., 2017) in humans, mice, and other animals. The data show that the aseptic mice colonized by the microbiota of obese mice showed more body fat (Turnbaugh et al., 2006) than lean mice, which provides credibility for the role of intestinal microflora in obesity. Therefore, obesity and fat deposition traits of pigs may also be one of the reasons for the difference in abundances between colonic microbial communities in Tibetan and Yorkshire pigs.

The colon is the primary site for microbial fermentation, and the core intestinal flora directly affects intestinal function (Luo et al., 2021). Tibetan pigs live in high-altitude and cold-plateau environments year-round, exhibiting plateau adaptability, resistance to the cold and rough feeding, and stress resistance. *Chlamydia* was found to be the dominant microflora in the colonic microflora of Tibetan pigs (semi-house feeding) and large York pigs (house feeding), and the relative abundance of Actinomycetes and *Spirulina* in Tibetan pigs was significantly higher than that of Yorkshire pigs. The ratio of Actinomycetes to Bacteroides in Tibetan pigs (11.93) was slightly higher than that in Yorkshire pigs (11.84). The changes in the abundance of Bacteroides and Bacteroides are related to changes in carcass fat deposition (Pedersen et al., 2013). In the core intestinal microbiome of obese and lean twins, *Chlamydia*/*Pseudomonas* ratio was associated with greater energy absorption and accumulation (Turnbaugh et al., 2009). Some studies further showed that the abundance of *Streptomyces* and *Streptomyces* was higher in the intestinal microbiota of obese pigs, whereas that of *Bacteroides* was lower (Guo et al., 2008; Koliada et al., 2017; Panasevich et al., 2018). At the genus level, the relative abundance

of *Bifidobacterium*, *Lactobacillus*, Family-XIII-AD3011-group, *Ruminococcaceae* UCG-005, and *Solobacterium* was greater than that in Yorkshire pigs. *Bifidobacterium*, an actinomycete, is a gram-positive bacterium that acts as an indicator of intestinal health, and can maintain the balance of intestinal microecology. *Bifidobacteria* can inhibit the reproduction of harmful microorganisms by forming intestinal biological barriers, producing organic acids and germicidal proteins, and secreting extracellular glycosidases. *Bifidobacteria* can also synthesize various digestive enzymes. Vitamin B and amino acids promote the digestion and absorption of nutrients (Binda et al., 2018; Wong et al., 2020). *Lactobacillus* plays an important role in metabolizing plant foods (Filannino et al., 2018) and participates in producing some antimicrobials with anticancer and anti-inflammatory effects (Fernández et al., 2016). Wang et al. (2017) reported that *Lactobacillus* was associated with growth and fat deposition traits in broilers. Some studies have screened individual microorganisms that play a critical role in the substantial effects of the cecum, colon, and jejunum on growth and fat-related traits in pigs. Among the 10 microorganisms screened, nine were located in the cecum and colon, indicating that the cecum and colon play a more important role than the jejunum, and *Ruminococcaceae* UCG-005 in the colon showed a highly positive correlation with body weight and average daily gain (Tang et al., 2020). They are widely present in different intestinal communities and can degrade plant polysaccharides (Biddle et al., 2013). They can also produce butyric acid and acetic acid (Vital et al., 2014) *via* the butyryl-coenzyme A (CoA): acetic acid CoA transferase pathway. Butyric acid is the main energy source for colonic mucosal epithelial cells, which can maintain the structural integrity of the intestinal mucosa and promote the growth of the large intestine. Butyrate also has a powerful effect on a variety of colonic mucosal functions, such as inhibiting inflammation and carcinogenicity and strengthening various components of the colon defense barrier (Peng et al., 2009). The reduction in short-chain fatty acids produced by intestinal microorganisms can lead to inflammation (Maslowski and Mackay, 2011). In addition, higher concentrations of short-chain fatty acids (Payne et al., 2011) were found in obese individuals. *Ruminococcaceae* UCG-005 also benefits hosts by preventing diabetes and increasing colonic levels of short-chain fatty acids (Andrade et al., 2020). In a study on goats, Wang et al. (2018) found that the abundance of *Ruminococcaceae* UCG-005 in the intestinal tract of kids with diarrhea was significantly lower than that in healthy goat kids. *Ruminococcaceae* and Family_XIII are members of Clostridium. The results showed that the relative abundance of *Bifidobacterium*, *Lactobacillus*, *Ruminococcaceae* UCG-005, and Family-XIII-AD3011-group in the colon of Tibetan pigs was higher than that in Yorkshire pigs, indicating that the fat deposition, intestinal health, and disease resistance of Tibetan pigs were higher than those of Yorkshire pigs. The main functions of colonic microflora in Tibetan and Yorkshire pigs are concentrated in the metabolism of amino acids, cofactors and vitamins, terpenes and holystones, and amino acids and lipids. For all functions, the comparative abundance of the colonic microbial community in the Tibetan pig group was higher than that in the Yorkshire pig group. This is consistent with the fact that fat deposition and disease resistance in Tibetan pigs are higher than in Yorkshire pigs.

## CONCLUSION

This study investigated the effects of colonic microbial communities, fat deposition traits, and disease resistance in Tibetan pigs. The relative abundance of colonic microflora in Tibetan pigs was higher than that of Yorkshire pigs. Particularly, the relative abundances of *Bifidobacterium*, *Ruminococcaceae*, and Family-XIII-AD3011-group in Tibetan pigs were significantly higher than that in Yorkshire pigs, which is the major microbial group responsible for the disease resistance of Tibetan pigs. The relative abundance of *Lactobacillus* and *Solobacterium* in Tibetan pigs was significantly higher than that in Yorkshire pigs, which mainly affected the fat deposition traits of Tibetan pigs. This study will provide a new reference for future development and utilization of Tibetan pigs.

## DATA AVAILABILITY STATEMENT

The data presented in this study are deposited in the NCBI repository, accession number PRJNA848282.

## ETHICS STATEMENT

The animal study was reviewed and approved by the rearing, slaughtering and experimental conditions for experimental were strictly followed the guidelines approved by the Animal Welfare Committee of the Tibet Agriculture and Animal Husbandry University (Approval Number: TAAHU256).

## AUTHOR CONTRIBUTIONS

PS and YC conceived and designed the experiments. MW and MD analyzed the data. MW, PS, YC, and FY provided manuscript editing. All authors statistically analyzed, discussed, critically revised the contents, and approved the final manuscript.

## FUNDING

This study was supported by the major science and technology projects of the Tibet autonomous region (XZ202101ZD0005N), National Natural Science Foundation of China (32160773), and Basic Research Funds of the China Agricultural University and Tibet Agriculture and Animal Husbandry University (2022TC125).

## REFERENCES


Ai, H., Yang, B., Li, J., Xie, X., Chen, H., and Ren, J. (2014). Population history and genomic signatures for high-altitude adaptation in Tibetan pigs. *BMC Genom.* 15:834. doi: 10.1186/1471-2164-15-834

Anand, S., and Mande, S. S. (2018). Diet, microbiota and gut-lung connection. *Front. Microbiol.* 9:2147. doi: 10.3389/fmicb.2018.02147

Andrade, B. G. N., Bressani, F. A., Cuadrat, R. R., Tizioto, P. C., de Oliveira, P. S., Mourão, G. B., et al. (2020). The structure of microbial populations in Nelore GIT reveals inter-dependency of methanogens in feces and rumen. *J. Anim. Sci. Biotechnol.* 11:6. doi: 10.1186/s40104-019-0422-x

Aßhauer, K. P., Wemheuer, B., Daniel, R., and Meinicke, P. (2015). Tax4Fun: predicting functional profiles from metagenomic 16S rRNA data. *Bioinformatics* 31, 2882–2884. doi: 10.1093/bioinformatics/btv287

Backhed, F., Ding, H., Wang, T., Hooper, L. V., Koh, G. Y., Nagy, A. et al. (2004). The gut microbiota as an environmental factor that regulates fat storage. *Proc. Natl. Acad. Sci. U.S.A.* 101, 1518–1523. doi: 10.1073/pnas.0407076101

Bergamaschi, M., Tiezzi, F., Howard, J., Huang, Y. J., Gray, K. A., Schillebeeckx, C., et al. (2020). Gut microbiome composition differences among breeds impact feed efficiency in swine. *Microbiome* 8:110. doi: 10.1186/s40168-020-00888-9

Biddle, A., Stewart, L., Blanchard, J., and Leschine, S. (2013). Untangling the genetic basis of fibrolytic specialization by Lachnospiraceae and Ruminococcaceae in diverse gut communities. *Diversity* 5, 627–640. doi: 10.3390/d5030627

Binda, C., Lopetuso, L. R., Rizzatti, G., Gibiino, G., Cennamo, V., and Gasbarrini, A. (2018). Actinobacteria: a relevant minority for the maintenance of gut homeostasis. *Dig. Liver Dis.* 50, 421–428. doi: 10.1016/j.dld.2018.02.012

Bokulich, N. A., Subramanian, S., Faith, J. J., Gevers, D., Gordon, J. I., Knight, R., et al. (2013). Quality-filtering vastly improves diversity estimates from Illumina amplicon sequencing. *Nat. Methods* 10, 57–59. doi: 10.1038/nmeth.2276

Camarinha-Silva, A., Maushammer, M., Wellmann, R., Vital, M., Preuss, S., and Bennewitz, J. (2017). Host genome influence on gut microbial composition and microbial prediction of complex traits in pigs. *Genetics* 206, 1637–1644. doi: 10.1534/genetics.117.200782

Candela, M., Perna, F., Carnevali, P., Vitali, B., Ciati, R., Gionchetti, P., et al. (2008). Interaction of probiotic lactobacillus and bifidobacterium strains with human intestinal epithelial cells: adhesion properties, competition against enteropathogens and modulation of il-8 production. *Int. J. Food Microbiol.* 125, 286–292. doi: 10.1016/j.ijfoodmicro.2008.04.012

Caporaso, J. G., Kuczynski, J., Stombaugh, J., Bittinger, K., Bushman, F. D., Costello, E. K., et al. (2010). QIIME allows analysis of high-throughput community sequencing data. *Nat. Methods* 7, 335–336. doi: 10.1038/nmeth.f.303

Chen, L., Xu, Y., Chen, X., Fang, C., Zhao, L., and Chen, F. (2017). The maturing development of gut microbiota in commercial piglets during the weaning transition. *Front. Microbiol.* 8:1688. doi: 10.3389/fmicb.2017.01688

Coleman, O. I., Lobner, E. M., Bierwirth, S., Sorbie, A., Waldschmitt, N., Rath, E., et al. (2018). Activated ATF6 induces intestinal dysbiosis and innate immune response to promote colorectal tumorigenesis. *Gastroenterology* 155, 1539.e–1552.e. doi: 10.1053/j.gastro.2018.07.028

Crespo-Piazuelo, D., Migura-Garcia, L., Estellé, J., Criado-Mesas, L., Revilla, M., Castelló, A., et al. (2019). Association between the pig genome and its gut microbiota composition. *Sci. Rep.* 9:8791. doi: 10.1038/s41598-019-45066-6

Edgar, R. (2013). UPARSE: highly accurate OTU sequences from microbial amplicon reads. *Nat. Methods* 10, 996–998. doi: 10.1038/nmeth.2604

Fernández, J., Redondo-Blanco, S., Gutiérrez-del-Río, I., Miguélez, E. M., Villar, C. J., and Lombó, F. (2016). Colon microbiota fermentation of dietary prebiotics towards short-chain fatty acids and their roles as anti-inflammatory and antitumour agents: a review. *J. Funct. Foods* 25, 511–522. doi: 10.1016/j.jff.2016.06.032

Fernandez, M. F., Boris, S., and Barbes, C. (2003). Probiotic properties of human lactobacilli strains to be used in the gastrointestinal tract. *J. Appl. Microbiol.* 94, 449–455. doi: 10.1046/j.1365-2672.2003.01850.x

Filannino, P., Di Cagno, R., and Gobbetti, M. (2018). Metabolic and functional paths of lactic acid bacteria in plant foods: get out of the labyrinth. *Curr. Opin. Biotechnol.* 49, 64–72. doi: 10.1016/j.copbio.2017.07.016

Ghosh, S., Whitley, C. S., Haribabu, B., and Jala, V. R. (2021). Regulation of Intestinal Barrier Function by Microbial Metabolites. *Cell Mol. Gastroenterol. Hepatol.* 11, 1463–1482. doi: 10.1016/j.jcmgh.2021.02.007

Gill, S. K., Rossi, M., Bajka, B., and Whelan, K. (2021). Dietary fibre in gastrointestinal health and disease. *Nat. Rev. Gastroenterol. Hepatol.* 18, 101–116. doi: 10.1038/s41575-020-00375-4

Gong, X., Zheng, M., Zhang, J., Ye, Y., Duan, M., Chamba, Y., et al. (2022). Transcriptomics-based study of differentially expressed genes related to fat deposition in Tibetan and Yorkshire pigs. *Front. Vet. Sci.* 9:919904. doi: 10.3389/fvets.2022.919904

Guo, X., Xia, X., Tang, R., and Wang, K. (2008). Real-time PCR quantification of the predominant bacterial divisions in the distal gut of Meishan and Landrace pigs. *Anaerobe* 14, 224–228. doi: 10.1016/j.anaerobe.2008.04.001

Hao, Z., Li, Z., Huo, J., Chu, Y., Li, J., Yu, X., et al. (2021). Effects of Chinese wolfberry and astragalus extracts on growth performance, pork quality, and unsaturated fatty acid metabolism regulation in Tibetan fragrant pigs. *Anim. Sci. J.* 92:e13581. doi: 10.1111/asj.13581

Hedemann, M. S., Eskildsen, M., Laerke, H. N., Pedersen, C., Lindberg, J. E., Laurinen, P., et al. (2006). Intestinal morphology and enzymatic activity in newly weaned pigs fed contrasting fiber concentrations and fiber properties. *J. Anim. Sci.* 84, 1375–1386. doi: 10.2527/2006.8461375x

Hillman, E. T., Lu, H., Yao, T., and Nakatsu, C. H. (2017). Microbial ecology along the gastrointestinal tract. *Microbes Environ.* 32, 300–313. doi: 10.1264/jsme2.ME17017

Judkins, T. C., Archer, D. L., Kramer, D. C., and Solch, R. J. (2020). Probiotics, nutrition, and the small intestine. *Curr. Gastroenterol. Rep.* 22:2. doi: 10.1007/s11894-019-0740-3

Just, S., Mondot, S., Ecker, J., Wegner, K., Rath, E., Gau, L., et al. (2018). The gut microbiota drives the impact of bile acids and fat source in diet on mouse metabolism. *Microbiome* 6:134. doi: 10.1186/s40168-018-0510-8

Kim, H. B., and Isaacson, R. E. (2015). The pig gut microbial diversity: understanding the pig gut microbial ecology through the next generation high throughput sequencing. *Vet. Microbiol.* 177, 242–213. doi: 10.1016/j.vetmic.2015.03.014

Koliada, A., Syzenko, G., Moseiko, V., Budovska, L., Puchkov, K., Perederiy, V., et al. (2017). Association between body mass index and Firmicutes/Bacteroidetes ratio in an adult Ukrainian population. *BMC Microbiol.* 17:120. doi: 10.1186/s12866-017-1027-1

Kumar, A., Vlasova, A. N., Deblais, L., Huang, H. C., Wijeratne, A., Kandasamy, S., et al. (2018). Impact of nutrition and rotavirus infection on the infant gut microbiota in a humanized pig model. *BMC Gastroenterol.* 18:93. doi: 10.1186/s12876-018-0810-2

Langille, M. G., Zaneveld, J., Caporaso, J. G., McDonald, D., Knights, D., Reyes, J. A., et al. (2013). Predictive functional profiling of microbial com-munities using 16S rRNA marker gene sequences. *Nat. Biotechnol.* 31, 814–821. doi: 10.1038/nbt.2676

Lei, L., Wang, Z., Li, J., Yang, H., Yin, Y., Tan, B., et al. (2021). Comparative microbial profiles of colonic digesta between ningxiang pig and large white pig. *Animals* 11:1862. doi: 10.3390/ani11071862

Liang, J., Sha, S. M., and Wu, K. C. (2014). Role of the intestinal microbiota and fecal transplantation in inflammatory bowel diseases. *J. Dig. Dis.* 15, 641–646. doi: 10.1111/1751-2980.12211

Lo, B. C., Chen, G. Y., Núñez, G., and Caruso, R. (2021). Gut microbiota and systemic immunity in health and disease. *Int. Immunol.* 33, 197–209. doi: 10.1093/intimm/dxaa079

Louca, S., Parfrey, L. W., and Doebeli, M. (2016). Decoupling function and taxonomy in the global ocean microbiome. *Science* 353:1272. doi: 10.1126/science.aaf4507

Lu, D., Tiezzi, F., Schillebeeckx, C., McNulty, N. P., Schwab, C., Shull, C., et al. (2018). Host contributes to longitudinal diversity of fecal microbiota in swine selected for lean growth. *Microbiome* 6:4. doi: 10.1186/s40168-017-0384-1

Lu, X. M., Lu, P. Z., and Zhang, H. (2014). Bacterial communities in manures of piglets and adult pigs bred with different feeds revealed by 16S rDNA 454 pyrosequencing. *Appl. Microbiol. Biotechnol.* 98, 2657–2665. doi: 10.1007/s00253-013-5211-4

Luo, Y., Li, J., Zhou, H., Yu, B., He, J., Wu, A., et al. (2021). The Nutritional significance of intestinal fungi: alteration of dietary carbohydrate composition triggers colonic fungal community shifts in a pig model. *Appl. Environ. Microbiol.* 87:e00038-21. doi: 10.1128/AEM.00038-21

Ma, Y. F., Han, X. M., Huang, C. P., Zhong, L., Adeola, A. C., Irwin, D. M., et al. (2019). Population genomics analysis revealed origin and high-altitude adaptation of tibetan pigs. *Sci. Rep.* 9:11463. doi: 10.1038/s41598-019-47711-6

Magoč, T., and Salzberg, S. L. (2011). FLASH: fast length adjustment of short reads to improve genome assemblies. *Bioinformatics* 27, 2957–2963. doi: 10.1093/bioinformatics/btr507

Maslowski, K. M., and Mackay, C. R. (2011). Diet, gut microbiota and immune responses. *Nat. Immunol.* 12, 5–9. doi: 10.1038/ni0111-5

Ngoc, T. T. B., Oanh, N. C., Hong, T. T. T., and Dang, P. K. (2021). Effects of dietary fiber sources on bacterial diversity in separate segments of the gastrointestinal tract of native and exotic pig breeds raised in Vietnam. *Vet. World* 10, 2579–2587. doi: 10.14202/vetworld.2021.2579-2587

Ondov, B. D., Bergman, N. H., and Phillippy, A. M. (2011). Interactive metagenomic visualization in a Web browser. *BMC Bioinf.* 12:385. doi: 10.1186/1471-2105-12-385

Panasevich, M. R., Wankhade, U. D., Chintapalli, S. V., Shankar, K., and Rector, R. S. (2018). Cecal versus fecal microbiota in Ossabaw swine and implications for obesity. *Physiol. Genom.* 50, 355–368. doi: 10.1152/physiolgenomics.00110.2017

Park, S. J., Kim, J., Lee, J. S., Rhee, S. K., and Kim, H. (2014). Characterization of the fecal microbiome in different swine groups by high-throughput sequencing. *Anaerobe* 28, 157–162. doi: 10.1016/j.anaerobe.2014.06.002

Payne, A. N., Chassard, C., Zimmermann, M., Müller, P., Stinca, S., and Lacroix, C. (2011). The metabolic activity of gut microbiota in obese children is increased compared with normal-weight children and exhibits more exhaustive substrate utilization. *Nutr. Diabetes* 1:e12. doi: 10.1038/nutd.2011.8

Pedersen, R., Ingerslev, H.-C., Sturek, M., Alloosh, M., Cirera, S., Christoffersen, B. Ø, et al. (2013). Characterisation of gut microbiota in Ossabaw and Göttingen minipigs as models of obesity and metabolic syndrome. *PLoS One* 8:e56612. doi: 10.1371/journal.pone.0056612

Peng, L., Li, Z. R., Green, R. S., Holzman, I. R., and Lin, J. (2009). Butyrate enhances the intestinal barrier by facilitating tight junction assembly via activation of AMP-activated protein kinase in Caco-2 cell monolayers. *J. Nutr.* 139, 1619–1625. doi: 10.3945/jn.109.104638

Pruesse, E., Quast, C., Knittel, K., Fuchs, B. M., Ludwig, W., Peplies, J., et al. (2007). SILVA: a comprehensive online resource for quality checked and aligned ribosomal RNA sequence data compatible with ARB. *Nucleic Acids Res.* 35, 7188–7196. doi: 10.1093/nar/gkm864

Shang, P., Li, W., Liu, G., Zhang, J., Li, M., Wu, L., et al. (2019). Identification of lncRNAs and Genes Responsible for Fatness and Fatty Acid Composition Traits between the Tibetan and Yorkshire Pigs. *Int. J. Genom.* 2019:5070975. doi: 10.1155/2019/5070975

Tan, Z., Yang, T., Wang, Y., Xing, K., Zhang, F., Zhao, X., et al. (2017). Metagenomic analysis of cecal microbiome identified microbiota and functional capacities associated with feed efficiency in landrace finishing pigs. *Front. Microbiol.* 8:1546. doi: 10.3389/fmicb.2017.01546

Tang, S., Xin, Y., Ma, Y., Xu, X., Zhao, S., and Cao, J. (2020). Screening of microbes associated with swine growth and fat deposition traits across the intestinal tract. *Front. Microbiol.* 11:586776. doi: 10.3389/fmicb.2020.586776

Turnbaugh, P. J., Hamady, M., Yatsunenko, T., Cantarel, B. L., Duncan, A., Ley, R. E., et al. (2009). A core gut microbiome in obese and lean twins. *Nature* 457, 480–484. doi: 10.1038/nature07540

Turnbaugh, P. J., Ley, R. E., Mahowald, M. A., Magrini, V., Mardis, E. R., and Gordon, J. I. (2006). An obesity-associated gut microbiome with increased capacity for energy harvest. *Nature* 444, 1027–1031. doi: 10.1038/nature05414

Vital, M., Howe, C., and Tiedje, M. (2014). Revealing the bacterial butyrate synthesis pathways by analyzing (meta) genomic data. *mBio* 5:e00889. doi: 10.1128/mBio.00889-14

Wang, H., Ni, X., Qing, X., Zeng, D., Luo, M., Liu, L., et al. (2017). Live Probiotic Lactobacillus johnsonii BS15 Promotes Growth Performance and Lowers Fat Deposition by Improving Lipid Metabolism, Intestinal Development, and Gut Microflora in Broilers. *Front. Microbiol.* 8:1073. doi: 10.3389/fmicb.2017.01073

Wang, Q., Garrity, G. M., Tiedje, J. M., and Cole, J. R. (2007). Naive Bayesian classifier for rapid assignment of rRNA sequences into the new bacterial taxonomy. *Appl. Environ. Microbiol.* 73, 5261–5267. doi: 10.1128/AEM.00062-07

Wang, X., Tsai, T., Deng, F., Wei, X., Chai, J., Knapp, J., et al. (2019). Longitudinal investigation of the swine gut microbiome from birth to market reveals stage and growth performance associated bacteria. *Microbiome* 7:109. doi: 10.1186/s40168-019-0721-7

Wang, Y., Zhang, H., Zhu, L., Xu, Y., Liu, N., Sun, X., et al. (2018). Dynamic distribution of gut microbiota in goats at different ages and health states. *Front. Microbiol.* 9:2509. doi: 10.3389/fmicb.2018.02509

Wong, C. B., Odamaki, T., and Xiao, J. Z. (2020). Insights into the reason of Human-Residential Bifidobacteria (HRB) being the natural inhabitants of the human gut and their potential health-promoting benefits. *FEMS Microbiol. Rev.* 44, 369–385. doi: 10.1093/femsre/fuaa010

Yang, H., Huang, X., Fang, S., He, M., Zhao, Y., Wu, Z., et al. (2017). Unraveling the fecal microbiota and metagenomic functional capacity associated with feed efficiency in pigs. *Front. Microbiol.* 8:1555. doi: 10.3389/fmicb.2017.01555

Yang, L., Bian, G., Su, Y., and Zhu, W. (2014). Comparison of faecal microbial community of lantang, bama, erhualian, meishan, xiaomeishan, duroc, landrace, and yorkshire sows. *Asian Austral. J. Anim. Sci.* 27, 898–906. doi: 10.5713/ajas.2013.13621

Zhang, B., Chamba, Y., Shang, P., Wang, Z., Ma, J., Wang, L., et al. (2017). Comparative transcriptomic and proteomic analyses provide insights into the key genes involved in high-altitude adaptation in the Tibetan pig. *Sci. Rep.* 7:3654. doi: 10.1038/s41598-017-03976-3

Zitvogel, L., Ma, Y., Raoult, D., Kroemer, G., and Gajewski, T. F. (2018). The microbiome in cancer immunotherapy: diagnostic tools and therapeutic strategies. *Science* 359, 1366–1370. doi: 10.1126/science.aar6918

**Conflict of Interest:** The authors declare that the research was conducted in the absence of any commercial or financial relationships that could be construed as a potential conflict of interest.

**Publisher's Note:** All claims expressed in this article are solely those of the authors and do not necessarily represent those of their affiliated organizations, or those of the publisher, the editors and the reviewers. Any product that may be evaluated in this article, or claim that may be made by its manufacturer, is not guaranteed or endorsed by the publisher.

frontiers | Frontiers in Microbiology

TYPE Original Research
PUBLISHED 07 September 2022
DOI 10.3389/fmicb.2022.1003905



OPEN ACCESS

EDITED BY
Hui Zhang,
South China Agricultural University, China

REVIEWED BY
Renhong Wan,
Tianjin University of Traditional Chinese Medicine, China
Yu Yin,
Changchun University of Chinese Medicine, China

*CORRESPONDENCE
Jinhong Guo
gjh1008611@126.com
Chuanbiao Wen
wcb106981630@126.com
Biao Huang
863653778@qq.com

†These authors have contributed equally to this work and share first authorship

SPECIALTY SECTION
This article was submitted to Microorganisms in Vertebrate Digestive Systems, a section of the journal Frontiers in Microbiology

RECEIVED 26 July 2022
ACCEPTED 19 August 2022
PUBLISHED 07 September 2022

CITATION
Zhang L, Xiong S, Jin F, Zhou F, Zhou H, Guo J, Wen C and Huang B (2022) Global trends in intestinal flora and ulcerative colitis research during the past 10 years: A bibliometric analysis.
*Front. Microbiol.* 13:1003905.
doi: 10.3389/fmicb.2022.1003905



# Global trends in intestinal flora and ulcerative colitis research during the past 10 years: A bibliometric analysis

Lu Zhang[1†], Shuai Xiong[1†], Fengchen Jin[1†], Fan Zhou[2†], Hongjun Zhou[1], Jinhong Guo[1*], Chuanbiao Wen[1*] and Biao Huang[3*]

[1]Chengdu University of Traditional Chinese Medicine, Chengdu, China, [2]North Sichuan Medical College, Nanchong, China, [3]Affiliated Hospital of Jiangxi University of Traditional Chinese Medicine, Nanchang, China

**Background and aim:** Ulcerative colitis is a chronic inflammatory bowel disease, and intestinal flora plays an important role in ulcerative colitis. In this study, we conducted a bibliometric analysis of publications in the field of intestinal flora and ulcerative colitis research in the past 10 years to summarize the current status of the field and analyze the trends in the field.

**Methods:** On July 15, 2022, we chose the Web of Science Core Collection database as the study's data source. CiteSpace.5.8.R3 and VOSviewer 1.6.17 were used to examine publications of research on intestinal flora and ulcerative colitis that were published between 2012 and 2021. We looked through the papers for journals, organizations, nations and regions, authors, and key terms.

**Results:** This analysis covered a total of 2,763 papers on studies into intestinal flora and ulcerative colitis. There were 13,913 authors, 93 nations, 3,069 organizations, and 759 journals in all of the articles. In the USA, 767 publications were the most. The university with the most publications was Harvard Medical School. The author with the most articles was Antonio Gasbarrini.

**Conclusion:** This study summarizes the global research trends in intestinal flora and ulcerative colitis. Publications in this field have increased year by year in the last decade and the field of research on intestinal flora and ulcerative colitis has good prospects for growth.

KEYWORDS

**intestinal flora, ulcerative colitis, trends, CiteSpace, VOSviewer**

## Introduction

Ulcerative colitis is a chronic inflammatory bowel disease, the pathogenesis of which is still unclear (Sonnenberg and Siegmund, 2016). The typical trait of ulcerative colitis is diffuse mucosal inflammation confined to the colonic region (Fell et al., 2016). Ulcerative colitis presents with bloody diarrhea, abdominal pain, fecal incontinence and fatigue (Segal

et al., 2021). The incidence and prevalence of ulcerative colitis is highest in North America and Northern Europe. The incidence of ulcerative colitis is bimodal in character, with the first peak between the ages of 15–30 years and the second peak between the ages of 50–70 years (Burisch and Munkholm, 2015). Treatment of ulcerative colitis includes corticosteroids (Rhen and Cidlowski, 2005), aminosalicylates (Habens et al., 2005) and immunosuppressive agents (van Dieren et al., 2006). The etiology of ulcerative colitis involves interactions between the environment, the immune system, the gut microbiota, and genetic susceptibility to disease (Kobayashi et al., 2020). Imbalance of the intestinal flora can lead to intestinal inflammation. Recent studies have highlighted the role of intestinal flora in ulcerative colitis (Khan et al., 2019). Regulation of intestinal flora can treat ulcerative colitis (Damaskos and Kolios, 2008).

In bibliometrics, publications in a certain topic are quantitatively analyzed using statistical techniques (Ellegaard and Wallin, 2015). In 1969, American academics developed bibliometric analysis (Ma C. 2021). Researchers may easily understand the trends in their field of study with the aid of bibliometrics (Ma D. 2021). It evaluates a field's state in terms of nations or regions, writers, institutions, etc. Numerous domains, such as cancer (Wang et al., 2021), pain (Luo et al., 2021), and infectious illnesses (Yang et al., 2020), have used bibliometrics. However, there has not been any bibliometric analysis done in the study on intestinal flora and ulcerative colitis. A bibliometric analysis of studies on intestinal flora and ulcerative colitis is necessary. We conducted a bibliometric analysis of publications on intestinal flora and ulcerative colitis from 2012 to 2021 with the intention of understanding the research trends in the area of intestinal flora and ulcerative colitis research during the last 10 years. We will summarize the current state of the field and analyze the trends in the field.

# Materials and methods

## Data collection and retrieval strategies

We obtained information from Clarivate Analytics' Web of Science Core Collection (WoSCC) database. We were able to accurately analyze the papers since the WoSCC offers more information than other databases (Ma et al., 2022). The Social Sciences Citation Index (SSCI), Arts and Humanities Citation Index (A&HCI), Conference Proceedings Citation Index—Social Sciences and Humanities (CPCI-SSH), and Emerging Science Citation Index were among the versions of WoSCC that we searched (ESCI). Topic = ("gastrointestinal microbiome*" or "gut microbiome*" or "gut microflora" or "gut microbiota" or "gastrointestinal flora" or "gastrointestinal microbial communit* "or "gastrointestinal microflora" or "gastric microbiome*" or "intestinal microbiome*" or "intestinal flora" "gastrointestinal microbial communit* "OR "gastrointestinal flora" OR "gastrointestinal microbiota*") AND Topic = ("ulcerative colitis" or "ulcerative colitis" or "ulcerous colitis "or "ulcerative colonitis" or "colitis ulcerosa" or "idiopathic proctocolitis" or "colitis gravis"). The article must be published between 2012-01-01 and 2021-12-31. The article can only be read in English. Only Article and Review articles could be found, and two researchers independently conducted the search. To lessen the bias brought on by automated database updates, the search was finished on July 15, 2022. Figure 1 depicts the literature screening procedure.

## Data analysis

To analyze the data from the literature, we utilized VOSviewer 1.6.17 and CiteSpace 5.8.R3. The literature's authors, organizations, keywords, and journals were examined. CiteSpace's specifications were configured, including the number of years in each slice (slice length = 1) and time slices from January 2012 to December 2021. The phrase "top 50 levels" is used as the threshold for the most commonly mentioned or cited in the relevant time slice, and all choices in the terminology source are verified. One node type is then chosen at a time based on particular criteria.

# Results

## Analysis of publication trends

Finally, we incorporated 2,763 papers, comprising 1779 articles and 984 reviews, on research into intestinal flora and ulcerative colitis. Figure 2 depicts a general upward trend in the number of publications on research into intestinal flora and ulcerative colitis from the years 2012 to 2021. Between 2016 and 2018, there were 200 and 300 yearly publications. The number of yearly publications grew from 366 to 570 between 2019 and 2021.

## Analysis of the contribution of major countries

Between 2012 and 2021, 93 nations will participate in research on gut flora and ulcerative colitis. Table 1 lists the top 10 nations in the previous 10 years for research on intestinal flora and ulcerative colitis publications. The two biggest contributions were the United States and China. China came in second with 621 publications, trailing the United States with 767. Three nations made up the Asian region: China, Australia, and Japan. Italy, the United Kingdom, Germany, France, and Netherlands are among the five countries in Europe. The United States and Canada are located in the Americas. The strength of the cooperation may be shown by centrality. The United Kingdom, Canada, and Netherlands have the highest centrality of 0.15 out of the top 10 nations.

## Analysis of major institutions

A total of 3,069 institutions were involved in studies related to intestinal flora and ulcerative neo-colitis from 2012 to 2021. The

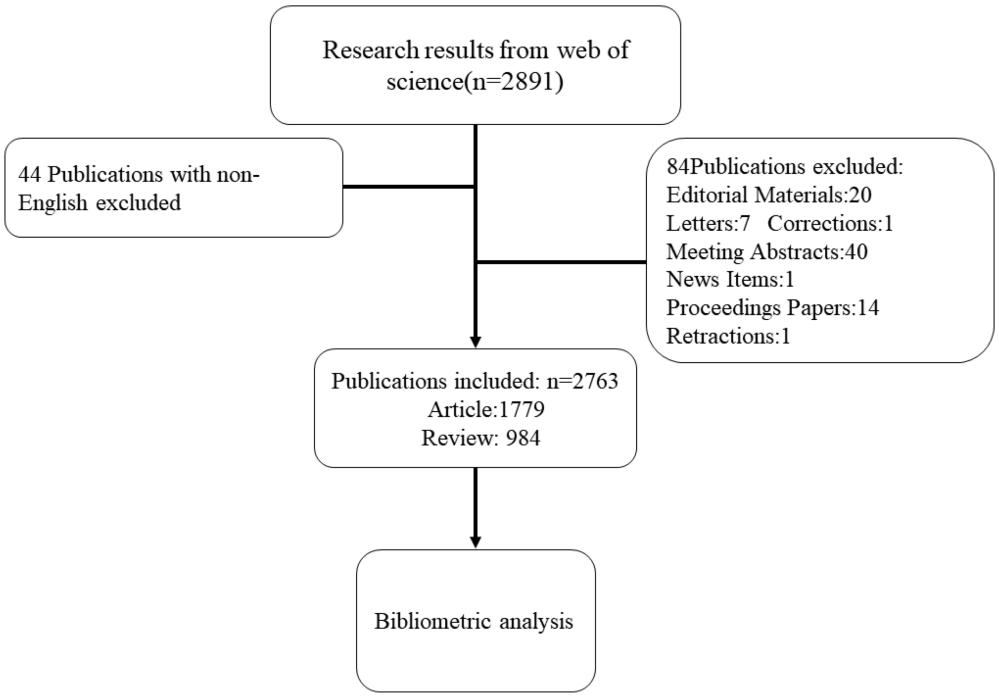


FIGURE 1
Flow chart of the study.

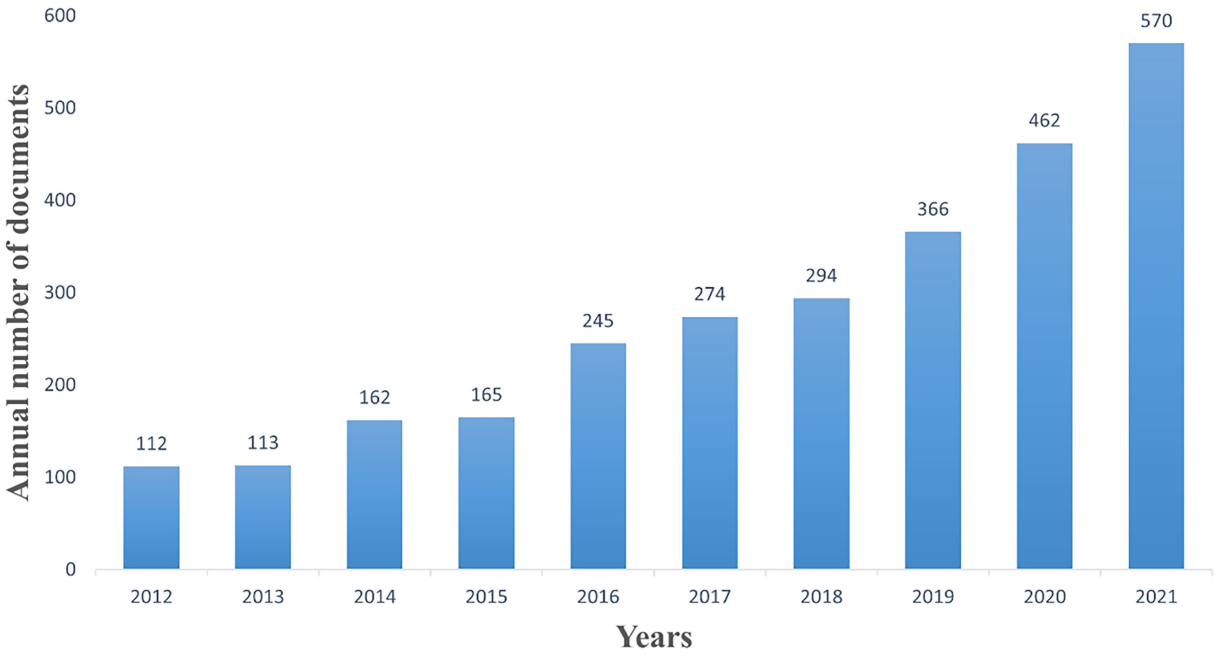


FIGURE 2
Trends in publications.

10 institutions with the highest number of publications are counted in Table 2. Those with > 30 publications were Harvard Medical School ($n = 47$), Massachusetts Hospital ($n = 43$), Harvard University (Walker et al., 2011), Nanjing Medical University (Kedia et al., 2021), University of Toronto (Cammarota et al., 2015), University of Alberta ($n = 31$) and Icahn School of Medicine

at Mount Sinai ($n = 31$). Figure 3 shows the network of collaborative relationships among the major publishing institutions in this field. Larger centrality indicates stronger collaborative relationships at that institution. Icahn School of Medicine at Mount Sinai has the largest centrality of 0.24, followed by Massachusetts State Hospital at 0.16.

TABLE 1 The ten countries with the most publications.

| Ranking | Countries | Centrality | Year | Publications |
|---|---|---|---|---|
| 1 | United States | 0.06 | 2012 | 767 |
| 2 | China | 0.00 | 2012 | 621 |
| 3 | Italy | 0.12 | 2012 | 197 |
| 4 | England | 0.15 | 2012 | 184 |
| 5 | Canada | 0.15 | 2012 | 180 |
| 6 | Germany | 0.00 | 2012 | 148 |
| 7 | Australia | 0.00 | 2012 | 129 |
| 8 | Japan | 0.06 | 2012 | 119 |
| 9 | France | 0.03 | 2012 | 109 |
| 10 | Netherlands | 0.15 | 2012 | 87 |

## Analysis of the main authors

Between 2012 and 2021, research on intestinal flora and ulcerative colitis had 13,913 authors in total. Table 3 includes a list of the top ten writers based on publications. Four of them, including Antonio Gasbarrini (Sokol et al., 2009), Ramnik J. Xavier (Marchesi et al., 2016), Ashwin N. Ananthakrishnan (Ma et al., 2022), and Harry Sokol (Ma et al., 2022), have published more than 15 publications. Figure 4 depicts the network of relationships that the leading authors in this subject have with one another. Collaboration exists between Jeanfrederic Colombel and Thomas J Borody. Benjamin H Mullish and Ailsa L Hart are

TABLE 2 Top ten institutions with the most publications.

| Ranking | Institution | Centrality | Year | Publications |
|---|---|---|---|---|
| 1 | Harvard Medical School | 0.00 | 2016 | 47 |
| 2 | Massachusetts General Hospital | 0.16 | 2012 | 43 |
| 3 | Harvard University | 0.04 | 2012 | 36 |
| 4 | Nanjing Medical University | 0.03 | 2016 | 35 |
| 5 | University of Toronto | 0.09 | 2012 | 32 |
| 6 | University of Alberta | 0.04 | 2012 | 31 |
| 7 | Icahn School of Medicine at Mount Sinai | 0.24 | 2014 | 31 |
| 8 | Sun Yat-sen University | 0.01 | 2015 | 28 |
| 9 | Università Cattolica del Sacro Cuore | 0.03 | 2014 | 26 |
| 10 | Zhejiang University | 0.01 | 2012 | 26 |

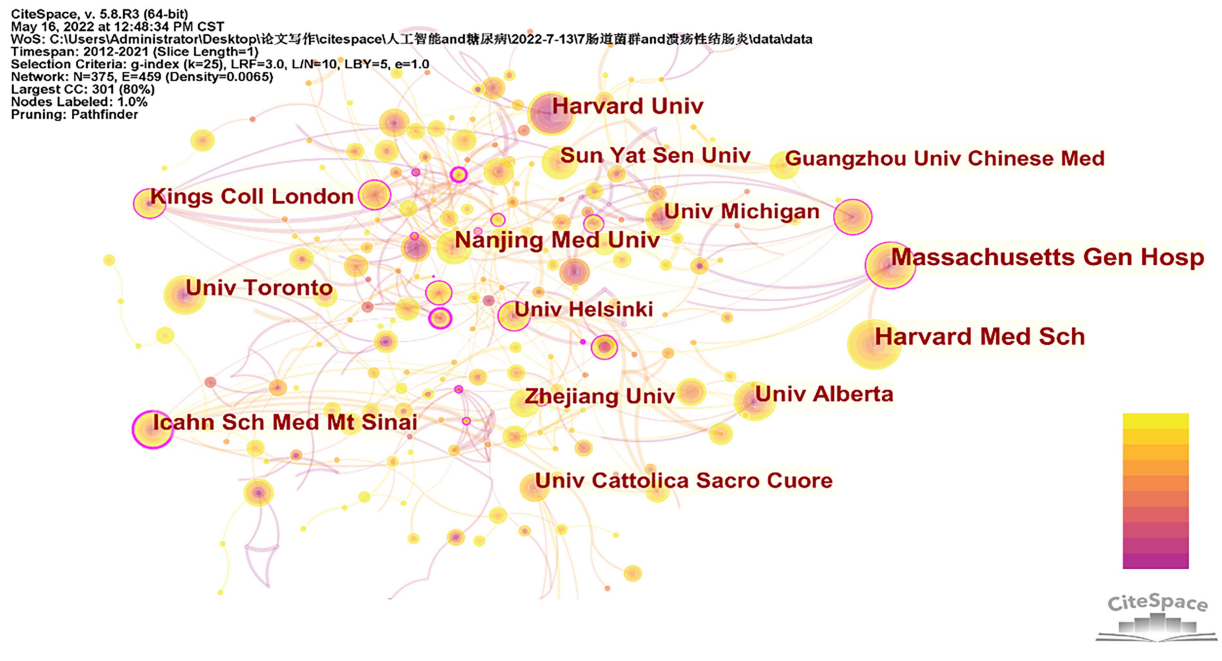


FIGURE 3
Institutional cooperation network.

TABLE 3 The ten authors with the highest number of articles.

| Ranking | Author | Centrality | Year | Publications |
|---|---|---|---|---|
| 1 | Antonio Gasbarrini | 0.02 | 2014 | 29 |
| 2 | Ramnik J Xavier | 0.05 | 2012 | 21 |
| 3 | Ashwin N Ananthakrishnan | 0.03 | 2013 | 17 |
| 4 | Harry Sokol | 0.04 | 2012 | 17 |
| 5 | Giovanni Cammarota | 0.03 | 2014 | 15 |
| 6 | Gerhard Rogler | 0.00 | 2014 | 14 |
| 7 | Jeanfrederic Colombel | 0.00 | 2017 | 13 |
| 8 | Eugene B Chang | 0.00 | 2013 | 12 |
| 9 | Wei Chen | 0.00 | 2019 | 12 |
| 10 | Gianluca Ianiro | 0.00 | 2014 | 11 |

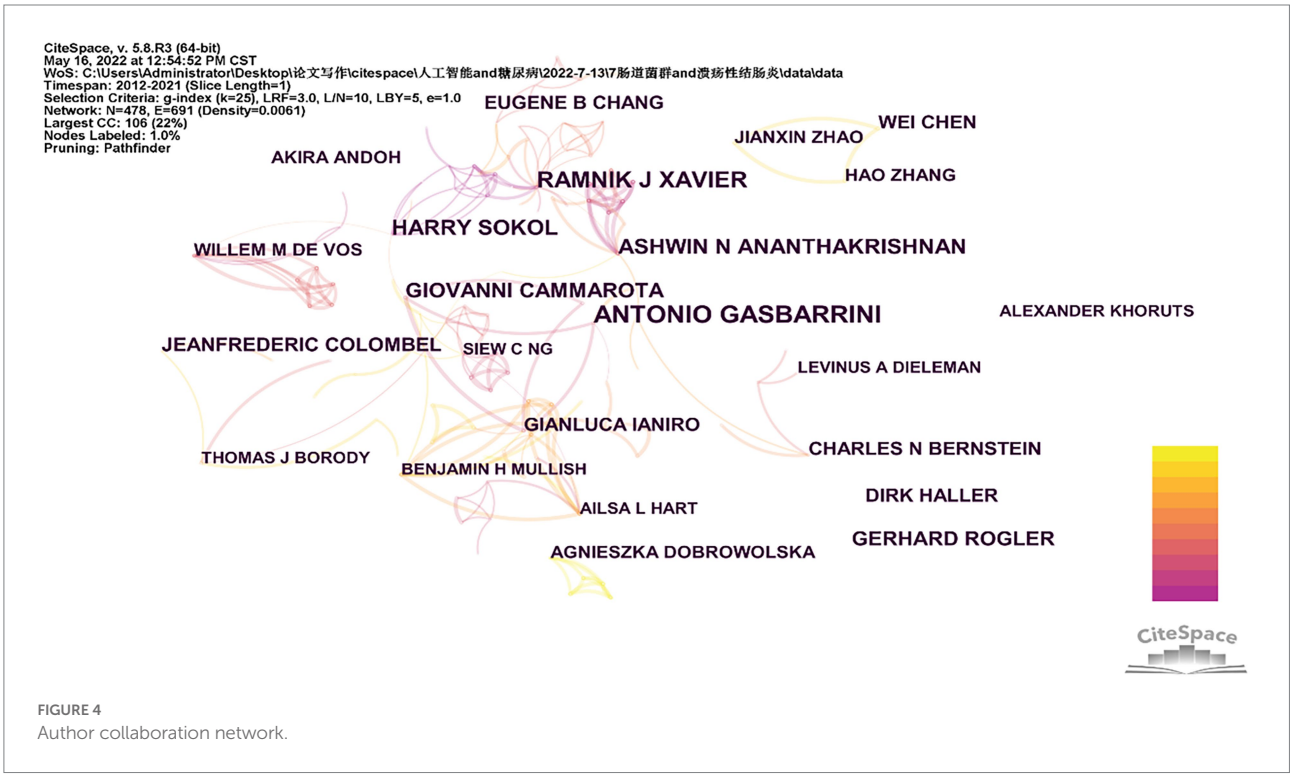


FIGURE 4
Author collaboration network.

working together. Hao Zhang, Wei Chen, and Jianxin Zhao work together on projects.

## Keyword analysis

The 7,808 keywords were found in the 2,763 papers on intestinal flora and ulcerative colitis research during the last 10 years. The top 20 terms in this field by frequency are listed in Table 4. There are four of them that have frequencies >300, including the terms "ulcerative colitis," "crohn's disease," "inflammatory bowel illness," and "gut microbiota." Figure 5 shows the co-occurrence network of keywords with frequencies over 100 in studies related to gut microbiota and ulcerative colitis. The 25 terms in the field with the greatest epidemic intensity are listed in Figure 6. Active ulcerative colitis, insulin sensitivity, and anxiety are a few of the epidemic keywords that started to surface after 2018. Figure 7 shows the relationship between keyword clustering and time. The top ten keyword clusters in the field of intestinal flora and ulcerative colitis research are "#0 th17," "#1 risk," "#2 diarrhea," "#3 probiotics," "#4 colitis," "#5 expression," "#6 host," "#7 ibd," "#8 remission" and "#9 sulfate-reducing bacteria."

## Analysis of high yielding journals

Figure 8 lists the journals with less than 20 publications out of the total 2,763 papers on intestinal flora and ulcerative colitis research that were published in 759 journals worldwide between

TABLE 4 The 20 keywords with the highest frequency.

| Ranking | Keywords | Centrality | Year | Count |
|---|---|---|---|---|
| 1 | ulcerative colitis | 0.02 | 2012 | 1,471 |
| 2 | crohn's disease | 0.00 | 2012 | 781 |
| 3 | inflammatory bowel disease | 0.00 | 2012 | 764 |
| 4 | gut microbiota | 0.00 | 2012 | 754 |
| 5 | intestinal microbiota | 0.03 | 2012 | 334 |
| 6 | fecal microbiota | 0.00 | 2012 | 265 |
| 7 | bacteria | 0.00 | 2012 | 218 |
| 8 | chain fatty acid | 0.04 | 2012 | 206 |
| 9 | clostridium difficile infection | 0.07 | 2012 | 188 |
| 10 | double blind | 0.01 | 2012 | 186 |
| 11 | active ulcerative colitis | 0.00 | 2015 | 179 |
| 12 | ibd | 0.03 | 2012 | 173 |
| 13 | diversity | 0.02 | 2012 | 164 |
| 14 | expression | 0.05 | 2012 | 160 |
| 15 | *Escherichia coli* | 0.00 | 2012 | 156 |
| 16 | pathogenesis | 0.03 | 2012 | 148 |
| 17 | remission | 0.05 | 2012 | 147 |
| 18 | inflammation | 0.05 | 2012 | 147 |
| 19 | disease | 0.21 | 2012 | 142 |
| 20 | mice | 0.06 | 2012 | 131 |

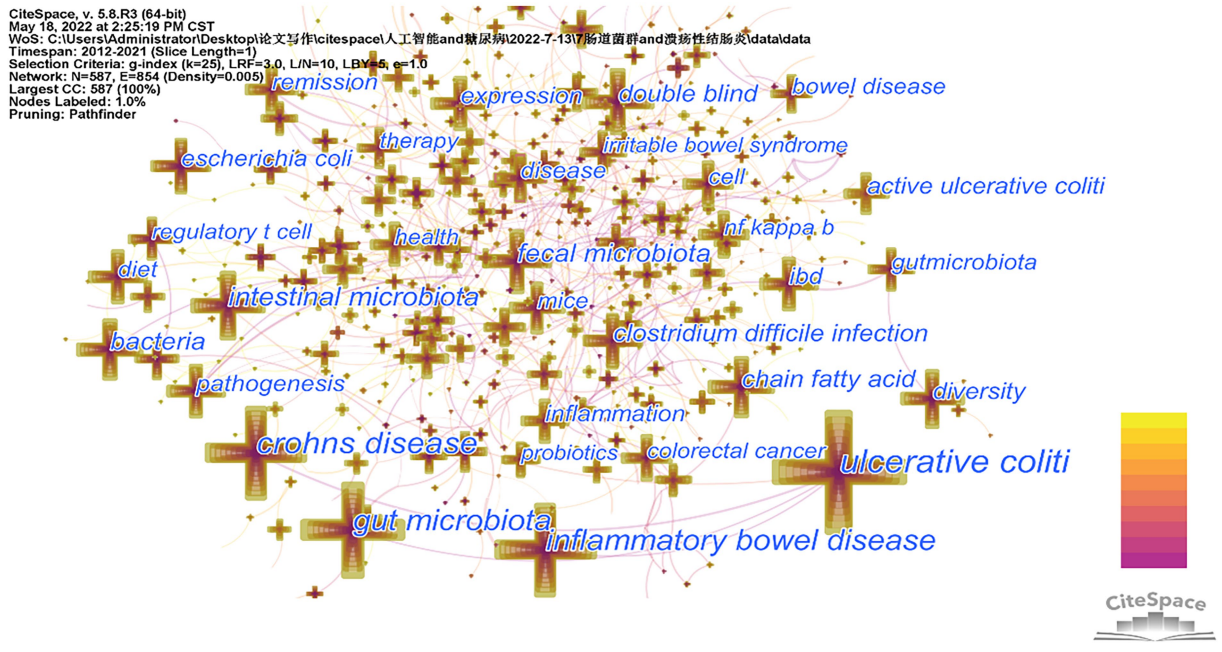


FIGURE 5
Keyword co-occurrence visualization.

2012 and 2021. Table 5 lists the ten journals that have published the most papers in this topic. Inflammatory Bowel Diseases ($n = 123$), World Journal of Gastroenterology ($n = 69$), Plos One ($n = 68$), Nutrients ($n = 67$), and Frontiers in Immunology ($n = 58$) were five journals with less than 50 articles. Inflammatory Bowel Diseases ($n = 4,648$), World Journal of Gastroenterology ($n = 3,498$), and Plos One ($n = 3,453$) were three journals with less than 3,000 citations each.

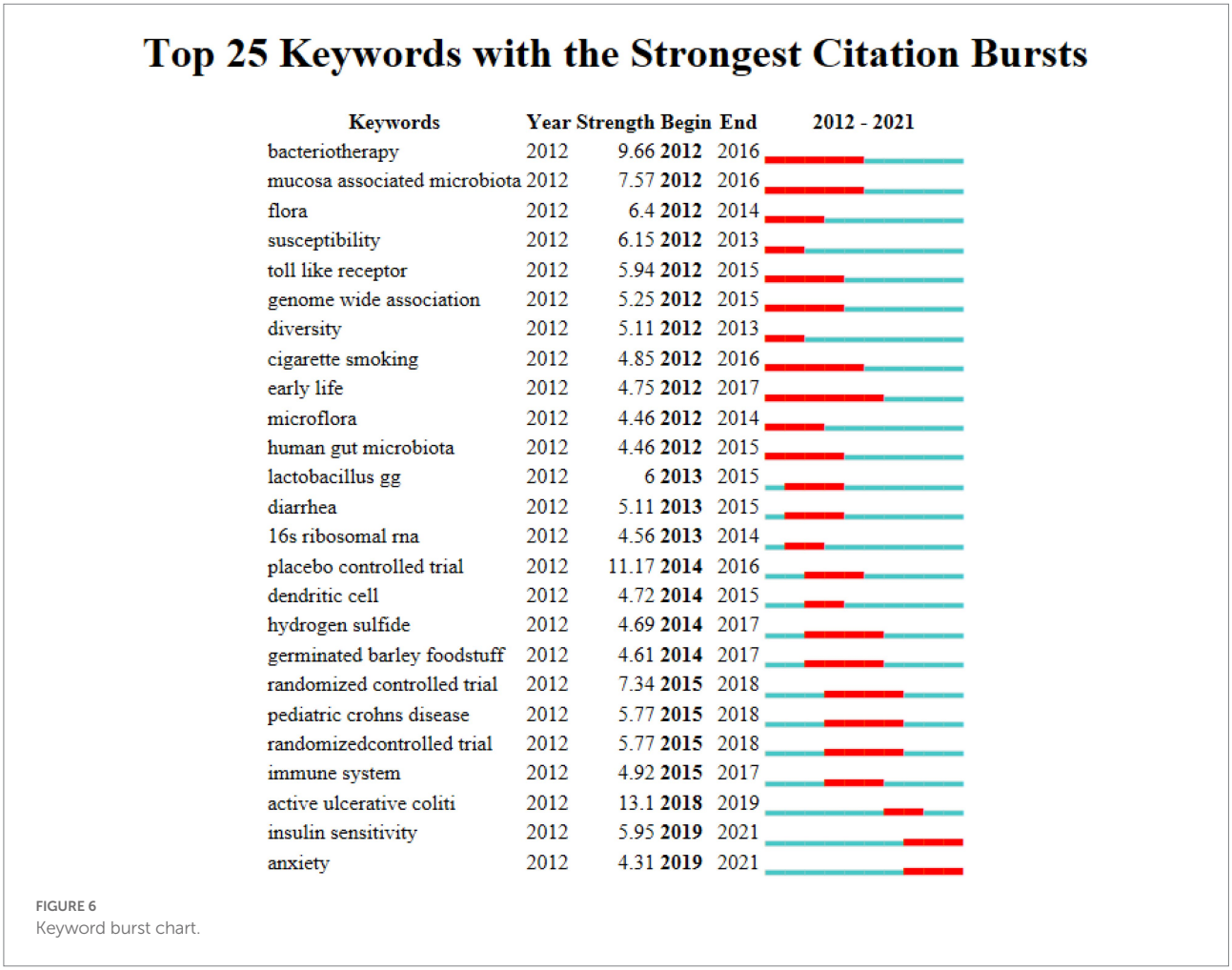


FIGURE 6
Keyword burst chart.

## Analysis of highly-cited papers

From 2012 to 2021, there were 2,763 articles on the topic of gut microbiota and ulcerative colitis. Of those, 23 studies had more than 500 citations. Table 6 displays the top ten articles in this field with the most citations. Four of them have citations in more than 1,000 publications. Include the article "The function of short-chain fatty acids in the interaction between food, gut microbiota, and host energy metabolism," by den Besten et al. (2013), which has 2070 citations in the Journal of Lipid Research. Clemente et al. (2012) article "The influence of the gut microbiota on human health: an integrated picture" from the journal Cell was mentioned in 1961. The article "Dysfunction of the intestinal microbiota in inflammatory bowel disease and therapy" by Morgan et al. (2012) had 1,576 citations. With 1,132 citations, Marchesi et al. (2016) published "The gut microbiota and host health: a new clinical frontier" in the Gut Journal.

# Discussion

It is crucial to research gut flora and ulcerative colitis. The bibliometric analysis of works in this topic has never been done before. We considered a total of 2,763 papers from 2012 to 2021 that dealt with studies on intestinal flora and ulcerative colitis. We discovered that there are more research being conducted in this area each year. In 2019, there were more publications than 300. One of the reasons of ulcerative colitis, according to theory, is dysbiosis of the gut flora (Venegas et al., 2019). The rise in publications indicates that this field of study is currently one of the most popular research hot topics.

From 2011 to 2021, the United States and China made the most progress in the field of research on intestinal flora and ulcerative colitis. 767 publications total, with 621 coming from China, were the most. Researchers from the United States examined the reduced variety and richness of gut flora in children with ulcerative colitis (Michail et al., 2012). In children with ulcerative colitis, the gut microbiome's composition and temporal alterations are linked to the disease process (Schirmer et al., 2018). Ursolic acid has been investigated by Chinese researchers to control the intestinal microbiota and inflammatory cell infiltration to avoid ulcerative colitis (Sheng et al., 2021). In ulcerative colitis patients, there was a reduction in beneficial bacteria and an increase in dangerous bacteria (He et al., 2021). In Xinjiang Uyghur, China, ulcerative colitis patients have lower levels of Clostridium, Bifidobacterium, Fusarium, and Proteus than

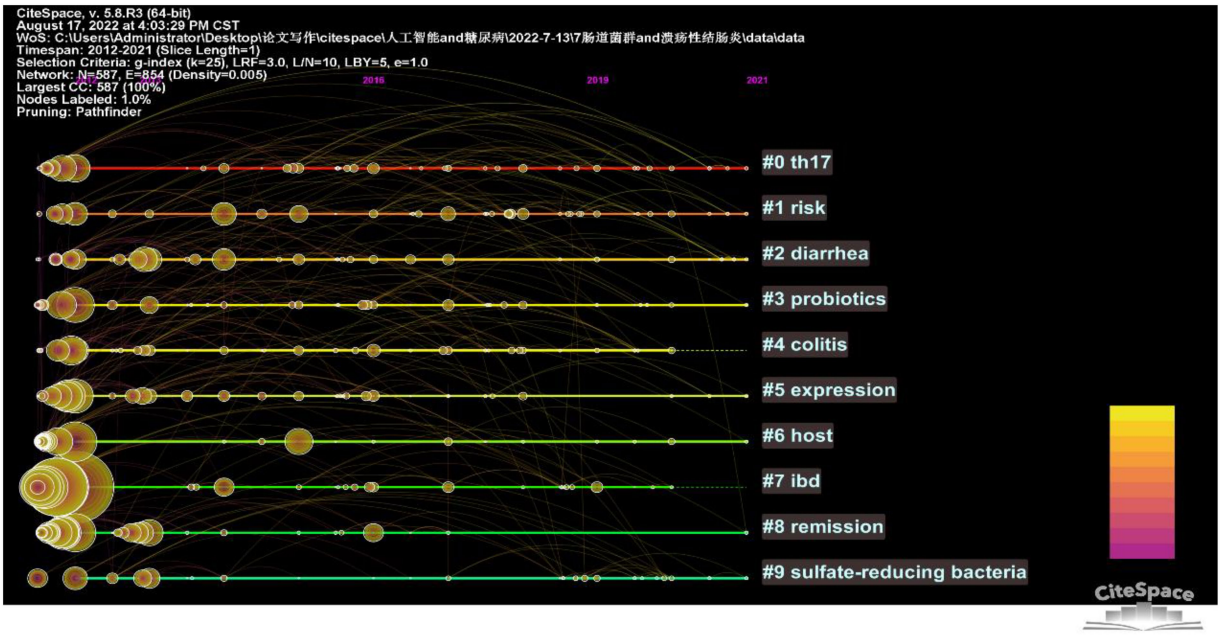


FIGURE 7
Keyword clustering timeline graph.

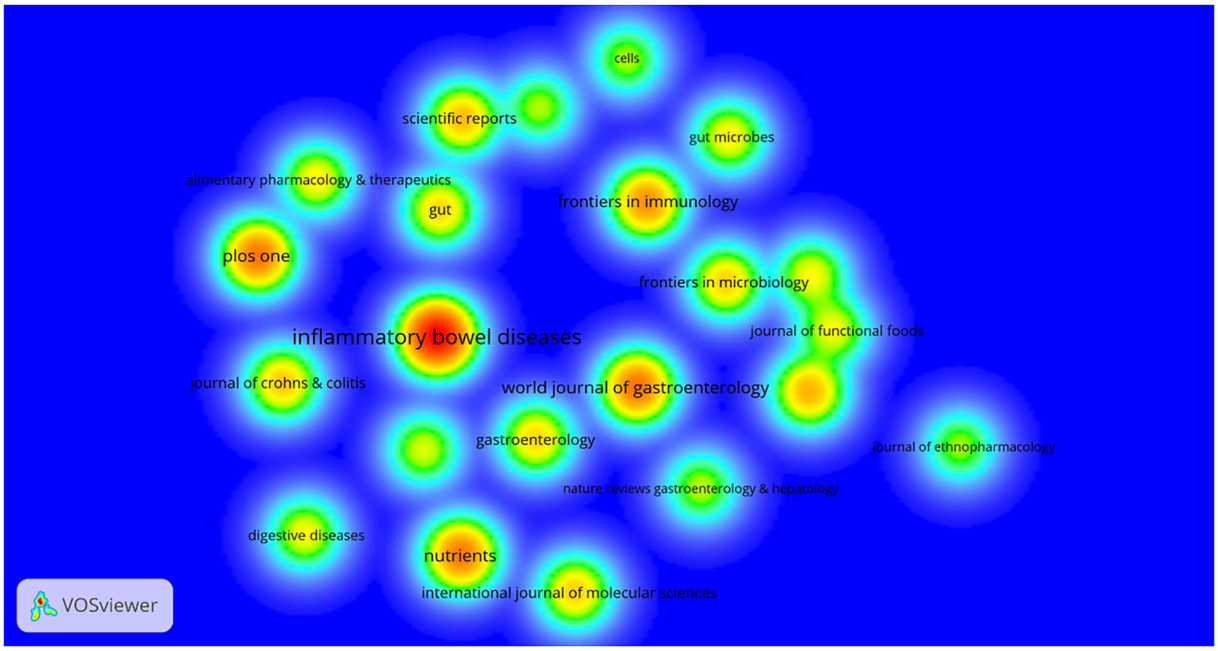


FIGURE 8
Journal density map.

healthy people (Yao et al., 2016). Harvard Medical School was the organization with the most amount of research papers on intestinal flora and ulcerative colitis published in this area47. The United States created the esteemed medical institution known as Harvard Medical School. DNA sequencing was used by researchers at Harvard Medical School to examine the gut flora in ulcerative colitis (Morgan et al., 2012). Changes in the gut flora can forecast how ulcerative colitis will develop (Ananthakrishnan

TABLE 5 Ten top journals.

| Ranking | Journal | Citations | Publications |
|---|---|---|---|
| 1 | Inflammatory Bowel Diseases | 4,648 | 123 |
| 2 | World Journal of Gastroenterology | 3,498 | 69 |
| 3 | Plos one | 3,453 | 68 |
| 4 | Nutrients | 2,029 | 67 |
| 5 | Frontiers in Immunology | 2,809 | 58 |
| 6 | Food and Function | 514 | 46 |
| 7 | Scientific Reports | 1,238 | 44 |
| 8 | Journal of Crohn's and Colitis | 1,557 | 41 |
| 9 | Frontiers in Microbiology | 1,721 | 39 |
| 10 | International Journal of Molecular Sciences | 612 | 39 |

TABLE 6 Ten highly cited articles.

| Rank | Title | Journals | First author | Year | Citations |
|---|---|---|---|---|---|
| 1 | The role of short-chain fatty acids in the interplay between diet, gut microbiota, and host energy metabolism | Journal of Lipid Research | Den Besten | 2013 | 2,070 |
| 2 | The impact of the gut microbiota on human health: an integrative view | Cell | Clemente | 2012 | 1,961 |
| 3 | Dysfunction of the intestinal microbiome in inflammatory bowel disease and treatment | Genome Biology | Morgan | 2012 | 1,576 |
| 4 | The gut microbiota and host health: a new clinical frontier | Gut | Marchesi | 2016 | 1,132 |
| 5 | The microbiome in inflammatory bowel disease: current status and the future ahead | Gastroenterology | Kostic | 2014 | 971 |
| 6 | The microbial metabolite butyrate regulates intestinal macrophage function *via* histone deacetylase inhibition | Proceedings of the National Academy of Sciences of the United States of America | Chang | 2014 | 939 |
| 7 | Short Chain Fatty Acids (SCFAs)-mediated gut epithelial and immune regulation and its relevance for inflammatory bowel diseases | Frontiers in Immunology | Parada Venegas | 2019 | 833 |
| 8 | Crohn's disease | Lancet | Torres | 2017 | 810 |
| 9 | Epidemiology and risk factors for IBD | Nature Reviews Gastroenterology and Hepatology | Ananthakrishnan | 2015 | 760 |
| 10 | Multi-omics of the gut microbial ecosystem in inflammatory bowel diseases | Nature | Lloyd-price | 2019 | 733 |

et al., 2017). With 123 articles, Inflammatory Bowel Diseases is the journal with the most publications in this area. Prausnitzii in Colitis Microbiota" (Sokol et al., 2009) and "Phylogenetic Analysis of Dysbiosis in Ulcerative Colitis During Remission" (Rajilic-Stojanovic et al., 2013). ANTONIO GASBARRINI, who has published the most articles on intestinal flora and ulcerative colitis, has investigated the beneficial effects of antibiotics in regulating intestinal flora (Ianiro et al., 2016). In the treatment of ulcerative colitis, ciprofloxacin is crucial (Cammarota et al., 2015).

The high frequency keywords in this field are "chain fatty acid" and "clostridium difficile infection." Intestinal flora and ulcerative colitis research both benefit from an understanding of chain fatty acids (Binder, 2010). According to research by laserna-Mendieta et al., a decline in chain fatty acids may be related to the onset of ulcerative colitis (Laserna-Mendieta et al., 2018). Anaerobic gut microbes fermenting generate chain fatty acids. Interestingly, ulcerative colitis has a diversified gut flora (Kedia et al., 2021). In acute ulcerative colitis, the gut flora is extremely unstable. In contrast to individuals with inflammatory bowel disease, the makeup of the intestinal flora fluctuates over time in normal persons. The microbial makeup of intestinal mucosa and feces differs significantly (Walker et al., 2011). Patients with ulcerative colitis are susceptible to clostridium difficile infection (Ananthakrishnan et al., 2013). Clostridium difficile infection is a gastrointestinal disease caused by Clostridium difficile, a Gram-positive, bacteriophage and toxin-producing anaerobic bacillus (Almeida et al., 2016). *Escherichia coli*

may induce ulcerative colitis in immunosuppressed hosts or when the natural gastrointestinal barrier is impaired (Darfeuille-Michaud and Colombel, 2008). The growth of research has enhanced the study of gut flora and ulcerative colitis.

Our one bibliometric analysis of the field of intestinal flora and ulcerative colitis, like other bibliometric studies, has some limitations. Our data were derived from the Web of Science Core Collection database, and automatic updates of the database can affect differences in data volume. In general, the trends in the field will not change much.

## Conclusion

For this study, we used CiteSpace.5.8.R3 and VOSviewer1.6.17 to evaluate the previous 10 years' worth of papers on intestinal flora and ulcerative colitis. 93 nations, 3,069 organizations, 13,913 authors, and 759 journals were represented in all articles. In the United States, there may be a maximum of 767 publications. With the most articles, Harvard Medical School tops the list of institutions. With the most articles, Antonio Gasbarrini is the author. The last 10 years have seen a rise in publications in this area, and the future of research on intestinal flora and ulcerative colitis is promising.

## Data availability statement

The original contributions presented in the study are included in the article/Supplementary material, further inquiries can be directed to the corresponding authors.

## Author contributions

SX and LZ wrote the manuscript and it was then revised by CW and BH. Additionally, FJ and HZ conducted a literature review and data analysis. All authors contributed to the article and approved the submitted version.

## Funding

This work was supported by the National Natural Science Foundation of China (82174236), Jiangxi Provincial Natural Science Foundation Youth Fund (20202BAL216065), Jiangxi Provincial Education Department Science Program (GJJ201259), and Jiangxi Provincial Science and Technology Department (20212BAG70037).

## Acknowledgments

We appreciate the data's availability *via* the Web of Science Core Ensemble Data as well as the cooperation of all authors.

## Conflict of interest

The authors declare that the research was conducted in the absence of any commercial or financial relationships that could be construed as a potential conflict of interest.

## Publisher's note



## Supplementary material

The Supplementary material for this article can be found online at: https://www.frontiersin.org/articles/10.3389/fmicb.2022.1003905/full#supplementary-material

## References

Almeida, R., Gerbaba, T., and Petrof, E. O. (2016). Recurrent Clostridium difficile infection and the microbiome. *J. Gastroenterol.* 51, 1–10. doi: 10.1007/s00535-015-1099-3

Ananthakrishnan, A. N., Luo, C. W., Yajnik, V., Khalili, H., Garber, J. J., Stevens, B. W., et al. (2017). Gut microbiome function predicts response to anti-integrin biologic therapy in inflammatory bowel diseases. *Cell Host Microbe* 21, 603–610.e3. doi: 10.1016/j.chom.2017.04.010

Ananthakrishnan, A. N., Oxford, E. C., Nguyen, D. D., Sauk, J., Yajnik, V., and Xavier, R. J. (2013). Genetic risk factors for Clostridium difficile infection in ulcerative colitis. *Aliment. Pharmacol. Ther.* 38, 522–530. doi: 10.1111/apt.12425

Binder, H. J. (2010). Role of colonic short-chain fatty acid transport in diarrhea. *Annu. Rev. Physiol.* 72, 297–313. doi: 10.1146/annurev-physiol-021909-135817

Burisch, J., and Munkholm, P. (2015). The epidemiology of inflammatory bowel disease. *Scand. J. Gastroenterol.* 50, 942–951. doi: 10.3109/00365521.2015.1014407

Cammarota, G., Ianiro, G., Cianci, R., Sibbo, S., Gasbarrini, A., and Curro, D. (2015). The involvement of gut microbiota in inflammatory bowel disease pathogenesis: potential for therapy. *Pharmacol. Ther.* 149, 191–212. doi: 10.1016/j.pharmthera.2014.12.006

Clemente, J. C., Ursell, L. K., Parfrey, L. W., and Knight, R. (2012). The impact of the gut microbiota on human health: An integrative view. *Cell* 148, 1258–1270. doi: 10.1016/j.cell.2012.01.035

Damaskos, D., and Kolios, G. (2008). Probiotics and prebiotics in inflammatory bowel disease: microflora 'on the scope'. *Br. J. Clin. Pharmacol.* 65, 453–467. doi: 10.1111/j.1365-2125.2008.03096.x

Darfeuille-Michaud, A., and Colombel, J. F. (2008). Pathogenic Escherichia coli in inflammatory bowel diseases. *J. Crohns Colitis* 2, 255–262. doi: 10.1016/j.crohns.2008.02.003

den Besten, G., van Eunen, K., Groen, A. K., Venema, K., Reijngoud, D. J., and Bakker, B. M. (2013). The role of short-chain fatty acids in the interplay between diet, gut microbiota, and host energy metabolism. *J. Lipid Res.* 54, 2325–2340. doi: 10.1194/jlr.R036012

Ellegaard, O., and Wallin, J. A. (2015). The bibliometric analysis of scholarly production: how great is the impact? *Scientometrics* 105, 1809–1831. doi: 10.1007/s11192-015-1645-z

Fell, J. M., Muhammed, R., Spray, C., Crook, K., Russell, R. K., and Grp, B. I. W. (2016). Management of ulcerative colitis. *Arch. Dis. Child.* 101, 469–474. doi: 10.1136/archdischild-2014-307218

Habens, F., Srinivasan, N., Oakley, F., Mann, D. A., Ganesan, A., and Packham, G. (2005). Novel sulfasalazine analogues with enhanced NF-kB inhibitory and apoptosis promoting activity. *Apoptosis* 10, 481–491. doi: 10.1007/s10495-005-1877-0

He, X. X., Li, Y. H., Yan, P. G., Meng, X. C., Chen, C. Y., Li, K. M., et al. (2021). Relationship between clinical features and intestinal microbiota in Chinese patients with ulcerative colitis. *World J. Gastroenterol.* 27, 4722–4737. doi: 10.3748/wjg.v27.i28.4722

Ianiro, G., Tilg, H., and Gasbarrini, A. (2016). Antibiotics as deep modulators of gut microbiota: between good and evil. *Gut* 65, 1906–1915. doi: 10.1136/gutjnl-2016-312297

Kedia, S., Ghosh, T. S., Jain, S., Desigamani, A., Kumar, A., Gupta, V., et al. (2021). Gut microbiome diversity in acute severe colitis is distinct from mild to moderate ulcerative colitis. *J. Gastroenterol. Hepatol.* 36, 731–739. doi: 10.1111/jgh.15232

Khan, I., Ullah, N., Zha, L. J., Bai, Y. R., Khan, A., Zhao, T., et al. (2019). Alteration of gut microbiota in inflammatory bowel disease (IBD): cause or consequence? IBD treatment targeting the gut microbiome. *Pathogens* 8:126. doi: 10.3390/pathogens8030126

Kobayashi, T., Siegmund, B., Le Berre, C., Wei, S. C., Ferrante, M., Shen, B., et al. (2020). Ulcerative colitis. *Nat. Rev. Dis. Primers* 6:74. doi: 10.1038/s41572-020-0205-x

Laserna-Mendieta, E. J., Clooney, A. G., Carretero-Gomez, J. F., Moran, C., Sheehan, D., Nolan, J. A., et al. (2018). Determinants of reduced genetic capacity for butyrate synthesis by the gut microbiome in Crohn's disease and ulcerative colitis. *J. Crohns Colitis* 12, 204–216. doi: 10.1093/ecco-jcc/jjx137

Luo, H. F., Cai, Z. L., Huang, Y. Y., Song, J. T., Ma, Q., Yang, X. W., et al. (2021). Study on pain Catastrophizing From 2010 to 2020: A Bibliometric analysis via CiteSpace. *Front. Psychol.* 12:6048. doi: 10.3389/fpsyg.2021.759347

Ma, L., Ma, J. X., Teng, M. Z., and Li, Y. M. (2022). Visual analysis of colorectal cancer immunotherapy: A Bibliometric analysis From 2012 to 2021. *Front. Immunol.* 13:1386. doi: 10.3389/fimmu.2022.843106

Ma, C. Q., Su, H., and Li, H. J. (2021). Global research trends on prostate diseases and erectile dysfunction: a Bibliometric and visualized study. *Front. Oncol.* 10:356. doi: 10.3389/fonc.2020.627891

Ma, D., Yang, B., Guan, B. Y., Song, L. X., Liu, Q. Y., Fan, Y. X., et al. (2021). A Bibliometric analysis of pyroptosis from 2001 to 2021. *Front. Immunol.* 12:731933. doi: 10.3389/fimmu.2021.731933

Marchesi, J. R., Adams, D. H., Fava, F., Hermes, G. D. A., Hirschfield, G. M., Hold, G., et al. (2016). The gut microbiota and host health: a new clinical frontier. *Gut* 65, 330–339. doi: 10.1136/gutjnl-2015-309990

Michail, S., Durbin, M., Turner, D., Griffiths, A. M., Mack, D. R., Hyams, J., et al. (2012). Alterations in the gut microbiome of children with severe ulcerative colitis. *Inflamm. Bowel Dis.* 18, 1799–1808. doi: 10.1002/ibd.22860

Morgan, X. C., Tickle, T. L., Sokol, H., Gevers, D., Devaney, K. L., Ward, D. V., et al. (2012). Dysfunction of the intestinal microbiome in inflammatory bowel disease and treatment. *Genome Biol.* 13, R79. doi: 10.1186/gb-2012-13-9-r79

Rajilic-Stojanovic, M., Shanahan, F., Guarner, F., and de Vos, W. M. (2013). Phylogenetic analysis of Dysbiosis in ulcerative colitis During remission. *Inflamm. Bowel Dis.* 19, 481–488. doi: 10.1097/MIB.0b013e31827fec6d

Rhen, T., and Cidlowski, J. A. (2005). Antiinflammatory action of glucocorticoids--new mechanisms for old drugs. *N. Engl. J. Med.* 353, 1711–1723. doi: 10.1056/NEJMra050541

Schirmer, M., Denson, L., Vlamakis, H., Franzosa, E. A., Thomas, S., Gotman, N. M., et al. (2018). Compositional and temporal changes in the gut microbiome of pediatric ulcerative colitis patients are linked to disease course. *Cell Host Microbe* 24, 600–610.e4. doi: 10.1016/j.chom.2018.09.009

Segal, J. P., LeBlanc, J. F., and Hart, A. L. (2021). Ulcerative colitis: an update. *Clin. Med.* 21, 135–139. doi: 10.7861/clinmed.2021-0080

Sheng, Q. S., Li, F., Chen, G. P., Li, J. C., Li, J., Wang, Y. F., et al. (2021). Ursolic acid regulates intestinal microbiota and inflammatory cell infiltration to prevent ulcerative colitis. *J. Immunol. Res.* 2021, 1–16. doi: 10.1155/2021/6679316

Sokol, H., Seksik, P., Furet, J. P., Firmesse, O., Nion-Larmurier, L., Beaugerie, L., et al. (2009). Low counts of *Faecalibacterium prausnitzii* in colitis microbiota. *Inflamm. Bowel Dis.* 15, 1183–1189. doi: 10.1002/ibd.20903

Sonnenberg, E., and Siegmund, B. (2016). Ulcerative colitis. *Digestion* 94, 181–185. doi: 10.1159/000452621

van Dieren, J. M., Kuipers, E. J., Samsom, J. N., Nieuwenhuis, E. E., and van der Woude, C. J. (2006). Revisiting the immunomodulators tacrolimus, methotrexate, and mycophenolate mofetil: their mechanisms of action and role in the treatment of IBD. *Inflamm. Bowel Dis.* 12, 311–327. doi: 10.1097/01.Mib.0000209787.19952.53

Venegas, D. P., De la Fuente, M. K., Landskron, G., Gonzalez, M. J., Quera, R., Dijkstra, G., et al. (2019). Short chain fatty acids (SCFAs)-mediated gut epithelial and immune regulation and its relevance for inflammatory bowel diseases. *Front. Immunol.* 10:277. doi: 10.3389/fimmu.2019.00277

Walker, A. W., Sanderson, J. D., Churcher, C., Parkes, G. C., Hudspith, B. N., Rayment, N., et al. (2011). High-throughput clone library analysis of the mucosa-associated microbiota reveals dysbiosis and differences between inflamed and non-inflamed regions of the intestine in inflammatory bowel disease. *BMC Microbiol.* 11:7. doi: 10.1186/1471-2180-11-7

Wang, X. Y., Li, D., Huang, X. H., Luo, Q., Li, X., Zhang, X. Q., et al. (2021). A bibliometric analysis and visualization of photothermal therapy on cancer. *Transl. Cancer Res.* 10, 1204–1215. doi: 10.21037/tcr-20-2961

Yang, W. T., Zhang, J. T., and Ma, R. L. (2020). The prediction of infectious diseases: A Bibliometric analysis. *Int. J. Environ. Res. Public Health* 17:6218. doi: 10.3390/ijerph17176218

Yao, P., Cui, M., Wang, H. K., Gao, H. L., Wang, L., Yang, T., et al. (2016). Quantitative analysis of intestinal Flora of Uygur and Han ethnic Chinese patients with ulcerative colitis. *Gastroenterol. Res. Pract.* 2016, 1–8. doi: 10.1155/2016/9186232

frontiers | Frontiers in Microbiology

TYPE Original Research
PUBLISHED 20 September 2022
DOI 10.3389/fmicb.2022.970563



OPEN ACCESS

EDITED BY
Tang Zhaoxin,
South China Agricultural University, China

REVIEWED BY
Abdel-Moneim Eid Abdel-Moneim,
Egyptian Atomic Energy Authority, Egypt
Kwang-Youn Whang,
Korea University, South Korea

*CORRESPONDENCE
Yuncai Xiao
xyc88@mail.hzau.edu.cn

†These authors have contributed equally to this work and share first authorship

SPECIALTY SECTION
This article was submitted to Microorganisms in Vertebrate Digestive Systems, a section of the journal Frontiers in Microbiology

RECEIVED 16 June 2022
ACCEPTED 22 August 2022
PUBLISHED 20 September 2022

CITATION
Xu P, Hong Y, Chen P, Wang X, Li S, Wang J, Meng F, Zhou Z, Shi D, Li Z, Cao S and Xiao Y (2022) Regulation of the cecal microbiota community and the fatty liver deposition by the addition of brewers' spent grain to feed of Landes geese. *Front. Microbiol.* 13:970563. doi: 10.3389/fmicb.2022.970563



# Regulation of the cecal microbiota community and the fatty liver deposition by the addition of brewers' spent grain to feed of Landes geese

Ping Xu[1,2,3†], Yuxuan Hong[1,2,3†], Pinpin Chen[1,2,3], Xu Wang[1,2,3], Shijie Li[1,2,3], Jie Wang[1,2,3], Fancong Meng[1,2,3], Zutao Zhou[1,2,3], Deshi Shi[1,2,3], Zili Li[1,2,3], Shengbo Cao[1,2,3] and Yuncai Xiao[1,2,3*]

[1]College of Veterinary Medicine, Huazhong Agricultural University, Wuhan, China, [2]State Key Laboratory of Agricultural Microbiology, Huazhong Agricultural University, Wuhan, China, [3]Key Laboratory of Preventive Veterinary Medicine in Hubei Province, Huazhong Agricultural University, Wuhan, China

The effects of brewers' spent grain (BSG) diets on the fatty liver deposition and the cecal microbial community were investigated in a total of 320 healthy 5-day-old Landes geese. These geese were randomly and evenly divided into 4 groups each containing 8 replicates and 10 geese per replicate. These four groups of geese were fed from the rearing stage (days 5–60) to the overfeeding stage (days 61–90). The Landes geese in group C (control) were fed with basal diet (days 5–90); group B fed first with basal diet in the rearing stage and then basal diet + 4% BSG in the overfeeding stage; group F first with basal diet + 4% BSG during the rearing stage and then basal diet in the overfeeding stage; and group W with basal diet + 4% BSG (days 5–90). The results showed that during the rearing stage, the body weight (BW) and the average daily gain (ADG) of Landes geese were significantly increased in groups F and W, while during the overfeeding stage, the liver weights of groups W and B were significantly higher than that of group C. The taxonomic structure of the intestinal microbiota revealed that during the overfeeding period, the relative abundance of *Bacteroides* in group W was increased compared to group C, while the relative abundances of *Escherichia–Shigella* and *prevotellaceae_Ga6A1_group* were decreased. Results of the transcriptomics analysis showed that addition of BSG to Landes geese diets altered the expression of genes involved in PI3K-Akt signaling pathway and sphingolipid metabolism in the liver. Our study provided novel experimental evidence based on the cecal microbiota to support the application of BSG in the regulation of fatty liver deposition by modulating the gut microbiota in Landes geese.

KEYWORDS

**brewers' spent grain, Landes goose, fatty liver, cecal microbiota community, differentially expressed gene, transcriptomics**

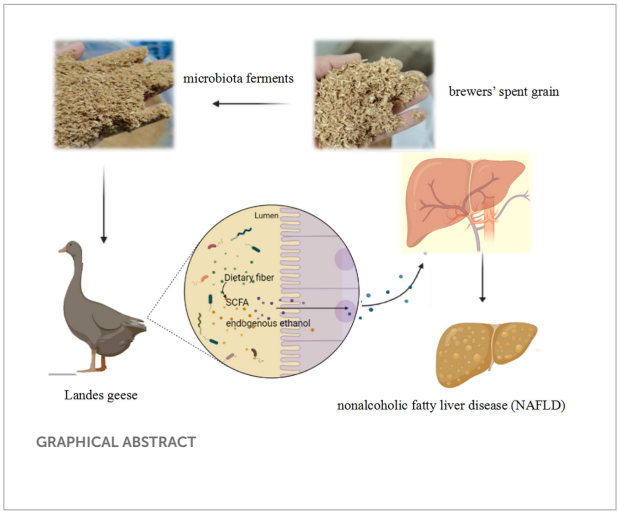


GRAPHICAL ABSTRACT

## Introduction

It is well-known that in the natural environment, some wild waterfowl (e.g., geese and ducks) would eat a large amount of food in a short period of time to deposit excess fat in the liver to form fatty liver prior to migration in order to meet the energy reserve needs of long-distance travel (Hermier et al., 1991). Studies showed that different from the human fatty liver, geese have shown a strong ability to store fat in their livers with the functional integrity of the liver cells preserved without the formation of fibrosis or hepatic necrosis (Lu et al., 2015). Therefore, geese are used extensively worldwide in the production of luxurious food based on their fatty liver products, e.g., foie gras. The foie gras is generally delicious and delicate in texture, favored by a large number of consumers worldwide, with an extremely large and increasing demand in the international market (Mozduri et al., 2021). In particular, as a world-renowned breed dedicated to fatty livers, the Landes geese are very popular and highly adaptable to their environment (Hermier et al., 1999; Mourot et al., 2000).

The brewers' spent grain (BSG) is the main by-product generated during the beer production (Mussatto, 2014), mainly composed of malt husk, insoluble protein, hemicellulose, fat, and a small amount of undecomposed starch (Cooray et al., 2017; Rachwał et al., 2020). Specifically, both compounds β-glucans and arabinoxylan detected in BSG are consumed by animals to help enhance the activities of beneficial microbiota (Lao et al., 2020). Studied showed that sun-dried BSG added to the diets for pigs at a dose of 17–25% improved the production margins (Amoah et al., 2017), while it was demonstrated that replacing 5% soybean meal with fermented BSG in the diet of Wanxi white geese increased both the feed intake and body weight of meat geese (Yang et al., 2020). Furthermore, studies showed that BSG contained microorganisms capable of producing endogenous ethanol (Bonifácio-Lopes et al., 2020), which promoted the accumulation of fat in the liver (Baraona and Lieber, 1979). These results strongly suggested the significant potential of BSG to promote liver fat deposition. However, the molecular mechanism underlying the liver fat deposition promoted by BSG is still unclear.

As the largest metabolic organ in body, the liver plays important roles in regulating the glucose and lipid metabolisms, while the intestine is the main place where the nutrient digestive absorption takes place and the gut microbiota colonizes, playing an important role in the growth and metabolism of the hosts (Safari and Gerard, 2019). The "gut-liver axis" refers to the bidirectional relationships among intestinal microbiome, intestine, and liver, attracting significant attention due to its involvement with intestinal microbiota in the occurrence and development of non-alcoholic fatty liver disease (NAFLD) (Bajaj and Hylemon, 2018). Studies have shown that overfeeding could cause significant variations in gut physiology and gut microbiota, thereby regulating the formation of fatty livers in geese (Knudsen et al., 2021). To date, the studies on the gut microbiome of Landes geese are sparse, while the investigations exploring the effects of BSG diets on the improvement of the liver production in Landes geese through the "gut-liver axis" are still lacking. Therefore, in this study, we performed the analyses of the intestinal physiology, intestinal microbiota, and liver transcriptomics of Landes geese to investigate the beneficial effects of BSG on the varied regulatory patterns of lipid deposition in Landes geese. The overall physiological and developmental benefits in the Landes geese generated by the addition of BSG in the feed were characterized based on the taxonomic composition of the intestinal microbiota before and after the overfeeding stage as well as changes in their body weight, liver weight, blood biochemical indices, and nutrient composition in the liver. The protective mechanism of the nutritional fatty liver in the Landes geese was further explored with the potential solutions to the problems related to fatty liver in animals. Our study provided novel experimental evidence to support the further investigations and applications of BSG in the promotion of fatty liver development in Landes geese.

It is noted that the overfeeding method is currently a controversial issue in the field. Interestingly, with the continuous improvement of modern overfeeding technology and equipment, the overfeeding method of geese is becoming

Abbreviations: BSG, brewers' spent grain; ALT, alanine aminotransferase; AST, aspartate aminotransferase; AKP, alkaline phosphatase; ACP, acid phosphatase; GLU, glucose; TG, triglycerides; CHO, cholesterol; HDL-C, high density liptein cholesterol; LDL-C, low density liptein cholesterol; VLDL, very low-density lipoprotein; VH, villus height; CD, crypt depth; VCR, villus height/crypt depth; BW, body weight; LW, liver weight; ADG, average daily gain; TPM, transcripts per million; DEG, differentially expressed gene; GO, Gene Ontology; KEGG, Kyoto Encyclopedia of Genes and Genomes; SCFA, short-chain fatty acids; NAFLD, non-alcoholic fatty liver disease; FGFs, fibroblast growth factors; HSP, heat shock proteins; ELOVL7, fatty acid elongase 7.

more and more mature and acceptable. In particular, during the entire feeding process, we followed closely the provisions of the Chinese Code of Practice for Testing the Performance of Geese with Fatty Liver (NT/T 3184-2018). Furthermore, the Landes geese are physiologically characterized by fatty deposits in the liver. It is expected that with the discovery of the relationships between liver fat deposition and intestinal microbiota through overfeeding, in the near future, it would be possible to directly achieve the liver fat deposition in geese by regular feeding of certain types of feed additions (e.g., BSG) without overfeeding the geese. This achievement would be of significant importance for fatty liver production.

# Materials and methods

## Laboratory animals

This study was performed by following strictly the Guide for the Care and Use of Laboratory Animals Monitoring Committee of Hubei Province, China. The experimental protocols were approved by the Committee on the Ethics of Animal Experiments of the College of Veterinary Medicine, Huazhong Agricultural University (NO. HZAUGE–2020–0001).

A total of 320 healthy 5-day-old Landes geese were randomly and evenly divided into 4 groups with each group containing 8 replicates and 10 geese per replicate. The geese were kept and fed in the brooding room for a total of 4 days prior to the start of the experiments. The Landes geese in group C (control) were fed with basal diet throughout the entire experiment in both the rearing stage (days 5–60) and the overfeeding stage (days 61–90); group B first with basal diet in the rearing stage and then with basal diet + 4% BSG in the overfeeding stage; group F first with basal diet + 4% BSG in the rearing stage and then basal diet in the overfeeding stage; and group W with basal diet + 4% BSG for the entire experiment (days 5–90). No animals were treated with antibiotics during the entire experiments. The Landes geese at different developmental stages were fed with different basal feeds with varied formula of nutritional compositions (**Supplementary Tables 1–3**).

The animal experiments were carried out at the Huaren Modern Farm (Anhui, China) according to the code of practice for performance testing of fatty liver goose in China (NT/T 3184–2018). The entire experimental procedures for four groups of Landes geese (i.e., C, B, F, and W) were divided into two stages. First, in the rearing stage (days 5–60), the temperature in the goose houses where the Landes geese were kept and fed was maintained at ∼33°C until the geese were 7 days old; then, the temperature was gradually decreased to and maintained at 23°C. It was noted that in days 45–60, reasonable feed consumption control was applied in order to prevent rapid excess body weight in the geese. The goose houses were disinfected with both potassium permanganate and formalin before the experiments started. Second, in the overfeeding stage (days 61–90), the temperature in the goose houses was maintained at ∼15°C. After the pre-feeding (days 61–67) in the overfeeding stage, the force feeding frequency and ration were gradually increased, i.e., force feeding for 2–3 times/day (days 68 and 69) with 140 g/time, 3–4 times/day (days 70–74) with 220 g/time, and 5–6 times/day (days 75–90) with 350 g/time. The feeds were softened with water during the overfeeding stage. On days 5, 15, 30, 45, 60, and 90, the geese and feeds were weighed to calculate the average daily gain (ADG) in body weight (BW) in each of the four groups of geese (n = 80) based on the following equation: ADG = (final body weight − initial body weight)/days of experiment.

## Brewers' spent grain

As the residue of barley malt extracted during the wort production process, the BSG was supplied by the Hubei Huada Real Technology Co., Ltd., Wuhan, China. The nutritional compositions of the BSG were shown in **Table 1**.

## Sample collection

A total of eight geese were sampled from each of the four groups of Landes geese on days 60 and 90 after 12 h of fasting with the pen number and weight of each individual goose recorded before euthanization. Blood samples (∼5 mL for each goose) were collected from the wing veins using the vacuum blood collection tubes and centrifuged for 10 min at 3000 rpm and 4°C to obtain the serum sample. The geese were euthanized with the liver tissues (on day 90) collected immediately, snap-frozen in liquid nitrogen, and stored at −80°C for further transcriptomics analysis. The duodenal, jejunal, and ileal tissues were collected and

TABLE 1 The nutritional compositions of brewers' spent grain (BSG).

| Ingredient | Percentage in the total weight |
|---|---|
| Water content | 36.97% |
| pH | 4.23 |
| Total acid | 2.08% |
| Crude protein | 13.26% |
| Crude fiber | 15.70% |
| Crude fat | 6.30% |
| Crude ash | 3.70% |
| Acid-soluble protein (as a percentage of the crude protein) | 25.73% |

immediately fixed in 4% paraformaldehyde (Biosharp Co., Ltd., Hefei, China) for subsequent morphological analysis.

## Serum analysis

The contents of a group of nine biochemical indices, including alanine aminotransferase (ALT), aspartate aminotransferase (AST), alkaline phosphatase (AKP), acid phosphatase (ACP), glucose (GLU), triglyceride (TG), cholesterol (CHO), high density liptein cholesterol (HDL-C), and low density liptein cholesterol (LDL-C), were measured by an automatic biochemical analyzer (BK-280, Shandong Blobase Biotechnology Co., Ltd., Shandong, China), while the contents of another biochemical index, i.e., the very low-density lipoprotein (VLDL-C), were measured using ELISA kits (Wuhan Meimian Biotechnology Co., Ltd., Wuhan, China). All experiments were performed with eight biological replicates in strict accordance with the protocols and instructions recommended by the manufacturers.

## Compositions of free amino acids in livers of Landes geese

The contents of amino acids in livers of Landes geese on day 90 were determined using an amino acid analyzer (L-8900, Hitachi, Japan). A total of ∼100 mg liver samples were dissolved in water with methanol (1:1) for 30 min at 4°C and then centrifuged for 10 min at 10,000 × g and 4°C. The supernatant was filtered through the glass wool and stored at −80°C for further analysis (Dong et al., 2020).

## Compositions of fatty acids in livers of Landes geese

The fatty acid compositions in livers of Landes geese on day 90 were measured using the gas chromatography (GC) based on the methods described previously (Li et al., 2015) using the gas chromatographer (Trace1310 ISQ, ThermoFisher, Waltham, CA, United States). The concentrations of individual fatty acids were quantified based on the peak area and presented as a percentage of the contents of the total fatty acids.

## Gut microorganism analysis

### Sample collection and DNA extraction and sequencing

The total genomic DNA of the microbial community was extracted from the cecal contents using the E.Z.N.A.® Soil DNA Kit (Omega Bio-tek, Norcross, GA, United States) by following the procedures recommended by the manufacturers. DNA quality was evaluated on 1% agarose gel with the DNA concentration and purity determined by the NanoDrop 2000 UV-vis spectrophotometer (Thermo Scientific, Wilmington, DE, United States). Then, the forward primer 338F (5′-ACTCCTACGGGAGGCAGCAG-3′) and the reverse primer 806R (5′-GGACTACHVGGGTWTCTAAT-3′) were used to amplify the hypervariable region (i.e., V3-V4) of the bacterial 16S rRNA gene on the PCR thermocycler (ABI GeneAmpR® 9700, Foster City, CA, United States) with the following procedures: denaturation for 3 min at 95°C, followed by a total of 27 cycles of denaturation for 30 s at 95°C, annealing for 30 s at 55°C, and extension for 45 s at 72°C, ended by the final extension for 10 min at 72°C, and kept at 4°C. The chemical mixture of PCR contained 4 μL 5 × TransStart FastPfu buffer, 2 μL 2.5 mM dNTPs, 0.8 μL forward primer (5 μM) and reverse primer (5 μM), 0.4 μL TransStart FastPfu DNA Polymerase, and 10 ng template DNA, with the final volume adjusted to 20 μL using $ddH_2O$. Each PCR analysis was repeated with three biological replicates. The PCR products were collected using 2% agarose gel and then purified using the AxyPrep DNA Gel Extraction Kit (Axygen Biosciences, Union City, CA, United States) by following the manufacturer's instructions. The concentrations of the purified PCR products were determined using the Quantus™ Fluorometer (Promega, United States). The paired-end sequencing (2 × 300 bp) of the purified amplicons pooled in equimolar was performed on an Illumina MiSeq platform (Illumina, San Diego, CA, United States) based on the standard procedures recommended by the Majorbio Bio-Pharm Technology Co., Ltd. (Shanghai, China).

### Sequencing data analysis

The paired-end reads of the transcriptomics analysis were processed using FLASH version 1.2.11 to generate the splicing sequences, i.e., the raw tags (Derakhshani et al., 2016). Further processing of raw reads was performed based on the quality control protocols of QIIME version 1.9.1 (Caporaso et al., 2010). The effective tags were clustered into the operational taxonomic units (OTUs) based on 97% identity with the representative sequences of the OTUs determined and annotated using the Uparse version 7.0.1090[1]. The taxonomy of each OTU representative sequence was determined by the RDP Classifier[2] based on the 16S rRNA database (Zhbannikov and Foster, 2015). The alpha diversity indices (i.e., Chao1, Shannon, and Simpson) were calculated based on the rarefaction analysis using Mothur v.1.30.2, while the relative abundance analyses at the phylum and genus levels were performed using the R software (version 3.3.1).

1 http://www.drive5.com/uparse/
2 http://rdp.cme.msu.edu/

## Transcriptomics analysis of liver in Landes geese

### RNA extraction and sequencing

The total RNA of each liver sample was extracted using the Ultrapure RNA Kit (CW0581M, CoWin Biosciences, Beijing, China) according to the manufacturer's instructions. The RNA samples meeting the quality requirements, i.e., bright and clear bands of the target RNA based on electrophoresis gel, no diffusion area in the swimming lane, no protein and DNA contaminations, with the RNA integrity number (RIN) close to 10, the 28S/18S ratio greater than or equal to 1.5, $1.8 < OD_{260/280} < 2.2$, and $OD_{260/230} \geq 2.0$, were used to construct the RNA-Seq transcriptomic library (Majorbio Co., Shanghai, China).

### Sequencing data analysis

The differentially expressed genes (DEGs) between the four different groups of liver samples of Landes geese on day 90 were identified based on fold change $> 2$ or $< -2$ and $Q$ value $\leq 0.05$ using DESeq2 (1.24.0)[3]. The expression level of each transcript was determined by the transcripts per million reads (TPM) method, while the gene abundances were evaluated based on RSEM[4]. Annotation and enrichment analyses of the DEGs based on the Gene Ontology (GO[5]) and the Kyoto Encyclopedia of Genes and Genomes (KEGG[6]) databases were performed by Goatools[7] and KOBAS[8], respectively, with the Bonferroni-corrected $P$-value $\leq 0.05$ compared with the entire transcriptome background.

In order to verify the molecular patterns revealed by the transcriptomic analysis, a total of six genes were randomly selected to perform the quantitative real-time PCR (qRT-PCR) analysis. The RNA sample (1 μg) was reverse-transcribed into cDNA using the PrimeScript$^{TM}$ RT Reagent Kit with gDNA Eraser (Vazyme, Nanjing, China) by following the manufacturer's protocols. Then, the cDNA was diluted 10-fold and mixing with ChamQ Universal SYBR qPCR Master Mix (Q711-02/03, Vazyme Biotech Co., Ltd., Nanjing, China) and specific primers, used for qRT-PCR analyses using the signal detection protocols provide by the manufacturers (Bio-Rad CFX96TM System, TaKaRa, Dalian, China). Each qRT-PCR experiment was repeated with three technical replicates using the house-keeping gene β-*Actin* as the endogenous control for the normalization of the expression of each gene. Primers used for qRT-PCR were shown in **Supplementary Table 4**. Data were analyzed using GraphPad Prism v 8.3.0 (GraphPad, Inc., La Jolla, CA, United States).

3 http://bioconductor.org/packages/stats/bioc/DESeq2/
4 http://deweylab.biostat.wisc.edu/rsem/
5 http://geneontology.org/
6 https://www.genome.jp/kegg/
7 https://github.com/tanghaibao/goatools
8 http://kobas.cbi.pku.edu.cn

## Statistical analysis

The significant differences between groups were analyzed by one-way analysis of variance (ANOVA) and Fisher's least significant difference (LSD) tests using the SPSS statistical software version 26.0 (SPSS, Inc., Chicago, IL, United States). Graphs were generated using GraphPad Prism 8.3. (GraphPad, Inc., La Jolla, CA, United States). The data were shown as the mean ± standard error of the mean (SEM) with the significance levels set at $P < 0.05$ (*) and $P < 0.01$ (**), respectively.

# Results

## Effect of brewers' spent grain on the growth performance of Landes geese

The results of growth performance in the Landes geese showed that the initial BWs were not significantly different ($P > 0.05$) among the 4 groups of Landes geese (**Table 2**). In the rearing stage (days 5–60), the geese in both groups F and W fed with diets supplemented with BSG showed higher BW and ADG than those of group C, with BW extremely significantly different at 15, 30, and 45 days ($P < 0.01$) and ADG extremely significantly different during 5–15 and 16–30 days ($P < 0.01$). During the overfeeding stage (days 61–90), the BSG was added to the diet of group B, but the BW and ADG were not changed significantly compared with group C. In 90 days, the average liver weight/body weight ratio of the geese in group W was increased by 21.36% compared with group C, while the liver weight/body weight ratio of group B also showed an increasing trend compared with groups C and F ($P > 0.05$) (**Table 2**). Overall, these results showed that addition of BSG during the rearing stage effectively increased the BW and ADG of Landes geese, while no significant difference was observed in BW with the addition of BSG during the overfeeding stage. Therefore, the addition of BSG during the overfeeding stage was beneficial to the liver fat deposition of the Landes geese.

## Effect of brewers' spent grain on the serum biochemical indices of Landes geese

The results of the effects of BSG on the serum biochemical indices of Landes geese were shown in **Table 3**. In 60 days, compared with group C, the contents of GLU were extremely significantly reduced in both groups F and W ($P < 0.01$), while the contents of HDL-C were significantly decreased ($P < 0.05$)

TABLE 2 Effects of brewers' spent grain (BSG) on the growth performance in four groups of Landes geese (i.e., groups C, B, F, and W).

| Growth | | Group C | Group B | Group F | Group W | *P*-value |
|---|---|---|---|---|---|---|
| BW (g) | 5 days | 218.7 ± 1.3 | 218.1 ± 1.3 | 218.1 ± 1.9 | 217.5 ± 1.3 | 0.952 |
| | 15 days | 703.0 ± 3.7$^{b}$ | 711.0 ± 3.9$^{b}$ | 726.2 ± 2.7$^{a}$ | 733.5 ± 3.4$^{a}$ | < 0.001 |
| | 30 days | 1913.7 ± 43.6$^{b}$ | 1916.1 ± 36.9$^{b}$ | 2080.0 ± 39.3$^{a}$ | 2087.5 ± 47.1$^{a}$ | 0.005 |
| | 45 days | 3385.6 ± 35.6$^{b}$ | 3383.1 ± 48.2$^{b}$ | 3698.1 ± 45.4$^{a}$ | 3603.8 ± 59.2$^{a}$ | 0.001 |
| | 60 days | 4531.3 ± 51.5 | 4522.5 ± 69.9 | 4678.9 ± 48.2 | 4671.9 ± 81.8 | 0.174 |
| | 90 days | 8066.7 ± 98.9 | 8300.0 ± 134.2 | 8480.0 ± 135.6 | 8400.0 ± 219.1 | 0.299 |
| LW (g) | 90 days | 946.7 ± 46.5$^{b}$ | 1089.2 ± 67.3$^{ab}$ | 943.3 ± 61.9$^{b}$ | 1192.5 ± 36.3$^{a}$ | 0.010 |
| LBR | 90 days | 11.7 ± 0.5 | 13.1 ± 0.8 | 11.6 ± 0.8 | 14.2 ± 0.7 | 0.053 |
| ADG (g/d) | 5–15 days | 48.5 ± 0.2$^{b}$ | 48.9 ± 0.3$^{b}$ | 51.4 ± 0.3$^{a}$ | 50.8 ± 0.2$^{a}$ | < 0.001 |
| | 16–30 days | 80.6 ± 2.8$^{b}$ | 80.5 ± 2.5$^{b}$ | 90.4 ± 3.2$^{a}$ | 90.2 ± 2.6$^{a}$ | 0.015 |
| | 31–45 days | 98.1 ± 1.0 | 97.8 ± 4.6 | 101.0 ± 4.7 | 101.3 ± 2.7 | 0.852 |
| | 46–60 days | 76.4 ± 1.1 | 75.9 ± 4.5 | 71.3 ± 6.1 | 71.9 ± 4.2 | 0.776 |
| | 61–90 days | 117.3 ± 1.9 | 125.7 ± 3.5 | 124.7 ± 6.3 | 124.3 ± 2.5 | 0.492 |

Data are expressed as mean ± standard error of the mean (SEM) ($n$ = 80 geese per group). $^{a,b}$Means within the same row with different superscripts differ. BW, body weight; LW, liver weight; LBR, liver weight/body weight ratio; ADG, average daily gain. Group C, control group; Group B, added with 4% BSG in the overfeeding stage (days 61–90); Group F, added with 4% BSG in the rearing stage (days 5–60); Group W, added with 4% BSG in the all stage (days 5–90).

TABLE 3 Effects of brewers' spent grain (BSG) on the serum biochemical indices in the four groups of Landes geese (i.e., groups C, B, F, and W) in 60 and 90 days.

| Biochemical index | Group C | Group B | Group F | Group W | *P*-value |
|---|---|---|---|---|---|
| **Day 60** | | | | | |
| ALT (U/L) | 23.1 ± 0.8 | 22.3 ± 0.7 | 23.2 ± 0.4 | 22.3 ± 1.4 | 0.834 |
| AST (U/L) | 62.4 ± 1.4 | 62.8 ± 1.9 | 58.9 ± 1.5 | 58.7 ± 1.3 | 0.139 |
| AKP (U/100 mL) | 61.8 ± 0.8 | 62.5 ± 0.8 | 61.5 ± 0.6 | 61.9 ± 0.5 | 0.749 |
| ACP (U/100 mL) | 20.9 ± 0.7 | 20.3 ± 0.9 | 19.7 ± 0.3 | 19.2 ± 0.9 | 0.434 |
| GLU (mmol/L) | 11.6 ± 0.3$^{a}$ | 11.4 ± 0.3$^{a}$ | 10.3 ± 0.3$^{b}$ | 10.4 ± 0.3$^{b}$ | 0.005 |
| TG (mmol/L) | 1.1 ± 0.1 | 1.1 ± 0.1 | 1.1 ± 0.1 | 1.0 ± 0.1 | 0.638 |
| CHO (mmol/L) | 4.6 ± 0.3 | 4.6 ± 0.2 | 4.4 ± 0.2 | 4.3 ± 0.1 | 0.158 |
| HDL-C (mmol/L) | 2.6 ± 0.2$^{a}$ | 2.6 ± 0.2$^{a}$ | 2.4 ± 0.1$^{b}$ | 2.5 ± 0.1$^{b}$ | 0.031 |
| LDL-C (mmol/L) | 1.2 ± 0.1$^{b}$ | 1.1 ± 0.1$^{b}$ | 1.3 ± 0.1$^{a}$ | 1.3 ± 0.1$^{a}$ | 0.008 |
| VLDL-C (nmol/L) | 291.7 ± 8.8 | 293.7 ± 26.6 | 320.6 ± 24.6 | 343.6 ± 22.7 | 0.323 |
| **Day 90** | | | | | |
| ALT (U/L) | 85.3 ± 1.5$^{a}$ | 68.1 ± 4.4$^{b}$ | 55.9 ± 3.7$^{b}$ | 76.7 ± 3.9$^{a}$ | < 0.001 |
| AST (U/L) | 189.4 ± 12.0$^{a}$ | 178.2 ± 13.1$^{a}$ | 184.1 ± 15.1$^{a}$ | 138.3 ± 5.5$^{b}$ | 0.041 |
| AKP (U/100 mL) | 191.4 ± 11.2$^{a}$ | 177.9 ± 17.3$^{a}$ | 195.1 ± 7.3$^{a}$ | 138.8 ± 7.3$^{b}$ | 0.018 |
| ACP (U/100 mL) | 25.1 ± 1.6$^{b}$ | 21.1 ± 1.7$^{b}$ | 24.2 ± 2.1$^{b}$ | 36.5 ± 1.2$^{a}$ | < 0.001 |
| GLU (mmol/L) | 16.4 ± 1.2$^{ab}$ | 14.7 ± 0.5$^{b}$ | 18.7 ± 1.5$^{a}$ | 13.6 ± 0.6$^{b}$ | 0.017 |
| TG (mmol/L) | 8.7 ± 0.8 | 6.7 ± 0.7 | 8.2 ± 0.5 | 6.8 ± 0.7 | 0.147 |
| CHO (mmol/L) | 7.2 ± 0.6 | 7.0 ± 0.3 | 6.4 ± 0.2 | 6.9 ± 0.4 | 0.478 |
| HDL-C (mmol/L) | 4.8 ± 0.2$^{b}$ | 4.9 ± 0.3$^{ab}$ | 4.5 ± 0.2$^{b}$ | 5.6 ± 0.3$^{a}$ | 0.032 |
| LDL-C (mmol/L) | 2.0 ± 0.3 | 2.5 ± 0.2 | 2.6 ± 0.3 | 2.5 ± 0.2 | 0.416 |
| VLDL-C (nmol/L) | 435.3 ± 24.4$^{c}$ | 511.9 ± 5.67$^{b}$ | 423.3 ± 7.1$^{c}$ | 587.5 ± 10.3$^{a}$ | < 0.001 |

Data are expressed as mean ± SEM. $^{a-c}$Means within the same row with different superscripts differ. Group C, control group; Group B, added with 4% BSG in the overfeeding stage (days 61–90); Group F, added with 4% BSG in the rearing stage (days 5–60); Group W, added with 4% BSG in the all stage (days 5–90).

and the contents of LDL-C ($P < 0.01$) and VLDL-C ($P > 0.05$) showed an increasing. In 90 days, compared with group C, the contents of both ALT and AST in the three experimental groups (i.e., groups B, F, and W) were reduced, while the contents of TP in all three experimental groups were increased. No significant difference was observed in the contents of TG and CHO among the four groups of Landes geese ($P > 0.05$). Compared with group C, the contents of three types of lipoproteins (i.e.,

HDL-C, LDL-C, and VLDL-C) in group W were increased by 16.60% ($P < 0.05$), 25.00% ($P > 0.05$), and 34.96% ($P < 0.01$), respectively.

## Effect of brewers' spent grain on the intestinal morphology of Landes geese

The results of the effects of BSG on the morphology of the small intestines of Landes goose were shown in **Table 4**. In 60 days, no significant difference was observed in VHs and CDs of the duodenum among the four groups of geese ($P > 0.05$). In the jejunum, both VHs and VCRs in groups F and W were significantly increased compared with those of group C ($P < 0.01$). For the ileum, the VCRs of geese fed with BSG were significantly increased in both groups F and W ($P < 0.01$), the VHs in groups F and W were significantly increased compared with group C ($P < 0.01$), while the CDs in groups F and W were significantly lower than that in group C ($P < 0.05$). In 90 days, both VH and VCR of the duodenum in group W were significantly increased compared with group C ($P < 0.05$), while the CD in group W was lower than that in group C ($P > 0.05$). In the jejunum, the VH in group W was significantly higher than those of the other three groups ($P < 0.05$), while no significant difference was observed in the CDs of the four groups of geese ($P > 0.05$). For the ileum, the CD of group F was significantly lower than that in group W ($P < 0.05$), while the VCR was extremely significantly increased ($P < 0.01$).

## Effect of brewers' spent grain on the compositions of amino acids in livers of Landes geese

The results of the effects of BSG on the compositions of amino acids in the livers of Landes geese in 90 days were shown in **Table 5**, revealing no significant difference in the contents of amino acids in the livers of the four groups of Landes geese ($P > 0.05$). It was noted that the contents of six types of amino acids, including glutamic acid, valine, histidine, and the three types of aromatic amino acids (i.e., phenylalanine, tryptophan, and tyrosine) in group W, tended to increase compared with group C.

## Effect of brewers' spent grain on the compositions of fatty acids in livers of Landes geese

The results of the effects of BSG on the compositions of fatty acids in the livers of Landes geese in 90 days were shown in **Table 6**. The results revealed the significant decrease in the contents of dodecanoic acid C12:0 ($P < 0.05$) and docosahexaenoic acid C22:2 ($P < 0.01$) in the livers of geese fed with BSG. The content of eleic acid C18:1 was significantly higher in group W than that of group C ($P < 0.05$), while the content of eicosadienoic acid C20:2 was significantly lower in both groups F and W than that of group C ($P < 0.05$). It was noted that compared with group C, the contents of the saturated fatty acid ΣSFA and unsaturated fatty acid ΣSFU in group W tended to decrease and increase, respectively.

## Effect of brewers' spent grain on the bacterial diversity of the intestinal microbiota in Landes geese

To explore the effects of BSG on the intestinal microbiota of Landes geese, the 16S rRNA gene was sequenced based on the genomic DNA extracted from the cecal contents of the Landes geese. After screening and splicing of the raw reads, a total of 3,055,821 valid reads were obtained with an average of 50,095 ± 1,155 reads per sample and an average length of 419 ± 0.28 bp (**Supplementary Table 5**). The clean reads were clustered based on 97% similarity to obtain the representative sequences of OTUs. The rarefaction curve of each sample generally tended to be flat, suggesting that the level of RNA-Seq analysis was sufficient to cover all taxa in the sample (**Supplementary Figure 1**). Three alpha diversity indices were determined based on the OTUs, i.e., the Chao1 index was evaluated to assess the community richness (**Figure 1A**), while both the Shannon (**Figure 1B**) and the Simpson (**Figure 1C**) indices were measured to evaluate the community diversity. The results showed that in 60 days, no significant difference was observed in the Chao1, Shannon, and Simpson indices in four groups of Landes geese ($P > 0.05$). In 90 days, it was noted that the alpha diversity indices showed an extremely significant difference compared with those of 60 days, showing that the community richness and diversity in cecum of Landes geese were decreased extremely significantly during the overfeeding stage.

In order to further explore the effects of BSG on the cecal microbiota of Landes geese, the cluster classification of OTUs was investigated at the phylum level (**Figures 2A,B**). The results revealed *Bacteroides* and *Firmicutes* as the top two bacterial phyla with the highest relative abundances in the cecal microbes of Landes geese during both the rearing and the overfeeding stages. Among the top seven abundant phyla (**Figure 2B**), the relative abundances of *Proteobacteria* in all four groups of Landes geese were significantly increased in 90 days compared with those in 60 days ($P < 0.01$), whereas the relative abundances of *Spirochaetota* in all four groups of Landes geese were significantly decreased in 90 days compared with those in 60 days ($P < 0.01$). In 90 days, the relative abundance of *Bacteroidetes* in group W was significantly higher than those in groups C, B, and F ($P < 0.05$; **Figure 2B**). In 60 days, the

TABLE 4 Effects of brewers' spent grain (BSG) on the intestinal morphology of the four groups of Landes geese (i.e., groups C, B, F, and W) in 60 and 90 days.

| Item | | Group C | Group B | Group F | Group W | *P*-value |
|---|---|---|---|---|---|---|
| **Day 60** | | | | | | |
| Duodenum (μm) | VH | 1083.3 ± 52.1 | 1091.1 ± 32.9 | 1145.9 ± 66.8 | 1140.5 ± 69.9 | 0.810 |
| | CD | 338.3 ± 7.8 | 332.3 ± 5.4 | 304.5 ± 8.0 | 306.5 ± 13.2 | 0.087 |
| | VCR | 3.4 ± 0.1$^{b}$ | 3.3 ± 0.1$^{b}$ | 3.9 ± 0.1$^{a}$ | 3.7 ± 0.1$^{a}$ | 0.010 |
| Jejunum (μm) | VH | 1258.8 ± 38.7$^{b}$ | 1242.1 ± 50.5$^{b}$ | 1498.8 ± 39.2$^{a}$ | 1481.1 ± 53.5$^{a}$ | 0.003 |
| | CD | 297.6 ± 9.7 | 299.3 ± 14.0 | 267.5 ± 6.8 | 262.4 ± 14.1 | 0.071 |
| | VCR | 4.3 ± 0.1$^{b}$ | 4.2 ± 0.1$^{b}$ | 5.6 ± 0.1$^{a}$ | 5.5 ± 0.2$^{a}$ | < 0.001 |
| Ileum (μm) | VH | 1110.9 ± 49.0 | 1115.9 ± 29.3 | 1170.7 ± 36.7 | 1178.6 ± 48.9 | 0.476 |
| | CD | 267.91 ± 17.7$^{b}$ | 264.8 ± 12.4$^{b}$ | 218.4 ± 4.5$^{b}$ | 221.3 ± 13.9$^{b}$ | 0.018 |
| | VCR | 4.28 ± 0.2$^{b}$ | 4.2 ± 0.1$^{b}$ | 5.4 ± 0.1$^{a}$ | 5.2 ± 0.1$^{a}$ | < 0.001 |
| **Day 90** | | | | | | |
| Duodenum (μm) | VH | 1240.6 ± 137.1$^{b}$ | 1793.6 ± 24.3$^{a}$ | 1460.9 ± 66.3$^{b}$ | 1726.8 ± 212.0$^{a}$ | 0.014 |
| | CD | 223.6 ± 12.1 | 260.6 ± 17.3 | 200.2 ± 7.6 | 213.5 ± 18.7 | 0.087 |
| | VCR | 5.5 ± 0.3$^{b}$ | 6.9 ± 0.5$^{ab}$ | 7.3 ± 0.5$^{ab}$ | 8.2 ± 0.5$^{a}$ | 0.029 |
| Jejunum (μm) | VH | 1579.9 ± 78.0$^{b}$ | 1544.3 ± 27.7$^{b}$ | 1495.9 ± 71.1$^{b}$ | 1772.4 ± 29.0$^{a}$ | 0.023 |
| | CD | 226.9 ± 13.8 | 266.2 ± 22.5 | 249.9 ± 24.2 | 232.5 ± 6.9 | 0.446 |
| | VCR | 7.0 ± 0.7 | 5.9 ± 0.4 | 6.1 ± 0.6 | 7.6 ± 0.1 | 0.123 |
| Ileum (μm) | VH | 1205.7 ± 92.5 | 1191.9 ± 46.1 | 1384.9 ± 113.4 | 1166.4 ± 58.3 | 0.270 |
| | CD | 246.9 ± 11.5$^{a}$ | 241.1 ± 13.8$^{a}$ | 196.7 ± 15.9$^{b}$ | 261.3 ± 26.5$^{a}$ | 0.015 |
| | VCR | 4.9 ± 0.6$^{b}$ | 5.0 ± 0.1$^{b}$ | 7.1 ± 0.2$^{a}$ | 4.8 ± 0.3$^{b}$ | 0.002 |

Data are expressed as mean ± SEM. $^{a,b}$Means within the same row with different superscripts differ. VH, villus height; CD, crypt depth; VCR, villus height/crypt depth ratio. Group C, control group; Group B, added with 4% BSG in the overfeeding stage (days 61–90); Group F, added with 4% BSG in the rearing stage (days 5–60); Group W, added with 4% BSG in the all stage (days 5–90).

TABLE 5 Effect of brewers' spent grain (BSG) on the compositions of amino acids in the livers of four groups of Landes geese (i.e., groups C, B, F, and W) in 90 days.

| Amino acid (mg/g) | Group C | Group B | Group F | Group W | *P*-value |
|---|---|---|---|---|---|
| Aspartic acid | 6.3 ± 0.4 | 6.5 ± 0.2 | 6.3 ± 0.3 | 6.5 ± 0.1 | 0.085 |
| Threonine | 3.4 ± 0.1 | 3.4 ± 0.1 | 3.4 ± 0.1 | 3.5 ± 0.1 | 0.924 |
| Serine | 3.2 ± 0.1 | 3.3 ± 0.1 | 3.1 ± 0.1 | 3.3 ± 0.1 | 0.348 |
| Glutamic acid | 10.9 ± 0.1 | 10.6 ± 0.5 | 11.9 ± 1.3 | 11.0 ± 0.7 | 0.827 |
| Glycine | 3.7 ± 0.1 | 3.6 ± 0.1 | 3.5 ± 0.1 | 3.7 ± 0.1 | 0.385 |
| Alanine | 4.6 ± 0.1 | 4.6 ± 0.2 | 4.4 ± 0.1 | 4.6 ± 0.1 | 0.297 |
| Cystine | 1.1 ± 0.2 | 1.2 ± 0.1 | 1.3 ± 0.3 | 1.2 ± 0.0 | 0.885 |
| Methionine | 0.3 ± 0.0 | 0.4 ± 0.0 | 0.3 ± 0.0 | 0.3 ± 0.0 | 0.969 |
| Isoleucine | 3.4 ± 0.1 | 3.3 ± 0.1 | 3.5 ± 0.5 | 3.4 ± 0.1 | 0.385 |
| Leucine | 6.5 ± 0.1 | 6.5 ± 0.2 | 6.3 ± 0.2 | 6.7 ± 0.2 | 0.268 |
| Tyrosine | 2.3 ± 0.0 | 2.4 ± 0.1 | 2.2 ± 0.1 | 2.6 ± 0.1 | 0.831 |
| Phenylalanine | 3.5 ± 0.1 | 3.5 ± 0.1 | 3.4 ± 0.1 | 3.7 ± 0.3 | 0.349 |
| Lysine | 5.3 ± 0.2 | 5.2 ± 0.3 | 5.2 ± 0.3 | 5.4 ± 0.2 | 0.879 |
| Histidine | 1.9 ± 0.1 | 1.9 ± 0.0 | 1.8 ± 0.1 | 2.1 ± 0.1 | 0.101 |
| Arginine | 4.4 ± 0.1 | 4.3 ± 0.1 | 4.3 ± 0.2 | 4.5 ± 0.2 | 0.606 |
| Proline | 3.0 ± 0.1 | 3.0 ± 0.1 | 2.9 ± 0.1 | 3.0 ± 0.0 | 0.530 |

Data are expressed as mean ± SEM. Group C, control group; Group B, added with 4% BSG in the overfeeding stage (days 61–90); Group F, added with 4% BSG in the rearing stage (days 5–60); Group W, added with 4% BSG in the all stage (days 5–90).

*Firmicutes/Bacteroidetes* (F/B) ratio in both groups W and F were increased, though not significantly ($P > 0.05$), compared with those of groups C and B (Figure 2C).We then evaluated the variations in the relative abundances of the cecal microbiota in four groups of Landes geese in 60 and 90 days at the genus level (Figures 3A,B). The results showed that the relative abundances

TABLE 6 Effects of brewers' spent grain (BSG) on the compositions of fatty acids in the livers of four groups of Landes geese (i.e., groups C, B, F, and W) in 90 days.

| Fatty acid | Group C | Group B | Group F | Group W | *P*-value |
|---|---|---|---|---|---|
| Decanoic acid C10:0 | 0.05 ± 0.01 | 0.06 ± 0.01 | 0.06 ± 0.02 | 0.08 ± 0.01 | 0.293 |
| Eleven carbonic acid C11:0 | 0.04 ± 0.01 | 0.04 ± 0.01 | 0.03 ± 0.01 | 0.064 ± 0.02 | 0.185 |
| Dodecanoic acid C12:0 | 0.06 ± 0.01$^{a}$ | 0.03 ± 0.00$^{b}$ | 0.03 ± 0.00$^{b}$ | 0.04 ± 0.00$^{b}$ | 0.020 |
| Myristic acid C14:0 | 0.51 ± 0.01 | 0.53 ± 0.00 | 0.42 ± 0.07 | 0.43 ± 0.05 | 0.060 |
| Palmitic acid C16:0 | 22.05 ± 0.35 | 21.56 ± 0.94 | 21.41 ± 0.22 | 20.43 ± 0.65 | 0.192 |
| Hexadecanoic acid C16:1 | 2.05 ± 0.71 | 1.84 ± 0.23 | 1.65 ± 0.25 | 1.64 ± 0.06 | 0.718 |
| Seventeen carbonic acid C17:0 | 0.07 ± 0.01 | 0.08 ± 0.03 | 0.07 ± 0.01 | 0.08 ± 0.01 | 0.803 |
| Stearic acid C18:0 | 14.71 ± 2.21 | 15.59 ± 1.33 | 15.31 ± 0.08 | 15.46 ± 0.11 | 0.905 |
| Eleic acid C18:1 | 53.52 ± 1.70$^{a}$ | 54.09 ± 0.13$^{a}$ | 56.32 ± 0.47$^{ab}$ | 57.17 ± 1.03$^{b}$ | 0.056 |
| Translinoleic acid C18:2 | 1.58 ± 0.45 | 1.58 ± 0.14 | 1.50 ± 0.09 | 1.61 ± 0.13 | 0.973 |
| α-linolenic acid C18:3 | 0.13 ± 0.05 | 0.09 ± 0.01 | 0.09 ± 0.01 | 0.08 ± 0.01 | 0.371 |
| λ-linolenic acid C18:3 | 0.09 ± 0.02 | 0.14 ± 0.02 | 0.07 ± 0.00 | 0.08 ± 0.01 | 0.450 |
| Arachidonic acid C20:0 | 0.14 ± 0.04 | 0.17 ± 0.04 | 0.16 ± 0.01 | 0.15 ± 0.01 | 0.766 |
| Eicosadienoic acid C20:2 | 0.30 ± 0.04$^{a}$ | 0.31 ± 0.04$^{a}$ | 0.21 ± 0.02$^{b}$ | 0.20 ± 0.01$^{b}$ | 0.047 |
| Eicosatetraenoic acid C20:3 | 0.19 ± 0.06 | 0.18 ± 0.11 | 0.10 ± 0.05 | 0.12 ± 0.01 | 0.535 |
| Arachidonic acid C20:4 | 1.80 ± 0.42 | 1.64 ± 0.00 | 1.26 ± 0.12 | 1.46 ± 0.01 | 0.115 |
| Eicosapentaenoic acid C20:5 | 0.08 ± 0.01 | 0.08 ± 0.06 | 0.07 ± 0.02 | 0.07 ± 0.03 | 0.935 |
| Docosanoic acid C22:0 | 0.37 ± 0.17 | 0.19 ± 0.21 | 0.64 ± 0.00 | 0.02 ± 0.01 | 0.104 |
| Docosyl monoenoic acid C22:1 | 0.04 ± 0.01 | 0.07 ± 0.01 | 0.05 ± 0.02 | 0.06 ± 0.03 | 0.537 |
| Docosahexadienoic acid C22:2 | 2.02 ± 0.04$^{a}$ | 1.61 ± 0.13$^{b}$ | 1.01 ± 0.04$^{c}$ | 0.95 ± 0.03$^{c}$ | < 0.001 |
| Docosahexaenoic acid C22:6 | 0.06 ± 0.11 | 0.08 ± 0.02 | 0.10 ± 0.01 | 0.10 ± 0.02 | 0.114 |
| Tricosanoic acid C23:0 | 0.13 ± 0.12 | 0.05 ± 0.03 | 0.01 ± 0.00 | 0.14 ± 0.16 | 0.399 |
| Saturated fatty acids ΣSFA | 38.17 ± 2.02 | 38.30 ± 0.14 | 37.57 ± 0.18 | 36.90 ± 0.64 | 0.638 |
| Unsaturated fatty acid ΣSFU | 61.87 ± 1.53 | 61.70 ± 0.14 | 62.43 ± 0.18 | 63.13 ± 0.64 | 0.423 |

Data presented as the percentage of the total content of fatty acids. Data are expressed as mean ± SEM. $^{a-c}$Means within the same row with different superscripts differ Group C, control group; Group B, added with 4% BSG in the overfeeding stage (days 61–90); Group F, added with 4% BSG in the rearing stage (days 5–60); Group W, added with 4% BSG in the all stage (days 5–90).

of *Bacteroides* ($P < 0.05$), *Lachnospiraceae* ($P < 0.01$), and *unclassified_f_Oscillospiraceae* ($P < 0.01$) in all four groups of Landes geese on day 90 were significantly increased compared to those on day 60. In 60 days, no significant difference was observed in the relative abundance at the genus level of the four groups of Landes geese. In 90 days, the relative abundances of *Escherichia-Shigella* in groups B, F, and W were decreased, though not significantly ($P > 0.05$), compared with that of group C. The relative abundances of *Lachnospiraceae* in groups F and W were significantly lower than that in group C ($P < 0.05$), whereas the relative abundances of *prevotellaceae_Ga6A1_group* in groups B ($P < 0.01$), F ($P < 0.05$), and W ($P < 0.01$) were significantly lower than that in group C.

## Transcriptomics analysis of fatty liver in Landes geese

The transcriptomics analysis was performed based on a total of 32 liver samples (n = 8 samples per group) for four groups of Landes geese (**Supplementary Table 6**). A total of 225.71 Gb of clean data were obtained with the exclusion of low-quality sequences, while the large portion of the filtered reads (>88%) showed a Phred quality score > 30 (i.e., base Q30). Results showed that the Pearson correlation coefficients ($R^2$) among the biological repeats in all four groups of Landes geese were high (**Figure 4A**), suggesting that the RNA-Seq data were reliable for further analyses. The expressions of a total of 10,033, 10,313, 10,252, and 10,426 genes were detected in the liver tissues of four groups of Landes geese, i.e., C, B, F, and W, respectively, with a total of 9,865 genes expressed commonly in all four groups of geese (**Figure 4B**).

The total number of DEGs varied in different pairwise comparisons (**Table 7**). A total of 866 DEGs were identified in the four groups of Landes geese using DESeq (**Supplementary Table 7**). The DEGs identified in the fatty livers of the Landes geese were further annotated based on the GO database (**Supplementary Table 8**). The results of GO annotation analysis showed that the functions of DEGs were classified into three categories, including biological process (BP), cellular component (CC), and molecular function (MF). Among the top five GO terms in each of these three categories (**Figure 5**), the

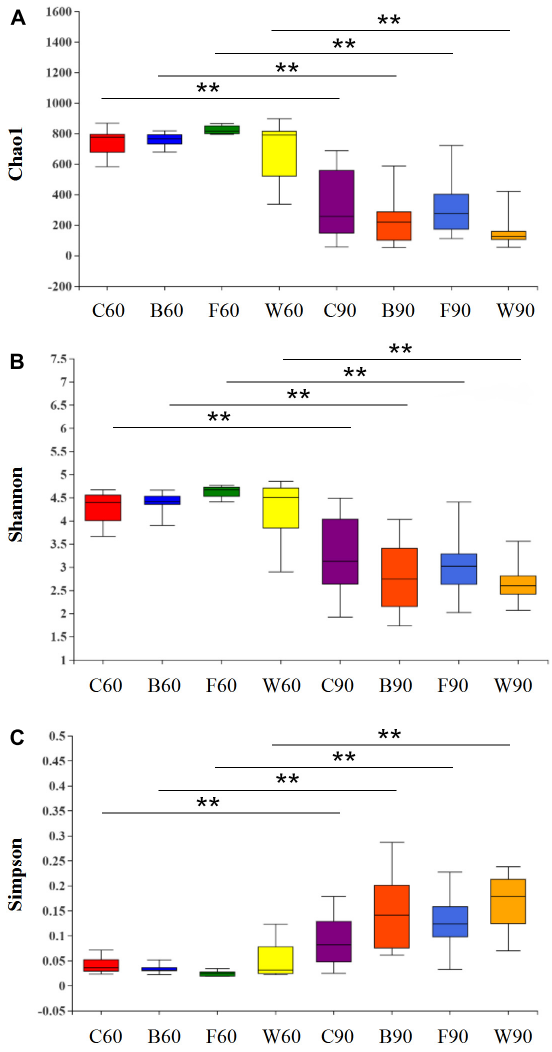


FIGURE 1
Effect of brewers' spent grain (BSG) on the alpha diversity of cecal microbiota in Landes geese in 60 and 90 days. **(A)** Chao1 index. **(B)** Shannon index. **(C)** Simpson index. Symbol "**" indicates the significant difference at $P < 0.01$. Group C=, control group; Group B, added with 4% BSG in the overfeeding stage (days 61–90); Group F, added with 4% BSG in the rearing stage (days 5–60); Group W, added with 4% BSG in the all stage (days 5–90).

highest number of genes were annotated in the GO term of signaling receptor binding in all three pairwise comparisons, followed by the GO terms of extracellular space and anatomical structure morphogenesis.

The enrichment analysis of DEGs identified in the fatty livers of the Landes geese were further performed based on the KEGG database (Figure 6). The results showed that the DEGs identified in group W compared with group C were highly enriched in three metabolic pathways (i.e., ECM-receptor interaction, PI3K-Akt signaling pathway, and sphingolipid signaling pathway), while the other three pathways (i.e., IL-17 signaling pathway, NF-kappa B signaling pathway, and B cell receptor signaling pathway) were highly enriched by DEGs identified in group F compared with group C. The *Q*-values of the KEGG enrichment analysis indicated that most of the genes enriched were involved in the biosynthesis of secondary metabolites.

## Kyoto encyclopedia of genes and genomes enrichment analysis of differentially expressed gene between groups C and W of Landes geese

Due to the extremely significant difference in the liver weight between groups W and C of Landes geese, the KEGG enrichment analysis of the DEGs identified between groups W and C was performed to further evaluate the functions of these genes involved in different metabolic pathways (Table 8). The results showed that in group W, the down-regulated DEGs were significantly enriched in two metabolic pathways (i.e., the protein processing in endoplasmic reticulum and the endocytosis), while the up-regulated DEGs were significantly enriched in four metabolic pathways, including PI3K-Akt signaling pathway, sphingolipid signaling pathway, sphingolipid metabolism, and biosynthesis of unsaturated fatty acids.

## Validation of differentially expressed genes

To validate the identification of DEGs between the groups C and W determined by RNA-Seq, a total of six DEGs (*CASQ2*, *SPR*, *PSPH*, *HTR2C*, *DGKI*, and *ELOVL7*) were randomly selected for qRT-PCR analysis (Figure 7). The results showed that in group W, three genes (i.e., *CASQ2*, *SPR*, and *PSPH*) were down-regulated, while the other three genes (i.e., *HTR2C*, *DGKI*, and *ELOVL7*) were up-regulated. These results were consistent with those of the RNA-Seq analysis, therefore validating the results of the RNA-Seq analysis.

# Discussion

Due to the increasing demand of various types of meat products worldwide, e.g., chicken, beef, and pork, the feed prices have been rapidly escalating. Therefore, it is practically and financially essential to identify feed supplements that are both nutritious and inexpensive. The BSG is the main by-product of the brewing industry and is commonly used in animal feeds, simply because the BSG is not only less expensive than most raw materials available on the market, but also rich in nutrients (Bianco et al., 2020). Furthermore, the

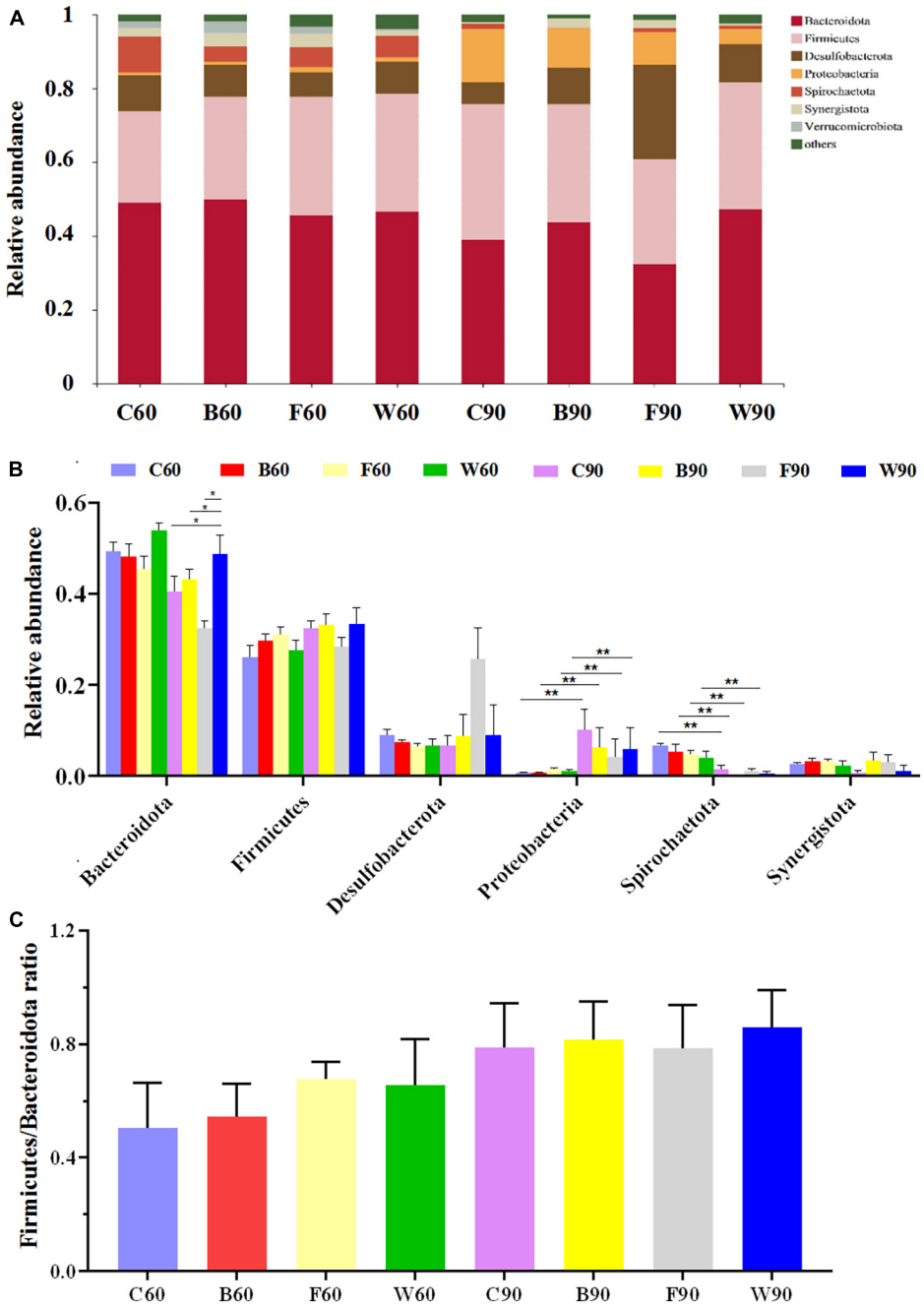


FIGURE 2
The microbiome compositions in cecum at the phylum level based on the 16S rRNA sequencing in four groups of Landes geese (i.e., groups C, B, F, and W) on both days 60 and 90. **(A)** The relative abundances of the top seven bacterial phyla in the microbiome of Landes geese on days 60 and 90. **(B)** The relative abundances of top seven bacterial phyla among the four groups of Landes geese on days 60 and 90 showing the statistical significance. **(C)** The *Firmicutes/Bacteroides* (F/B) ratio in four groups of Landes geese on days 60 and 90. Values are represented as the mean ± stand error of the mean (SEM) ($n$ = 8 geese per group). The significant difference is set at $P < 0.05$ (*) and $P < 0.01$ (**), respectively. Group C, control group; Group B, added with 4% BSG in the overfeeding stage (days 61–90); Group F, added with 4% BSG in the rearing stage (days 5–60); Group W, added with 4% BSG in the all stage (days 5–90).

BSG may contain microbes capable of producing endogenous ethanol. For example, studies reported a strong correlation between the amount of endogenous ethanol produced in the intestine of obese patients and the pathogenesis of NAFLD (Nair et al., 2001), showing the high relative abundance of alcohol-producing bacteria in the microbiota of NAFLD

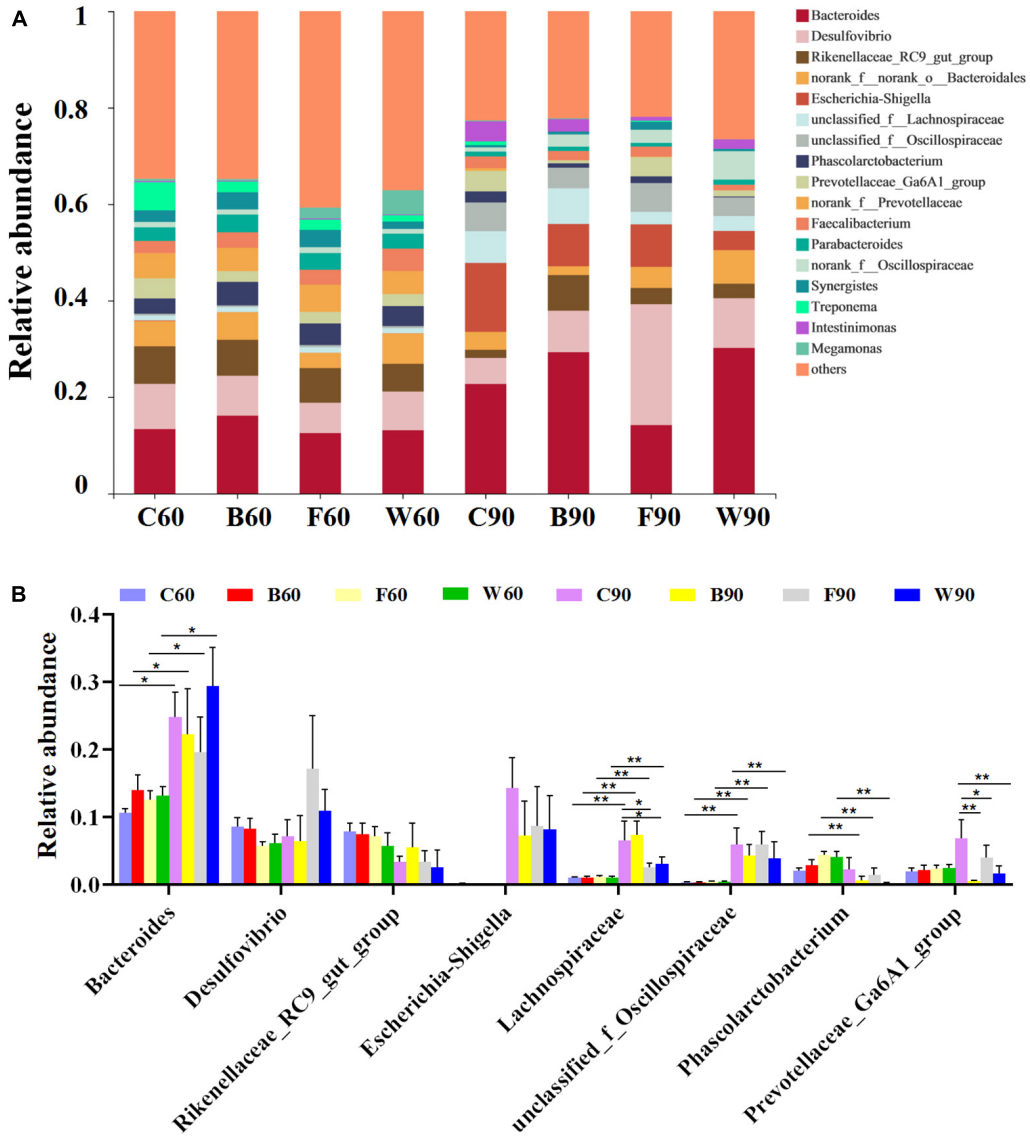


FIGURE 3
The microbiome compositions in cecum at the genus level based on the 16S rRNA sequencing in four groups of Landes geese (i.e., groups C, B, F, and W) on both day 60 and 90. **(A)** The relative abundances of the top 18 bacterial taxa in the microbiome of the Landes geese on day 60 and 90. **(B)** The relative abundances of the top 18 bacterial taxa in the microbiome of the Landes geese on day 60 and 90 showing the statistical significance. Values are represented as the mean ± stand error of the mean (SEM) ($n$ = 8 geese per group). The significant difference is set at $P < 0.05$ (*) and $P < 0.01$ (**), respectively. Group C, control group; Group B, added with 4% BSG in the overfeeding stage (days 61–90); Group F, added with 4% BSG in the rearing stage (days 5–60); Group W, added with 4% BSG in the all stage (days 5–90).

patients. Moreover, it was suggested that the endogenous ethanol production could promote liver steatosis by stimulating the inflammatory signals (Jandhyala et al., 2015; Boursier and Diehl, 2016). In our study, the beneficial effects of BSG, used as the feed additives, on the liver production performance of Landes geese through the "gut-liver axis" and on the growth performance, intestinal morphological structure, serum biochemical indicators of Landes geese, were investigated based on transcriptomics analysis. Our study provided novel experimental evidence to support the further investigations and applications of BSG in the fat deposition regulation by modulating the gut microbiota in the Landes geese.

## Effects of brewers' spent grain on the growth performance of Landes geese

Previous studies reported that the addition of 20% brewers' dried grain to the diets of Vanaraja chicks significantly improved

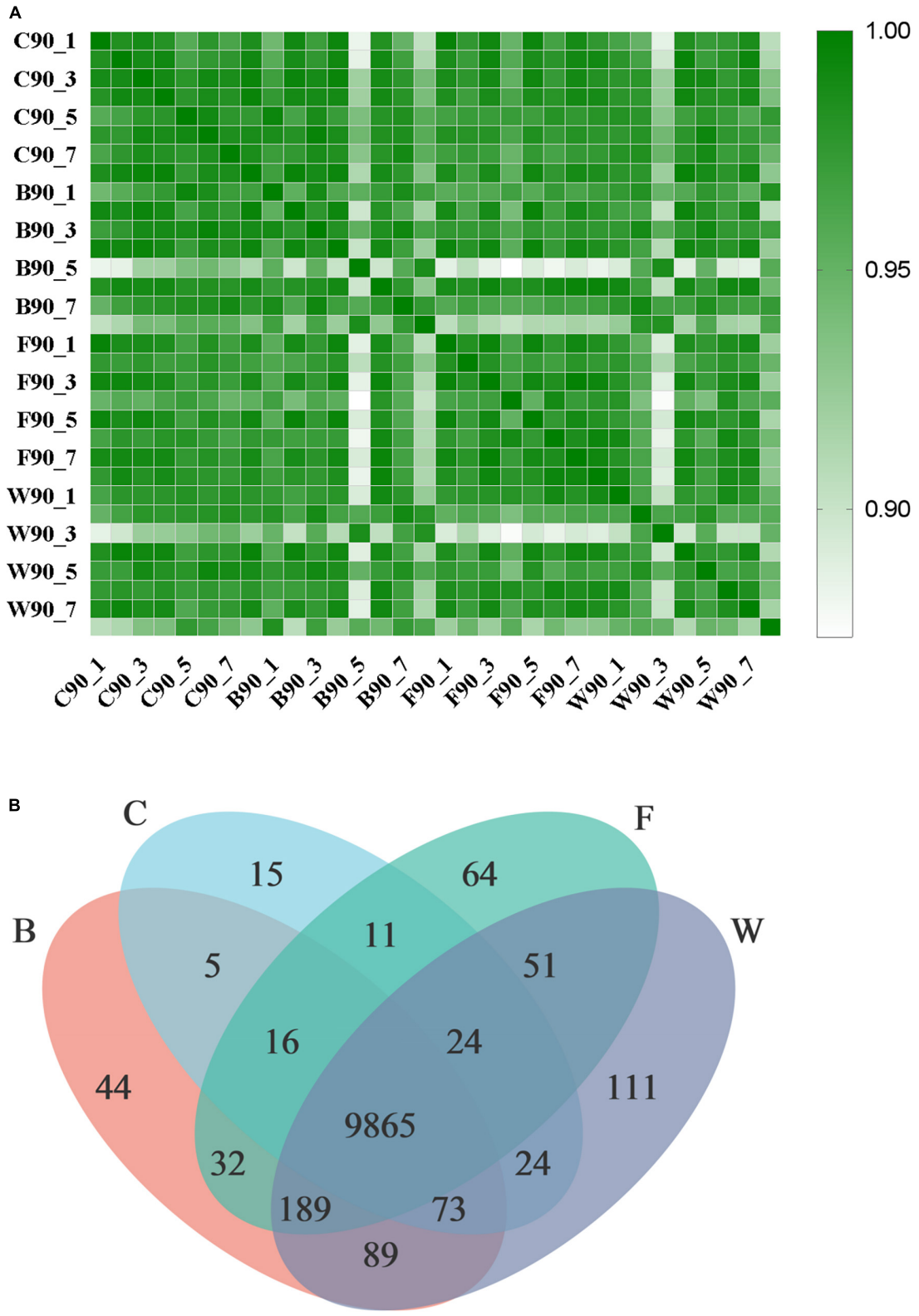


FIGURE 4
Transcriptomic profiles of liver tissues in four groups of Landes geese (i.e., groups C, B, F, and W) on day 90. **(A)** The Pearson correlation coefficient ($R^2$) heat map among individual samples in four groups of Landes geese ($P < 0.01$). **(B)** Venn diagram showing the number of expressed genes detected in four groups of Landes geese. Group C, control group; Group B, added with 4% BSG in the overfeeding stage (days 61–90); Group F, added with 4% BSG in the rearing stage (days 5–60); Group W, added with 4% BSG in the all stage (days 5–90).

TABLE 7 Differentially expressed genes (DEGs) identified in three pairwise comparisons between the control (group C) and each of the three experiments groups of Landes geese (i.e., groups F, B, and W) treated with brewers' spent grain (BSG) on day 90 based on transcriptomics analysis.

| | Groups C vs. F | Groups C vs. B | Groups C vs. W |
|---|---|---|---|
| Up-regulated | 169 | 143 | 296 |
| Down-regulated | 131 | 43 | 84 |
| Total | 300 | 186 | 380 |

Group C, control group; Group B, added with 4% BSG in the overfeeding stage (days 61–90); Group F, added with 4% BSG in the rearing stage (days 5–60); Group W, added with 4% BSG in the all stage (days 5–90).

the carcass yield and enhanced profit margins without affecting the growth performance in birds (Denstadli et al., 2010). Furthermore, studies showed that BSG could be used to replace portion of the diet of growing pigs without causing adverse effects on daily weight gain and economic benefits (Mukasafari et al., 2018). However, these results were not consistent with the findings revealed in our study. In particular, our results showed that the addition of BSG in the feeds caused an increasing trend in both BW and ADG of Landes geese during the rearing period (**Table 2**). These conflicting results were probably because that the BSG used in our study was already fermented by microorganisms, and there were a large number of probiotics and enzymes in the fermented BSG, which could improve the digestibility of nutritional components, ultimately reducing the anti-nutritional factors and harmful components in the raw materials, as previously reported (Al-Khalaifah et al., 2020). Moreover, studies showed that the BSG could produce a type of unique fragrance derived from the probiotic fermentation, improving the feed intake and weight gain of lambs (Frasson et al., 2018), while the addition of 40% fermented brewers' dried grain to the diet of Meihua pigs resulted in rapid weight gain and high feed remuneration, largely decreasing the feeding costs of Meihua pigs as well as effectively preventing diarrhea and reducing stool odor (Wu et al., 2018). These results suggested that the fermented BSG not only reduced the feeding costs but also improved the animal growth performance, showing significant potential of feed additives in animal feed industry.

## Effects of brewers' spent grain on the fatty liver deposition in Landes geese

It is well-known that beer fermentation is a metabolic process converting both monosaccharides and disaccharides into ethanol under anaerobic or micro-oxygen conditions by microorganisms such as yeast, while a large number of alcohol-producing microorganisms are identified in the BSG (Zabed et al., 2017; Rojas-Chamorro et al., 2020). For example, studies showed that the high gravity brewing yeast *Saccharomyces cerevisiae* BLGII 1762 and *S. cerevisiae* PE-2 isolated from the bioethanol industry produced ethanol with yields of 42.27 g/L and 40.3 g/L, respectively (Pinheiro et al., 2019). Furthermore, it was previously reported that the ethanol produced by high alcohol-producing bacteria was an important factor causing liver lipid accumulation and ultimately NAFLD (Chen et al., 2020). Studies have shown that in the obese mice, ethanol could be detected in exhaled gas even in the absence of ethanol intake, and the increased level of exhaled ethanol indicated the increased production of ethanol by the gut microbiota, which could contribute to the development of fatty liver (Cope et al., 2000). Moreover, studies showed that gut microbiota rich in alcohol-producing bacteria (e.g., *Klebsiella pneumoniae*) constantly produced more alcohol through 2,3-butanediol fermentation pathway involved in fatty liver disease (Li N. N. et al., 2021). In our study, the results showed that the addition of BSG in feeds caused significant increase in liver weight of Landes geese during the overfeeding stage (**Table 2**). This could be explained by the presence of endogenous ethanol-producing microorganisms in BSG causing the increased liver weight, suggesting the positive effect of microorganisms capable of producing endogenous ethanol to enhance the fatty liver deposition in Landes geese.

## Effects of brewers' spent grain on the serum biochemical index in Landes geese

Blood biochemical indices are generally considered sensitive indicators used to evaluate the body's systemic or local metabolic changes and the physiological functions of various types of tissues (Kani et al., 2013). In our study, the BSG significantly reduced the serum GLU level during the rearing stage (**Table 3**), while previous studies identified the correlation between the increased level of hunger and the observed decrease in blood GLU level (Campfield and Smith, 2003). Therefore, the significantly higher ADG in geese fed with BSG was not only due to the fermentation process that improved the palatability of the feeds, but also associated with the lower blood GLU level. Both AST and ALT are two important amino acid transferases that are generally detected at low levels in the blood, released from cells into the blood when tissue damage or necrosis occurs in organs such as the liver, resulting in the increased enzymatic activities in the serum (Kunde et al., 2005). Therefore, the serum levels of AST and ALT could reflect the health status of the liver and heart. In our study, the increased serum levels of both ALT

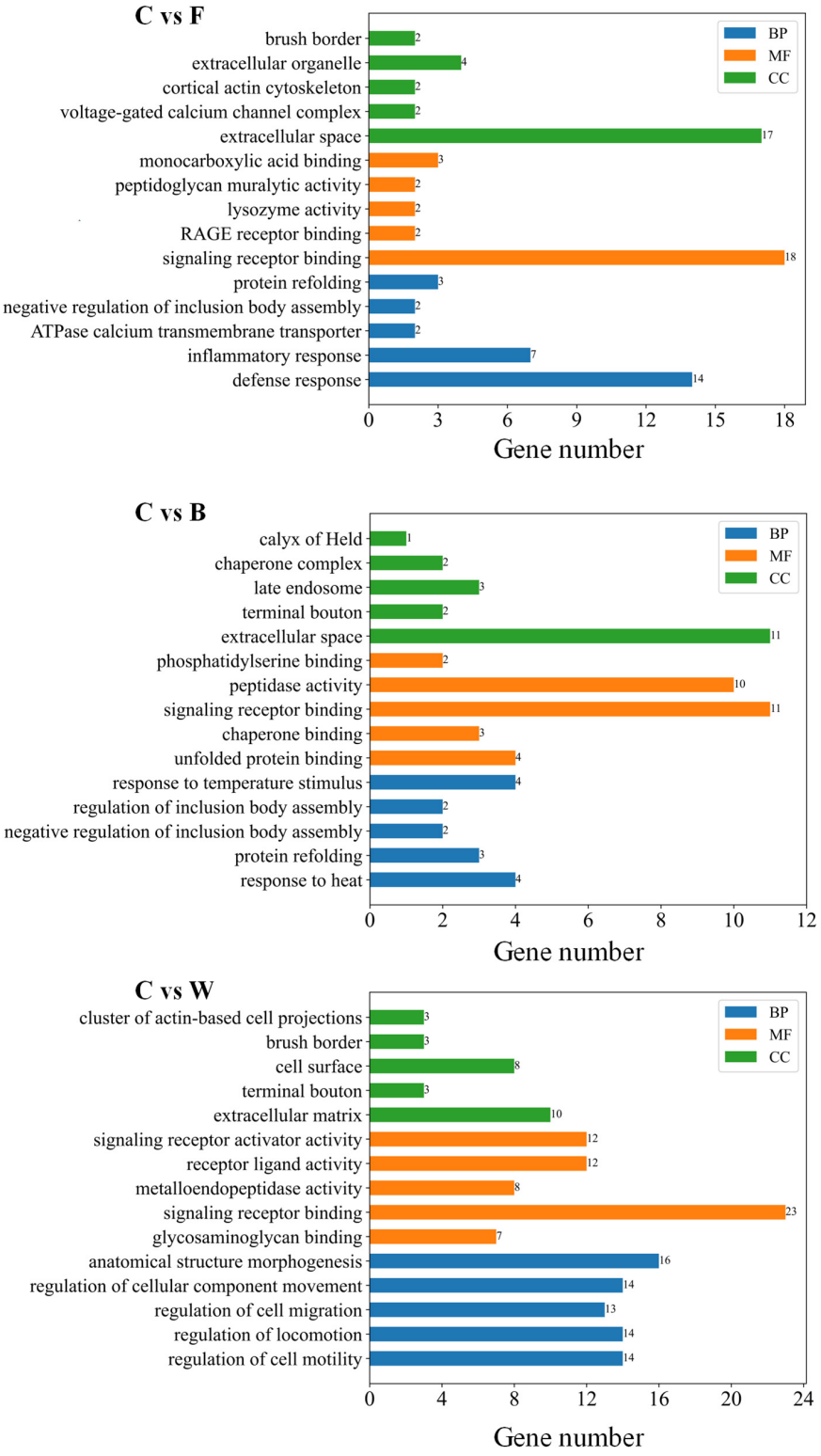


FIGURE 5
Gene Ontology (GO) annotation of the differentially expressed genes (DEGs) identified between the control (group C) and each of the three experimental groups of Landes geese (i.e., groups F, B, and W) on day 90 showing the top five GO terms in each of the three categories of GO terms, including molecular function (MF), cellular component (CC), and biological process (BP). Group C, control group; Group B, added with 4% BSG in the overfeeding stage (days 61–90); Group F, added with 4% BSG in the rearing stage (days 5–60); Group W, added with 4% BSG in the all stage (days 5–90).

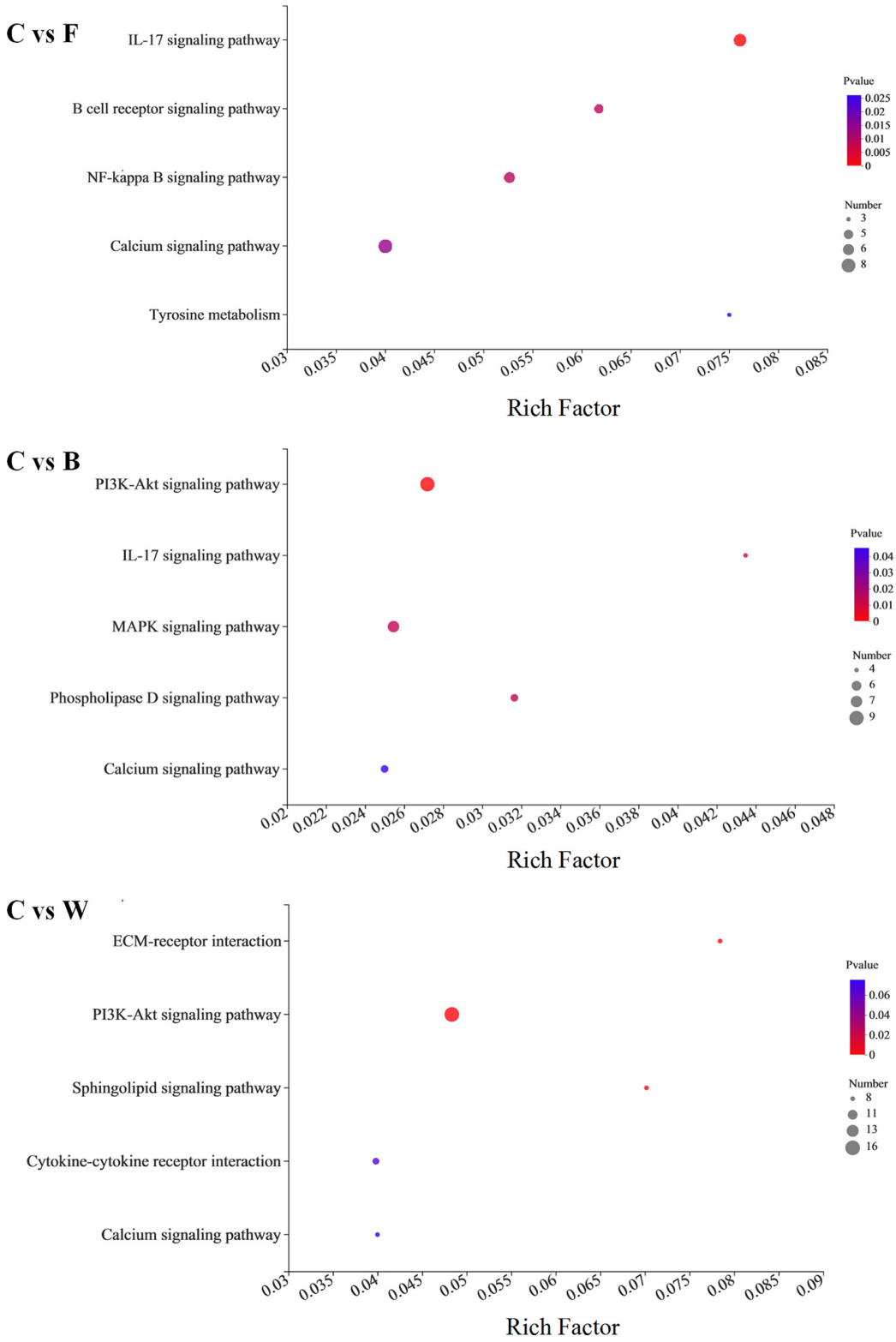


FIGURE 6
Enrichment analysis based on the Kyoto Encyclopedia of Genes and Genomes (KEGG) database of the differentially expressed genes (DEGs) identified between the control (group C) and each of the three experimental groups of Landes geese (i.e., groups F, B, and W) on day 90. The larger Rich factor value indicates the greater enrichment. The size of the dots indicates proportionally the number of genes enriched in the pathway; the color of the dots corresponds to the *P*-value ranges. Group C, control group; Group B, added with 4% BSG in the overfeeding stage (days 61–90); Group F, added with 4% BSG in the rearing stage (days 5–60); Group W, added with 4% BSG in the all stage (days 5–90).

TABLE 8 Enrichment analysis of differentially expressed genes (DEGs) identified between groups C and W of Landes geese on day 90 based on the Kyoto Encyclopedia of Genes and Genomes (KEGG) database.

| DEG | *P*-value | Number of gene | KEGG pathway |
|---|---|---|---|
| Up-regulated | | 28 | |
| *PPP2R2B, BCL2, PPP2R3B, LAMC2, LAMA2, LAMA4, COL6A1, HGF, THBS2, KIT, FGF10, ANGPT4, IL2RA, COL6A3, PDGFRA* | 0.000571 | 15 | PI3K-Akt signaling pathway |
| *PPP2R2B, PLCB4, BCL2, PPP2R3B, SGPP1, ASAH2, CERS6* | 0.003413 | 7 | Sphingolipid signaling pathway |
| *GAL3ST1, SGPP1, ASAH2, CERS6* | 0.011893 | 4 | Sphingolipid metabolism |
| *ELOVL7, LOC106048282* | 0.150318 | 2 | Biosynthesis of unsaturated fatty acids |
| Down-regulated | | 8 | |
| *HSPA8, LOC106048968, HSPA2, HSPH1* | 0.005821 | 4 | Protein processing in endoplasmic reticulum |
| *HSPA8, IQSEC3, LOC106044678, HSPA2* | 0.021602 | 4 | Endocytosis |

Group C, control group; Group W, added with 4% BSG in the all stage (days 5–90).

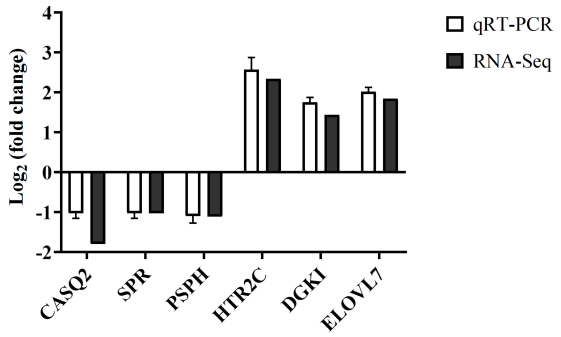


FIGURE 7
The expression fold changes in six randomly selected differentially expressed genes (DEGs) between groups C and W of Landes geese based on the quantitative real-time PCR (qRT-PCR) analysis validating the expression patterns revealed by the RNA-Seq analysis. Group C, control group; Group W, added with 4% BSG in the all stage (days 5–90).

and AST were observed in 90-day-old Landes geese compared with those of the 60-day-old geese (Table 3), suggesting that the force-feeding process caused the abnormal liver function, i.e., formation of fatty liver, as reported previously (Locsmándi et al., 2007).

The lipids synthesized in goose liver are either stored in hepatocytes as cytoplasmic droplets or secreted as lipoproteins into blood (Hermier, 1997). Our results showed that the overfeeding of Landes geese with BSG caused the significantly increased serum lipid concentration in Landes geese, with the contents of both HDL and VLDL increased considerably. However, no significant difference was observed in the contents of TG and CHO among the four groups of Landes geese (Table 3). These results were consistent with those reported previously. For example, due to the dramatic increase in new hepatic lipogenesis caused by overfeeding, both TG and CHO did not fully enter the secretory pathway with a large amount of TG remained and stored in the liver (Liu et al., 2020). Studies have shown that HDL could lower the blood cholesterol level mainly by transporting cholesterol from peripheral tissues and plasma to the liver for both metabolism and excretion through apolipoproteins (i.e., APOA1 and APOC3), while as the main form of endogenous cholesterol synthesized by the liver and transported to other tissues, the LDL is rich in cholesterol esters to release cholesterol through its APOB100 protein binding to receptors on non-hepatocyte plasma membranes (Ikonen, 2008; Min et al., 2012). Furthermore, studies reported that the increased rate of cholesterol synthesis in the liver in comparison to that of VLDL-C secretion resulted in a large amount of cholesterol deposition in the liver (Han et al., 2008; Griffin et al., 2009). Moreover, a positive correlation between VLDL-C concentration and liver weight was revealed in Polish geese (Mourot et al., 2000). These results indicated that the high VLDL-C concentration indicated the enhanced fat deposition in the liver tissue. In our study, increased HDL-C and VLDL-C secretion rates caused by the addition of BSG strongly indicated that BSG could make significant impact on the lipoproteins, which in turn affected the deposition of TG in the liver, ultimately increasing the weight of the fatty liver in Landes geese.

## Effects of brewers' spent grain on the intestinal morphology in Landes geese

The small intestine is the main organ for digestion and absorption, which are crucial to the growth performance of the Landes geese. Studies have shown that as the main microstructures functioning in nutrient absorption and transport, the villi with increased height obtained an enhanced nutrient absorption capacity, while the crypt depth (CD) reflected the turnover rate of the intestinal epithelium (Gu et al., 2020). Therefore, the villus height/crypt depth ratio (VCR) is commonly used as an important factor for evaluating

the absorption capacity of small intestine. For example, it was reported that the addition of wine lees and soluble matter to broiler diets significantly ($P < 0.05$) increased the jejunal villus height (VH) (Alizadeh et al., 2016), while the supplementation of diets with 2.5% fermented feed increased the proximal jejunal VH in geese, ultimately causing the beneficial effect on growth performance and nutrient digestibility (Yan et al., 2019). These results were consistent with our findings, showing that the BSG treatment markedly increased the VCRs of the duodenum, jejunum, and ileum of Landes geese (**Table 4**). These results strongly indicated that the fermented BSG enhanced the villus development and the absorption of nutrients in the small intestine, leading to the significantly increased BW and ADG in the Landes geese fed with BSG in comparison with those of the control group.

## Effects of brewers' spent grain on the compositions of liver amino acids and fatty acids in Landes geese

As two of the important indicators for evaluating the nutritional value of the goose liver, both the compositions and ratios of various amino acids and fatty acids affect the physicochemical properties and flavor of goose liver (Liu et al., 2011; Zhu et al., 2011). Amino acids could activate G protein-coupled receptors (GPCRs) to control the ion channels in the umami and sweet taste pathways, directly affecting the mammalian taste ability (Oike et al., 2006). In our study, no significant differences were observed in each amino acid in the livers of four groups of Landes geese (**Table 5**). However, the levels of glutamic acid, valine, histidine, and three types of aromatic amino acids (i.e., phenylalanine, tryptophan, and tyrosine) in the experimental groups of geese were slightly increased compared with those of the control group, suggesting that the addition of BSG could improve the flavor of goose liver.

As people's living standards rapidly improve, the polyunsaturated fatty acids (PUFAs) are increasingly demanded in the world market due to their health benefits. As the essential types of nutrient, the PUFAs have shown a preventive effect against chronic diseases (Gillingham et al., 2011). Therefore, it is now widely recommended to increase the intake of PUFAs in human diets (Chen et al., 2016). For example, it was reported that the addition of distillers' dried grains in the laying duck diet significantly ($P < 0.01$) increased the ratio of oleic acid (C18:1) and the total monounsaturated fatty acids in egg yolk (Ruan et al., 2018), while the concentration of the total PUFAs in the bull muscles fed with distillers' grains was higher than that of the control group (He et al., 2015). In our study, the results showed that both C16:0 and C18:1 were the predominant fatty acids in the liver of Landes geese, with C18:1 accounted for more than 50% of the total fatty acids, while the addition of BSG increased the content of C18:1 to the highest levels in goose livers of group W compared to the control group (**Table 6**). In summary, the addition of BSG to the diets of Landes geese significantly increased the concentrations of unsaturated fatty acids in the livers of Landes geese.

## Effects of brewers' spent grain on the microbial diversity of the intestinal microbiota in Landes geese

It is important to understand the relationship between gut microbiota and growth performance in order to effectively improve the growth and production performance of Landes geese. In our study, the bacterial communities of the cecal samples were comparatively investigated among the four groups of geese on both day 60 and 90. The results showed that species richness and diversity of the microbial communities were not significantly altered by the addition of BSG during the entire experiment of both the rearing and overfeeding stages (**Figure 1**). However, the alpha diversity indices (i.e., Chao1, Shannon, and Simpson) of Landes geese were decreased after the overfeeding stage. Studies reported that in both the ileal and cecal samples, the probiotic addition showed no significant effect on species richness and diversity before overfeeding, whereas both diversity and species richness tended to decrease after the overfeeding (Even et al., 2018). These results were consistent with the findings revealed in our study, suggesting that the overfeeding could modulate the intestinal microbiota in Landes geese.

Our results revealed that all cecal samples were relatively dominated by both Bacteroidota and Firmicutes at the phylum level (**Figure 2A**), similar to the results previously reported (Waite and Taylor, 2014), and were dominated by *Bacteroides*, *Desulfovibrio*, and *Rikenellaceae_RC9_gut_group* at the genus level (**Figure 3A**). As a generally predominant genus in the poultry intestine, *Bacteroides* shows its unique physiological characteristics (Aruwa et al., 2021), e.g., regulating the intestinal redox level (Wexler and Goodman, 2017), participating in the carbohydrate metabolism, and generating the main end-products (i.e., acetate, propionate, and butyrate) in sugar fermentation (Fu et al., 2019). Studies have shown that the relative abundance of *Bacteroidetes* was increased in the laying hens as a model group for NASH (Hamid et al., 2019). Furthermore, it was reported that the gut *Firmicutes*/*Bacteroidetes* ratio was positively correlated with steatosis in the obese patient group (Jasirwan et al., 2021). Moreover, studies have shown that an increase in the proportion of *Proteobacteria* is the most significant change in gut-liver axis induced hepatic steatosis in mice

(Vasques-Monteiro et al., 2021). In our study, the relative abundances of *Proteobacteria* in all four groups of Landes geese were significantly increased after the overfeeding stage (**Figure 2B**). However, there was no significant difference in the relative abundance of *Proteobacteria* between the four groups of Landers geese (i.e., groups C, B, F, and W) in 90 days. These results suggested that future studies should also evaluate the microbial taxa at both genus and family levels in the phylum *Proteobacteria* in order to explore the development of NAFLD. Studies have shown that *Phascolarctobacterium* was a substantially main acetate propionate producer that could be dramatically increased by berberine and metformin (Wu et al., 2017). Moreover, it was suggested that the high relative abundance of *Phascolarctobacterium* in low-aerobic-capacity rats could contribute to their susceptibility to acute high fat diet-induced hepatic steatosis (Panasevich et al., 2016). Furthermore, *Lachnospiraceae* have been recognized as fermentative commensals that produce short-chain fatty acids (SCFAs), which are involved in the maintenance of intestinal health (Sorbara et al., 2020). Our results showed that the relative abundances of both *Phascolarctobacterium* and *Lachnospiraceae* were increased after the overfeeding stage (**Figure 3B**). However, the relative abundances of *Phascolarctobacterium* and *Lachnospiraceae* were decreased with the addition of BSG in feeds, which was inconsistent with our results of growth performance in Landes geese, probably due to the consumption of the nutrients by *Bacillus subtilis* and yeast entering the intestinal tract, suggesting that feeding fermented BSG was not conducive to the growth of *Phascolarctobacterium* and *Lachnospiraceae*. Indeed, studies showed that the relative abundance of *Phascolarctobacterium* and *Lachnospiraceae_uncultured* were decreased by adding fermented feed to geese diets (Yuan et al., 2019). Furthermore, studies showed that both β-glucans and arabinoxylan inhibited the proliferation of *Lachnospiraceae_XPB_1014_group* to enhance the production of butyrate (Bai et al., 2021), while the BSG contained large amounts of β-glucans and arabinoxylan.

It has been reported that the high-meat protein diet could increase the relative abundances of *Desulfovibrio* in both cecum and colon to cause the metabolic defects in liver (Shi et al., 2020), while a high relative abundance of *Desulfovibrio* was revealed in the pig model of NASH (Panasevich et al., 2018). Furthermore, the richness of *Desulfovibrio_Otu047* was increased with the increased activities of the NAFLD-HCC process (Zhang et al., 2021a). The Shiga toxin-producing *Escherichia–Shigella* are pathogenic bacteria that cause the bloody diarrheal diseases of bacillary dysentery and hemorrhagic colitis (Lee et al., 2020). It was reported that the harmful bacteria such as *Escherichia–Shigella* and *Helicobacter* were prevalent in the intestine of rats with alcohol-related liver injury (Yu et al., 2020), while the *Prevotellaceae_Ga6A1_group* was enriched in the gastric mucosal microbiota of patients with gastric intraepithelial neoplasia (Zhang et al., 2021b). In our study, no significant differences were observed in the relative abundances of these three groups of bacteria (i.e., *Desulfovibrio, Escherichia–Shigella*, and *Prevotellaceae_Ga6A1_group*) among the four groups of Landes geese during the rearing stage, whereas the relative abundances of these taxa were significantly increased during the overfeeding stage as the fatty liver was formed (**Figure 3B**). The addition of BSG caused the decrease in the relative abundances of these three groups of bacteria, suggesting that the probiotic properties of fermented BSG were involved in the protective mechanism in Landes geese preventing the progression of steatosis to steatohepatitis in their livers.

## Regulatory functions of brewers' spent grain in the fatty liver development in Landes geese based on the transcriptomics analysis

It has been reported that the fatty livers of geese composed of adipose tissue are achieved with significant weight gain after overfeeding (Wang et al., 2019). This phenomenon is generally considered being related to the long-distance migration of migratory birds. Domestic geese are descendants of migratory birds, suggesting their high tolerance for energy intake (Lu et al., 2015). Our study indicated that the addition of BSG in feed caused an increasing trend in liver weight, suggesting the intrinsic variations in transcriptional regulation during the liver development. Furthermore, our results of KEGG enrichment analysis showed that with the addition of BSG only in the rearing stage (i.e., group F), the DEGs were most significantly enriched in three metabolic pathways, including the NF-kappa B signaling pathway, IL-17 signaling pathway, and B cell receptor signaling pathway (**Figure 6**). Previous studies showed that the transcription factor NF-κB played a key role in the host response to microbial infection by coordinating innate and adaptive immune functions (Peng et al., 2020), while the IL-17 was a host defense cytokine located in barrier mucosal tissues, playing an important role in immunity against fungal and other extracellular pathogens (Conti et al., 2009). These results suggested that the feeding of the Landes geese with BSG at the rearing stage generated a positive regulatory effect on activating the immune system in the geese. When the BSG was added only in the overfeeding stage (i.e., group B), the DEGs were most significantly enriched in the PI3K-Akt signaling pathway, MAPK signaling pathway, and phospholipase D signaling pathway, while the Landes geese were fed with BSG in both the rearing and overfeeding stages (i.e., group W), the DEGs were most significantly enriched in PI3K-Akt signaling pathway, sphingolipid signaling pathway,

and cholinergic synapse (**Figure 6**). Previous studies showed that the formation of fatty liver in geese by overfeeding was accompanied by the activation of the PI3K-Akt-MTOR pathway, suggesting that the PI3K-Akt-MTOR pathway played a key role in regulating the lipid metabolism (Han et al., 2015). Furthermore, it was reported that with the essential feature of an aliphatic amino alcohol sphingolipid skeleton, the sphingolipids were involved in the development of NAFLD (Gorden et al., 2015). Moreover, the sphingolipids were reported to play the critical roles in the physiological functions of *Bacteroidetes*, which were capable of performing activities related to symbiotic functions in the gut (An et al., 2011). In our study, the results showed that the sphingolipid signaling pathway was significantly enriched in the livers of Landes geese of group W, suggesting that the addition of BSG aggravated the hepatic steatosis, which was probably caused by the intestinal bacteria. Notably, our results revealed a relatively high abundance of bacteria in group W of Landes geese in comparison with group C. These results were consistent with those derived from the liver transcriptomics analysis in our study.

Our results of differential gene expression analysis showed that the expressions of several genes, e.g., *BCL-2*, *ELOVL7*, *FGF10*, and *HGF*, were up-regulated in liver tissues when BSG was added to feed during both the rearing and overfeeding stages (i.e., group W). It was reported that the activation of the BCL-2 protein family induced the hepatocyte apoptosis, which played important roles in the formation of NAFLD (Kanda et al., 2018). Compared with the NAFLD patients, the NASH patients showed lowered level of the anti-apoptotic BCL-2 protein, with a strong negative correlation between BCL-2 level and lobular inflammation (El Bassat et al., 2014), which could be explained by the increased BCL-2 concentration in hepatic steatosis, while the hepatic steatosis was a detoxification process because the free fatty acids (FFA) were directly cytotoxic to hepatocytes. The anti-apoptotic processes enhanced the triglyceride formation and inhibited the FFA toxicity, while the high levels of anti-apoptotic BCL-2 revealed in NAFLD suggested its protective role in disease progression (Tarantino et al., 2011). These results indicated that in our study, the significantly up-regulated expression of *BCL-2* in the livers of Landes geese in group W compared to group C suggested that the BSG supplementation reduced the liver damage (i.e., liver inflammation pressure) and enhanced deposition of lipids in the livers. The FA elongase, also known as a long-chain fatty acid-like fatty acid elongase (ELOVL), cooperates with desaturases to synthesize either monounsaturated fatty acids or PUFAs. Studies have shown that the FA elongase 7 (ELOVL7) played an important role in the synthesis of long-chain saturated fatty acids (Green et al., 2010; Naganuma et al., 2011), while the overexpression of *ELOVL7* significantly decreased the concentrations of palmitoleic acid (C16:1) and increased the concentrations of vaccine (C18:1) (Shi et al., 2019). These results were consistent with the findings revealed in our study (**Table 6**).

The fibroblast growth factors (FGFs) are a polypeptide family, with the FGF10 as an important intercellular signaling molecule in adipogenesis and highly expressed in adipose tissue (Itoh and Ornitz, 2011). Furthermore, the FGF10 stimulated cell proliferation of white adipose tissue and played an essential role in adipogenesis (Matsubara et al., 2013). It was reported that the overexpression of *FGF10* mainly activated the PI3K-Akt pathway to play a protective role in mouse liver (Li S. T. et al., 2021). These results suggested that the hepatocyte growth factor (HGF) played an important role in liver adipose tissue. In our study, the significantly up-regulated expressions of the *FGF10* and *HGF* genes in the group W of Landes geese indicated the enhanced synthesis of active glycogen and protein and lipid differentiation in the livers of these geese. Our results were consistent with those previously reported, strongly indicating that FGF10 was involved in adipose expression and played an important role in the formation of fatty liver in geese.

The heat shock proteins (HSPs) constitute a large family of highly homologous chaperone proteins that are induced in response to elevated temperature, and more generally in response to environmental, physical, and chemical stresses (Bonam et al., 2019). Previous studies showed that the heat stress could increase the HSP70 levels in goats, while the cell metabolism was accelerated and the respiratory function was enhanced (Dangi et al., 2015). Furthermore, it was reported that the probiotics reduced the *HSP60* gene and protein expression levels in mouse model of alcoholic liver (Barone et al., 2016). Our results of the KEGG enrichment analysis showed that under the treatment of BSG, the down-regulated genes were predominantly enriched in the protein processing in endoplasmic reticulum and endocytosis (**Table 8**), in particular, the expressions of *HSPA8*, *HSPA2*, and *HSPH1* were significantly down-regulated in the group W of Landes geese. These results indicated that overfeeding could lead to chronic stress in the Landes geese. However, the heat stress genes were down-regulated in the group W of Landes geese, probably due to the alleviation of oxidative stress caused by the microorganisms in the fermented BSG.

In recent years, due to the rapid increases in global feed prices, there has been a rapidly growing interest in the use of industrial by-products as alternative feeds. However, the by-products of grains are generally not favored due to their rich anti-nutritional factors and the difficulties to preserve under regular practical conditions (Jackowski et al., 2020). With the rapid development of the microbial fermentation technology, the solutions to the problems of waste of resources and the production performance of geese have been gradually identified and established. In our study, the results showed that the addition of BSG in feed of Landes geese generated the optimal effect on liver fat deposition in the group W of Landes geese

during the entire experiment, probably due to the production of endogenous ethanol by the microorganisms in BSG and the secondary sphingolipid metabolism involved in the adaptation of the gut to overfeeding and maintaining the structural integrity of the gut, as reported previously (Gu et al., 2020). Consistently, the cecal microbiota was closely involved in the sphingolipid metabolism (Li et al., 2019). These results suggested that the cecal microbiota contributed significantly to the regulation of fat deposition, benefiting the development of technical strategies for the significant advancement of the foie gras industry.

## Conclusion

In conclusion, our study revealed the beneficial effects of BSG as the feed additives on the growth performance during the rearing stage (days 5–60) of Landes geese, with both the BW and ADG of the Landes geese significantly increased, whereas the optimal effect of BSG on liver fat deposition was achieved during the overfeeding stage (days 61–90). The intestinal microbiota compositions of Landes geese on day 90 were altered by the addition of BSG, mainly increasing the relative abundance of *Bacteroides* and inhibiting Gram-negative pathogenic bacteria such as members of *prevotellaceae_Ga6A1_group*. Results of the transcriptomics analysis showed that addition of BSG to Landes geese diets altered the expression of genes involved in PI3K-Akt signaling pathway and sphingolipid metabolism in the liver. These beneficial effects were probably caused by either the endogenous ethanol-producing microorganisms in BSG or the fermentation products of BSG mitigating the development of NAFLD. Further studies are necessary to explicitly explore the molecular mechanism underlying the formation of NAFLD with the involvement of microorganisms in BSG. Our study provided novel experimental evidence based on the cecal microbiota to support the investigations and applications of BSG in the regulation of the fat deposition by modulating the gut microbiota in the Landes geese.

## Data availability statement

The datasets presented in this study can be found in online repositories. The names of the repository/repositories and accession number(s) can be found in the article/**Supplementary material**.

## Ethics statement

This animal study was reviewed and approved by The Committee on the Ethics of Animal Experiments of the College of Veterinary Medicine, Huazhong Agricultural University (NO. HZAUGE–2020–0001).

## Author contributions

PX, DS, ZZ, ZL, and YX: conceptualization. PX, YH, PC, XW, SL, JW, FM, and YX: methodology. PX and PC: validation. PX: formal analysis, investigation, and data curation. YX: resources. PX and YH: software and writing—original draft preparation. YX and SC: writing—review and editing. All authors have read and agreed to the published version of the manuscript.

## Funding

This research was funded by the Innovative Job Funds of Agricultural Science and Technology of Hubei Province, China (Grant number: 2021-620-000-001-030).

## Acknowledgments

The authors thank Qiuyuan Li and Hongxia Ding at the Huazhong Agricultural University for their laboratory assistance.

## Conflict of interest

The authors declare that the research was conducted in the absence of any commercial or financial relationships that could be construed as a potential conflict of interest.

## Publisher's note



## Supplementary material

The Supplementary Material for this article can be found online at: https://www.frontiersin.org/articles/10.3389/fmicb.2022.970563/full#supplementary-material

SUPPLEMENTARY FIGURE 1
The rarefaction curves of the cecal microbial communities in the control (group C) and three experimental groups (B, F, and W) of Landes geese in 60 and 90 days. Group B, added with 4% BSG in the overfeeding

stage (days 61–90); Group F, added with 4% BSG in the rearing stage (days 5–60); Group W, added with 4% BSG in the all stage (days 5–90).

SUPPLEMENTARY TABLE 1
Ingredients and nutrient compositions of diets (%) in the control (group C) and three experimental groups (B, F, and W) of Landes geese during the rearing stage (days 5–15).

SUPPLEMENTARY TABLE 2
Ingredients and nutrient compositions of diets (%) in the control (group C) and three experimental groups (B, F, and W) of Landes geese during the rearing stage (days 16–60).

SUPPLEMENTARY TABLE 3
Ingredients and nutrient compositions of diets (%) in the control (group C) and three experimental groups (B, F, and W) of Landes geese during the overfeeding stage (days 61–90).

SUPPLEMENTARY TABLE 4
Primers and their sequences used in the quantitative real-time PCR (qRT-PCR) analysis in this study. "F" and "R" at the end of each primer name indicate the forward and reverse primers, respectively.

SUPPLEMENTARY TABLE 5
Summary of 16S rRNA sequencing data based on the cecal contents in the control (group C) and three experimental groups (B, F, and W) of Landes geese in 60 and 90 days.

SUPPLEMENTARY TABLE 6
Summary of sequencing data based on the liver transcriptomics analysis the control (group C) and three experimental groups (B, F, and W) of Landes geese in 60 and 90 days.

SUPPLEMENTARY TABLE 7
Differentially expressed genes between the control and experimental groups.

SUPPLEMENTARY TABLE 8
Gene Ontology terms annotated based on the DEGs between control and experimental groups.

# References

Alizadeh, M., Rodriguez-Lecompte, J. C., Rogiewicz, A., Patterson, R., and Slominski, B. A. (2016). Effect of yeast-derived products and distillers dried grains with solubles (DDGS) on growth performance, gut morphology, and gene expression of pattern recognition receptors and cytokines in broiler chickens. *Poult. Sci.* 95, 507–517. doi: 10.3382/ps/pev362

Al-Khalaifah, H. S., Shahin, S. E., Omar, A. E., Mohammed, H. A., Mahmoud, H. I., and Ibrahim, D. (2020). Effects of graded levels of microbial fermented or enzymatically treated dried brewer's grains on growth, digestive and nutrient transporter genes expression and cost effectiveness in broiler chickens. *BMC Veter. Res.* 16:424. doi: 10.1186/s12917-020-02603-0

Amoah, K. O., Asiedu, P., Wallace, P., Bumbie, G. Z., and Rhule, S. (2017). The performance of pigs at different phases of growth on sun-dried brewers spent grain. *Livestock Res. Rural Dev.* 29:90.

An, D. D., Na, C. Z., Bielawski, J., Hannun, Y. A., and Kasper, D. L. (2011). Membrane sphingolipids as essential molecular signals for *Bacteroides* survival in the intestine. *Proc. Natl. Acad. Sci. U.S.A.* 108, 4666–4671. doi: 10.1073/pnas.1001501107

Aruwa, C. E., Pillay, C., Nyaga, M. M., and Sabiu, S. (2021). Poultry gut health - microbiome functions, environmental impacts, microbiome engineering and advancements in characterization technologies. *J. Anim. Sci. Biotechnol.* 12:119. doi: 10.1186/s40104-021-00640-9

Bai, Y., Zhou, X., Li, N., Zhao, J., Ye, H., Zhang, S., et al. (2021). In vitro fermentation characteristics and fiber-degrading enzyme kinetics of cellulose, arabinoxylan, β-glucan and glucomannan by pig fecal microbiota. *Microorganisms* 9:1071. doi: 10.3390/microorganisms9051071

Bajaj, J. S., and Hylemon, P. B. (2018). Gut-liver axis alterations in alcoholic liver disease: Are bile acids the answer? *Hepatology* 67, 2074–2075. doi: 10.1002/hep.29760

Baraona, E., and Lieber, C. S. (1979). Effects of ethanol on lipid-metabolism. *J. Lipid Res.* 20, 289–315.

Barone, R., Rappa, F., Macaluso, F., Bavisotto, C. C., Sangiorgi, C., Di Paola, G., et al. (2016). Alcoholic liver disease: A mouse model reveals protection by *Lactobacillus fermentum*. *Clin. Transl. Gastroenterol.* 7:e138. doi: 10.1038/ctg.2015.66

Bianco, A., Budroni, M., Zara, S., Mannazzu, I., Fancello, F., and Zara, G. (2020). The role of microorganisms on biotransformation of brewers' spent grain. *Appl. Microbiol. Biotechnol.* 104, 8661–8678. doi: 10.1007/s00253-020-10843-1

Bonam, S. R., Ruff, M., and Muller, S. (2019). HSPA8/HSC70 in immune disorders: A molecular rheostat that adjusts chaperone-mediated autophagy substrates. *Cells* 8:849. doi: 10.3390/cells8080849

Bonifácio-Lopes, T., Vilas Boas, A. A., Coscueta, E. R., Costa, E. M., Silva, S., Campos, D., et al. (2020). Bioactive extracts from brewer's spent grain. *Food Funct.* 11, 8963–8977. doi: 10.1039/d0fo01426e

Boursier, J., and Diehl, A. M. (2016). Nonalcoholic fatty liver disease and the gut microbiome. *Clin. Liver Dis.* 20, 263–275. doi: 10.1016/j.cld.2015.10.012

Campfield, L. A., and Smith, F. J. (2003). Blood glucose dynamics and control of meal initiation: A pattern detection and recognition theory. *Physiol. Rev.* 83, 25–58. doi: 10.1152/physrev.00019.2002

Caporaso, J. G., Kuczynski, J., Stombaugh, J., Bittinger, K., Bushman, F. D., Costello, E. K., et al. (2010). QIIME allows analysis of high-throughput community sequencing data. *Nat. Methods* 7, 335–336. doi: 10.1038/nmeth.f.303

Chen, X., Du, X., Shen, J., Lu, L., and Wang, W. (2016). Original research: Effect of various dietary fats on fatty acid profile in duck liver: Efficient conversion of short-chain to long-chain omega-3 fatty acids. *Exp. Biol. Med.* 242, 80–87. doi: 10.1177/1535370216664031

Chen, X., Zhang, Z., Li, H., Zhao, J., Wei, X., Lin, W., et al. (2020). Endogenous ethanol produced by intestinal bacteria induces mitochondrial dysfunction in non-alcoholic fatty liver disease. *J. Gastroenterol. Hepatol.* 35, 2009–2019. doi: 10.1111/jgh.15027

Conti, H. R., Shen, F., Nayyar, N., Stocum, E., Sun, J. N., Lindemann, M. J., et al. (2009). Th17 cells and IL-17 receptor signaling are essential for mucosal host defense against oral candidiasis. *J. Exp. Med.* 206, 299–311. doi: 10.1084/jem.20081463

Cooray, S. T., Lee, J. J. L., and Chen, W. N. (2017). Evaluation of brewers' spent grain as a novel media for yeast growth. *AMB Express* 7:117. doi: 10.1186/s13568-017-0414-1

Cope, K., Risby, T., and Diehl, A. M. (2000). Increased gastrointestinal ethanol production in obese mice: Implications for fatty liver disease pathogenesis. *Gastroenterology* 119, 1340–1347. doi: 10.1053/gast.2000.19267

Dangi, S. S., Gupta, M., Dangi, S. K., Chouhan, V. S., Maurya, V. P., Kumar, P., et al. (2015). Expression of HSPs: An adaptive mechanism during long-term heat stress in goats (*Capra hircus*). *Int. J. Biometeorol.* 59, 1095–1106. doi: 10.1007/s00484-014-0922-5

Denstadli, V., Westereng, B., Biniyam, H. G., Ballance, S., Knutsen, S. H., and Svihus, B. (2010). Effects of structure and xylanase treatment of brewers' spent grain on performance and nutrient availability in broiler chickens. *Br. Poult. Sci.* 51, 419–426. doi: 10.1080/00071668.2010.495745

Derakhshani, H., Tun, H. M., and Khafipour, E. (2016). An extended single-index multiplexed 16S rRNA sequencing for microbial community analysis on MiSeq illumina platforms. *J. Basic Microbiol.* 56, 321–326. doi: 10.1002/jobm.201500420

Dong, L., Zhong, Z. X., Cui, H. H., Wang, S. N., Luo, Y., Yu, L. H., et al. (2020). Effects of rumen-protected betaine supplementation on meat quality and the composition of fatty and amino acids in growing lambs. *Animal* 14, 435–444. doi: 10.1017/S1751731119002258

El Bassat, H., Ziada, D. H., Hasby, E. A., Nagy, H., and Abo Ryia, M. H. (2014). Apoptotic and anti-apoptotic seromarkers for assessment of disease severity of non-alcoholic steatohepatitis. *Arab J. Gastroenterol.* 15, 6–11. doi: 10.1016/j.ajg.2014.01.009

Even, M., Davail, S., Rey, M., Tavernier, A., Houssier, M., Bernadet, M. D., et al. (2018). Probiotics strains modulate gut microbiota and lipid metabolism in mule ducks. *Open Microbiol. J.* 12, 71–93. doi: 10.2174/1874285801812010071

Frasson, F. M., Carvalho, S., Jaurena, G., Menegon, A. M., Machado Severo, M., Henriques da Motta, J., et al. (2018). Intake and performance of lambs finished in feedlot with wet brewer's grains. *J. Anim. Sci. Technol.* 60:12. doi: 10.1186/s40781-018-0166-8

Fu, X. D., Liu, Z. M., Zhu, C. L., Mou, H. J., and Kong, Q. (2019). Nondigestible carbohydrates, butyrate, and butyrate-producing bacteria. *Crit. Rev. Food Sci. Nutr.* 59, S130–S152. doi: 10.1080/10408398.2018.1542587

Gillingham, L. G., Harris-Janz, S., and Jones, P. J. (2011). Dietary monounsaturated fatty acids are protective against metabolic syndrome and cardiovascular disease risk factors. *Lipids* 46, 209–228. doi: 10.1007/s11745-010-3524-y

Gorden, D. L., Myers, D. S., Ivanova, P. T., Fahy, E., Maurya, M. R., Gupta, S., et al. (2015). Biomarkers of NAFLD progression: A lipidomics approach to an epidemic. *J. Lipid Res.* 56, 722–736. doi: 10.1194/jlr.P056002

Green, C. D., Ozguden-Akkoc, C. G., Wang, Y., Jump, D. B., and Olson, L. K. (2010). Role of fatty acid elongases in determination of de novo synthesized monounsaturated fatty acid species. *J. Lipid Res.* 51, 1871–1877. doi: 10.1194/jlr.M004747

Griffin, H. D., Butterwith, S. C., and Goddard, C. (2009). Contribution of lipoprotein-lipase to differences in fatness between broiler and layer-strain chickens. *Br. Poult. Sci.* 28, 197–206. doi: 10.1080/00071668708416953

Gu, W., Wen, K., Yan, C. C., Li, S., Liu, T. J., Xu, C., et al. (2020). Maintaining intestinal structural integrity is a potential protective mechanism against inflammation in goose fatty liver. *Poult. Sci.* 99, 5297–5307. doi: 10.1016/j.psj.2020.08.052

Hamid, H., Zhang, J. Y., Li, W. X., Liu, C., Li, M. L., Zhao, L. H., et al. (2019). Interactions between the cecal microbiota and non-alcoholic steatohepatitis using laying hens as the model. *Poult. Sci.* 98, 2509–2521. doi: 10.3382/ps/pey596

Han, C. C., Wang, J. W., Xu, H. Y., Li, L., Ye, J. Q., Jiang, L., et al. (2008). Effect of overfeeding on plasma parameters and mRNA expression of genes associated with hepatic lipogenesis in geese. *Asian Austral. J. Anim. Sci.* 21, 590–595. doi: 10.5713/ajas.2008.70472

Han, C. C., Wei, S. H., He, F., Liu, D. D., Wan, H. F., Liu, H. H., et al. (2015). The regulation of lipid deposition by insulin in goose liver cells is mediated by the PI3K-AKT-mTOR signaling pathway. *PLoS One* 10:e0098759. doi: 10.1371/journal.pone.0098759

He, Z. X., He, M. L., Zhao, Y. L., Xu, L., Walker, N. D., Beauchemin, K. A., et al. (2015). Effect of wheat dried distillers grains and enzyme supplementation on growth rates, feed conversion ratio and beef fatty acid profile in feedlot steers. *Animal* 9, 1740–1746. doi: 10.1017/S1751731115000944

Hermier, D. (1997). Lipoprotein metabolism and fattening in poultry. *J. Nutr.* 127, S805–S808. doi: 10.1093/jn/127.5.805S

Hermier, D., Saadoun, A., Salichon, M.-R., Sellier, N., Rousselot-Paillet, D., and Chapman, M. J. (1991). Plasma lipoproteins and liver lipids in two breeds of geese with different susceptibility to hepatic steatosis: Changes induced by development and force-feeding. *Lipids* 26, 331–339. doi: 10.1007/bf02537194

Hermier, D., Salichon, M. R., Guy, G., and Peresson, R. (1999). Differential channelling of liver lipids in relation to susceptibility to hepatic steatosis in the goose. *Poult. Sci.* 78, 1398–1406. doi: 10.1093/ps/78.10.1398

Ikonen, E. (2008). Cellular cholesterol trafficking and compartmentalization. *Nat. Rev. Mol. Cell Biol.* 9, 125–138. doi: 10.1038/nrm2336

Itoh, N., and Ornitz, D. M. (2011). Fibroblast growth factors: From molecular evolution to roles in development, metabolism and disease. *J. Biochem.* 149, 121–130. doi: 10.1093/jb/mvq121

Jackowski, M., Niedzwiecki, L., Jagiello, K., Uchanska, O., and Trusek, A. (2020). Brewer's spent grains-valuable beer industry by-product. *Biomolecules* 10:1669. doi: 10.3390/biom10121669

Jandhyala, S. M., Talukdar, R., Subramanyam, C., Vuyyuru, H., Sasikala, M., and Nageshwar Reddy, D. (2015). Role of the normal gut microbiota. *World J. Gastroenterol.* 21, 8787–8803. doi: 10.3748/wjg.v21.i29.8787

Jasirwan, C. O. M., Muradi, A., Hasan, I., Simadibrata, M., and Rinaldi, I. (2021). Correlation of gut Firmicutes/Bacteroidetes ratio with fibrosis and steatosis stratified by body mass index in patients with non-alcoholic fatty liver disease. *Biosci. Microbiota Food Health* 40, 50–58. doi: 10.12938/bmfh.2020-046

Kanda, T., Matsuoka, S., Yamazaki, M., Shibata, T., Nirei, K., Takahashi, H., et al. (2018). Apoptosis and non-alcoholic fatty liver diseases. *World J. Gastroenterol.* 24, 2661–2672. doi: 10.3748/wjg.v24.i25.2661

Kani, A. H., Alavian, S. M., Esmaillzadeh, A., Adibi, P., and Azadbakht, L. (2013). Dietary quality indices and biochemical parameters among patients with non alcoholic fatty liver disease (NAFLD). *Hepat. Mon.* 13:e10943. doi: 10.5812/hepatmon.10943

Knudsen, C., Arroyo, J., Even, M., Cauquil, L., Pascal, G., Fernandez, X., et al. (2021). The intestinal microbial composition in Greylag geese differs with steatosis induction mode: Spontaneous or induced by overfeeding. *Anim. Microbiome* 3:6. doi: 10.1186/s42523-020-00067-z

Kunde, S. S., Lazenby, A. J., Clements, R. H., and Abrams, G. A. (2005). Spectrum of NAFLD and diagnostic implications of the proposed new normal range for serum ALT in obese women. *Hepatology* 42, 650–656. doi: 10.1002/hep.20818

Lao, E. J., Dimoso, N., Raymond, J., and Mbega, E. R. (2020). The prebiotic potential of brewers' spent grain on livestock's health: A review. *Trop. Anim. Health Product.* 52, 461–472. doi: 10.1007/s11250-019-02120-9

Lee, M. S., Yoon, J. W., and Tesh, V. L. (2020). Editorial: Recent advances in understanding the pathogenesis of shiga toxin-producing *Shigella* and *Escherichia coli*. *Front. Cell Infect. Microbiol.* 10:620703. doi: 10.3389/fcimb.2020.620703

Li, F. N., Duan, Y. H., Li, Y. H., Tang, Y. L., Geng, M. M., Oladele, O. A., et al. (2015). Effects of dietary n-6:n-3 PUFA ratio on fatty acid composition, free amino acid profile and gene expression of transporters in finishing pigs. *Br. J. Nutr.* 113, 739–748. doi: 10.1017/S0007114514004346

Li, N. N., Li, W., Feng, J. X., Zhang, W. W., Zhang, R., Du, S. H., et al. (2021). High alcohol-producing *Klebsiella pneumoniae* causes fatty liver disease through 2,3–butanediol fermentation pathway in vivo. *Gut Microbes* 13:1979883. doi: 10.1080/19490976.2021.1979883

Li, S. T., Zhu, Z. X., Xue, M., Pan, X. B., Tong, G. Z., Yi, X. C., et al. (2021). The protective effects of fibroblast growth factor 10 against hepatic ischemia-reperfusion injury in mice. *Redox Biol.* 40:101859. doi: 10.1016/j.redox.2021.101859

Li, W., Edwards, A., Riehle, C., Cox, M. S., Raabis, S., Skarlupka, J. H., et al. (2019). Transcriptomics analysis of host liver and meta-transcriptome analysis of rumen epimural microbial community in young calves treated with artificial dosing of rumen content from adult donor cow. *Sci. Rep.* 9:790. doi: 10.1038/s41598-018-37033-4

Liu, W. M., Lai, S. J., Lu, L. Z., Shi, F. X., Zhang, J., Liu, Y., et al. (2011). Effect of dietary fatty acids on serum parameters, fatty acid compositions, and liver histology in Shaoxing laying ducks. *J. Zhejiang Univ. Sci. B* 12, 736–743. doi: 10.1631/jzus.B1000329

Liu, X., Li, P., He, C., Qu, X., and Guo, S. (2020). Comparison of overfed Xupu and Landes geese in performance, fatty acid composition, enzymes and gene expression related to lipid metabolism. *Asian Austral. J. Anim. Sci.* 33, 1957–1964. doi: 10.5713/ajas.19.0842

Locsmándi, L., Hegedüs, G., Andrássy-Baka, G., Bogenfürst, F., and Romvári, R. (2007). Following the goose liver development by means of cross-sectional digital imaging, liver histology and blood biochemical parameters. *Acta Biol. Hung.* 58, 35–48. doi: 10.1556/ABiol.58.2007.1.4

Lu, L., Chen, Y., Wang, Z., Li, X., Chen, W., Tao, Z., et al. (2015). The goose genome sequence leads to insights into the evolution of waterfowl and susceptibility to fatty liver. *Genome Biol.* 16:89. doi: 10.1186/s13059-015-0652-y

Matsubara, Y., Aoki, M., Endo, T., and Sato, K. (2013). Characterization of the expression profiles of adipogenesis-related factors, ZNF423, KLFs and FGF10, during preadipocyte differentiation and abdominal adipose tissue development in chickens. *Comp. Biochem. Physiol. B Biochem. Mol. Biol.* 165, 189–195. doi: 10.1016/j.cbpb.2013.04.002

Min, H. K., Kapoor, A., Fuchs, M., Mirshahi, F., Zhou, H. P., Maher, J., et al. (2012). Increased hepatic synthesis and dysregulation of cholesterol metabolism is associated with the severity of nonalcoholic fatty liver disease. *Cell Metab.* 15, 665–674. doi: 10.1016/j.cmet.2012.04.004

Mourot, J., Guy, G., Lagarrigue, S., Peiniau, P., and Hermier, D. (2000). Role of hepatic lipogenesis in the susceptibility to fatty liver in the goose (*Anser anser*). *Comp. Biochem. Physiol. Part B Biochem. Mol. Biol.* 126, 81–87. doi: 10.1016/s0305-0491(00)00171-1

Mozduri, Z., Lo, B., Marty-Gasset, N., Masoudi, A. A., Arroyo, J., Morisson, M., et al. (2021). Application of metabolomics to identify hepatic biomarkers of foie gras qualities in duck. *Front. Physiol.* 12:694809. doi: 10.3389/fphys.2021.694809

Mukasafari, M. A., Ambula, M. K., Karege, C., and King'ori, A. M. (2018). Effects of substituting sow and weaner meal with brewers' spent grains on the performance of growing pigs in Rwanda. *Trop. Anim. Health Product.* 50, 393–398. doi: 10.1007/s11250-017-1446-x

Mussatto, S. I. (2014). Brewer's spent grain: A valuable feedstock for industrial applications. *J. Sci. Food Agric.* 94, 1264–1275. doi: 10.1002/jsfa.6486

Naganuma, T., Sato, Y., Sassa, T., Ohno, Y., and Kihara, A. (2011). Biochemical characterization of the very long-chain fatty acid elongase ELOVL7. *FEBS Lett.* 585, 3337–3341. doi: 10.1016/j.febslet.2011.09.024

Nair, S., Cope, K., Terence, R. H., and Diehl, A. M. (2001). Obesity and female gender increase breath ethanol concentration: Potential implications for the pathogenesis of nonalcoholic steatohepatitis. *Am. J. Gastroenterol.* 96, 1200–1204. doi: 10.1111/j.1572-0241.2001.03702.x

Oike, H., Wakamori, M., Mori, Y., Nakanishi, H., Taguchi, R., Misaka, T., et al. (2006). Arachidonic acid can function as a signaling modulator by activating the TRPM5 cation channel in taste receptor cells. *Biochim. Biophys. Acta Mol. Cell Biol. Lipids* 1761, 1078–1084. doi: 10.1016/j.bbalip.2006.07.005

Panasevich, M. R., Meers, G. M., Linden, M. A., Booth, F. W., Perfield, J. W., Fritsche, K. L., et al. (2018). High-fat, high-fructose, high-cholesterol feeding causes severe NASH and cecal microbiota dysbiosis in juvenile Ossabaw swine. *Am. J. Physiol. Endocrinol. Metab.* 314, E78–E92. doi: 10.1152/ajpendo.00015.2017

Panasevich, M. R., Morris, E. M., Chintapalli, S. V., Wankhade, U. D., Shankar, K., Britton, S. L., et al. (2016). Gut microbiota are linked to increased susceptibility to hepatic steatosis in low-aerobic-capacity rats fed an acute high-fat diet. *Am. J. Physiol. Gastrointest. Liver Physiol.* 311, G166–G179. doi: 10.1152/ajpgi.00065.2016

Peng, C., Ouyang, Y., Lu, N., and Li, N. (2020). The NF-κB signaling pathway, the microbiota, and gastrointestinal tumorigenesis: Recent advances. *Front. Immunol.* 11:1387. doi: 10.3389/fimmu.2020.01387

Pinheiro, T., Coelho, E., Romaní, A., and Domingues, L. (2019). Intensifying ethanol production from brewer's spent grain waste: Use of whole slurry at high solid loadings. *New Biotechnol.* 53, 1–8. doi: 10.1016/j.nbt.2019.06.005

Rachwał, K., Waśko, A., Gustaw, K., and Polak-Berecka, M. (2020). Utilization of brewery wastes in food industry. *PeerJ* 8:e9427. doi: 10.7717/peerj.9427

Rojas-Chamorro, J. A., Romero-Garcia, J. M., Cara, C., Romero, I., and Castro, E. (2020). Improved ethanol production from the slurry of pretreated brewers' spent grain through different co-fermentation strategies. *Bioresour. Technol.* 296:122367. doi: 10.1016/j

Ruan, D., Fouad, A. M., Fan, Q. L., Chen, W., Xia, W. G., Wang, S., et al. (2018). Effects of corn dried distillers' grains with solubles on performance, egg quality, yolk fatty acid composition and oxidative status in laying ducks. *Poult. Sci.* 97, 568–577. doi: 10.3382/ps/pex331

Safari, Z., and Gerard, P. (2019). The links between the gut microbiome and non-alcoholic fatty liver disease (NAFLD). *Cell. Mol. Life Sci.* 76, 1541–1558. doi: 10.1007/s00018-019-03011-w

Shi, H. B., Wang, L., Luo, J., Liu, J. X., Loor, J. J., and Liu, H. Y. (2019). Fatty acid elongase 7 (ELOVL7) plays a role in the synthesis of long-chain unsaturated fatty acids in goat mammary epithelial cells. *Animals* 9:389. doi: 10.3390/ani9060389

Shi, J., Zhao, D., Song, S., Zhang, M., Zamaratskaia, G., Xu, X., et al. (2020). High-Meat-protein high-fat diet induced dysbiosis of gut microbiota and tryptophan metabolism in Wistar rats. *J. Agric. Food Chem.* 68, 6333–6346. doi: 10.1021/acs.jafc.0c00245

Sorbara, M. T., Littmann, E. R., Fontana, E., Moody, T. U., Kohout, C. E., Gjonbalaj, M., et al. (2020). Functional and genomic variation between human-derived isolates of lachnospiraceae reveals inter- and intra-species diversity. *Cell Host Microbe* 28, 134–146.e4. doi: 10.1016/j.chom.2020.05.005

Tarantino, G., Scopacasa, F., Colao, A., Capone, D., Tarantino, M., Grimaldi, E., et al. (2011). Serum Bcl-2 concentrations in overweight-obese subjects with nonalcoholic fatty liver disease. *World J. Gastroenterol.* 17, 5280–5288. doi: 10.3748/wjg.v17.i48.5280

Vasques-Monteiro, I. M. L., Silva-Veiga, F. M., Miranda, C. S., de Andrade Gonçalves, ÉC. B., Daleprane, J. B., and Souza-Mello, V. (2021). A rise in Proteobacteria is an indicator of gut-liver axis-mediated nonalcoholic fatty liver disease in high-fructose-fed adult mice. *Nutr. Res.* 91, 26–35. doi: 10.1016/j.nutres.2021.04.008

Waite, D. W., and Taylor, M. W. (2014). Characterizing the avian gut microbiota: Membership, driving influences, and potential function. *Front. Microbiol.* 5:223. doi: 10.3389/fmicb.2014.00223

Wang, G. S., Jin, L., Li, Y., Tang, Q. Z., Hu, S. L., Xu, H. Y., et al. (2019). Transcriptomic analysis between normal and high-intake feeding geese provides insight into adipose deposition and susceptibility to fatty liver in migratory birds. *BMC Genomics* 20:372. doi: 10.1186/s12864-019-5765-3

Wexler, A. G., and Goodman, A. L. (2017). An insider's perspective: *Bacteroides* as a window into the microbiome. *Nat. Microbiol.* 2:17026. doi: 10.1038/nmicrobiol.2017.26

Wu, F. F., Guo, X. F., Zhang, J. C., Zhang, M., Ou, Z. H., and Peng, Y. Z. (2017). Phascolarctobacterium faecium abundant colonization in human gastrointestinal tract. *Exp. Therap. Med.* 14, 3122–3126. doi: 10.3892/etm.2017.4878

Wu, S., Wang, Y., Huang, C., Zhang, Y., Lan, Z., Wang, X., et al. (2018). Feeding effect of brewer's grains fermented feed on Meihua pig. *Feed Industry* 39, 43–45. doi: 10.13302/j.cnki.fi.2018.02.008

Yan, J., Zhou, B., Xi, Y., Huan, H., Li, M., Yu, J., et al. (2019). Fermented feed regulates growth performance and the cecal microbiota community in geese. *Poult. Sci.* 98, 4673–4684. doi: 10.3382/ps/pez169

Yang, J., Yao, G., Ji, X., and Sui, F. (2020). Effects of solid-state fermentation of brewer's grains on growth performance, immune organ index and meat quality of hybrid Wanxi White goose. *Chin. J. Anim. Sci.* 52, 93–98.

Yu, L., Wang, L., Yi, H., and Wu, X. (2020). Beneficial effects of LRP6-CRISPR on prevention of alcohol-related liver injury surpassed fecal microbiota transplant in a rat model. *Gut Microbes* 11, 1015–1029. doi: 10.1080/19490976.2020.1736457

Yuan, J., Chen, C., Cui, J., Lu, J., Yan, C., Wei, X., et al. (2019). Fatty liver disease caused by high-alcohol-producing *Klebsiella pneumoniae*. *Cell Metab.* 30, 675–688. doi: 10.1016/j.cmet.2019.08.018

Zabed, H., Sahu, J. N., Suely, A., Boyce, A. N., and Faruq, G. (2017). Bioethanol production from renewable sources: Current perspectives and technological progress. *Renew. Sustain. Energy Rev.* 71, 475–501. doi: 10.1016/j.rser.2016.12.076

Zhang, X., Coker, O. O., Chu, E. S., Fu, K., Lau, H. C. H., Wang, Y. X., et al. (2021a). Dietary cholesterol drives fatty liver-associated liver cancer by modulating gut microbiota and metabolites. *Gut* 70, 761–774. doi: 10.1136/gutjnl-2019-319664

Zhang, X., Li, C., Cao, W., and Zhang, Z. (2021b). Alterations of gastric microbiota in gastric cancer and precancerous stages. *Front. Cell Infect. Microbiol.* 11:559148. doi: 10.3389/fcimb.2021.559148

Zhbannikov, I. Y., and Foster, J. A. (2015). MetAmp: Combining amplicon data from multiple markers for OTU analysis. *Bioinformatics* 31, 1830–1832. doi: 10.1093/bioinformatics/btv049

Zhu, L. H., Meng, H., Duan, X. J., Xu, G. Q., Zhang, J., and Gong, D. Q. (2011). Gene expression profile in the liver tissue of geese after overfeeding. *Poult. Sci.* 90, 107–117. doi: 10.3382/ps.2009-00616

frontiers | Frontiers in Microbiology

TYPE Original Research
PUBLISHED 04 October 2022
DOI 10.3389/fmicb.2022.1017804



OPEN ACCESS

EDITED BY
Hui Zhang,
South China Agricultural University, China

REVIEWED BY
Teng-Gen Hu,
Guangdong Academy of Agricultural Sciences (GDAAS), China
Pissared Khuituan,
Prince of Songkla University, Thailand

*CORRESPONDENCE
Jun Sheng
shengjun_ynau@163.com
Yang Tian
tianyang1208@163.com
Yuanhong Fan
2247888136@qq.com

†These authors have contributed equally to this work

SPECIALTY SECTION
This article was submitted to Frontiers in Microbiology | Microorganisms in Vertebrate Digestive Systems, a section of the journal Frontiers in Microbiology

RECEIVED 12 August 2022
ACCEPTED 09 September 2022
PUBLISHED 04 October 2022

CITATION
Gao X, Hu Y, Tao Y, Liu S, Chen H, Li J, Zhao Y, Sheng J, Tian Y and Fan Y (2022) *Cymbopogon citratus* (DC.) Stapf aqueous extract ameliorates loperamide-induced constipation in mice by promoting gastrointestinal motility and regulating the gut microbiota.
*Front. Microbiol.* 13:1017804.
doi: 10.3389/fmicb.2022.1017804



# *Cymbopogon citratus* (DC.) Stapf aqueous extract ameliorates loperamide-induced constipation in mice by promoting gastrointestinal motility and regulating the gut microbiota

Xiaoyu Gao[1†], Yifan Hu[1,2†], Yafei Tao[3], Shuangfeng Liu[3], Haowen Chen[2], Jiayi Li[2], Yan Zhao[4], Jun Sheng[5*], Yang Tian[5*] and Yuanhong Fan[6*]

[1]Engineering Research Center of Development and Utilization of Food and Drug Homologous Resources, Ministry of Education, Yunnan Agricultural University, Kunming, China, [2]College of Agronomy and Biotechnology, Yunnan Agricultural University, Kunming, China, [3]College of Food Science and Technology, Yunnan Agricultural University, Kunming, China, [4]Department of Science and Technology, Yunnan Agricultural University, Kunming, China, [5]Yunnan Provincial Engineering Research Center for Edible and Medicinal Homologous Functional Food, Yunnan Agricultural University, Kunming, China, [6]Yunnan Plateau Characteristic Agricultural Industry Research Institute, Yunnan Agricultural University, Kunming, China

Slow transit constipation (STC) is the most common type of functional constipation. Drugs with good effects and few side effects are urgently needed form the treatment of STC. *Cymbopogon citratus* (DC.) Stapf (CC) is an important medicinal and edible spice plant. The wide range of biological activities suggested that CC may have laxative effects, but thus far, it has not been reported. In this study, the loperamide-induced STC mouse model was used to evaluate the laxative effect of the aqueous extract of CC (CCAE), and the laxative mechanism was systematically explored from the perspectives of the enteric nervous system (ENS), neurotransmitter secretion, gastrointestinal motility factors, intestinal inflammation, gut barrier and gut microbiota. The results showed that CCAE not only decreased the serum vasoactive intestinal polypeptide (VIP), induced nitric oxide synthases (iNOS), and acetylcholinesterase (AchE) in STC mice but also increased the expression of gastrointestinal motility factors in colonic interstitial cells of Cajal (ICCs) and smooth muscle cells (SMCs), thereby significantly shortening the defecation time and improving the gastrointestinal transit rate. The significantly affected gastrointestinal motility factors included stem cell factor receptor (*c-Kit*), stem cell factor (*SCF*), anoctamin 1 (*Ano1*), ryanodine receptor 3 (*RyR3*), smooth muscle myosin light chain kinase (*smMLCK*) and Connexin 43 (*Cx43*).

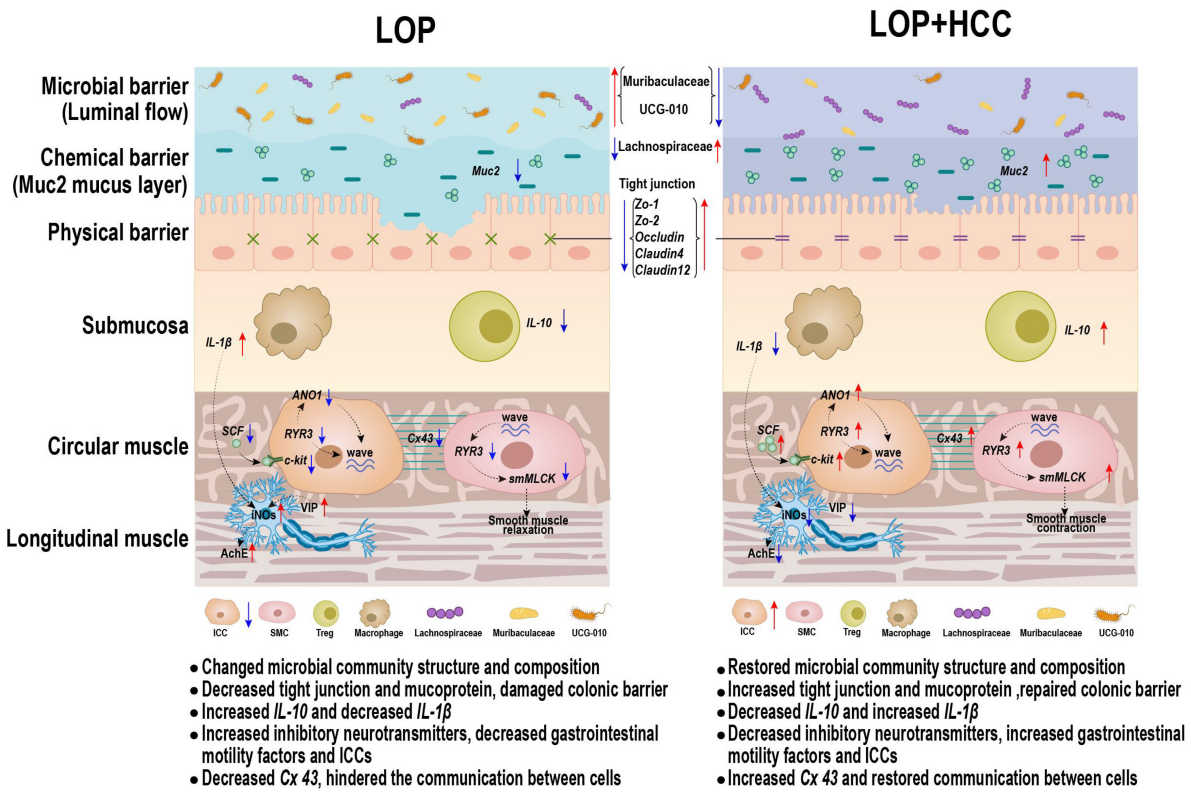


GRAPHICAL ABSTRACT
CCAE might promote intestinal motility by modulating the ENS-ICCs-SMCs network, intestinal inflammation, intestinal barrier, and gut microbiota.

Meanwhile, CCAE could repair loperamide-induced intestinal inflammation and intestinal barrier damage by reducing the expression of the pro-inflammatory factor *IL-1β* and increasing the expression of the anti-inflammatory factor *IL-10*, chemical barrier (*Muc-2*) and mechanical barrier (*Cldn4*, *Cldn12*, *Occludin*, *ZO-1,* and *ZO-2*). Interestingly, CCAE could also partially restore loperamide-induced gut microbial dysbiosis in various aspects, such as microbial diversity, community structure and species composition. Importantly, we established a complex but clear network between gut microbiota and host parameters. Muribaculaceae, Lachnospiraceae and UCG-010 showed the most interesting associations with the laxative phenotypes; several other specific taxa showed significant associations with serum neurotransmitters, gastrointestinal motility factors, intestinal inflammation, and the gut barrier. These findings suggested that CCAE might promote intestinal motility by modulating the ENS-ICCs-SMCs network, intestinal inflammation, intestinal barrier and gut microbiota. CC may be an effective and safe therapeutic choice for STC.

KEYWORDS

**gut microbiota, lemon grass, constipation, gastrointestinal motility, enteric nervous system, intestinal inflammation, gut barrier, Muribaculaceae**

## Introduction

In recent years, due to changes in the human diet and lifestyle, constipation has become increasingly common and has gradually reduced people's quality of life (Bharucha and Lacy, 2020). Constipation can be roughly divided into secondary constipation and functional constipation. Slow transit constipation (STC) is the most common type of functional constipation. STC is characterized by prolonged colonic transit time and reduced colonic high amplitude propulsion and contraction after eating, and the main symptoms are dry stool, difficulty in defecation, and a decrease in stool weight and frequency. At present, most scholars believe that the pathophysiological mechanism of STC may be related to nervous system diseases, abnormal hormone levels *in vivo*, smooth muscle dysfunction, abnormal interstitial cells of Cajal (ICCs), and gut microbiota imbalance.

Medications are still the main method for the treatment of STC, and they can be divided into Western medicine, traditional Chinese medicine and microbial drugs. Mainstream Western medicine therapies represented by various laxatives, prokinetic drugs and secretagogues often fail or have only short-term efficacy and induce side effects (Vriesman et al., 2020). For the treatment of STC, drugs with good effects, few side effects and clearly defined functional components are urgently needed. An innovative and efficacious drug for the treatment of STC may be found in food and natural drug resources.

*Cymbopogon citratus* (DC.) Stapf (CC) is a spice commonly used in soups and grills in Asian countries such as China, India, Thailand, Singapore, Sri Lanka and Vietnam. CC is also a traditional Chinese medicinal plant. Ancient books in China record its effects of dredging wind and collaterals, reducing swelling and pain, and gastric ventilation (Li et al., 2020). Recent scientific studies have shown that CC has antibacterial (Iram et al., 2019), antioxidant (Tiwari et al., 2010), anti-inflammatory (Figueirinha et al., 2010), anti-anxiety (Mendes Hacke et al., 2020) and antidepressant (Umukoro et al., 2017) activities, and it is beneficial in the treatment of diabetes (Borges et al., 2021), liver damage (Uchida et al., 2017), and even cancers (Rojas-Armas et al., 2020; Gomes et al., 2021; Pan et al., 2022).

Although CC has a variety of biological activities, its protective effect on the gastrointestinal tract is the most noteworthy. Volatile CC oil can effectively alleviate gastric ulcers in mice induced by absolute ethanol and aspirin (Fernandes et al., 2012; Venzon et al., 2018) and shows relatively effective inhibition of acetylcholinesterase activity (Madi et al., 2021). CC is also popular as a lemongrass tea in North and South America, West Africa and other countries and can be used to aid digestion (Kieling and Prudencio, 2019), which indicates that the water-soluble part of CC also has good gastrointestinal regulatory function. The research progress of CC in gastrointestinal regulatory activities suggests that it may be effective in relieving constipation. However, whether CC can alleviate constipation and how CC alleviates constipation is still unclear. To this end, the loperamide-induced STC mouse model was used to evaluate the laxative effect of the aqueous extract of CC, and the mechanism was systematically explored from the perspectives of the enteric nervous system (ENS), neurotransmitter secretion, gastrointestinal motility factors, gut barrier, intestinal inflammation and gut microbiota in this study.

Abbreviations: STC, slow transit constipation; CC, *Cymbopogon citratus* (DC.) Stapf; CCAE, aqueous extract of *Cymbopogon citratus* (DC.) Stapf; ENS, enteric nervous system; VIP, vasoactive intestinal polypeptide; iNOS, induced nitric oxide synthases; AchE, acetylcholinesterase; 5-HT, serotonin; ICCs, interstitial cells of Cajal; SMCs, smooth muscle cells; c-Kit, stem cell factor receptor; SCF, stem cell factor; Ano1, anoctamin 1; RyR3, ryanodine receptor 3; smMLCK, smooth muscle myosin light chain kinase; Cx43, connexin 43; FBS, the defecation time of the first black stool; FW, fecal wet weight; FN, fecal number; GTR, gastrointestinal transit rate; TNF-α, tumor necrosis factor-alpha; IL-1β, interleukin-1β; IL-6, interleukin-6; IL-10, interleukin-10; MCP-1, monocyte chemotactic protein-1; Muc2, mucin 2; Occludin, occluding; ZO-1, zonula occludens protein 1; ZO-2, zonula occludens protein 2; Cldn4, claudin 4; Cldn12, claudin 12; LEfSe, linear discriminant analysis effect size; PCoA, principal coordinate analysis; CON, control group; POS, positive control group; LOP, model group, received loperamide; LCC, LCC group (received loperamide and low dosage of CCAE); MCC, MCC group (received loperamide and medium dosage of CCAE); HCC, HCC (received loperamide and high dosage of CCAE).

## Materials and methods

### Preparation and chemical composition determination of *Cymbopogon citratus* (DC.) Stapf aqueous extract

Ultramicro-powder of CC leaves was obtained from a local company in Nujiang City, Yunnan Province (China). Then, 200 g ultramicro-powder was boiled for 3 min in 2 L ultrapure water (pH = 6.8). After cooling to room temperature, the extraction solution was immediately centrifuged at 5,000 rpm for 5 min. The precipitates were collected twice under the same conditions and then discarded. All the supernatants were combined and dried in vacuum freeze-drying equipment for 2–3 days. The final product was greenish brown in color, with a yield of 17.6%. The dried extract was weighed and dissolved in distilled water just before administration to experimental animals. The main nutritional components and phytochemical composition of CC aqueous extract (CCAE) were determined by various methods. The methods are described briefly in **Supplementary Table 1**.

### Animal experimental design

Six-week-old male KM mice (20–25 g) were purchased from Chengdu Dossy Experimental Animals Co., Ltd., China. All mice were housed in specific pathogen-free barrier conditions

(24 ± 1°C, 30–50% humidity, 12-h daylight cycle, lights off at 20:00) with a normal chow diet (10.8% fat, 68.7% carbohydrates, and 20.5% protein, according to caloric intake) and water *ad libitum*. After 7 days of acclimation, the mice were divided into six groups of 12 mice according to their body weights. Three mice were housed together in each cage, and the weight, food intake, and water consumption of the mice were recorded every day. Importantly, 6 mg/kg·bw loperamide (LOP, mg/kg·body weight, Sigma) was used to generate the STC mouse model.

The groups were designed as follows: CON group (control group, received saline solution as vehicle), LOP group (model group, received loperamide), POS group (positive control group, received 900 mg/kg·bw Maren pill from Beijing Tongrentang Pharmaceutical Co., Ltd, Beijing, China), LCC group (received loperamide and 300 mg/kg·bw CCAE, low dosage), MCC group (received loperamide and 600 mg/kg·bw CCAE, medium dosage) and HCC (received loperamide and 900 mg/kg·bw CCAE, high dosage). STC model mice were induced by administration of LOP for 8 days, and at the same time, the mice were gavaged with daily oral doses of 300 μL of solutions designated by their experimental group assignment. Required doses of the Maren pill and CCAE were dissolved in 300 μL of saline solution (**Figure 1A**). All mice were deprived of food but not water overnight before the defecation test and gastrointestinal transit test. All procedures were previously approved by Animal Ethics Committee of Yunnan Agriculture University.

## Defecation test

At 08:00 on the seventh day of the animal experiment, mice were given the normal dose of the drugs by gavage, the homemade ink (300 μL) was given by gavage 30 min later, and the defecation experiment of mice was officially started. The defecation time of the first black stool (FBS) of each mouse was recorded carefully, and the fecal wet weight (FW), fecal number (FN) and water content of stools were also analyzed for each mouse for 6 h from the start of the defecation test to evaluate the laxative effect.

## Gastrointestinal transit test and tissue collection

At 08:00 on the eighth day of the animal experiment, mice were administered the normal dose of the drugs. Thirty minutes later, the ink (300 μL) was given to each mouse. After 20 min, the mice were sacrificed quickly in a chamber saturated with $CO_2$, the abdominal cavity was opened, and the blood was collected from the abdominal aorta. The mesentery of each gastrointestinal tract was carefully stripped, and then the length of the whole small intestine and the length marked by the ink were measured to calculate the gastrointestinal transit rate (GTR).

Meanwhile, the distal ileum, cecum, and proximal colon were accurately dissected from each mouse. The contents of the ileum and colon segments were thoroughly flushed with cold PBS to remove feces. Ceca contents were washed from the cecum in a 2-mL Eppendorf tube containing 1.0 mL cold Milli-Q water. The liver, kidney, and cecum tissues were weighed. Cleaned tissues were subsequently placed in individual cryogenic tubes. Tissues and ceca contents were all flash-frozen in liquid nitrogen and stored at −80°C until analysis.

## Enzyme-linked immunosorbent assay

After the mice were sacrificed, blood was collected immediately and incubated at 37°C for 30 min and centrifuged at 4°C at 3,500 rpm for 10 min, and serum was collected. The contents of neurotransmitters, including vasoactive intestinal polypeptide (VIP), induced nitric oxide synthases (iNOS), acetylcholinesterase (AchE), and serotonin (5-HT), in the serum of mice were determined by using an ultrasensitive enzyme-linked immunosorbent assay (ELISA) kit (Cusabio, China).

## RNA preparation and quantitative PCR analysis of gene expression

FastPure Cell/Tissue Total RNA Isolation Kits (RC101-01, Vazyme, China) were used for the total RNA extraction from mouse tissues. HiScript III RT SuperMix for qPCR (plus gDNA wiper, R323-01, Vazyme, China) was used for RNA reverse transcription, and ChamQ Universal SYBR qPCR Master Mix (Q711-02, Vazyme, China) was used for the quantitative PCR analysis of gene expression. The relative amount of the target mRNA was normalized to the *RPL-19* level, and the results were calculated by the $2^{--\Delta\Delta Ct}$ method. The detailed method has been described previously (Gao et al., 2017). The primer sequences are presented in **Supplementary Table 2**.

## Histopathological examination and immunohistochemistry assay

After the mice of each group were sacrificed, the proximal colon was collected immediately, fixed with 10% formalin, embedded in paraffin, sectioned to a thickness of 5 mm, deparaffinized and submitted to hematoxylin and eosin (H&E, Sigma-Aldrich, Shanghai, China) staining. Immunohistochemistry was performed using a previously

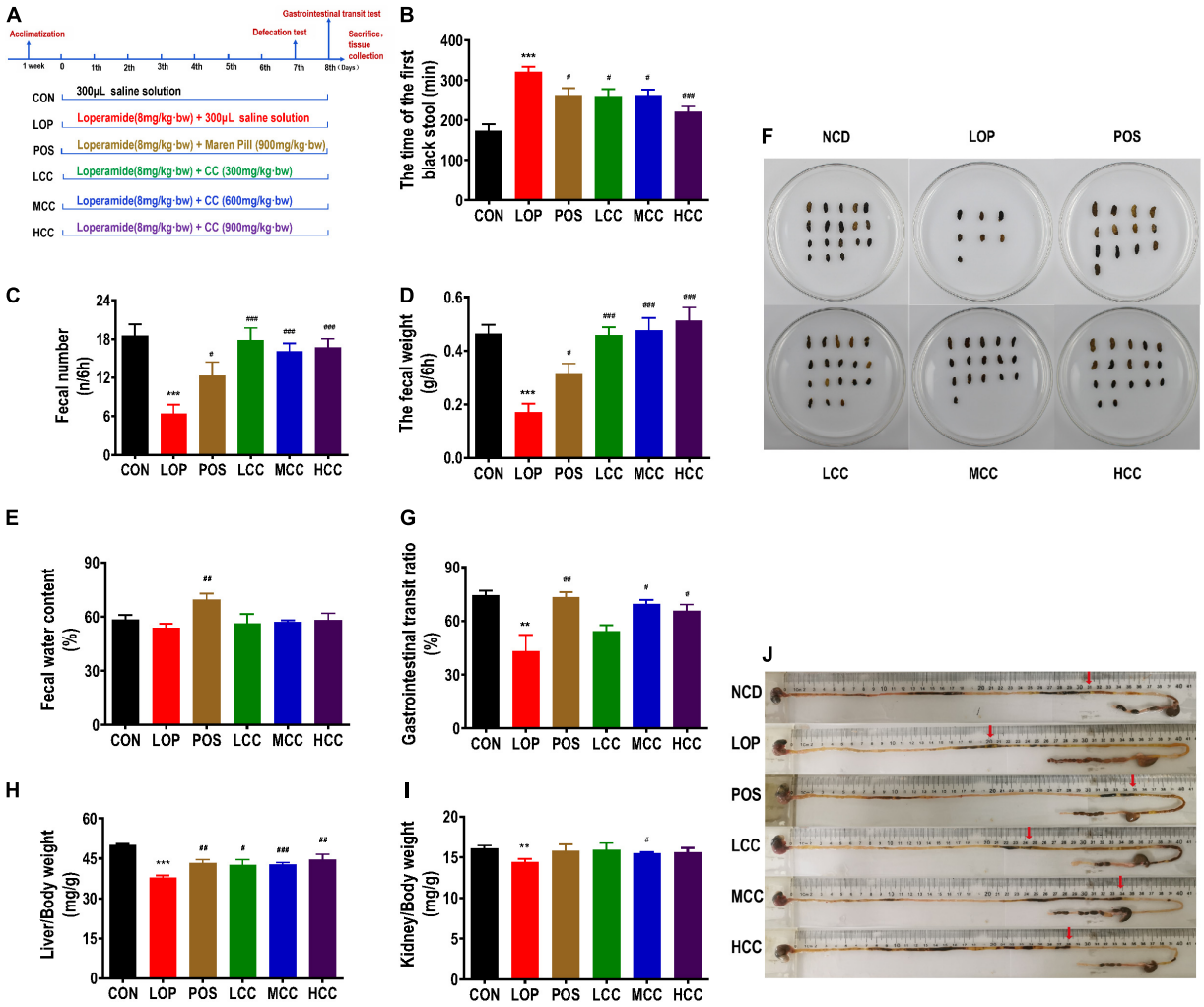


FIGURE 1
Influences of CCAE on loperamide-induced constipation symptoms in mice. **(A)** Grouping and basic workflow of animal experiment. **(B)** The defecation time of the first black stool, FBS. **(C)** Number of feces excreted in 6 h, FN. **(D)** Wet weight of feces excreted in 6 h, FW. **(E)** Fecal water content. **(F)** Representative fecal morphology of each group. **(G)** Gastrointestinal transit rate, GTR. **(H)** Liver index. **(I)** Kidney index. **(J)** Ink advancing distance and intestinal length. The data are expressed as the means ± SEMs ($n$ = 10-12). *, Compared with the CON group; #, compared with the LOP group. $^{**}P < 0.01$, $^{***}P < 0.001$. $\#P < 0.05$, $\#\#P < 0.01$, $\#\#\#P < 0.001$.

described method (Huang et al., 2019). Briefly, 3 μm sections were deparaffinized in xylene and rehydrated in graded alcohol. After quenching endogenous peroxidase activity and blocking non-specific binding, the sections were incubated with a rabbit monoclonal antibody [EPR22566-344] against c-Kit (Abcam, ab256345) overnight at 4°C and then incubated with the secondary antibody goat anti-rabbit IgG (H + L) HRP (ab0101, Abways) at room temperature for 30 min. Finally, the slides were incubated with reagents from the Avidin-Biotin Complex Kit (Vector Laboratories, Inc., Burlingame, USA) and a 3,3′-diaminobenzidine kit (Tiangen, China) according to the manufacturer's instructions. Images were captured with a Nikon Ci-S microscope and Nikon DS-U3 imaging system. The proportion of c-Kit-positive cells in the colonic muscle layer was determined using an image analyzer (Image-Pro Plus 6.0, Media Cybernetics, Inc., Rockville, USA).

## Ceca content DNA extraction and 16S rRNA gene sequencing

After the mice of each group were sacrificed, the contents of the cecum were collected immediately, and the total microbial genomic DNA was extracted by the E.Z.N.A.® soil DNA Kit (Omega Bio-Tek, Norcross, GA, USA) according to the manufacturer's instructions. Agarose gel electrophoresis (1.0%) and a NanoDrop® ND-2000 spectrophotometer (Thermo Scientific Inc., Shanghai, United States) were

used to check the quality and concentration of DNA. Qualified DNA was kept at −80°C until further use. The hypervariable region V3–V4 of the bacterial 16S rRNA gene was amplified with the primer pairs 338F (5′-ACTCCTACGGGAGGCAGCAG-3′) and 806R (5′-GGACTACHVGGGTWTCTAAT-3′) by an ABI GeneAmp® 9700 PCR thermocycler (ABI, Arlington, USA). The PCR conditions and the purification of the PCR products were performed using a previously described method (Gao et al., 2020).

According to the standard protocols by Majorbio Bio-Pharm Technology Co. Ltd. (Shanghai, China), purified amplicons were pooled in equimolar amounts and paired-end sequenced on an Illumina MiSeq PE300 platform (Illumina, San Diego, CA, United States). The raw sequencing reads were deposited into the NCBI Sequence Read Archive database.

## Amplicon sequence processing and analysis

After demultiplexing, the resulting sequences were quality filtered with Fastp and merged with FLASH. Then, the high-quality sequences were de-noised using DADA2 (plugin in the QIIME2 pipeline with recommended parameters), which obtains single nucleotide resolution based on error profiles within samples. DADA2 de-noised sequences are usually called amplicon sequence variants (ASVs). To minimize the effects of sequencing depth on alpha and beta diversity measurements, the number of sequences from each sample was rarefied to 20,000, which still yielded an average Good's coverage of 97.90%. Taxonomic assignment of ASVs was performed using the Naive Bayes consensus taxonomy classifier implemented in QIIME2 and the SILVA 16S rRNA database.

## Bioinformatics analysis

The Majorbio Cloud platform[1] was used to analyze the gut microbiota. Based on the ASV information, rarefaction curves and alpha diversity indices, including observed ASVs, were calculated with Mothur v1.30.1. The similarity among the microbial communities in different samples was determined by principal coordinate analysis (PCoA) based on Bray-Curtis dissimilarity using the Vegan v2.5-3 package. Linear discriminant analysis (LDA) effect size (LEfSe)[2] was performed to identify the significantly abundant taxa (phylum to genera) of bacteria among the different groups (LDA score $> 2.0$, $P < 0.05$).

## Statistical analysis

The data are expressed as the means ± standard errors of the means (SEMs). The unpaired two-tailed Student's *t*-test was performed to analyze two independent groups. Bivariate correlations were calculated using Spearman's *r* coefficients. Heatmaps were constructed using HemI 1.0 software[3]. Unless otherwise specified in the figure legends, the results were considered statistically significant at a *P*-value of $< 0.05$.

# Results

## Nutritional components and phytochemical composition of aqueous extract of *Cymbopogon citratus* (DC.) Stapf

The contents of the main nutritional components are shown in **Supplementary Table 1**. The macronutrients included protein (8.54%), carbohydrate (60.10%), fat (1.99%), water (4.06%), dietary fiber (11.79%), and crude polysaccharide (0.65%). The ash, total acid, and sodium contents were 13.52, 0.26, and 0.11%, respectively.

The phytochemical compositions of CCAE were also examined by widely targeted metabolomics (HPLC-QQQ-MS/MS). As shown in **Supplementary Table 3**, among the top ten chemical compound categories found in CCAE, flavonoids showed the highest relative abundance, accounting for 24.30%. Other compounds that accounted for more than 10% of the total were nucleotides (19.66%), amino acids (15.81%), organ oxygen compounds and carboxylic acids (14.85%), and alkaloids (13.51%).

There were 23 compounds with a relative abundance of more than 1% (**Supplementary Table 4**). Unexpectedly, the compound with the highest abundance belonged to the alkaloid betaine (13.59%). The compounds that accounted for more than 5% of the total are pyrrolidonecarboxylic acid (9.91%), vidarabine (7.45%), proline (6.50%), and homoorientin (5.74%).

## Aqueous extract of *Cymbopogon citratus* (DC.) Stapf alleviated loperamide-induced slow transit constipation symptoms

During the experiments, all mice appeared healthy and showed no abnormal behaviors. Loperamide and CCAE treatment did not show an obvious influence on body weight,

1 https://cloud.majorbio.com

2 http://huttenhower.sph.harvard.edu/LEfSe

3 http://hemi.biocuckoo.org/down.php

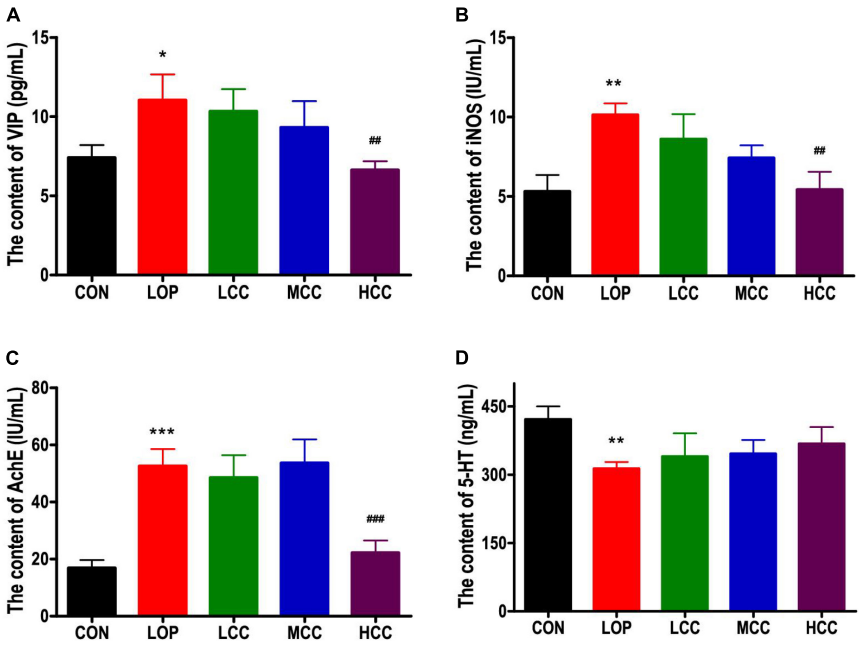


FIGURE 2
**(A)** Vasoactive intestinal polypeptide (VIP), **(B)** induced nitric oxide synthases (iNOS), **(C)** acetylcholinesterase (AchE), and **(D)** serotonin (5-HT) in serum. The data are expressed as the means ± SEMs ($n$ = 8). *, compared with the CON group; #, compared with the LOP group. $^{*}P < 0.05$; $^{**}P < 0.01$; $^{***}P < 0.001$; $^{\#\#}P < 0.01$; $^{\#\#\#}P < 0.001$.

food intake, or water consumption (**Supplementary Figure 1**). Compared with the CON group, FBS in the LOP group was significantly increased, and CCAE treatment shortened the time (**Figure 1B**). In addition, FW and FN in the LOP group were significantly reduced, and CCAE treatment significantly reversed these characteristics of feces (**Figures 1C,D**). However, CCAE did not increase the water content of the feces significantly (**Figure 1E**).

In the gastrointestinal transit test, the medium and high doses of CCAE (MCC and HCC groups) significantly reduced the symptoms of lower GTR induced by loperamide in mice (**Figure 1G**). Notably, CCAE reversed the decrease in liver and kidney indices induced by loperamide (**Figures 1H,I**). In general, CCAE not only alleviated a series of STC symptoms but also reversed the possible negative effects on mouse organs caused by loperamide. CCAE showed a mild and good laxative effect, which was comparable to the effect of the traditional Chinese drug Maren pill.

## Aqueous extract of *Cymbopogon citratus* (DC.) Stapf reversed the changes in serum neurotransmitters induced by loperamide

We investigated whether loperamide-induced defecation delay were accompanied by alterations in the molecular regulators for STC, including iNOS, AchE, VIP, and 5-HT, because they are associated with the proliferation of interstitial cells of Cajal and gastrointestinal mobility. Similar expression patterns were observed for VIP, iNOS, and AchE. These levels were significantly increased only in the LOP, whereas the HCC mice showed reduced levels of these molecules (**Figures 2A–C**). However, the neurotransmitter 5-HT did not have a significant reversal trend in the CCAE treatment groups. In general, LOP increased the serum level of inhibitory neurotransmitters and AchE, and the high dosage of CCAE (HCC group) reduced them to the control level.

## Aqueous extract of *Cymbopogon citratus* (DC.) Stapf enhanced the reduced gastrointestinal motility factors induced by loperamide

Interstitial cells of Cajal (ICCs) and smooth muscle cells (SMCs) play a very important role in regulating gastrointestinal motility. The contraction and relaxation of smooth muscle is controlled by the slow wave of smooth muscle. As the pacemaker cells of smooth muscle and mediators of neurotransmitters, ICCs exist in the muscle layer. Stem cell factor receptor (c-Kit) is a biomarker of ICC. The stem cell factor (SCF) and c-Kit signaling pathways play vital roles in maintaining the development, differentiation and phenotype of ICCs. In

mice in the LOP group, loperamide significantly reduced the mRNA expression of *c-Kit* and *SCF* in the colon; interestingly, CCAE treatment significantly increased their expression (**Figures 3A,B**). The immunohistochemistry results showed that c-Kit expression in colon muscle was decreased with the onset of STC induced by loperamide and increased with CCAE treatment (**Figures 3C,D**).

In ICCs, calcium channels and calcium-activated chloride channels are mainly used to generate $Ca^{2+}$ transients and then generate slow-wave currents, which are transmitted to smooth muscle cells through the network structure. The opening up of ryanodine receptor 3 (RyR3) in calcium channels can increase the release of $Ca^{2+}$, activate myosin light chain kinase (MLCK), and finally cause smooth muscle contraction. Anoctamin 1 (Ano1), a calcium-activated chloride channel, also exists in ICCs. Connexin 43 (Cx43) is the most important connexin constituting gap junctions, which widely exist between ICCs and SMCs and play an important role in slow wave transmission. Mutation and reduction of Cx43 affect the number of gap junction channels on the cell membrane, thereby hindering the transmission of intercellular signals and resulting in gastrointestinal motility dysfunction. In this study, we found that loperamide significantly or nearly significantly reduced the mRNA expression levels of *Ano1*, *RyR3*, *Cx43* and smooth muscle myosin light chain kinase (*smMLCK*), while CCAE significantly restored the expression levels of these genes to varying degrees, even exceeding the expression levels of the CON group (**Figures 3E–H**). In general, CCAE might promote defecation in STC mice by increasing the expression of key gastrointestinal motility factors present in colonic ICCs and SMCs.

## Aqueous extract of *Cymbopogon citratus* (DC.) Stapf improved the intestinal inflammation and intestinal barrier damage induced by loperamide

Intestinal barrier function is essential for maintaining intestinal homeostasis. Dysfunction of the intestinal barrier may trigger an excessive immune response and prolong the inflammatory state, resulting in a variety of gastrointestinal diseases. The mRNA expression of *IL-1*β in the LOP group was higher than that in the CON group, while CCAE treatment significantly reduced it (**Figure 4A**). However, loperamide and CCAE treatment did not have an obvious influence on the mRNA expression of *MCP-1*, *TNF*-α or *IL-6* (**Supplementary Figures 2A–C**). Interestingly, the gene expression of the anti-inflammatory factor *IL-10* was significantly inhibited by loperamide, and CCAE effectively restored the expression level of *IL-10* in the colon of the STC model mice (**Figure 4B**). The regulatory effect on iNOS also suggests that CCAE has a certain anti-inflammatory ability (**Figure 2B**).

The mucus layer is mainly lined with the muco-protein (Muc) skeleton and complex O-linked oligosaccharides, which can separate the bacteria in the intestinal lumen from the intestinal epithelial cells and allow the absorption of nutrients. We found that the mRNA expression of *Muc-2* in the LOP group was inhibited, and CCAE treatment could prevent this inhibition and restore the expression of *Muc-2* to the control level (**Figure 4C**).

Claudin, Occludin, and ZO family proteins play an important role in maintaining the normal physiological functions of epithelial cells. The mRNA expression of tight junction proteins, including *Claudin4*, *Claudin12*, *Occludin*, *ZO-1*, and *ZO-2,* showed similar trends among the groups, all of which were significantly lower in the LOP group than in the CON group, and the CCAE treatment groups had higher levels than the LOP group (**Figures 4D–H**). In general, CCAE showed a good ability to prevent loperamide-induced intestinal inflammation and impaired barrier function.

## Aqueous extract of *Cymbopogon citratus* (DC.) Stapf partially restored loperamide-induced gut microbial dysbiosis

The gut microbiota plays an important role in the progression of STC. The V3–V4 regions of the 16S rRNA genes were sequenced to determine the effect of CCAE (HCC group) on the STC model mice. We obtained 532,597 sequences in a total of 18 samples from the CON, LOP, and HCC groups, each with more than 21,571 valid sequences for subsequent taxonomic analysis. Through systematic bioinformatics analysis, we identified 591 ASVs, 84 genera, 40 families, and 9 phyla. The rarefaction curve of the Sobs index of each sample plateau with the current sequencing indicated that the sequencing result was credible (**Figure 5A**).

The community diversity (Shannon, Sobs, Chao, and Ace) and community evenness (Shannoneven, Simpsoneven) indices were all reduced in the LOP group compared with the CON group (**Figure 5B** and **Supplementary Figure 3**). CCAE administration reversed these loperamide-induced diversity index changes to varying degrees. Notably, CCAE administration significantly improved the loperamide-induced decrease in the Shannon, Shannoneven, and Simpsoneven indices ($P < 0.05$, **Figure 5B** and **Supplementary Figures 3A,B**). These results indicated that CCAE could increase the α diversity of the gut microbiota in STC mice. CCAE also altered β diversity in STC mice (**Figure 5C**). Although the administration of high-dose CCAE could not completely reverse the significant changes induced by loperamide, CCAE still appeared to regulate the abnormal gut microbiota in STC mice. Moreover, CCAE changed the cecal microbial composition of STC mice (**Supplementary Figures 4A–C**), and the microbial

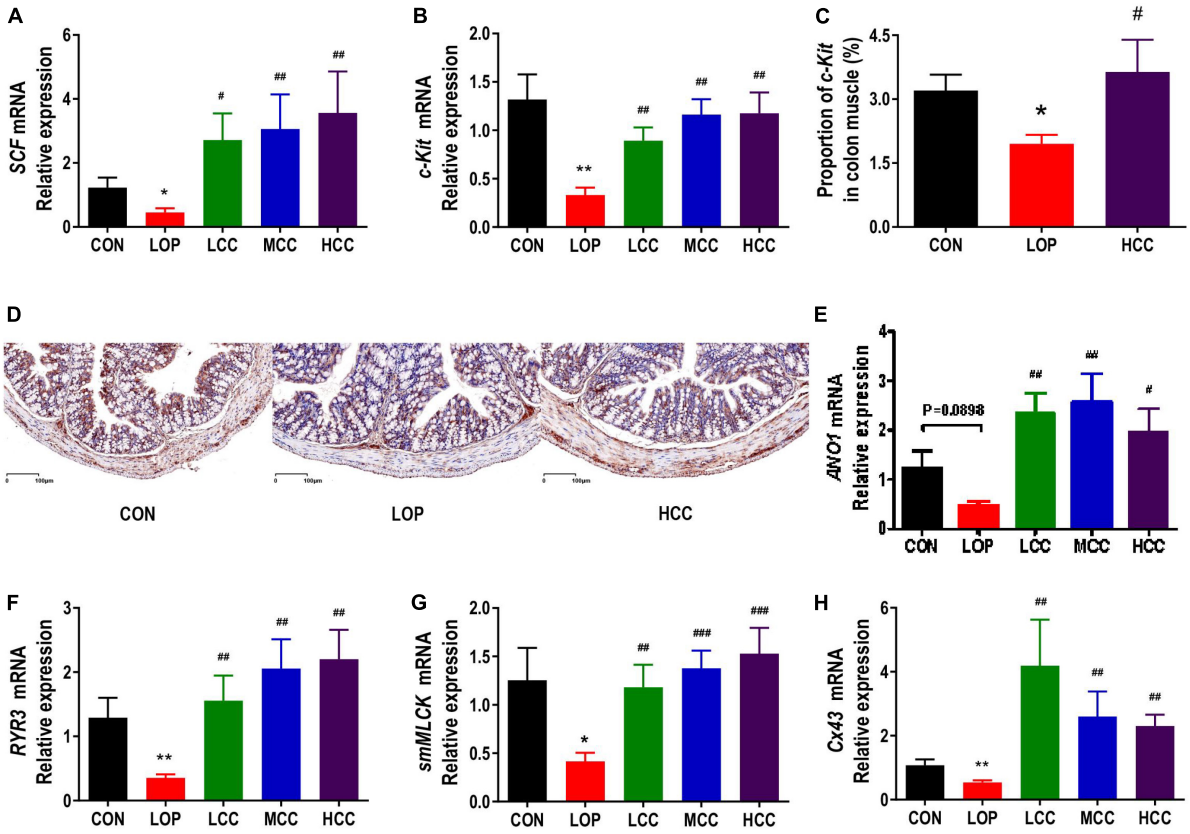


FIGURE 3
Aqueous extract of *Cymbopogon citratus* (DC.) Stapf (CCAE) increased the expression of gastrointestinal motility factors in the colon of STC mice. **(A,B)** The mRNA expression of stem cell factor (*SCF*) and stem cell factor receptor (*c-Kit*) in the colon. **(C)** Percentage of c-Kit-positive area in colon muscle. **(D)** Representative immunostaining images of colon sections stained for c-Kit. **(E–H)** The mRNA expression of *Anoctamin 1* (*Ano1*), *Ryanodine receptor 3* (*RyR3*), *smooth muscle myosin light chain kinase* (*smMLCK*), and *Connexin 43* (*Cx43*) in the colon. The data are expressed as the means ± SEMs ($n$ = 8). *, Compared with the CON group; #, compared with the LOP group. $^{*}P < 0.05$, $^{**}P < 0.01$, $^{***}P < 0.001$. $^{\#}P < 0.05$, $^{\#\#}P < 0.01$, $^{\#\#\#}P < 0.001$.

composition of CCAE-treated mice was clustered with that of the CON group (Supplementary Figures 4D–F).

Linear discriminant analysis (LDA) effect size (LEfSe) analyses were used to obtain the dominant microbiota at different levels for each group (Figure 5D and Supplementary Figures 5A–D). Here, a total of 43 different taxa from the 3 groups are displayed, including 5 phyla, 5 classes, 6 orders, 10 families, and 17 genera (Supplementary Figures 5A–C). We focused on the taxa that were significantly affected by LOP or HCC, especially those significantly changed by HCC treatment (Supplementary Figure 5D).

At the phylum level (Figure 5E), the relative abundances of six phyla were all significantly altered by loperamide treatment, including Firmicutes, Bacteroidota, Proteobacteria, Actinobacteriota, Desulfobacterota, and Patescibacteria. This finding suggests a comprehensive effect of loperamide on the gut microbiota in mice. CCAE treatment had different degrees of reversal effects on five phyla, except for Patescibacteria, but these reversal effects did not reach statistical significance (Figure 5E).

At the family level, the dominant families of gut bacteria, Muribaculaceae and Lachnospiraceae, belonging to Firmicutes and Bacteroidota, respectively, were significantly upregulated and downregulated in relative abundance under loperamide induction, respectively; importantly, CCAE could significantly reverse the loperamide-induced changes (Figure 5F). Similarly, CCAE significantly reduced the relative abundance of Flavobacteriaceae and UCG-010 compared to the LOP group, although loperamide was not able to increase their abundances significantly (Figure 5G). There were also some other families that were significantly upregulated or downregulated under the induction by loperamide, and CCAE treatment had a certain reversal effect on them, but there was no statistical significance (Figures 5G,H). Among them, Eubacterium coprostanoligenes group and Sutterellaceae were significantly upregulated (Figure 5G); Desulfovibrionaceae, Lactobacillaceae, Ruminococcaceae, Saccharimonadaceae, Anaerovoracaceae, and Eggerthellaceae were significantly downregulated (Figure 5H).

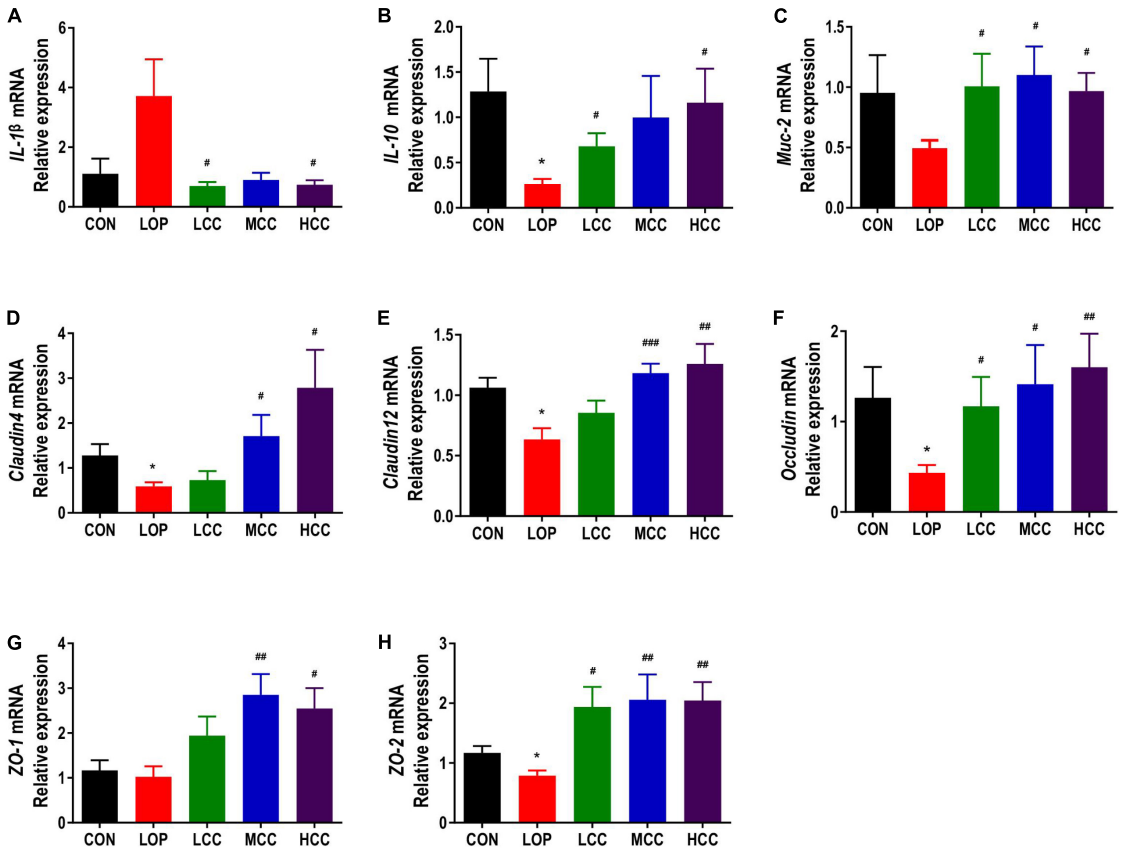


FIGURE 4
Effects of CCAE administration on the mRNA expression of inflammation- and intestinal barrier-related factors in the colons of mice. **(A–H)** *IL-1β*, *IL-10*, *Muc-2*, *Cldn4*, *Cldn12*, *Occludin*, *ZO-1*, and *ZO-2*. The data are expressed as the means ± SEMs ($n$ = 8). *, Compared with the NCD group; #, compared with the LOP group. *$P$ < 0.05, **$P$ < 0.01, ***$P$ < 0.001. #$P$ < 0.05, ##$P$ < 0.01, ###$P$ < 0.001.

At the genus level, the most interesting taxa still belonged to Firmicutes and Bacteroidota. *Unclassified_f__Lachnospiraceae*, *Lachnospiraceae_UCG-006* and *GCA-900066575* belong to Lachnospiraceae, and their relative abundances were all significantly reduced in mice of the LOP group but reversed significantly in the HCC group (**Figures 5I,J**). Notably, *norank_f__Muribaculaceae* (belonging to Bacteroidota) and *Anaeroplasma* (belonging to Firmicutes) showed the opposite variation (**Figures 5I,N**). Some other genera in Firmicutes also showed nearly the same patterns as Lachnospiraceae, including Family_XIII_UCG-001 and *UCG-005* (**Figure 5J**). CCAE treatment significantly increased the relative abundance of *Paludicola*, *UCG-009*, *Eubacterium xylanophilum group*, and *norank_f__Lachnospiraceae*, although loperamide did not reduce their abundances significantly. Interestingly, *Prevotellaceae_UCG-001* and *Rikenellaceae_RC9_gut_group* (belonging to Bacteroidota) showed a similar pattern with Lachnospiraceae (**Figure 5K**). *Anaerotruncus*, *unclassified_f__Oscillospiraceae*, *Lactobacillus*, and *Lachnospiraceae_NK4A136_group* were also significantly reduced by loperamide, while the reversal effects of CCAE did not reach statistical significance (**Figure 5L**). The same pattern was exhibited in some genera belonging to Actinobacteriota, Desulfobacterota and Patescibacteria, including *unclassified_f__Eggerthellaceae*, *Enterorhabdus*, *Bilophila*, *Desulfovibrio*, and *Candidatus_Saccharimonas* (**Figure 5M**). In addition, loperamide treatment enhanced the relative abundance of *norank_f__Flavobacteriaceae*, *norank_f__UCG-010* and *Parasutterella* to varying extents; CCAE treatment significantly reduced the abundance of the first two of them (**Figure 5N**). These results fully demonstrated that CCAE could partially restore loperamide-induced gut microbial dysbiosis in many aspects, such as microbial diversity, community structure, and species composition.

## Correlations between specific gut bacteria and core host parameters

To further clarify the possible role of gut microbiota in the amelioration of loperamide-induced STC progression by CCAE, we systematically analyzed the correlations between

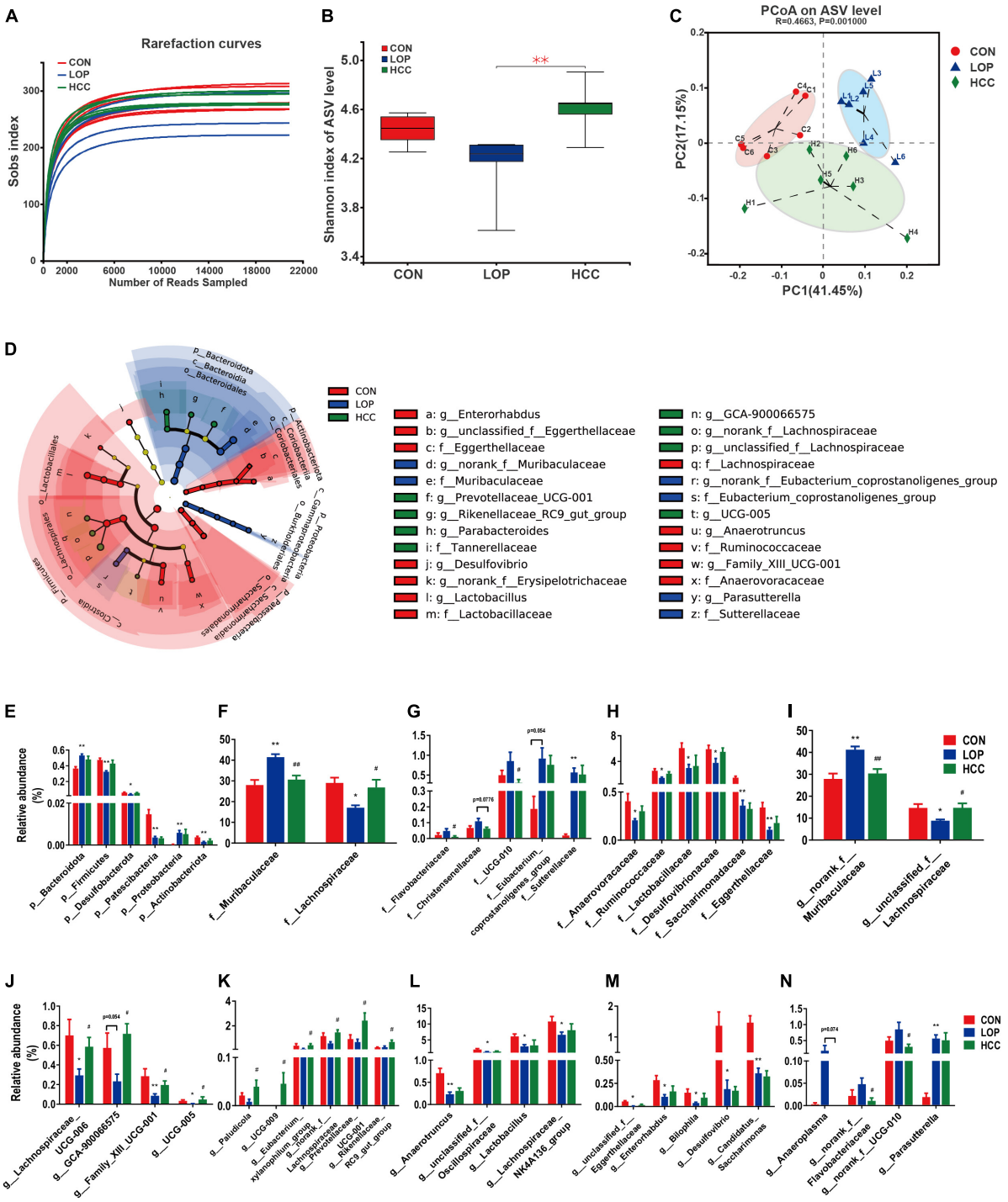


FIGURE 5
HCC restores the LOP-induced gut microbial community structural and compositional shift. **(A)** The rarefaction curve of the Sobs index of each sample plateau at the ASV level. **(B)** Alpha diversity estimated by the Shannon index. **(C)** PCoA (principal coordinate analysis) plot based on weighted UniFrac distance. **(D)** Linear discriminant analysis effect size (LEfSe) analyses (LDA score of > 2.0). **(E–N)** Relative abundances of gut microbiota at the phylum, family, and genus levels, which were significantly affected by LOP or HCC, especially those reversed by HCC treatment. The data are expressed as the means ± SEMs ($n$ = 6). *, Compared with the CON group; #, compared with the LOP group. *$P$ < 0.05, **$P$ < 0.01. #$P$ < 0.05, ##$P$ < 0.01.

taxa-specific gut bacteria and core host parameters, such as laxative phenotypic indicators, serum neurotransmitters, gastrointestinal motility factors, intestinal inflammation, and intestinal barrier function, at the phylum, family, and genus levels.

Correlations between the specific gut bacteria and the laxative phenotypic indicators are shown in **Figures 6A–C** and **Supplementary Figure 6**. FBS is the core host parameter that could directly reflect the laxative effect of CCAEs on mice. At the phylum level (**Figure 6A**), correlations between Firmicutes, Bacteroidota and FBS showed opposite trends. Firmicutes and Desulfobacterota were significantly negatively correlated with FBS, and Bacteroidota and Proteobacteria were significantly positively correlated with FBS. Actinobacteriota and Patescibacteria were significantly positively correlated with FN.

At the family level, Anaerovoracaceae and Lachnospiraceae were significantly negatively correlated with FBS and positively correlated with FN and FW. Muribaculaceae, Flavobacteriaceae, and UCG-010 show completely opposite correlations. Ruminococcaceae and Desulfovibrionaceae were also significantly negatively correlated with FBS, while Sutterellaceae and Peptococcaceae also showed a positive correlation with FBS. Notably, there was also a significant negative correlation between UCG-010 and GTR.

At the genus level, correlations between the microbial groups and defecation phenotype are relatively complex, but the correlation laws are still clear. The genera with a strong correlation mainly belonged to Firmicutes and Bacteroidota. The important genera with a significant negative correlation with FBS mainly included *unclassified_f__Lachnospiraceae*, *Lachnospiraceae_UCG-006*, *norank_f__Ruminococcaceae*, *UCG-005*, *Roseburia*, *unclassified_f__Eggerthellaceae*, and *GCA-900066575*; meanwhile, they showed a significant positive correlation with FN or FW. The important genera with a significant positive correlation with FBS mainly included *norank_f__Muribaculaceae*, *norank_f__Flavobacteriaceae*, *Parasutterella*, and *norank_f__UCG-010*; meanwhile, they showed a significant negative correlation with FN or FW. It is worth mentioning that *unclassified_f__Eggerthellaceae* (belonging to Actinobacteriota) also exhibited a strong negative correlation with FBS and a positive correlation with GTR and FN. Interestingly, GTR showed significant correlations with a few genera, only negatively correlated with *norank_f__UCG-010*, *Muribaculum*, and *norank_f__Peptococcaceae* and positively correlated with *unclassified_f__Eggerthellaceae* and *unclassified_f__Lachnospiraceae*. Of course, some other genera of gut bacteria also showed strong associations with mouse laxative phenotypes, such as FN and FW. All these numerous correlations suggest that gut microbiota might play an important role in regulating the laxative phenotype.

Correlations between the specific gut bacteria and intestinal inflammation and gut barrier function are shown in **Figure 6D**. Interestingly and importantly, the anti-inflammatory factor *IL-10* was only significantly positively correlated with the highly abundant genus *unclassified_f__Lachnospiraceae*; moreover, both *unclassified_f__Lachnospiraceae* and *IL-10* were significantly reversed by CCAE in STC mice. Among the gut barrier function factors, *ZO-1* showed the most correlations with the microbial taxa. Several taxa of Actinobacteria had a strong negative correlation with *ZO-1*, and the Eubacterium_coprostanoligenes_group of Firmicutes had a strong positive correlation with *ZO-1*. Ruminococcaceae and *UCG-009* also showed a strong positive correlation with *Cldn4*. This suggests that some specific groups of Firmicutes and Actinobacteria might play important and positive roles in CCAE against loperamide-induced colonic inflammation and impaired barrier function.

The heatmap in **Figure 6E** clearly shows the correlations between the specific gut bacteria and serum neurotransmitters and gastrointestinal motility factors. *c-kit, RyR3,* and *iNOS* showed more correlations with gut microbes. At the family and genus levels, *Eubacterium_coprostanoligenes_group*, *Parabacteroides*, *Parasutterella,* and *norank_f__Muribaculaceae* were negatively correlated with *c-kit* and *RyR3*, while *Candidatus_Saccharimonas*, *Enterorhabdus*, Eggerthellaceae, *Lactobacillus*, *unclassified_f__Oscillospiraceae*, and *Anaerotruncus* exhibited the opposite correlation. Except for Desulfovibrionaceae, the taxa with significant negative correlations with iNOS all belong to Firmicutes, mainly including *norank_f__Lachnospiraceae*, *GCA-900066575*, Lachnospiraceae, *Eubacterium_xylanophilum_group*, *Paludicola*, *UCG-005*, and *Family_XIII_UCG-001*, in which *norank_f__Lachnospiraceae* and GCA-900066575 belong to Lachnospiraceae. Notably, the genus *Lachnospiraceae_NK4A136_group* and family UCG-010 were negatively correlated with gap junction *Cx43*, which also belongs to Firmicutes. Interestingly, the genus *Prevotellaceae_UCG-001* showed a significantly positive correlation. These results implied that some specific groups of Firmicutes, Bacteroidota, and Actinobacteriota might play different and important roles in CCAE regulating gastrointestinal peristalsis in STC mice.

## Discussion

Prolonged constipation often produces a variety of adverse reactions, causing serious distress to the affected people. Loperamide is an opioid receptor agonist that is used for the treatment of acute and chronic diarrhea caused by various etiologies. Therefore, it is widely used to induce constipation in animals (Hu et al., 2021). Loperamide mainly inhibits intestinal motility by blocking calcium channels, inhibiting calmodulin, reducing cell bypass permeability, and reducing the release of acetylcholine from intestinal nerve endings (Baker, 2007). In

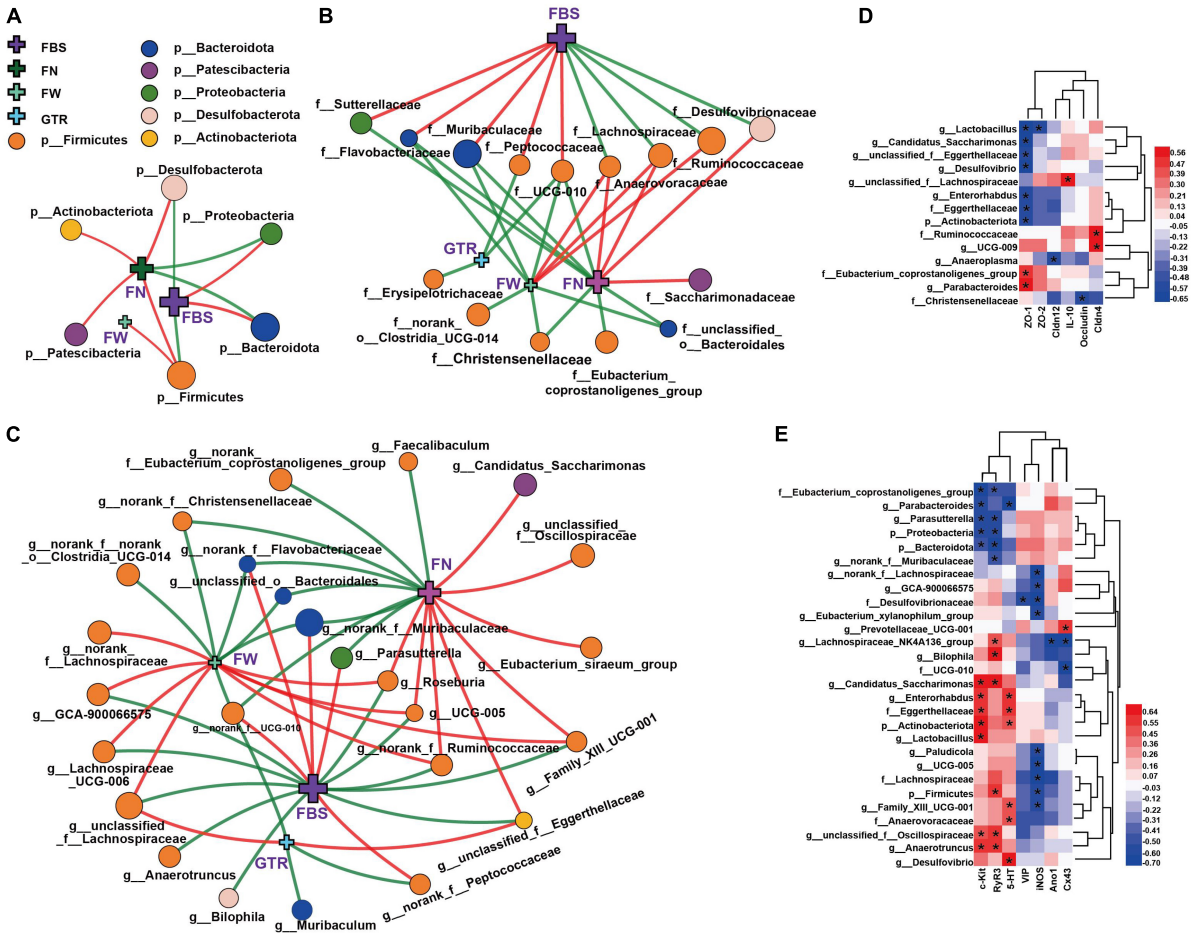


FIGURE 6
Network and heatmaps showing correlations between specific gut bacteria and core host parameters in STC mice. **(A–C)** Two-factor correlation network analysis ($P < 0.05$; Spearman, $n = 6$ in each group). Red lines represent $r$ values $\geq 0.4$, and green lines represent $r$ values $\leq 0.4$. Correlations between gut bacteria and the laxative phenotypic indicators, including **(A)** at the phylum level, **(B)** at the family level, and **(C)** at the genus level. FBS, the defecation time of the first black stool; the wet weight of the feces (FW) and the number of feces excreted in 6 h (FN); the gastrointestinal transit rate (GTR). **(D,E)** Bivariate correlations ($P < 0.05$, $n = 6$ in each group), including correlations between gut bacteria and intestinal inflammation, gut barrier function in the colon of mice **(D)**, correlations between gut bacteria and serum neurotransmitters, gastrointestinal motility factors **(E)**. *IL-10*, *ZO-1*, *ZO-2*, *Cldn4*, *Cldn12*, *Occludin*, *c-Kit*, *SCF*, *Ano1*, and *Cx43* indicate their mRNA expression levels in the colons of mice. 5-HT, iNOS, and VIP indicate their expression levels in serum. The color at each intersection indicates the value of the $r$ coefficient; $P$ -alues were adjusted for multiple testing according to the *Bonferroni and Hochberg* procedures. * Indicates a significant correlation between these two parameters.

this study, loperamide also showed an excellent ability to shape the STC model.

Intestinal homeostasis plays an extremely important role in intestine-related diseases. Studies have shown that loperamide-induced STC animals generally have impaired intestinal homeostasis (Lin et al., 2021). Therefore, we systematically evaluated the effect of CCAE on loperamide-induced STC from three aspects, including intestinal movement, intestinal barrier and gut microbiota. We found that CCAE not only significantly decreased the expression of VIP, iNOS, and AchE (Figure 2), but also significantly increased the expression of the gastrointestinal motility factors *SCF*, *c-Kit*, *Ano1*, *RyR3*, and *smMLCK* (Figure 3), thereby improving the gastrointestinal transport rate and shortening the defecation time (Figure 1). At the same time, CCAE decreased the mRNA expression of the inflammatory factor *IL-1*β and increased the mRNA expression of the anti-inflammatory factor *IL-10*, chemical barrier *Muc-2*, mechanical barrier *Cldn4*, *Cldn12*, *Occludin*, *ZO-1*, and *ZO-2* to repair the gut barrier and maintain intestinal homeostasis (Figure 4). Interestingly, CCAE also changed the intestinal microbial community structure and composition in loperamide-induced STC mice, and some important taxa of gut microbiota were significantly regulated by CCAE (Figure 5).

In recent years, the above neurotransmitters and gastrointestinal functional factors have received increasing attention in the research of STC, but there are few

comprehensive reports that connect the important factors of each part of the ENS-ICCs-SMCs network. The ENS-ICCs-SMCs network is the basic functional unit of gastrointestinal movement, and it is mainly organized through the functions of ICCs. As a pacemaker cell for gastrointestinal activity, ICCs are also promoters of gastrointestinal electrical activity transmission and regulators of neurotransmitter transmission (Zhu et al., 2021). There are a large number of neurotransmitter receptors on the cell membrane of ICCs. When some neurotransmitters bind to the corresponding nerve receptors on ICCs, they can transmit excitatory or inhibitory nerve signals to SMCs through ICCs to regulate the relaxation and contraction of smooth muscle (Kim et al., 2006, 2013; Choi et al., 2010; Cipriani et al., 2011; Liu et al., 2020). Our results indicated that CCAE could reverse the loperamide-induced decrease in the expression of ICC cell marker c-Kit and changes in serum neurotransmitters to a certain extent. The pacing effect of ICCs on SMCs depends on the generation of slow waves, which are generated by $Ca^{2+}$-induced potential changes in ICCs (Drumm et al., 2019). In this study, the mRNA expression of *RyR3* of calcium channels and *Ano1* of calcium-activated chloride channels was significantly inhibited in the LOP group, which was significantly reversed by CCAE. After the slow wave is generated, it is transmitted to SMCs via Cx43 to contract smooth muscle (Sancho et al., 2011). smMLCK is a key regulatory enzyme that controls the initiation of smooth muscle contraction and is widely present in smooth muscle (Zhang et al., 2016). We found that loperamide could significantly inhibit the expression of *smMLCK* and *Cx43* in the mouse colon, while CCAE could significantly upregulate them. Therefore, we believe that CCAE can alleviate loperamide-induced STC by regulating the ENS-ICCs-SMCs network.

Intestinal homeostasis is mainly maintained by intestinal barrier function (Salinas et al., 2021). The normal intestinal mucosal barrier is mainly composed of four parts: mechanical barrier, chemical barrier, immune barrier and biological barrier. The occludin family, claudin family and ZO family are important protein molecules that constitute the tight junctions between cells (Zhang J. et al., 2021). The basic structure of the chemical barrier is the mucus layer, which is mainly composed of mucus and other substances secreted by the intestinal epithelium (Lu et al., 2021). When the mechanical barrier and chemical barrier are dysfunctional, bacteria and toxic products enter the immune barrier and induce production of inflammatory factors (Stolfi et al., 2022). The mRNA expression levels of *ZO-1*, *Occludin*, *Cldn1,* and *Muc-2* could be significantly downregulated in the colon of constipated animals, and their expression levels were significantly upregulated after probiotic treatment (Eor et al., 2019; Lee et al., 2019; Lu et al., 2021). CCAE can also repair the intestinal barrier and maintain intestinal homeostasis by enhancing the mRNA expression levels of chemical barriers (*Muc-2*), mechanical barriers (*Cldn4*, *Cldn12*, *Occludin*, *ZO-1,* and *ZO-2*) and anti-inflammatory factors (*IL-10*).

The gut microbiota is an important part of the intestinal barrier and belongs to the biological barrier. The importance of the gut microbiota to health is now well known. Accumulating evidence supports the critical role of gut microbiota in regulating gut motility (Ohkusa et al., 2019; Zhang S. et al., 2021). Studies have confirmed that bacterial colonization in the gut is critical for the development and maturation of the ENS (Joly et al., 2021). Abnormal gastrointestinal microbiota composition may lead to disruption of "microbiota-gut-brain axis" signaling, leading to altered gut motility (Kennedy et al., 2012; Carabotti et al., 2015). Metabolites of gut microbiota could stimulate the ENS and affect gut motility (Barbara et al., 2005). Therefore, altering the gut microbiota may affect defecation behavior by regulating intestinal motility and secretion. In this study, CCAE partially reversed the gut microbiota changes induced by loperamide.

According to the analysis results of gut microbiota, we speculate that some high-abundance families and genera might play vital roles in the process of CCAE alleviating STC. For example, Muribaculaceae, Lachnospiraceae, *norank_f__Muribaculaceae*, and *unclassified_f__Lachnospiraceae* (**Figures 5F,I**) not only showed significant reversal-type changes during CCAE treatment but were also significantly associated with the laxative phenotypes, serum neurotransmitters, gastrointestinal motility factors, intestinal barrier, and intestinal inflammation (**Figure 6**). A series of previous clinical research results confirmed the rationality of our findings and speculations in mice. For example, a clinical study of irritable bowel syndrome showed that a higher Firmicutes to Bacteroidetes ratio was positively associated with loose stools in patients (Hollister et al., 2020). Parthasarathy et al. (2016) found that genera from Bacteroidetes were more abundant in the colonic mucosal microbiota of patients with constipation, and that the profile of the fecal microbiota was associated with colonic transit; genera from Firmicutes correlated with faster colonic transit; there was a decrease in the proportion of Firmicutes and an increase in Bacteroidetes in subjects with functional constipation, while ID-HWS1000 (composed of probiotics and prebiotics) directly improved the discomfort associated with bowel movements, decreased the proportion of Lachnospiraceae, and increased the proportion of Bacteroidaceae (Kim M. C. et al., 2021).

Previous animal experimental studies also agreed with our findings. Phlorotannins derived from *Ecklonia cava* could improve the constipation phenotype and restore the abundance of Muribaculaceae in the fecal microbiota of STC rats (Kim J. E. et al., 2021). Goji Berry and soluble fiber dextrin from tapioca promote the growth of butyrate-producing bacteria, including Lachnospiraceae and Ruminococcaceae, while reducing

proinflammatory factors in IL-10-deficient mice (Valcheva et al., 2015; Kang et al., 2018). We found that both *unclassified_f__Lachnospiraceae* and *IL-10* were significantly reversed by CCAE in STC mice, and *IL-10* was only significantly positively correlated with the highly abundant genus *unclassified_f__Lachnospiraceae*.

Although the abovementioned high abundance families and genera performed well in the correlation analysis with the phenotypic indicators of constipation, they generally performed well in the correlation analysis with serum neurotransmitters, gastrointestinal motility factors and intestinal barrier. In contrast, the comprehensive performance of some low abundance taxa is remarkable, including Flavobacteriaceae, UCG-010, Anaerovoracaceae, *norank_f__Flavobacteriaceae*, *Lachnospiraceae_UCG-006*, *GCA-900066575*, *Family_XIII_UCG-001*, *UCG-005*, *Paludicola*, *UCG-009*, and *Prevotellaceae_UCG-001*, although some of these taxa did not show the most prominent abundance changes in this study. We could hardly find literature reports of these taxa related to constipation. Only Lachnospiraceae_UCG-006 was found to be associated with yellow tea extract interventions for constipation relief (Cao et al., 2021), which is consistent with our findings. In addition, several low abundance taxa of Actinobacteria (*unclassified_f__Eggerthellaceae*, Eggerthellaceae and *Enterorhabdus*) had a strong correlation with intestinal barrier and gastrointestinal motility factors in this study. The correlation between the taxa and intestinal barrier has been mentioned in previous studies (Chen et al., 2021; Han et al., 2021), but there is no report on their association with gastrointestinal motility factors. This also suggests that our study may reveal more potential associations between microbes and constipation-related markers that have not yet been addressed.

Overall, we believe that gut microbiota play a very important role in regulating the laxative phenotype; some specific taxa of Firmicutes and Actinobacteria might play positive roles in CCAE against loperamide-induced colonic inflammation and impaired barrier function; some specific taxa of Firmicutes, Bacteroidota and Actinobacteriota might play different and important roles in CCAE regulating gastrointestinal peristalsis.

CCAE is a nutrient-rich, phytochemically diverse complex (**Supplementary Tables 1**, **3**,**4**). Although we have systematically evaluated the laxative effect of CCAE, the laxative active components and *in vivo* pharmacodynamic substance of CCAE are still unclear. However, some main components of CCAE exhibit laxative-related biological activity. For example, dietary fiber intake can obviously increase stool frequency in patients with constipation (Yang et al., 2012); as a metabolite, the betaine content decreased in constipated rats and increased significantly after the symptoms of constipation were relieved (Kim et al., 2019); betaine can also ameliorate intestinal injury in heat-challenged broilers by suppressing inflammatory responses and enhancing mucosal barrier function (Alhotan et al., 2021); vitexin exerted neural protective effects via antioxidant, anti-inflammatory and gut microbiota modulating properties (Li et al., 2021); and crotonoside, cordycepin, and cynaroside have significant anti-inflammatory effects (Lin et al., 2020; Pei et al., 2021; Tan et al., 2021). These results on major bioactive components of CCAE not only provide evidence for our research results of CCAE relieving constipation but also provide references for us to further clarify the molecular basis how CCAE relieves constipation.

## Conclusion

In summary, we systematically studied the effect of CCAE on host parameters and the gut microbiota in loperamide-induced STC mice. We found that CCAE could significantly improve loperamide-induced constipation symptoms. We believe that CCAE might promote intestinal motility by modulating the ENS-ICCs-SMCs network, intestinal inflammation, intestinal barrier and gut microbiota, thereby relieving constipation. Meanwhile, the established correlation networks between the gut microbiota and the laxative phenotypic indicators in STC mice provided a foundation for further clarifying the relationship between the gut microbiota and host metabolism in STC mice.

## Data availability statement

The data presented in this study are deposited in the SRA repository, accession number PRJNA840843.

## Ethics statement

The animal study was reviewed and approved by Animal Ethics Committee of Yunnan Agriculture University.

## Author contributions

XG: conceptualization, data curation, formal analysis, methodology, and writing – original draft, review and editing. YH: data curation, formal analysis, methodology, visualization, and writing – original draft. YTa, SL, HC, and

JL: methodology. YZ: visualization. JS: conceptualization and funding acquisition. YTi: conceptualization and supervision. YF: resources, supervision, and funding acquisition. All authors read and approved the final manuscript.

## Funding

This research was funded by the Major Project of Science and Technology Department of Yunnan Province (202102AE090027-2), YEFICRC project of Yunnan provincial key programs (2019ZG009), and Yunnan Fundamental Research Projects (202001AT070123).

## Conflict of interest

The authors declare that the research was conducted in the absence of any commercial or financial relationships that could be construed as a potential conflict of interest.

## Publisher's note

All claims expressed in this article are solely those of the authors and do not necessarily represent those of their affiliated organizations, or those of the publisher, the editors and the reviewers. Any product that may be evaluated in this article, or claim that may be made by its manufacturer, is not guaranteed or endorsed by the publisher.

## Supplementary material

The Supplementary Material for this article can be found online at: https://www.frontiersin.org/articles/10.3389/fmicb.2022.1017804/full#supplementary-material

SUPPLEMENTARY FIGURE 1
Effects of CCAE on loperamide-induced constipation symptoms in mice. **(A)** The body weight. **(B)** Food intake. **(C)** The water consumption. **(D)** Spleen index. **(E)** The small intestine length. **(F)** Cecum index.

SUPPLEMENTARY FIGURE 2
Gene expression of intestinal inflammatory factors in colon of STC mice. **(A–C)** Inflammatory factor *MCP-1*, *TNF-α*, and *IL-6*.

SUPPLEMENTARY FIGURE 3
**(A–F)** Shannoneven, simpsoneven, ace, chao, sobs, simpson index of ASV level. *compared with the NCD group, using the Kruskal-Wallis *H* test. $^{**}P < 0.01$.

SUPPLEMENTARY FIGURE 4
Effect of CCAE on the cecum microbial composition in STC mice. **(A)** Phylum level. **(B)** Family level. **(C)** Genus level. **(D–F)** Cluster heatmaps of gut microbiota in different groups.

SUPPLEMENTARY FIGURE 5
Linear discriminant analysis effect size (LEfSe) analyses (LDA score > 2.0). **(A–C)** LEfSe analyses based on the CON, LOP and HCC groups. **(A)** At the phylum, class and order level. **(B)** At the family level. **(C)** At the genus level. **(D)** LEfSe analyses based on the LOP and HCC groups, from the phylum level to the genus level.

SUPPLEMENTARY FIGURE 6
Heat maps showing correlations between specific gut bacteria and the core laxative phenotypic indicators in STC mice. Bivariate correlations ($P < 0.05$, $n = 6$ in each group), including correlations between gut bacteria and the core laxative phenotypic indicators. FBS, the defecation time of the first black stool; the fecal wet weight (FW) and the fecal number (FN) in 6 h; the gastrointestinal transit rate (GTR). The color at each intersection indicates the value of the *r* coefficient; *P*-values were adjusted for multiple testing according to the *Bonferroni and Hochberg* procedures. * indicates a significant correlation between these two parameters ($P < 0.05$).

## References

Alhotan, R. A., Al Sulaiman, A. R., Alharthi, A. S., and Abudabos, A. M. (2021). Protective influence of betaine on intestinal health by regulating inflammation and improving barrier function in broilers under heat stress. *Poult. Sci.* 100:101337. doi: 10.1016/j.psj.2021.101337

Baker, D. E. (2007). Loperamide: A pharmacological review. *Rev. Gastroenterol. Disord.* 7(Suppl. 3), S11–S18.

Barbara, G., Stanghellini, V., Brandi, G., Cremon, C., Di Nardo, G., De Giorgio, R., et al. (2005). Interactions between commensal bacteria and gut sensorimotor function in health and disease. *Am. J. Gastroenterol.* 100, 2560–2568. doi: 10.1111/j.1572-0241.2005.00230.x

Bharucha, A. E., and Lacy, B. E. (2020). Mechanisms, evaluation, and management of chronic constipation. *Gastroenterology* 158, 1232–1249. doi: 10.1053/j.gastro.2019.12.034

Borges, P., Pedreiro, S., Baptista, S. J., Geraldes, C., Batista, M. T., Silva, M., et al. (2021). Inhibition of α-glucosidase by flavonoids of cymbopogon citratus (DC) Stapf. *J. Ethnopharmacol.* 280:114470. doi: 10.1016/j.jep.2021.114470

Cao, P. Q., Li, X. P., Ou-Yang, J., Jiang, R. G., Huang, F. F., Wen, B. B., et al. (2021). The protective effects of yellow tea extract against loperamide-induced constipation in mice. *Food Funct.* 12, 5621–5636. doi: 10.1039/d0fo02969f

Carabotti, M., Scirocco, A., Maselli, M. A., and Severi, C. (2015). The gut-brain axis: Interactions between enteric microbiota, central and enteric nervous systems. *Ann. Gastroenterol.* 28, 203–209.

Chen, K. J., Chen, Y. L., Ueng, S. H., Hwang, T. L., Kuo, L. M., and Hsieh, P. W. (2021). Neutrophil elastase inhibitor (MPH-966) improves intestinal mucosal damage and gut microbiota in a mouse model of 5-fluorouracil-induced intestinal mucositis. *Biomed. Pharmacother.* 134:111152. doi: 10.1016/j.biopha.2020.111152

Choi, S., Sun, J. M., Shahi, P. K., Zuo, D. C., Kim, H. I., and Jun, J. Y. (2010). Capsaicin inhibits the spontaneous pacemaker activity in interstitial cells of cajal from the small intestine of mouse. *J. Neurogastroenterol. Motil.* 16, 265–273. doi: 10.5056/jnm.2010.16.3.265

Cipriani, G., Serboiu, C. S., Gherghiceanu, M., Faussone-Pellegrini, M. S., and Vannucchi, M. G. (2011). NK receptors, substance P, Ano1 expression and ultrastructural features of the muscle coat in Cav-1(-/-) mouse ileum. *J. Cell. Mol. Med.* 15, 2411–2420. doi: 10.1111/j.1582-4934.2011.01333.x

Drumm, B. T., Hwang, S. J., Baker, S. A., Ward, S. M., and Sanders, K. M. (2019). Ca2+ signaling behaviors of intramuscular interstitial cells of Cajal in the murine colon. *J. Physiol.* 597, 3587–3617. doi: 10.1113/JP278036

Eor, J. Y., Tan, P. L., Lim, S. M., Choi, D. H., Yoon, S. M., Yang, S. Y., et al. (2019). Laxative effect of probiotic chocolate on loperamide-induced constipation in rats. *Food Res. Int.* 116, 1173–1182. doi: 10.1016/j.foodres.2018.09.062

Fernandes, C., De Souza, H., De Oliveria, G., Costa, J., Kerntopf, M., and Campos, A. (2012). Investigation of the mechanisms underlying the gastroprotective effect of *Cymbopogon citratus* essential oil. *J. Young Pharm. JYP* 4, 28–32. doi: 10.4103/0975-1483.93578

Figueirinha, A., Cruz, M. T., Francisco, V., Lopes, M. C., and Batista, M. T. (2010). Anti-inflammatory activity of *Cymbopogon citratus* leaf infusion in lipopolysaccharide-stimulated dendritic cells: Contribution of the polyphenols. *J. Med. Food* 13, 681–690. doi: 10.1089/jmf.2009.0115

Gao, X., Chang, S., Liu, S., Peng, L., Xie, J., Dong, W., et al. (2020). Correlations between α-Linolenic acid-improved multitissue homeostasis and gut microbiota in mice fed a high-fat diet. *mSystems* 5, e00391–20. doi: 10.1128/mSystems.00391-20

Gao, X., Xie, Q., Liu, L., Kong, P., Sheng, J., and Xiang, H. (2017). Metabolic adaptation to the aqueous leaf extract of *Moringa oleifera* Lam.-supplemented diet is related to the modulation of gut microbiota in mice. *Appl. Microbiol. Biotechnol.* 101, 5115–5130. doi: 10.1007/s00253-017-8233-5

Gomes, L. F., Longhi, P., Machado, L., da Cruz, I., Montano, M., Martins, M., et al. (2021). Lemongrass (*Cymbopogon citratus* (D.C.) Stapf) presents antitumoral effect and improves chemotherapy activity in prostate cancer cells. *Anti-Cancer Agents Med. Chem.* 21, 2337–2350. doi: 10.2174/1871520621666210112111711

Han, R., Ma, Y., Xiao, J., You, L., Pedisiæ, S., and Liao, L. (2021). The possible mechanism of the protective effect of a sulfated polysaccharide from *Gracilaria* Lemaneiformis against colitis induced by dextran sulfate sodium in mice. *Food Chem. Toxicol.* 149:112001. doi: 10.1016/j.fct.2021.112001

Hollister, E. B., Cain, K. C., Shulman, R. J., Jarrett, M. E., Burr, R. L., Ko, C., et al. (2020). Relationships of microbiome markers with extra-intestinal, psychological distress and gastrointestinal symptoms, and quality of life in women with irritable bowel syndrome. *J. Clin. Gastroenterol.* 54, 175–183. doi: 10.1097/MCG.0000000000001107

Hu, M., Fang, C., Liu, Y., Gao, M., Zhang, D., Shi, G., et al. (2021). Comparative study of the laxative effects of Konjac oligosaccharides and Konjac glucomannan on loperamide-induced constipation in rats. *Food Funct.* 12, 7709–7717. doi: 10.1039/d1fo01237a

Huang, Y. W., Zhu, Q. Q., Yang, X. Y., Xu, H. H., Sun, B., Wang, X. J., et al. (2019). Wound healing can be improved by (-)-epigallocatechin gallate through targeting Notch in streptozotocin-induced diabetic mice. *FASEB J.* 33, 953–964. doi: 10.1096/fj.201800337R

Iram, F., Tariq, M., and Sobia Kanwal. (2019). Microbiostatic, antioxidative and cytotoxic potentiation of some grasses of Bahawalpur, Pakistan. *J. Tradit. Chine. Med.* 39, 482–491.

Joly, A., Leulier, F., and De Vadder, F. (2021). Microbial modulation of the development and physiology of the enteric nervous system. *Trends Microbiol.* 29, 686–699. doi: 10.1016/j.tim.2020.11.007

Kang, Y., Yang, G., Zhang, S., Ross, C. F., and Zhu, M. J. (2018). Goji Berry modulates gut microbiota and alleviates colitis in IL-10-Deficient Mice. *Mol. Nutr. Food Res.* 62:e1800535. doi: 10.1002/mnfr.201800535

Kennedy, P. J., Clarke, G., Quigley, E. M., Groeger, J. A., Dinan, T. G., and Cryan, J. F. (2012). Gut memories: Towards a cognitive neurobiology of irritable bowel syndrome. *Neurosci. Biobehav. Rev.* 36, 310–340. doi: 10.1016/j.neubiorev.2011.07.001

Kieling, D. D., and Prudencio, S. H. (2019). Blends of lemongrass derivatives and lime for the preparation of mixed beverages: Antioxidant, physicochemical, and sensory properties. *J. Sci. Food Agric.* 99, 1302–1310. doi: 10.1002/jsfa.9305

Kim, B. J., Kim, H. W., Lee, G. S., Choi, S., Jun, J. Y., So, I., et al. (2013). *Poncirus trifoliate* fruit modulates pacemaker activity in interstitial cells of Cajal from the murine small intestine. *J. Ethnopharmacol.* 149, 668–675. doi: 10.1016/j.jep.2013.07.017

Kim, B. J., Lee, J. H., Jun, J. Y., Chang, I. Y., So, I., and Kim, K. W. (2006). Vasoactive intestinal polypeptide inhibits pacemaker activity via the nitric oxide-cGMP-protein kinase G pathway in the interstitial cells of Cajal of the murine small intestine. *Mol. Cells* 21, 337–342.

Kim, J. E., Choi, Y. J., Lee, S. J., Gong, J. E., Jin, Y. J., Park, S. H., et al. (2021). Laxative effects of phlorotannins derived from Ecklonia cava on loperamide-induced constipation in SD Rats. *Molecules* 26:7209. doi: 10.3390/molecules26237209

Kim, J. E., Lee, Y. J., Ryu, S. H., Park, J. W., Kang, M. J., Choi, H. J., et al. (2019). Metabolomics approach to serum biomarker for laxative effects of red *Liriope platyphylla* in loperamide-induced constipation of SD rats. *Lab. Anim. Res.* 35:9. doi: 10.1186/s42826-019-0009-x

Kim, M. C., Lee, S., Park, J. K., Park, J., Lee, D., Park, J., et al. (2021). Effects of ID-HWS1000 on the perception of bowel activity and microbiome in subjects with functional constipation: A randomized, double-blind placebo-controlled study. *J. Med. Food* 24, 883–893. doi: 10.1089/jmf.2020.4746

Lee, C. S., Tan, P. L., Eor, J. Y., Choi, D. H., Park, M., Seo, S. K., et al. (2019). Prophylactic use of probiotic chocolate modulates intestinal physiological functions in constipated rats. *J. Sci. Food Agric.* 99, 3045–3056. doi: 10.1002/jsfa.9518

Li, M., Liu, B., Bernigaud, C., Fischer, K., Guillot, J., and Fang, F. (2020). Lemongrass (*Cymbopogon citratus*) oil: A promising miticidal and ovicidal agent against *Sarcoptes scabiei*. *PLoS Negl. Trop. Dis.* 14:e0008225. doi: 10.1371/journal.pntd.0008225

Li, S., Liang, T., Zhang, Y., Huang, K., Yang, S., Lv, H., et al. (2021). Vitexin alleviates high-fat diet induced brain oxidative stress and inflammation via anti-oxidant, anti-inflammatory and gut microbiota modulating properties. *Free Rad. Biol. Med.* 171, 332–344. doi: 10.1016/j.freeradbiomed.2021.05.028

Lin, S. C., Lin, C. C., Li, S., Lin, W. Y., Lehman, C. W., Bracci, N. R., et al. (2020). Alleviation of collagen-induced arthritis by crotonoside through modulation of dendritic cell differentiation and activation. *Plants* 9:1535. doi: 10.3390/plants9111535

Lin, X., Liu, Y., Ma, L., Ma, X., Shen, L., Ma, X., et al. (2021). Constipation induced gut microbiota dysbiosis exacerbates experimental autoimmune encephalomyelitis in C57BL/6 mice. *J. Trans. Med.* 19:317. doi: 10.1186/s12967-021-02995-z

Liu, J., Du, P., and Rudd, J. A. (2020). Acetylcholine exerts inhibitory and excitatory actions on mouse ileal pacemaker activity: Role of muscarinic versus nicotinic receptors. *Am. J. Physiol. Gastroint. Liver Physiol.* 319, G97–G107. doi: 10.1152/ajpgi.00003.2020

Lu, Y., Yu, Z., Zhang, Z., Liang, X., Gong, P., Yi, H., et al. (2021). *Bifidobacterium animalis* F1-7 in combination with Konjac glucomannan improves constipation in mice via humoral transport. *Food Funct.* 12, 791–801. doi: 10.1039/d0fo02227f

Madi, Y. F., Choucry, M. A., Meselhy, M. R., and El-Kashoury, E. A. (2021). Essential oil of *Cymbopogon citratus* cultivated in Egypt: Seasonal variation in chemical composition and anticholinesterase activity. *Nat. Prod. Res.* 35, 4063–4067. doi: 10.1080/14786419.2020.1713125

Mendes Hacke, A. C., Miyoshi, E., Marques, J. A., and Pereira, R. P. (2020). Anxiolytic properties of *Cymbopogon citratus* (DC.) stapf extract, essential oil and its constituents in Zebrafish (*Danio rerio*). *J. Ethnopharmacol.* 260:113036. doi: 10.1016/j.jep.2020.113036

Ohkusa, T., Koido, S., Nishikawa, Y., and Sato, N. (2019). Gut microbiota and chronic constipation: A review and update. *Front. Med.* 6:19. doi: 10.3389/fmed.2019.00019

Pan, D., Machado, L., Bica, C. G., Machado, A. K., Steffani, J. A., and Cadoná, F. C. (2022). In vitro evaluation of antioxidant and anticancer activity of lemongrass (*Cymbopogon citratus* (D.C.) Stapf). *Nutr. Cancer* 74, 1474–1488. doi: 10.1080/01635581.2021.1952456

Parthasarathy, G., Chen, J., Chen, X., Chia, N., O'Connor, H. M., Wolf, P. G., et al. (2016). Relationship between microbiota of the colonic mucosa vs feces and symptoms, colonic transit, and methane production in female patients with chronic Constipation. *Gastroenterology* 150, 367–379.e1. doi: 10.1053/j.gastro.2015.10.005

Pei, L., Le, Y., Chen, H., Feng, J., Liu, Z., Zhu, J., et al. (2021). Cynaroside prevents macrophage polarization into pro-inflammatory phenotype and alleviates cecal ligation and puncture-induced liver injury by targeting PKM2/HIF-1α axis. *Fitoterapia* 152:104922. doi: 10.1016/j.fitote.2021.104922

Rojas-Armas, J. P., Arroyo-Acevedo, J. L., Palomino-Pacheco, M., Herrera-Calderón, O., Ortiz-Sánchez, J. M., Rojas-Armas, A., et al. (2020). The essential oil of *Cymbopogon citratus* Stapt and Carvacrol: an approach of the antitumor effect on 7,12-Dimethylbenz-[α]-anthracene (DMBA)-induced breast cancer in female rats. *Molecules* 25:3284. doi: 10.3390/molecules25143284

Salinas, E., Reyes-Pavón, D., Cortes-Perez, N. G., Torres-Maravilla, E., Bitzer-Quintero, O. K., Langella, P., et al. (2021). Bioactive compounds in food as a current therapeutic approach to maintain a healthy intestinal epithelium. *Microorganisms* 9:1634. doi: 10.3390/microorganisms9081634

Sancho, M., Triguero, D., and Garcia-Pascual, A. (2011). Direct coupling through gap junctions is not involved in urethral neurotransmission. *Am. J. Physiol. Renal Physiol.* 300, F864–F872. doi: 10.1152/ajprenal.00641.2010

Stolfi, C., Maresca, C., Monteleone, G., and Laudisi, F. (2022). Implication of intestinal barrier fysfunction in gut fysbiosis and diseases. *Biomedicines* 10:289. doi: 10.3390/biomedicines10020289

Tan, L., Song, X., Ren, Y., Wang, M., Guo, C., Guo, D., et al. (2021). Anti-inflammatory effects of cordycepin: A review. *Phytother. Res.* 35, 1284–1297. doi: 10.1002/ptr.6890

Tiwari, M., Dwivedi, U. N., and Kakkar, P. (2010). Suppression of oxidative stress and pro-inflammatory mediators by *Cymbopogon citratus* D. Stapf extract in lipopolysaccharide stimulated murine alveolar macrophages. *Food Chem. Toxicol.* 48, 2913–2919. doi: 10.1016/j.fct.2010.07.027

Uchida, N. S., Silva-Filho, S. E., Aguiar, R. P., Wiirzler, L., Cardia, G., Cavalcante, H., et al. (2017). Protective effect of *Cymbopogon citratus* essential oil in experimental model of acetaminophen-induced liver injury. *Am. J. Chine. Med.* 45, 515–532. doi: 10.1142/S0192415X17500318

Umukoro, S., Ogboh, S. I., Omorogbe, O., Adekeye, A. A., and Olatunde, M. O. (2017). Evidence for the involvement of monoaminergic pathways in the antidepressant-like activity of *Cymbopogon citratus* in mice. *Drug Res.* 67, 419–424. doi: 10.1055/s-0043-106586

Valcheva, R., Hotte, N., Gillevet, P., Sikaroodi, M., Thiessen, A., and Madsen, K. L. (2015). Soluble dextrin fibers alter the intestinal microbiota and reduce proinflammatory cytokine secretion in male IL-10-deficient mice. *J. Nutr.* 145, 2060–2066. doi: 10.3945/jn.114.207738

Venzon, L., Mariano, L., Somensi, L. B., Boeing, T., de Souza, P., Wagner, T. M., et al. (2018). Essential oil of *Cymbopogon citratus* (lemongrass) and geraniol, but not citral, promote gastric healing activity in mice. *Biomed. Pharmacother.* 98, 118–124. doi: 10.1016/j.biopha.2017.12.020

Vriesman, M. H., Koppen, I., Camilleri, M., Di Lorenzo, C., and Benninga, M. A. (2020). Management of functional constipation in children and adults. *Nat. Rev. Gastroenterol. Hepatol.* 17, 21–39. doi: 10.1038/s41575-019-0222-y

Yang, J., Wang, H. P., Zhou, L., and Xu, C. F. (2012). Effect of dietary fiber on constipation: A meta-analysis. *World J. Gastroenterol.* 18, 7378–7383. doi: 10.3748/wjg.v18.i48.7378

Zhang, C. H., Wang, P., Liu, D. H., Chen, C. P., Zhao, W., Chen, X., et al. (2016). The molecular basis of the genesis of basal tone in internal anal sphincter. *Nat. Commun.* 7:11358. doi: 10.1038/ncomms11358

Zhang, J., Cao, L., Sun, Y., Qing, D. G., Xu, X. Q., Wang, J. C., et al. (2021). The regulatory effects of Licochalcone A on the intestinal epithelium and gut microbiota in murine colitis. *Molecules* 26:4149. doi: 10.3390/molecules26144149

Zhang, S., Wang, R., Li, D., Zhao, L., and Zhu, L. (2021). Role of gut microbiota in functional constipation. *Gastroenterol. Rep.* 9, 392–401. doi: 10.1093/gastro/goab035

Zhu, G. Y., Jia, D. D., Yang, Y., Miao, Y., Wang, C., and Wang, C. M. (2021). The Effect of Shaoyao Gancao decoction on sphincter of oddi dysfunction in hypercholesterolemic rabbits via protecting the enteric nervous system-interstitial cells of Cajal-smooth muscle cells network. *J. Inflamm. Res.* 14, 4615–4628. doi: 10.2147/JIR.S326416

frontiers | Frontiers in Microbiology

TYPE Original Research
PUBLISHED 11 October 2022
DOI 10.3389/fmicb.2022.1007609



OPEN ACCESS

EDITED BY
Hui Zhang,
South China Agricultural University, China

REVIEWED BY
Xueying Tao,
Nanchang University, China
Hongxia Zhang,
Yantai University, China

*CORRESPONDENCE
Zhoujin Tan
tanzhjin@sohu.com

SPECIALTY SECTION
This article was submitted to Microorganisms in Vertebrate Digestive Systems, a section of the journal Frontiers in Microbiology

RECEIVED 30 July 2022
ACCEPTED 15 September 2022
PUBLISHED 11 October 2022

CITATION
Zhu J, Li X, Deng N, Peng X and Tan Z (2022) Diarrhea with deficiency kidney-yang syndrome caused by adenine combined with *Folium senna* was associated with gut mucosal microbiota.
*Front. Microbiol.* 13:1007609.
doi: 10.3389/fmicb.2022.1007609



# Diarrhea with deficiency kidney-yang syndrome caused by adenine combined with *Folium senna* was associated with gut mucosal microbiota

Jiayuan Zhu[1], Xiaoya Li[2], Na Deng[2], Xinxin Peng[3] and Zhoujin Tan[2]*

[1]College of Pharmacy, Hunan University of Chinese Medicine, Changsha, China, [2]College of Chinese Medicine, Hunan University of Chinese Medicine, Changsha, China, [3]The First Affiliated Hospital of Hunan University of Chinese Medicine, Changsha, China

The present study aims to study and analyze the characteristics of gut mucosal microbiota in diarrhea mice with deficiency kidney-yang syndrome. Ten male mice were randomly divided into the control group and the model group. Diarrhea mice model with deficiency kidney-yang syndrome was established by adenine combined with *Folium sennae*. The kidney structure was observed by hematoxylin-eosin (HE) staining. Serum $Na^+$-$K^+$-ATP-ase and $Ca^{2+}$-$Mg^{2+}$-ATP-ase were detected by enzyme-linked immunosorbent assay (ELISA). The characteristics of gut mucosal microbiota were analyzed by performing third-generation high-throughput sequencing. The results showed that the model mice exhibit obvious structural damage to the kidney. Serum $Na^+$-$K^+$-ATP-ase and $Ca^{2+}$-$Mg^{2+}$-ATP-ase levels showed a decreased trend in the model group. The diversity and community structure of the gut mucosal microbiota improved in the model group. Dominant bacteria like *Candidatus Arthromitus*, *Muribaculum,* and *Lactobacillus reuteri* varied significantly at different taxonomic levels. The characteristic bacteria like *Bacteroides*, *Erysipelatoclostridium, Anaerotignum, Akkermansia muciniphila*, *Clostridium cocleatum*, *Bacteroides vulgatus,* and *Bacteroides sartorii* were enriched in the model group. A correlation analysis described that *Erysipelatoclostridium* was positively correlated with $Na^+$-$K^+$-ATP-ase and $Ca^{2+}$-$Mg^{2+}$-ATP-ase levels, while *Anaerotignum* exhibited an opposite trend. Together, adenine combined with *Folium sennae* damaged the structure of the kidney, affected energy metabolism, and caused disorders of gut mucosal microbiota in mice. *Bacteroides*, *Erysipelatoclostridium,* and *Anaerotignum* showed significant inhibition or promotion effects on energy metabolism. Besides, *Akkermansia muciniphila*, *Clostridium cocleatum*, *Bacteroides vulgatus,* and *Bacteroides sartorii* might be the characteristic species of gut mucosal microbiota responsible for causing diarrhea with deficiency kidney-yang syndrome.

KEYWORDS

**adenine combined with *Folium sennae*, diarrhea with deficiency kidney-yang syndrome, gut mucosal microbiota, kidney, energy metabolism**

# Introduction

Diarrhea is defined as reduced stool consistency, increased water content, and the number of evacuations per day, which is highly associated with gut microbiota dysbiosis (Mendez et al., 2019; Xie et al., 2019; Shao et al., 2020; Li Y. X. et al., 2021). Currently, with the change in people's lifestyle and diet structure, the number of patients with diarrhea is increasing year by year (Huang et al., 2019). The earliest discussion of diarrhea in traditional Chinese medicine (TCM) was found in the "Yellow Emperor's Classic of Internal Medicine". Ancient and modern medical practitioners mostly believed that the key internal organ of diarrhea was the spleen, which also involves the liver, kidney, and other internal organs. Due to the differences in etiology, pathogenesis, and clinical manifestations of patients, different types of diarrhea could be found in TCM, among which the deficiency kidney-yang syndrome was a common syndrome of diarrhea (Li Y. L. et al., 2021). As early as in the "Yellow Emperor's Classic of Internal Medicine", the theory of "treating diarrhea from the kidney" was mentioned (Wang et al., 2016). TCM emphasized that the human body is a whole system and that the tissues of the internal organs are interrelated. The theory of "treating diarrhea from the kidney" explained that the spleen and kidney were physiologically related and pathologically connected. In the process of syndrome differentiation and treatment of diarrhea, the regulation of kidney functions should not be neglected (Chen et al., 2021). Hence, the development of diarrhea was closely related to the kidney.

Gut microbiota consists of a variety of microorganisms that reside in the gastrointestinal tract, and they are host-specific and evolve with the individual. The composition and diversity of this microbial community are susceptible to a variety of factors (such as diet, drugs, pathogens, and environmental factors), which in turn affect human and animal health (Wu et al., 2020). There is evidence that imbalances in the gut microbiota increase susceptibility to a wide range of pathogens and contribute to many diseases, including diarrhea, irritable bowel syndrome, allergies, cardiovascular disease, and obesity (Zhu et al., 2021). Besides, intestinal diseases may have multiple effects on the host, such as altering the composition of the gut microbiota (Meng et al., 2020; Zhou et al., 2020). Therefore, it is very meaningful to investigate the correlation between diarrhea with kidney-yang deficiency syndrome and changes in gut microbiota.

Adenine is a drug that is mainly used clinically in tumor radiation therapy, tumor chemotherapy, and psychotherapy (Su W. W. et al., 2020). Orally ingested adenine is rapidly metabolized to water-insoluble 2,8-dihydroxyadenine, which is deposited and crystallized in the microvilli and the apical domains of the epithelia in proximal renal tubules, causing renal tubule obstruction, leading to renal failure, and affecting the energy metabolism of renal tissue, thus resulting in the manifestation of kidney-yang deficiency (Jia and Jia, 2016; Sueyoshi et al., 2019). *Folium sennae is* a bitter-cold laxative commonly used in TCM, with the main laxative component being senna glycosides A and B, which can cause intestinal hyperfunction and lead to diarrhea (Guan et al., 2021). Our group has found significant diarrheal symptoms in mice after *Folium sennae* modeling and disturbances in the gut mucosal microbiota of the model mice (Zhang et al., 2020a). In addition, we compared the effects of adenine combined with *Folium sennae* at different doses and days on kidney and intestinal function in mice and found that adenine (50 mg/(kg·d), gavaged for 14 days) combined with *Folium sennae* (10 g/(kg·d), gavaged for 7 days) significantly caused impairment of the kidney and intestinal functions in mice (Li et al., 2022a). Subsequently, we have successfully constructed and validated a mouse model of diarrhea with deficiency kidney-yang syndrome using the same modeling method described above, thus confirming the reliability of the model (Li et al., 2022b). In this study, adenine combined with *Folium sennae* was used to construct a model of diarrhea with deficiency kidney-yang syndrome. By exploring the characteristics of gut mucosal microbiota and the correlation between differential bacteria and energy metabolism, this study provided a basis for exploring the treatment of diarrhea with kidney-yang deficiency syndrome from the perspective of gut mucosal microbiota. The specific process is shown in Figure 1.

# Materials and methods

## Animals

Ten 4-week-old Kunming male mice (weighing 18–22 g) were purchased from Slack Jingda Experimental Animal Co, Ltd. (Hunan, China, license number: SCXK [Xiang] 2016-0002). All mice were housed in the Animal Experiment Center of the Hunan University of Chinese Medicine with free access to food and drinking water (room temperature 23–25°C, relative humidity 50–70%, and 12 h of light/darkness). All animal experiments were performed according to the guidelines approved by the Institutional Animal Care and Use Committee of Hunan University of Chinese Medicine (license number: SYXK [Xiang] 2019-0009). Animal experiments were approved by the Animal Ethics and Welfare Committee of the Hunan University of Chinese Medicine (LLBH-202106120002). To exclude the effect of gender on gut microbiota, only male rats were used in this study (Wu et al., 2022).

## Medicine

Adenine (Changsha Yaer Biology Co., LTD, EZ2811A135) suspension preparation (Xiao et al., 2008): adenine was prepared in sterile water to a final concentration of 5 mg/mL in proportion to the concentration of the suspension, which

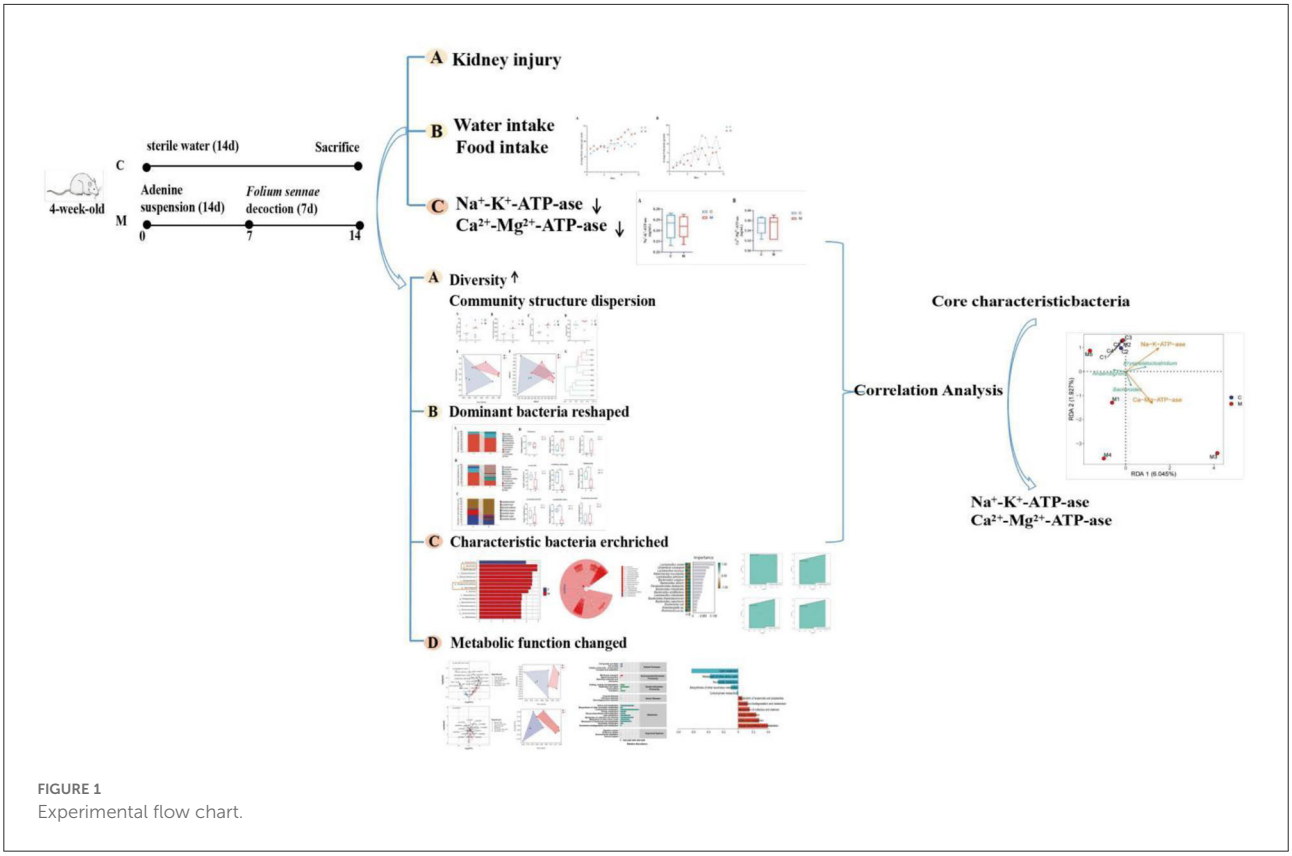


FIGURE 1
Experimental flow chart.

is ready to use preparation for daily use. *Folium senna* (Anhui Puren Chinese Herbal Beverage Co., LTD, 2005302) decoction preparation (Xie et al., 2022): Appropriate amount of *Folium sennae* was placed in a decoction vessel, and then appropriate amount of water was added (over the *Folium sennae*) and soaked for 30 min. After 30 min, the water was poured off, and five times the amount of water was added to the vessel and boiled for 30 min. Then filtered dregs were added to an appropriate amount of water, and the boiling of the decoction was continued for 15 min. The decoction was mixed with the two decoctions and then boiled for 15 min. The decoction was further concentrated to form a decoction containing 1 g/mL of raw herbs and stored in a refrigerator at 4°C.

## Reagents

$Na^+$-$K^+$-ATP-ase enzyme-linked immunosorbent assay (ELISA) Kit (Jiangsu Jingmei Biotechnology Co., LTD, number: JM-11845M1) and $Ca^{2+}$-$Mg^{2+}$-ATP-ase ELISA Kit (Jiangsu Jingmei Biotechnology Co., LTD, number: JM-12156M1) were used in the experiments.

## Grouping and modeling of animals

After 3 days of acclimatization feeding, 10 male mice were randomly divided into the control (C) group and model (M) group, with five mice in each group. After the modeling method was improved in reference to the literature (Xiao et al., 2008, 2016), mice in the M group were gavaged with adenine suspension (50 mg/(kg·d), 0.4 mL per time) once a day for 14 consecutive days. From the 8th day of modeling, mice in the M group were gavaged with the *Folium sennae* decoction (10 g/(kg·d), 0.4 mL per time) once a day for 7 days. Mice in the C group were intragastrically gavaged with an equal volume of sterile water, once a day, for 14 days.

## Model evaluation criteria

According to the clinical manifestations of diarrhea with deficiency of kidney-yang syndrome (Spleen and Stomach Branch of China Association of Traditional Chinese Medicine, 2017), the diagnostic criteria of macroscopic symptoms in mice diarrhea with deficiency of kidney-yang syndrome were dilute feces, or incomplete pellets, cold extremities, curved and arched

back, decreased appetite and body weight, and depression. On the basis of the manifestation of macroscopic signs, combined with histopathological sections of the kidney, a reliable basis for model evaluation was provided.

## General behavioral observations

During the experiment, mice were observed for their mental state, activity frequency, and fecal characteristics. The amount of water consumed and the amount of food ingested by the mice were tested and recorded daily (Li et al., 2022c).

## Pathological slides of kidney

Under aseptic conditions, the connective tissue of the kidney was removed on an ultra-clean bench, fixed in 4 % paraformaldehyde solution, dehydrated by gradient ethanol, made transparent by xylene, embedded in paraffin, sliced, stained with HE, and the histopathological changes of the kidney were observed under a light microscope.

## ELISA analysis

The blood sample for the ELISA was left to stand for 30 min at room temperature. After centrifugation at 3,000 r/min for 10 min, the serum was separated and the test samples were loaded into a sterilized centrifuge tube. The method for setting plate layout, adding samples, adding enzymes, incubation, washing plate, color, termination reaction, and machine detection was performed according to the instructions provided by the manufacturer of the ELISA kit.

## 16S rRNA gene high-throughput sequencing

After the experiment, the mice were sacrificed by cervical dislocation. Under aseptic conditions, the abdominal cavity of mice was opened and the small intestine was removed. The small intestine was cut open along the long axis, rinsed with saline, and dried with filter paper, and then the intestinal mucosa was scraped and collected on a sterilized coverslip (He et al., 2019). The samples were separately loaded into 1.5 mL sterilized centrifuge tubes, numbered, weighed, and then stored in a −80°C refrigerator for the detection of gut mucosal microbiota. The total genomic DNA of the samples was extracted from the intestinal mucosa samples using the bacterial DNA Kit (OMEGA, USA). The quantity and quality of the extracted DNA were determined by NanoDrop NC2000 spectrophotometer (Thermo Fisher Scientific, Waltham, MA, USA) and agarose gel electrophoresis. Forward primer 27F (5′-AGAGTTTGATCMTGGCTCAG-3′) and reverse primer 1492R (5′-GGACTACHVGGGTWTCTAAT-3′) were used for PCR amplification of bacterial 16S rRNA near the full-length gene. The 16S rRNA gene was amplified by polymerase chain reaction (PCR) using Q5 high-fidelity DNA polymerase (New England BioLabs, USA). PCR products were detected by 2% agarose gel electrophoresis and purified by the Axygen® AxyPrep DNA gel extraction kit. The recovered PCR amplification products were quantified by fluorescence intensity using the Quant-it PicoGreen dsDNA Assay Kit. According to the fluorescence quantitative results, the samples were mixed in proportion to the sequencing requirements of each sample (Yuan et al., 2020). Sequencing was completed by Paiseno Biological Co., LTD (Shanghai, China).

## Bioinformatics and statistical analysis

Gut mucosal microbiota was analyzed by high-throughput sequencing of 16S rRNA, and sequences with similarity higher than 97% were assigned to an OTU (Wang et al., 2018). Species accumulation curves were used to test the sequencing depth and evaluate the quality of sequence data. Chao1 and Observed_species indexes reflect the abundance of the community, and the larger the index, the higher the abundance of the community. Simpson and Shannon indexes reflect community diversity, and higher index values indicate higher community diversity. The beta diversity analysis examines the similarity of community structure among different samples. Three main methods, that is, principal coordinate analysis (PCoA), non-metric multidimensional scaling (NMDS), and clustering analysis, are used to naturally decompose the community data structure and rank the samples by ordination to observe the differences between samples (Bray and Curtis, 1957). LEfSe and random forest analysis detected groups that differ significantly in the abundance of gut mucosa and also identify potential biomarkers (Breiman, 2001; Edgar, 2013). The receiver operating characteristic curve (ROC) was plotted, and the area under the curve (AUC) was calculated to analyze the role of differential flora in predicting the disease. Redundant analysis (RDA) was used to investigate the association of biochemical indicators with gut mucosal microbiota (Zhang et al., 2021).

The SPSS 21.00 software was used for statistical analysis, and the data obtained from each group were expressed as mean ± standard deviation. If the data of the two groups were in line with normal distribution and homogeneity of variance, an independent sample *t*-test was used. If the data did not conform to a normal distribution and variance was uneven, Wilcoxon rank-sum test was used. $P < 0.05$ indicates a statistical difference, and $p < 0.01$ indicates a very strong statistical difference; otherwise, there was no statistical significance (Li X. Y. et al., 2021).

# Results

## Modeling induced behavioral changes in mice

During the modeling period, mice in the C group had normal mental status and autonomic activity, with smooth and responsive fur. Mice in the M group were in poor mental status, with sparse and dull fur, wet bedding, and loose feces stuck to the bedding. On the 9th day of modeling (Figure 2A), the average daily water intake of the M group was much higher than the C group ($p < 0.05$). From the 4th day of modeling (Figure 2B), the average daily food intake of the M group was consistently lower than the C group ($p > 0.05$). The results suggested that modeling induced behavioral changes in mice.

## Modeling damaged the kidney structure in mice

The structural morphology of the kidney of mice in the C group showed no abnormal pathological manifestations. In the M group, glomerular thylakoid hyperplasia, interstitial edema, congestion, aggregation of inflammatory cells, different degrees of dilatation of renal tubules, lumen enlargement, tubular wall degeneration, and edema (Figure 3) were observed, indicating that modeling damaged the kidney structure of mice.

## Modeling affected energy metabolism in mice

The levels of $Na^{+}$-$K^{+}$-ATP-ase and $Ca^{2+}$-$Mg^{2+}$-ATP-ase were reduced in the M group when compared with the C group ($p > 0.05$; $p > 0.05$) (Figure 4), suggesting that adenine combined with *Folium sennae* affected the energy metabolism of mice to a certain extent.

## Sequencing data quality assessment and OTU count of gut mucosal microbiota in mice

An inflection point occurred and then the curve flattened out with increasing sequencing depth to reach a plateau. The results indicated that the two sets of samples were sequenced at a sufficient and reasonable depth to cover most biological species and that the species richness of the samples tested was sufficient for subsequent studies (Figures 5A–D). Figure 5E depicts the species accumulation curve, which shows that with the increase in the sample size, the number of detected species increases significantly, and the curve becomes relatively steep. When the sample size increased to a certain level, further increase in the sample size does not detect new species and the curve tends to flatten out. These findings indicate that the sample size of this experiment was sufficient to reflect the richness of the community.

Venn diagram analyzes the unique or common OTUs between different sample groups, visually showing the similarity and uniqueness of the samples at the OTU level. The common OTUs in the C and M groups were 80. There were 200 OTUs unique to the C group and 329 OTUs unique to the M group. The total number of OTUs in the normal group was 280, and the total number of OTUs in the model group was 409 (Figure 5F), suggesting that modeling increased the number of species of the gut mucosal microbiota and taxonomic units in mice.

## Modeling affected the diversity and the microbiota structure in mice

In order to comprehensively assess the alpha diversity of microbial communities, Chao1 and Observed_species indexes were used to determine the richness of species. Shannon and Simpson indexes were used to evaluate community diversity (Figures 6A–D). The Simpson index in the C group was slightly lower than that in the M group ($p > 0.05$), and the Chao1, Shannon, and Observed_species indexes in the C group were slightly higher in the M group ($p > 0.05$, $p > 0.05$, and $p > 0.05$, respectively). As could be seen from Figures 6E,F, the M samples were efficiently separated from the C samples and presented the phenomenon of grouping and aggregation. All these findings suggest that adenine combined with *Folium sennae* modeling altered the homogeneity of gut mucosal microbiota. From the clustering analysis (Figure 6G), it could be seen that the distance between the samples in the C group was relatively small. It reflected the small intra-group variation. Several samples in the M group, except for the M2 sample, could be well clustered into one group. In addition, M1 and M4 clustered more easily with the rest of the samples of the M group than with the C group, which reflected that the intra-group variation of the samples in the M group was larger than that in the C group, but they still could be well separated from the samples of the C group. Together, modeling affected the diversity and microbiota structure in mice.

## Modeling reshaped the dominant bacteria composition of the gut mucosal microbiota in mice

The horizontal coordinates of the bars indicated groups, and the vertical coordinates, respectively, indicated the relative

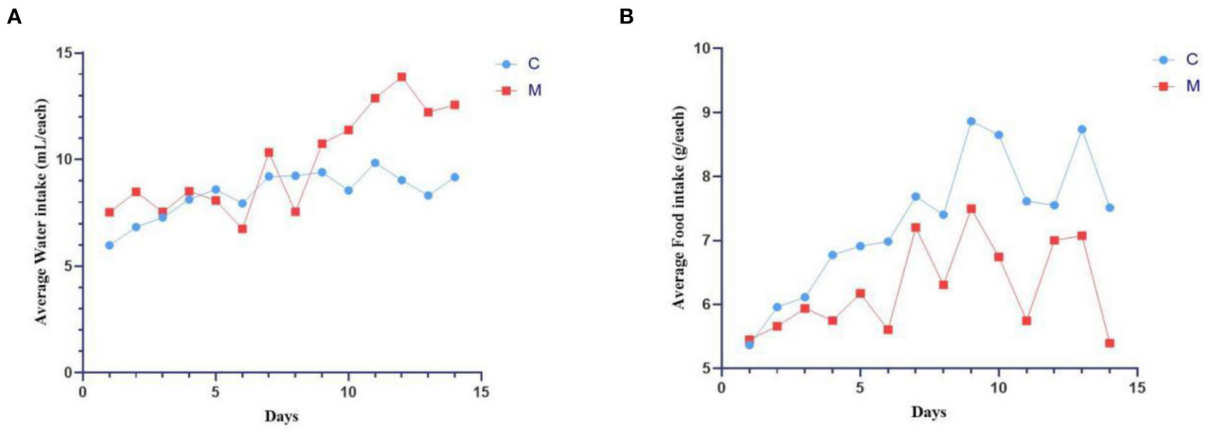


FIGURE 2
Modeling induced behavioral changes in mice. **(A)** Average water intake. **(B)** Average food intake. C, Control group ($n = 5$); M, Model group ($n = 5$). The values are expressed as mean ± standard deviation.

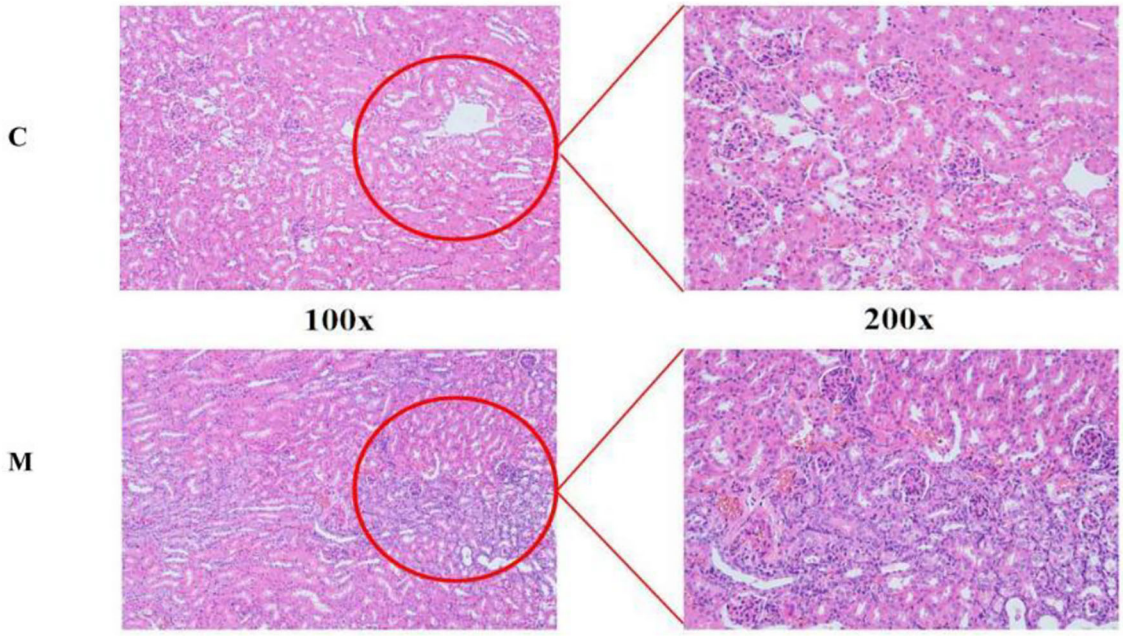


FIGURE 3
HE staining sections of kidney tissue. C, Control group; M, Model group.

abundance of gut mucosal microbiota at the phylum, genus, and species levels. We performed a taxonomic histological analysis in the C group and the M group and compared the differences at the phylum, genus, and species levels. Figure 7A indicates that the top three phyla were Firmicutes, Bacteroidetes, and Proteobacteria in both the C group and the M group (87.99, 10.06, and 1.09% in the C group, but 69.73, 19.65, and 7.31% in the M group, respectively).

*Lactobacillus*, *Candidatus Arthromitus,* and *Muribaculum* were the top three genera in the C group, and the dominant genera in the M group were *Lactobacillus*, *Bacteroides*, and *Helicobacter*. The M group had a lower proportion of *Lactobacillus, Candidatus Arthromitus,* and *Muribaculum* and

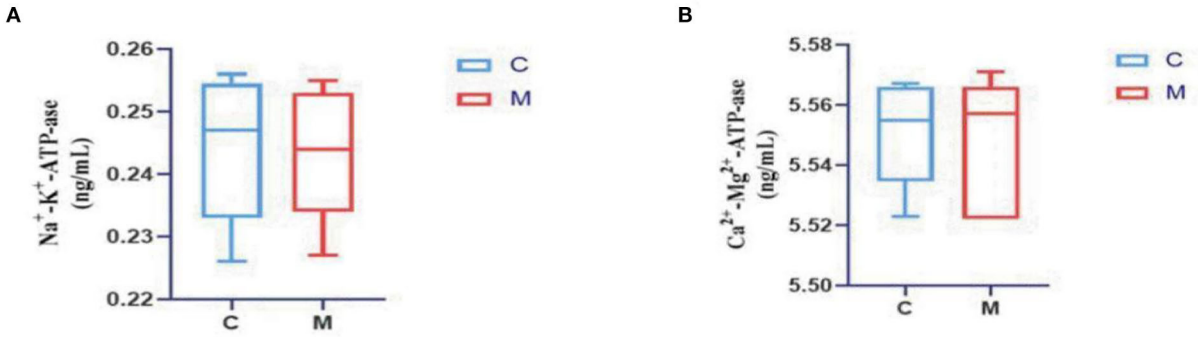


FIGURE 4
Modeling affected energy metabolism in mice. **(A)** $Na^{+}$-$K^{+}$-ATP-ase. **(B)** $Ca^{2+}$-$Mg^{2+}$-ATP-ase. C, Control group ($n = 5$); M, Model group ($n = 5$). The values are expressed as mean ± standard deviation.

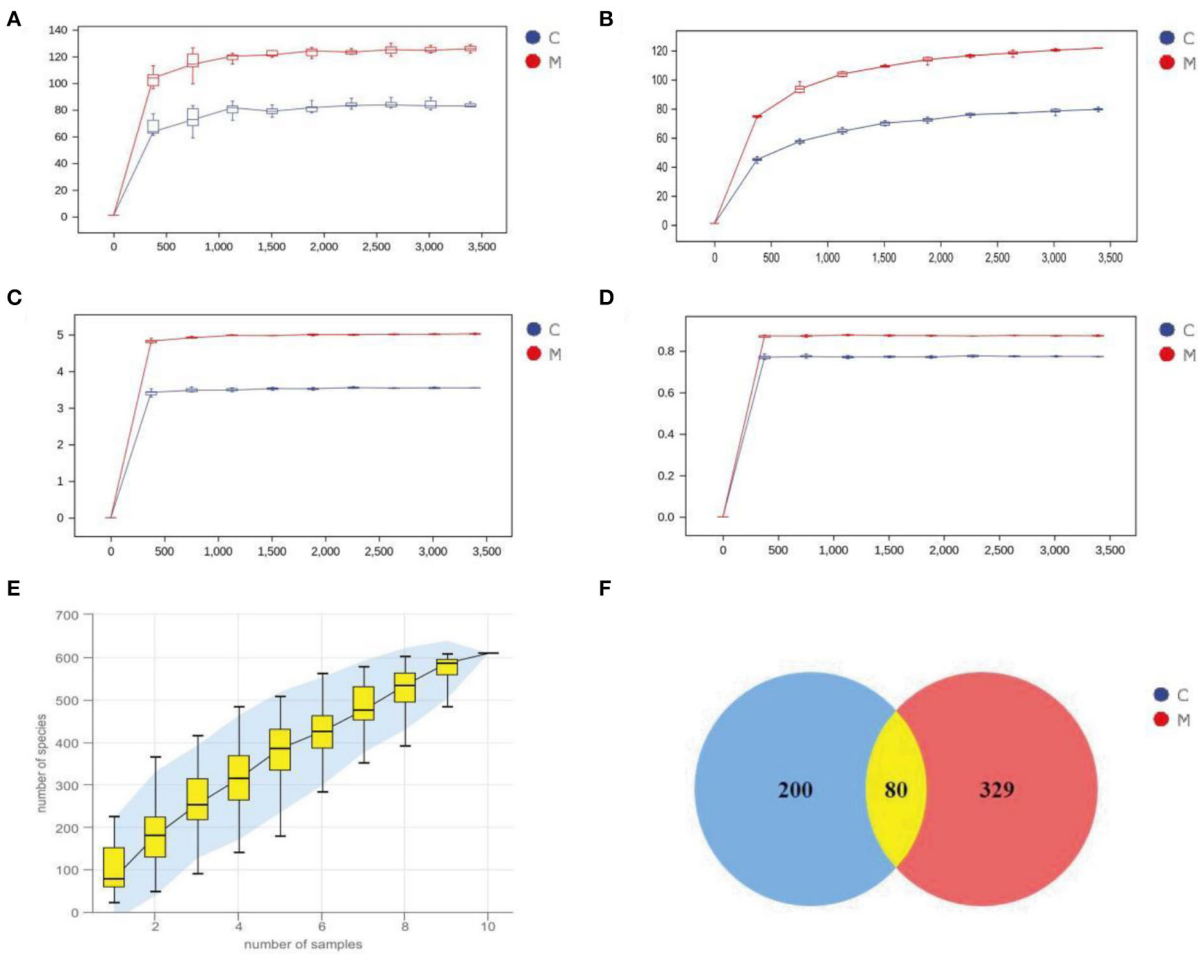


FIGURE 5
Sequencing data quality assessment and OTU count of gut mucosal microbiota. **(A)** Dilution curve of Chao1. **(B)** Dilution curve of Observed_species. **(C)** Dilution curve of Simspon. **(D)** Dilution curve of Shannon. **(E)** Species accumulation curves. **(F)** Venn diagram. C, Control group ($n = 5$); M, Model group ($n = 5$).

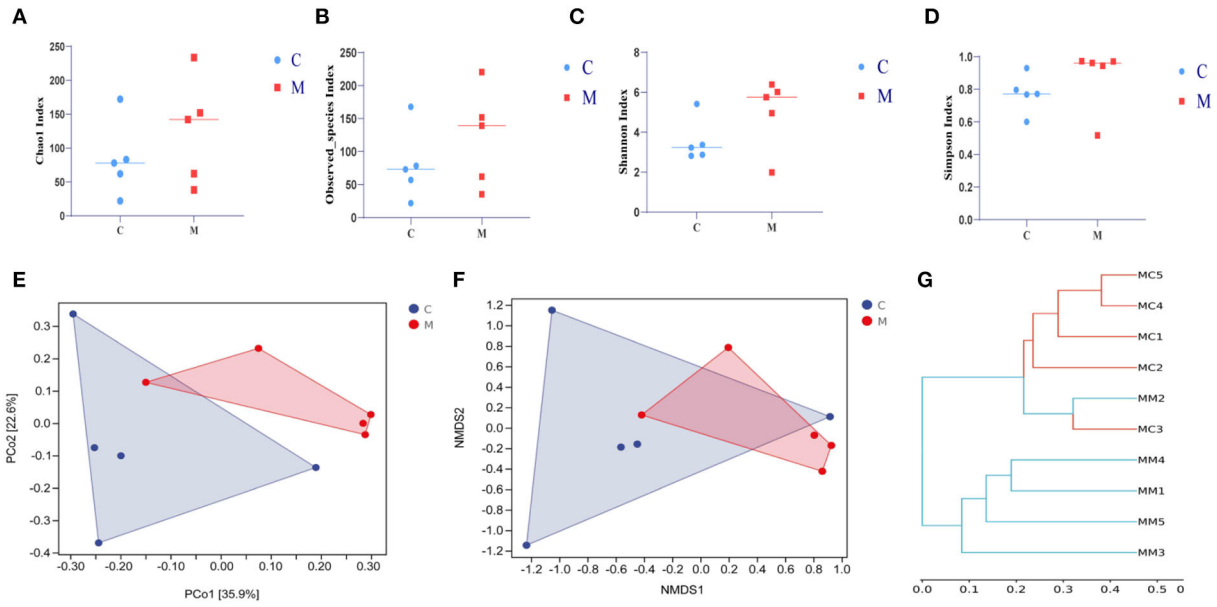


FIGURE 6
Effect of modeling on the diversity of the gut mucosal microbiota in mice. **(A)** Chao1 index. **(B)** Observed_species index. **(C)** Shannon index. **(D)** Simpson index. **(E)** PCoA analysis. **(F)** NMDS analysis. **(G)** Clustering analysis. C, Control group ($n = 5$); M, Model group ($n = 5$).

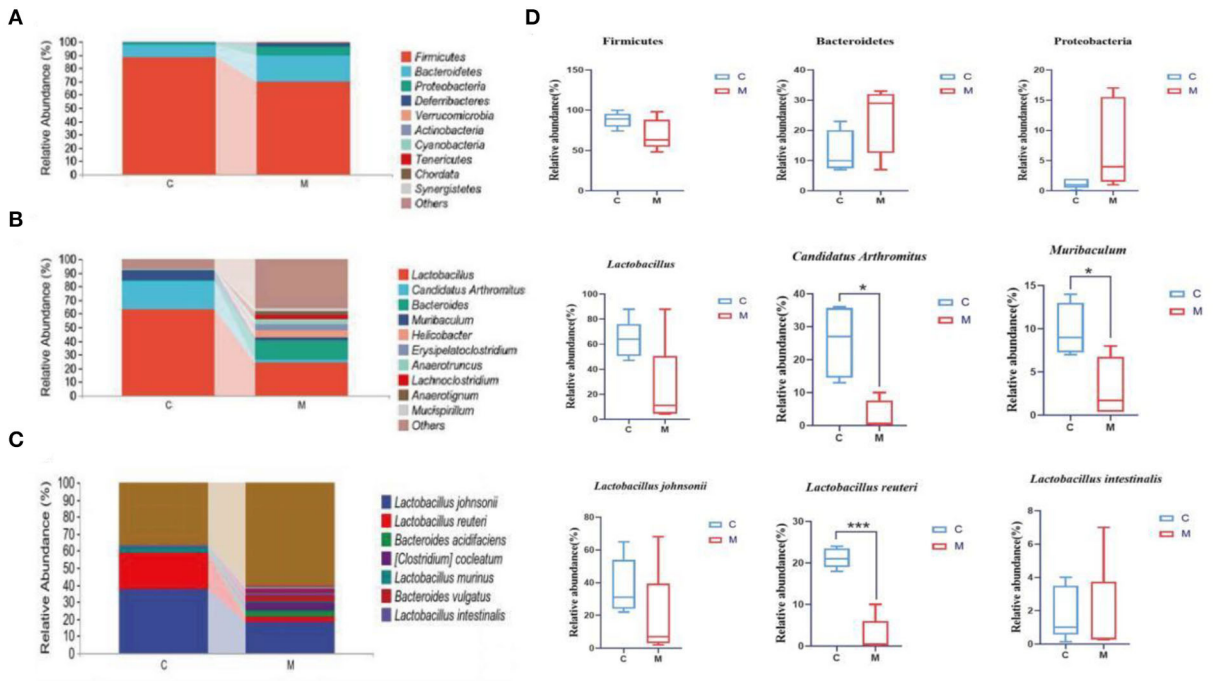


FIGURE 7
Effect of modeling on the relative abundance of gut mucosal microbiota in mice. **(A)** Relative abundance of gut mucosal microbiota at the phylum level. **(B)** Relative abundance of gut mucosal microbiota at the genus level. **(C)** Relative abundance of gut mucosal microbiota at the species level. **(D)** Phylum, genus, and species levels of dominant bacteria of gut mucosal microbiota in mice. C, Control group ($n = 5$); M, Model group ($n = 5$). The values are expressed as mean ± standard deviation. $^{*}p < 0.05$, $^{***}p < 0.01$.

a higher proportion of *Bacteroides* and *Helicobacter* than the C group (Figure 7B), indicating the changes in the composition of the dominant bacteria at the genus level.

Specific for species level analysis (Figure 7C) indicated that the abundance of *Lactobacillus johnsonii*, *Lactobacillus reuteri,* and *Lactobacillus murinus* in the C group was markedly higher than that in the M group. The dominant bacteria in the M group specifically were *Lactobacillus johnsonii*, *Bacteroides acidifaciens,* and *Bacteroides vulgatus*. The population of *Bacteroides vulgatus* and *Bacteroides sartorii* was significantly higher in the M group than in the C group, which indicated the changes in the composition of the dominant bacteria at the species level.

We further performed a statistical analysis of the bacteria with a relative abundance >1% in both the C group and the M group at the phylum, genus, and species levels (Figure 7D). Compared with the C group, the relative abundance of Bacteroidetes and Proteobacteria in the M group was increased ($p > 0.05$; $p > 0.05$), while that of Firmicutes decreased ($p > 0.05$). *Lactobacillus, Candidatus Arthromitus,* and *Muribaculum* in the M group decreased significantly ($p > 0.05$, $p < 0.05$, and $p < 0.05$, respectively). At the species level, *Lactobacillus johnsonii*, *Lactobacillus intestinalis*, and *Lactobacillus reuteri* in the M group decreased ($p > 0.05$, $p > 0.05$, and $p < 0.01$, bacteria). In summary, Bacteroidetes, Proteobacteria, Firmicutes, *Lactobacillus, Candidatus Arthromitus*, *Muribaculum, Lactobacillus johnsonii*, *Lactobacillus intestinalis*, and *Lactobacillus reuteri* might play important an role as the dominant bacteria in diarrhea with kidney-yang deficiency syndrome.

## Significant enrichment of core differential bacteria of gut mucosal microbiota in mice

The LEfSe method was used to directly search for key species that were statistically different between groups at all taxonomic levels. In the experiment, LDA = 4 was set as the cut-off point. The C group showed no significant enrichment of any bacterial taxon. The M group showed significant enrichment of eight bacterial taxa. Of these, *Bacteroides*, *Erysipelatoclostridium*, and *Anaerotignum* were involved at the genus level (Figures 8A,B). Then, we constructed a random forest diagnostic model to distinguish the C group from the M group by using 20 bacteria at the species levels (Figure 8C). The ROC results displayed (Figure 8D) that *Akkermansia muciniphila*, *Clostridium cocleatum*, *Bacteroides vulgatus*, and *Bacteroides sartorii* presented large AUC values, denoting that *Akkermansia muciniphila*, *Clostridium cocleatum*, *Bacteroides vulgatus*, and *Bacteroides sartorii* might be used as potential biomarkers at the species level of gut mucosal microbiota for the diagnosis of diarrhea with deficiency kidney-yang syndrome.

## Modeling altered the function of the gut mucosal microbiota in mice

A phylogenetic investigation of communities by reconstruction of unobserved states2 (Picrust2) software was applied to predict 396 EC enzyme labels of microbiota (including 59 upregulated ECs and 18 downregulated ECs, $p < 0.05$) and 170 KEGG homologous genes (including 35 upregulated KOs and 14 downregulated KOs, $p < 0.05$) (Figures 9A,C). The samples in the two databases showed significant separation (Figures 9B,D). Also, the gut mucosal microbiota function was generally divided into six categories, and the second level included 29 sub-functional categories, with the metabolic function accounting for a greater abundance. Among them, the gut mucosal microbiota of mice had a significant role in regulating carbohydrate metabolism, amino acid metabolism, and energy metabolism (Figure 9E).

## Modeling affected the interaction between differential bacteria of gut mucosal microbiota and energy metabolism in mice

The RDA results pointed out that *Bacteroide*s was positively correlated with $Ca^{2+}$-$Mg^{2+}$-ATP-ase and negatively correlated with $Na^{+}$-$K^{+}$-ATP-ase. *Erysipelatoclostridium* was positively correlated with $Na^{+}$-$K^{+}$-ATP-ase and $Ca^{2+}$-$Mg^{2+}$-ATP-ase. *Anaerotignum* was negatively correlated with $Na^{+}$-$K^{+}$-ATP-ase and $Ca^{2+}$-$Mg^{2+}$-ATP-ase (Figure 10). These results indicated that there was a correlation between the populations of *Bacteroides*, *Erysipelatoclostridium*, and *Anaerotignum* and the energy metabolism after mice were modeled with adenine combined with *Folium sennae*.

# Discussion

Observation of the animal behavioral characteristics defining the syndrome of TCM in animal models is an important support for TCM research (Ren and Peng, 2020). Behavioral changes in the mice were recorded and assessed during the modeling process. The mice in the M group showed increased water intake, cool tail, arching back and lethargy, piling up, loose stools, decreased anal temperature and filthy perianal area, and feces stuck to the bedding. From the 4th day of modeling, the average daily water intake in the M group was much higher than that in the C group. The average daily food intake in the M group was persistently lower than that in the C group since the 4th day. In conjunction with the kidney histopathological sections, we also observed that the glomerulus and renal tubules of mice in the M group were obviously damaged. The renal interstitium was edematous,

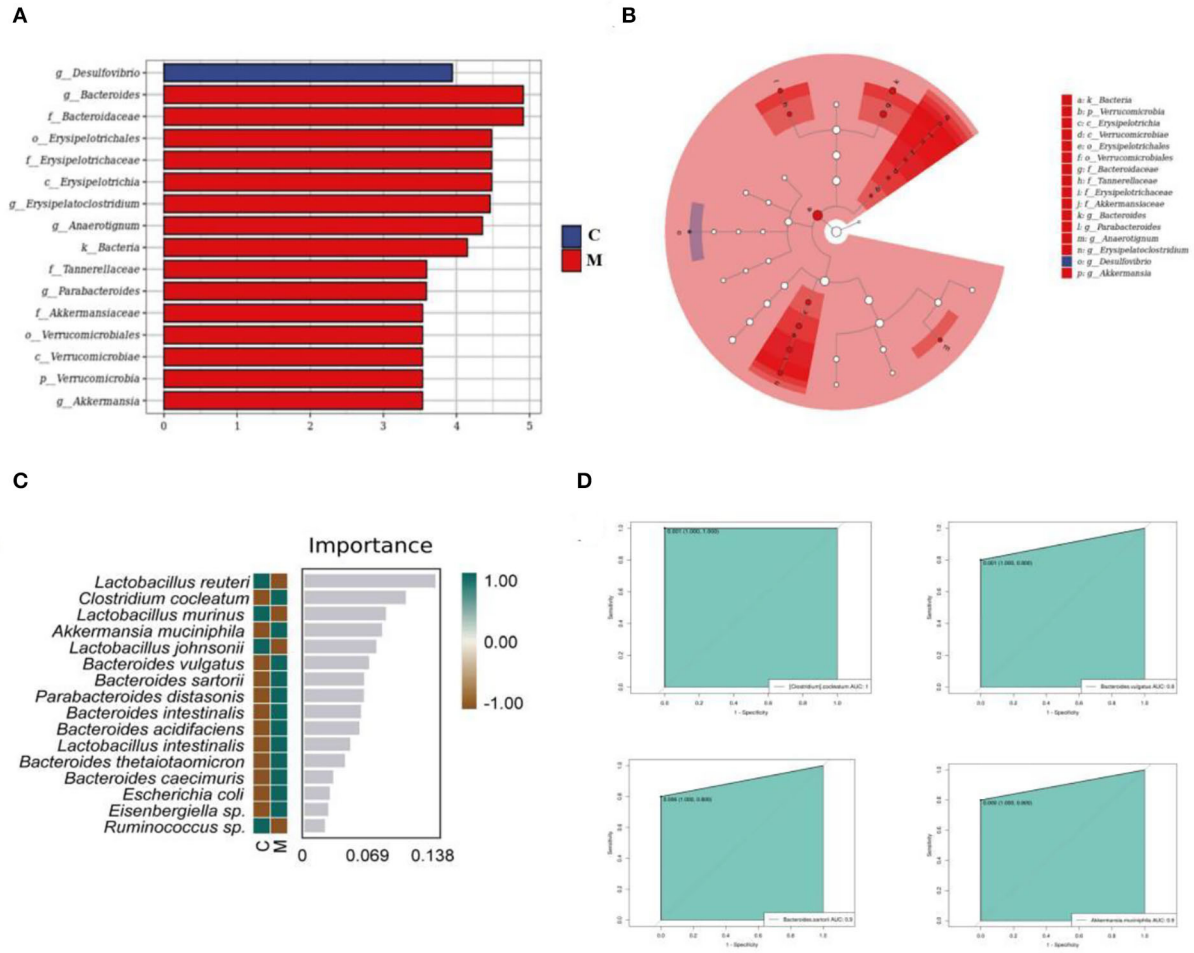


FIGURE 8
Core characteristic bacterial analysis of gut mucosal microbiota. **(A)** LDA diagram. **(B)** Cladogram diagram. **(C)** Random forest diagram of species level. **(D)** ROC curve of species. C, Control group ($n = 5$); M, Model group ($n = 5$).

and inflammatory cells were aggregated. It suggested that adenine combined with *Folium senna* damaged the structure of the kidney in mice. $Na^+$-$K^+$-ATP-ase and $Ca^{2+}$-$Mg^{2+}$-ATP-ase are membrane-bound proteins located in the inner mitochondrial and cellular membranes, and they are important indicators of mitochondrial function and energy metabolism levels (Simão et al., 2011). It was demonstrated that the activity of $Na^+$-$K^+$-ATP-ase and $Ca^{2+}$-$Mg^{2+}$-ATP-ase in the rats with kidney-yang deficiency syndrome was reduced and the mitochondrial structure was impaired, leading to the reduction in energy metabolism (Qiu et al., 2019). In the present study, the activity of both enzymes was affected in the serum of mice, which proved that the animal model of diarrhea with deficiency kidney-yang syndrome was successfully constructed.

The relationship between diarrhea and gut mucosal dysbiosis is gradually being understood (Zhang et al., 2020b, 2021). Both adenine and *Folium senna* caused gut mucosal barrier damage and an imbalance of microbial communities (Blander et al., 2017; Huang et al., 2022). Combined with the experimental results, the richness of gut mucosal microbiota (Chao1 and Observed_species indexes) and the diversity (Simpson and Shannon indexes) were higher in the M group than in the C group. Beta diversity also confirmed that modeling caused impressive dispersion of community structure of gut mucosal microbiota in mice, suggesting that modeling influenced the richness, diversity, and structure of gut mucosal microbiota.

Patients with kidney injury had an imbalance in gut mucosal microbiota, with an upregulation in Firmicutes, Actinobacteria, and Proteobacteria, and downregulation in *Bifidobacteria* and *Lactobacilli* (Vaziri et al., 2013). Studies have confirmed that diarrhea rats with spleen deficiency induced significant changes in the abundance of Firmicutes and Proteobacteria, and upgraded several genera, such as

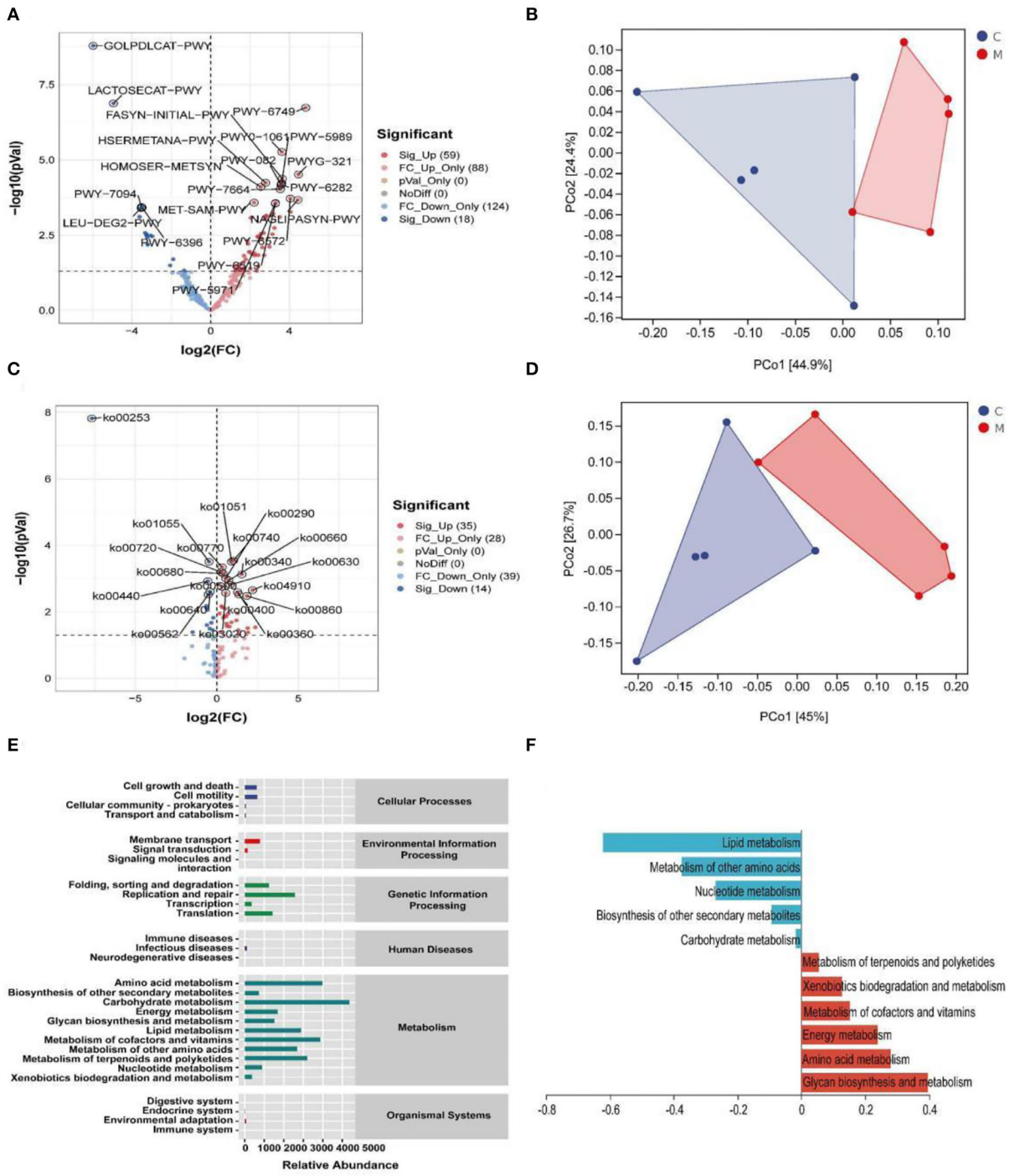


FIGURE 9
Functional analysis of gut mucosal microbiota. **(A)** Volcano map of MetaCyc pathway. **(B)** MetaCyc functional unit PCoA map. **(C)** KEGG pathway volcanoes. **(D)** PCoA diagram of KEGG functional units. **(E)** Predicted abundance of KEGG function. **(F)** Histogram of metabolic function in positive and negative coordinates. C, Control group ($n = 5$); M, Model group ($n = 5$).

*Clostridium*, *Bacteroides*, *Parabacteroides*, *Alloprevotella,* and *Helicobacter* (Shi et al., 2020). The preliminary experiments showed that the abundance of Actinobacteria, Proteobacteria, *Veillonococcus, Mycoplasma, Escherichia coli,* and *Enterococci* was elevated in diarrhea mice with deficiency kidney-yang syndrome, while *Bifid bacteria and Lactobacillus* were decreased

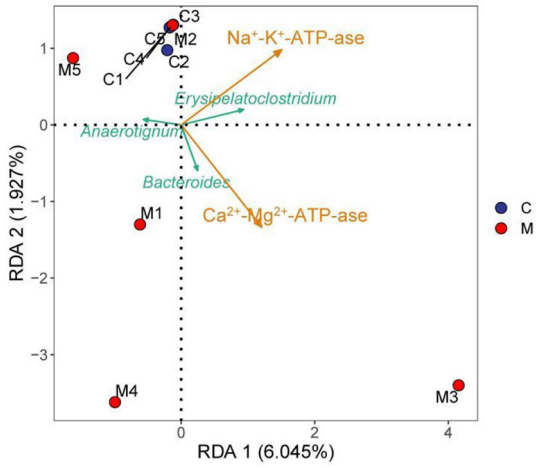


FIGURE 10
RDA analysis. C, Control group ($n = 5$); M, Model group ($n = 5$).

(Li X. Y. et al., 2021). In our experiments, the taxonomic composition of gut mucosal microbiota in mice changed after the animal was modeled. Compared to the C group, *Lactobacillus*, *Candidatus Arthromitus,* and *Muribaculum* in the M group decreased significantly. Besides, we found that *Lactobacillus johnsonii*, *Lactobacillus intestinalis,* and *Lactobacillus reuteri* in the M group presented notable downregulation, while *Clostridium* showed pronounced upregulation. It could be seen that modeling significantly altered gut mucosal microbiota composition at the phylum, genus, and species levels. LEfSe analysis revealed at the genus level that *Erysipelatoclostridium,Bacteroides*, and *Anaerotignum* were markedly enriched in the M group as differentiated bacteria. *Erysipelatoclostridium* is a genus of pathogenic bacteria that cause a variety of serious infections in immunocompromised patients (Milosavljevic et al., 2021). Previous studies have confirmed that green tea leaf powder promoted fatty acid catabolism and reduced the abundance of *Erysipelatoclostridium*, and its abundance was negatively correlated with lipid metabolism (Wang et al., 2020). It was reported that *Anaerotignum* produced acetate, propionate, and butyrate to provide energy to the host (Choi et al., 2019). In our study, *Erysipelatoclostridium* presented positive correlations with $Na^+$-$K^+$-ATP-ase and $Ca^{2+}$-$Mg^{2+}$-ATP-ase. *Anaerotignum* was negatively correlated with $Na^+$-$K^+$-ATP-ase and $Ca^{2+}$-$Mg^{2+}$-ATP-ase. The reasons for these results were presumed to be related to the interactions between the differential bacteria and the specific mechanism of action, which still needs further investigation. *Bacteroides* is usually a "friendly" commensal in the gut, which transfers through the gut mucosa and multiplies in normal sterile tissues, thus leading to abdominal inflammation, diarrhea, and abscess in the abdominal cavity (Zafar and Saier, 2021). Studies confirmed that in a balanced state of gut microbiota, *Bacteroides* used complex dietary polysaccharides and host glycans to provide energy to the body and promote the breakdown and metabolism of adipose tissue (Ito et al., 2020; Yoshida et al., 2021). When the gut mucosal barrier was damaged, the gut microbiota was disturbed and bacteria appeared to translocate. *Bacteroides* facilitated pathogen growth by producing virulence factors and depriving the host of nutrients (Zafar and Saier, 2021). *Folium sennae* has been found to cause intestinal mucosal barrier damage and intestinal mucosal permeability changes (Su P. et al., 2020). In this experiment, *Bacteroides* showed a positive regulation with $Ca^{2+}$-$Mg^{2+}$-ATP-ase but negative regulation with $Na^+$-$K^+$-ATP-ase. Therefore, we hypothesized that adenine combined with *Folium senna* might cause the migration of *Bacteroides* and thus the facilitation or inhibition of host energy metabolism. In summary, the study of specific gut-related functional microorganisms will be an essential direction (Long et al., 2017, 2018a,b; He et al., 2018).

## Conclusion

Adenine combined with *Folium senna* caused behavioral changes in mice, significantly damaged the structure of the kidney, affected energy metabolism, and caused disorders of gut mucosal microbiota. Furthermore, the correlation between *Bacteroides*, *Erysipelatoclostridium*, and *Anaerotignum* and diarrhea with deficiency kidney-yang syndrome was revealed to have a more of a synergistic or competitive effect on energy metabolism.

## Data availability statement

The datasets presented in this study can be found in online repositories. The names of the repository/repositories and accession number(s) can be found below: https://www.ncbi.nlm.nih.gov/, PRJNA851244.

## Ethics statement

Animal experiments were approved by the Animal Ethics and Welfare Committee of Hunan University of Chinese Medicine (LLBH-202106120002).

## Author contributions

JZ and XL: conceptualization, methodology, and writing of the original draft. XL: data curation, methodology, and

visualization. ND and XP: investigation and visualization. ZT: supervision, funding acquisition, reviewing, and editing. All authors contributed to manuscript revision and read and approved the submitted version.

## Funding

This study was supported by grants from the National Natural Science Foundation of China (No: 81874460) and the Natural Science Foundation of Hunan Province (2022JJ30440).

## Acknowledgments

The authors acknowledge all the scholars who provided relevant guidance for the study.

## Conflict of interest

The authors declare that the research was conducted in the absence of any commercial or financial relationships that could be construed as a potential conflict of interest.

## Publisher's note



## References

Blander, J. M., Longman, R. S., Iliev, I. D., Sonnenberg, G. F., and Artis, D. (2017). Regulation of inflammation by microbiota interactions with the host. *Nat. Immunol.* 18, 851–860. doi: 10.1038/ni.3780

Bray, J. R., and Curtis, J. T. (1957). An ordination of the upland forest communities of southern wisconsin. *Ecol. Monogr.* 27, 326–349. doi: 10.2307/1942268

Breiman, L. (2001). Random Forests. *Mach Learn.* 45, 5–32. doi: 10.1023/A:1010933404324

Chen, Y. Q., Li, F., Fan, Q. F., and Yang, X. J. (2021). Experience in treating chronic diarrhea based on syndrome differention of Yin and Yang and five internal organs. *Asia-Pacific Tradit. Med.* 17, 123–125.

Choi, S. H., Kim, J. S., Park, J. E., Lee, K. C., Eom, M. K., Oh, B. S., et al. (2019). Anaerotignum faecicola sp. nov., isolated from human faeces. *J. Microbiol.* 57, 1073–1078. doi: 10.1007/s12275-019-9268-3

Edgar, R. (2013). UPARSE: Highly Accurate OTU Sequences from Microbial Amplicon Reads. *Nat. Methods.* 10, 996–998. doi: 10.1038/nmeth.2604

Guan, Z. Y., Zhao, Q., and Zhao, Z. H. (2021). Study on Dose Time Effect Relationship of Diarrhea Model in Young Rats Induced by *Folium sennae*. *Lishizhen Med. Mater. Medica. Res.* 32, 1806–1809.

He, L., Liu, Y. W., Guo, Y. F., Shen, K. J., Hui, H. Y., Tan, Z. J., et al. (2018). Diversity of intestinal bacterial lactase gene in antibiotics-induced diarrhea mice treated with Chinese herbs compound Qi Wei Bai Zhu San. *3 Biotech.* 8, 4. doi: 10.1007/s13205-017-1024-y

He, Y. S., Tang, Y., Peng, M. J., Xie, G. Z., Li, W. G., Tan, Z. J., et al. (2019). Influence of *Debaryomyces hansenii* on bacterial lactase gene diversity in intestinal mucosa of mice with antibiotic-associated diarrhea. *PLoS ONE.* 14, e022580. doi: 10.1371/journal.pone.0225802

Huang, H. R., Liu, Q. Y., and Han, X. Q. (2019). Therapeutic Effect of Salt-separated Moxibustion Combined with Acupoint Application on Diabetic Diarrhea of Spleen and Kidney-Yang Deficiency Type. *Fujian J. Tradit. Chin. Med.* 50, 72–73.

Huang, Y., Xin, W., Xiong, J., Yao, M., Zhang, B., Zhao, J., et al. (2022). The intestinal microbiota and metabolites in the gut-kidney-heart axis of chronic kidney disease. *Front. Pharmacol.* 13, 1–17. doi: 10.3389/fphar.2022.837500

Ito, T., Gallegos, R., Matano, L. M., Butler, N. L., Hantman, N., Kaili, M., et al. (2020). Genetic and biochemical analysis of anaerobic respiration in *Bacteroides fragilis* and its importance *in vivo*. *mBio.* 11, e03238–19. doi: 10.1128/mBio.03238-19

Jia, K. J., and Jia, T. Z. (2016). Comparison of antidiuretic activity of ootheca mantidis before and after processing and its medicinal part against insufficiency of kidney-Yang and Diuresis Rats. *China Phar.* 27, 879–882.

Li, X. Y., Deng, N., Zheng, T., Qiao, B., Peng, M. J., Tan, Z. J., et al. (2022c). Importance of *Dendrobium officinale* in improving the adverse effects of high-fat diet on mice associated with intestinal contents microbiota. *Front. Nutr.* 9, 957334. doi: 10.3389/fnut.2022.957334

Li, X. Y., Zhang, C. Y., Hui, H. Y., and Tan, Z. J. (2021). Effect of Gegenqinlian decoction on intestinal mucosal flora in mice with diarrhea induced by high temperature and humidity treatment. *3 Biotech.* 11, 83. doi: 10.1007/s13205-020-02628-0

Li, X. Y., Zhu, J. Y., Wu, Y., Liu, Y. W., Hui, H. Y., Tan, Z. J., et al. (2022b). Model Building and Validation of Diarrhea Mice with Kidney-yang Depletion Syndrome. *J. Tradit. Chin. Med.* 63:1368–1373.

Li, X. Y., Zhu, J. Y., Wu, Y., and Tan, Z. J. (2022a). Correlation between kidney function and intestinal biological characteristics of adenine and folium sennae-induced diarrhea model in mice. *Turk. J. Gastroenterol.* doi: 10.5152/tjg.2022.211010. [Epub ahead of print].

Li, Y. L., Yuan, Z. Y., and Tan, Z. J. (2021). Correlation between intestinal flora and traditional chinese medicine syndromes of diarrhea: a review. *Chin. J. Exp. Tradit. Med. Formul.* 27, 209–216.

Li, Y. X., Xia, S. T., Jiang, X. H., Feng, C., Gong, S. M., Ma, J., et al. (2021). Gut Microbiota and Diarrhea: An Updated Review. *Front. Cell Infect. Microbiol.* 11, 1–8. doi: 10.3389/fcimb.2021.625210

Long, C. X., He, L., Guo, Y. F., Liu, Y. W., Xiao, N. Q., Tan, Z. J., et al. (2017). Diversity of bacterial lactase genes in intestinal contents of mice with antibiotics-induced diarrhea. *World J. Gastroenterol.* 23, 7584–7593. doi: 10.3748/wjg.v23.i42.7584

Long, C. X., Liu, Y. W., He, L., Tan, Q. Q., Yu, Z. Z., Xiao, N. Q., et al. (2018b). Bacterial lactase genes diversity in intestinal mucosa of mice with dysbacterial diarrhea induced by *antibiotics*. *3 Biotech.* 8, 176. doi: 10.1007/s13205-018-1191-5

Long, C. X., Liu, Y. W., He, L., Yu, R., Tan, Z. J., et al. (2018a). Bacterial lactase genes diversity in intestinal mucosa of dysbacterial diarrhea mice treated with Qiweibaizhu powder. *3 Biotech.* 8, 423. doi: 10.1007/s13205-018-1460-3

Mendez, R., Banerjee, S., Bhattacharya, S. K., and Banerjee, S. (2019). Lung Inflammation and disease: a Perspective on Microbial Homeostasis and Metabolism. *IUBMB Life.* 71, 152–165. doi: 10.1002/iub.1969

Meng, X., Zhang, G., Cao, H., Yu, D., Fang, X., de Vos, W. M., et al. et al. (2020). Gut Dysbacteriosis and Intestinal Disease: Mechanism and Treatment. *J Appl Microbiol.* 129, 787–805. doi: 10.1111/jam.14661

Milosavljevic, M. N., Kostic, M., Milovanovic, J., Zaric, R. Z., et al. (2021). Antimicrobial treatment of erysipelatoclostridium ramosum invasive

infections: A systematic review. *Rev. Inst. Med. Trop. São Paulo*. 63, 1–12. doi: 10.1590/s1678-9946202163030

Qiu, L., Zhao, Q. J., and Dai, Z. L. (2019). Exploration of the formulation mechanism of Kidney Qi Pill "Shao Huo Qi" based on mitochondrial energy metabolism. *Lishizhen Med Mater Med Res*. 30, 1850–1853.

Ren, Z., and Peng, M. F. (2020). The Current Situation and Consideration of Animal Model Evaluation Methods in Traditional Chinese Medicine. Pharmacol. *Clin Chin Mater*. 36, 219–222.

Shao, H. Q., Zhang, C. Y., Xiao, N. Q., and Tan, Z. J. (2020). Gut microbiota characteristics in mice with antibiotic-associated diarrhea. *BMC Microbiol*. 20, 313. doi: 10.1186/s12866-020-01999-x

Shi, K., Qu, L. H., Lin, X., Xie, Y., Tu, J. Y., Liu, X. Q., et al. (2020). Deep-fried atractylodis rhizoma protects against spleen deficiency-induced diarrhea through regulating intestinal inflammatory response and gut microbiota. *Int. J. Mol. Sci*. 21, 124. doi: 10.3390/ijms21010124

Simão, F., Matté, A., Matté, C., Soares, F. M. S., Wyse, A. T. S., Netto, C. A., et al. (2011). Resveratrol prevents oxidative stress and inhibition of Na(+)K(+)-ATPase activity induced by transient global cerebral ischemia in rats. *J. Nutr. Biochem*. 22, 921–928. doi: 10.1016/j.jnutbio.2010.07.013

Spleen and Stomach Branch of China Association of Traditional Chinese Medicine. (2017). Consensus opinion on TCM Diagnosis and Treatment of Diarrhea. *J. Tradit. Chin. Med*. 58, 1256–1259.

Su, P., Chen, Y., Zhang, H. J., Ye, Z. G., and Zhang, G. P. (2020). Effect and Mechanism Study of Ganbao Capsule on the Liver Injury Induced by Anti-Tuberculosis Drugs. *Pharmacol. Clin. Chin. Mat. Med*. 36, 176–181.

Su, W. W., Huang, J. Y., Chen, H. M., Lin, J. T., and Kao, S. H. (2020). Adenine inhibits growth of hepatocellular carcinoma cells via AMPK-mediated S phase arrest and apoptotic cascade. *Int J Med Sci*. 17, 678–684. doi: 10.7150/ijms.42086

Sueyoshi, M., Fukunaga, M., Mei, M., Nakajima, A., Tanaka, G., Murase, T., et al. (2019). Effects of lactulose on renal function and gut microbiota in adenine-induced chronic kidney disease rats. *Clin. Exp. Nephrol*. 23, 908–919. doi: 10.1007/s10157-019-01727-4

Vaziri, N. D., Wong, J., Pahl, M., Piceno, Y. M., Yuan, J., DeSantis, T. Z., et al. (2013). Chronic kidney disease alters intestinal microbial flora. *Kidney. Int*. 83, 308–315. doi: 10.1038/ki.2012.345

Wang, B., Dai, M., Zhang, S. X., Lin, Y., and Dai, Y. C. (2016). *Yellow Emperor's Classic of Internal Medicine* (Nanning: Guangxi Science and Technology Press).

Wang, J., Li, P., Liu, S., Zhang, B. W., Hu, Y. Z., Ma, H., et al. (2020). Green tea leaf powder prevents dyslipidemia in high-fat diet-fed mice by modulating gut microbiota. *Food. Nutr. Res*. 64, 1–10. doi: 10.29219/fnr.v64.3672

Wang, W. Y., Srivathsan, A., Foo, M., Yamane, S. K., and Meier, R. (2018). Sorting specimen-rich invertebrate samples with cost-effective NGS barcodes: Validating a reverse workflow for specimen processing. *Mol. Ecol. Resour*. 18, 490–501. doi: 10.1111/1755-0998.12751

Wu, Y., Peng, X. X., Li, X. Y., Li, D. D., Tan, Z. J., Yu, R., et al. (2022). Sex hormones influences intestinal microbiota composition in mice. *Front Microbiol*. doi: 10.3389/fmicb.2022.964847

Wu, Y., Tang, Y., and Liu, Y. W., Hui, H.,Y., and Tan, Z. J. (2020). Effects of tongxie yaofang prescription on activity of digestive enzymes in intestinal mucosa and contents in Gan-qi-cheng Diarrhea mice -pi diarrhea mice. *Chin J Microecol*. 32, 745–749.

Xiao, J., He, L. Q., Gao, J. D., and Huang, D. (2008). Comparison of the model establishment method of syndrome of deficiency of Kidney-yang between adenine and hydrocortisone. *Chin. J. Comp. Med*. 18, 77–80.

Xiao, X. Y., Deng, Y. L., Liu, Y. J., Li, D. D., and Tan, Z. J. (2016). Effects of *Folium sennae* on Blood Routine in Rats with Diarrhea of Splenic Deficiency Type. *J. Hubei Univ. Chin. Med*. 18, 49–51.

Xie, G. Z., Tan, K., Peng, M. J., Long, C. X., Li, D. D., Tan, Z. J., et al. (2019). Bacterial diversity in intestinal mucosa of antibiotic-associated diarrhea mice. *3 Biotech*. 9, 444. doi: 10.1007/s13205-019-1967-2

Xie, Y. A., Hu, X. F., Li, S. L., Qiu, Y., Cao, R., Xu, C., et al. (2022). Pharmacological targeting macrophage phenotype via gut-kidney axis ameliorates renal fibrosis in mice. *Pharmacol. Res*. 178, 106161. doi: 10.1016/j.phrs.2022.106161

Yoshida, N., Yamashita, T., Osone, T., Hosooka, T., Shinohara, M., Kitahama, S., et al. (2021). *Bacteroides spp*. promotes branched-chain amino acid catabolism in brown fat and inhibits obesity. *iScience*. 24, 103342. doi: 10.1016/j.isci.2021.103342

Yuan, Z., Zhang, C. Y., Peng, X. X., Shu, L., Long, C. X., Tan, Z. J., et al. (2020). Intestinal microbiota characteristics of mice treated with *Folium senna* decoction gavage combined with restraint and tail pinch stress. *3 Biotech*. 10, 180. doi: 10.1007/s13205-020-02172-x

Zafar, H., and Saier, M. H. (2021). Gut *Bacteroides* species in health and disease. *Gut Microbes*. 13, 1–20. doi: 10.1080/19490976.2020.1848158

Zhang, C. Y., Peng, X. X., Shao, H. Q., Li, X. Y., Wu, Y., Tan, Z. J., et al. (2021). Gut microbiota comparison between intestinal contents and mucosa in mice with repeated stress-related diarrhea provides novel insight. *Front. Microbiol*. 12, 626691. doi: 10.3389/fmicb.2021.626691

Zhang, C. Y., Shao, H. Q., Li, D. D., Xiao, N. Q., and Tan, Z. J. (2020a). Role of tryptophan-metabolizing microbiota in mice diarrhea caused by *Folium sennae* extracts. *BMC Microbiol*. 20, 185. doi: 10.1186/s12866-020-01864-x

Zhang, C. Y., Shao, H. Q., Peng, X. X., Liu, T. H., and Tan, Z. J. (2020b). Microbiotal characteristics colonized in intestinal mucosa of mice with diarrhoea and repeated stress. *3 Biotech*. 10, 372. doi: 10.1007/s13205-020-02368-1

Zhou, B., Yuan, Y., Zhang, S., Guo, C., Li, X., Li, G., et al. (2020). Intestinal flora and disease mutually shape the regional immune system in the intestinal tract. *Front. Immunol*. 11, 575. doi: 10.3389/fimmu.2020.00575

Zhu, J. Y., Xiao, N. Q., and Tan, Z. J. (2021). Research progress on intestinal mucosal injury induced by traditional chinese medicine. *World Chin. J. Digestol*. 29, 449–454. doi: 10.11569/wcjd.v29.i9.449

frontiers | Frontiers in Microbiology

TYPE Original Research
PUBLISHED 28 October 2022
DOI 10.3389/fmicb.2022.1036042



OPEN ACCESS

EDITED BY
Tang Zhaoxin,
South China Agricultural University, China

REVIEWED BY
Yun peng Fan,
Northwest A&F University, China
Jingui Li,
Yangzhou University, China

*CORRESPONDENCE
Yi Wu
wuyi2001cn@163.com
Kun Li
lk3005@njau.edu.cn

†These authors have contributed equally to this work

SPECIALTY SECTION
This article was submitted to Microorganisms in Vertebrate Digestive Systems, a section of the journal Frontiers in Microbiology

RECEIVED 03 September 2022
ACCEPTED 29 September 2022
PUBLISHED 28 October 2022

CITATION
Chen X, Kong Q, Zhao X, Zhao C, Hao P, Irshad I, Lei H, Kulyar MF-e-A, Bhutta ZA, Ashfaq H, Sha Q, Li K and Wu Y (2022) Sodium acetate/sodium butyrate alleviates lipopolysaccharide-induced diarrhea in mice *via* regulating the gut microbiota, inflammatory cytokines, antioxidant levels, and NLRP3/Caspase-1 signaling. *Front. Microbiol.* 13:1036042. doi: 10.3389/fmicb.2022.1036042



# Sodium acetate/sodium butyrate alleviates lipopolysaccharide-induced diarrhea in mice *via* regulating the gut microbiota, inflammatory cytokines, antioxidant levels, and NLRP3/Caspase-1 signaling

Xiushuang Chen[1,2†], Qinghui Kong[3†], Xiaoxiao Zhao[1,2], Chenxi Zhao[1,2], Pin Hao[1,2], Irfan Irshad[4], Hongjun Lei[1,2], Muhammad Fakhar-e-Alam Kulyar[5,6], Zeeshan Ahmad Bhutta[7], Hassan Ashfaq[4], Qiang Sha[8], Kun Li[1,2*] and Yi Wu[1,2*]

[1]Institute of Traditional Chinese Veterinary Medicine, College of Veterinary Medicine, Nanjing Agricultural University, Nanjing, China, [2]MOE Joint International Research Laboratory of Animal Health and Food Safety, College of Veterinary Medicine, Nanjing Agricultural University, Nanjing, China, [3]College of Animal Science, Tibet Agricultural and Animal Husbandry University, Nyingchi, China, [4]Institute of Continuing Education and Extension, University of Veterinary Animal Sciences, Lahore, Pakistan, [5]Department of Animal Nutrition and Feed Science, College of Animal Science and Technology, Huazhong Agricultural University, Wuhan, China, [6]College of Veterinary Medicine, Huazhong Agricultural University, Wuhan, China, [7]College of Veterinary Medicine, Chungbuk National University, Cheongju, Chungbuk, South Korea, [8]Jiangsu Key Laboratory of Pesticide Science, Department of Chemistry, College of Sciences, Nanjing Agricultural University, Nanjing, China

Diarrhea is a word-widely severe disease coupled with gastrointestinal dysfunction, especially in cattle causing huge economic losses. However, the effects of currently implemented measures are still not enough to prevent diarrhea. Previously we found that dropped short-chain fatty acids in diarrhea yaks, and butyrate is commonly known to be related to the epithelial barrier function and intestinal inflammation. However, it is still unknown whether sodium acetate/sodium butyrate could alleviate diarrhea in animals. The present study is carried out to explore the potential effects of sodium acetate/sodium butyrate on lipopolysaccharide-induced diarrhea in mice. Fifty ICR mice were randomly divided into control (C), LPS-induced (L), and sodium acetate/sodium butyrate (D, B, A)-treated groups. Serum and intestine samples were collected to examine inflammatory cytokines, antioxidant levels, relative gene expressions *via* real-time PCR assay, and gut microbiota changes through high-throughput sequencing. Results indicated that LPS decreased the villus height ($p < 0.0001$), increased the

crypt depth ($p < 0.05$), and lowered the villus height to crypt depth ratio ($p < 0.0001$), while sodium acetate/sodium butyrate supplementation caused a significant increase in the villus height ($p < 0.001$), decrease in the crypt depth ($p < 0.01$), and increase in the villus height to crypt depth ratio ($p < 0.001$), especially. In mice treated with LPS, it was found that the serum level of IL-1β, TNF-α ($p < 0.001$), and MDA ($p < 0.01$) was significantly higher; however, sodium acetate/sodium butyrate supplementation significantly reduced IL-1β ($p < 0.001$), TNF-α ($p < 0.01$), and MDA ($p < 0.01$), respectively. A total of 19 genera were detected among mouse groups; LPS challenge decreased the abundance of *Lactobacillus, unidentified F16, unidentified_S24-7, Adlercreutzia, Ruminococcus, unclassified Pseudomonadales, [Ruminococcus], Acetobacter, cc 1, Rhodococcus, unclassified Comamonadaceae, Faecalibacterium,* and *Cupriavidus*, while increased *Shigella, Rhodococcus, unclassified Comamonadaceae,* and *unclassified Pseudomonadales* in group L. Interestingly, sodium acetate/sodium butyrate supplementation increased *Lactobacillus, unidentified F16, Adlercreutzia, Ruminococcus, [Ruminococcus], unidentified F16, cc 115, Acetobacter, Faecalibacterium,* and *Cupriavidus,* while decreased *Shigella, unclassified Enterobacteriaceae, unclassified Pseudomonadales, Rhodococcus,* and *unclassified Comamonadaceae*. LPS treatment upregulated the expressions of ZO-1 ($p < 0.01$) and NLRP3 ($p < 0.0001$) genes in mice; however, sodium acetate/sodium butyrate solution supplementation downregulated the expressions of ZO-1 ($p < 0.05$) and NLRP3 ($p < 0.05$) genes in treated mice. Also, the LPS challenge clearly downregulated the expression of Occludin ($p < 0.001$), Claudin ($p < 0.0001$), and Caspase-1 ($p < 0.0001$) genes, while sodium acetate/sodium butyrate solution supplementation upregulated those gene expressions in treated groups. The present study revealed that sodium acetate/sodium butyrate supplementation alleviated LPS-induced diarrhea in mice *via* enriching beneficial bacterium and decreasing pathogens, which could regulate oxidative damages and inflammatory responses *via* NLRP3/Caspase-1 signaling. The current results may give insights into the prevention and treatment of diarrhea.

KEYWORDS

**sodium acetate, sodium butyrate, LPS, diarrhea, microbiota**

## Introduction

Diarrhea is a severe disease coupled with gastrointestinal dysfunction that has a global impact on fertility rate, milk production, and immunity in livestock (Coura et al., 2015; Li et al., 2022). Nowadays diarrhea in dairy cows and yak is very serious. It has a high incidence rate, especially neonatal calf diarrhea is found usually with high morbidity and mortality, causing considerable economic damage to the industry due to the heavy treatment expenses and impairments in the growth of animal (Coura et al., 2015; Schmoeller et al., 2021). Despite measures such as improved hygiene and scientific feeding management with the use of extensive drugs, this disease, i.e., diarrhea, remains serious (Li et al., 2022). The imbalance in gut microbiota was commonly recognized as the primary cause of diarrhea (Schmoeller et al., 2021), and many studies found changed intestine microbiota in diarrhea of cattle (Chuang et al., 2022; Coelho et al., 2022; Li et al., 2022; Liu J. et al., 2022).

Gut microflora is composed of millions of microorganisms that contribute remarkably to physiological processes, i.e., functions of nutrition absorption, metabolism, and immunity of the host by producing various metabolites (Wei et al., 2020). The anaerobic bacterial fermented short-chain fatty acids (SCFAs) are six carbon-containing fatty acids in the gut (Du et al., 2021).

Acetate and butyrate are mainly produced through bacterial catabolism of dietary fibers in the host colon (Ezzine et al., 2022), which are a primary source of energy for colonic epithelial cells (Fu et al., 2019). Previous studies found that acetate could promote small intestinal barrier function in mice (Yosi et al., 2022) and regulate IgA reactivity (Takeuchi et al., 2021). As an important short-chain fatty acid, butyrate can not only provide energy for enterocyte regeneration but also modulate the intestine microbial community and contribute to the host's health (Jiminez et al., 2017). Some of the studies reported that butyrate has an important role in the proper functioning of the immune system, nervous system, and energy metabolism (Koh et al., 2016; Fu et al., 2019). It was observed in the previous study that intestinal disease like ulcerative colitis is highly related to inadequate use of butyrate (Leonel and Alvarez-Leite, 2012). Butyrate could enhance epithelial barrier function, promote goblet cells mucus secretion, and reduce intestinal inflammation by reducing pro-inflammatory cytokines' levels (Hamer et al., 2008; Gaudier et al., 2009; Guilloteau et al., 2010).

In our previous study, we found a significant decrease in concentrations of SCFAs, especially acetic acid and butyric acid in yaks (Li et al., 2022). We hypothesized that sodium acetate/sodium butyrate supplementation could alleviate diarrhea in animals, similar to how *Lactobacillus plantarum* alleviated diarrhea in a previous study by balancing gut microbiota and regulating SCFAs (Yue et al., 2020). The widely known lipopolysaccharide is an important membrane component of gram-negative bacteria, causing the inflammatory reaction, oxidative damage, and gut dysbiosis in hosts (Xu et al., 2021). Previous studies found that ROS were an important second messenger of the atypical domain (NOD)-like receptor containing pyrin domain 3 inflammasomes, and Caspase-1 was activated by NLRP3 and then cause inflammation reaction (Dashdorj et al., 2013; Sho and Xu, 2019; He et al., 2022). Hence, we conducted this study to explore the alleviation effect and potential mechanism of sodium acetate/sodium butyrate supplementation on LPS-induced diarrhea in mice *via* NLRP3/Caspase-1 signaling.

# Materials and methods

## Experiment design

A total of 50, four weeks of age, ICR mice with an equal number of male and female animals (average weight of 18 ± 2 g) were purchased from Qing Long Shan Dong Wu Fan Zhi (Nanjing, China). After 30 days of rearing, mice were randomly divided into five groups, namely control (C), LPS (L), and treatment groups (A, B, and D). Group D (400: 200), B (300:300), and A (200: 400) were treated with 600 mg/kg sodium acetate/sodium butyrate solution *via* gavage for 18 days, while mice in C and L were treated with equal volume of normal saline. On day 19, mice in groups L, A, B, and D were treated with 20 mg/kg LPS (Solarbio life science, China), and after 24 hours mice were euthanized to collect serum, small intestine, and rectum samples (**Figure 1**). All animals were given normal water and feeds, and kept in the laboratory animal center of Nanjing Agricultural University. The body weights and diarrhea were documented.

## Hematoxylin and eosin staining

Duodenum, jejunum, and ileum samples from all the groups were preserved in 4% paraformaldehyde for at least 48 hrs and then processed for commercial H&E staining (Wuhan Pinuofei Biological Technology Co., Ltd., China). On an Olympus CX23 microscope with an integrated digital imaging analysis system, histological slices were examined (Olympus Co., Japan). The villus height and crypt depth were measured as depicted in the previous study (Xu et al., 2021).

## Antioxidative indices, cytokine levels, and NOs levels in serum

Blood samples of mice were centrifuged at 4,000 g for 10 min and stored at −20°C for future analysis. Antioxidant capacity was examined by detecting the levels of superoxide dismutase (SOD), glutathione peroxidase (GSH-px), total anti-oxidation capacity (T-AOC), and malondialdehyde (MDA) by utilizing commercial assay kits (Nanjing Jiancheng Bioengineering Institute, China). Meanwhile, the NO concentrations were determined *via* commercial assay kits (Nanjing Jiancheng Bioengineering Institute, China). The concentration of cytokines including interleukin 1 beta (IL-1β), interleukin 6 (IL-6), interleukin 10 (IL-10), and tumor necrosis factor-alpha (TNF-α) was measured by using commercial ELISA kits (Solarbio life science, China).

## Gut microbiota sequencing and analysis

The total microbial genomic DNA was extracted from the rectum contents of each mouse. The samples from groups C ($n$ = 4), L ($n$ = 4), and A ($n$ = 4) were extracted utilizing the fast DNA Stool Mini Kit (Qiagen, German) according to the manufacturer's specifications. The quantity and quality of all extracted DNA samples were examined by using NanoDrop 2000 UV-vis spectrophotometer (Thermo Scientific, USA) and agarose gel electrophoresis, respectively. Gene amplification of bacterial 16S rRNA gene was performed using the V3–V4 regions primers 338F (5′-ACTCCTACGGGAGGCAGCAG-3′) and 806R (5′-GGACTACHVGGGTWTCTAAT-3′).

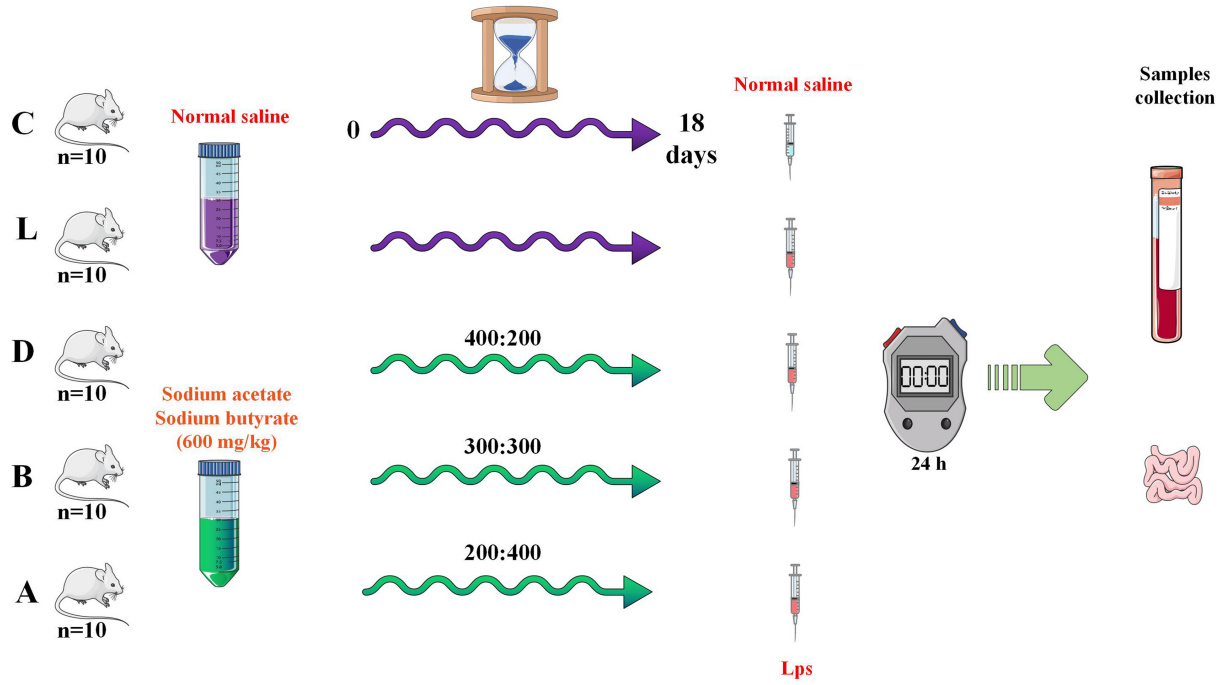


FIGURE 1
Study design for the experiment.

Then all amplicon products were purified by employing Vazyme VAHTSTM DNA Clean Beads (Vazyme, China) and quantified using the QuantiFluor™-ST (Promega, USA). At last, all samples were sequenced by using the Illumina MiSeq platform (Bioyi Biotechnology Co., Ltd. China) with MiSeq Reagent Kit v3.

All of the achieved sequencing raw data were cleaned using the DADA2 (Callahan et al., 2016) and Vsearch (Rognes et al., 2016) to generate accurate and reliable results for microbiome bioinformatic analysis through QIIME2 (2019.4)[1] (Bokulich et al., 2018). Phylogenetic trees were constructed *via* mafft (Katoh et al., 2002) and FastTree (Price et al., 2010). Alpha-diversity metrics of Chao1 (Chao, 1984), observed species, Shannon (Shannon, 1948), Simpson (Simpson, 1997), Faith's PD (Faith, 1992), Pielou's evenness (Pielou, 1966), and Good's coverage (Good, 1953) were estimated among samples. Beta diversity metrics of principal coordinate analysis (PCoA) (Alban, 2010), non-metric multidimensional scaling (NMDS) (Legendre and Montréal, 2003), and unweighted pair-group method with arithmetic means (UPGMA) were estimated among samples. Taxonomy was assigned to non-singleton amplicon sequence variants (ASVs) using the classify-sklearn naïve Bayes taxonomy classifier in the feature-classifier plugin (Bokulich et al., 2018) against the SILVA Release 132 Database[2] (Quast et al., 2012). Tree diagram of classification levels and GraPhlAn evolutionary was generated *via* ggtree[3]. Krona species composition map was generated *via* KronaTools (v2.7)[4] (Ondov et al., 2011). Significant difference analyses among different mouse groups were performed *via* PERMANOVA and Adonis in QIIME2 (2019.4). Venn[5], heatmap, metagenomeSeq, LEFSe (Mahadevan et al., 2008; Segata et al., 2011), OPLS-DA (Mahadevan et al., 2008), and random forest analysis were carried to explore the significant difference in species. Network analysis (Faust and Raes, 2012) was performed to find potential keystone. The functional potential prediction was carried through the phylogenetic investigation of communities by the reconstruction of unobserved states (PICRUSt2) (Gavin et al., 2019) using MetaCyc[6] and KEGG[7] databases.

## RNA extraction and RT-qPCR analysis

Intestinal tissue RNA extraction from all mouse groups was performed by utilizing TRIzol reagent (Life Technologies, USA). All of the RNA samples were examined *via* denaturing

1 https://github.com/QIIME2/q2-feature-classifier
2 http://www.arb-silva.de
3 https://yulab-smu.github.io/treedata-book
4 https://github.com/marbl/Krona/wiki
5 https://en.wikipedia.org/wiki/Venn_diagram
6 https://metacyc.org/
7 https://www.kegg.jp/

formaldehyde gel electrophoresis and NanoDrop 2000 analyzer (Thermo Fisher Scientific, China) to validate their integrity and concentrations, respectively. Then commercial SuperScript$^{TM}$IV first strand cDNA synthesis kits (Invitrogen$^{TM}$, Thermo Fisher Scientific, USA) were used for translating RNA samples into cDNA under the guidance of the manufacturer's specifications. Finally, qRT-PCR for all groups was carried out by using 25 uL of reaction mixtures consisting of 2 uL of intestinal tissues cDNA, 12.5 uL of Hieff UNICON® Universal Blue qPCR SYBR Green Master Mix (Yeasen, China), 2uL of primers, and 8.5 uL nuclease-free water, then the procedure was performed in the StepOnePlus$^{TM}$ Real-Time PCR System (Applied Biosystems, USA). All sample reactions were repeated three times and the method of $2^{-\Delta\Delta CT}$ was utilized for calculating gene relative quantification. All primer pairs used in the present study were synthesized by Sangon Biotech (China) and are shown in Table 1.

## Statistical analysis

All the generated data were evaluated *via* ANOVA, Student's t-test, Kruskal–Wallis, and Dunn's test *via* IBM SPSS (22.0) software. Data presented as means ± SD and statistically significant are considered when $P < 0.05$.

# Results

## Effects of sodium acetate/sodium butyrate supplementation on body weights and intestinal damage induced by LPS

The mice were weighed on a daily basis and the weight of the mice in group A was slightly higher than mice in other groups (Figure 2A). The diarrhea was found in the mouse of group L (induced by LPS), whereas sodium acetate/sodium butyrate supplementation alleviated diarrhea, especially in mice of group A. The intestines' morphology was examined *via* H&E staining and found that LPS caused a decrease in the villus height ($p < 0.0001$), an increase in the crypt depth ($p < 0.05$), and it also lowered the villus height to crypt depth ratio ($p < 0.0001$). Whereas, sodium acetate/sodium butyrate supplementation resulted in a significant increase in the villus height ($p < 0.001$), decrease in the crypt depth ($p < 0.01$), and increase in the villus height to crypt depth ratio ($p < 0.001$), especially in the mice of groups B and A (Figure 2).

TABLE 1 Primers used in the present study.

| Genes | Primer sequence (5′–3′) | Product size (bp) | Tm (°C) |
|---|---|---|---|
| ZO-1 | F: CTGGTGAAGTCTCGGAAAAATG<br>R: CATCTCTTGCTGCCAAACTATC | 97 | 54 |
| Occludin | F: TGCTTCATCGCTTCCTTAGTAA<br>R: GGGTTCACTCCCATTATGTACA | 155 | 54 |
| Claudin | F: AGATACAGTGCAAAGTCTTCGA<br>R: CAGGATGCCAATTACCATCAAG | 86 | 54 |
| Caspase-1 | F: TGCCCTCATTATCTGCAACA<br>R: GATCCTCCAGCAGCAACTTC | 95 | 56 |
| NLRP3 | F: CATCAATGCTGCTTCGACAT<br>R: TCAGTCCCACACACAGCAAT | 118 | 56 |
| β-actin | F: CTACCTCATGAAGATCCTGACC<br>R: CACAGCTTCTCTTTGATGTCAC | 90 | 54 |

## Effects of sodium acetate/sodium butyrate on the inflammation response and oxidative stress of mouse induced by LPS

In mice serum, no obvious difference was found in IL-6, IL-10, NO, GSH-px, and SOD levels among the control group and LPS-induced groups, respectively. T-AOC in group L was significantly low than in group C ($p < 0.05$), while there was no marked difference between group L and treated groups D, B, and A, respectively. In group C, the serum level of mice induced by LPS was found prominently high for IL-1β ($p < 0.001$), TNF-α ($p < 0.001$), and MDA ($p < 0.01$), respectively. However, in the serum of groups D, B, and A, sodium acetate/sodium butyrate supplementation caused a remarkable decrease in IL-1β ($p < 0.001$), TNF-α ($p < 0.01$), and MDA ($p < 0.01$), respectively (Figure 3).

## Effects of sodium acetate/sodium butyrate supplementation on the structure and diversity of mouse gut microbiota

In the current study, over 110 000, 95 000, 90 000, 94 000, 69 000, and 69 000 of input, filtered, denoised, merged, non-chimeric, and non-singleton data were achieved, respectively, in different mouse samples (Table 2). A significant difference in non-chimeric ($p < 0.05$) and non-singleton ($p < 0.05$) was found between groups C and L (Figure 4A). The majority of sequence lengths were around 430 bp (Figure 4B). As shown in Figure 4C, flatness broken lines were present in all samples, which reflected the evenness of OTUs composition in samples. Alpha-diversity index of Chao1, Simpson, Shannon, Pielou's evenness, observed species, Faith's PD, and Goods coverage is shown in Table 3. There was a significant difference in only Pielou's evenness between groups C and A ($p < 0.05$) (Figure 4D). Beta diversity analysis indicated a far distance of

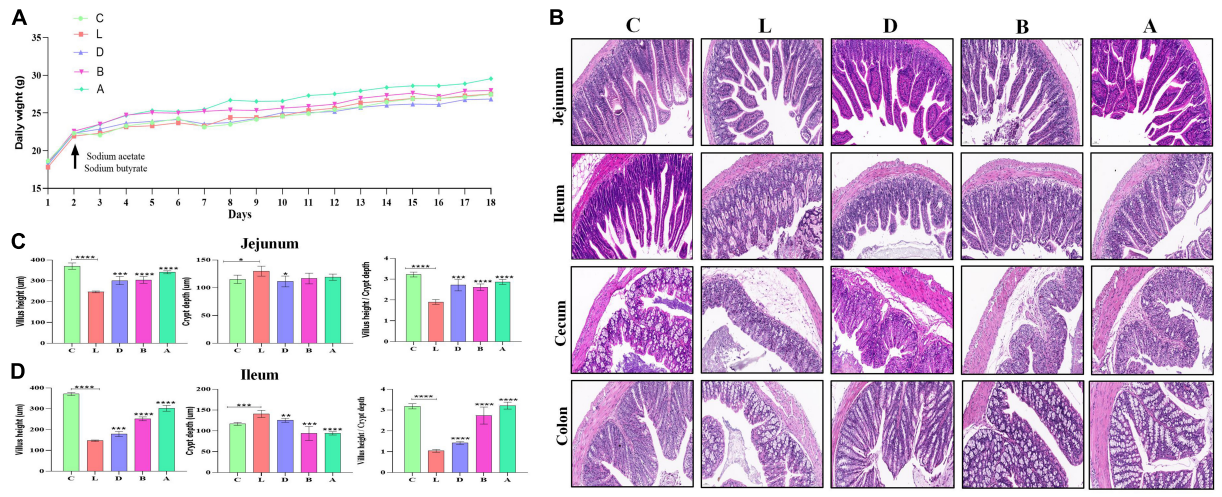


FIGURE 2
Effects of sodium acetate/sodium butyrate supplementation on body weight, diarrhea score, and intestinal damage induced by LPS. **(A)** Mouse daily weights, **(B)** H&E staining analysis of small intestine of mouse, **(C)** villus height, crypt depth, and villus height/crypt depth ratio of Jejunum, and **(D)** villus height, crypt depth, and villus height/crypt depth ratio of Ileum. Scale bar 50 μm. Significance is presented as *$p < 0.05$, **$p < 0.01$, ***$p < 0.001$, and ****$p < 0.0001$; data are presented as the mean ± SEM ($n = 3$).

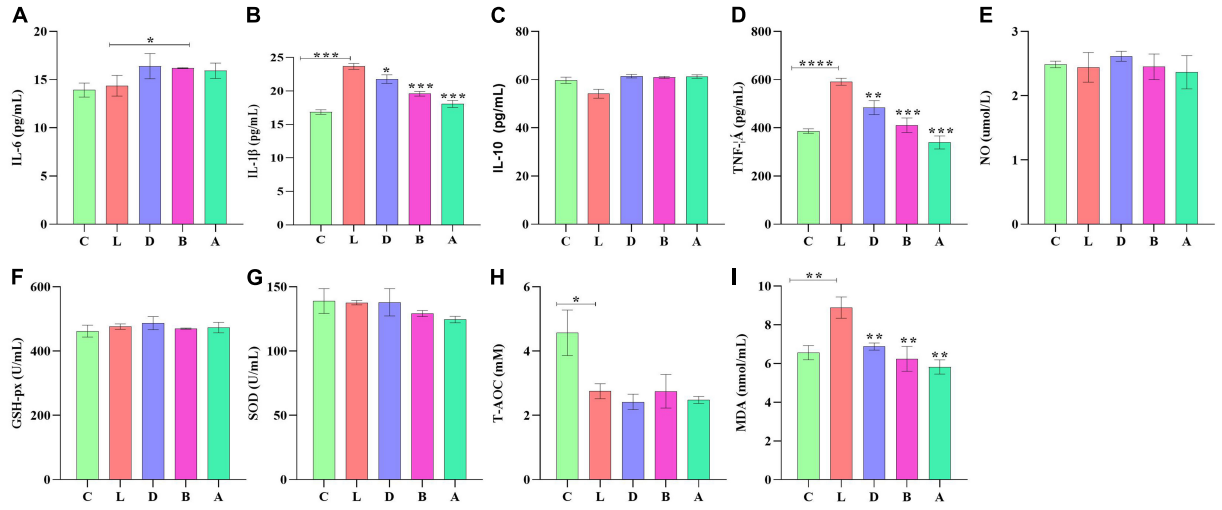


FIGURE 3
Sodium acetate/sodium butyrate supplementation improved the inflammation response and oxidative stress of mouse induced by LPS. The concentrations of inflammatory cytokines IL-6 **(A)**, IL-1β **(B)**, IL-10 **(C)**, TNF-α **(D)**, and NO **(E)** in serums. Oxidative status indices levels of GSH-px **(F)**, SOD **(G)**, T-AOC **(H)**, and MDA **(I)** in serums. Significance is presented as *$p < 0.05$, **$p < 0.01$, ***$p < 0.001$, and ****$p < 0.0001$; data are presented as the mean ± SEM ($n = 3$).

points in samples of group L, whereas relatively near points were found in group A *via* PCoA and NMDS analyses, respectively (Figure 4E). UPGMA analysis found that the branch length in group C was relatively shorter in group A compared with samples in group L (Figure 4E). Significant differences between groups were found in groups A and C through PERMANOVA ($p < 0.05$), ANOSIM ($p < 0.05$), and PERMDISP ($p < 0.05$), respectively (Figure 4F).

## Effects of sodium acetate/sodium butyrate solution supplementation on the taxon composition of mouse gut microbiota

The number of taxa contained in different levels of phylum, class, order, family, genus, and species is shown in Figure 5. At the phylum level, the dominating phyla in group

10.3389/fmicb.2022.1036042

TABLE 2 Statistical analysis of sample sequencing data.

| Sample ID | Input | Filtered | Denoised | Merged | Non-chimeric | Non-singleton |
|---|---|---|---|---|---|---|
| CZ1 | 117228 | 103506 | 102080 | 98791 | 70298 | 69958 |
| CZ2 | 110721 | 95414 | 94891 | 94063 | 87694 | 87636 |
| CZ3 | 127184 | 110284 | 109548 | 107874 | 81870 | 81757 |
| CZ4 | 124309 | 108080 | 107080 | 105393 | 79170 | 79009 |
| LZ1 | 138930 | 118886 | 118448 | 118127 | 112023 | 111994 |
| LZ2 | 136031 | 120329 | 120002 | 119787 | 117181 | 117170 |
| LZ3 | 119805 | 107500 | 106496 | 104659 | 87609 | 87411 |
| LZ4 | 120971 | 108244 | 107518 | 106137 | 90221 | 90048 |
| AZ1 | 114290 | 102104 | 101618 | 100822 | 90342 | 90275 |
| AZ2 | 117460 | 102209 | 101350 | 100174 | 85482 | 85389 |
| AZ3 | 123722 | 110608 | 110272 | 110016 | 108806 | 108790 |
| AZ4 | 121781 | 107460 | 106791 | 105671 | 69110 | 69002 |

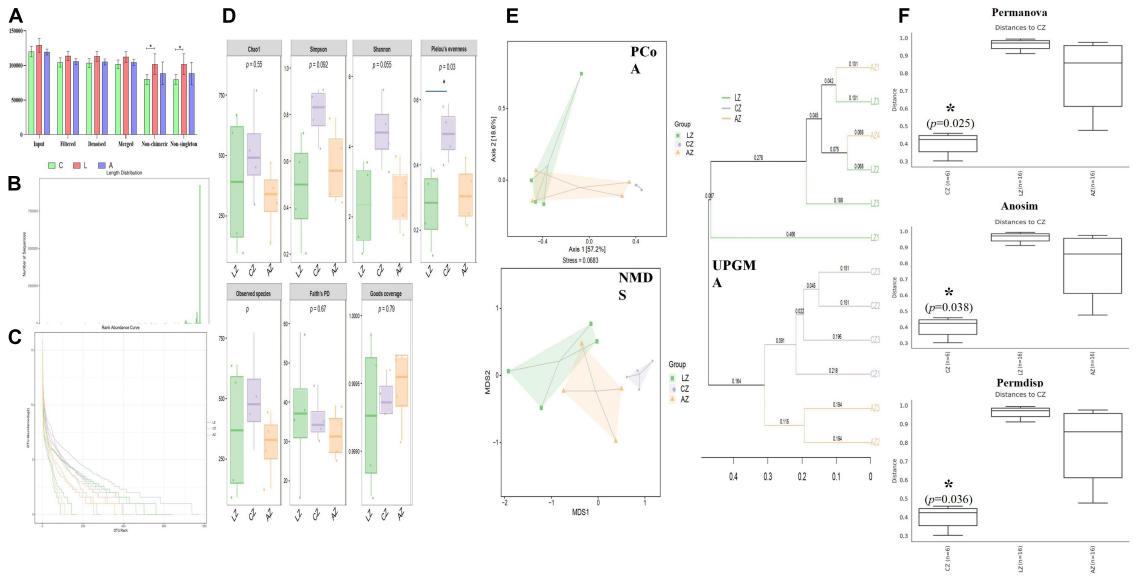


FIGURE 4
Sodium acetate/sodium butyrate supplementation restored the structure and diversity of mouse gut microbiota affected by LPS. **(A)** Sequencing data statistical analysis, **(B)** length distribution of sequencing data, **(C)** rank abundance curve, **(D)** alpha-diversity index analysis, **(E)** beta diversity analysis, and **(F)** group difference analysis. Significance is presented as *$p < 0.05$, **$p < 0.01$, ***$p < 0.001$, and ****$p < 0.0001$; data are presented as the mean ± SEM ($n = 4$).

L were *Proteobacteria* (83.02%) and *Bacteroidetes* (13.00%). While *Firmicutes* (83.36%), *Bacteroidetes* (12.80%), *Firmicutes* (45.35%), and *Proteobacteria* (46.88%) were the main phyla in groups C and A. At the Class level, the main classes were *Gammaproteobacteria* (81.28%) and *Bacteroidia* (12.99%) in group L, while *Bacilli* (74.72%), *Bacteroidia* (12.80%), Clostridia (8.08%), *Gammaproteobacteria* (45.90%), *Bacilli* (44.04%), and *Bacteroidia* (6.80%) were the dominant classes in groups C and A, respectively. At the order level, the primary classes were *Enterobacteriales* (55.60%), *Pseudomonadales* (25.65%), and *Bacteroidales* (12.99%), while *Lactobacillales* (72.68%), *Bacteroidales* (12.80%), Clostridiales (8.08%), *Lactobacillales* (43.52%), *Enterobacteriales* (41.07%), and *Bacteroidales* (6.80%) were the staple orders in groups C and A, respectively. At the family level, the dominating families in group L were *Enterobacteriaceae* (55.59%), *Pseudomonadaceae* (25.47%), and *Bacteroidaceae* (9.09%), while the main families were *Lactobacillales* (72.47%) and *S24-7* (12.50%) in group C, whereas *Lactobacillales* (43.35), *Enterobacteriaceae* (41.07%), and *Bacteroidaceae* (4.84%) in group A, respectively. At the genus level, the major genera in group L were *Shigella* (54.62%), *Pseudomonas* (25.42%), and *Bacteroides* (9.09%), while *Lactobacillus* (72.45%), *unidentified_S24-7* (12.50), *Lactobacillus* (43.34%), *Shigella* (40.71), and *Bacteroides*

10.3389/fmicb.2022.1036042

TABLE 3 Statistical analysis of alpha-diversity index.

| Sample | Chao1 | Simpson | Shannon | Pielou's evenness | Observed species | Faith's PD | Goods coverage |
|---|---|---|---|---|---|---|---|
| CZ1 | 776.424 | 0.910572 | 5.64342 | 0.588308 | 772.1 | 44.4865 | 0.999433 |
| CZ2 | 301.297 | 0.655669 | 3.32679 | 0.406681 | 290.1 | 30.4710 | 0.999602 |
| CZ3 | 456.026 | 0.881407 | 4.67368 | 0.53205 | 440.9 | 33.3046 | 0.999271 |
| CZ4 | 525.863 | 0.782378 | 4.13132 | 0.458692 | 514.4 | 35.1551 | 0.999288 |
| LZ1 | 182.193 | 0.204933 | 0.978133 | 0.132322 | 168.0 | 57.6407 | 0.999628 |
| LZ2 | 97.6659 | 0.398078 | 1.464920 | 0.22345 | 94.1 | 15.9611 | 0.999873 |
| LZ3 | 672.409 | 0.600411 | 3.21118 | 0.344443 | 640.4 | 38.3927 | 0.998668 |
| LZ4 | 600.000 | 0.722918 | 3.59158 | 0.392133 | 571.7 | 35.7839 | 0.998896 |
| AZ1 | 309.775 | 0.457996 | 2.07760 | 0.253912 | 290.5 | 25.4681 | 0.999414 |
| AZ2 | 472.144 | 0.788589 | 3.72562 | 0.422906 | 448.7 | 34.7309 | 0.999080 |
| AZ3 | 139.305 | 0.426415 | 1.52562 | 0.217816 | 128.4 | 39.1726 | 0.999709 |
| AZ4 | 372.352 | 0.6599 | 3.01108 | 0.352894 | 370.3 | 27.8166 | 0.999680 |

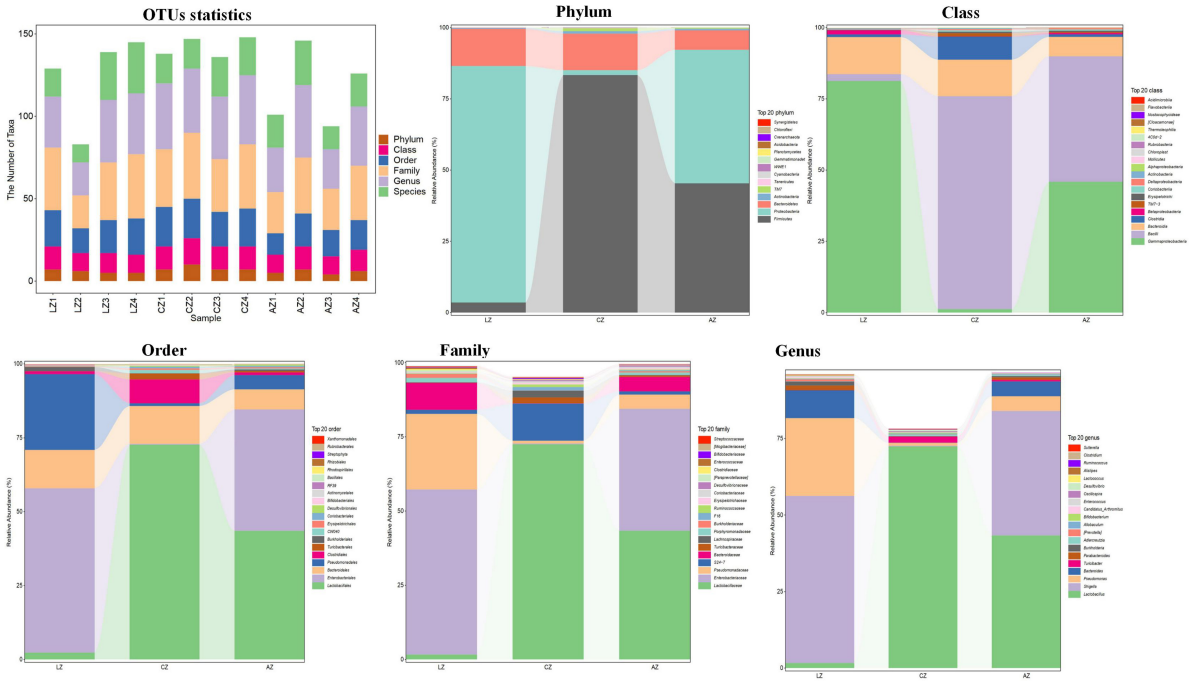


FIGURE 5
Effect of dietary sodium acetate/sodium butyrate supplementation on the relative abundance of gut microbiota in different taxa levels.

(4.84%) were the dominating genera in groups C and A (Figure 5).

The classification levels tree diagram showed that larger sectors of *Ruminococcus*, *Oscillospira*, *Lactobacillus vaginalis*, *Lactobacillus helveticus*, *Lactobacillus hamsteri*, *Turicibacter*, *Allobaculum*, *Adlercreutzia,* and *F16* with light orange and lavender color in groups A and C, respectively, while larger sectors of *Candidatus Arthromitus, Lactococcus, Enterococcus, Bacteroides uniformis, Bacteroides caccae, Bacteroides acidifaciens, Parabacteroides gordonii, Parabacteroides distasonis, Alistipes finegoldii, Prevotella, Shigella, Pseudomonas syringae,* and *Pseudomonas Pseudomonas* with green color were found in group L (Figure 6A). GraPhlAn evolutionary tree diagram showed that the abundance of *Lactobacillus*, *Shigella*, *Pseudomonas Pseudomonas, Bacteroides, Turicibacter, Parabacteroides, Burkholderia, Adlercreutzia, Prevotella,* and *Enterobacteriaceae Pseudomonas* depicted with various colors were found significantly different among different mouse groups (Figure 6B). Krona species composition diagram indicated that the main genera were *Shigella* (72%), *Bacteroides* (9%), and *Pseudomonas* (8%) in group L, while *Shigella* (56%), *Pseudomonas* (26%), and *Bacteroides* (9%) in group A, and

unidentified *S34-7* (45%), unidentified *Clostridia* (15%), *Lachnospiraceae* (7%), and *Turicibacter* (7%) in group C, respectively (Figure 6C).

To find different species and markers, species in mouse microbiota induced by LPS, we performed the Venn diagram, bar chart of ASV/OTU numbers in different regions of the Venn diagram, bar graphs of ASV/OTU abundance in different regions of the Venn diagram, Genera composition heatmap, PCA, and OPLS-DA analysis. Results showed that 216 (7.71%) OTUs were shared in groups C and L, while 335 (11.96%) OTUs were shared in groups C and A (Figure 7A). Then ASV/OTU abundance was explored in different regions of the Venn diagram. The results showed that at the phylum level, groups C and A shared *Firmicutes, Proteobacteria, Bacteroidetes, Actinobacteria,* and *TM7* Phyla, while groups C and L shared *Firmicutes, Proteobacteria,* and *Bacteroidetes* Phyla. At the genus level, groups C and L shared *Shigella*, *Lactobacillus, Pseudomonas, Bacteroides, Parabacteroides, Oscillospira, Allobaculum,* and *Ruminococcus* Genera, while groups C and A shared *Lactobacillus, Adlercreutzia, Oscillospira, Ruminococcus,* and *Allobaculum* genera (Figure 7B). ASV/OTU number analysis found that at the Phylum level, groups C and L shared *Firmicutes, Bacteroidetes, Proteobacteria, Actinobacteria,* and *Cyanobacteria*, while groups C and A shared *Firmicutes, Bacteroidetes, Proteobacteria, Actinobacteria, TM7,* and *Tenericutes* Phyla. At the genus level, groups C and L shared *Lactobacillus, Bacteroides, Shigella, Oscillospira, Parabacteroides, Pseudomonas, Adlercreutzia, Ruminococcus,* and *Enterococcus,* while groups C and A shared *Lactobacillus, Bacteroides, Oscillospira, Pseudomonas, Adlercreutzia, Ruminococcus, Bifidobacterium,* and *Enterococcus* genera (Figure 7C). It is depicted in the heatmap that the abundance of *Bacteroides, Parabacteroides, Shigella, Prevotella, Phenylobacterium, Candidatus Arthromitus, Prevotella, Rhodococcus, Burkholderia, Blautia, Dorea, Enterococcus, Pseudomonas, Melissococcus, Rubrobacter, Acinetobacter, Butyricimonas, Prauserella, Anaerotruncus, Alistipes,* and *Subdoligranulum* shown in red color in group L were obviously higher than in groups C and A, while *Lactobacillus, Adlercreutzia, Ruminococcus, Coprobacillus*, and *Faecalibacterium* shown in blue color in group L were significantly lower than in groups C and A (Figure 7D). PCA analysis represents that the main genera among mouse groups were *Lactobacillus, Shigella,* and *Pseudomonas*. The distance between points of group A (green) projected on the coordinate axis was clearly farther than groups A (light orange) and C (lavender), which revealed a difference between group L, and groups A and C, respectively (Figure 7E). Also, OPLS-DA analysis revealed similar results to PCA analysis (Figure 7F).

For further investigation, MetagenomeSeq analysis was performed and different genera like *Bacteroidales* and *Lactobacillales* were found significantly on the upside of the broken lines with decreased ASV 102 ($p < 0.05$), ASV 23 ($p < 0.05$), ASV 14 ($p < 0.05$), and ASV 53 ($p < 0.05$), increased ASV 73 ($p < 0.05$), ASV 1 ($p < 0.01$), ASV 194 ($p < 0.05$), ASV 50 ($p < 0.05$), ASV 18 ($p < 0.01$), and ASV 5 ($p < 0.001$) between groups C and A. Different genera like *Bacteroidales*, *Lactobacillales*, *Clostridiales*, *Burkholderiales*, *Desulfovibrionales*, *Enterobacteriales,* and *Pseudomonadales* were found significantly in groups C and L, with 107 decreased ASV and 86 increased ASV (Figure 8A). Biomarker bacteria in mouse groups were uncovered by using LEfSe analysis, which were from the class *Gammaproteobacteria*, phylum *Proteobacteria*, genus *Shigella*, family *Enterobacteriaceae*, order *Enterobacteriales, Rhizobiales*, order *Burkholderiales,* class *Betaproteobacteria*, and genus *Pseudomonas* in group L (green color), family *S24-7,* order *Clostridiales,* class *Clostridia*, genus *Gemella*, order *Gemellales*, family *Gemellaceae*, phylum *Tenericutes*, class *Mollicutes*, family *Lachnospiraceae*, order *RF39*, family *F16*, class *TMT-3*, order *CW040*, phylum *TM7*, and genus *Ruminococcus* in group C (lavender), genus *Faecalibacterium*, family *Acetobacteraceae*, and order *Rhodospirillales* in group A (light orange) (Figure 8B).

Random forest analysis was performed with an accuracy ratio of 2 (Figure 9A). Important genera among mouse groups are shown in Figure 9B including *Clostridium*, *Ruminococcus*, *Lactococcus*, *Gemella*, etc. Network analysis revealed that there were more edges between groups A and C than between groups L and C, which inferred a higher similarity between groups A and C (Figure 9C). The dominant genera in the network were *unidentified F16*, *Lactobacillus*, *Adlercreutzia*, *unidentified S24-7,* and *Turicibacter* between groups A and C, while *Lactococcus* and *Allobaculum* were the main genera in the network between groups L and C (Figure 9D).

By comparing the abundance of genera of mouse microbiota, 19 genera were detected among mouse groups. The abundance of *Lactobacillus* ($p < 0.0001$), *unidentified F16* ($p < 0.0001$), *Adlercreutzia* ($p < 0.01$), *Ruminococcus* ($p < 0.05$), [*Ruminococcus*] ($p < 0.05$), *Acetobacter* ($p < 0.05$), *cc 115* ($p < 0.05$), and *Cupriavidus* ($p < 0.05$) in group L was obviously lower than group C, respectively. While *Shigella* ($p < 0.05$) was prominently higher in group L than in group C. *Unidentified_S24-7* and *unclassified RF39* were significantly higher in group C than in groups A ($p < 0.05$) and L ($p < 0.05$), respectively, while *unclassified Enterobacteriaceae* was significantly lower in group C than in groups A ($p < 0.05$) and L ($p < 0.05$), respectively. The abundance of unclassified *Pseudomonadales* ($p < 0.05$), *Rhodococcus* ($p < 0.05$), unclassified *Comamonadaceae* ($p < 0.05$), and *Lysobacter* ($p < 0.05$) in group L was conspicuously higher than group A, respectively. The abundance of *Faecalibacterium* in group L was clearly lower than groups A ($p < 0.05$) and L ($p < 0.01$), respectively. The abundance of *Gluconacetobacter* in group A was prominently higher than groups L ($p < 0.05$) and C ($p < 0.01$), respectively. The abundance of *unclassified*

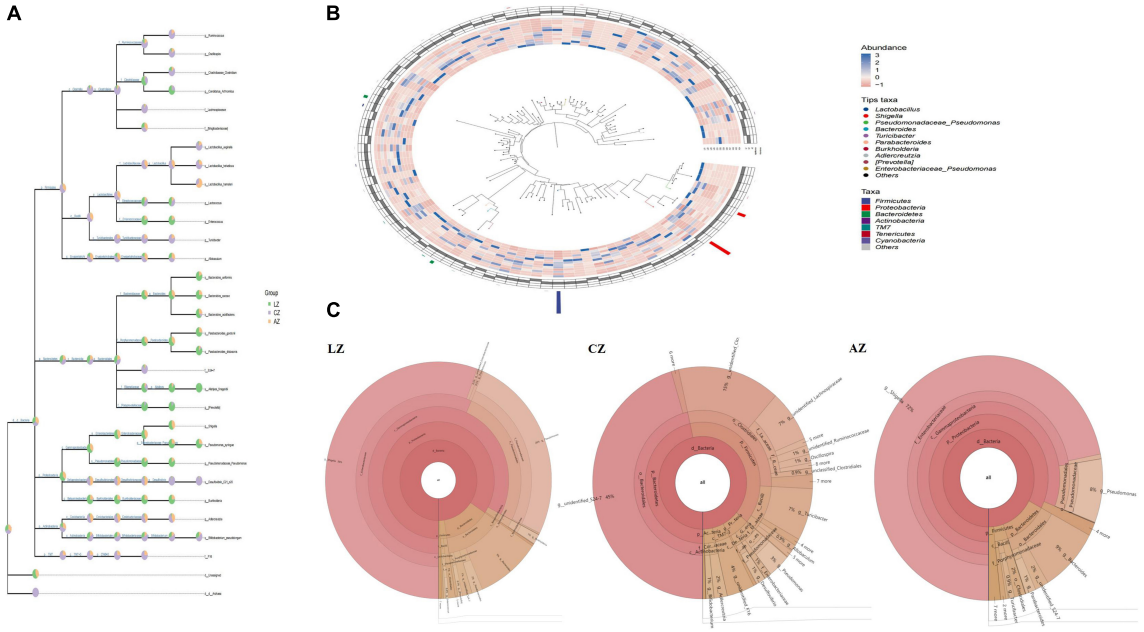


FIGURE 6
Species composition analysis of mouse gut microbiota. **(A)** Classification levels tree diagram, **(B)** GraPhlAn evolutionary tree diagram, and **(C)** Krona species composition diagram.

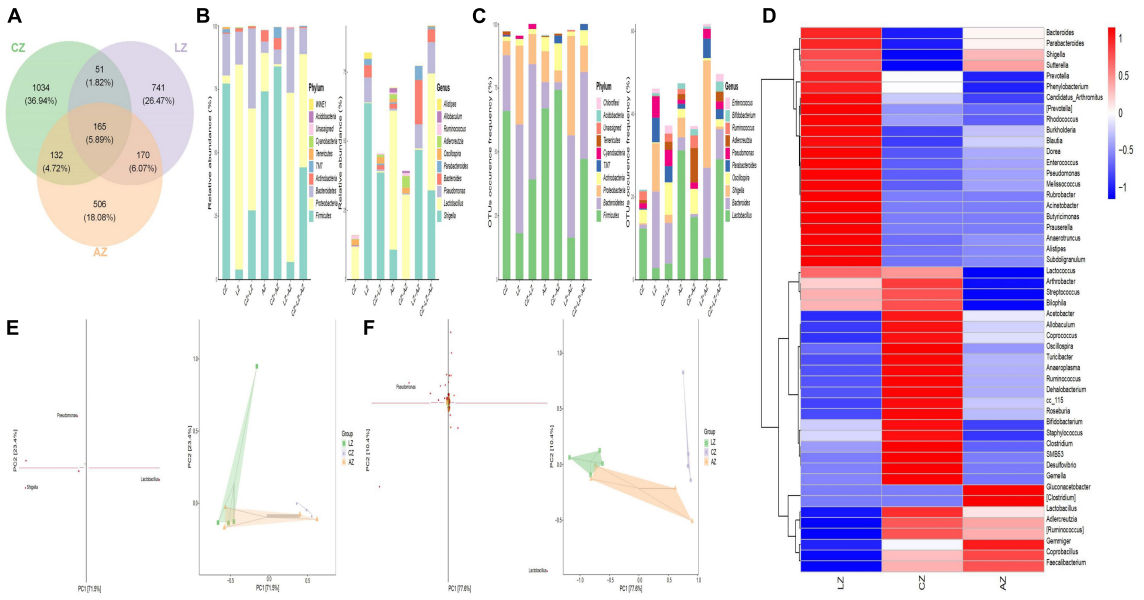


FIGURE 7
Different species and marker species analysis in mouse microbiota induced by LPS. **(A)** Venn diagram, **(B)** bar chart of ASV/OTU numbers in different regions of Venn diagram, **(C)** bar graphs of ASV/OTU abundance in different regions of the Venn diagram, **(D)** genera composition heatmap, **(E)** PCA, and **(F)** OPLS-DA.

*Bradyrhizobiaceae* in group C was clearly higher than in group A ($p < 0.05$) (Figure 10).

In summary, different analysis methods include relative abundance taxa, classification levels tree diagram, GraPhlAn evolutionary tree diagram, Krona species composition diagram, Venn Diagram, Genera composition heatmap, PCA, OPLS-DA, metagenomeSeq analysis, LEfSe analysis, and random forests and network analyses demonstrated that LPS challenge

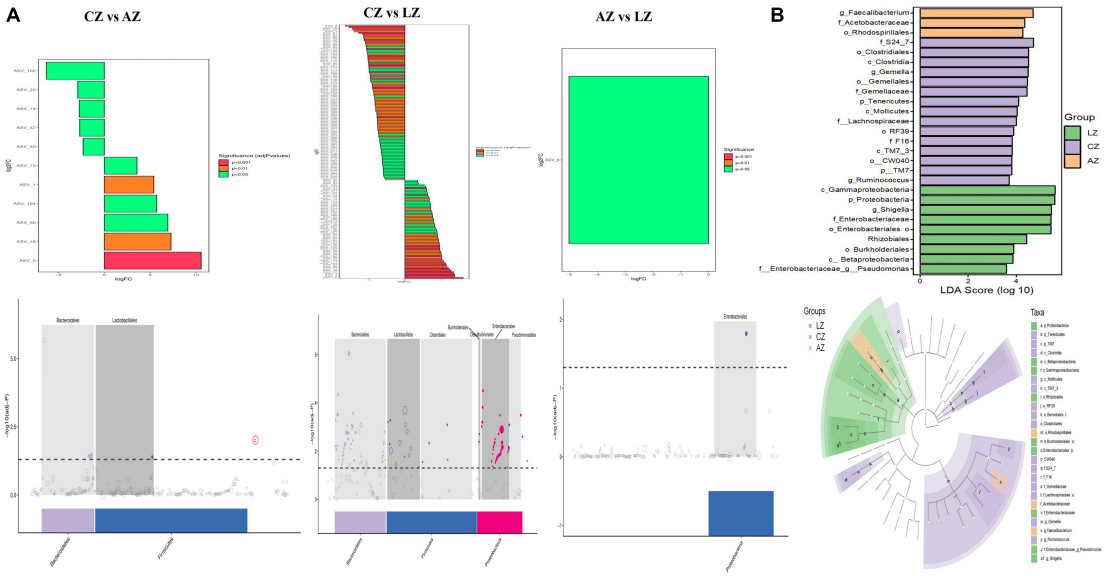


FIGURE 8
Gut microbiota difference analysis between mouse groups. **(A)** MetagenomeSeq analysis and **(B)** LEfSe analysis.

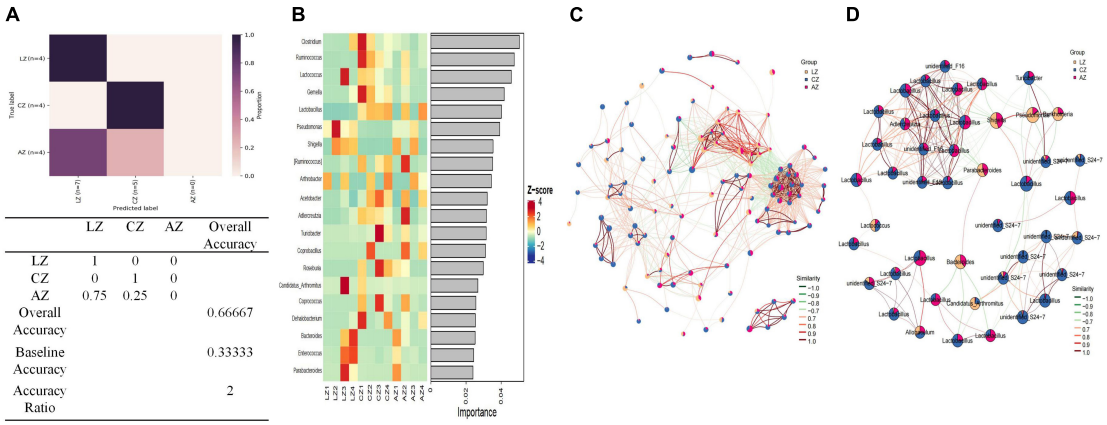


| | LZ | CZ | AZ | Overall Accuracy |
|---|---|---|---|---|
| LZ | 1 | 0 | 0 | |
| CZ | 0 | 1 | 0 | |
| AZ | 0.75 | 0.25 | 0 | |
| Overall Accuracy | | | | 0.66667 |
| Baseline Accuracy | | | | 0.33333 |
| Accuracy Ratio | | | | 2 |

FIGURE 9
Random Forests and network analysis. **(A)** Model accuracy, **(B)** ASV taxa heatmap, **(C)** network analysis, and **(D)** subnetwork analysis of dominant genera.

changed microbiota composing in mice; however, sodium acetate/sodium butyrate supplementation could partly restore the gut microbiota in animals.

## Effects of sodium acetate/sodium butyrate solution supplementation on the function of mouse gut microbiota

PICRUSt2 was utilized for potential function prediction analysis of mouse microbiota. PCoA analysis found that closer points are projected on the coordinate axis in groups A and L in both functional units of KO and EC (Figure 11A), which revealed a more similar functional composition in these groups. KEGG analysis showed that the main pathways were related to metabolism (Figure 11B). MetaCyc analysis showed that the main pathways were related to biosynthesis, degradation/utilization/assimilation, and generation of precursor metabolite and energy (Figure 11C). MetaCyc metabolic pathways comparing analysis found 44 ($p < 0.05$), 9 ($p < 0.01$), and 20 ($p < 0.001$) significant different pathways between groups C and L, 37 ($p < 0.05$), 27 ($p < 0.01$), and 53 ($p < 0.001$) significant different pathways between groups A and C, respectively (Figure 11D). KEGG metabolic pathways

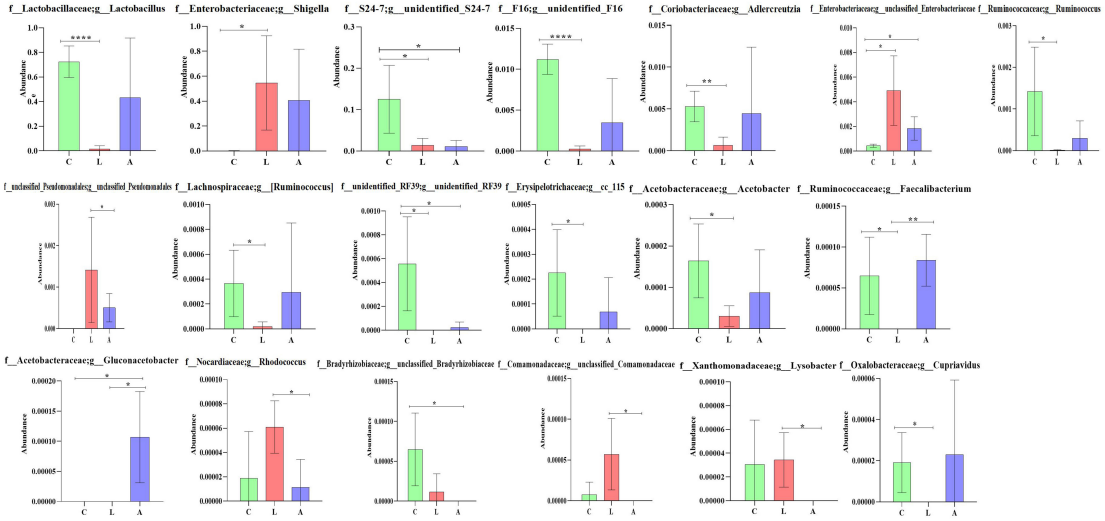


FIGURE 10
Comparing genera difference of mouse microbiota. Significance is presented as $^{*}p < 0.05$, $^{**}p < 0.01$, $^{***}p < 0.001$, and $^{****}p < 0.0001$; data are presented as the mean ± SEM ($n = 4$).

comparing analysis revealed that 15 ($p < 0.05$), 15 ($p < 0.01$), and 51 ($p < 0.001$) significant different pathways between groups C and L, while one ($p < 0.001$) significant different pathway between groups A and C was examined (Figure 11E).

## Expression of ZO-1, Occludin, Claudin, Caspase-1, and NLRP3 genes in mouse intestines

Relative gene expression of Zonula occludens 1 (ZO-1), Occludin, Claudin, Caspase-1, and NLRP3 were detected by employing qRT-PCR. LPS induction prominently upregulated the expression of ZO-1 ($p < 0.01$) and NLRP3 ($p < 0.0001$) in mice of group L; however, sodium acetate/sodium butyrate solution supplementation downregulated the expression of ZO-1 ($p < 0.05$) and NLRP3 ($p < 0.05$) genes in treated mice. Furthermore, change in LPS clearly downregulated the expression of Occludin ($p < 0.001$), Claudin ($p < 0.0001$), and Caspase-1 ($p < 0.0001$) genes in group L, while sodium acetate/sodium butyrate solution supplementation upregulated those gene expressions in treated groups of D, B, and A (Figure 11).

## The correlation among differential bacteria, detection indices, and gene expressions

Correlation assessment between differential bacteria (abundance of top 20 genera), intestine morphology indices, inflammatory cytokines, oxidative indices, and gene expressions was performed through Statistical Analysis System. Results showed that *Lactobacillus*, *Turicibacter*, *Roseburia*, *Allobaculum*, *Bifidobacterium*, *Faecalibacterium*, *Ruminococcus*, *Coprococcus*, *cc_15*, *Gemella*, *Pediococcus*, *Butyricicoccus,* and *Cupriavidus* were positively related to villus height and villus height to crypt depth ratio, while *Rhodococcus*, *Phenylobacterium*, *Lysobacter,* and *W22* were positively related to villus height. *Lactobacillus*, *Allobaculum*, *Rhodococcus*, *Butyricicoccus*, and *Ralstonia* were found positively related to antioxidant ability. *Pseudomonas*, *Faecalibacterium*, *Faecalibacterium*, *Candidatus Arthromitus*, *Ruminococcus*, *Roseburia*, *Gemella*, *Faecalibacterium*, *Gluconacetobacter*, *Rhodococcus*, *Anaeroplasma*, (*Clostridium*), *Phenylobacterium*, and *Aminobacter* were positively related to inflammatory cytokines. *Pseudomonas*, *Faecalibacterium*, *Gluconacetobacter*, *Rhodococcus*, (*Clostridium*), and *Gluconobacter* were positively related to tight junction proteins, while *Adlercreutzia*, *Candidatus Arthromitus*, *Lactococcus*, *Ruminococcus*, *Coprococcus*, *Acinetobacter*, *cc_115*, *Gemella*, *Anaeroplasma*, *Phenylobacterium*, *Lysobacter,* and *W22* were negatively related to tight junction proteins. Adlercreutzia, Ruminococcus, Coprococcus, cc_115, Roseburia, Gemella, and Anaeroplasma were negatively related to expressions of Caspase-1 and NLRP3 (Figure 12).

# Discussion

Though various kinds of measures have been implemented so far to fight against diarrhea, there is still a long way

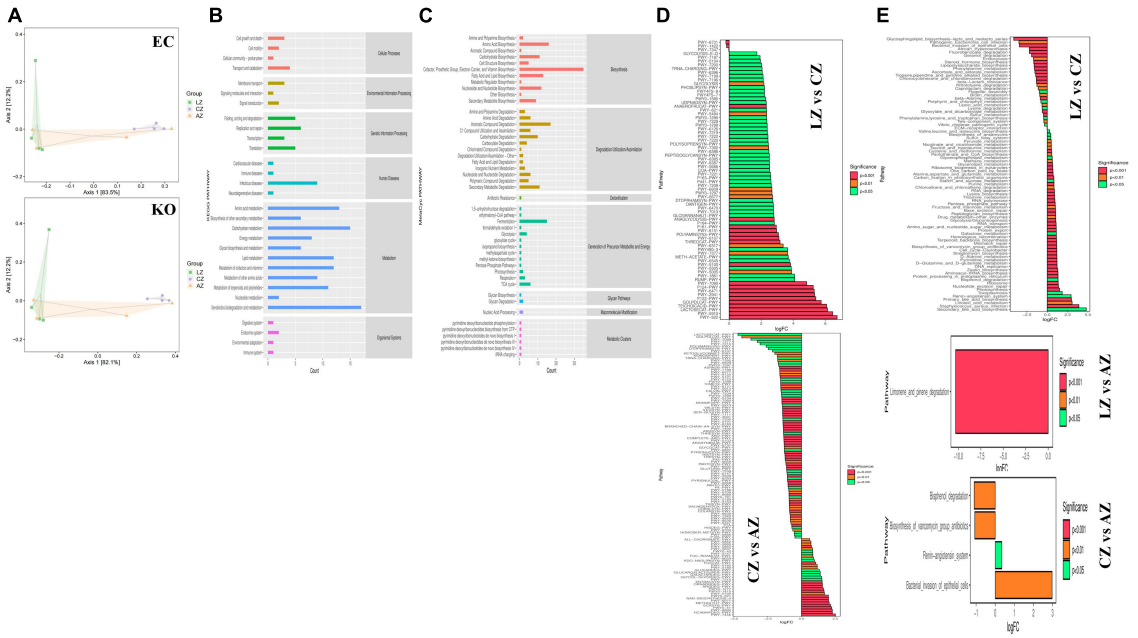


FIGURE 11
Potential function prediction analysis of mouse microbiota. **(A)** PCoA, **(B)** KEGG, **(C)** MetaCyc, **(D)** MetaCyc metabolic pathways, and **(E)** KEGG metabolic pathways.

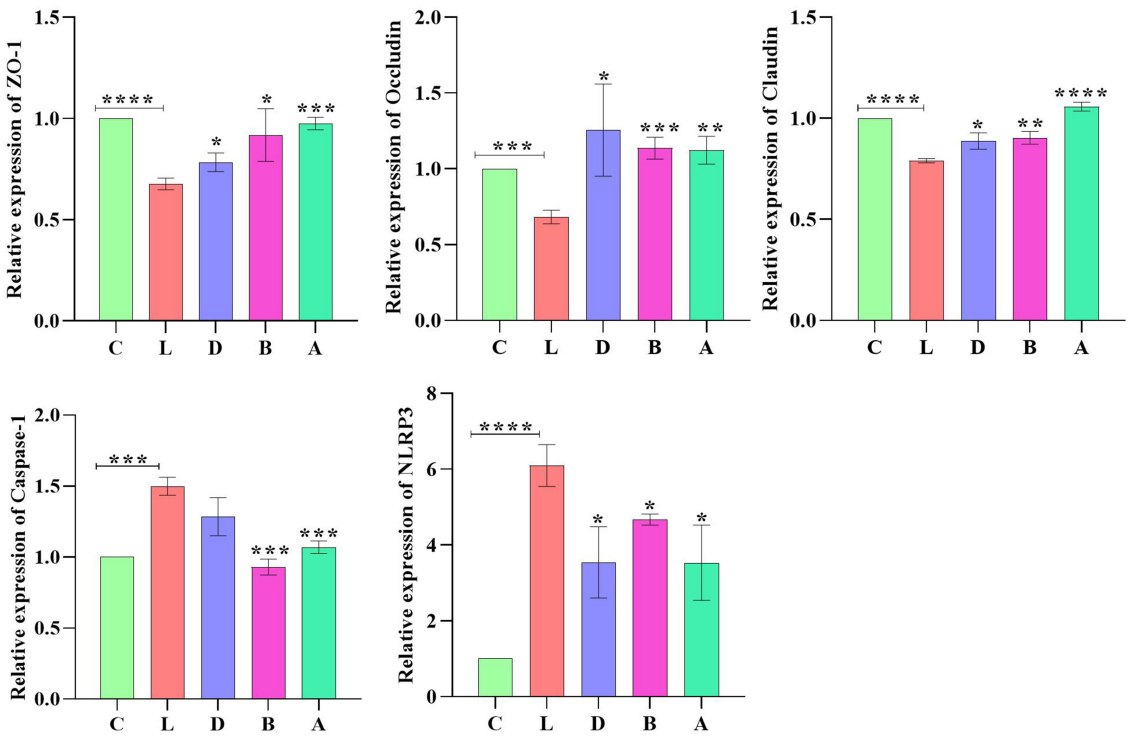


FIGURE 12
Relative expression analysis of ZO-1, Occludin, Claudin, Caspase-1, and NLRP3 *via* qRT-PCR. Significance is presented as $*p < 0.05$, $**p < 0.01$, $***p < 0.001$, and $****p < 0.0001$; data are presented as the mean ± SEM ($n = 3$).

to go (Cho et al., 2013). A recent review found that higher antimicrobial resistance was associated with the drugs being used for the treatment of diarrhea (Zhang H. et al., 2022; Zhang X. et al., 2022); therefore, establishing a method to positively regulate the gut microbiota to ameliorate diarrhea is of great importance and meaningful (Coelho et al., 2022).

In the present study, mice were supplemented with sodium acetate/sodium butyrate before inducing diarrhea by utilizing LPS. Serve damage to intestines particularly jejunum, ileum, cecum, and colon was examined (**Figure 1B**), which was in accordance with previous results (He et al., 2022). An obvious decrease in villus height, increase in crypt depth, and lowered villus height to crypt depth ratio were uncovered in group C, while interestingly, sodium acetate/sodium butyrate supplementation could significantly increase the villus height, decrease the crypt depth, and increase the villus height to crypt depth ratio in both jejunum and ileum, especially in groups B and A (**Figures 1C,D**). The current results demonstrated that sodium acetate/sodium butyrate could improve intestinal integrity deteriorated by LPS, as intestinal barrier integrity is considered an important indicator of intestinal health (Liu H. et al., 2022). The current results may reveal that sodium acetate/sodium butyrate supplementation is a hopeful and effective method to alleviate diarrhea in animals.

To explore the potential mechanisms, we detected the gene expressions of tight junction proteins in intestines. Among them Occludin and Claudins were recognized as important components of intestinal permeability (Chen et al., 2015). The expression of Occludin in group L was significantly lower than in group C, while expression levels of Occludin increased in sodium acetate/sodium butyrate-treated groups (**Figure 11**). The current results were in line with a study on inflammatory bowel disease in humans with the downregulation of Occludin (Chen et al., 2015). The expression of Claudin in group L was significantly lower, which is in line with previous results (He et al., 2022); however, with the treatment of sodium acetate/sodium butyrate, the expression of Claudin upregulated significantly. The plaque protein ZO1 is an adaptor connecting trans-membrane protein with the peri-junctional actomyosin ring (Ulluwishewa et al., 2011). Like previous results found lower expressions of ZO-1 (Cao et al., 2022; He et al., 2022), the expression of ZO-1 in group L was significantly higher than in group C, while expression levels of ZO-1 decreased in sodium acetate/sodium butyrate-treated groups. The current findings suggested that acetate/sodium butyrate could improve intestinal barrier function by modulating tight junction gene expressions.

Reactive oxygen species are widely known for their important role in inflammatory diseases like colitis. The intestinal tissue injury is mediated through the administration of the antioxidants (Dashdorj et al., 2013; Aziz et al., 2021; Hassan et al., 2021; Liu et al., 2021; Murtaza et al., 2021). Oxidative agents of SOD, T-AOC, GSH-Px, and MDA are commonly known important enzymes related to oxidative stress, which may cause intestinal damage (Mehmood et al., 2019; Liu J. et al., 2022). In mice serums, no obvious difference was found in GSH-px and SOD between the control group and LPS-induced groups, respectively, while a prominently higher level of MDA ($p < 0.01$) was detected in group L; however, there was a significant decrease in MDA ($p < 0.01$) levels in sodium acetate/sodium butyrate supplemented groups D, B, and A, respectively (**Figure 3**), suggesting that sodium acetate/sodium butyrate improves intestinal oxidative damage by reducing MDA contents. Previous studies found that the activation of Caspase-1 by NLRP3 inflammasome could cause inflammation reaction by promoting the maturation of IL-1β, and ROS was a generally accepted second key messenger of NLRP3 inflammasome (Dashdorj et al., 2013; Sho and Xu, 2019; He et al., 2022). LPS inducing obviously upregulated the expression of NLRP3 ($p < 0.0001$) in mice in group L; however, sodium acetate/sodium butyrate solution supplementation downregulated the expression of NLRP3 ($p < 0.05$) genes in treated mice. Also, the LPS challenge

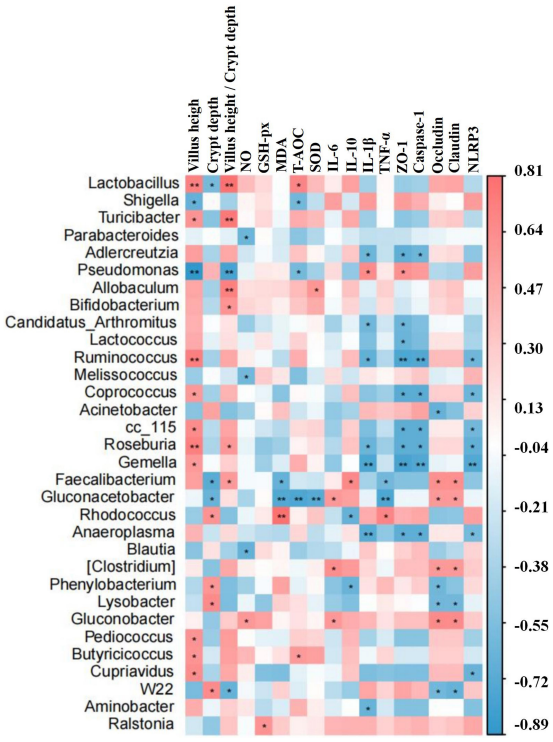


FIGURE 13
The differential bacteria of mouse were notably corrected with the indices of inflammatory cytokines, oxidative status, intestine morphology, and gene expressions by the statistical analysis system. Significance is presented as $*p < 0.05$ and $**p < 0.01$; data are presented as the mean ± SEM ($n = 4$).

clearly upregulated the Caspase-1 ($p < 0.0001$) gene in group L, while sodium acetate/sodium butyrate solution supplementation downregulated it in treated groups D, B, and A (**Figure 11**). TNF-α is an important cytokine in inflammation (Zelová and Hošek, 2013), Significantly higher IL-1β and TNF-α ($p < 0.001$) were found in group C, which was consistent with previous results found higher inflammatory factors and upregulation of NLRP3 in HUVEC cells (Liu et al., 2021). However, sodium acetate/sodium butyrate supplementation significantly decreased IL-1β and TNF-α in groups D, B, and A, respectively (**Figure 3**), demonstrating that sodium acetate/sodium butyrate could reduce intestine inflammation caused by LPS by alleviating oxidative damage *via* the downregulation of NLRP3 and Caspase-1.

Previous study found that LPS-induced ROS caused gut microbiota dysbiosis in piglets (Xu et al., 2021). Similar results were found in the current results in mice. The structure and diversity of mouse gut microbiota were significantly altered in LPS-induced mice, as determined by alpha and beta diversity analysis (**Figure 13**), taxa analysis at different levels (**Figure 5**), Classification levels tree diagram, and GraPhlAn evolutionary tree diagram analysis (**Figures 6A,C**). Potential function prediction analysis by PICRUSt2 and KEGG analysis found that LPS significantly changed the main pathways of mice (**Figure 11**). In consistent with previous studies (Yue et al., 2020; Xu et al., 2021; Chang et al., 2022), sodium acetate/sodium butyrate supplementation restored the structure, diversity, and partly function of mouse gut microbiota. Venn diagram, heatmap, PCA, OPLS-DA (**Figure 7**), metagenomeSeq (**Figure 8**), and random forests and network analysis (**Figure 9**) analyses were performed to reveal different species and their markers in mice microbiota induced by LPS. A total of 19 genera were detected among mouse groups (**Figure 10**). LPS challenge decreased the abundance of *Lactobacillus, unidentified F16, unidentified_S24-7, Adlercreutzia, Ruminococcus, unclassified Pseudomonadales, (Ruminococcus), Acetobacter, cc 1, Rhodococcus, unclassified Comamonadaceae, Faecalibacterium,* and *Cupriavidus*, while increased *Shigella, Rhodococcus, unclassified Comamonadaceae,* and *unclassified Pseudomonadales* in group L. Interestingly sodium acetate/sodium butyrate supplementation increased *Lactobacillus, unidentified F16, Adlercreutzia, Ruminococcus, (Ruminococcus), unidentified F16, cc 115, Acetobacter,*

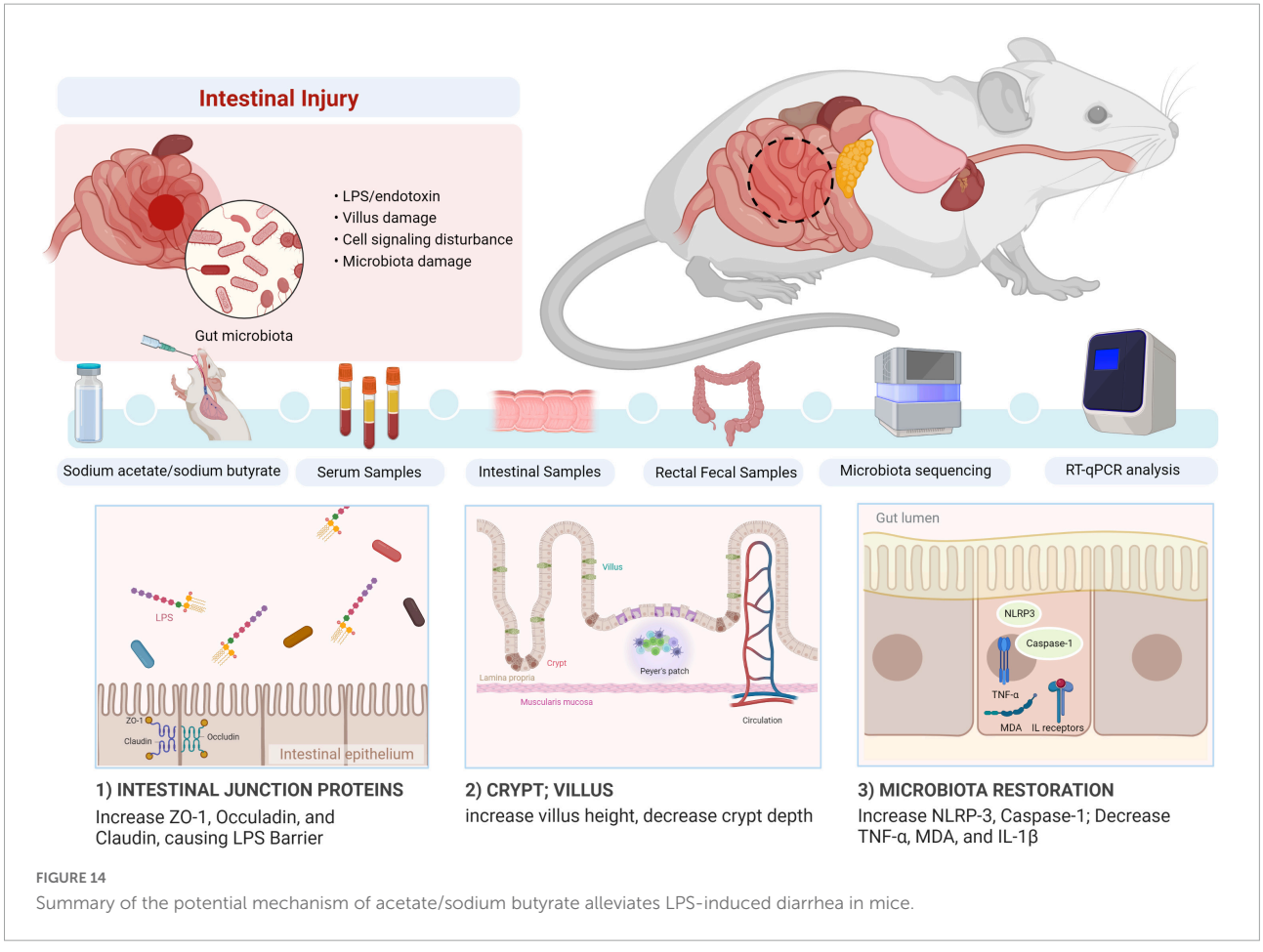


FIGURE 14
Summary of the potential mechanism of acetate/sodium butyrate alleviates LPS-induced diarrhea in mice.

*Faecalibacterium,* and *Cupriavidus,* while decreased *Shigella, unclassified Enterobacteriaceae, unclassified Pseudomonadales, Rhodococcus,* and *unclassified Comamonadaceae*. *Lactobacillus* genus bacteria are probiotic microorganisms that have beneficial effects on to host (Rajab et al., 2020), and previous studies demonstrated that *Lactobacillus* could improve diarrhea in infants and piglets (Hu et al., 2019; Wang et al., 2020). A previous study reported that the genus *Adlercreutzia* was related to body weight loss (Liu Z. et al., 2022), the abundance of *Ruminococcus* was significantly decreased in diarrhea piglets (Liu C. et al., 2019; Liu G. et al., 2019). The changes of Adlercreutzia and Ruminococcus in the current study were consistent with previous findings. Bacteria from the *Acetobacter* genus are related to lignin degradation and intestine metabolism (Wu et al., 2022), and the decreasing of this genus may affect the metabolism of animals. Also, these bacteria can generate acetate (Zhang H. et al., 2022), which confirmed that diarrhea was related to the inefficiency of acetate. Bacteria of *Rhodococcus* are from natural environments (Alvarez et al., 2021), which may contrite little to diarrhea. A previous study reported that *unclassified Comamonadaceae* were related to the degradation of organics (Zhang et al., 2020), which may infer that LPS inducing could affect organics metabolism. The lower abundance of *Faecalibacterium* was consistent with the previous study observed in patients with colitis and Crohn's disease (Ponziani et al., 2020). *Faecalibacterium* could cause inflammation through decreased SCFAs (Nishiwaki et al., 2020), which showed that LPS-induced diarrhea may attribute to the absence of SCFAs. Bacteria from *Cupriavidus* genus are related to biodegradation and biodetoxifcation, which may indicate that LPS could reduce the degradation (Al-Nussairawi et al., 2020) and detoxification ability of mouse. *Shigella spp.* are well-known pathogens causing bacterial dysentery (Liu C. et al., 2019), which should reveal the reason of diarrhea caused by LPS. Bacteria from the top 20 abundance genera related to intestine damage, oxidation resistance, inflammatory factor, and gene expressions are shown in **Figure 12**, which demonstrated that sodium acetate/sodium butyrate could regulate microbiota to improve diarrhea induced by LPS in mice.

## Conclusion

In conclusion, we revealed that sodium acetate/sodium butyrate could alleviate LPS-induced diarrhea in mice by increasing beneficial bacteria and decreasing pathogens, which could regulate oxidative damage and inflammatory responses *via* NLRP3/Caspase-1 signaling (**Figure 14**). The current results may give insights into the prevention and treatment of diarrhea.

## Data availability statement

The data presented in this study are deposited in the https://www.ncbi.nlm.nih.gov/ repository, accession numbers: PRJNA872847 and SAMN30471364-SAMN30471375.

## Ethics statement

This animal study was reviewed and approved by Laboratory Animals Research Centre of Jiangsu, China and the Ethics Committee of Nanjing Agricultural University (NJAU.No20220520108).

## Author contributions

KL and QK: research idea, methodology, visualization, and supervision. XC, QK, XZ, CZ, PH, and HL: reagents, materials, and analysis tools. KL: writing—original draft and preparation. MK, ZB, II, HA, QS, and KL: writing—review and editing. All authors contributed to the article and approved the submitted version.

## Funding

This study was supported by the Basic Research Funds for Central Universities (Tibet Joint Fund) (KYYZ2022003) and the National Natural Science Foundation of China (Nos. 31872514 and 32172900).

## Acknowledgments

We thank Bioyi Biotechnology Co., Ltd., (Wuhan, China) for providing sequencing help in our research.

## Conflict of interest

The authors declare that the research was conducted in the absence of any commercial or financial relationships that could be construed as a potential conflict of interest.

## Publisher's note

# References

Alban, R. (2010). Multivariate analyses in microbial ecology. *FEMS Microbiol. Ecol.* 62, 142–160. doi: 10.1111/j.1574-6941.2007.00375.x

Al-Nussairawi, M., Risa, A., Garai, E., Varga, E., Szabó, I., Csenki-Bakos, Z., et al. (2020). Mycotoxin biodegradation ability of the *Cupriavidus* Genus. *Curr. Microbiol.* 77, 2430–2440. doi: 10.1007/s00284-020-02063-7

Alvarez, H. M., Hernández, M. A., Lanfranconi, M. P., Silva, R. A., and Villalba, M. S. (2021). Rhodococcus as biofactories for microbial oil production. *Molecules* 26:4871. doi: 10.3390/molecules26164871

Aziz, S., Abdullah, S., Anwar, H., Latif, F., and Mustfa, W. (2021). Effect of engineered nickel oxide nano particles on antioxidant enzymes in fresh water fish, *Labeo rohita*. *Pak. Vet. J.* 41, 424–428. doi: 10.29261/pakvetj/2021.044

Bokulich, N. A., Kaehler, B. D., Rideout, J. R., Dillon, M., Bolyen, E., Knight, R., et al. (2018). Optimizing taxonomic classification of marker-gene amplicon sequences with QIIME 2's q2-feature-classifier plugin. *Microbiome* 6:90. doi: 10.1186/s40168-018-0470-z

Callahan, B. J., Mcmurdie, P. J., Rosen, M. J., Han, A. W., Johnson, A. J. A., and Holmes, S. P. (2016). DADA2: High-resolution sample inference from Illumina amplicon data. *Nat. Methods* 13, 581–583. doi: 10.1038/nmeth.3869

Cao, Z., Gao, J., Huang, W., Yan, J., Shan, A., and Gao, X. (2022). Curcumin mitigates deoxynivalenol-induced intestinal epithelial barrier disruption by regulating Nrf2/p53 and NF-κB/MLCK signaling in mice. *Food Chem. Toxicol.* 167:113281. doi: 10.1016/j.fct.2022.113281

Chang, M., Wang, F., Ma, F., Jin, Y., and Sun, P. (2022). Supplementation with galacto-oligosaccharides in early life persistently facilitates the microbial colonization of the rumen and promotes growth of preweaning Holstein dairy calves. *Anim. Nutr.* 10, 223–233. doi: 10.1016/j.aninu.2022.04.009

Chao, A. (1984). Nonparametric estimation of the number of classes in a population. *Scand. J. Stat.* 11, 265–270.

Chen, J., Tellez, G., Richards, J. D., and Escobar, J. (2015). Identification of potential biomarkers for gut barrier failure in broiler chickens. *Front. Vet. Sci.* 2:14. doi: 10.3389/fvets.2015.00014

Cho, Y., Han, J., Wang, C., Cooper, V., Schwartz, K., Engelken, T., et al. (2013). Case-control study of microbiological etiology associated with calf diarrhea. *Vet. Microbiol.* 166, 375–385. doi: 10.1016/j.vetmic.2013.07.001

Chuang, S., Chen, C., Hsieh, J., Li, K., Ho, S., and Chen, M. (2022). Development of next-generation probiotics by investigating the interrelationships between gastrointestinal Microbiota and Diarrhea in Preruminant Holstein Calves. *Animals* 12:695. doi: 10.3390/ani12060695

Coelho, M. G., Virgínio Júnior, G. F., Tomaluski, C. R., de Toledo, A. F., Reis, M. E., Dondé, S. C., et al. (2022). Comparative study of different liquid diets for dairy calves and the impact on performance and the bacterial community during diarrhea. *Sci. Rep.* 12:13394. doi: 10.1038/s41598-022-17613-1

Coura, F. M., Freitas, M. D., Ribeiro, J., de Leme, R. A., de Souza, C., Alfieri, A. A., et al. (2015). Longitudinal study of *Salmonella* spp., diarrheagenic *Escherichia coli*, Rotavirus, and Coronavirus isolated from healthy and diarrheic calves in a Brazilian dairy herd. *Trop. Anim. Health Prod.* 47, 3–11. doi: 10.1007/s11250-014-0675-5

Dashdorj, A., Jyothi, K. R., Lim, S., Jo, A., Nguyen, M. N., Ha, J., et al. (2013). Mitochondria-targeted antioxidant MitoQ ameliorates experimental mouse colitis by suppressing NLRP3 inflammasome-mediated inflammatory cytokines. *BMC Med.* 11:178. doi: 10.1186/1741-7015-11-178

Du, K., Bereswill, S., and Heimesaat, M. M. (2021). A literature survey on antimicrobial and immune-modulatory effects of butyrate revealing non-antibiotic approaches to tackle bacterial infections. *Eur. J. Microbiol. Immunol.* 11, 1–9. doi: 10.1556/1886.2021.00001

Ezzine, C., Loison, L., Montbrion, N., Bole-Feysot, C., Dechelotte, P., Coeffier, M., et al. (2022). Fatty acids produced by the gut microbiota dampen host inflammatory responses by modulating intestinal SUMOylation. *Gut Microbes* 14:2108280. doi: 10.1080/19490976.2022.2108280

Faith, D. P. (1992). Conservation evaluation and phylogenetic diversity. *Biol. Conserv.* 61, 1–10. doi: 10.1016/0006-3207(92)91201-3

Faust, K., and Raes, J. (2012). Microbial interactions: From networks to models. *Nat. Rev. Microbiol.* 10, 538–550. doi: 10.1038/nrmicro2832

Fu, X., Liu, Z., Zhu, C., Mou, H., and Kong, Q. (2019). Nondigestible carbohydrates, butyrate, and butyrate-producing bacteria. *Crit. Rev. Food Sci.* 59, S130–S152. doi: 10.1080/10408398.2018.1542587

Gaudier, E., Rival, M., Buisine, M., Robineau, I., and Hoebler, C. (2009). Butyrate enemas upregulate Muc genes expression but decrease adherent mucus thickness in mice colon. *Physiol. Res.* 58, 111–119. doi: 10.33549/physiolres.931271

Gavin, M. D., Vincent, J. M., Jesse, Z., Svetlana, N. Y., James, R. B., Christopher, M. T., et al. (2019). PICRUSt2: An improved and customizable approach for metagenome inference. *bioRxiv* [Preprint]. doi: 10.1101/672295

Good, I. J. (1953). The population frequencies of species and the estimation of population parametes. *Biometrika* 40, 237–264. doi: 10.1093/biomet/40.3-4.237

Guilloteau, P., Martin, L., Eeckhaut, V., Ducatelle, R., Zabielski, R., and Van Immerseel, F. (2010). From the gut to the peripheral tissues: The multiple effects of butyrate. *Nutr. Res. Rev.* 23, 366–384. doi: 10.1017/S0954422410000247

Hamer, H. M., Jonkers, D., Venema, K., Vanhoutvin, S., Troost, F. J., and Brummer, R. J. (2008). Review article: The role of butyrate on colonic function. *Aliment. Pharm. Ther.* 27, 104–119. doi: 10.1111/j.1365-2036.2007.03562.x

Hassan, M., Ali, A., Wajid, M., Ahmad, A., Saleemi, M. K., Sarwar, Y., et al. (2021). Purification and antigenic detection of lipopolysaccharides of *Salmonella enterica* serovar Typhimurium isolate from Faisalabad, Pakistan. *Pak. Vet. J.* 41, 434–438.

He, Y., Li, Z., Xu, T., Luo, D., Chi, Q., Zhang, Y., et al. (2022). Polystyrene nanoplastics deteriorate LPS-modulated duodenal permeability and inflammation in mice via ROS drived-NF-κB/NLRP3 pathway. *Chemosphere* 307:135662. doi: 10.1016/j.chemosphere.2022.135662

Hu, P., Zhao, F., Zhu, W., and Wang, J. (2019). Effects of early-life lactoferrin intervention on growth performance, small intestinal function and gut microbiota in suckling piglets. *Food Funct.* 10, 5361–5373. doi: 10.1039/C9FO00676A

Jiminez, J. A., Uwiera, T. C., Abbott, D. W., Uwiera, R. R. E., and Inglis, G. D. (2017). Butyrate supplementation at high concentrations alters enteric bacterial communities and reduces intestinal inflammation in mice infected with *Citrobacter rodentium*. *mSphere* 2:e00243-17. doi: 10.1128/mSphere.00243-17

Katoh, K., Misawa, K., Kuma, K., and Miyata, T. (2002). MAFFT: A novel method for rapid multiple sequence alignment based on fast Fourier transform. *Nucleic Acids Res.* 30, 3059–3066. doi: 10.1093/nar/gkf436

Koh, A., De Vadder, F., Kovatcheva-Datchary, P., and Bäckhed, F. (2016). From dietary fiber to host physiology: Short-chain fatty acids as key bacterial metabolites. *Cell* 165, 1332–1345. doi: 10.1016/j.cell.2016.05.041

Legendre, P., and Montréal, U. D. (2003). *Numerical ecology*, 2nd English Edn. *Developments in environmental modelling,* Vol. 20. Amsterdam: Elsevier.

Leonel, A., and Alvarez-Leite, J. (2012). Butyrate implications for intestinal function. *Curr. Opin. Clin. Nutr. Metab. Care* 15, 474–479. doi: 10.1097/MCO.0b013e32835665fa

Li, K., Zeng, Z., Liu, J., Pei, L., Wang, Y., Li, A., et al. (2022). Effects of short-chain fatty acid modulation on potentially Diarrhea-causing pathogens in Yaks Through Metagenomic Sequencing. *Front. Cell. Infect. Microbiol.* 12:805481. doi: 10.3389/fcimb.2022.805481

Liu, C., Liang, X., Wei, X., Jin, Z., Chen, F., Tang, Q., et al. (2019). Gegen Qinlian decoction treats Diarrhea in piglets by modulating gut microbiota and short-chain fatty Acids. *Front. Microbiol.* 10:825. doi: 10.3389/fmicb.2019.00825

Liu, G., Pilla, G., and Tang, C. M. (2019). Shigellahost: Pathogen interactions: Keeping bacteria in the loop. *Cell. Microbiol.* 21:e13062. doi: 10.1111/cmi.13062

Liu, H., Li, X., Shi, S., Zhou, Y., Zhang, K., Wang, Y., et al. (2022). Chlorogenic acid improves growth performance and intestinal health through autophagy-mediated nuclear factor erythroid 2-related factor 2 pathway in oxidatively stressed broilers induced by dexamethasone. *Poult. Sci.* 101:102036. doi: 10.1016/j.psj.2022.102036

Liu, J., Wang, X., Zhang, W., Kulyar, M. F., Ullah, K., Han, Z., et al. (2022). Comparative analysis of gut microbiota in healthy and diarrheic yaks. *Microb. Cell Fact.* 21:111. doi: 10.1186/s12934-022-01836-y

Liu, X., Lu, B., Fu, J., Zhu, X., Song, E., and Song, Y. (2021). Amorphous silica nanoparticles induce inflammation via activation of NLRP3 inflammasome and HMGB1/TLR4/MYD88/NF-kb signaling pathway in HUVEC cells. *J. Hazard. Mater.* 404:124050. doi: 10.1016/j.jhazmat.2020.124050

Liu, Z., Peng, Y., Zhao, L., and Li, X. (2022). MFE40—the active fraction of Mume Fructus alcohol extract—alleviates Crohn's disease and its complications. *J. Ethnopharmacol.* 296:115465. doi: 10.1016/j.jep.2022.115465

Mahadevan, S., Shah, S. L., Marrie, T. J., and Slupsky, C. M. (2008). Analysis of metabolomic data using support vector machines. *Anal. Chem.* 80, 7562–7570. doi: 10.1021/ac800954c

Mehmood, K., Zhang, H., Yao, W., Jiang, X., Waqas, M., Li, A., et al. (2019). Protective effect of Astragaloside IV to inhibit thiram-induced tibial

dyschondroplasia. *Environ. Sci. Pollut. Res.* 26, 16210–16219. doi: 10.1007/s11356-019-05032-1

Murtaza, S., Khan, J. A., Aslam, B., and Faisal, M. N. (2021). Pomegranate peel extract and quercetin possess antioxidant and hepatoprotective activity against concanavalin A-induced liver injury in mice. *Pak. Vet. J.* 41, 197–202.

Nishiwaki, H., Ito, M., Ishida, T., Hamaguchi, T., Maeda, T., Kashihara, K., et al. (2020). Meta-Analysis of Gut Dysbiosis in Parkinson's disease. *Mov. Disord.* 35, 1626–1635. doi: 10.1002/mds.28119

Ondov, B. D., Bergman, N. H., and Phillippy, A. M. (2011). Interactive metagenomic visualization in a Web browser. *BMC Bioinformatics* 12:385. doi: 10.1186/1471-2105-12-385

Pielou, E. C. J. (1966). The measurement of diversity in different types of biological collections. *J. Theor. Biol.* 13, 131–144. doi: 10.1016/0022-5193(66)90013-0

Ponziani, F. R., Scaldaferri, F., Siena, M., Mangiola, F., Matteo, M., Pecere, S., et al. (2020). Increased Faecalibacterium abundance is associated with clinical improvement in patients receiving rifaximin treatment. *Benef. Microbes* 11, 519–525. doi: 10.3920/BM2019.0171

Price, M. N., Dehal, P. S., and Arkin, A. P. (2010). FastTree 2–approximately maximum-likelihood trees for large alignments. *PLoS One* 5:e9490. doi: 10.1371/journal.pone.0009490

Quast, C., Pruesse, E., Yilmaz, P., Gerken, J., Schweer, T., Yarza, P., et al. (2012). The SILVA ribosomal RNA gene database project: Improved data processing and web-based tools. *Nucleic Acids Res.* 41, D590–D596. doi: 10.1093/nar/gks1219

Rajab, S., Tabandeh, F., Shahraky, M. K., and Alahyaribeik, S. (2020). The effect of lactobacillus cell size on its probiotic characteristics. *Anaerobe* 62:102103. doi: 10.1016/j.anaerobe.2019.102103

Rognes, T., Flouri, T., Nichols, B., Quince, C., and Mahé, F. (2016). VSEARCH: A versatile open source tool for metagenomics. *PeerJ* 4:e2584. doi: 10.7717/peerj.2584

Schmoeller, E., Matos, A. D. C. D., Rahal, N. M., Feijo, J. O., Brauner, C. C., Pino, F. A. B. D., et al. (2021). Diarrhea duration and performance outcomes of pre-weaned dairy calves supplemented with bacteriophage. *Can. J. Anim. Sci.* 102, 165–174. doi: 10.1139/cjas-2021-0074

Segata, N., Izard, J., Waldron, L., Gevers, D., Miropolsky, L., Garrett, W. S., et al. (2011). Metagenomic biomarker discovery and explanation. *Genome Biol.* 12:R60. doi: 10.1186/gb-2011-12-6-r60

Shannon, C. E. (1948). A mathematical theory of communication, 1948. *Bell Syst. Tech. J.* 27, 3–55. doi: 10.1002/j.1538-7305.1948.tb01338.x

Sho, T., and Xu, J. (2019). Role and mechanism of ROS scavengers in alleviating NLRP3-mediated inflammation. *Biotechnol. Appl. Biochem.* 66, 4–13. doi: 10.1002/bab.1700

Simpson, E. H. (1997). Measurement of diversity. *J. Cardiothor. Vasc. Anesth.* 11, 812–812.

Takeuchi, T., Miyauchi, E., Kanaya, T., Kato, T., Nakanishi, Y., Watanabe, T., et al. (2021). Acetate differentially regulates IgA reactivity to commensal bacteria. *Nature* 595, 560–564. doi: 10.1038/s41586-021-03727-5

Ulluwishewa, D., Anderson, R. C., Mcnabb, W. C., Moughan, P. J., Wells, J. M., and Roy, N. C. (2011). Regulation of tight junction permeability by intestinal bacteria and dietary. *J. Nutr.* 141, 769–776. doi: 10.3945/jn.110.135657

Wang, X., Zhang, M., Wang, W., Lv, H., Zhang, H., Liu, Y., et al. (2020). The *in vitro* effects of the probiotic strain, *Lactobacillus casei* ZX633 on gut microbiota composition in infants with Diarrhea. *Front. Cell. Infect. Microbiol.* 10:576185. doi: 10.3389/fcimb.2020.576185

Wei, H., Li, X., Tang, L., Yao, H., Ren, Z., Wang, C., et al. (2020). 16S rRNA gene sequencing reveals the relationship between gut microbiota and ovarian development in the swimming crab *Portunus trituberculatus*. *Chemosphere* 254:126891. doi: 10.1016/j.chemosphere.2020.126891

Wu, X., Wang, J., Amanze, C., Yu, R., Li, J., Wu, X., et al. (2022). Exploring the dynamic of microbial community and metabolic function in food waste composting amended with traditional Chinese medicine residues. *J. Environ. Manage.* 319:115765. doi: 10.1016/j.jenvman.2022.115765

Xu, B., Yan, Y., Yin, B., Zhang, L., Qin, W., Niu, Y., et al. (2021). Dietary glycyl-glutamine supplementation ameliorates intestinal integrity, inflammatory response, and oxidative status in association with the gut microbiota in LPS-challenged piglets. *Food Funct.* 12, 3539–3551. doi: 10.1039/D0FO03080E

Yosi, F., Sharma, S., Sener-Aydemir, A., Koger, S., Baskara, A. P., and Metzler-Zebeli, B. U. (2022). Short-chain fatty acids promote jejunal barrier function and caecal muscle contractibility in laying hens ex vivo. *Br. Poult. Sci.* 63, 406–413. doi: 10.1080/00071668.2021.2008312

Yue, Y., He, Z., Zhou, Y., Ross, R. P., Stanton, C., Zhao, J., et al. (2020). Lactobacillus plantarum relieves diarrhea caused by enterotoxin-producing *Escherichia coli* through inflammation modulation and gut microbiota regulation. *Food Funct.* 11, 10362–10374. doi: 10.1039/D0FO02670K

Zelová, H., and Hošek, J. (2013). TNF-α signalling and inflammation: Interactions between old acquaintances. *Inflamm. Res.* 62, 641–651. doi: 10.1007/s00011-013-0633-0

Zhang, B., Yue, J., Guo, Y., Liu, T., Zhou, M., Yang, Y., et al. (2020). Effects of bioporous carriers on the performance and microbial community structure in side-stream anaerobic membrane bioreactors. *Can. J. Microbiol.* 66, 475–489. doi: 10.1139/cjm-2019-0632

Zhang, H., Elolimy, A. A., Akbar, H., Thanh, L. P., Yang, Z., and Loor, J. J. (2022). Association of residual feed intake with peripartal ruminal microbiome and milk fatty acid composition during early lactation in Holstein dairy cows. *J. Dairy Sci.* 105, 4971–4986. doi: 10.3168/jds.2021-21454

Zhang, X., Yi, X., Zhuang, H., Deng, Z., and Ma, C. (2022). Invited review: Antimicrobial use and antimicrobial resistance in pathogens associated with Diarrhea and Pneumonia in Dairy Calves. *Animals* 12:771. doi: 10.3390/ani12060771

frontiers | Frontiers in Microbiology

TYPE Original Research
PUBLISHED 31 October 2022
DOI 10.3389/fmicb.2022.964847



OPEN ACCESS

EDITED BY
Tang Zhaoxin,
South China Agricultural University, China

REVIEWED BY
José Antonio Moreno Muñoz, Laboratorios Ordesa, Spain
Minyi Huang,
Hunan University of Humannities, Science and Technology, China

*CORRESPONDENCE
Zhoujin Tan
tanzhjin@sohucom
Rong Yu
yuron@21cn.com

SPECIALTY SECTION
This article was submitted to Microorganisms in Vertebrate Digestive Systems, a section of the journal Frontiers in Microbiology

RECEIVED 09 June 2022
ACCEPTED 26 August 2022
PUBLISHED 31 October 2022

CITATION
Wu Y, Peng X, Li X, Li D, Tan Z and Yu R (2022) Sex hormones influence the intestinal microbiota composition in mice. *Front. Microbiol.* 13:964847. doi: 10.3389/fmicb.2022.964847



# Sex hormones influence the intestinal microbiota composition in mice

Yi Wu[1,2], Xinxin Peng[3], Xiaoya Li[1,2], Dandan Li[1,2], Zhoujin Tan[1,2]* and Rong Yu[1,2]*

[1]College of Chinese Medicine, Hunan University of Chinese Medicine, Changsha, China, [2]Hunan Key Laboratory of Chinese Medicine Prescription and Syndromes Translational Medicine, Changsha, China, [3]Department of Pediatrics, The First Affiliated Hospital of Hunan University of Chinese Medicine, Changsha, China

Sex hormone secretion difference is one of the main reasons for sexually dimorphic traits in animals, which affects the dimorphism of the intestinal microbiota; however, their interaction is still unknown. Intestinal mucosa-associated microbiota (MAM) and intestinal luminal content microbiota (LM) belong to two different habitats according to the difference in interactions between bacteria and host intestinal epithelium/nutrients. To clarify the sexually dimorphic characteristics of MAM and LM and their correlation with sex hormones, 12 specific pathogen-free (SPF) Kunming mice from the same nest were fed separately according to sex. After 8 weeks, samples from the male intestinal mucosa group (MM group), the female intestinal mucosa group (FM group), the male intestinal content group (MC group), and the female intestinal content group (FC group) were collected and then, the next-generation sequencing of 16S ribosomal ribonucleic acid (rRNA) gene was performed. Our results showed that the sexual dimorphism of MAM was more obvious than that of LM and the relative abundance of *Muribaculaceae*, *Turicibacter*, and *Parasutterella* was significantly higher in the FM group than in the MM group ($p < 0.001$, $p < 0.05$, $p < 0.05$). Next, we measured the level of serum sex hormones in mice and calculated the correlation coefficient between major bacteria and sex hormones. The results showed that the correlation between MAM and sex hormones was more prominent, and finally, three bacterial genera (*Muribaculaceae*, *Turicibacter*, and *Parasutterella*) were obtained, which could better represent the relationship between sexual dimorphism and sex hormones. The abundance of *Parasutterella* is positively and negatively correlated with estradiol and testosterone (T), respectively, which may be related to the differences in the metabolism of bile acid and glucose. A decrease in the abundance of *Turicibacter* is closely related to autism. Our results show that the abundance of *Turicibacter* is negatively and positively correlated with T and estradiol, respectively, which can provide a hint for the prevalence of male autism. In conclusion, it is proposed in our study that intestinal microbiota is probably the biological basis of physiological and pathological differences due to sex, and intestinal MAM can better represent the sexual dimorphism of mice.

KEYWORDS

**intestinal mucosa-associated microbiota, intestinal luminal content microbiota, sex hormones, sex dimorphism traits, gender-associated diseases**

# Introduction

Significant differences in mammalian health and disease exist between males and females, that is, sexual dimorphism (Britannica, 2022). For example, in most mammalian species, males are slightly larger than females (Naqvi et al., 2019), and differences in longevity and aging processes have been observed between males and females (Sampathkumar et al., 2020). Sexually dimorphic traits are also evident in the incidence, epidemic, and mortality of diseases, such as autoimmune disorders and autism (Alshammari, 2021; Manuel and Liang, 2021). In recent years, gut microbiota has become a hotspot for various studies. Coincidentally, these studies found sex differences in gut microbiota composition between humans and rodents (Ding and Schloss, 2014; Falony et al., 2016; Borgo et al., 2018; Sinha et al., 2019). It has also been suggested that sex hormones play an important role in building and maintaining the characteristics of the gut microbiome associated with sex (Zhang X. et al., 2021).

Sexual dimorphism is controlled by sex hormones, which have a bidirectional interaction with the intestinal microbiota. On the one hand, sex hormones affect the intestinal microbiota by regulating the permeability and integrity of an intestinal barrier and adjusting sex hormone receptors, β-glucuronidase, bile acid, intestinal immunity, etc. (Braniste et al., 2009; Looijer-van Langen et al., 2011; Li and Chiang, 2015; Laffont et al., 2017; Pellock and Redinbo, 2017; Miranda-Ribera et al., 2019; Barroso et al., 2020). On the other hand, the intestinal microbiota also influences the secretion of sex hormones, for example, androgen. Testosterone (T) and ovaries are the major production sources of male and female androgen, respectively, and the intestinal microbiota is the major regulator of androgen metabolism in the intestinal tract (Pernigoni et al., 2021). Some bacterial strains have been shown to metabolize androgen *in vitro*. For example, *Aggregatibacter actinomycetecomitans* and *Porphyromonas gingivalis* convert T to dihydrotestosterone (Bélanger et al., 1989). Pathologically, abnormal fluctuations in androgen contribute to the development and progression of diseases by affecting the intestinal microbiota (Yurkovetskiy et al., 2013; Moreno-Indias et al., 2016). Female rats with pathological androgen levels were found to have different intestinal microbiota from normal rats. Studies showed that abnormal androgen levels can lead to intestinal dysbacteria, including enzymes involved in androgen metabolism, which further interfere with androgen metabolism, and are associated with diseases such as polycystic ovary syndrome (Lindheim et al., 2017; Liu et al., 2017; Torres et al., 2018; Zeng et al., 2018), type 1 diabetes (Markle et al., 2013; Yurkovetskiy et al., 2013), and obesity (Kelly and Jones, 2015; Harada et al., 2016). Therefore, intestinal microbiota dimorphism is also a part of sexual dimorphism, in which sex hormones play a crucial role.

In recent years, sufficient animal experiments and clinical trials have confirmed differences in composition and function between luminal content microbiota (LM) and mucosa-associated microbiota (MAM) (Van den Abbeele et al., 2011; Yang et al., 2020). MAM is believed to interact directly or indirectly with the host intestinal epithelium and is therefore critical to the formation of the host immune system. LM is mainly involved in the digestion of nutrients and does not interact directly with the intestinal mucosa. Therefore, the composition and function of MAM is closely related to the host and its immune system, while LM is closely related to nutrients (Van den Abbeele et al., 2011). Due to this difference, LM and MAM have different roles in the initiation and progression of diseases. MAM played the most important role in the pathogenesis of diarrhea-predominant irritable bowel syndrome (IBS-D) (Maharshak et al., 2018), MAM is highly susceptible to disruption in patients with diarrhea because it participates in neurological responses (Zhang C. et al., 2021). Functional MAM and LM differ from each other (He et al., 2019; Wu et al., 2020). According to Francesca Borgo, microbial diversity in these two niches might be influenced by host factors such as body mass index (BMI), diet, and sex. Thus, in our study, we controlled all variables except sex and focused on the effects of sex and sex hormones on intestinal microbiota diversity (Borgo et al., 2018).

In summary, we attempted to clarify the following questions: (i) Are host sex hormones involved in intestinal microbiota diversity? (ii) Is there a difference in the impact of host sex on MAM and LM diversity? (iii) Could the intestinal microbiota be one of the biological bases of sex-associated diseases?

# Materials and methods

## Materials

### Animals and feeding

A total of 12 specific pathogen-free (SPF) Kunming mice (3 weeks of age, half male, half female) were purchased from Hunan Slike Jingda Laboratory Animal Co., Ltd. and fed in a regulated barrier system with light and dark cycles of 12 h, 23–25°C, and 50–70% relative humidity. After 1 week of adaptive feeding, animals were divided into male and female groups and fed for 8 weeks. Mice were fed by the Animal Experiment Center of Hunan University of Chinese Medicine with nutritional standards in line with GB/14924.3 and sanitation standards in line with GB/T149.24.2 to support their growth and reproduction. All animal experiments were licensed by the Animal Experiment of Hunan University of Chinese Medicine (Changsha, China), and the protocol was approved by the Animal Ethics Committee of Hunan University of Chinese Medicine [Facility use permit number: SYXK (Xiang) 2019-0009].

# Methods

## Serum sex steroid-level testing

Post experiment, all mice were sacrificed by sampling orbital blood after fasting for 12 h; then, small intestinal contents and mucosa were collected according to the method established by our research group (Wu et al., 2021). Four serum sex hormones (estradiol, T, prolactin, and progesterone) were detected using chemiluminescence immunoassay. The operating instrument was the Abbott AXSYM automatic chemiluminescence instrument equipped with matching reagents. The nuclear medicine department of the First Affiliated Hospital of the Hunan University of Chinese Medicine is responsible for the detection. In the female group, intestinal contents were labeled as FC 1, FC 2, FC 3, FC 4, FC 5, and FC 6 and the intestinal mucosa was labeled as FM 1, FM 2, FM 3, FM 4, FM 5, and FM 6. In the male group, intestinal contents were labeled as MC 1, MC 2, MC 3, MC 4, MC 5, and MC 6 and the intestinal mucosa was labeled as MM 1, MM 2, MM 3, MM 4, MM 5, and MM 6. All samples were stored at −80°C for the high-throughput sequencing of the 16S ribosomal ribonucleic acid (rRNA) gene.

## Extraction and polymerase chain reaction amplification of total DNA

The total microbial genomic deoxyribonucleic acid (DNA) from each sample was extracted as per the directives of the DNA extraction kit (MN NucleoSpin 96 So), and the steps were included as follows. The sample was precipitated to remove impurities and filtered to remove inhibitors, followed by DNA binding, membrane washing, drying, and elution. Quantity and mass of the extracted DNA were detected using NanoDrop ND-2000 ultramicro spectrophotometer (Thermo Fisher Scientific, Waltham, MA, USA) and Qubit 3.0 Fluorometer (Life Technologies, CA, USA), *via* agarose gel electrophoresis, respectively. All samples were processed by Beijing Biomac Biotechnology Co., Ltd. (Beijing, China).

## Bridge polymerase chain reaction and 16S rRNA gene sequencing

Flow cells are the channels for adsorption of flowing DNA fragments. Adapter-added DNA fragments on a chip containing adapters are bound to flow cells and bridge-amplified. The primers, 338F5'-ACTCCTACGGGAGGCAGCA-3' and 806R5'-GGACTACHVGGGTWTCTAAT-3', were designed according to the conservative region of 16S r DNA V3-V4. The amplification reaction system was as follows: 50 ng of gene DNA, 0.3 μl of Vn F, 0.3 μl of Vn R, 5 μl of KOD FX Neo Buffer, 2 μl of deoxynucleoside triphosphate (dNTP), 0.25 μl of KOD FX Neo, and finally a total reaction volume to 10 μl of double pure water ($ddH_2O$). Polymerase chain reaction (PCR) reaction conditions were given as follows: DNA was rapidly denatured at 95°C for 30 s and rapidly cooled to 50°C for 30 s, and the primers were annealed and bound to the target sequence and rapidly heated to 72°C for 40 s. After the last cycle, the primer strands were extended along the template for 7 min and were maintained at 4°C.

Library preparation and 16S rRNA gene sequencing were performed using the Solexa Genome Analyzer platform. When a complementary chain extends into a lateral column cluster family, each inserted dNTP can release corresponding fluorescence, which is immediately detected by a sequencer and then converted into fragment sequence information. Next-generation sequencing features a bridge polymerase chain reaction along with 16S rRNA gene sequencing. The basic principle is DNA polymerase and fluorescently labeled dNTPs and adapter primers in the amplification reaction system when a complementary chain extends into a lateral column cluster family.

## Data processing

The raw sequencing data are processed with quality filtering, double-ended sequence splicing, and chimera elimination. The reads of each sample are spliced using the USEARCH (version 10) (Edgar Robert, 2013) with a minimum overlap length of 10 bp and a maximum mismatch ratio in the overlap area of 0.2 (Default), and the resulting splicing sequence is the Raw Tags. After quality inspection, tags with a length of less than 75% are filtered to get Clean Tags using the Trimmomatic program. To extract the final tag sequence, the chimera was eliminated using UCHIME (version 8.1) (Bokulich et al., 2013).

# Bioinformatics analysis and statistical methods

Sequences were clustered using USEARCH (version 10.0) (Edgar Robert, 2013) with a similarity criterion of 97% and the default OTU filtering threshold of 0.005% of all sequences. OTU (operational taxonomic units) were then aligned in the Silva database, and the species were annotated using the blast method. The α and β diversities were demonstrated by Chao 1, Shannon, ACE, Simpson index, non-metric multi-dimensional scaling (NMDS) analysis, and analysis of similarities (ANOSIM). The abundance of microbiota at all levels is calculated based on the OTU and is presented in a histogram. The random forest algorithm is an integrated algorithm that integrates multiple decision trees and can avoid the problem of overfitting a single decision tree. The Gini index calculates the influence of each variable on the observed heterogeneity at each node of the classification tree, and larger values indicate that the variables are more important. Our study uses line discriminant analysis effect size (LEfSe) and random forest algorithm analysis at the same time to find the biomarker for different groups. To further analyze the correlation between the intestinal microbiota and sex hormones, we calculated Spearman's rank correlation coefficient

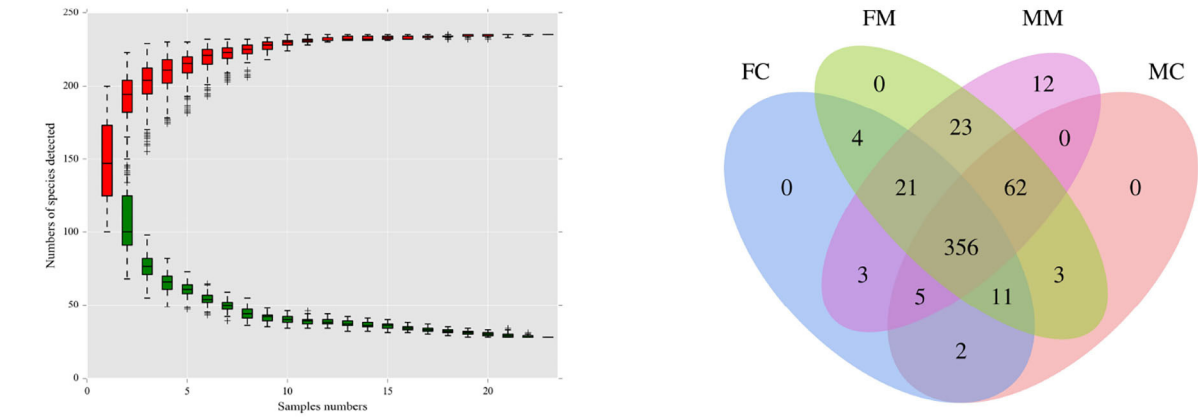


FIGURE 1
**(A)** The species accumulation curve was used to evaluate whether the sequencing volume was sufficient to cover all taxa and reflects the species richness of the intestinal microbiota. **(B)** Venn diagram of each group based on the number of OTUs. FC, luminal content of female mice; FM, mucosa of female mice; MM, mucosa of male mice; MC, luminal content of male mice.

and plotted the heatmap. Compared to PICRUSt 1, PICRUSt 2 (Douglas et al., 2020) has the advantages of richer genomic information, more realistic prediction settings, and more rigorous functional prediction methods. The abovementioned analysis was performed using BMKCloud (www.biocloud.net).

Scatter and linear correlation plots (Pearson correlation method) were drawn using Graph pad Prism 9.0. Statistical data were analyzed using SPSS 24.0 software (IBM, Almonk, NY, USA). The independent sample *t*-test was used when the two groups of data were in agreement with the normal distribution. Otherwise, the nonparametric test (the Mann–Whitney *U* test) was used. The test criterion was a $p$-value $< 0.05$ or a $p$-value $< 0.01$.

# Results

## DNA sequence and the number of OTUs

As shown in Figure 1A, when the number of species approaches 230, the curve flattens, indicating that the number of species meets the analysis criteria. As shown in Figure 1B, the four groups had 356 shared OTUs; the MC and FC groups found 65 and 28 unique OTUs, respectively. MM and MC groups had 20 and 18 unique OTUs, respectively.

## Bacterial diversity analysis

α and β diversities explain the richness and diversity of microbial communities from different dimensions. α diversity refers to the richness and diversity of microbial communities and species within a living territory, expressed in four indicators: Chao 1, Shannon, ACE, and Simpson. As shown in Figure 2, there are no significant sex differences between LM and MM in the Chao 1, Shannon, ACE, and Simpson indices.

β diversity refers to the difference in the number and distribution of species in different environmental communities, reflecting not only the diversity distance between samples but also the degree of differentiation between bacterial communities. As shown in the NMDS analysis (Figure 3A), there was a small distance between the FM and MM groups (stress = 0.1365). The ANOSIM analysis (Figures 3B–D) showed significant differences between the FC and MC groups and the FM and MM groups ($p < 0.01$). The phylogenetic tree combined with a histogram of species distribution (Figure 3E) intuitively indicates subtle differences among groups, with the MC group being distinguishable from others.

## Bacterial composition analysis of intestinal microbiota

To further investigate the differences in the intestinal microbiota of mice of different sexes, the relative abundance of microbial communities at the phylum and genus level in each group was counted. The combined abundance of Firmicutes, Bacteroidetes, Proteobacteria, and Actinobacteria exceeded 98% in LM (Figure 4A). The relative abundance of Firmicutes was higher in males than in females ($p < 0.05$, Figure 4B), while in the case of Bacteroidetes the opposite was true ($p$

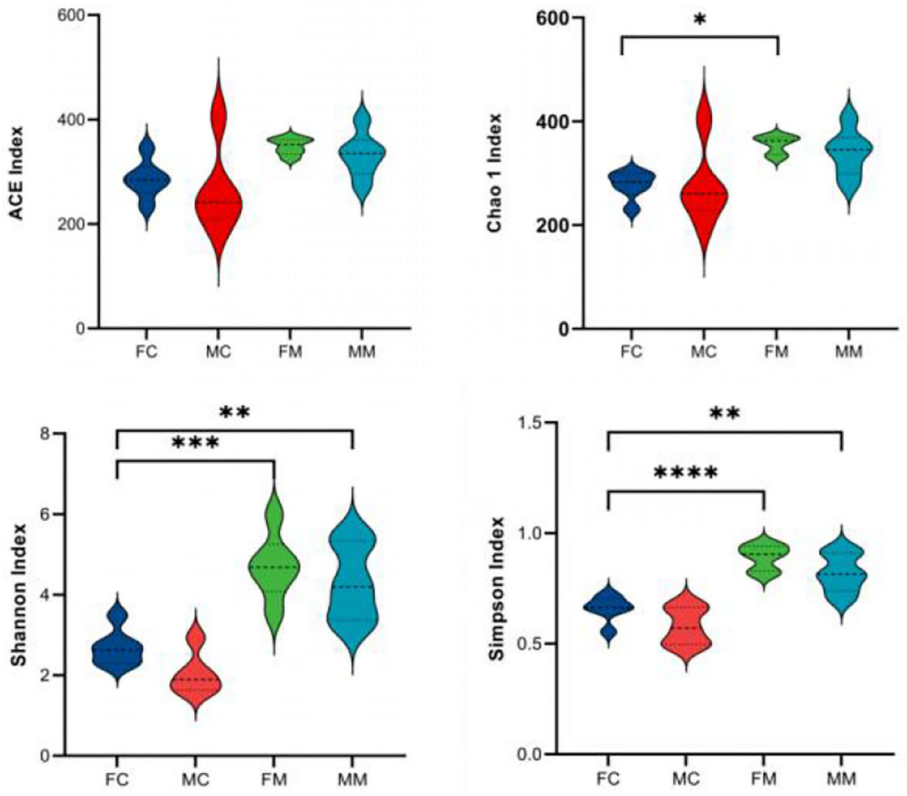


FIGURE 2
The α diversity index was calculated based on the OTU classification level, consisting of ACE, Chao 1, Shannon, and Simpson. *$p < 0.05$, **$p < 0.01$, ***$p < 0.001$, ****$p < 0.0001$.

$< 0.05$, Figure 4B). The four phyla were also dominated in MAM, and the relative abundance of Bacteroidetes was also higher in females than in males ($p < 0.05$, Figure 4B). The Firmicutes/Bacteroidetes (F/B) ratio of MAM and LM was higher in males than in females ($p < 0.05$, $p < 0.05$, Figure 4C).

Figure 5 shows the relative abundance of each group of bacterial species at the genus level. The results showed that *Lactobacillus*, *Muribaculaceae*, *Candidatus Arthromitus*, *Bifidobacterium*, and *Desulfovibrio* were enriched, of which *Lactobacillus* had the highest relative abundance. The relative abundance of *Muribaculaceae*, *Turicibacter*, and *Faecalibaculum* was significantly higher in the FC group than in the MC group ($p < 0.01$, $p < 0.05$, $p < 0.05$). A total of seven of the top 30 relative abundance had a significant sex difference in MAM. Specifically, the relative abundance of *Muribaculaceae*, *Turicibacter*, and *Parasutterella* was significantly higher in the FM group than in the MM group ($p < 0.001$, $p < 0.05$, $p < 0.05$), while the relative abundance of *Bifidobacterium*, *Gammaproteobacteria*, *Enterococcus*, and *Streptococcus* was significantly higher in the MM group ($p < 0.05$) than in the FM group. Overall, sex differences were more prominent in MAM than LM.

## Intestinal differential bacterial species analysis in each group

To further identify the species with the greatest differences in each group, we performed the LESef analysis (SCORE > 4, $p < 0.05$). The results (Figure 6A) showed that *Bifidobacterium longum* subsp. was a differential bacterium in the MC group, *Prevotella*, *Muribaculacea*, and *Bacteroidales* were the differential bacteria in the FC group. As shown in Figure 6B, *Lactobacillus* was a differential bacterium in the MM group and *Muribaculaceae*, *Erysipelotrichaceae*, *Turicibacter*, and *Anaerococcus* were the differential bacteria in the FM group.

The random forest algorithm analysis showed that *Parasutterella*, *Turicibacter*, and *Muribaculaceae* had the highest Gini index in the MAM group (Figure 7A), and *Muribaculaceae* and *Pleomorphomonadaceae* had the highest in the LM group (Figure 7B). In summary, *Parasutterella*, *Muribaculaceae*, and *Turicibacter* were the differential species identified in the FM and MM groups, and *Muribaculaceae* was the differential species identified in the FC and MC groups, which further

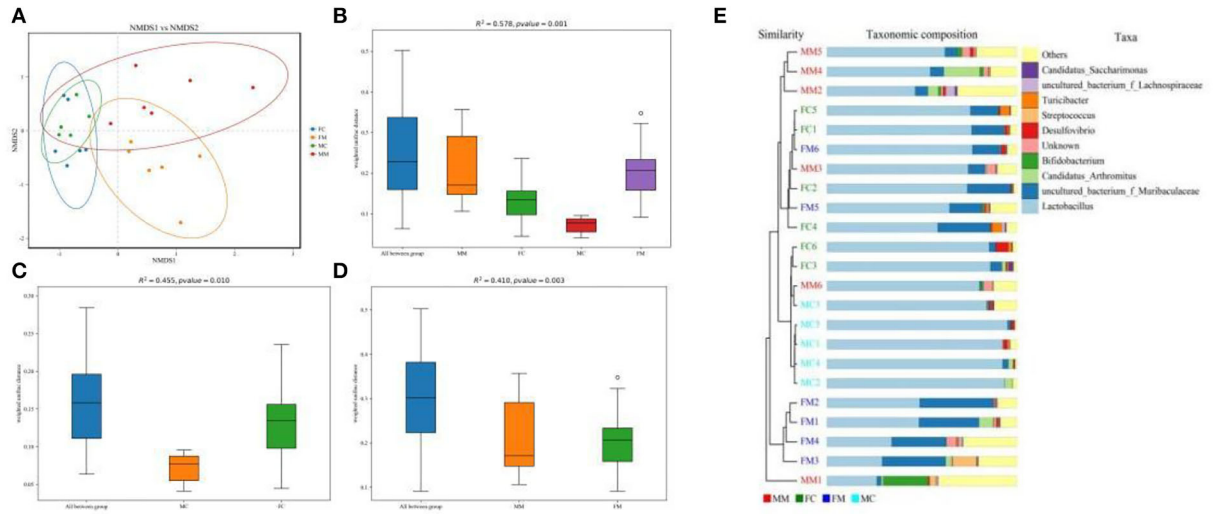


FIGURE 3
**(A)** Non-metric multidimensional scaling (NMDS) analysis (based on weighted UniFrac distance). Different groups of samples were colored differently. Distance between the dots presented a difference. NMDS with stress levels of less than 0.2 is acceptable. The closer the sample is to the coordinates, the higher the similarity. **(B–D)** Analysis of similarities (ANOSIM) (based on weighted UniFrac distance) can test for a significant difference in β-diversity among samples of different groups. The y-axis represents β-distance; the box above "All between *" represents the β-distance data of samples of all groups, while the box above "All within *" represents the β-distance data of samples within all groups. The closer the *R*-value is to 1, the difference between groups is higher than the difference within groups; the smaller the *R*-value is, the smaller difference between groups; and the value of $p < 0.05$ indicates high reliability of the test. **(E)** Combination of the phylogenetic tree and histogram based on the unweighted group average clustering method.

confirmed that the sexual dimorphism of MAM was greater than that of LM.

## Correlation analysis of serum sex steroid hormones and the intestinal microbiota

To confirm whether the serum levels of sex hormones were related to the sexual dimorphism of the intestinal microbiota, we detected four serum sex hormone levels and found (Table 1) significant differences in serum levels of estradiol (E2) and T of male and female mice ($p < 0.01$). It could be seen in Figures 8A–C that, in MAM, *Parasutterella*, *Muribaculaceae*, *Enterorhabdus*, and E2 were significantly positively correlated ($p < 0.05$), especially since *Muribaculaceae* and *Parasutterella* had extremely significant differences ($R > 0.073$, $p < 0.01$; $R > 0.089$, $p < 0.001$). Moreover, *Brachybacterium*, *Bacteroides*, *Gammaproteobacteria*, *Brevibacterium*, and *Haemophilus* were positively correlated with T ($p < 0.05$), while *Candidatus Saccharimonas*, *Parasutterella*, and *Muribaculaceae* were negatively correlated with T ($p < 0.05$). In LM (Figures 8B,D), *Faecalibaculum*, *Turicibacter*, *Parasutterella*, *Muribaculaceae*, and *Lachnospiraceae* were positively correlated with E2 ($p < 0.05$), while *Lactobacillus* showed the opposite ($R < -0.84$, $p \leq 0.001$) and *Turicibacter* was negatively correlated with T ($R = -0.79$, $p < 0.05$).

## Functional prediction of MAM in mice of different sexes

To further explore whether the sexual dimorphism of MAM affects the potential function, we performed a functional prediction analysis of each group. As showed in Table 2 , the glycosphingolipid biosynthesis—globo and isoglobo series is the only metabolic pathway with significant sex differences in MAM ($p < 0.05$).

# Discussion

## Differences in the characteristics of the intestinal microbiota in mice of different sexes

One of the important conclusions of this study is that MAM is more sex-sensitive than LM. As reported in the study, sex has a major influence on MAM (Borgo et al., 2018) than on LM, which is further confirmed in our experiment. First of all, β analysis showed sex differences only in the MAM.Secondly, among the top 30 bacteria with relative abundance at the genus level, the number of bacteria with sex differences in LM was 5, while the number of bacteria with sex differences in MAM was 7. Moreover, seven bacterial genera were associated with E2 secretion and only one with T secretion in LM, and four

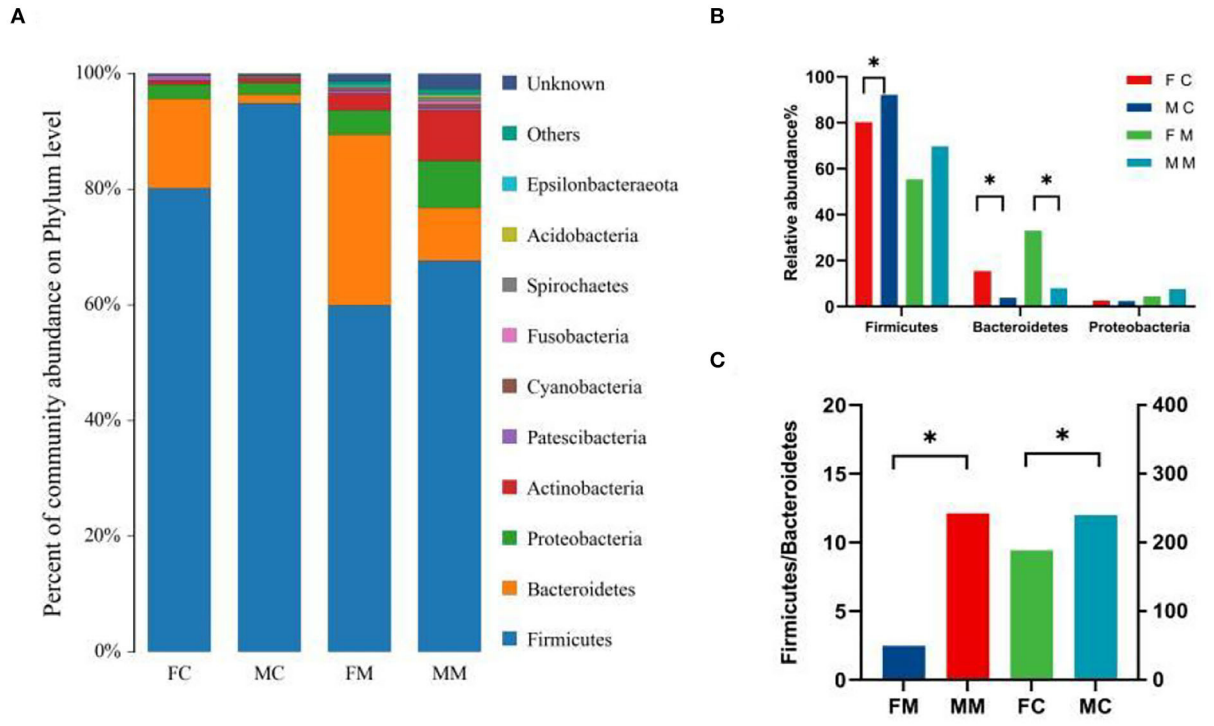


FIGURE 4
**(A)** The composition and relative abundance of species at the phylum level of each group, **(B)** the abundance of Bacteroidetes, Firmicutes, and Proteobacteria in each group (*$p < 0.05$), and **(C)** the Firmicutes/Bacteroidetes (F/B) ratio for each group.

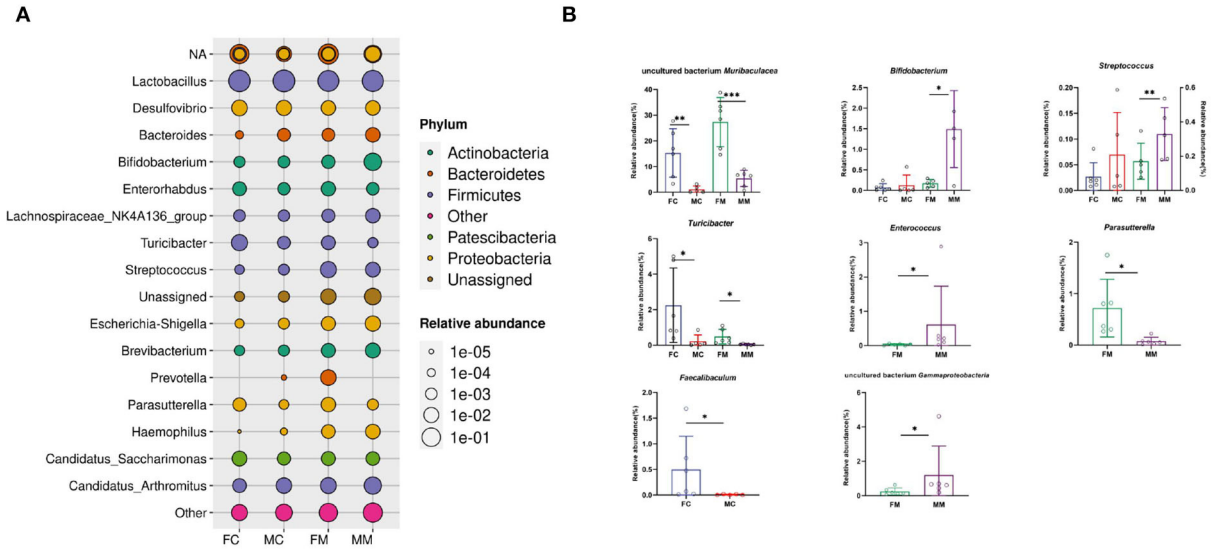


FIGURE 5
**(A)** The bacterial species and relative abundance of each group at the genus level, **(B)** illustration of sex differences in the relative abundance of the top 30 major genera (*$p < 0.05$, **$p < 0.01$, ***$p < 0.01$).

bacterial genera were associated with E2 secretion and nine with T secretion in MAM. In both physiology and pathology, MAM seems to be more susceptible to the host than to LM, which is attributed to the fact that MAM is less affected by food rather than LM. Zhang C. et al. (2021) proved that MAM is more susceptible to repeated stress-related diarrhea in comparison

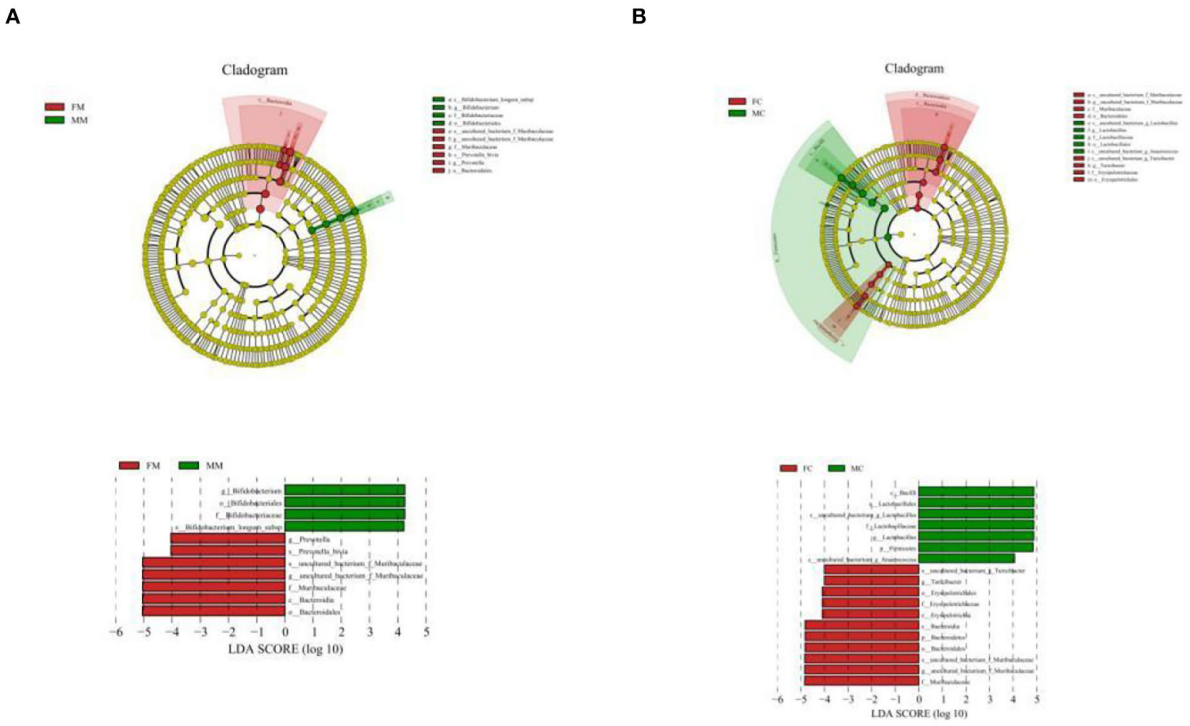


FIGURE 6
Cladogram based on the line discriminant analysis effect size (LEfSe) analysis and linear discriminant analysis (LDA) value distribution histogram of MAM **(A)** and LM **(B)**. In this figure, species with no significant differences are colored in yellow, and other colors stand for different groups. The LDA histogram showed the species whose LDA score is higher than the set value (the default is 4.0). The length of the histogram represents the impact of different species (i.e., LDA score), and different colors represent species in different groups. Different colors represent species in different groups, and nodes with different colors represent microbial groups that play an important role in the group represented by the color.

to LM. We conclude that MAM is more influenced by sex hormones, which can better represent sexual dimorphism. In further research, it is best to consider whether MAM is more suitable for the experiment. Unlike other studies, we did not find that the α diversity of female mice was higher than that of male mice, which was probably due to the different locations from which the samples were collected (Roager et al., 2016).

## The intestinal microbiota of mice with different sexes provides a new perspective on sexually dimorphic diseases

Our study found that the intestinal microbiota may be one of the important biological bases of sexual dimorphism in physiology and pathology. LEfSe and random forest algorithm analyses showed that *Muribaculaceae* and *Parasutterella* were the key genera to distinguish mice with different sexes. The relative abundance analysis of the intestinal microbiota revealed the highest concentration of *Muribaculaceae*, *Parasutterella*, and *Turicibacter* in the intestine of female mice. The correlation analysis of serum sex hormones with the intestinal microbiota illustrated that, in LM, both *Muribaculaceae* and *Parasutterella* were positively and negatively correlated with E2 and T, respectively, and *Turicibacter* was negatively correlated with T. All results demonstrate that *Muribaculaceae*, *Parasutterella*, and *Turicibacter* are the key species of intestinal sexual dimorphism.

*Parasutterella* may be involved in intestinal bile acid metabolism as the core intestinal microbiota of mice and humans (Ju et al., 2019). Bile acid synthesis rate and bile acid pool have been shown to be higher in females than in males (Turley et al., 1998). Related studies (Org et al., 2016) showed that bile acid metabolism changes significantly with hormonal changes, especially in high-fat and high-sugar diets. In our study, females of *Parasutterella* were highly abundant than male parasites, further suggesting that sex differences in bile acid metabolism might be related to intestinal *Parasutterella*. In addition, we found a positive correlation between the abundance of *Parasutterella* and E2, suggesting that sex hormones influenced bile acid metabolism in females by regulating the abundance of *Parasutterella*. Type 2 diabetes is a glucose metabolism disorder with significant sexual

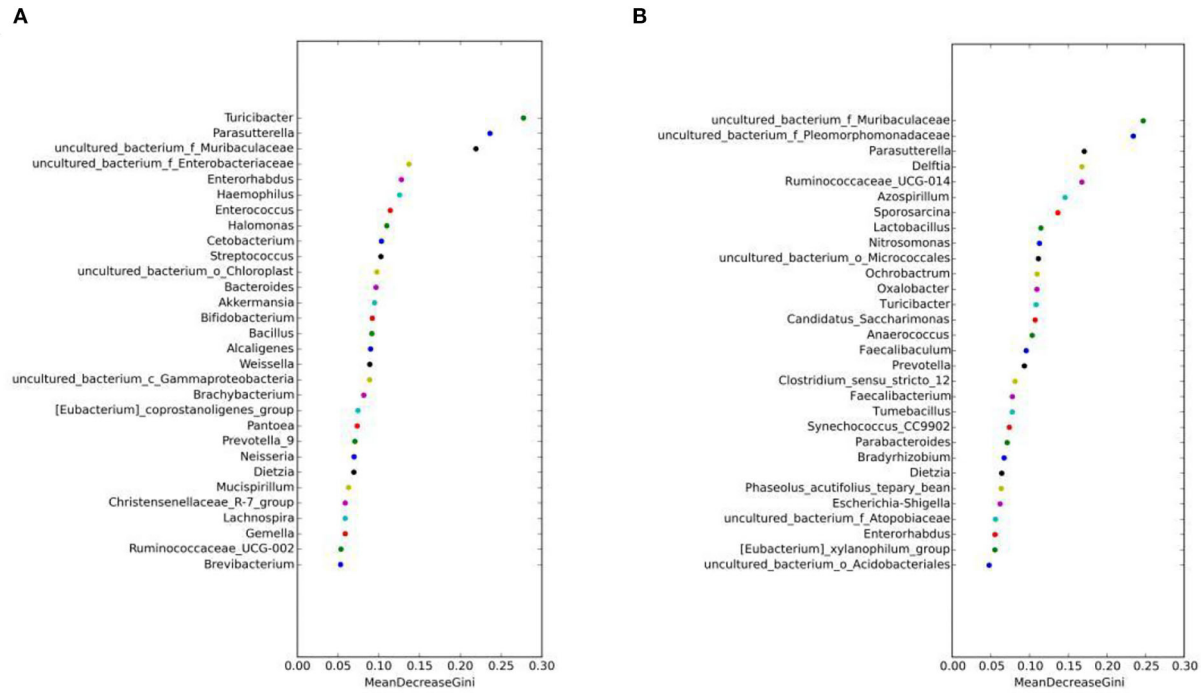


FIGURE 7
Random forest algorithm analysis of MAM **(A)** and intestinal LM **(B)**. The horizontal axis is the mean decrease Gini, and the vertical axis is the top 30 genera with the highest relative abundance. The larger the mean decrease Gini, the higher the contribution of bacteria.

TABLE 1 Differences in serum sex steroid levels in mice ($\bar{X} \pm S$, $n = 6$).

| Sex steroid | E2 (Pg/mL) | Test (nmol/L) | Prolactin (ng/mL) | Progesterone (ng/mL) |
|---|---|---|---|---|
| Female | 29.33 ± 3.27 | 1.46 ± 0.72 | 234.83 ± 15.89 | 33.35 ± 11.13 |
| Male | 22.67 ± 2.88 | 9.62 ± 7.51 | 225.00 ± 15.30 | 22.14 ± 8.80 |
| *P* value | 0.004 | 0.004 | 0.326 | 0.093 |

dimorphism; however, there is no clear mechanism to explain how this sex difference occurs. In animal studies, researchers proved that male mice have lower glucose tolerance compared to females, which is associated with intestinal microbiota and sex hormones (Gao et al., 2021). *Parasutterella* is a producer of succinate, which improves glucose homeostasis through intestinal gluconeogenesis (De Vadder et al., 2016; Canfora et al., 2019). Therefore, we hypothesize that sex hormones may be involved in the sexual dimorphism of glucose metabolism by regulating the abundance of *Parasutterella*.

Muribaculaceae is the dominant family in the intestine of mice. Studies showed that Muribaculaceae degrades dietary carbohydrates and rapidly adapts to carbohydrate-enriched diets to resist obesity (Obanda et al., 2018; Lagkouvardos et al., 2019). In our study, the abundance of *Bacteroides* and *Muribaculaceae* is significantly higher in females than in males and is positively and negatively correlated with E2 level and T, respectively. In addition, we found that the ratio of F/B (Jasirwan et al., 2021) used to evaluate the energy metabolism capacity was lower in female mice than in male mice (Figure 4C), which indicated that female mice had higher energy metabolism ability than male mice. As mentioned above, how sex hormones successfully and synthetically regulate the body's energy balance with *Muribaculaceae*, which will help to shed light on the formation mechanism of obesity and its prevalence in specific populations, is shown.

*Turicibacter* belonging to Firmicutes is involved in the metabolism of bile acids and cholesterol (Kemis et al., 2019). According to studies, *Turicibacter* may also be related to obesity, its abundance is positively correlated with high-density lipoproteins, and it may be involved in the formation mechanism of obesity by regulating cholesterol metabolism (Zheng et al., 2020). *Turicibacter* is therefore another important bacterium that reveals the biological basis of sex differences

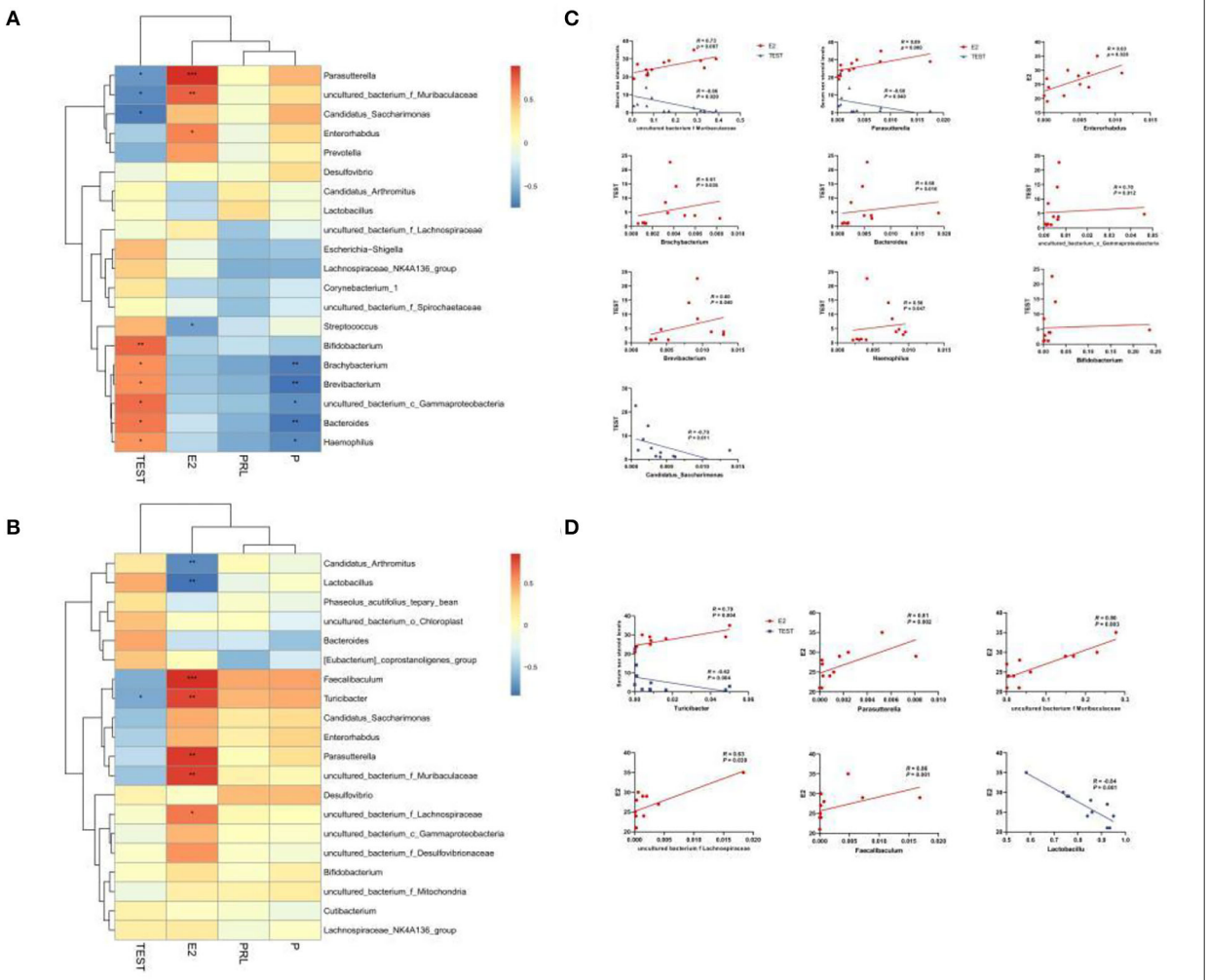


FIGURE 8
Heatmap of MAM **(A)** and LM **(B)** correlations with sex steroid levels. In the heat map, red represents a positive correlation, and blue represents a negative correlation; the closer to red, the closer the *R*-value is to 1; the closer to blue, the closer the *R*-value is to −1. In the linear correlation diagram of MAM **(C)** and LM **(D)**, the closer the *R*-value is to 1, the more obvious the correlation. $*p < 0.05$, $**p < 0.01$, $***p < 0.001$.

in obesity between males and females. There is a sex bias in mental disorders, which the sex-selective sex hormone theory seeks to uncover (Singh et al., 2021). Similarly, many studies demonstrated that the intestinal microbiota participates in the development of mental diseases through the brain-gut axis (Sharon et al., 2019; Qin et al., 2022). An interesting phenomenon is that males are more likely to exhibit the aggravation of autism symptoms with changes in their intestinal microbiota in times of adversity, but these have a limited impact on females (Rincel et al., 2019). In addition, the intestinal microbiota of male mice with autism showed a decrease in *Turicibacter*, and the lower the abundance of *Turicibacter*, the greater the social deficit (Szyszkowicz et al., 2017); however, the abundance of *Turicibacter* was reversed after intake of *Lactobacillus* (Kong et al., 2021). In our study, we further found that male mice had a significantly lower abundance of *Turicibacter* than female mice and were correlated with T. These results suggest that the development of autism in males may be related to congenital hormone levels and the intestinal microbiota, of which *Turicibacter* is worth exploring.

The abundance of *Bifidobacterium*, *Gammaproteobacteria*, and *Enterococcus* was significantly higher in the MM group than in the FM group and positively correlated with T, indicating that *Bifidobacterium*, *Gammaproteobacteria*, and *Enterococcus* were significantly regulated by sex hormones. Studies showed a marked increase in serum androgens and a lack of intestinal probiotics like *Bifidobacterium* in polycystic ovarian syndrome, but taking *Bifidobacterium* can reverse this trend. Unfortunately, the current experiment lacks evidence related to MAM (Zhang et al., 2019). The incidence of Crohn's disease is slightly higher in males than in females, but males had a milder disease severity than females. Studies confirm that this may be related to estrogen

TABLE 2 Functional prediction table of Kyoto Encyclopedia of Genes and Genomes (KEGG) level 3 of mucosa-associated microbiota (MAM).

| Level 1 | Level 2 | Level 3 | *P* value (adjusted) |
|---|---|---|---|
| Metabolism | Lipid metabolism | Linoleic acid metabolism | 0.614 |
| | | Sphingolipid metabolism | 0.116 |
| | | Steroid hormone biosynthesis | 0.293 |
| | | Biosynthesis of unsaturated fatty acids | 0.584 |
| | Glycan biosynthesis and metabolism | Glycosphingolipid biosynthesis - ganglio series | 0.532 |
| | | Glycosphingolipid biosynthesis - globo and isoglobo series | 0.022 |
| | | Glycosaminoglycan degradation | 0.474 |
| | | Other glycan degradation | 0.468 |
| | Amino acid metabolism | Cyanoamino acid metabolism | 0.302 |
| | | Selenocompound metabolism | 0.514 |
| | Metabolism of other amino acids | Alanine, aspartate and glutamate metabolism | 0.527 |
| | Energy metabolism | Photosynthesis - antenna proteins | 0.613 |
| Human diseases | Infectious diseases: Bacterial | Vibrio cholerae infection | 0.458 |
| Genetic information processing | Folding, sorting and degradation | Protein processing in endoplasmic reticulum | 0.604 |
| Environmental information processing | Membrane transport | ABC transporters | 0.088 |
| | | Bacterial secretion system | 0.609 |
| | Transport and catabolism | Lysosome | 0.465 |
| Cellular processes | Cell growth and death | Apoptosis | 0.628 |
| | Cellular community - prokaryotes | Quorum sensing | 0.547 |

(Goodman et al., 2020). Studies showed that proteus plays a key role in the development of Crohn's disease by attacking the intestinal mucosa (Zhang J. et al., 2021). Other research also showed that *Gammaproteobacteria* are enriched within $CD14^{+}$ macrophages from the intestinal lamina propria of patients with Crohn's disease vs. mucus (Sekido et al., 2020). However, in our research, *Proteus* has little correlation with estrogen, and its abundance is higher in the MM group than in the FM group. *Enterococcus* is a physiologically dominant species in the intestine of mice and humans, with strong tolerance and the ability to colonize the intestinal mucosa and inhibit pathogen damage to intestinal mucosal epithelial cells (O' Shea et al., 2012). So far, however, no link between *Enterococcus* and sex or sex hormones has been reported.

## Conclusion

Our study concluded that MAM is more sexually dimorphic than LM. We identified that various bacteria were prone to a certain sex and were highly correlated with E2 and T levels. *Parasutterella*, *Muribaculacea,* and *Turicibacter* are considered the best representatives of the intestinal microbiota associated with sex hormones. In addition, our study further found that *Parasutterella*, *Muribaculacea*, and *Turicibacter* are the key bacteria that cause intestinal sexual dimorphism. It is speculated that sex hormones may be involved in sexual dimorphism in bile acid metabolism by regulating the abundance of these bacteria. The dimorphism of *Turicibacter* in the intestinal microbiota also provides insight into how neurological diseases are more common in males than in females. Furthermore, our study also found that the glycosphingolipid metabolism of MAM had significant sex differences, which provided new clues for the mechanisms underlying sex differences in glucose metabolism.

However, our study only compared the differences in the intestinal microbiota in physiological mice and lacked experiments or data analysis for specific sex-associated diseases. Future studies should be based on open databases or more animal experiments to provide some reference for accurate clinical use.

## Data availability statement

The datasets presented in this study can be found in online repositories. The names of the repository/repositories and accession number(s) can be found below: NCBI, PRJNA847180.

## Ethics statement

The animal study was reviewed and approved by Animal Ethics Committee of Hunan University of Chinese

Medicine. The number of the facility use permit: SYXK (Xiang) 2019-0009.

## Author contributions

YW: animal experiments, data analysis, and original draft writing. XP and XL: validation, review, and editing. DL: data analysis. ZT and RY: project administration and funding acquisition. All authors contributed to this article and approved the submitted version.

## Funding

This research was financially supported by the National Natural Science Foundation of China (Grant No. 81874460), the National Natural Science Foundation of China Regional Innovation and Development Joint Fund Key Support Project (Grant No. U21A20411), and the Provincial Natural Science Foundation of Hunan (Grant No. 2022JJ30440).

## Conflict of interest

The authors declare that the research was conducted in the absence of any commercial or financial relationships that could be construed as a potential conflict of interest.

## Publisher's note

All claims expressed in this article are solely those of the authors and do not necessarily represent those of their affiliated organizations, or those of the publisher, the editors and the reviewers. Any product that may be evaluated in this article, or claim that may be made by its manufacturer, is not guaranteed or endorsed by the publisher.

## Supplementary material

The Supplementary Material for this article can be found online at: https://www.frontiersin.org/articles/10.3389/fmicb.2022.964847/full#supplementary-material

## References

Alshammari, T. K. (2021). Sexual dimorphism in pre-clinical studies of depression. *Prog. Neuropsychopharmacol. Biol. Psychiatry* 105, 110120. doi: 10.1016/j.pnpbp.2020.110120

Barroso, A., Santos-Marcos, J. A., Perdices-Lopez, C., Vega-Rojas, A., Sanchez-Garrido, M. A., Krylova, Y., et al. (2020). Neonatal exposure to androgens dynamically alters gut microbiota architecture. *J. Endocrinol.* 247, 69–85. doi: 10.1530/JOE-20-0277

Bélanger, B., Bélanger, A., Labrie, F., Dupont, A., Cusan, L., and Monfette, G. (1989). Comparison of residual C-19 steroids in plasma and prostatic tissue of human, rat and guinea pig after castration: unique importance of extratesticular androgens in men. *J. Steroid. Biochem.* 5, 695–698. doi: 10.1016/0022-4731(89)90514-1

Bokulich, N. A., Subramanian, S., Faith, J. J., Gevers, D., Gordon, J. I., Knight, R., et al. (2013). Quality-filtering vastly improves diversity estimates from Illumina amplicon sequencing. *Nat. Method* 10, 57–59. doi: 10.1038/nmeth.2276

Borgo, F., Garbossa, S., Riva, A., Severgnini, M., Luigiano, C., Benetti, A., et al. (2018). Body Mass index and sex affect diverse microbial niches within the gut. *Front. Microbiol.* 9, 213. doi: 10.3389/fmicb.2018.00213

Braniste, V., Leveque, M., Buisson-Brenac, C., Bueno, L., Fioramonti, J., and Houdeau, E. (2009). Oestradiol decreases colonic permeability through oestrogen receptor beta-mediated up-regulation of occludin and junctional adhesion molecule-A in epithelial cells. *J. Physiol.* 587, 3317–3328. doi: 10.1113/jphysiol.2009.169300

Britannica, The Editors of Encyclopaedia. (2022). "sexual dimorphism". Encyclopedia Britannica, 14 Feb. 2020, Available online at: https://www.britannica.com/science/sexual-dimorphism (accessed 6 June 2022).

Canfora, E. E., Meex, R. C. R., Venema, K., and Blaak, E. E. (2019). Gut microbial metabolites in obesity, NAFLD and T2DM. *Nat. Rev. Endocrinol.* 15, 261–273. doi: 10.1038/s41574-019-0156-z

De Vadder, F., Kovatcheva-Datchary, P., Zitoun, C., Duchampt, A., Bäckhed, F., and Mithieux, G. (2016). Microbiota-produced succinate improves glucose homeostasis via intestinal gluconeogenesis. *Cell Metab.* 24, 151–157. doi: 10.1016/j.cmet.2016.06.013

Ding, T., and Schloss, P. D. (2014). Dynamics and associations of microbial community types across the human body. *Nature* 509, 357–360. doi: 10.1038/nature13178

Douglas, G. M., Maffei, V. J., Zaneveld, J. R., Yurgel, S. N., Brown, J. R., Taylor, C. M., et al. (2020). PICRUSt2 for prediction of metagenome functions. *Nat. Biotechnol.* 38, 685–688. doi: 10.1038/s41587-020-0548-6

Edgar Robert, C. (2013). UPARSE: highly accurate OTU sequences from microbial amplicon reads. *Nat. Method* 10, 996–998. doi: 10.1038/nmeth.2604

Falony, G., Joossens, M., Vieira-Silva, S., Wang, J., Darzi, Y., Faust, K., et al. (2016). Population-level analysis of gut microbiome variation. *Science* 352, 560–564. doi: 10.1126/science.aad3503

Gao, A., Su, J., Liu, R., Zhao, S., Li, W., Xu, X., et al. (2021). Sexual dimorphism in glucose metabolism is shaped by the androgen-driven gut microbiome. *Nat. Commun.* 12, 7080. doi: 10.1038/s41467-021-27187-7

Goodman, W. A., Erkkila, I. P., and Pizarro, T. T. (2020). Sex matters: impact on pathogenesis, presentation and treatment of inflammatory bowel disease. *Nat. Rev. Gastroenterol. Hepatol.* 17, 740–754. doi: 10.1038/s41575-020-0354-0

Harada, N., Hanaoka, R., Horiuchi, H., Kitakaze, T., Mitani, T., Inui, H., et al. (2016). Castration influences intestinal microflora and induces abdominal obesity in high-fat diet-fed mice. *Sci. Rep.* 6, 23001. doi: 10.1038/srep23001

He, Y., Tang, Y., Peng, M., Xie, G., Li, W., and Tan, Z. (2019). Influence of Debaryomyces hansenii on bacterial lactase gene diversity in intestinal mucosa of mice with antibiotic-associated diarrhea. *PLoS ONE* 14, e022580. doi: 10.1371/journal.pone.0225802

Jasirwan, C. O. M., Muradi, A., Hasan, I., Simadibrata, M., and Rinaldi, I. (2021). Correlation of gut Firmicutes/Bacteroidetes ratio with fibrosis and steatosis stratified by body mass index in patients with non-alcoholic fatty liver disease. *Biosci. Microbiota. Food Health* 40, 50–58. doi: 10.12938/bmfh.2020-046

Ju, T., Kong, J. Y., Stothard, P., and Willing, B. P. (2019). Defining the role of Parasutterella, a previously uncharacterized member of the core gut microbiota. *ISME J.* 13, 1520–1534. doi: 10.1038/s41396-019-0364-5

Kelly, D. M., and Jones, T. H. (2015). Testosterone and obesity. *Obes. Rev.* 16, 581–606. doi: 10.1111/obr.12282

Kemis, J. H., Linke, V., Barrett, K. L., Boehm, F. J., Traeger, L. L., Keller, M. P., et al. (2019). Genetic determinants of gut microbiota composition and bile acid profiles in mice. *PLoS Genet.* 15, e1008073. doi: 10.1371/journal.pgen.1008073

Kong, Q., Wang, B., Tian, P., Li, X., Zhao, J., Zhang, H., et al. (2021). Daily intake of Lactobacillus alleviates autistic-like behaviors by ameliorating the

5-hydroxytryptamine metabolic disorder in VPA-treated rats during weaning and sexual maturation. *Food Funct.* 12, 2591–2604. doi: 10.1039/D0FO02375B

Laffont, S., Seillet, C., and Guéry, J. C. (2017). Estrogen receptor-dependent regulation of dendritic cell development and function. *Front. Immunol.* 10, 108. doi: 10.3389/fimmu.2017.00108

Lagkouvardos, I., Lesker, T. R., Hitch, T. C. A., Gálvez, E. J. C., Smit, N., Neuhaus, K., et al. (2019). Sequence and cultivation study of Muribaculaceae reveals novel species, host preference, and functional potential of this yet undescribed family. *Microbiome.* 7:28. doi: 10.1186/s40168-019-0637-2

Li, T., and Chiang, J. Y. (2015). Bile acids as metabolic regulators. *Curr. Opin. Gastroenterol.* 31, 159–165. doi: 10.1097/MOG.0000000000000156

Lindheim, L., Bashir, M., Münzker, J., Trummer, C., Zachhuber, V., Leber, B., et al. (2017). Alterations in gut microbiome composition and barrier function are associated with reproductive and metabolic defects in women with polycystic ovary syndrome (PCOS): a pilot study. *PLoS ONE* 12, e0168390. doi: 10.1371/journal.pone.0168390

Liu, R., Zhang, C., Shi, Y., Zhang, F., Li, L., Wang, X., et al. (2017). Dysbiosis of gut microbiota associated with clinical parameters in polycystic ovary syndrome. *Front. Microbiol.* 8, 324. doi: 10.3389/fmicb.2017.00324

Looijer-van Langen, M., Hotte, N., Dieleman, L. A., Albert, E., Mulder, C., and Madsen, K. L. (2011). Estrogen receptor-β signaling modulates epithelial barrier function. *Am. J. Physiol. Gastrointest. Liver Physiol.* 300, 621–626. doi: 10.1152/ajpgi.00274.2010

Maharshak, N., Ringel, Y., Katibian, D., Lundqvist, A., Sartor, R. B., Carroll, I. M., et al. (2018). Fecal and mucosa-associated intestinal microbiota in patients with diarrhea-predominant irritable bowel syndrome. *Dig. Dis. Sci.* 63, 1890–1899. doi: 10.1007/s10620-018-5086-4

Manuel, R. S. J., and Liang, Y. (2021). Sexual dimorphism in immunometabolism and autoimmunity: Impact on personalized medicine. *Autoimmun. Rev.* 20, 102775. doi: 10.1016/j.autrev.2021.102775

Markle, J. G., Frank, D. N., Mortin-Toth, S., Robertson, C. E., Feazel, L. M., Rolle-Kampczyk, U., et al. (2013). Sex differences in the gut microbiome drive hormone-dependent regulation of autoimmunity. *Science* 339, 1084–1088. doi: 10.1126/science.1233521

Miranda-Ribera, A., Ennamorati, M., Serena, G., Cetinbas, M., Lan, J., Sadreyev, R. I., et al. (2019). Exploiting the zonulin mouse model to establish the role of primary impaired gut barrier function on microbiota composition and immune profiles. *Front. Immunol.* 10, 2233. doi: 10.3389/fimmu.2019.02233

Moreno-Indias, I., Sánchez-Alcoholado, L., Sánchez-Garrido, M. Á., Martín-Núñez, G. M., Pérez-Jiménez, F., Tena-Sempere, M., et al. (2016). Neonatal androgen exposure causes persistent gut microbiota dysbiosis related to metabolic disease in adult female rats. *Endocrinology* 157, 4888–4898. doi: 10.1210/en.2016-1317

Naqvi, S., Godfrey, A. K., Hughes, J. F., Goodheart, M. L., Mitchell, R. N., and Page, D. C. (2019). Conservation, acquisition, and functional impact of sex-biased gene expression in mammals. *Science.* 365, eaaw7317. doi: 10.1126/science.aaw7317

O' Shea, E. F., Cotter, P. D., Ross, R. P., and Hill, C. (2012). Strategies to improve the bacteriocin protection provided by lactic acid bacteria. *Curr. Opin. Biotechnol.* 24, 130–134. doi: 10.1016/j.copbio.2012.12.003

Obanda, D., Page, R., Guice, J., Raggio, A. M., Husseneder, C., Marx, B., et al. (2018). CD obesity-prone rats, but not obesity-resistant rats, robustly ferment resistant starch without increased weight or fat accretion. *Obesity* 26, 570–577. doi: 10.1002/oby.22120

Org, E., Mehrabian, M., Parks, B. W., Shipkova, P., Liu, X., Drake, T. A., et al. (2016). Sex differences and hormonal effects on gut microbiota composition in mice. *Gut. Microbes.* 7, 313–322. doi: 10.1080/19490976.2016.1203502

Pellock, S. J., and Redinbo, M. R. (2017). Glucuronides in the gut: Sugar-driven symbioses between microbe and host. *J. Biol. Chem.* 292, 8569–8576. doi: 10.1074/jbc.R116.767434

Pernigoni, N., Zagato, E., Calcinotto, A., Troiani, M., Mestre, R. P., Cal,ì B., et al. (2021). Commensal bacteria promote endocrine resistance in prostate cancer through androgen biosynthesis. *Science* 374, 216–224. doi: 10.1126/science.abf8403

Qin, Y., Havulinna, A. S., Liu, Y., Jousilahti, P., Ritchie, S. C., Tokolyi, A., et al. (2022). Combined effects of host genetics and diet on human gut microbiota and incident disease in a single population cohort. *Nat. Genet.* 54, 134–142. doi: 10.1038/s41588-021-00991-z

Rincel, M., Aubert, P., Chevalier, J., Grohard, P. A., Basso, L., Monchaux de Oliveira, C., et al. (2019). Multi-hit early life adversity affects gut microbiota, brain and behavior in a sex-dependent manner. *Brain Behav. Immun.* 80, 179–192. doi: 10.1016/j.bbi.2019.03.006

Roager, H. M., Hansen, L. B., Bahl, M. I., Frandsen, H. L., Carvalho, V., Gøbel, R. J., et al. (2016). Colonic transit time is related to bacterial metabolism and mucosal turnover in the gut. *Nat. Microbiol.* 1, 16093. doi: 10.1038/nmicrobiol.2016.93

Sampathkumar, N. K., Bravo, J. I., Chen, Y., Danthi, P. S., Donahue, E. K., Lai, R. W., et al. (2020). Widespread sex dimorphism in aging and age-related diseases. *Hum. Genet.* 139, 333–356. doi: 10.1007/s00439-019-02082-w

Sekido, Y., Nishimura, J., Nakano, K., Osu, T., Chow, C. T., Matsuno, H., et al. (2020). Some Gammaproteobacteria are enriched within CD14+ macrophages from intestinal lamina propria of Crohn's disease patients versus mucus. *Sci. Rep.* 10, 2988. doi: 10.1038/s41598-020-59937-w

Sharon, G., Cruz, N. J., Kang, D. W., Gandal, M. J., Wang, B., Kim, Y. M., et al. (2019). Human gut microbiota from autism spectrum disorder promote behavioral symptoms in mice. *Cell* 177, 1600–1618.e17. doi: 10.1016/j.cell.2019.05.004

Singh, R. S., Singh, K. K., and Singh, S. M. (2021). Origin of sex-biased mental disorders: an evolutionary perspective. *J. Mol. Evol.* 89, 195–213. doi: 10.1007/s00239-021-09999-9

Sinha, T., Vich Vila, A., Garmaeva, S., Jankipersadsing, S. A., Imhann, F., Collij, V., et al. (2019). Analysis of 1135 gut metagenomes identifies sex-specific resistome profiles. *Gut. Microbes* 10, 358–366. doi: 10.1080/19490976.2018.1528822

Szyszkowicz, J. K., Wong, A., Anisman, H., Merali, Z., and Audet, M. C. (2017). Implications of the gut microbiota in vulnerability to the social avoidance effects of chronic social defeat in male mice. *Brain Behav. Immun.* 66, 45–55. doi: 10.1016/j.bbi.2017.06.009

Torres, P. J., Siakowska, M., Banaszewska, B., Pawelczyk, L., Duleba, A. J., Kelley, S. T., et al. (2018). Gut microbial diversity in women with polycystic ovary syndrome correlates with hyperandrogenism. *J. Clin. Endocrinol. Metab.* 103, 1502–1511. doi: 10.1210/jc.2017-02153

Turley, S. D., Schwarz, M., Spady, D. K., and Dietschy, J. M. (1998). Gender-related differences in bile acid and sterol metabolism in outbred CD-1 mice fed low- and high-cholesterol diets. *Hepatology* 28, 1088–1094. doi: 10.1002/hep.510280425

Van den Abbeele, P., Van de Wiele, T., Verstraete, W., and Possemiers, S. (2011). The host selects mucosal and luminal associations of coevolved gut microorganisms: a novel concept. *FEMS Microbiol. Rev.* 35, 681–704. doi: 10.1111/j.1574-6976.2011.00270.x

Wu, Y., Tang, Y., Xiao, N., Wang, C., and Tan, Z. (2020). Bacterial lactase gene characteristics in intestinal contents of antibiotic-associated diarrhea mice treated with Debaryomyces hansenii. *Med. Sci. Monitor* 26, e920879. doi: 10.12659/MSM.920879

Wu, Y., Zhang, C., Shao, H., Luo, H., and Tan, Z. (2021). Characteristics of intestinal microbiota and enzyme activities in mice fed with lily bulb. *Biotech.* 3, 17. doi: 10.1007/s13205-020-02597-4

Yang, M., Hong, G., Jin, Y., Li, Y., Li, G., and Hou, X. (2020). Mucosal-associated microbiota other than luminal microbiota has a close relationship with diarrhea-predominant irritable bowel syndrome. *Front. Cell Infect. Microbiol.* 10, 515614. doi: 10.3389/fcimb.2020.515614

Yurkovetskiy, L., Burrows, M., Khan, A. A., Graham, L., Volchkov, P., Becker, L., et al. (2013). Gender bias in autoimmunity is influenced by microbiota. *Immunity* 39, 400–412. doi: 10.1016/j.immuni.2013.08.013

Zeng, B., Lai, Z., Sun, L., Zhang, Z., Yang, J., Li, Z., et al. (2018). Structural and functional profiles of the gut microbial community in polycystic ovary syndrome with insulin resistance (IR-PCOS): a pilot study. *Res. Microbiol.* 170, 43–52. doi: 10.1016/j.resmic.2018.09.002

Zhang, C., Peng, X., Shao, H., Li, X., Wu, Y., and Tan, Z. (2021). Gut microbiota comparison between intestinal contents and mucosa in mice with repeated stress-related diarrhea provides novel insight. *Front. Microbiol.* 12, 626691. doi: 10.3389/fmicb.2021.626691

Zhang, J., Hoedt, E. C., Liu, Q., Berendsen, E., Teh, J. J., Hamilton, A., et al. (2021). Elucidation of proteus mirabilis as a key bacterium in crohn's disease inflammation. *Gastroenterology* 160, 317–330.e11. doi: 10.1053/j.gastro.2020.09.036

Zhang, J., Sun, Z., Jiang, S., Bai, X., Ma, C., Peng, Q., et al. (2019). Probiotic bifidobacterium lactis v9 regulates the secretion of sex hormones in polycystic ovary syndrome patients through the gut-brain axis. *mSystems* 4, e00017–19. doi: 10.1128/mSystems.00017-19

Zhang, X., Zhong, H., Li, Y., Shi, Z., Ren, H., Zhang, Z., et al. (2021). Sex-and age-related trajectories of the adult human gut microbiota shared across populations of different ethnicities. *Nat. Aging.* 1, 87–100. doi: 10.1038/s43587-020-00014-2

Zheng, B., Wang, T., Wang, H., Chen, L., and Zhou, Z. (2020). Studies on nutritional intervention of rice starch-oleic acid complex (resistant starch type V) in rats fed by high-fat diet. *Carbohydr. Polym.* 246, 116637. doi: 10.1016/j.carbpol.2020.116637

frontiers | Frontiers in Microbiology

TYPE Original Research
PUBLISHED 21 November 2022
DOI 10.3389/fmicb.2022.1024822



OPEN ACCESS

EDITED BY
Tang Zhaoxin,
South China Agricultural University, China

REVIEWED BY
Zhaolai Dai,
China Agricultural University, China
Huantian Cui,
Shandong University, China

*CORRESPONDENCE
Jianye Yuan
yuanjianye@hotmail.com

SPECIALTY SECTION
This article was submitted to Microorganisms in Vertebrate Digestive Systems, a section of the journal Frontiers in Microbiology

RECEIVED 22 August 2022
ACCEPTED 07 November 2022
PUBLISHED 21 November 2022

CITATION
Hang L, Wang E, Feng Y, Zhou Y, Meng Y, Jiang F and Yuan J (2022) Metagenomics and metabolomics analysis to investigate the effect of Shugan decoction on intestinal microbiota in irritable bowel syndrome rats.
*Front. Microbiol.* 13:1024822.
doi: 10.3389/fmicb.2022.1024822



# Metagenomics and metabolomics analysis to investigate the effect of Shugan decoction on intestinal microbiota in irritable bowel syndrome rats

Lu Hang, Enkang Wang, Ya Feng, Yan Zhou, Yangyang Meng, Fengru Jiang and Jianye Yuan*

Institute of Digestive Diseases, Longhua Hospital, Shanghai University of Traditional Chinese Medicine, Shanghai, China

**Background:** The effect of Shugan Decoction (SGD) on intestinal motility and visceral hypersensitivity in Water avoid stress (WAS)-induced diarrhea predominant irritable bowel syndrome (IBS-D) model rats has been confirmed. However, the mechanisms of its action involved in the treatment of IBS-D need to be further studied. Intestinal microbiota plays an important role in maintaining intestinal homeostasis and normal physiological function. Changes in the intestinal microbiota and its metabolites are thought to participate in the pathophysiological process of IBS.

**Aim:** This study aimed to analyze the influence of SGD on intestinal microbiota and fecal metabolites in IBS-D rats by multiple omics techniques, including metagenomic sequencing and metabolomics.

**Methods:** We measured the intestinal motility and visceral sensitivity of three groups of rats by fecal pellets output and colorectal distension (CRD) experiment. In addition, metagenome sequencing analysis was performed to explore the changes in the number and types of intestinal microbiota in IBS-D model rats after SGD treatment. Finally, we also used untargeted metabolomic sequencing to screen the metabolites and metabolic pathways closely related to the therapeutic effect of SGD.

**Results:** We found that compared with the rats in the control group, the fecal pellets output of the rats in the WAS group increased and the visceral sensitivity threshold was decreased ($P < 0.05$). Compared with the rats in the WAS group, the fecal pellets output of the SGD group was significantly decreased, and the visceral sensitivity threshold increased ($P < 0.05$). Besides, compared with the rats in the WAS group, the relative abundance of *Bacteroidetes* increased in SGD group, while that of *Firmicutes* decreased at the phylum level, and at the species level, the relative abundance

of *Bacteroides sp. CAG:714*, *Lactobacillus reuteri* and *Bacteroides Barnesiae* in SGD group increased, but that of *bacterium D42-87* decreased. In addition, compared with the WAS group, several metabolic pathways were significantly changed in SGD group, including Taurine and hypotaurine metabolism, Purine metabolism, Sulfur metabolism, ABC transporters, Arginine and proline metabolism and Bile secretion.

**Conclusion:** SGD can regulate specific intestinal microbiota and some metabolic pathways, which may explain its effect of alleviating visceral hypersensitivity and abnormal intestinal motility in WAS-induced IBS-D rats.

KEYWORDS

**Shugan decoction, IBS-D, intestinal microbiota, metabonomics, metagenomics**

# Introduction

Irritable bowel syndrome (IBS) is a functional bowel disorder manifested in abdominal pain, abdominal distention, changed bowel habits and fecal appearance (Botschuijver et al., 2017), and its symptoms tend to be persist and recurrent (Shariati et al., 2019). According to the latest Roman IV criteria, the global prevalence of this disorder is about 4.1% (Sperber et al., 2021). At present, IBS can be roughly divided into four types: diarrhea predominant IBS (IBS-D), constipation predominant IBS (IBS-C), mixed IBS (IBS-M) and unsubtyped IBS (IBS-U) (Ford et al., 2017). Notably, IBS-D is the most common subtype (Oka et al., 2020). Although IBS is not a fatal disease, it seriously affects the life, study and work of patients, and also causes a serious economic burden to the society (Sebastián Domingo, 2022). Therefore, how to effectively prevent and treat IBS is an important problem to be solved urgently.

So far, the pathogenesis of IBS is unclear. The known pathophysiological mechanisms of IBS mainly include gastrointestinal motility abnormalities, visceral hypersensitivity, intestinal barrier dysfunction, intestinal microbiota disorders, *etc*. In recent years, more and more studies have confirmed that visceral hypersensitivity and intestinal dysmotility caused by enteric dysbacteriosis are the important pathological basis of IBS (Pimentel and Lembo, 2020). 5-hydroxytryptamine (5-HT) mediation is one of the pathways by which intestinal microbiota play its role in gastrointestinal function and the disturbances or disorders of 5-HT signal can induce IBS-like symptoms (Mishima and Ishihara, 2021; Murciano-Brea et al., 2021).

Treating IBS with traditional Chinese medicine can not only effectively improve its clinical symptoms, but also has the advantages of low cost and relatively small toxic and side effects (Teschke et al., 2015). Traditional Chinese medicine compound Shugan decoction (SGD) is an empirical prescription based on the traditional Chinese medicine syndrome differentiation of IBS-D patients in modern society. The formula consists of *white Atractylodes macrocephala*, *paeony root*, *tangerine peel*, *parsnip* and *Bupleurum*. Early studies confirmed that SGD can improve abdominal pain, diarrhea, defecation changes and other single symptoms in patients with IBS-D of liver spleen disharmony type, and the total effective rate can reach 86.67% (Xie et al., 2004). Further research found that SGD was more effective than Dicetel in relieving flatulence, and had better safety and tolerance (Pan and Xie, 2006). The latest randomized controlled clinical trial shows that SGD can not only effectively improve symptoms such as diarrhea, abdominal distension and bowel ringing, but also effectively relieve patients' anxiety, depression and other mental states (Lu L. et al., 2020). Animal experiments showed that SGD could improve visceral hypersensitivity and gastrointestinal motility abnormalities in Water avoid stress (WAS)-induced IBS-D model rats by regulating 5-HT content and SERT expression in colon tissue (Shi et al., 2015; Lu et al., 2018). In recent years, it has been proved that SGD may regulate intestinal microbiota, thereby affecting intestinal 5-HT synthesis to improve symptoms such as abdominal pain and diarrhea (Shi et al., 2015).

In this study, metagenomic sequencing and untargeted metabolomics analysis were performed on rat feces to observe the effects of SGD treatment on intestinal microbiota and specific metabolic pathways in WAS-induced IBS model rats. On this basis, we aim to elucidate the role of SGD in IBS-D model rats on specific intestinal microbiota and the regulation of endogenous metabolites.

# Materials and methods

## Agents and materials

The components of SGD, i.e., *White attractylodes rhizome* (Baizhu) (Shang Hai De Hua GuoYao; Lot number:

2018061101), *white peony root* (Baishao) (Shang Hai Hua Pu Zhong Yao; Lot number: 2018042901), *dried old orange peel* (Chenpi) (Shang Hai Lei Yun Shang Zhong Yao; Lot number: 1805037), *ledebouriella root* (Fangfeng) (Shang Hai Yu Tian Cheng Zhong Yao; Lot number:2017022706), and *Radix bupleuri* (Chaihu) (Ma Chen Jiu Zhou; Lot number: E2018050101), were purchased as crude herbs from JinKe Pharmacy (Shanghai, China). Saikosaponin A (National Institute for Food and Drug Control; Lot number: 110777-201912), paeoniflorin (National Institute for Food and Drug Control; Lot number: 110736-201943), 5-O-Methylvisammioside (National Institute for Food and Drug Control; Lot number: 111523-201811), hesperidin (National Institute for Food and Drug Control; Lot number: 110721-201818), and cimicifugoside (National Institute for Food and Drug Control; Lot number: 111522-201913) were purchased from Shanghai Zhaorui Biological Technology Co. (Shanghai, China).

## Preparation of Shugan decoction extract

The quality ratios of White attractylodes rhizome (Baizhu), white peony root (Baishao), dried old orange peel (Chenpi), ledebouriella root (Fangfeng), and Radix bupleuri (Chaihu) are 6:4:3:4:6. SGD extract was prepared by decoction and water extraction in the Herbal Chemistry Lab in Shanghai University of TCM. The extraction process has been described previously (Wang Y. et al., 2020): herbal pieces were first soaked in distilled water for 30 min, then they were boiled in 6 times of water for 1 h. Next, the mixture was filtrated with 4 layers of gauze, and the filtrate was collected. The procedure was repeated twice, and the filtrate was freeze-dried to obtain the powder. The steps of freeze-drying are as follows: First, we freeze the drug into a solid state, and then sublimate and dry it to remove the ice crystals in the drug by sublimation. Next, we desorb and dry it to evaporate some of the water remaining in the product at a higher temperature, so that the residual water can meet the requirements. Finally, the dried products are sealed and packaged under vacuum or filled with inert gas for storage.

## Analysis and identification of Shugan decoction by high-performance liquid chromatography

According to the procedure described in our previous study (Wang Y. et al., 2020): Saikosaponin A, paeoniflorin, 5-*O*-Methylvisammioside, hesperidin, and cimicifugoside was dissolved in methanol and obtained 1 mg/mL standard solution separately. 500 mg SGD extract power was weighed and dissolved in distilled water. After ultrasonic shock for 40 min, the SGD solution was fixed at a constant volume of 10 mL. Then, 1 mL solution was injected into the activated $C_{18}$ column, eluted with 10 mL water, and then eluted with 10 mL methanol. The methanol eluent was collected, concentrated to dry, dissolved with 1 mL methanol, and 50.89 mg/mL SGD sample solution was obtained through 0.45 μm microporous membrane. The standard solution and the SGD sample solution were analyzed using the Dionex UltiMate$^{TM}$ 3000 RSLC nano system (Thermo Scientific, MA, USA) equipped with a Corona® ultra$^{TM}$CAD detector, Luna® C18 Column (Phenomenex, 250 mm × 4.6 mm, 5 mm), and a data station with analytical software (CHROMELEON®). Mobile phases consisted of A-Purified water and B-acetonitrile. Gradient was set as follows: 0 min, 5% B; 35 min 65.5% B; 35.001 min, 100% B; 40 min, 100% B. Column temperature was set at 25°C, DAD detection wavelength: 203, 254, 366 nm.

## Animals and treatments

Thirty male Sprague-Dawley (SD) rats, weighing 200g ± 20g, provided by Shanghai Bikai Experimental Animal Co., Ltd. [production license No.: SCXK (Shanghai) 2018-0006], raised in the Experimental Animal Center of Shanghai University of TCM under the standard temperature (21–24°C), humidity (50% ± 5%), light and dark cycle (12 h/12 h), and they had free access to standard rat chow and tap water. All the experiments in this study are in accordance with the regulations of the Animal Ethics Committee of Shanghai University of TCM (No. PZSHUTCM190906001). All the experiments were carried out between 8:00 and11:00 AM to minimize potential confounding effects of diurnal variations.

After a week of adaptive feeding, rats were randomly divided into 3 groups ($n$=10 in each group). SGD group: 10 days WAS and gavage with SGD (1.28 g/kg body weight, lyophilized powder dosage, once per day) since the 4th day; WAS group: 10 days WAS and gavage with the same dose of saline; Control group: gavage with the same dose of saline.

## Water avoidance stress

Refer to the method pioneered by Bradesi et al. and used in our previous studies (Bradesi et al., 2005), rats were placed on the platform (10 cm long, 8 cm wide, 8 cm high) which was fixed in the center of a organic glass pool (45 cm long, 25 cm wide, 25 cm high) filled with water (25°C) to suffer from WAS for 1 h every day in 10 consecutive days.

## Fecal pellets counting

As described before (Bradesi et al., 2006), fecal pellets output in the one hour of WAS were counted to assess colonic motility every day for 10 consecutive days.

## Colorectal distension

On the 10th day after WAS, the pressure threshold to induce abdominal withdrawal reflex (AWR) in rats was measured by colorectal distension (CRD) test. The methods were as previously described (Spence and Moss-Morris, 2007): a balloon (5 mm diameter and 1 cm long) with catheter (2 mm diameter) was inserted into the colorectum 1 cm above the anus. The catheter was fixed to the root of the rat tail with adhesive tape. Then the balloon was inflated gradually by one experimenter; the abdominal wall reactions of the rats were observed by another experimenter and a voice command was issued by him when the first AWR appeared; then the pressure value at this moment was recorded. Every two measurements were done with an interval of 3 min, and the average value was calculated after 3 times of measurement.

## Fecal sample collection

After SGD treatment and WAS, feces from the Control, WAS, and SGD groups were obtained under sterile conditions and stored at −80°C. The fecal samples were divided into two parts, one part was used to perform Metagenomics analysis, and another part was used for untargeted metabolomics analysis.

## Hematoxylin eosin staining

The colon tissues were fixed in 4% paraformaldehyde for 48 h after the luminal content was washed off with ice normal saline. Then the paraffin sections were made by dehydration, transparency, wax soaking, embedding and sectioning. Hematoxylin eosin (H&E) solution staining, neutral gum sealing, and observation under ordinary optical microscope (Nikon Corporation, Japan) were done in sequence.

## Metagenomics analysis

DNA was extracted from rat fecal samples, then microbial DNA was fragmented, metagenomic sequencing was performed based on Illumina NovaSeq high-throughput sequencing platform, Whole Genome Shotgun (WGS) strategy was adopted. The extracted metagenomic total DNA was randomly interrupted into short fragments and inserted fragment libraries of appropriate length were constructed. These libraries were paired with PE sequencing. FastQC was used to test data quality. MEGAHIT was used for metagenomic sequence splicing. Meta GeneMark[1] was used for gene prediction and the identification of Open Reading Frame (ORF), the corresponding gene prediction files and protein sequences were obtained. The non-redundant protein sequence set was compared with the common protein database to annotate and analyze the gene function in each sample. QIIME (Quantitative Insights Into Microbial Ecology) software was used to obtain the relative abundance distribution table of each sample corresponding to each functional level of each database. By using the software MEGAN,[2] each sample and taxonomy of species abundance information of data can map to NCBI Taxonomy provided by the microbial classification tree,[3] which can be in a standard classification system, uniformly present the specific composition of all samples at each classification level. Next, with the help of the "random forest" toolkit of R software, the random forest algorithm is used to select the functions/species with significant differences in abundance distribution among different groups. Specifically, in order to compare the diversity of different samples, the abundance spectrum of underlying functional groups or the composition spectrum of species level annotated in each functional database of all samples were firstly randomly resampled according to the lowest sequencing depth (i.e., "sequence volume leveling"), so as to correct the diversity differences caused by sequencing depth. Subsequently, QIIME software was used to calculate four diversity indices including Shannon index for each sample. On the basis of the above analysis, we conducted Beta diversity analysis on the abundance spectrum of functional annotation and the composition spectrum of species annotation respectively, so as to investigate the differences between samples at the two levels of bacterial flora function and species composition. Mainly through three methods: Principal Component analysis (PCA), Multidimensional Scaling analysis (MDS) and Clustering analysis, the metagenomic multi-dimensional data structure was decomposed naturally and the samples were ordinated to observe the differences between samples. R software and QIIME software were used to perform PCA analysis on the abundance spectrum or species level composition spectrum of the underlying functional groups annotated in each functional database of metagenomic samples, and 2D and 3D images were used to describe the natural distribution characteristics among samples. QIIME software was used to map the first two- or three-dimensional data obtained from PCoA analysis, so as to know the spatial distribution characteristics of community samples based on metagenomic functional abundance spectrum or species composition spectrum, and quantify the size of

1 http://exon.gatech.edu/GeneMark/
2 http://ab.inf.uni-tuebingen.de/software/megan5/
3 https://www.ncbi.nlm.nih.gov/taxonomy

differences between samples (groups). R software was used to perform NMDS analysis on the Bray-Curtis distance matrix obtained, and the structure distribution of community samples was described by two-dimensional ranking map. Using QIIME software, the Bray-Curtis distance matrix obtained was analyzed by UPGMA clustering and visualized by R software. According to the abundance spectrum or species-level composition spectrum of the underlying functional groups annotated in the functional database of each sample (group), R software was used to calculate the number of common taxa of each sample (group), and the number of common and unique functions/species of each sample (group) was visually presented by Venn diagram.

## Untargeted metabolomics analysis

The metabolites in feces were extracted and analyzed by UHPLC (Ultra high-performance liquid chromatography) platform of Shanghai Paiseno Technology Co., LTD. The specific steps of untargeted metabolomics mainly include: sample preparation, QC preparation, sample LC-MS/MS mass spectrometry, data analysis and experimental report, etc. In order to control the quality of this experiment, the researchers prepared QC samples at the same time, and QC samples were samples mixed with equal amounts of all samples. QC samples were used in the balanced chromatography-mass spectrometry system and the state of the instrument, and were used to evaluate the stability of the system throughout the experiment. After the liquid nitrogen was ground, 400 μl of pre-cooled methanol/acetonitrile/aqueous solution (4:4:2, V/V) was added to the sample, mixed by vortexing, stood at −20°C for 60 min, centrifuged at 14,000 *g* at 4°C for 20 min, and the supernatant was dried under vacuum. For mass spectrometry analysis, 100 μL acetonitrile aqueous solution (acetonitrile: Water = 1:1, v/v) were redissolved, vortexed, centrifuged at 14,000 *g* for 15 min at 4°C, and 2 μL of the supernatant was taken for sample analysis. The samples were separated on Agilent 1290 Infinity LC ultra-high performance liquid chromatography (UHPLC) HILIC column. The column temperature is 25°C; Flow rate 0.3 mL/min; Injection volume 2 μL; Mobile phase composition: A: water + 25 mM ammonium acetate + 25 mM ammonia, B: acetonitrile; The gradient elution procedure was as follows: 0–1 min, 95%b; 1–14 min, B changed linearly from 95 to 65%; 14–16 min, B changed linearly from 65 to 40%; 16–18 min, B maintained at 40%; 18–18.1 min, B changed linearly from 40 to 95%; 18.1– 23 min, B maintained at 95%; The samples were placed in an autosampler at 4°C during the whole analysis. Electrospray ionization (ESI) positive ion mode and negative ion mode were used for detection. The samples were separated by UHPLC and analyzed by mass spectrometry using a Triple TOF 6600 mass spectrometer (AB SCIEX). The ESI Source conditions after HILIC chromatographic separation were as follows: Ion Source Gas1 (Gas1): 60, Ion Source Gas2 (Gas2): 60, Curtain Gas (CUR): 30, Source temperature: 600°C, IonSapary Voltage Floating (ISVF) ± 5,500 V (both positive and negative modes); TOF MS Scan M/Z Range: 60–1,000 Da, Product ION Scan M/Z Range: 25–1,000 Da, TOF MS scan accumulation time is 0.20 s/spectra, Product ion scan accumulation time is 0.05 s/spectra; The secondary mass spectra were obtained using Information dependent acquisition (IDA) and their high sensitivity mode, Declustering potential (DP): *In situ*: ± 60 V (positive and negative modes), Collision Energy: 35 ± 15 eV, IDA non-frontiers within 4 Da, Candidate ions to monitor per cycle: 6. The final Data set was imported into SIMCA 16.0.2 software using an internal standard normalization method (Sartorius Stedim Data Analytics AB, Umea, Sweden; RRID:SCR_014688) was applied to principal component analysis (PCA) and orthogonal partial least squares discriminant analysis (OPLS-DA). One-dimensional statistical analysis including Student's *t*-test and multiple variation analysis, R software was used to draw the volcano map. VIP > 1 and *P* value < 0.05 in OPLS-DA model were used as screening criteria, and then cluster analysis and KEGG metabolic pathway analysis were performed on the differentially expressed metabolites.

## Statistical analysis

SPSS version 25.0 (SPSS, Chicago, IL, USA) and GraphPad Prism 9.0 (La Jolla, CA, USA) were used for data analysis. Each value was expressed as mean ± SE. If data were subject to normality and homogeneity of variance, one-way analysis of variance (One-way ANOVA) and followed LSD-t test was use for analyzing the differences among the groups. If disobedient, the rank-sum test was used. $P < 0.05$ was considered statistically significant.

# Results

## Effects of Shugan decoction on irritable bowel syndrome model rats

It was found that compared with control group, the amount of fecal pellets output of rats in WAS group was significantly increased. Compared with WAS group, the SGD group had reduced amount of fecal pellets output ($P < 0.05$, **Figure 1A**). In addition, we found that compared with control group, visceral sensitivity threshold of rats in WAS group was decreased. Compared with WAS group, visceral sensitivity threshold of rats increased in SGD group ($P < 0.001$, **Figure 1B**). No significant pathological changes were found in colonic mucosa in WAS and SGD groups, compared with control group (**Figure 1C**).

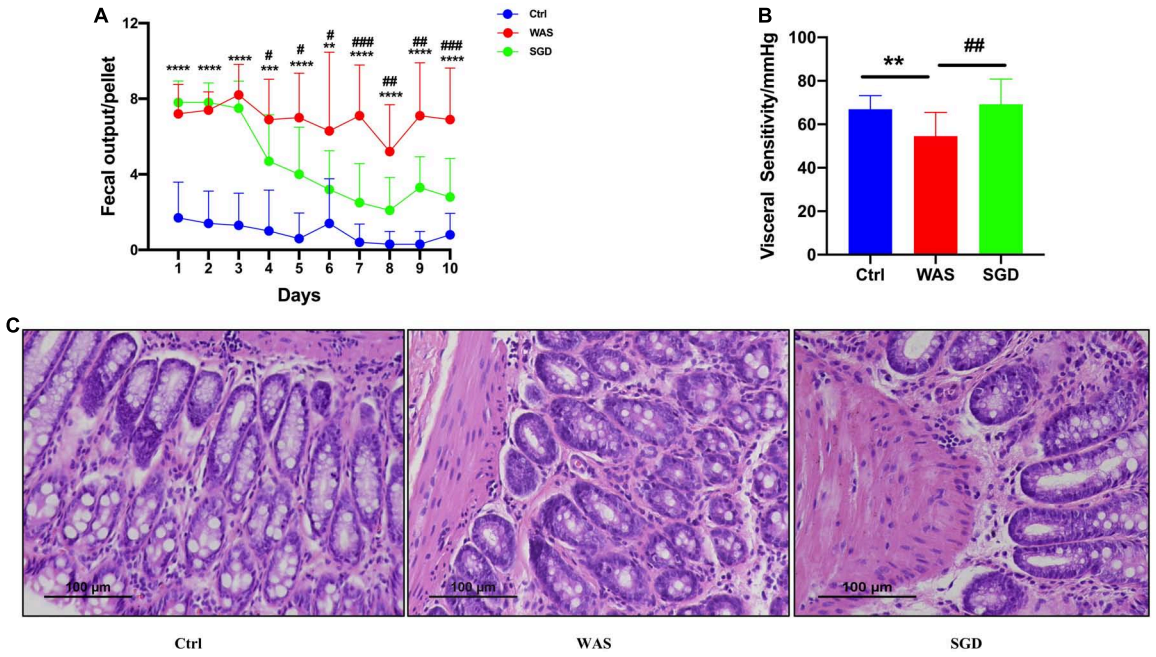


FIGURE 1
Effects of SGD on daily fecal pellets output, visceral sensitivity and colon histology in WAS-induced IBS-D model rats. **(A)** Daily fecal pellets output of rats. The daily fecal pellets output in the WAS group was higher than that in the control group, and SGD reduced daily fecal pellets output in the WAS group. **(B)** Visceral sensitivity in rats. The visceral sensitivity threshold of the WAS group was lower than that of the control group, and SGD improved the visceral sensitivity threshold of the rats in the WAS group. **(C)** Histology of the colon of the rats. H&E staining showed that there were no pathological changes in the colon tissues of rats in each group. Control group; WAS group; SGD + WAS group ($n$ = 10 per group). Data are presented as mean ± standard deviation (*$P < 0.05$, **$P < 0.01$, ***$P < 0.001$, ****$P < 0.0001$; $^{\#}P < 0.05$, $^{\#\#}P < 0.01$, $^{\#\#\#}P < 0.001$).

## Effects of Shugan decoction on intestinal microbiota of irritable bowel syndrome model rats

We used a sequencing platform to conduct metagenomic sequencing of rat fecal bacteria DNA, aiming to study the changes of intestinal microbiota species in IBS-D model rats before and after SGD treatment. The results showed that shannon index in WAS group was significantly higher than that in control and SGD group, while there is no significant difference among the three groups in Simpson index (Figure 2A). In addition, Venn diagram analysis indicated that the three groups shared 19,748 OTUs, with 857 OTUs peculiar to control group, 1,050 OTUs peculiar to WAS group and 1,166 OTUs peculiar to SGD group (Figure 2B). The results of principal coordinate analysis (PCA) and systematic clustering tree both manifested that the intestinal microbiota of the three groups were significantly different (Figures 2C,D).

Next, we studied the changes of intestinal microbiota and its abundance at phylum and species level in each group. Firstly, at the phylum level, 20 phyla could be found in each group (Figure 3A) and the most abundant phyla in each group were *Bacteroidetes* and *Firmicutes*. Compared with control group, the relative abundance of *Bacteroidetes* in WAS group decreased ($P < 0.05$, Figure 3B) and *Firmicutes* increased ($P < 0.05$, Figure 3C). Compared with WAS group, the relative abundance of *Bacteroidetes* in SGD group increased ($P < 0.05$, Figure 3B). Secondly, at the species level, we found that, compared to control group, the relative abundance of *Parabacteroides sp. CAG:409*, *Akkermansia muciniphila*, *Bacteroides sp. CAG:714* and *Bacteroides Barnesiae* decreased, and the relative abundance of *Bacterium D42-87* increased in WAS group. Compared with WAS group, the relative abundance of *Bacteroides sp. CAG:714*, *Lactobacillus reuteri* and *Bacteroides Barnesiae* increased, and the relative abundance of *Bacterium D42-87* decreased in SGD group ($P < 0.05$ and $P < 0.01$, Figures 4A,B). Besides, the possible function related to the differential intestinal microbiota has been analyzed. The results are shown in Figure 5.

To further investigate whether the improvement of VH and intestinal motility by SGD is related to the effect of significantly altered intestinal microbiota, we conducted correlation analysis between these significantly changed intestinal strains and visceral sensitivity threshold and amount of fecal pellets output in rats, respectively. On this basis, the heatmap is used to further analyze the correlation between significantly altered intestinal microbiota and rat phenotype parameters. As illustrated in the correlation heatmap, the abundances of *Parabacteroides sp.*

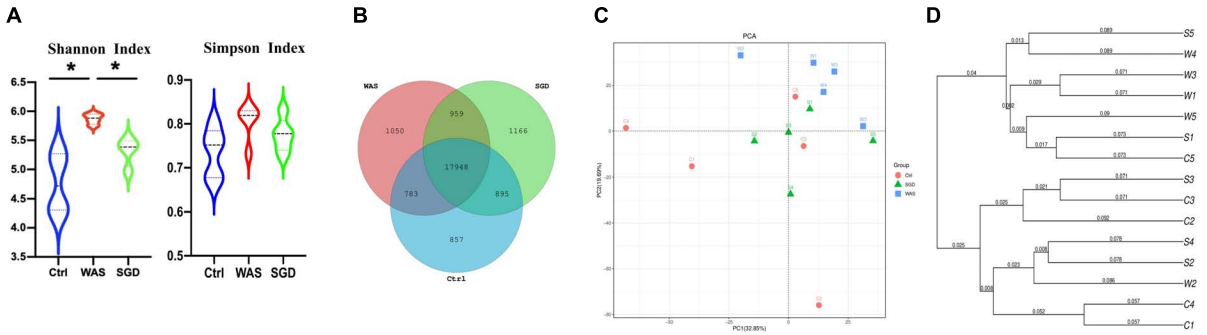


FIGURE 2
Effects of SGD on the intestinal microbiota of IBS-D model rats. **(A)** Shannon index and Simpson index were calculated after refining to an equal number of sequence reads for all samples. The Shannon index of the WAS group was higher than that of the control and SGD groups, while Simpson index has no significant difference among the three groups. **(B)** Venn diagram represented OTUs in each group. **(C)** PCA scores based on the weighted Unifrac index were different among groups. **(D)** The weighted Unifrac index based PCA score phylogenetic tree of gut microbiota. Control group; WAS group; SGD group ($n$ = 5 per group) (*$P$ < 0.05).

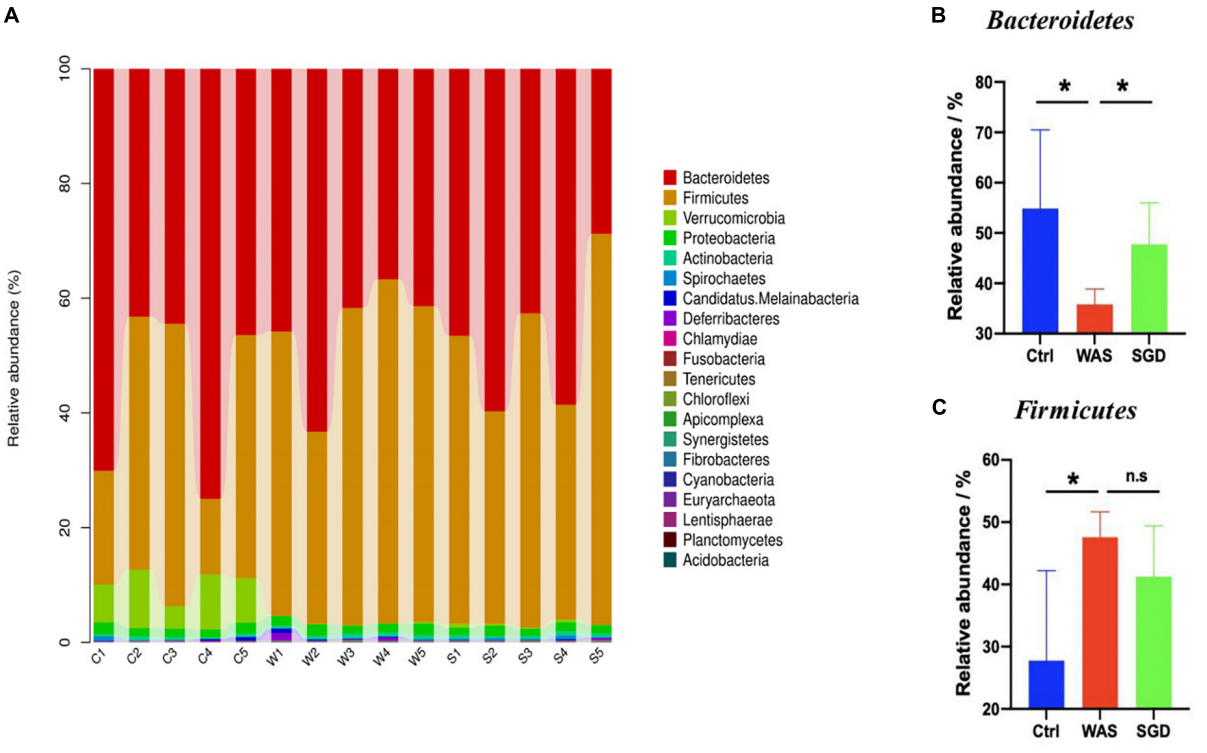


FIGURE 3
Effects of SGD on the intestinal microbiota of IBS-D model rats at the phylum level. **(A)** SGD treatment changed the intestinal microbiota at the phylum level. **(B)** The relative abundance of *Bacteroidetes* was decreased in the WAS group compared with the control group; compared with the WAS group, the relative abundance of *Bacteroidetes* increased in the SGD group. **(C)** Compared with the control group, the relative abundance of *Firmicutes* in the WAS group increased; compared with the WAS group, the relative abundance of *Firmicutes* in the SGD group decreased (*$P$ < 0.05).

*CAG:409*, *Akkermansia muciniphila*, *Bacteroides sp. CAG:714*, *Bacterium D42-87*, *Lactobacillus reuteri* and *Bacteroides Barnesiae* were positively correlated with visceral sensitivity threshold. Moreover, except for *Bacterium D42-87*, the abundances of *Parabacteroides sp. CAG:409*, *Akkermansia muciniphila*, *Bacteroides sp. CAG:714*, *Lactobacillus reuteri* and *Bacteroides Barnesiae* were all negatively associated with the amount of fecal pellets output (Figure 6).

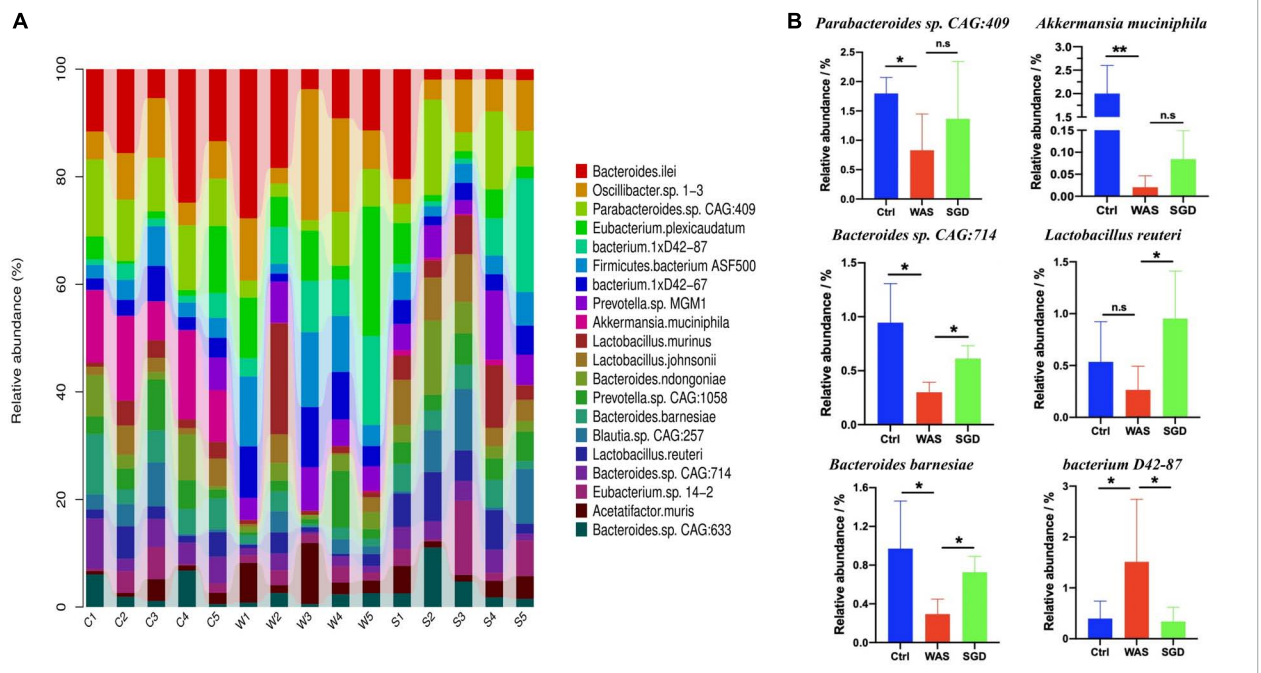


FIGURE 4
Effects of SGD on the intestinal microbiota of IBS-D model rats at the species level. **(A)** SGD treatment changed the intestinal microbiota at the species level. **(B)** Compared with the control group, the relative abundance of *Parabacteroides sp. CAG: 409*, *Akkermansia muciniphila*, *Bacteroides sp. CAG*: 714 and *Bacteroides barnesiae* decreased, and the relative abundance of *bacterium 1xD42-87* increased in the WAS group; compared with the WAS group, the relative abundance of *Bacteroides sp. CAG: 714*, *Lactobacillus reuteri*, and *Bacteroides barnesiae* increased and the relative abundance of *bacterium 1xD42-87* decreased in the SGD group. Control group; WAS group; SGD group ($n$ = 5 per group) (*$P$ < 0.05, **$P$ < 0.01).

## Effects of Shugan decoction on the metabolites of intestinal microbiota in fecal of irritable bowel syndrome model rats

Untargeted metabolomics analysis was performed by ultra-high performance liquid chromatography-Q-TOF MS. Volcanic map showed that there were 26 significantly upregulated metabolites in WAS group (The red dots in the figure are metabolites with FC > 2.0 and $P$ value <0.05, that is, the difference metabolites screened by univariate statistical analysis) compared with control group (Figure 7A), 14 metabolites were significantly up-regulated in the feces of the SGD group compared with the control group (Figure 7B), and 44 significantly upregulated metabolites in SGD compared with the WAS group (Figure 7C).

In addition, we performed cluster analysis on all metabolites detected and constructed a heat map (Figure 8). The results showed that, compared with control group, *N*-acetyl-D-Galactosamine 4-sulfate, PG (18:0/22:6 (4Z,7Z,10Z,13Z,16Z,19Z), Brassylic acid, gibberellinA51-catabolite were significantly up-regulated in WAS group, while 5-amino-4-imidazolecarboxylate, (8R,9R,11Z)-1-carboxy-9-hydroxy-11-heptadecen-8-yl alpha-L-talopyranosiduronic acid, 2_2-iminodipropanoate, Piceatannol, 4-indolecarbaldehyde, ?-Cyano-3-hydroxycinnamic acid, 3″-hydroxy-geranylhydroquinone, GibberellinA8, Gentisic acid, Gallic acid, 1-methylProlinamide, Creatinine, 1-Linoleoyl-sn-glycero-3-phosphoethanolamine, Dezaguanine, 5-[(Z)-2-(3-hydroxy-4-methoxyphenylvinyl-1,3-benzenediol, Oleocanthal, Isorhapontigenin decreased significantly (Figure 8A). In addition, compared with control group, the 3-Hydroxysebacic acid, Letosteine, Dezaguanine, (2S,3S)-2,3-dihydro-3-hydroxyanthranilic acid zwitterion, trans-4-Hydroxy-L-proline, (8R,9R,11Z)-1-Carboxy-9-hydroxy-11-heptadecen-8-yl alpha-L-talopyranosiduronic acid, Creatinine, 1-linoleoyl-sn-glycero-3-phosphoethanolamine, Piceatannol, [FAhydroxy(22:0)]13-hydroxy-docosanoicacid in SGD group decreased significantly, while (5beta)-Chola-7,9(11)-dien-24-oic acid, Adrenic acid, Ethylenediaminetetraacetic acid, Karwinaphthol B, Brassylic acid,Gynocardin, 2-Hydroxyquinoline, (4S)-Cholest-5-ene-3beta_7alpha_24-triol, 5-Hydroxy-8-methoxy-2,2-dimethyl-7-(3-methyl-2-buten-1-yl)-2H,6H-pyrano[3,2-blxanthen-6-one, 3-tert-Butyladipic acid were significantly up-regulated (Figure 8B). Besides,

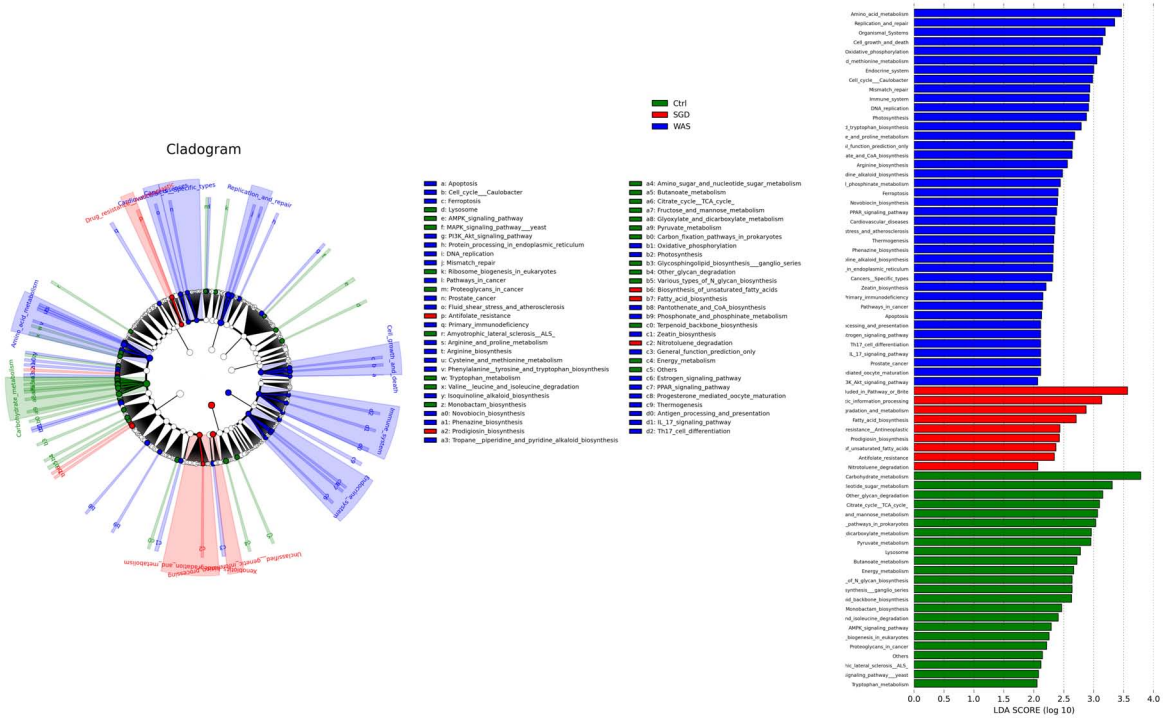


FIGURE 5
Effect of SGD on microbial function. LEfSe analysis shows significantly different function between the three groups **(left panel)** and function with significantly different abundances (LDA scores >2) **(right panel)**. LDA, linear discriminant analysis; LEfSe, LDA effect size.

compared with WAS group, the levels of 1H-lMidazole-4-carboxylic acid, D-Mannose 6-phosphate barium salt hydrate and Creatinine were significantly decreased, while Pentadecanedioic acid, Digitoxigenin, 3beta, 17beta-diacetoxy-5alpha-androstane, 2R_4S-2_4-Diaminopentanoate, [FAmethyl (14:O)]12-methyl-tetradecanoicacid, (9Z)-(13S)-12_13-Epoxyoctadeca-9_11-dienoicacid, 2-Hydroxyethanesulfonate, Sarmentosin, 3_4-Dihydroxy-L-phenylalanine (L-DOPA), Fluocinolone, Uric acid, Fluvastatin, Fortimicin FU-10, *N*-Acetyl-D-glucosamine and Neuraminicacid increased significantly in SGD group (**Figure 8C**).

Finally, Bioinformatics analysis showed that compared to control group, the metabolic pathways with significant differences in WAS group were as follows: endocrine resistance, tryptophan metabolism, prostate cancer and prolactin signaling pathway (**Figure 9A** and **Table 1**). In addition, compared to control group, the metabolic pathways that were significantly different in SGD group were as follows: purine metabolism, nicotinate and nicotinamide metabolism, biosynthesis of unsaturated fatty acids, and arginine and proline metabolism (**Figure 9B** and **Table 1**). What's more, compared to WAS group, the metabolic pathways with significant differences in SGD group were as follows: taurine and hypotaurine metabolism, purine metabolism, sulfur metabolism, ABC transporters and bile secretion (**Figure 9C** and **Table 1**).

## Discussion

In this study, the results showed that compared with control group, the amount of fecal pellets output in WAS group was significantly increased, accompanied by an increase in visceral sensitivity, and there were no pathological changes in colonic epithelial tissues, indicating that the model was successfully established. Consistent with previous study (Shang et al., 2013; Wang Y. et al., 2020), SGD reduced the amount of fecal pellets output of WAS rats and restored their visceral sensitivity.

Next, we conducted metagenomic sequencing of fecal bacteria DNA in each group to study changes in microbial composition. The results showed that compared with the control group, the α-diversity of the intestinal microbiota of the rats in the WAS group was increased, mainly manifested as a significant increase in the shannon index. In addition, both PCA analysis and phylogenetic clustering tree showed significant differences among the groups, indicating that the β-diversity of the intestinal microbiota was significantly different among the three groups. On this basis, when we studied the changes of intestinal microbiota at the phylum level, we found that compared with the control group, the relative abundance of *Bacteroidetes* in the WAS group was significantly lower, which was consistent with previous research results (Jacobs et al., 2021). *Bacteroides* is a kind of beneficial bacteria and is considered to be the main

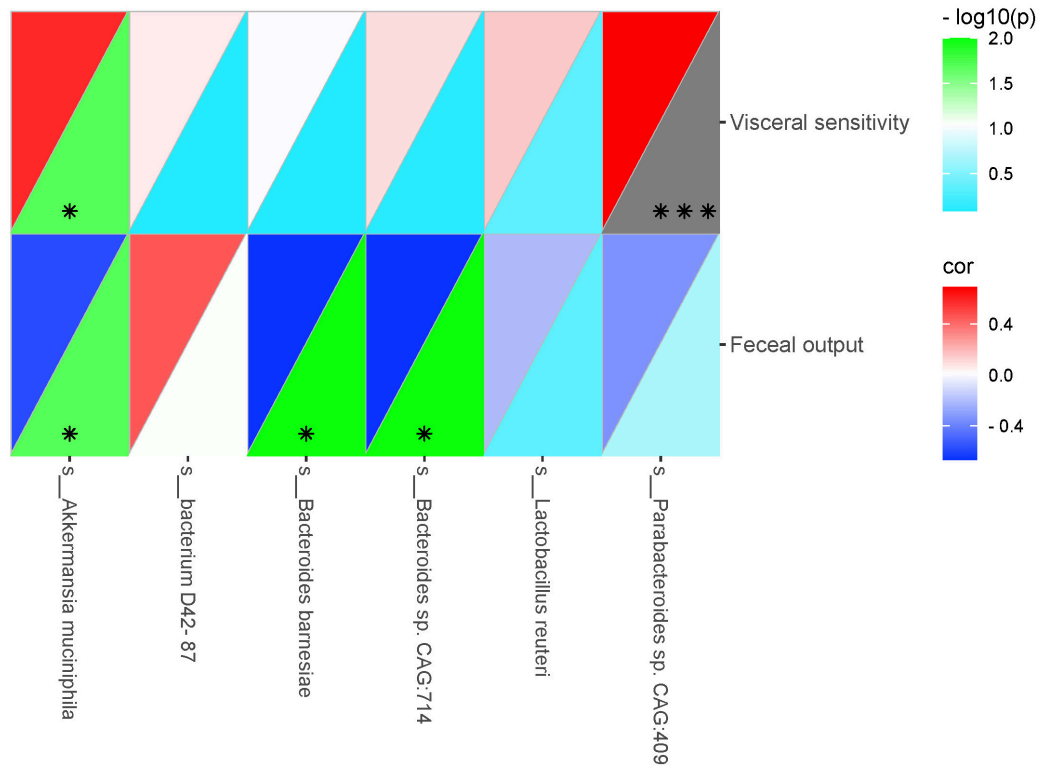


FIGURE 6
Heatmap showing correlations between significantly altered intestinal microbiota and rat phenotype parameters. Color intensity indicates the degree of correlation. The top left represents the correlation, and the bottom right represents −log10(*P*). Red, positive correlation; blue, negative correlation ($n$ = 5 rats per group) (*$P < 0.05$, ***$P < 0.001$).

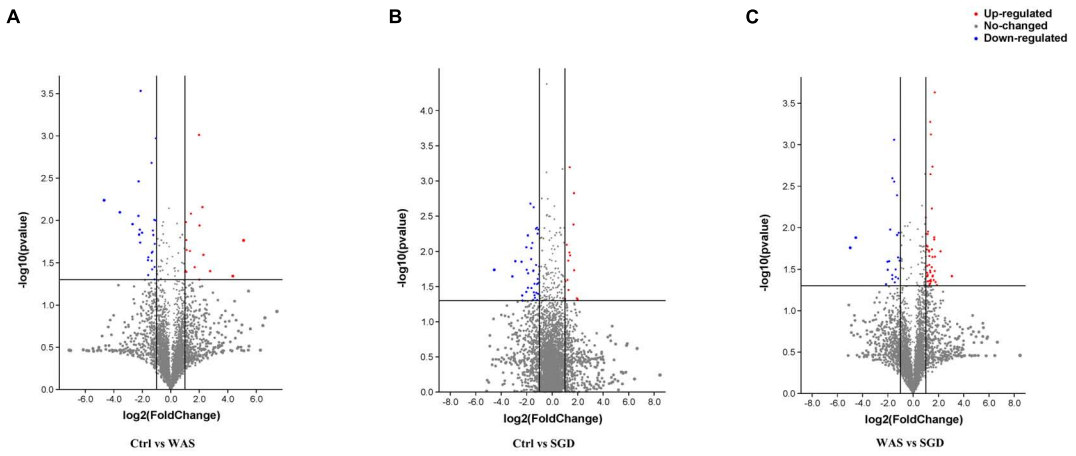


FIGURE 7
Metabolic profiling: volcano plot. **(A)** 26 metabolites (red dots) were significantly up-regulated in the feces of the WAS group compared with the control group; **(B)** 14 metabolites (red dots) were significantly up-regulated in the feces of the SGD group compared with the control group; **(C)** 44 metabolites (red dots) were significantly up-regulated in the feces of the SGD group compared with the WAS group. The red dots in the figure indicate FC > 2.0 and $P < 0.05$. The differential metabolites were screened by univariate statistical analysis.

synthesizer of vitamin K. what's more, it can maintain host intestinal homeostasis by regulating the level of short-chain fatty acids (SCFAs) (Nagpal et al., 2018), and it may also reduce the production of lipopolysaccharide in intestinal microorganisms, inhibiting inflammatory response (Yoshida et al., 2018). At last, it can not only down-regulate the level of interleukin-6

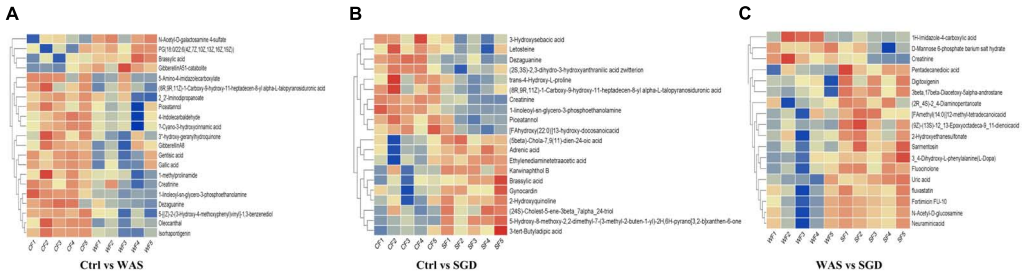


FIGURE 8
Metabolic profiling: hierarchical clustering results. **(A)** Significantly different metabolites between control group and WAS group. **(B)** Significantly different metabolites between control group and SGD group. **(C)** Significantly different metabolites between WAS group and SGD group. The abscissa represents different samples, and the ordinate represents significantly different metabolites.

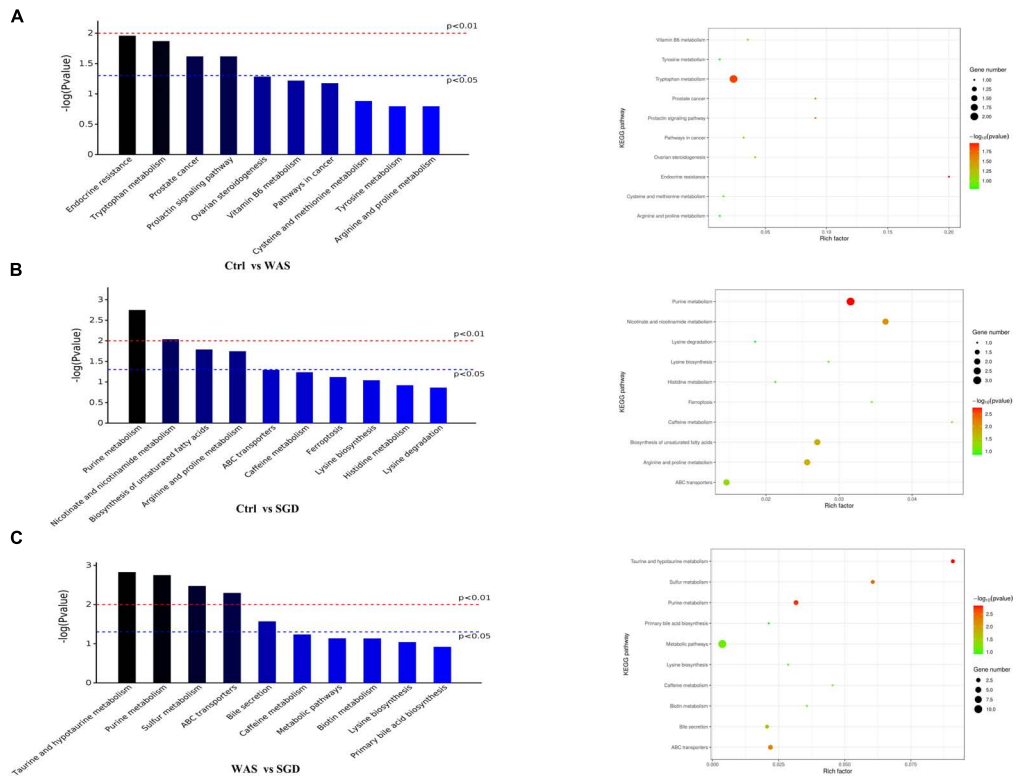


FIGURE 9
Metabolic profiling: KEGG pathway. **(A)** KEGG pathways with significant differences between control and WAS groups. **(B)** KEGG pathways with significant differences between control and SGD groups. **(C)** KEGG pathways with significant differences between WAS and SGD groups. (Left) Histogram of enriched KEGG pathways statistics. The *x*-axis indicates KEGG metabolic pathways with significant differences and the *y*-axis indicates the *P* value of each KEGG pathway. (Right) Bubble chart of enriched KEGG pathways statistics. Rich factor is the ratio of the differentially expressed gene number to the total gene number in a certain pathway. The color and size of the dots represent the range of the −log(*P*-value) and the number of genes mapped to the indicated pathways, respectively. pathways that $P < 0.05$ are shown in the figure.

(IL-6), but also up-regulate the expression of occludin, playing an important role in the treatment of antibiotic-associated diarrhea (Guo et al., 2021). Existing studies have pointed out that *Bacteroides* in the rectal mucosa can be used as a microbial marker to distinguish patients with IBS-D from normal people (Zhu et al., 2021). Interestingly, we observed increased abundance of *Bacteroidetes* after administration of SGD. This suggests that SGD may improve the diarrhea symptoms of IBS patients by increasing the abundance of *Bacteroidetes*, but the specific mechanisms need to be studied further. As sequencing technology continues to improve, we have been able to observe changes in intestinal microbiota

at the species level. As mentioned above, several strains in WAS group changed significantly compared with control group. Regarding them, it has been found that *Parabacteroides* can produce acetate to reduce the infiltration of neutrophils, which plays a role in acute pancreatitis (Lei et al., 2021). *Akkermansia Muciniphila* can directly regulate the integrity of host intestinal epithelial cells and the thickness of mucus layer to promote intestinal health. In addition, its metabolite propionic acid can bind with G protein-coupled receptor (GPR) 43 to mediate changes in downstream pathways, thus playing a key role in immunomodulatory, and is closely related to metabolic diseases such as metabolic syndrome (Zhang et al., 2019). What's more, *Akkermansia muciniphila* was also negatively correlated with pain (Cruz-Aguliar et al., 2019). Interestingly, *Lactobaccillus Reuteri* is mainly used for the treatment of IBS-C, functional abdominal pain or constipation related diseases (Pärtty et al., 2018; Hojsak, 2019). As a kind of probiotics, it can not only regulate intestinal microbiota to relieve the symptoms of gastroenteritis patients, but also promote intestinal movement to relieve chronic constipation (Saviano et al., 2021). *Bacteroides Barnesiae* is mainly related to immune function (Su et al., 2021). Notably, the abundance of these significantly reduced intestinal microbiota recovered after the administration of SGD. Therefore, we speculated that increasing in the abundance of these strains was closely related to the relief of abdominal pain and diarrhea symptoms after SGD administration. In the future, we should conduct further studies on these strains to develop new biomarkers and/or probiotics for the diagnosis and treatment on IBS.

On this basis, we conducted a metabolomics study on rat fecal samples to screen out metabolites with statistical and biological significance, clarify the mechanism of metabolic process and expression changes in IBS model rats, and further explore the correlation between them. For example, whether they are in the same metabolic pathway, or whether they are upstream and downstream metabolites. When analyzing the differential metabolites between two groups of samples, Volcano Plot, as a univariate analysis method, can intuitively show the significance of metabolite changes. It helped us to screen metabolites as potential markers. We found that 26 metabolites were significantly up-regulated in the WAS group compared with the control group, and 44 metabolites were significantly up-regulated in the SGD group compared with the WAS group. After observing this phenomenon, we conducted Hierarchical Clustering for each group of samples, so as to accurately screen out marker metabolites and study the changes of related metabolic processes. The results revealed that most of the significantly changed metabolites in the WAS group showed a downward trend compared with the control group. Among them, Oleocanthal can act as an anti-inflammatory agent, a heat shock protein (HSP) 90 inhibitor, a cyclooxygenase (COX)1 and 2 inhibitor and an antioxidant. Dezaguanine is a purine nucleoside analog with antitumor and viral activity. While Gallic acid is mainly used in veterinary medicine as a bowel astringent and antidiarrheal. In addition, Gentisic acid is a metabolite of human salicylic acid, which is associated with the occurrence and development of colorectal cancer (Brown et al., 2016). Notably, most of the significantly changed metabolites in the SGD group showed an upward trend compared with the WAS group. N-Acetyl-D-glucosamine is related to amino acid metabolism pathway and is involved in the occurrence and development of colon cancer (Brown et al., 2016; Sinha et al., 2016) and diverticulum-related diseases (Tursi et al., 2016). Fluvastatin is a commonly used cholesterol-lowering agent, which can act by inhibiting 3-hydroxy-3-methyl glutaryl coenzyme A reductase (HMGR), and associated with abdominal pain, anorexia (Li et al., 2016), indigestion (Greten et al., 1994) and other digestive system diseases. Besides, uric acid (UA) is the main antioxidant in human plasma, which can inhibit or delay the oxidation reaction, and is related to diseases such as acute kidney injury and colorectal cancer (Wang et al., 2017). Fluocinolone is an anti-inflammatory glucocorticoid. Levodopa, an amino acid precursor of dopamine, is associated with aromatic L-amino acid decarboxylase deficiency (Abdenur et al., 2006). It can cross the blood-brain barrier through various pathways and decarboxylate to form dopamine. Pentadecanedioic acid, as a long-chain fatty acid, is the basic component of phospholipids, triglycerides and cholesterol, as well as the main substrate in energy metabolic reactions, and is closely related to metabolic syndrome such as obesity, hypertension and dyslipidemia (Wang L. et al., 2020). By analyzing these metabolites, we can see that WAS can cause a decrease in the expression of metabolites related to anti-inflammatory, antioxidant, antidiarrheal, and anti-tumor, and SGD administration can increase the expression of some specific metabolites to treat abdominal pain, indigestion, colon cancer and other digestive system diseases.

There is a certain relationship between the significantly changed intestinal microbiota and the differentially expressed metabolites. Existing studies have found that N-Acetyl-D-glucosamine is indispensable for the growth of Akkermansia muciniphila (Ouwerkerk et al., 2016; Ropot et al., 2020). In addition, UA is the end-product of purine metabolism in the liver, and when purine metabolism is impaired, serum UA levels will increase, further forming hyperuricemia, which will eventually lead to gout. However, Lactobacillus reuteri can stabilize serum uric acid level and prevent hyperuricemia (Kuo et al., 2021). Other studies have pointed out that the abundance of Akkermansia mucinphila in the intestine is related to the levels of uric acid and xanthine, and plays an important role in fatty acid synthesis and energy metabolism (Lu C. et al., 2020; Han et al., 2021; Liao et al., 2022).

After screening out these obviously different metabolites, cluster analysis and KEGG metabolic pathway analysis on them were performed and we obtained the metabolic pathways with significant differences in each group of rats

TABLE 1 KEGG pathway with significant differences between different groups are as follows ($P < 0.05$).

| Groups (A vs B) | KEGG metabolic pathways' name | *P* value |
|---|---|---|
| Ctrl vs WAS | Endocrine resistance | 0.011 |
| | Tryptophan metabolism | 0.0135 |
| | Prostate cancer | 0.0241 |
| | Prolactin signaling pathway | 0.0241 |
| Ctrl vs SGD | Purine metabolism | 0.00178 |
| | Nicotinate and nicotinamide metabolism | 0.00914 |
| | Biosynthesis of unsaturated fatty acids | 0.0162 |
| | Arginine and proline metabolism | 0.0179 |
| WAS vs SGD | Taurine and hypotaurine metabolism | 0.00149 |
| | Purine metabolism | 0.00178 |
| | Sulfur metabolism | 0.00336 |
| | ABC transporters | 0.00506 |
| | Bile secretion | 0.0269 |

(important metabolites in this pathway are in brackets). Compared with control group, there were remarkable differences in endocrine resistance (Androstenedione), tryptophan metabolism pathways (2-Aminophenol, 4-Hydroxy-2-quinolinecarboxylic acid), prostate cancer (Androstenedione) and Prolactin signaling pathway (Androstenedione) in WAS rats. To begin with, endocrine resistance is mainly related to colon function. Some studies have found that IL-6, a pro-inflammatory cytokine, is significantly elevated in patients with IBS, which can regulate intestinal secretion and participate in the development of IBS (O'Brien et al., 2021). Regarding the Tryptophan metabolism pathway, studies have found that the decreased serum tryptophan concentration exhibited by SERT $^{-/-}$ rats is associated with visceral hypersensitivity and abnormal gastrointestinal motility (Bi et al., 2021). In addition, the tryptophan metabolic pathway is considered to be one of the main metabolic pathways in the WAS-induced IBS model rats, and the changes in the intestinal microbiota of the model rats are closely related to the changes in tryptophan metabolism (Mishima and Ishihara, 2021). Recent studies indicate that dysregulation of tryptophan/serotonin metabolism in feces and serum is closely related to the severity of IBS. The kynurenine pathway is thought to be the main pathway for the metabolism of L-tryptophan (Fila et al., 2021; Han et al., 2022). 2-Aminophenol (2AP) is the structural precursor of L-3-hydroxy kanurine (L-3HOK) and 3-hydroxy anthranilic acid (3HAA), whose oxidative autodimerization can induce neurotoxicity of Kynurenines, the oxidative degradation products of tryptophan (Zhuravlev et al., 2018). We can see that Androstenedione is the major metabolite of both Prostate cancer and Prolactin signaling pathway. Existing studies suggest that they are related to prostate cancer (Hettel et al., 2018) and adrenal cortical function (Kaminska et al., 2002), respectively. Compared with WAS group, SGD group showed significant differences in metabolic pathways such as taurine

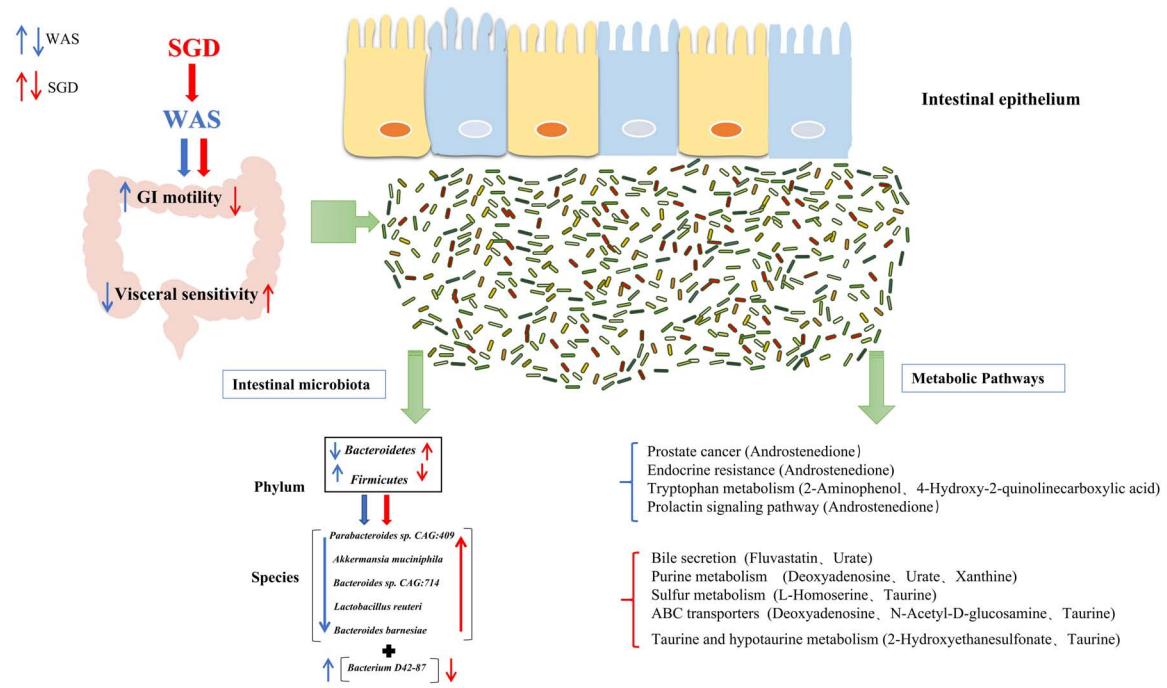


FIGURE 10
Effect of SGD on intestinal microbiota in IBS-D rats.

and hypotaurine metabolism (2-Hydroxyethanesulfonate, Taurine), purine metabolism (Deoxyadenosine, Urate, Xanthine), sulfur metabolism (L-Homoserine, Taurine), ABC transporters (Deoxyadenosine, *N*-Acetyl-D-glucosamine, Taurine) and bile secretion (Fluvastatin, Urate). Among them, taurine and hypotaurine metabolism can play an important role in bile acid metabolism pathway, leading to intestinal microbiota disturbance by inhibiting the growth of beneficial bacteria and causing intestinal inflammation (Schliess et al., 1997; Cerdó et al., 2018). Studies have pointed out that its important metabolite Taurine is involved in the occurrence and development of chronic transport constipation, UC and colorectal cancer (Liu et al., 2019; Zhou et al., 2019; Zhu et al., 2022). Purine metabolism is linked to the occurrence and development of colitis (Wu et al., 2020) and type 2 diabetes (Zhao et al., 2020). Interestingly, rhein, as a major metabolite in Purine metabolism, can reduce uric acid levels and thus alleviate Dextran sulfate sodium salt (DSS)-induced chronic colitis (Wu et al., 2020). As for sulfur metabolism, studies have confirmed that the energy and lipid metabolism capacity of the gut microbes in WAS group decreased, while the fatty acid and sulfur metabolism capacity increased (Fourie et al., 2017). The marked increase in the content of exogenous hydrogen sulfide, a major component involved in sulfur metabolism, is considered a potential player in the etiology of IBS, inflammatory bowel disease (IBD), and colorectal cancer (Carbonero et al., 2012; Chassard et al., 2012). Taurine, as its important metabolite, can promote the growth of sulfur-producing bacteria and lead to the occurrence of IBD (Walker and Schmitt-Kopplin, 2021). In addition, ABC transporters are key bacterial proteins affecting nutrient absorption and drug resistance (Zhang et al., 2021). Notably, Bile secretion can regulate visceral pain perception and improve visceral hypersensitivity in IBS patients (Ní Dhonnabháin et al., 2021). The increased expression of bile acid in fecal, primary bile acid in liver and bile acid receptor Takeda G protein-coupled receptor 5 (TGR5) in colon in most patients with IBS-D is closely related to the severity of diarrhea symptoms (Walters, 2021; Wei et al., 2021), and the TGR5-ECS-5-HT signaling pathway may play an important role in the pathophysiology of IBS (Tao et al., 2022). Bile acids can control the circadian variation of the metabolite uric acid through the regulation of xanthine oxidase by PPARα (Kanemitsu et al., 2017). In addition, it has been proposed that bile acid malabsorption is caused by changes in intestinal microbiota (Reynaud et al., 2016). Therefore, the interaction between bile acid secretion imbalance and intestinal microbiota can be a potential research point for the pathogenesis of IBS (Fuchs and Trauner, 2022). In conclusion, the discovery of these metabolic pathways is helpful to further clarify the mechanism of SGD in the treatment of IBS, and provide new ideas for the clinical use of SGD in the treatment of IBS patients in the future. In order to better summarize the effect of SGD on intestinal microbiota in IBS-D rats, we drew a graphic summary (**Figure 10**).

## Data availability statement

The original contributions presented in this study are included in the article/**Supplementary material**, further inquiries can be directed to the corresponding author.

## Ethics statement

This animal study was reviewed and approved by Animal Ethics Committee of Shanghai University of TCM.

## Author contributions

LH carried out the animal experiments, analyzed the experimental data, and wrote the draft of the manuscript. EW, YF, YZ, YM, and FJ carried out the animal experiments. JY designed the experiments and revised the manuscript. All authors contributed to the article and approved the submitted version.

## Funding

This work was supported by the National Natural Science Foundation of China (No. 81874391).

## Conflict of interest

The authors declare that the research was conducted in the absence of any commercial or financial relationships that could be construed as a potential conflict of interest.

## Publisher's note

All claims expressed in this article are solely those of the authors and do not necessarily represent those of their affiliated organizations, or those of the publisher, the editors and the reviewers. Any product that may be evaluated in this article, or claim that may be made by its manufacturer, is not guaranteed or endorsed by the publisher.

## Supplementary material

The Supplementary Material for this article can be found online at: https://www.frontiersin.org/articles/10.3389/fmicb.2022.1024822/full#supplementary-material

# References


Abdenur, J. E., Abeling, N., Specola, N., Jorge, L., Schenone, A. B., van Cruchten, A. C., et al. (2006). Aromatic l-aminoacid decarboxylase deficiency: Unusual neonatal presentation and additional findings in organic acid analysis. *Mol. Genet. Metab.* 87, 48–53. doi: 10.1016/j.ymgme.2005.09.007

Bi, Z., Zhang, S., Meng, Y., Feng, Y., Wang, Y., Wang, E., et al. (2021). Female serotonin transporter-knockout rat: A potential model of irritable bowel syndrome. *FASEB J.* 35:e21701. doi: 10.1096/fj.202000007RRR

Botschuijver, S., Roeselers, G., Levin, E., Jonkers, D. M., Welting, O., Heinsbroek, S. E. M., et al. (2017). Intestinal fungal dysbiosis is associated with visceral hypersensitivity in patients with irritable bowel syndrome and rats. *Gastroenterology* 153, 1026–1039. doi: 10.1053/j.gastro.2017.06.004

Bradesi, S., Kokkotou, E., Simeonidis, S., Patierno, S., Ennes, H. S., Mittal, Y., et al. (2006). The role of neurokinin 1 receptors in the maintenance of visceral hyperalgesia induced by repeated stress in rats. *Gastroenterology* 130, 1729–1742. doi: 10.1053/j.gastro.2006.01.037

Bradesi, S., Schwetz, I., Ennes, H. S., Lamy, C. M., Ohning, G., Fanselow, M., et al. (2005). Repeated exposure to water avoidance stress in rats: A new model for sustained visceral hyperalgesia. *Am. J. Physiol. Gastrointest. Liver Physiol.* 289, G42–G53. doi: 10.1152/ajpgi.00500.2004

Brown, D. G., Rao, S., Weir, T. L., O'Malia, J., Bazan, M., Brown, R. J., et al. (2016). Metabolomics and metabolic pathway networks from human colorectal cancers, adjacent mucosa, and stool. *Cancer Metab.* 4:11. doi: 10.1186/s40170-016-0151-y

Carbonero, F., Benefiel, A. C., Alizadeh-Ghamsari, A. H., and Gaskins, H. R. (2012). Microbial pathways in colonic sulfur metabolism and links with health and disease. *Front. Physiol.* 3:448. doi: 10.3389/fphys.2012.00448

Cerdó, T., Ruiz, A., Jáuregui, R., Azaryah, H., Torres-Espínola, F. J., García-Valdés, L., et al. (2018). Maternal obesity is associated with gut microbial metabolic potential in offspring during infancy. *J. Physiol. Biochem.* 74, 159–169. doi: 10.1007/s13105-017-0577-x

Chassard, C., Dapoigny, M., Scott, K. P., Crouzet, L., Del'homme, C., Marquet, P., et al. (2012). Functional dysbiosis within the gut microbiota of patients with constipated-irritable bowel syndrome. *Aliment. Pharmacol. Ther.* 35, 828–838. doi: 10.1111/j.1365-2036.2012.05007.x

Cruz-Aguliar, R. M., Wantia, N., Clavel, T., Vehreschild, M., Buch, T., Bajbouj, M., et al. (2019). An open-labeled study on fecal microbiota transfer in irritable bowel syndrome patients reveals improvement in abdominal pain associated with the relative abundance of *Akkermansia muciniphila*. *Digestion* 100, 127–138. doi: 10.1159/000494252

Fila, M., Chojnacki, J., Pawlowska, E., Szczepanska, J., Chojnacki, C., and Blasiak, J. (2021). Kynurenine pathway of tryptophan metabolism in migraine and functional gastrointestinal disorders. *Int. J. Mol. Sci.* 22:10134. doi: 10.3390/ijms221810134

Ford, A. C., Lacy, B. E., and Talley, N. J. (2017). Irritable bowel syndrome. *N. Engl. J. Med.* 376, 2566–2578. doi: 10.1056/NEJMra1607547

Fourie, N. H., Wang, D., Abey, S. K., Creekmore, A. L., Hong, S., Martin, C. G., et al. (2017). Structural and functional alterations in the colonic microbiome of the rat in a model of stress induced irritable bowel syndrome. *Gut Microbes* 8, 33–45. doi: 10.1080/19490976.2016.1273999

Fuchs, C. D., and Trauner, M. (2022). Role of bile acids and their receptors in gastrointestinal and hepatic pathophysiology. *Nat. Rev. Gastroenterol. Hepatol.* 19, 432–450. doi: 10.1038/s41575-021-00566-7

Greten, H., Beil, F. U., Schneider, J., Weisweiler, P., Armstrong, V. W., Keller, C., et al. (1994). Treatment of primary hypercholesterolemia: Fluvastatin versus bezafibrate. *Am. J. Med.* 96, 55s–63s. doi: 10.1016/0002-9343(94)90233-x

Guo, H., Yu, L., Tian, F., Zhao, J., Zhang, H., Chen, W., et al. (2021). Effects of *Bacteroides*-based microecologics against antibiotic-associated diarrhea in mice. *Microorganisms* 9:2492. doi: 10.3390/microorganisms9122492

Han, L., Zhao, L., Zhou, Y., Yang, C., Xiong, T., Lu, L., et al. (2022). Altered metabolome and microbiome features provide clues in understanding irritable bowel syndrome and depression comorbidity. *ISME J.* 16, 983–996. doi: 10.1038/s41396-021-01123-5

Han, R., Qiu, H., Zhong, J., Zheng, N., Li, B., Hong, Y., et al. (2021). Si Miao Formula attenuates non-alcoholic fatty liver disease by modulating hepatic lipid metabolism and gut microbiota. *Phytomedicine* 85:153544. doi: 10.1016/j.phymed.2021.153544

Hettel, D., Zhang, A., Alyamani, M., Berk, M., and Sharifi, N. (2018). AR signaling in prostate cancer regulates a feed-forward mechanism of androgen synthesis by way of HSD3B1 upregulation. *Endocrinology* 159, 2884–2890.

Hojsak, I. (2019). Probiotics in functional gastrointestinal disorders. *Adv. Exp. Med. Biol.* 1125, 121–137. doi: 10.1007/5584_2018_321

Jacobs, J. P., Gupta, A., Bhatt, R. R., Brawer, J., Gao, K., Tillisch, K., et al. (2021). Cognitive behavioral therapy for irritable bowel syndrome induces bidirectional alterations in the brain-gut-microbiome axis associated with gastrointestinal symptom improvement. *Microbiome* 9:236. doi: 10.1186/s40168-021-01188-6

Kaminska, B., Ciereszko, R. E., Opalka, M., and Dusza, L. (2002). Prolactin signaling in porcine adrenocortical cells: Involvement of protein kinases. *Domest. Anim. Endocrinol.* 23, 475–491. doi: 10.1016/s0739-7240(02)00173-x

Kanemitsu, T., Tsurudome, Y., Kusunose, N., Oda, M., Matsunaga, N., Koyanagi, S., et al. (2017). Periodic variation in bile acids controls circadian changes in uric acid *via* regulation of xanthine oxidase by the orphan nuclear receptor PPARα. *J. Biol. Chem.* 292, 21397–21406. doi: 10.1074/jbc.M117.791285

Kuo, Y. W., Hsieh, S. H., Chen, J. F., Liu, C. R., Chen, C. W., Huang, Y. F., et al. (2021). *Lactobacillus reuteri* TSR332 and *Lactobacillus fermentum* TSF331 stabilize serum uric acid levels and prevent hyperuricemia in rats. *PeerJ* 9:e11209. doi: 10.7717/peerj.11209

Lei, Y., Tang, L., Liu, S., Hu, S., Wu, L., Liu, Y., et al. (2021). Parabacteroides produces acetate to alleviate heparanase-exacerbated acute pancreatitis through reducing neutrophil infiltration. *Microbiome* 9:115. doi: 10.1186/s40168-021-01065-2

Li, L., Ma, Y., Geng, X. B., Song, Y. X., Tan, Z., Shang, X. M., et al. (2016). Drug-induced acute liver injury within 12 hours after fluvastatin therapy. *Am. J. Ther.* 23, e318–e320. doi: 10.1097/mjt.0000000000000012

Liao, C. A., Huang, C. H., Ho, H. H., Chen, J. F., Kuo, Y. W., Lin, J. H., et al. (2022). A combined supplement of probiotic strains AP-32, bv-77, and CP-9 increased *Akkermansia mucinphila* and reduced non-esterified fatty acids and energy metabolism in HFD-induced obese rats. *Nutrients* 14:527. doi: 10.3390/nu14030527

Liu, J., Li, H., Zheng, B., Sun, L., Yuan, Y., and Xing, C. (2019). Competitive endogenous RNA (ceRNA) regulation network of lncRNA-miRNA-mRNA in colorectal carcinogenesis. *Dig. Dis. Sci.* 64, 1868–1877. doi: 10.1007/s10620-019-05506-9

Lu, L., Zhu, Y., and Zhu, Y. (2020). Clinical observation of Shugan decoction in the treatment of irritable bowel syndrome with liver stagnation and spleen deficiency. *Chin. J. Integr. Tradit. West. Med.* 28, 901–905.

Lu, C., Li, Y., Li, L., Kong, Y., Shi, T., Xiao, H., et al. (2020). Alterations of serum uric acid level and gut microbiota after roux-en-Y gastric bypass and sleeve gastrectomy in a hyperuricemic rat model. *Obes. Surg.* 30, 1799–1807. doi: 10.1007/s11695-019-04328-y

Lu, L., Yan, L., Yuan, J., Ye, Q., and Lin, J. (2018). Shuganyin decoction improves the intestinal barrier function in a rat model of irritable bowel syndrome induced by water-avoidance stress. *Chin. Med.* 13:6. doi: 10.1186/s13020-017-0161-x

Mishima, Y., and Ishihara, S. (2021). enteric microbiota-mediated serotonergic signaling in pathogenesis of irritable bowel syndrome. *Int. J. Mol. Sci.* 22:10235. doi: 10.3390/ijms221910235

Murciano-Brea, J., Garcia-Montes, M., Geuna, S., and Herrera-Rincon, C. (2021). Gut microbiota and neuroplasticity. *Cells* 10:2084. doi: 10.3390/cells10082084

Nagpal, R., Wang, S., Ahmadi, S., Hayes, J., Gagliano, J., Subashchandrabose, S., et al. (2018). Human-origin probiotic cocktail increases short-chain fatty acid production *via* modulation of mice and human gut microbiome. *Sci. Rep.* 8:12649. doi: 10.1038/s41598-018-30114-4

Ní Dhonnabháin, R., Xiao, Q., and O'Malley, D. (2021). Aberrant gut-to-brain signaling in irritable bowel syndrome–the role of bile acids. *Front. Endocrinol. (Lausanne)* 12:745190. doi: 10.3389/fendo.2021.745190

O'Brien, R., Buckley, M. M., and O'Malley, D. (2021). Divergent effects of exendin-4 and interleukin-6 on rat colonic secretory and contractile activity are associated with changes in regional vagal afferent signaling. *Neurogastroenterol. Motil.* 33:e14160. doi: 10.1111/nmo.14160

Oka, P., Parr, H., Barberio, B., Black, C. J., Savarino, E. V., and Ford, A. C. (2020). Global prevalence of irritable bowel syndrome according to Rome III or IV criteria: A systematic review and meta-analysis. *Lancet Gastroenterol. Hepatol.* 5, 908–917. doi: 10.1016/s2468-1253(20)30217-x

Ouwerkerk, J. P., Aalvink, S., Belzer, C., and de Vos, W. M. (2016). *Akkermansia glycaniphila* sp. nov., an anaerobic mucin-degrading bacterium isolated from reticulated python faeces. *Int. J. Syst. Evol. Microbiol.* .66, 4614–4620. doi: 10.1099/ijsem.0.001399

Pan, X., and Xie, Q. (2006). Observation on the clinical efficacy of Shugan Yin in treating irritable bowel syndrome. *Acta Univ. Tradit. Med. Sin. Pharmacol. Shanghai* 4, 48–50.

Pärtty, A., Rautava, S., and Kalliomäki, M. (2018). Probiotics on pediatric functional gastrointestinal disorders. *Nutrients* 10:1836. doi: 10.3390/nu10121836

Pimentel, M., and Lembo, A. (2020). Microbiome and its role in irritable bowel syndrome. *Dig. Dis. Sci.* 65, 829–839. doi: 10.1007/s10620-020-06109-5

Reynaud, Y., Fakhry, J., Fothergill, L., Callaghan, B., Ringuet, M., Hunne, B., et al. (2016). The chemical coding of 5-hydroxytryptamine containing enteroendocrine cells in the mouse gastrointestinal tract. *Cell Tissue Res.* 364, 489–497. doi: 10.1007/s00441-015-2349-7

Ropot, A. V., Karamzin, A. M., and Sergeyev, O. V. (2020). Cultivation of the next-generation probiotic *Akkermansia muciniphila*, methods of its safe delivery to the intestine, and factors contributing to its growth in vivo. *Curr. Microbiol.* 77, 1363–1372. doi: 10.1007/s00284-020-01992-7

Saviano, A., Brigida, M., Migneco, A., Gunawardena, G., Zanza, C., Candelli, M., et al. (2021). *Lactobacillus reuteri* DSM 17938 (*Limosilactobacillus reuteri*) in diarrhea and constipation: Two sides of the same coin? *Medicina (Kaunas)* 57:643. doi: 10.3390/medicina57070643

Schliess, F., Kurz, A. K., vom Dahl, S., and Häussinger, D. (1997). Mitogen-activated protein kinases mediate the stimulation of bile acid secretion by tauroursodeoxycholate in rat liver. *Gastroenterology* 113, 1306–1314. doi: 10.1053/gast.1997.v113.pm9322526

Sebastián Domingo, J. J. (2022). Irritable bowel syndrome. *Med. Clin. (Barc)* 158, 76–81. doi: 10.1016/j.medcli.2021.04.029

Shang, J. J., Yuan, J. Y., Xu, H., Tang, R. Z., Dong, Y. B., and Xie, J. Q. (2013). Shugan-decoction relieves visceral hyperalgesia and reduces TRPV1 and SP colon expression. *World J. Gastroenterol.* 19, 8071–8077. doi: 10.3748/wjg.v19.i44.8071

Shariati, A., Fallah, F., Pormohammad, A., Taghipour, A., Safari, H., Chirani, A. S., et al. (2019). The possible role of bacteria, viruses, and parasites in initiation and exacerbation of irritable bowel syndrome. *J. Cell Physiol.* 234, 8550–8569. doi: 10.1002/jcp.27828

Shi, H. L., Liu, C. H., Ding, L. L., Zheng, Y., Fei, X. Y., Lu, L., et al. (2015). Alterations in serotonin, transient receptor potential channels and protease-activated receptors in rats with irritable bowel syndrome attenuated by Shugan decoction. *World J. Gastroenterol.* 21, 4852–4863. doi: 10.3748/wjg.v21.i16.4852

Sinha, R., Ahn, J., Sampson, J. N., Shi, J., Yu, G., Xiong, X., et al. (2016). Fecal microbiota, fecal metabolome, and colorectal cancer interrelations. *PLoS One* 11:e0152126. doi: 10.1371/journal.pone.0152126

Spence, M. J., and Moss-Morris, R. (2007). The cognitive behavioural model of irritable bowel syndrome: A prospective investigation of patients with gastroenteritis. *Gut* 56, 1066–1071. doi: 10.1136/gut.2006.108811

Sperber, A. D., Bangdiwala, S. I., Drossman, D. A., Ghoshal, U. C., Simren, M., Tack, J., et al. (2021). Worldwide prevalence and burden of functional gastrointestinal disorders, results of Rome foundation global study. *Gastroenterology* 160, 99–114.e3. doi: 10.1053/j.gastro.2020.04.014

Su, Y., Tian, S., Li, D., Zhu, W., Wang, T., Mishra, S. K., et al. (2021). Association of female reproductive tract microbiota with egg production in layer chickens. *Gigascience* 10:giab067. doi: 10.1093/gigascience/giab067

Tao, E., Zhu, Z., Hu, C., Long, G., Chen, B., Guo, R., et al. (2022). Potential roles of enterochromaffin cells in early life stress-induced irritable bowel syndrome. *Front. Cell Neurosci.* 16:837166. doi: 10.3389/fncel.2022.837166

Teschke, R., Wolff, A., Frenzel, C., Eickhoff, A., and Schulze, J. (2015). Herbal traditional Chinese medicine and its evidence base in gastrointestinal disorders. *World J. Gastroenterol.* 21, 4466–4490. doi: 10.3748/wjg.v21.i15.4466

Tursi, A., Mastromarino, P., Capobianco, D., Elisei, W., Miccheli, A., Capuani, G., et al. (2016). Assessment of fecal microbiota and fecal metabolome in symptomatic uncomplicated diverticular disease of the colon. *J. Clin. Gastroenterol.* 50(Suppl. 1), S9–S12. doi: 10.1097/mcg.0000000000000626

Walker, A., and Schmitt-Kopplin, P. (2021). The role of fecal sulfur metabolome in inflammatory bowel diseases. *Int. J. Med. Microbiol.* 311:151513. doi: 10.1016/j.ijmm.2021.151513

Walters, J. R. F. (2021). The role of bile acids and their TGR5 receptor in irritable bowel syndrome and diarrhoea. *Dig. Liver Dis.* 53, 1118–1119. doi: 10.1016/j.dld.2021.06.017

Wang, Y., Dong, Y., Wang, E., Meng, Y., Bi, Z., Sun, S., et al. (2020). Shugan decoction alleviates colonic dysmotility in female SERT-knockout rats by decreasing M(3) receptor expression. *Front. Pharmacol.* 11:01082. doi: 10.3389/fphar.2020.01082

Wang, L., Li, G., and Deng, Y. (2020). Diamine biosynthesis: Research progress and application prospects. *Appl. Environ. Microbiol.* 86, e1972–e1920. doi: 10.1128/aem.01972-20

Wang, X., Wang, J., Rao, B., and Deng, L. (2017). Gut flora profiling and fecal metabolite composition of colorectal cancer patients and healthy individuals. *Exp. Ther. Med.* 13, 2848–2854. doi: 10.3892/etm.2017.4367

Wei, W., Wang, H., Zhang, Y., Zhang, Y., Niu, B., Chen, S., et al. (2021). Faecal bile acids and colonic bile acid membrane receptor correlate with symptom severity of diarrhoea-predominant irritable bowel syndrome: A pilot study. *Dig. Liver Dis.* 53, 1120–1127. doi: 10.1016/j.dld.2021.04.022

Wu, J., Wei, Z., Cheng, P., Qian, C., Xu, F., Yang, Y., et al. (2020). Rhein modulates host purine metabolism in intestine through gut microbiota and ameliorates experimental colitis. *Theranostics* 10, 10665–10679. doi: 10.7150/thno.43528

Xie, Q., Zheng, Y., Fei, Y., Pan, X., Yuan, Y., and Xue, Y. (2004). Clinical study of Shugan decoction in the treatment of diarrhea-type irritable bowel syndrome with disharmony between liver and spleen. *Acta Univ. Trait. Med. Sin. Pharm. Shanghai* 4, 11–13. doi: 10.16306/j.1008-861x.2004.04.004

Yoshida, N., Emoto, T., Yamashita, T., Watanabe, H., Hayashi, T., Tabata, T., et al. (2018). *Bacteroides vulgatus* and *Bacteroides dorei* reduce gut microbial lipopolysaccharide production and inhibit atherosclerosis. *Circulation* 138, 2486–2498. doi: 10.1161/circulationaha.118.033714

Zhang, T., Li, Q., Cheng, L., Buch, H., and Zhang, F. (2019). *Akkermansia muciniphila* is a promising probiotic. *Microb. Biotechnol.* 12, 1109–1125. doi: 10.1111/1751-7915.13410

Zhang, X., Yang, Y., Zhang, F., Yu, J., Sun, W., Wang, R., et al. (2021). Traditional Chinese medicines differentially modulate the gut microbiota based on their nature (Yao-Xing). *Phytomedicine* 85:153496. doi: 10.1016/j.phymed.2021.153496

Zhao, X. Q., Guo, S., Lu, Y. Y., Hua, Y., Zhang, F., Yan, H., et al. (2020). *Lycium barbarum* L. leaves ameliorate type 2 diabetes in rats by modulating metabolic profiles and gut microbiota composition. *Biomed. Pharmacother.* 121:109559. doi: 10.1016/j.biopha.2019.109559

Zhou, J., Yao, N., Wang, S., An, D., Cao, K., Wei, J., et al. (2019). *Fructus Gardeniae*-induced gastrointestinal injury was associated with the inflammatory response mediated by the disturbance of vitamin B6, phenylalanine, arachidonic acid, taurine and hypotaurine metabolism. *J. Ethnopharmacol.* 235, 47–55. doi: 10.1016/j.jep.2019.01.041

Zhu, G., Wu, X., Jiang, S., Wang, Y., Kong, D., Zhao, Y., et al. (2022). The application of omics techniques to evaluate the effects of Tanshinone IIA on dextran sodium sulfate induced ulcerative colitis. *Mol. Omics* 18, 666–676. doi: 10.1039/d2mo00074a

Zhu, X., Hong, G., Li, Y., Yang, P., Cheng, M., Zhang, L., et al. (2021). Understanding of the site-specific microbial patterns towards accurate identification for patients with diarrhea-predominant irritable bowel syndrome. *Microbiol. Spectr.* 9:e0125521. doi: 10.1128/Spectrum.01255-21

Zhuravlev, A. V., Vetrovoy, O. V., and Savvateeva-Popova, E. V. (2018). Enzymatic and non-enzymatic pathways of kynurenines' dimerization: The molecular factors for oxidative stress development. *PLoS. Comput. Biol.* 14:e1006672. doi: 10.1371/journal.pcbi.1006672

frontiers | Frontiers in Microbiology

TYPE Original Research
PUBLISHED 30 November 2022
DOI 10.3389/fmicb.2022.1055146



OPEN ACCESS

EDITED BY
Tang Zhaoxin,
South China Agricultural University, China

REVIEWED BY
Wenting Li,
Henan Agricultural University, China
Adeel Sattar,
University of Veterinary and Animal Sciences, Pakistan

*CORRESPONDENCE
Peng Shang
nemoshpmh@126.com

†These authors have contributed equally to this work

SPECIALTY SECTION
This article was submitted to Microorganisms in Vertebrate Digestive Systems, a section of the journal Frontiers in Microbiology

RECEIVED 27 September 2022
ACCEPTED 07 November 2022
PUBLISHED 30 November 2022

CITATION
Chang Z, Bo S, Xiao Q, Wang Y, Wu X, He Y, Iqbal M, Ye Y and Shang P (2022) Remodeling of the microbiota improves the environmental adaptability and disease resistance in Tibetan pigs.
*Front. Microbiol.* 13:1055146.
doi: 10.3389/fmicb.2022.1055146



# Remodeling of the microbiota improves the environmental adaptability and disease resistance in Tibetan pigs

Zhenyu Chang[1,2,3†], Suxue Bo[1,2†], Qingqing Xiao[1,2], Yu Wang[1,2], Xi Wu[1,2], Yuxuan He[1,2], Mujahid Iqbal[4], Yourong Ye[1,2] and Peng Shang[1,2*]

[1]College of Animal Science, Tibet Agriculture and Animal Husbandry University, Linzhi, China, [2]The Provincial and Ministerial Co-founded Collaborative Innovation Center for R & D in Tibet Characteristic Agricultural and Animal Husbandry Resources, Linzhi, China, [3]Key Laboratory of Clinical Veterinary Medicine in Tibet, Tibet Agriculture and Animal Husbandry University, Linzhi, China, [4]Department of Pathology, Cholistan University of Veterinary and Animal Sciences (CUVAS), Bahawalpur, Pakistan

**Introduction:** The establishment of intestinal microbiota and the maintenance of its equilibrium structure plays an important role in Tibetan pigs during different growth stages. Understanding the structure and function of the intestinal microbiota at different growth stages of Tibetan pigs can provide a theoretical basis for guiding nutritional regulation and feeding management in different stages.

**Methods:** Fecal samples were collected from the Tibetan piglets at different growth stages, and the 16S rRNA was sequenced to analyze the changes of intestinal microbiota.

**Results:** Alpha and Beta diversity indexes showed that the diversity of the intestinal microbiota did not change during the three growth stages, and the main components of intestinal microbiota were not significantly different. At the phylum level, Firmicutes and Bacteroidetes were dominant and abundant at different growth stages and were not restricted by age. At the genus level, Streptococcus, Lactobacillus, and Bifidobacterium were the most dominant in the TP10d and TP40d groups, Streptococcus was the most dominant in the TP100d group, followed by Treponema_2 and Lactobacillus. Fusobacteria, Gluconobacter, and Synergistetes were found to be specific genera of 10-day-old Tibetan piglets by LEfSe combined with LDA score. The change of diet made Tenericutes and Epsilonbacteraeota, which are closely related to digestive fiber, become specific bacteria at the age of 40 days. With the consumption of oxygen in the intestine, obligate anaerobes, such as Verrucomicrobia, Fibrobacter, and Planctomycetes, were the characteristic genera of 100 days. KEGG function prediction analysis showed that the intestinal microbiota function of Tibetan pigs changed dynamically with the growth and development of Tibetan piglets.

**Discussion:** In conclusion, the structure and composition of the intestinal microbiota of Tibetan pigs are significantly different at different growth and development stages, which plays an important role in their immune performance.

KEYWORDS

Tibetan pig, growth stage, intestinal microbiota, 16S rRNA sequencing, Tibet

## Introduction

Tibetan pig is a unique and geographically isolated pig breed living in the high-altitude area of the Qinghai–Tibet Plateau in China (Zhao et al., 2019). It is a typical highland miniature pig breed and is often used as an experimental material in the study of pig growth traits. Tibetan pigs are widely distributed in southeast Tibet, Sichuan Ganzi and Aba, Yunnan Diqing, and Gannan region. These pigs mainly live in the mountains, valleys, forests, and grassland. Their excellent features such as bearing high-altitude weather environment and disease resistance are closely related to the unique Tibetan pig intestinal flora (Yang et al., 2011; Shang et al., 2021). However, harsh natural conditions combined with extensive feeding and management also lead to a slow growth rate and low reproductive performance (Chen et al., 2014; Wang et al., 2017). For a long time, Tibetan pigs have been one of the main sources of meat for the Tibetan people. It is reported that these pigs are being raised in Tibet since the seventh century (Ma et al., 2019). Their population has experienced a lot of genetic differentiation, but Tibetan pigs of different populations can well adapt to the harsh plateau environment (Ai et al., 2014). For example, crude feeding tolerance is generally considered to be related to the ability of Tibetan pigs to digest fiber foods. As far as Tibetan pigs are concerned, digestive enzymes secreted by themselves cannot decompose fibrous substances, and can only rely on the function of microorganisms in the gut, especially in the cecum and colon.

Intestinal microbial flora composition of pig and human are similar, mostly including bacteria, archaea, eukaryotic organisms. There are about 1,000 kinds of intestinal microbes mainly anaerobic bacteria and facultative anaerobic bacteria. Anaerobic bacteria such as lactobacillus are accounted for more than 99% in the maintenance of physical health, improvement of immunity and nutrients absorption metabolism. However, aerobic bacteria and facultative anaerobic bacteria account only for about 1% (Kim and Isaacson, 2015; Donaldson et al., 2016; Xiao et al., 2017). There are significant differences in the intestinal microbiota of pigs at different stages. During the embryonic period, the intestinal tract is in a sterile state. During parturition, microorganisms, mainly *E. coli* and Staphylococcus, begin to appear under the influence of the maternal birth canal, feces, and the surrounding environment (Pluske, 2016). At different growth stages, the dominant bacteria in the intestinal tract of pigs are mainly Firmicutes and Bacteroides. The dominant bacteria in the intestinal tract of pigs are closely related to the regulation of autoimmunity. These dominant bacteria in the intestinal tract see a change with age and external environment accordingly (Isaacson and Kim, 2012).

The gastrointestinal microbiota of pigs is a heterogeneous ecosystem dominated by bacteria (Yang H. et al., 2017), and intestinal bacteria exert a significant impact on the host nutrition, physiology and immune processes in a variety of ways (Maltecca et al., 2020). With the emergence of low-cost and high-throughput sequencing technology, studies on animal intestinal microbiota have increased dramatically. Commercial pigs are expensive to feed, have a long growth cycle, and are difficult to deal with. Therefore, many studies mainly focus on the composition and diversity of intestinal microbiota in pigs at a certain stage, but there are few studies on the overall longitudinal changes of intestinal microbiota dynamics in Tibetan pigs at different growth stages (Armougom and Raoult, 2009; Crespo-Piazuelo et al., 2018; Bergamaschi et al., 2020). Therefore, studying the characteristics of intestinal microbiota at different growth stages of Tibetan pigs can play an important role in the healthy growth of Tibetan pigs, and can better reveal the composition and balance mechanism of intestinal microbiota at different growth stages, which is of great significance for the development of plateau animal husbandry.

With the development of microbiome, metabolomics, aseptic technology, and fecal microbiota transplantation (FMT) technology, the role of porcine intestinal microbiota in nutrient digestion, absorption and utilization has gradually become a hot topic. The dynamic balance of intestinal microbiota in pigs is an important prerequisite to ensure the normal digestion, absorption, and metabolism of nutrients. Therefore, this study aims to explore the characteristics of intestinal microbiota in Tibetan pigs at different growth stages, in order to provide a reference study of the interaction mechanism between intestinal microbiota and host and to provide a basis for using intestinal microbiota as a regulatory target to improve intestinal health and improve production performance of pigs. In this study, we collected fecal samples from Tibetan piglets at 10 days (piglet), 40 days (nursery period), and 100 days (finishing period), and

16S rRNA gene high-throughput sequencing method was used to explore the longitudinal changes of intestinal microbiota at different growth stages.

# Materials and methods

## Sample collection

The current study was conducted on the Tibetan Plateau, the highest distribution of grazing pig species in the world. The experimental samples were collected from the experimental base of Tibet Agriculture and Animal Husbandry College in Nyingchi City, Tibet Autonomous Region (average altitude 2,980 m, longitude 94.34°, latitude 29.67°). Fresh fecal samples were collected from 6 Tibetan pigs with similar body weight in each litter at three time points of birth day 10 (piglet), day 40 (nursery period), and day 100 (finishing period). There were 6 Tibetan piglets, 6 nursery pigs, and 6 finishing pigs (labeled as TP10d-1, TP10d-2, TP10d-3, TP10d-4, TP10d-5, TP10d-6, TP40d-1, TP40d-2, TP40d-3, TP40d-4, TP40d-5, TP40d-6, TP100d-1, TP100d-2, TP100d-3, TP100d-4, TP100d-5, TP100d-6). These pigs were fed in half indoor feeding way, feeding without antibiotic with fodder, raising management were in accordance with the conventional procedures. Insect repellent and vaccination were done regularly, all pigs were free to gather at the feed and drinking water points. Stool samples were collected on the same day after getting target age and were mixed with litter of piglets samples as a group, cryopreserved in tubes at −80°C.

## Total DNA extraction, PCR amplification, high throughput sequencing

Fecal genomic DNA extraction kit (Guangzhou Meiji Biotechnology Co., LTD., D3141) was used to extract the total DNA from fecal samples. The concentration and purity of DNA were detected by 1% agarose gel. The total amount of DNA was determined using a Nano Drop NC 2000 (Thermo Fisher Scientific). The V3–V4 region of 16S rRNA gene was selected as the target fragment for amplification. For PCR the pre-primer sequence used was: 341F (5′-CCTACGG GNGGCWGCAG-3′) and 806R was: (5′-GGACTACHVGGGTATCTAAT-3′). The samples were uniformly diluted to 20 ng $\mu L^{-1}$ as a template for PCR amplification. Amplification system (25 μL) was: PCR-Mix 12 μL, upstream primer (10 μm) 1 μL, downstream primer (10 μm) 1 μL, DNA template 2 μL, DD $H_2O$ 9 μL. The amplification parameters were as follows: pre-denaturation at 98°C for 2 min, denaturation at 98°C for 15 s, annealing at 55°C for 30 s, extension at 72°C for 30 s, 30 cycles, and extension at 72°C for 5 min. PCR products from the same sample were mixed and recovered on 2% agarose gel. AxyPrep DNA Gel Extraction Kit (Axygen Biosciences, Union City, CA, USA) was used to purify the recovered products. The recovered products were detected by 2% agarose gel electrophoresis and quantified by Quantus™ Fluorometer (Promega, USA). Illumina Mi Seq PE250 sequencer was used for sequencing.

## Bioinformatics and statistical analysis

In order to obtain accurate and reliable results in subsequent bioinformatics analysis, paired-end clean reads were merged as raw tags using FLSAH (Magoč and Salzberg, 2011) (version 1.2.11) with a minimum overlap of 10 bp and mismatch error rates of 2%. Noisy sequences of raw tags were filtered by QIIME (Caporaso et al., 2010) (version 1.9.1) pipeline under specific filtering conditions (Bokulich et al., 2013) to obtain the high-quality clean tags. Clean tags were searched against the reference database[1] to perform reference-based chimera checking using the UCHIME algorithm.[2] All chimeric tags were removed and finally obtained effective tags were used for further analysis. The effective tags were clustered into operational taxonomic units (OTUs) of ≥ 97% similarity using UPARSE (Edgar, 2013) pipeline. The tag sequence with the highest abundance was selected as a representative sequence within each cluster. Between groups Venn analysis was performed in R project (version 3.4.1) to identify unique and common OTUs. The effective tags were clustered into OTUs of ≥ 97% similarity using UPARSE [4] pipeline. The tag sequence with the highest abundance was selected as a representative sequence within each cluster. Between groups Venn analysis was performed in R project (version 3.4.1) to identify unique and common OTUs. The representative sequences were classified into organisms by a naive Bayesian model using RDP classifier (Wang et al., 2007) (version 2.2) based on SILVA (Pruesse et al., 2007) Database,[3] with the confidence threshold values ranged from 0.8 to 1. The abundance statistics of each taxonomy were visualized using Krona (Ondov et al., 2011) (version 2.6). Biomarker features in each group were screened by Metastats (White et al., 2009) (version 20090414) and LEfSe software (Segata et al., 2011) (version 1.0). Chao1, Simpson, and all other alpha diversity index were calculated in QIIME. OTU rarefaction curve and rank abundance curves were plotted in QIIME. Alpha index comparison between groups was calculated by Welch's *t*-test and Wilcoxon rank test in R project. Alpha index comparison among groups was computed by Tukey's HSD test and Kruskal-Wallis *H*-test in R project. Weighted and unweighted unifrac distance matrix were generated by QIIME. Multivariate statistical techniques including PCA (principal

1 http://drive5.com/uchime/uchime_download.html
2 http://www.drive5.com/usearch/manual/uchime_algo.html
3 https://www.arb-silva.de/

component analysis), PCoA (principal coordinates analysis) and NMDS (non-metric multi-dimensional scaling) of (Un) weighted unifrac distances were calculated and plotted in R project. Statistical analysis of Welch's *t*-test, Wilcoxon rank test, Tukey's HSD test, Kruskal-Wallis *H*-test, Adonis (also called Permanova) and Anosim test were calculated using R project.v. The KEGG pathway analysis of the OTUs was inferred using Tax4Fun (Aßhauer et al., 2015) (version 1.0).

In order to explore the differences of bacterial community structure and diversity in three different growth stages, IBM SPSS 21.0 software was used to analyze the variance of each data. If the variance was significant, Duncan's method was used for multiple comparisons, and the results were expressed as mean ± standard deviation, $P < 0.05$ means significant difference, $P > 0.05$ indicates no significant difference.

# Results

## Sequence analysis

In the current study, 18 samples from three groups were used to conduct amplicon sequencing to investigate the changes in gut microbiota. Results indicated that a total of 2,098,941 (TP10 = 741,257, TP40 = 708,960, TP100 = 648,724) raw sequences were generated (**Table 1**). Furthermore, 1,756,695 (TP10 = 623,221, TP40 = 592,483, TP100 = 540,991) valid sequences were obtained after quality assessment, with an effective rate of over 80%. According to 97% nucleotide-sequence similarity, the effective sequences were clustered into 1,781 OTUs and 654 OTUs were in common. Moreover, the number of unique OTUs in the TP10, TP40, and TP100 groups were 384, 207, and 182, respectively. Notably, rarefaction curves and species rank curve of all samples showed a tendency to saturate, indicating sufficient sequencing evenness and richness.

## Analysis of microbial composition and structure

At the phylum level, the Firmicutes (60.53, 67.37, and 56.51%) and Bacteroidetes (20.88, 13.32, and 25.45%) were abundantly present in TP10d, TP40d, and TP100d groups, regardless of age, which accounted for over 80% of the total taxonomic composition. Other phyla such as Planctomycetes (0.096, 0.23, and 0.52%), Patescibacteria (0.26, 0.33, and 0.15%), Cyanobacteria (0.33, 0.24, and 0.16%), and Kiritimatiellaeota (0.11, 0.15, and 0.28%) in TP10d, TP40d, and TP100d groups were identified in low abundances (**Figures 1A–E**). Among recognized genera, Streptococcus (11.44%, 20.47%), Lactobacillus (10.77%, 11.40%), and Bifidobacterium (4.93%, 7.96%) were the most predominant genus in the TP10d and TP40d groups, whereas the predominant genera observed in the TP100d group was Streptococcus (17.61%), followed by Treponema_2 (8.67%) and Lactobacillus (6.26%) (**Figures 2A–F**).

## Analysis of intestinal microflora diversity in Tibetan pigs at different growth stages

The qualified sequences were aligned to evaluate multiple alpha-diversity indexes that could describe the diversity and abundance of the community. Good's coverage estimations of each group varied from 99.06 to 99.59%, suggesting almost all bacterial phenotypes were identified. Statistical analysis of alpha diversity revealed that there were no obvious differences in the Chao1 (1503.31 ± 175.12 vs. 1622.74 ± 93.44 vs. 1557.03 ± 194.20), ACE (1601.99 ± 193.13 vs. 1729.90 ± 100.53 vs. 1669.86 ± 202.54), Simpson (0.941 ± 0.029 vs. 0.93 ± 0.013 vs. 0.94 ± 0.017), and Shannon (6.17 ± 0.43 vs. 6.32 ± 0.41 vs. 6.53 ± 0.39) indices between the TP10d, TP40d, and TP100d groups, suggesting that the diversity of gut microbiota did not change in Tibetan pigs at this stage. Furthermore, beta diversity analysis showed that the dots in the TP10d, TP40d, and TP100d groups were clustered together, indicating that there was no significant difference in the main components of gut microbiota among the three groups (**Figures 3A–J**).

## Analysis of microbial representation species of Tibetan pig at different growth stages

The previous analysis showed that there were great differences between Tibetan pig group and Yorkshire pig group at the gate level and genus level, so the microbial community composition of the two levels was analyzed, and the results are shown in **Figure 4**. As it can be observed in **Figure 4A**, the top 10 phyla are Firmicutes, Bacteroidetes, Euryarchaeota, Actinobacteria, Fusobacteria, Spirochaetes, Proteobacteria, Synergistetes, Patescibacteria, and Kiritimatiellaeota. The actinomycetes and spirochetes in the colon of Tibetan and Yorkshire pigs were the dominant communities, accounting for 81.15 and 76.26%, respectively. The relative abundance of actinomycetes and spirochetes in Tibetan pigs was significantly higher than that in Yorkshire pigs ($P < 0.05$). There were no significant differences in the relative abundance of other bacteria between Tibetan pigs and Yorkshire pigs ($P > 0.05$). It can be seen from **Figure 4B** that there are great differences in the composition of microflora at the genus level between Tibetan pigs and Yorkshire pigs, and the relative abundance of most microflora in Tibetan pig colon is higher than that of Yorkshire pig group. The relative abundance of Clostridium_sensu_stricto_1 (21.08%),

10.3389/fmicb.2022.1055146

TABLE 1 Quantitative statistics of tags and OTUs.

| Samples name | Raw reads | Clean reads | Raw tags | Clean tags | Chimera | Effective tags | Effective ratio (%) | OTUs |
|---|---|---|---|---|---|---|---|---|
| TP40-1 | 125,780 | 125,681 | 124,108 | 123,296 | 18,320 | 104,976 | 83.46 | 1,644 |
| TP40-2 | 125,197 | 125,091 | 123,632 | 122,970 | 18,363 | 104,607 | 83.55 | 1,568 |
| TP40-3 | 129,850 | 129,726 | 128,063 | 127,361 | 18,699 | 108,662 | 83.68 | 1,524 |
| TP40-4 | 117,609 | 117,482 | 116,084 | 115,272 | 16,278 | 98,994 | 84.17 | 1,381 |
| TP40-5 | 115,966 | 115,839 | 114,410 | 113,822 | 17,423 | 96,399 | 83.13 | 1,422 |
| TP40-6 | 94,558 | 94,474 | 93,342 | 92,961 | 14,116 | 78,845 | 83.38 | 1,402 |
| TP100-1 | 96,350 | 96,263 | 95,089 | 94,616 | 14,612 | 80,004 | 83.03 | 1,171 |
| TP100-2 | 76,337 | 76,283 | 75,270 | 74,952 | 10,903 | 64,049 | 83.9 | 1,203 |
| TP100-3 | 114,888 | 114,778 | 113,447 | 112,769 | 17,182 | 95,587 | 83.2 | 1,622 |
| TP100-4 | 116,116 | 116,013 | 114,499 | 113,713 | 16,959 | 96,754 | 83.33 | 1,392 |
| TP100-5 | 123,126 | 123,035 | 121,522 | 120,787 | 18,626 | 102,161 | 82.97 | 1,620 |
| TP100-6 | 121,907 | 121,825 | 120,413 | 119,582 | 17,146 | 102,436 | 84.03 | 1,463 |
| TP10-1 | 131,700 | 131,605 | 129,911 | 129,284 | 19,352 | 109,932 | 83.47 | 1,476 |
| TP10-2 | 134,758 | 134,668 | 133,054 | 132,312 | 20,231 | 112,081 | 83.17 | 1,530 |
| TP10-3 | 120,261 | 120,189 | 118,720 | 117,858 | 16,431 | 101,427 | 84.34 | 1,141 |
| TP10-4 | 128,071 | 127,968 | 126,198 | 125,622 | 18,784 | 106,838 | 83.42 | 1,598 |
| TP10-5 | 109,240 | 109,137 | 107,768 | 107,222 | 15,332 | 91,890 | 84.12 | 1,312 |
| TP10-6 | 117,227 | 117,121 | 115,330 | 114,819 | 13,766 | 101,053 | 86.2 | 1,393 |

Lactobacillus (10.44%), Sporobacillus (6.98%), Streptococcus (6.50%), and Ruminococcaceae_UCG-005 (3.36%) in the colon microbiota of Tibetan pigs was significantly higher than that of Yorkshire pigs (Clostridium_sensu_stricto_1 7.73%, Lactobacillus 1.83%, Bacillus 4.53%). Streptococcus 2.90% and Ruminococcaceae_UCG-005 2.36%) ($P < 0.05$).

To further assess the changes in the gut microbiota of piglets at different ages, LEfSe combined with LDA scores were used for identifying the specific taxa associated with age change (**Figure 5**). At the phylum level, Verrucomicrobia, Fibrobacteres, and Planctomycetes were significantly more preponderant in the TP100d group than in the TP40d and TP10d groups, while the abundances of the Fusobacteria, Gluconobacter, and Synergistetes were dramatically increased in TP10d group in comparison with TP100d and TP40d groups. Additionally, the levels of Tenericutes and Epsilonbacteraeota tended to be higher in the TP40d group than TP100d and TP10d groups. We also observed that several genera such as Frateuria, Bacteroides, Prevotellaceae_UCG_004, Prevotellaceae_UCG_001, Oscillibacter, Chlamydia, Fructobacillus, Quinella, Prevotellaceae_NK3B31_group, Lachnospiraceae_UCG_001, Cetobacterium, Ruminococcus_1, Tatumella, Coprobacter, Lachnospiraceae_NK4B4_group, Family_XIII_UCG_001, Methylotenera, Ruminococcaceae_UCG_010, Anaerorhabdus_furcosa_group, Sphaerochaeta, Thiobacillus, Ruminococcaceae_UCG_009, Gluconobacter, Oenococcus, Family_XIII_AD3011_group, p_1088_a5_gut_group, Lachnospiraceae_NK4A136_group, Fibrobacter, Ruminococcaceae_UCG_013, Akkermansia, Marvinbryantia, and Lachnospiraceae_XPB1014_group were the most dominant bacteria in the TP100d group as compared to TP10d and TP40d groups, whereas the proportions of Geobacillus, Escherichia_Shigella, Bradyrhizobium, Marivita, Megamonas, Marivivens, Acetobacter, Prauserella, LD29, Candidatus_Arthromitus, Helicobacter, Staphylococcus, Clostridium_sensu_stricto_15, NS3a_marine_group, Rubrobacter, Ureaplasma, Enterococcus, Cloacibacterium, Saccharofermentans, Erysipelatoclostridium, Caproiciproducens, Leuconostoc, dgA_11_gut_group, Eubacterium_eligens_group, Stenotrophomonas, DTU089, Ralstonia, Alteribacillus, Clostridium_sensu_stricto_7, Paraburkholderia, and CHKCI001 were significantly higher in the TP40d group than in the other two groups. Moreover, the TP10d group was significantly found enriched in Pasteurella, Rothia, Olsenella, Coprococcus_1, Fluviicola, Holdemanella, Globicatella, Candidimonas, Pseudomonas, Parvimonas, Dorea, Gemella, Lachnospiraceae_FCS020_group, Dietzia, Agathobacter, Erysipelotrichaceae_UCG_002, Erysipelotrichaceae_UCG_007, Erysipelotrichaceae_UCG_006, Erysipelotrichaceae_UCG_009, CPla_4_termite_group, Eggerthellaceae.DNF00809, Tissierella, Ruminococcus_gauvreauii_group, Fermentimonas, Roseburia, CAG_873, Actinomyces, Prevotella_7, Blautia, Dialister, Proteiniphilum, Taibaiella, Sediminibacterium, Denitrobacterium, Arcanobacterium, Leucobacter, Aequorivita, Ruminococcaceae_UCG_003, Pelomonas, Synergistia, Cloacibacillus, Atopobium, Peptostreptococcus, Shuttleworthia, Paeniglutamicibacter, Sharpea, Fusobacterium, Odoribacter, Enterorhabdus, Pseudoscardovia, Proteiniclasticum,

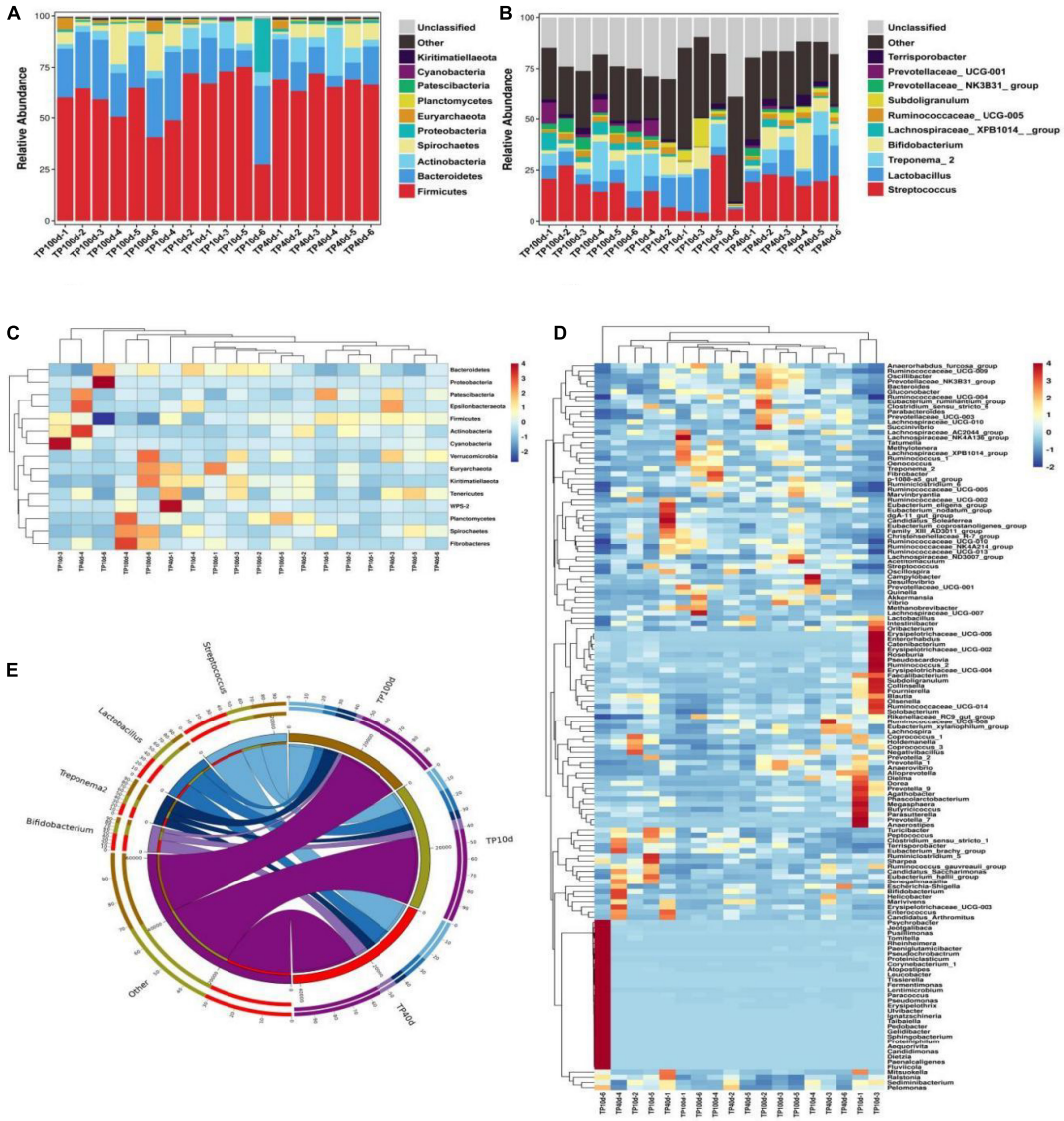


FIGURE 1
Relative abundance and heat map of intestinal microflora in Tibetan pig at phylum and genus levels at different growth stages. **(A,B)** Represent the community distribution at the phylum and genus level, respectively. **(C)** Heat maps of the top 17 common gates in different communities. **(D)** Heat maps of the top 96 common genera in different communities. Each color block in the heat map represents the relative abundance of a genus in the sample. Clustering can distinguish taxons with different abundance, and color gradient and similarity is reflecting the similarities and differences of multiple samples at different classification levels. The blue-red gradient shows the change of abundance from low to high. **(E)** The composition of microorganisms among horizontal species.

Senegalimassilia, Acidaminococcus, Filifactor, Catenibacterium, and Collinsella compared with TP100d and TP40d group.

## Prediction of microbial ecological function of Tibetan pigs at different growth stages

Principal coordinate analysis was performed to analyze the differences of intestinal flora at different growth stages. At the phylum level, the intestinal microbiota structure of suckling and nursery piglets slightly crossed but could be completely separated from that of newborn piglets (Figure 6A). At the genus level, piglets were able to fully separate their gut organisms at the three stages (Figure 6B).

In conclusion, the succession of intestinal microbiota changed significantly with increase in the age of pig. After using PICRUSt to predict the function of microorganisms, it was found that the function of intestinal microbiota changed dynamically with the growth and development of

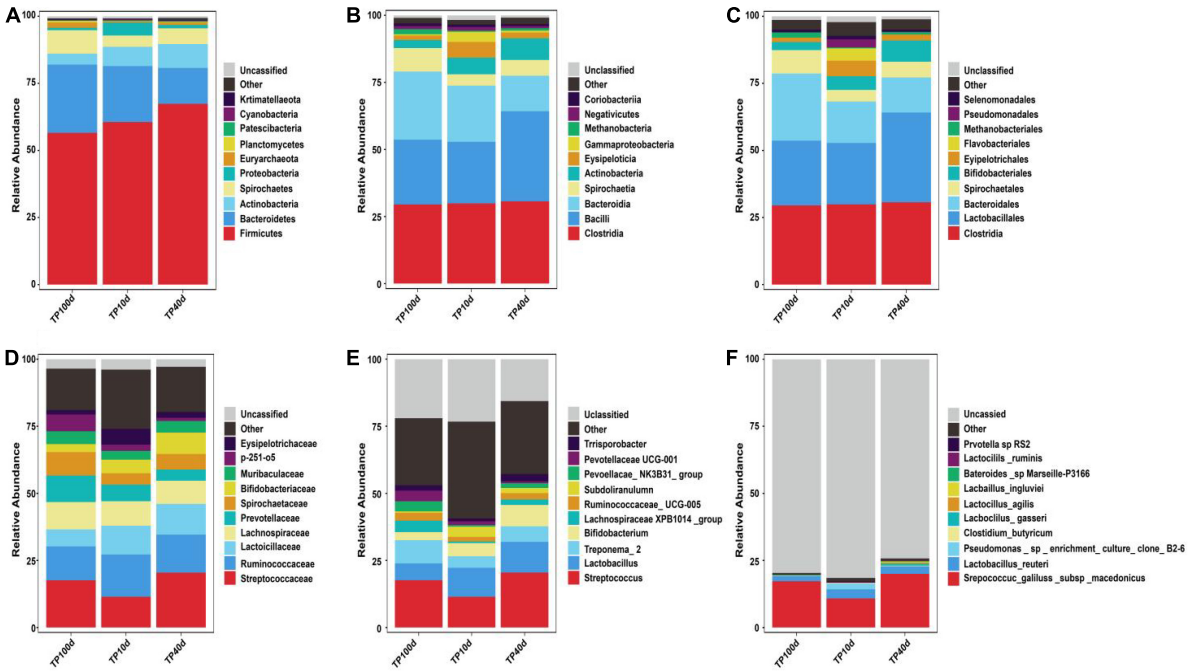


FIGURE 2
Relative abundance (Top10) of intestinal microflora in Tibetan pigs. At boundary **(A)**, phylum **(B)**, class **(C)**, order **(D)**, family **(E)**, and genus **(F)** levels at different growth stages.

Tibetan pigs, and the microbial communities of the three groups of Tibetan pigs were mainly related to metabolism, disease function, cell transformation, genetic information processing, and environmental information processing, etc. The abundance of microbial communities for infectious diseases and immune diseases was the highest on the 10th day, and then showed a downward trend. Opposite pathways such as immune system, transcription, cellular community—Prokaryotes, transport and catabolism, and neurodegenerative diseases showed an increasing trend and reached the highest abundance at 100 days (**Figure 6C** and **Table 2**).

## Discussion

Tibetan pigs are the main pig species on the Qinghai–Tibet Plateau, distributed in mountains, valleys, forests, and grasslands with an altitude of 2,900–4,100 m (Zhang et al., 2015). Age and microecological space of the host dynamically change under the influence of dietary composition, nutrient level, and environmental factors. Age, intake of solid feed, and weaning were the main driving forces of succession and establishment of intestinal microbial population in piglets (10 days). The stable intestinal microbiota was not established in piglets at early weaning. The introduction of solid diet and environmental changes disrupted the balance of intestinal microbiota in piglets, resulting in the deterioration of their health status and growth performance. The growth process of nursery pigs (40 days) accompanied by a series of adverse factors, such as house transfer, feeding mode, and feed change leads to the disorder of intestinal flora of nursery pigs. Diet was the dominant factor (57%) affecting the number and composition of intestinal microorganisms in finishing pigs (100 days), which was related to the health level and growth performance of finishing pigs. There are few studies on the longitudinal changes of intestinal microbiota in Tibetan pigs at different growth stages. Understanding the structure and function of intestinal microbiota in Tibetan pigs at different growth stages can provide a theoretical basis for guiding nutritional regulation and feeding management at different stages. With the increasing demand, Tibetan pig farming is gradually developing to a larger scale (Zhang et al., 2017). The gastrointestinal tract of pig has diverse and complex microbial communities. However, the composition of gut microbiota is not immutable, and its composition and ecological succession are determined by many complex internal and external factors. The gastrointestinal microbiome of pigs contains thousands of different microbial species, such as Firmicutes, Bacteroidetes, and Proteobacteria (Holman et al., 2017). The gastrointestinal tract of pigs begins to be colonized by microorganisms shortly after birth and gradually becomes stable over the time (Faith et al., 2013). The changes of intestinal microbiota structure can affect the health status and growth performance of pigs. Metagenomic analysis of fecal microbiota of piglets with diarrhea by Yang Q. et al. (2017) showed

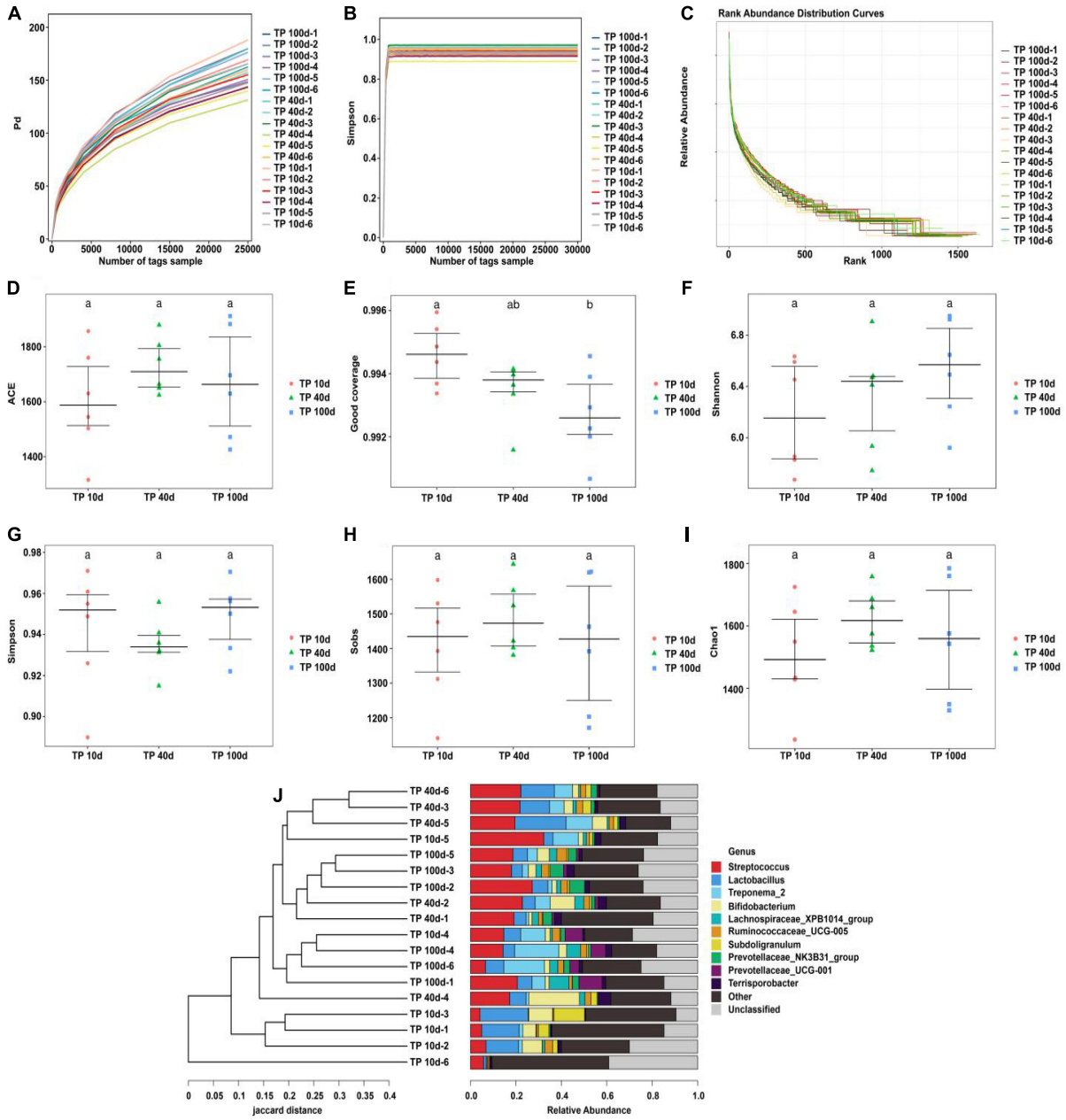


FIGURE 3
Microbial diversity in colon of Tibetan pig at different growth stages. **(A)** PD diversity index curve. **(B)** Simpson diversity index curve. **(C)** Rank abundance curve. **(D–I)** Alpha diversity index (Simpson, PD, Good's coverage, Shannon, Chao1, and ACE). **(J)** UPGMA cluster tree. Each curve represents a sample.

that diarrhea was associated with increased relative abundance of Prevotella, Sudella, Campylobacter, and Fusobacteriaceae bacteria. Therefore, it is important to understand the changes in intestinal microbiota during pig growth and development. Liu et al. (2019) found in their study that the intestinal microbes of piglets changed a lot before and after weaning. Bacteroides had the highest content in the intestinal tract within 1 week of birth. After weaning, this dominant position was replaced by Prevotella, which was closely related to fiber digestion. The finishing period occupies a large proportion in the whole breeding cycle of pigs. Although the composition and structure of intestinal microorganisms in pigs in the finishing period remain relatively stable, they are still in a state of dynamic change. With the progress of the finishing period, the level of Firmicutes in pig manure increases while the level of Bacteroides decreases (Ban-Tokuda et al., 2017). It is well

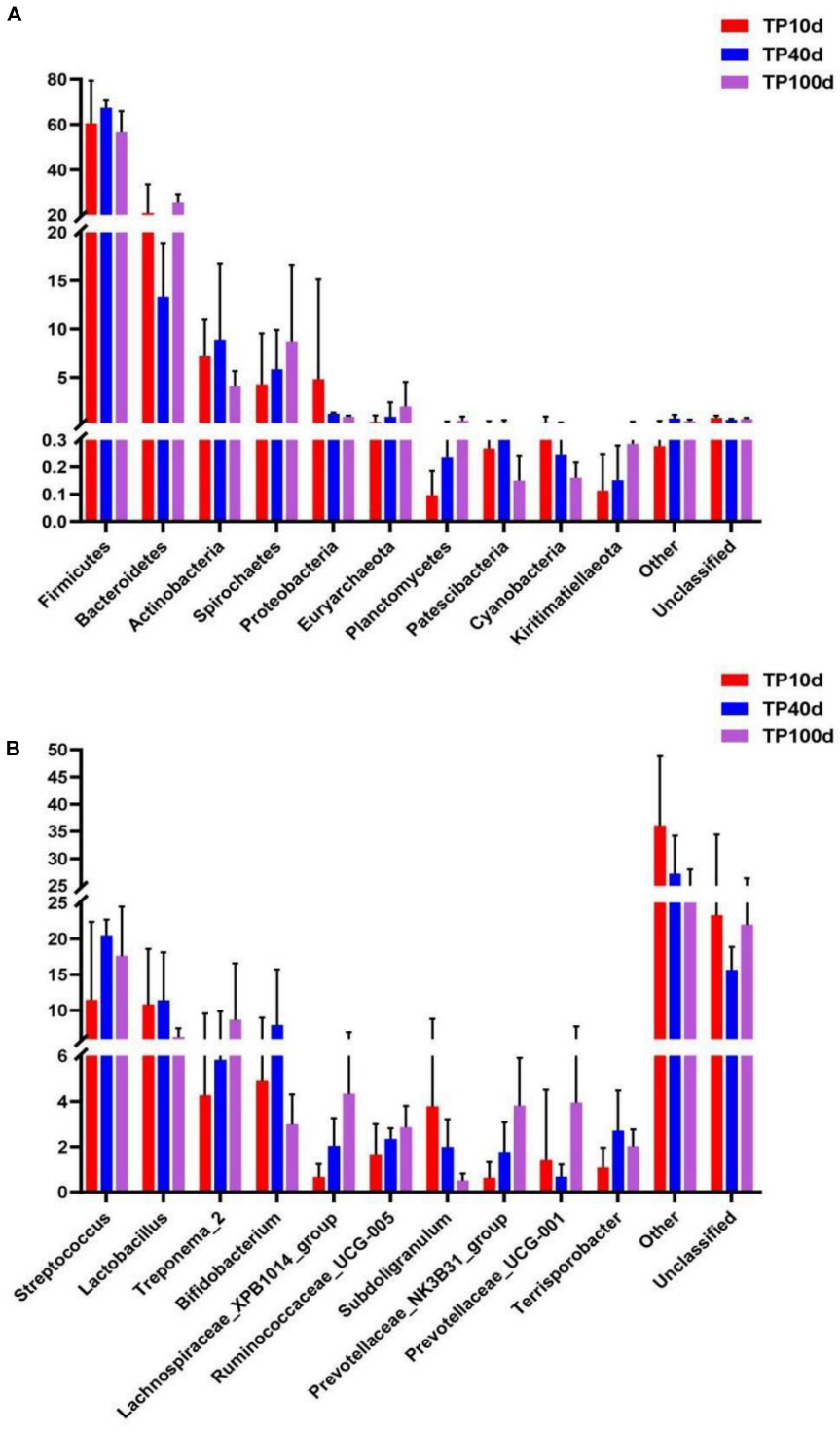


FIGURE 4
Comparison of community differences in intestinal microbial composition between Tibetan pigs. At phyla level **(A)** and genus level **(B)**. All data represent averages.

known that diversity can improve the stability and function of gut microbiota, and in particular, gut microbiota diversity has been considered as a novel biomarker of health and metabolic activity (Clarke et al., 2014). At present, the gut microbiome of pigs at a certain growth stage is well understood, but still there is a lack of comprehensive longitudinal studies on the

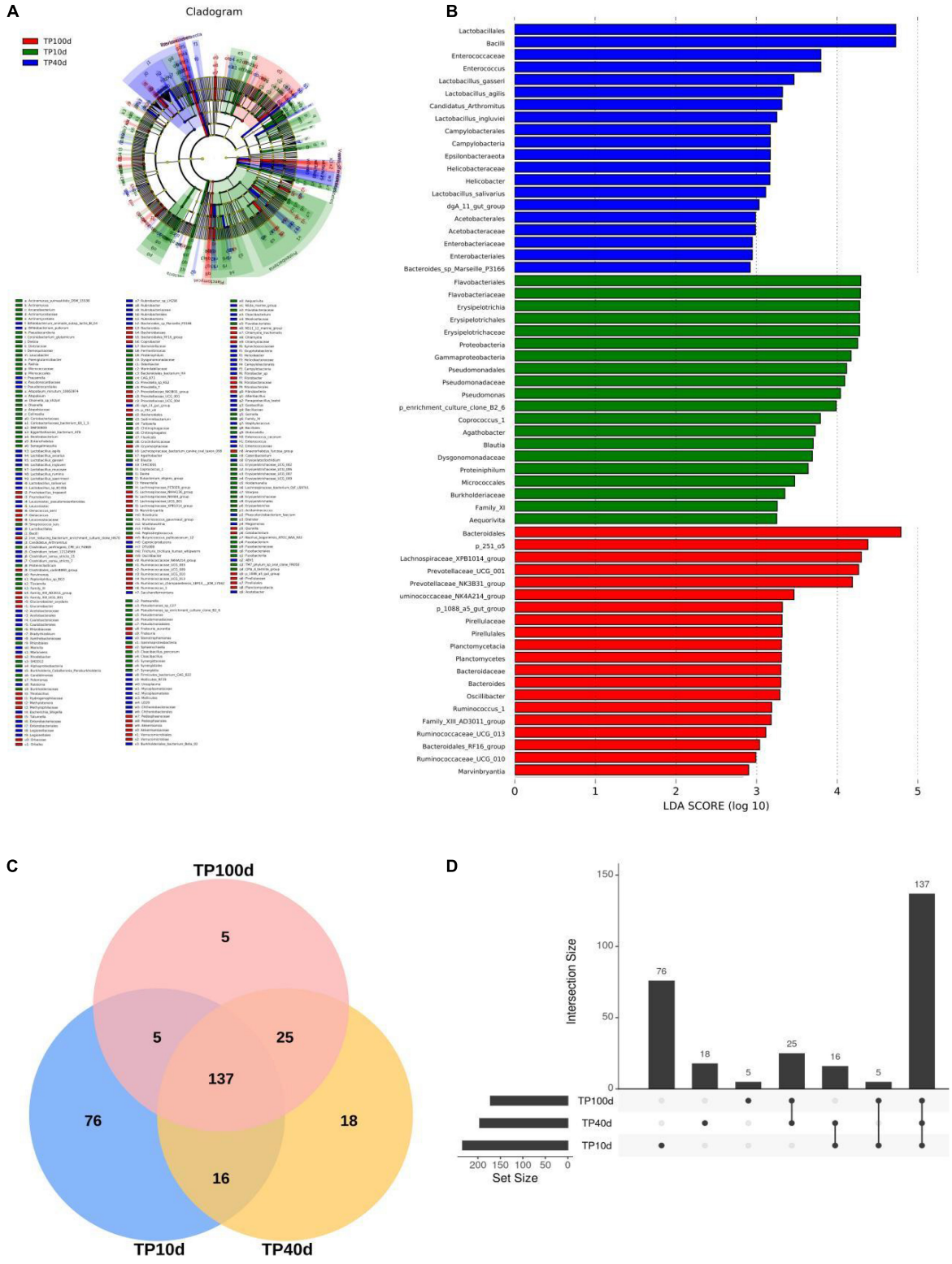


FIGURE 5
Comparison of differences in gut microbiota of pigs at different days of age. **(A)** and **(B)** are LEfSe analysis plots. **(C)** Venn plots of different age groups; **(D)** Figure shows the difference of gut microbiota between different days of age.

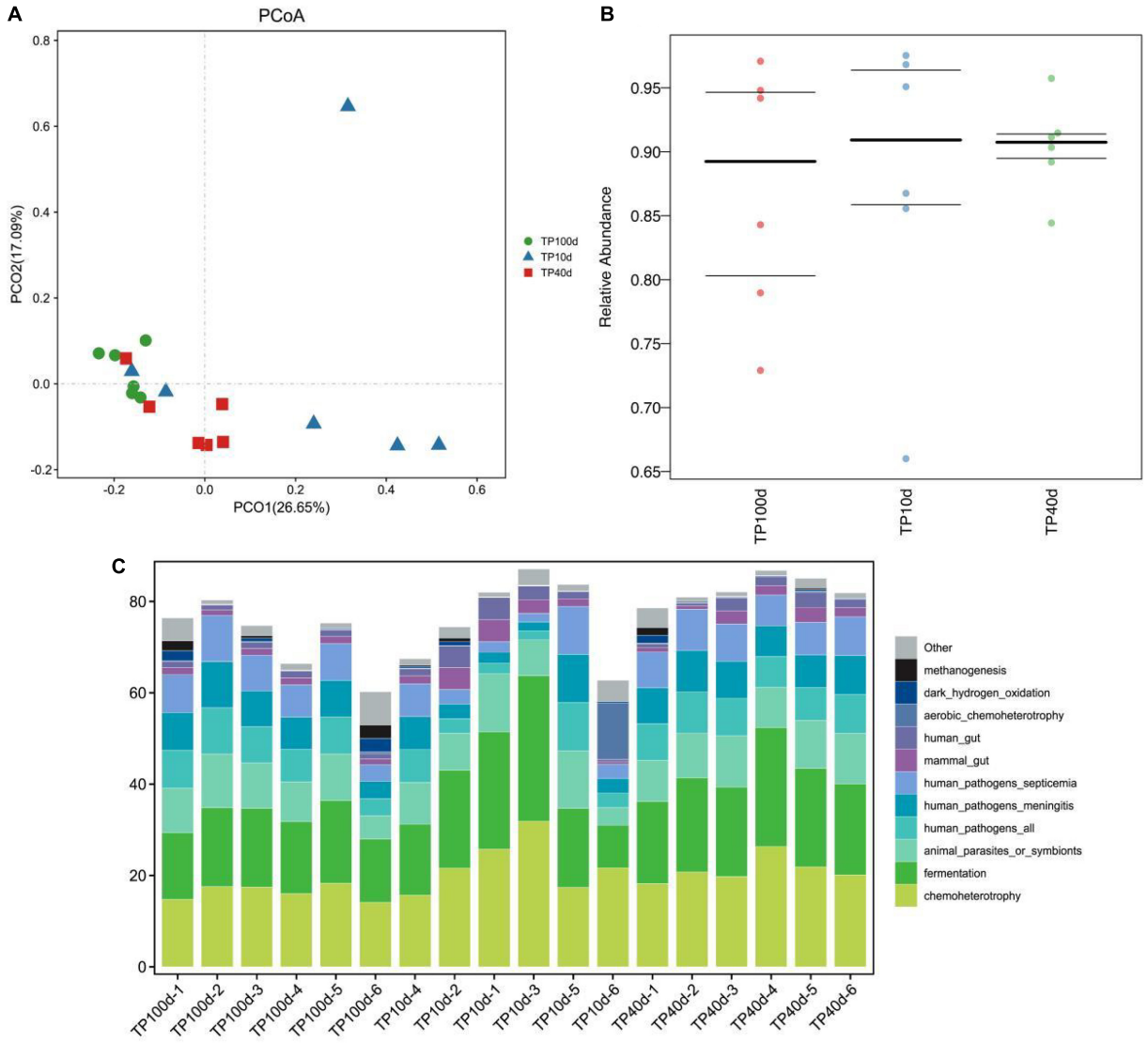


FIGURE 6
Prediction of intestinal microbial ecological function of Tibetan pig at different growth stages. **(A,B)** PCoA analysis of group TP10d, TP40d, and group TP100d at the genus level. Each point represents a sample. The distance between the two points indicates the difference in fecal microbiota. (CmurF) TP10d, TP40d, and TP100d intestinal microbial ecological function prediction **(C)**.

dynamics of gut microbiome in Tibetan pigs at different growth stages. Therefore, we collected fecal samples of Tibetan pig at three growth stages, 10, 40, and 100 days in order to observe gut microbes and its influencing factors for the sake of adopting new strategies to regulate the intestinal microbiome, thereby enhancing the Tibetan pig intestinal health and growth performance.

The results of this study showed that there was no significant change in the diversity of intestinal microbiota of Tibetan pigs at three growth stages of Tibetan piglets, nursery pigs, and finishing pigs. According to the Alpha diversity of intestinal microbiota in Tibetan pigs at three developmental stages, the intestinal microbiota diversity of piglets increased significantly from birth to 10 days, and reached the highest level at the time of conservation. Mi et al. (2019) found that the Alpha diversity of gut microbiota in miniature pigs increased dramatically with the age, increasing to about 20 weeks and then fluctuating slightly throughout life. Similar diversity results have been found in human infant gut microbiota studies (Chernikova et al., 2018). This indicates that the development of intestinal microbiota of newborn piglets is basically the same as that of human beings. When exposed to various bacteria in the environment, the number and diversity of intestinal microbiota will increase rapidly, which is also the key to the development of intestinal microbiota. The research results of Backhed et al. (2005) and Leamy et al. (2014) showed that intestinal microbes have a wide

TABLE 2 Functional prediction of three groups of Tibetan pigs at different growth stages.

| Level_1 | Level_2 | TP40d | TP100d | TP10d |
|---|---|---|---|---|
| M | Carbohydrate metabolism | 260258.26 | 235265.96 | 265604.65 |
| M | Amino acid metabolism | 226694.69 | 213477.11 | 237281.99 |
| M | Metabolism of cofactors and vitamins | 214941.12 | 212421.52 | 221398.83 |
| M | Metabolism of terpenoids and polyketides | 162783.19 | 156734.83 | 172590.53 |
| M | Metabolism of other amino acids | 130978.09 | 117769.43 | 135952.77 |
| M | Lipid metabolism | 115140.38 | 94428.19 | 117474.1 |
| M | Energy metabolism | 96341.41 | 93074.48 | 101534.38 |
| M | Xenobiotics biodegradation and metabolism | 68869.13 | 57360.06 | 79682.61 |
| M | Glycan biosynthesis and metabolism | 56872.72 | 62626.92 | 61897.43 |
| M | Biosynthesis of other secondary metabolites | 41830.91 | 39899.42 | 41342.17 |
| M | Nucleotide metabolism | 40132.12 | 37772.72 | 40656.26 |
| GIP | Replication and repair | 118594.29 | 110072.92 | 121111.32 |
| GIP | Translation | 67531.76 | 63224.36 | 67091.48 |
| GIP | Folding, sorting, and degradation | 56622.48 | 53839.83 | 59120.81 |
| GIP | Transcription | 17936.21 | 18581.63 | 19640.47 |
| CP | Cell motility | 37998.58 | 41324.13 | 40583.28 |
| CP | Cell growth and death | 28246.43 | 27082.34 | 29229.23 |
| CP | Transport and catabolism | 4071.36 | 4109.7 | 4538.6 |
| CP | Cellular community—prokaryotes | 3155.53 | 3228.19 | 3518.75 |
| EIP | Membrane transport | 41220.89 | 34078.72 | 43818.69 |
| EIP | Signal transduction | 6546.61 | 6040.1 | 7256.9 |
| EIP | Signaling molecules and interaction | 0.32 | 0.11 | 0.63 |
| OS | Environmental adaptation | 3435.12 | 3466.01 | 3764.5 |
| OS | Endocrine system | 1832.36 | 1757.39 | 1840.6 |
| OS | Immune system | 898.55 | 1079.07 | 1126.72 |
| OS | Digestive system | 498.84 | 788.5 | 584.71 |
| OS | Excretory system | 0.02 | 0.01 | 0.26 |
| HD | Infectious diseases | 5316.17 | 4497.89 | 4761.07 |
| HD | Neurodegenerative diseases | 219.83 | 503.03 | 715.67 |
| HD | Cardiovascular diseases | 0.27 | 0 | 6.34 |
| HD | Immune diseases | 0.09 | 0.04 | 0.08 |

M, Metabolism; GIP, Genetic Information Processing; CP, Cellular Processes; EIP, Environmental Information Processing; OS, Organismal Systems; HD, Human Diseases.

range of functions and are involved in almost all life processes, including resistance against potential pathogens, absorption of different kinds of nutrients, regulation of host immune system, fat deposition traits, chronic diseases, etc. Gut microbiota contributes greatly to the host health and nutrient digestion (Coleman et al., 2018; Kumar et al., 2018; Zitvogel et al., 2018; Lei et al., 2021). The results of PCoA analysis also showed that the composition of intestinal microbiota was different at different time periods from 10 to 100 days of birth, indicating that the structure and composition of intestinal microbiota may change greatly with the passage of time.

At the genus level, Ruminococcus appeared during lactation and reached its highest abundance during the finishing period. Ruminococcus is the main producer of butyric acid in the intestine, which can provide about 70% of the energy for intestinal epithelial cells (Serpa et al., 2010). Butyrate, a type of short-chain fatty acid, has been shown to be beneficial for intestinal development and maintenance of intestinal health in mammals and has immune defense functions (Ratajczak et al., 2019). The main bacteria producing butyrate are anaerobic bacteria, and the low oxygen concentration in the intestine creates a favorable environment for anaerobic bacteria. At the same time, butyrate absorbed and metabolized by the epithelium can consume oxygen in the intestine, thereby stabilizing hypoxia-inducible factor (HIF, a transcription factor that orchestrates barrier protection) and protect the barrier function of the epithelium (Kelly and Colgan, 2016). In addition, this study found that Lactobacillus was present in all three time periods. However, its abundance reached the highest in the fattening period. This is maybe due to change in feed, from breastfeeding to fattening period, the piglets feed change from milk to difficult feed digestion and

absorption of solid particles. So, they were in need of more lactobacillus. This also illustrates the lactic acid bacteria help in maintaining the stability of the intestinal bacteria of piglets and increase the beneficial effects of piglet adaptability to the environment.

In this study, LEfSe combined with LDA score method was used to analyze and identify the specific microorganisms of intestinal flora of different age pigs at the phyla level. It was found that the intestinal specific bacteria at 10 days were mainly Fusobacteria, Gluconobacter, and Synergistetes. The pattern of nutrient intake has a big impact on the development of gut microbiota. For example, when piglets switch from breast feeding to a solid diet, the abundance of microbes associated with digestive fiber in their gut microbiota changes significantly. In this study, it was found that Tenericutes and Epsilonbacteraeota were specific bacteria for the nursing pigs (TP40d), and Verrucomicrobia, microbacillus, and Planctomycetes were specific bacteria for the finishing pigs (TP100d). Wang et al. (2019) found that the abundance of Prevotella was low in the lactation period and significantly increased after weaning, and continued to increase in the nursery and growth period, and got decreased in the fattening period. Prevotella is a Gram-negative anaerobe of the Bacteroidete phylum, which can ferment dietary fiber to produce short-chain fatty acids (Franke and Deppenmeier, 2018). The intestinal microbiota is closely related to the digestive function and dietary pattern of the host, which together exert an important influence on the growth and development of the host.

During growth and development, the development of mammalian gut microbiota is affected by breed, age, and diet, and reaches stability at maturity. The results of this study showed that Firmicutes (60.53, 67.37, and 56.51%) and Bacteroides (20.88, 13.32, and 25.45%) were the dominant phyla of intestinal flora in Tibetan pigs during the three growth stages. Pajarillo et al. (2014) explored the similarities and differences of fecal microbial communities of Duroc, Landrace, and Yorkshire pig by 16S rRNA gene sequencing, and found that at the phylum level, most sequences were classified into Firmicutes and Bacteroides regardless of pig breeds. But the abundance of gut microbiota changes during pig development. At the phylum level, Firmicutes and Bacteroidetes showed an increasing trend at different growth stages.

In this study, KEGG functional prediction analysis showed that the function of intestinal microbiota changed dynamically with the growth and development of piglets, among which the abundance of metabolic pathways such as cancer, neurodeformation disease and drug resistance was the highest at 0 day, and then decreased. This indicates that the gastrointestinal tract of piglets is immature at birth, and the intestinal microbiota is not fully developed, and the diversity is low, which is easy to be invaded by pathogens. On the contrary, pathways of immune system, biosynthesis, replication and repair of other secondary metabolites increased with the growth and development of piglets, and the highest abundance was observed at 40 days. Mi et al. (2019) also found that the relative abundance of secondary metabolism such as terpenoids and polyketides increased significantly with increasing age. This indicates that with the growth and development, the diversity of intestinal flora increases, and the abundance of microorganisms related to nutrient digestion increases, which promotes the metabolism and absorption of nutrients and maintains the health and normal development of the body.

At present, there are few studies on the effects of vitamin and mineral metabolism in Tibetan pigs. Future studies can also strengthen the understanding mechanism of Tibetan pig gut microbes' interaction with the host nutrition, liver and brain gut shaft axis, to find the effective gut microbes control targets, and can help in proving the regulatory mechanism of Tibetan pig nutrition metabolism.

## Conclusion

In this study, Tibetan pigs in Nyingchi City, Tibet Autonomous Region were selected as subjects to analyze the diversity and functional changes of intestinal microbiota in three different growth stages. It was found that there was no significant change in the diversity of intestinal microbiota in Tibetan piglets. The relative abundance of specific gut microorganisms changes dynamically with the age. For example, at the genus level, aerobic and facultative anaerobic bacteria first appear in the gut of newborn piglets, and then are replaced by obligate anaerobic bacteria. With the increase in age and the development of gut microbiota, the function of gut microbiota also changes significantly. This study expands our understanding of the dynamic migration of intestinal microbiota in Tibetan pigs at different growth stages and provides a theoretical reference for studying the changes of intestinal microbiota colonization and succession in piglets.

## Data availability statement

The datasets presented in this study can be found in online repositories. The names of the repository/repositories and accession number(s) can be found below: NCBI—PRJNA894839.

## Author contributions

PS: study conception and design. ZC, SB, QX, YW, XW, YH, and YY: experimentation and data analysis. ZC, SB, QX, YW,

XW, and YH: contribution toward reagents, materials, and analysis tools. PS, QX, SB, and ZC: writing and revising of the manuscript. All authors contributed to the article and approved the submitted version.

## Funding

This study was supported by the Major Science and Technology Projects of the Tibet Autonomous Region (XZ202101ZD0005N), the National Natural Science Foundation of China (32160773), and the Basic Research Funds of the China Agricultural University and Tibet Agriculture and Animal Husbandry University (2022TC125).

## Conflict of interest

The authors declare that the research was conducted in the absence of any commercial or financial relationships that could be construed as a potential conflict of interest.

## Publisher's note

All claims expressed in this article are solely those of the authors and do not necessarily represent those of their affiliated organizations, or those of the publisher, the editors and the reviewers. Any product that may be evaluated in this article, or claim that may be made by its manufacturer, is not guaranteed or endorsed by the publisher.

## References

Ai, H., Yang, B., Li, J., Xie, X., Chen, H., and Ren, J. (2014). Population history and genomic signatures for high-altitude adaptation in *Tibetan pigs*. *BMC Genom.* 15:834. doi: 10.1186/1471-2164-15-834

Armougom, F., and Raoult, D. (2009). Exploring microbial diversity using 16S r RNA high-throughput methodsJ. *J. Comp. Sci. Systems Biol.* 2, 74–92.

Aßhauer, K. P., Wemheuer, B., Daniel, R., and Meinicke, P. (2015). Tax4Fun: predicting functional profiles from metagenomic 16S rRNA data. *Bioinformatics* 31, 2882–2884. doi: 10.1093/bioinformatics/btv287

Backhed, F., Ley, R. E., Sonnenburg, J. L., Peterson, D. A., and Gordon, J. I. (2005). Host-bacterial mutualism in the human intestine. *Science* 307, 1915–1920. doi: 10.1126/science.1104816

Ban-Tokuda, T., Maekawa, S., Miwa, T., Ohkawara, S., and Matsui, H. (2017). Changes in faecal bacteria during fattening in finishing swine. *Anaerobe* 47, 188–193. doi: 10.1016/j.anaerobe.2017.06.006

Bergamaschi, M., Tiezzi, F., Howard, J., Huang, Y. J., Gray, K. A., Schillebeeckx, C., et al. (2020). Gut microbiome composition differences among breeds impact feed effificiency in swine. *J. Microbiome* 8:110. doi: 10.1186/s40168-020-00888-9

Bokulich, N. A., Subramanian, S., Faith, J. J., Gevers, D., Gordon, J. I., Knight, R., et al. (2013). Quality-filtering vastly improves diversity estimates from Illumina amplicon sequencing. *Nat. Methods* 10, 57–59. doi: 10.1038/nmeth.2276

Caporaso, J. G., Kuczynski, J., Stombaugh, J., Bittinger, K., Bushman, F. D., Costello, E. K., et al. (2010). QIIME allows analysis of high-throughput community sequencing data. *Nat. Methods* 7, 335–336. doi: 10.1038/nmeth.f.303

Chen, L., Guo, G., Yuan, X. J., Shimojo, M., Yu, C. Q., and Shao, T. (2014). Effect of applying molasses and propionic acid on fermentation quality and aerobic stability of total mixed ration silage prepared with whole-plant corn in Tibet. *Asian-Australasian J. Animal Sci.* 27, 349–356. doi: 10.5713/ajas.2013.13378

Chernikova, D. A., Madan, J. C., Housman, M. L., Zain-Ul-Abideen, M., Lundgren, S. N., Morrison, H. G., et al. (2018). The premature infant gut microbiome during the fifirst 6 weeks of life differs based on gestational maturity at birth. *Pediatr. Res.* 84, 71–79. doi: 10.1038/s41390-018-0022-z

Clarke, S. F., Murphy, E. F., O'Sullivan, O., Lucey, A. J., Humphreys, M., Hogan, A., et al. (2014). Exercise and associated dietary extremes impact on gut microbial diversity. *Gut* 63, 1913–1920. doi: 10.1136/gutjnl-2013-306541

Coleman, O. I., Lobner, E. M., Bierwirth, S., Sorbie, A., Waldschmitt, N., and Rath, E. (2018). Activated ATF6 induces intestinal dysbiosis and innate immune response to promote colorectal tumorigenesis. *Gastroenterology* 155, 1539–1552.e12. doi: 10.1053/j.gastro.2018.07.028.

Crespo-Piazuelo, D., Estellé, J., Revilla, M., Criado-Mesas, L., Ramayo-Caldas, Y., Óvilo, C., et al. (2018). Characterization of bacterial microbiota compositions along the intestinal tract in pigs and their interactions and functions. *Sci. Rep.* 8:12727. doi: 10.1038/s41598-018-30932-6

Donaldson, G. P. S., Melanie, L., and Mazmanian, S. K. (2016). Gut biogeography of the bacterial microbiota. *Nat. Rev. Mic.* 14, 20–32. doi: 10.1038/nrmicro3552

Edgar, R. C. (2013). UPARSE: highly accurate OTU sequences from microbial amplicon reads. *Nat. Methods* 10, 996–998. doi: 10.1038/nmeth.2604

Faith, J. J., Guruge, J. L., Charbonneau, M., Subramanian, S., Seedorf, H., Goodman, A. L., et al. (2013). The long-term stability of the human gut microbiota. *Science* 341:1237439. doi: 10.1126/science.1237439

Franke, T., and Deppenmeier, U. (2018). Physiology and central carbon metabolism of the gut bacterium *Prevotella copri*. *Mol. Microbiol.* 109, 528–540. doi: 10.1111/mmi.14058

Holman, D. B., Brunelle, B. W., Trachsel, J., and Allen, H. K. (2017). Meta-analysis to define a core microbiota in the swine gut. *mSystems* 2:e00004-17. doi: 10.1128/mSystems.00004-17

Isaacson, R., and Kim, H. B. (2012). The intestinal microbiome of the pig. *Anim. Health Res. Rev.* 13, 100–109. doi: 10.1017/S1466252312000084

Kelly, C. J., and Colgan, S. P. (2016). Breathless in the gut: implications of luminal o2 for microbial pathogenicity. *Cell Host Microbe* 19, 427–428. doi: 10.1016/j.chom.2016.03.014

Kim, H. B., and Isaacson, R. E. (2015). The pig gut microbial diversity: understanding the pig gut microbial ecology through the next generation high throughput sequencing. *Vet. Microbiol.* 177, 242–251. doi: 10.1016/j.vetmic.2015.03.014

Kumar, A., Vlasova, A. N., Deblais, L., Huang, H. C., Wijeratne, A., Kandasamy, S., et al. (2018). Impact of nutrition and rotavirus infection on the infant gut microbiota in a humanized pig model. *BMC Gastroenterol.* 18:93. doi: 10.1186/s12876-018-0810-2

Leamy, L. J., Kelly, S. A., Nietfeldt, J., Legge, R. M., Ma, F., Hua, K., et al. (2014). Host genetics and diet, but not immunoglobulin a expression, converge to shape compositional features of the gut microbiome in an advanced intercross population of mice. *Genome Biol.* 15:552.

Lei, L., Wang, Z., Li, J., Yang, H., Yin, Y., Tan, B., et al. (2021). Comparative microbial profiles of colonic digesta between ningxiang pig and large white pig. *Animals* 23:1862. doi: 10.3390/ani11071862

Liu, Y., Zheng, Z., Yu, L., Wu, S., Sun, L., Wu, S., et al. (2019). Examination of the temporal and spatial dynamics of the gut microbiome in newborn piglets reveals distinct microbial communities in six intestinal segments. *Sci. Rep.* 9:3453. doi: 10.1038/s41598-019-40235-z

Ma, Y., Han, X., Huang, C., Zhong, L., Adeola, A. C., Irwin, D. M., et al. (2019). Population genomics analysis revealed origin and high-altitude adaptation of *Ttibetan pigs*. *Sci. Rep.* 9, 11463–11474. doi: 10.1038/s41598-019-47711-6

Magoč, T., and Salzberg, S. L. (2011). FLASH: fast length adjustment of short reads to improve genome assemblies. *Bioinformatics* 27, 2957–2963. doi: 10.1093/bioinformatics/btr507

Maltecca, C., Bergamaschi, M., and Tiezzi, F. (2020). The interaction between microbiome and pigefficiency: a review. *J. Animal Breed. Genet.* 137, 4–13. doi: 10.1111/jbg.12443

Mi, Y. L., Song, E. J., Kang, K. S., and Nam, Y. D. (2019). Age-related compositional and functional changes in micro-pig gut microbiome. *Gero Sci.* 41, 935–944. doi: 10.1007/s11357-019-00121-y

Ondov, B. D., Bergman, N. H., and Phillippy, A. M. (2011). Interactive metagenomic visualization in a Web browser. *BMC Bioinform.* 12:385. doi: 10.1186/1471-2105-12-385

Pajarillo, E. A. B., Chae, J. P., Balolong, M. P., Kim, H. B., Seo, K. S., and Kang, D. K. (2014). Pyrosequencing-based analysis of fecal microbial communities in three purebred pig lines. *J. Microbiol.* 52, 646–651. doi: 10.1007/s12275-014-4270-2

Pluske, J. R. (2016). Invited review: aspects of gastrointestinal tract growth and maturation in the pre- and postweaning period of pigs. *J. Anim. Sci.* 94, 399–411. doi: 10.2527/jas.2015-9767

Pruesse, E., Quast, C., Knittel, K., Fuchs, B. M., Ludwig, W., Peplies, J., et al. (2007). SILVA: a comprehensive online resource for quality checked and aligned ribosomal RNA sequence data compatible with ARB. *Nucleic Acids Res.* 35, 7188–7196. doi: 10.1093/nar/gkm864

Ratajczak, W., Rył, A., Mizerski, A., Walczakiewicz, K., Sipak, O., and Laszczyńska, M. (2019). Immunomodulatory potential of gut microbiome-derived short-chain fatty acids (SCFAs). *Acta Biochim. Polonica* 66, 1–12. doi: 10.18388/abp.2018_2648

Segata, N., Izard, J., Waldron, L., Gevers, D., Miropolsky, L., Garrett, W. S., et al. (2011). Metagenomic biomarker discovery and explanation. *Genome Biol.* 12:R60. doi: 10.1186/gb-2011-12-6-r60

Serpa, J., Caiado, F., Carvalho, T., Torre, C., Gonçalves, L. G., Casalou, C., et al. (2010). Butyrate-rich colonic microenvironment is a relevant selection factor for metabolically adapted tumor cells. *J. Biol. Chem.* 285, 39211–39223. doi: 10.1074/jbc.M110.156026

Shang, P., Li, W., Tan, Z., Zhang, J., Dong, S., Wang, K., et al. (2021). Population genetic analysis of tengeographically isolated tibetan pig populations. *Animals* 10:1297. doi: 10.3390/ani10081297

Wang, Q., Garrity, G. M., Tiedje, J. M., and Cole, J. R. (2007). Naive Bayesian classifier for rapid assignment of rRNA sequences into the new bacterial taxonomy. *Appl. Environ. Microbiol.* 73, 5261–5267. doi: 10.1128/AEM.00062-07

Wang, S. R., Yuan, X. J., Dong, Z. H., Li, J. F., Guo, G., Bai, Y. F., et al. (2017). Characteristics of isolated lactic acid bacteria and their effects on the silage quality. *Asian-Australasian J. Animal Sci.* 30, 819–827. doi: 10.5713/ajas.16.0589

Wang, X., Tsai, T., Deng, F., Wei, X., Chai, J., Knapp, J., et al. (2019). Longitudinal investigation of the swine gut microbiome from birth to market reveals stage and growth performance associated bacteria. *Microbiome* 7, 109–127. doi: 10.1186/s40168-019-0721-7

White, J. R., Nagarajan, N., and Pop, M. (2009). Statistical methods for detecting differentially abundant features in clinical metagenomic samples. *PLoS Comput. Biol.* 5:e1000352. doi: 10.1371/journal.pcbi.1000352

Xiao, Y., Li, K., Xiang, Y., Zhou, W., Gui, G., et al. (2017). The fecal microbiota composition of boar duroc, yorkshire, landrace and hampshire pigs. *Asian-Australas J. Anim. Sci.* 30, 1456–1463. doi: 10.5713/ajas.16.0746

Yang, H., Huang, X., Fang, S., He, M., Zhao, Y., Wu, Z., et al. (2017). Unraveling the fecal microbiota and metagenomicfunctional capacity associated with feed efficiency in pigs. *Front. Microbiol.* 8:1555. doi: 10.3389/fmicb.2017.01555

Yang, Q., Huang, X., Zhao, S., Sun, W., Yan, Z., Wang, P., et al. (2017). Structure and function of the fecal microbiota in diarrheic neonatal piglets. *Front. Microbiol.* 8:502. doi: 10.3389/fmicb.2017.00502

Yang, S., Zhang, H., Mao, H., Yan, D., Lu, S., Lian, L., et al. (2011). The local origin of the Tibetan pig and additional insights into the origin of Asian pigs. *PLoS One* 6:e28215. doi: 10.1371/journal.pone.0028215

Zhang, B., Chamba, Y., Shang, P., Wang, Z., Ma, J., Wang, L., et al. (2017). Comparative transcriptomic and proteomic analyses provide insights into the key genes involved in high-altitude adaptation in the *Tibetan pig*. *Sci. Rep.* 7:3654. doi: 10.1038/s41598-017-03976-3

Zhang, B., Qiangba, Y., Shang, P., Wang, Z., Ma, J., Wang, L., et al. (2015). A comprehensive Micro RNA expression profile related to hypoxia adaptation in the Tibetan pig. *PLoS One* 10:e0143260. doi: 10.1371/journal.pone.0143260

Zhao, Y., Lu, X., Cheng, Z., Tian, M., Qiangba, Y., Fu, Q., et al. (2019). Comparative proteomic analysis of *Tibetan pig* spermatozoa at high and low altitudes. *BMC Genom.* 20:569. doi: 10.1186/s12864-019-5993-6

Zitvogel, L., Ma, Y., Raoult, D., Kroemer, G., and Gajewski, T. F. (2018). The microbiome in cancer immunotherapy: diagnostic tools and therapeutic strategies. *Science* 359, 1366–1370. doi: 10.1126/science.aar6918

frontiers | Frontiers in Microbiology

TYPE Original Research
PUBLISHED 05 January 2023
DOI 10.3389/fmicb.2022.1091116



OPEN ACCESS

EDITED BY
Yung-Fu Chang,
Cornell University,
United States

REVIEWED BY
Nisha Kannan,
Cornell University,
United States
Yi Wu,
Nanjing Agricultural University,
China
Juan Liu,
Southwest University,
China

*CORRESPONDENCE
Dayou Shi
✉ shidayou@scau.edu.cn

†These authors have contributed equally to this work

SPECIALTY SECTION
This article was submitted to Microorganisms in Vertebrate Digestive Systems, a section of the journal Frontiers in Microbiology

RECEIVED 06 November 2022
ACCEPTED 13 December 2022
PUBLISHED 05 January 2023

CITATION
Lin R, Zhi C, Su Y, Chen J, Gao D, Li S and Shi D (2023) Effect of Echinacea on gut microbiota of immunosuppressed ducks. *Front. Microbiol.* 13:1091116. doi: 10.3389/fmicb.2022.1091116



# Effect of Echinacea on gut microbiota of immunosuppressed ducks

Renzhao Lin[1†], Chanping Zhi[2†], Yalin Su[1], Jiaxin Chen[1], Debao Gao[3], Sihan Li[1] and Dayou Shi[1*]

[1]College of Veterinary Medicine, South China Agricultural University, Guangzhou, China, [2]Guangdong Maoming Agriculture and Forestry Technical College, Maoming, China, [3]Guangzhou Technician College, Guangzhou, China

**Introduction:** Immunosuppression puts animals in a susceptible state and disrupts the balance of intestinal flora, which can increase the risk of disease and cause serious harm to the farm. Echinacea can exert its immunomodulatory effect in various ways, but its influence on intestinal flora is unclear.

**Methods:** Therefore, we investigated the effect of Echinacea extract (EE) on gut microbiota in immunosuppressed ducks by 16s-RNA sequencing in this experiment.

**Results:** The results showed that EE significantly improved the weight gain of immunosuppressed ducks ($p<0.001$). It also increased the immune organ index ($p<0.01$) and upregulated the levels of TNF-α and IFN-γ ($p<0.05$) as well as IL-2 in the serum. The lesions of the bursa were evident compared to the spleen and thymus. After treatment in the EE group, the lymphocyte count of the bursa returned to healthy levels and the lesions were significantly improved. The diversity analysis showed that neither of the alpha-diversity indices showed a significant difference ($p>0.05$). However, the EE group had a trend closer to the healthy group compared to the M group. β-diversity analysis revealed a high degree of sample separation between the healthy and immunosuppressed groups. The sequencing result showed a significantly higher relative abundance of *Prevotella* and *Prevotella_UCG_001* in the dexamethasone-treated group, which could be potential biomarkers of dexamethasone-induced immunosuppression. EE increased the relative abundance of *Akkermansia*, *Bacteroides*, and *Alistipes* and significantly decreased the relative abundance of *Megamonas*, *Streptococcus*, and *Enterococcus* ($p<0.05$).

**Conclusion:** The results showed that Echinacea extract improves the development of immunosuppressed ducks and modulates intestinal immune function by increasing the abundance of beneficial bacterial genera in the intestine.

KEYWORDS

**gut microbiota, immunosuppression, Echinacea extract, duck, *Prevotella***

# 1. Introduction

China is the world's largest producer and consumer of waterfowl, including the meat duck, egg duck, and meat goose industries. The total value of waterfowl production has exceeded $100 billion, with duck farming accounting for 74.3% of world production and goose farming for 93.3%. They can provide large quantities of high-quality meat and down. In recent years, diseases caused by immunosuppression have become more and more prevalent in large intensive farms, and the direct or indirect losses and hazards caused by them are quite huge. Immunosuppression can lead to retarded weight gain, decreased egg production in laying hens, and decreased litter size in breeding pigs by affecting animal intake and reducing feed conversion ratios. Meanwhile, the animals are vulnerable to infection, erosion by pathogenic microorganisms, and secondary diseases, which can be fatal in serious cases. However, there is still a gap in studies related to immunosuppression in waterfowl compared to reports in chickens, pigs, and rats. The factors leading to immunosuppression are mainly divided into disease factors, human factors, and feeding environment factors. Most of the factors causing immunosuppression in ducks are viral diseases, such as duck circovirus (DCV) (Hong et al., 2018), duck euthero virus (Wang et al., 2020), duck influenza virus, duck herpesvirus type 2, duck distemper virus (DPV) (Dhama et al., 2017), etc. These diseases are characterized by damage to the immune organs and hinder the process of the humoral immune response.

Dexamethasone can cause an immunosuppressive state in animals, and it was selected as an immunosuppressive drug in this test. In experiments studying animal models of dexamethasone-induced immunosuppression pathology, more attention has been paid to changes in leukocytes and immune cells, and a lack of focus on clinical signs such as body weight (Lo et al., 2005; Harada et al., 2011; Hundakova et al., 2022). Immunosuppression led to atrophy of the thymus and the bursin, organ function was affected, and organ indexes showed a significant decrease after modeling, whereas the spleen showed no difference. It was found that dexamethasone-induced immunosuppression significantly reduced splenic lymphoid follicles in the spleen of house sparrows. But did not affect their CD3 immune effect and had a minimal effect on splenic lymphocytes in mice (Jeklova et al., 2008; Crouch et al., 2022).

Research on natural herbal medicines is critical to reducing the risk of drug resistance on farms. Echinacea, as a natural herb, possesses a wide range of medicinal effects, and it contains a great potential medical value that is worth exploring. Echinacea was already used to treat traumatic injuries, septicemia, and toothache by Indians in the 18th century. Nowadays, it is more commonly used to treat skin diseases and to combat respiratory diseases such as influenza and asthma in Western countries (Aarland et al., 2017). A large number of studies have also reported that EE can exert immunomodulatory effects by affecting immune system mechanisms in different ways (Block and Mead, 2003; Randolph et al., 2003; Sharifi-Rad et al., 2018), such as activating immune cells and promoting the secretion of interferon-α (Zhai et al., 2007). However, the effects of its interaction with the intestinal flora on the immune system are still inconclusive.

It has been found that the immune regulation of the body is inseparably related to gut microbiota (Hansen et al., 2010). The gut microbiota is a system composed of a large variety of bacteria, including beneficial, harmful, and neutral bacteria. These microbiotas play a key role in digestion and absorption, growth and development, immune regulation, and physiological and structural changes in the intestine (Liu et al., 2009; Quinteiro-Filho et al., 2012). The immune function of the host is closely linked to the dynamic balance of the gut microbiota (Yamashiro, 2017; Liu et al., 2021). Normal flora has an important role in promoting the maturation of immune cells and tissues, while the presence of imbalances in the flora, is associated with the development of infectious and inflammatory diseases such as bacterial vaginosis, inflammatory bowel disease, and rheumatoid arthritis (Srinivasan et al., 2012; Ferreira et al., 2014; Trompette et al., 2014; Wagenaar et al., 2021). The gut microbiota can affect the host's immune system in direct or indirect ways. The flora directly eradicates pathogenic competitors by competing for nutrients and ecological niches, acting as a biological barrier together with the intestinal mucosa; or indirectly influencing the host's immune system through flora metabolites, enhancing its defense mechanisms (Kamada et al., 2013). For example, SCFAs are common metabolites of the flora, mainly produced by Firmicutes and Bacteroidota. They provide energy to intestinal epithelial cells, maintain the integrity of the intestinal mucosa, balance the pH of the intestinal microenvironment, have a positive regulatory effect on intestinal immune cells, and exert an inhibitory effect on intestinal inflammation (Correa-Oliveira et al., 2016; Parada et al., 2019; Blaak et al., 2020).

Abnormalities in the species, ratio, and the number of gut microbiota could occur due to medical origin, drug abuse, and other problems. The immune regulation and metabolic function of gut microbiota will be affected as the homeostasis of the microbial population are out of order. As a result, changes in the intestinal flora may lead to disruption of the normal immune response process and even immunosuppression. It may also lead to changes in the microenvironment in the intestinal tract and abnormalities in the digestive and absorption functions of the animal. This effect can affect the increase in body weight, decrease in meat yield, increase in feed weight ratio, etc., causing economic losses to the farm (Choi et al., 2014).

In this experiment, we analyzed the effect of EE on the treatment of the dexamethasone immunosuppressed duck model by the 16 s-RNA intestinal flora sequencing method and explored the relationship between the immunomodulatory effect of EE and intestinal flora.

# 2. Materials and methods

## 2.1. Animals and treatment

The protocol was performed after the approval of the Institutional Animal Welfare and Research Ethics Committee of

South China Agricultural University, Guangzhou, China, and every effort was made to minimize animals suffering during the experiments. A total of 60 healthy 7-day-old Pekin ducks (purchased from Foshan Guiliu Poultry Co., Ltd.) were randomly divided into three groups of 20 ducks each. They were divided into a blank group (K), a model control group (M) and an Echinacea extract treatment group (EE). In the M and EE groups, dexamethasone (purchased from Chongqing Buur Animal Pharmaceutical Co., Ltd.) was injected intramuscularly at a dose of 3.5 mg/kg for 7 days to construct an immunosuppressed animal model, with no dexamethasone injection in group K. After the animal model was established, the EE group added 0.6 g/kg of Echinacea purpurea extract powder (purchased from Sichuan Hengrui Tongda Veterinary Medicine Co., Ltd.) to the basic diet, while the K and M groups had no addition to the basic diet. During the experiment, all three groups were fed and watered *ad libitum*.

## 2.2. Body weight, immune organ index, and serum cytokines

We randomly selected six ducks from each group and sampled them at 0, 7, and 14 days after EE administration. The ducks were euthanized. And the weight of the body, spleen, thymus, and bursa of each duck was measured and recorded.

The immune organ index is calculated as follows. Immune organ index = immune organ weight (mg)/body weight (g). Their blood was obtained from the jugular vein, centrifuged at 3000 rpm/min for 10 min, and the serum was collected to detect the TNF-α, IFN-γ, and IL-2 levels in it by Elisa.

## 2.3. Pathological histological sections

After modeling, the spleen, thymus, and bursa of ducks in the healthy and immunosuppressed groups were randomly dissected and placed in 10% neutral formalin fixation, paraffin-embedded and HE stained to observe histopathology. According to the pathological changes, test ducks were randomly selected for dissection at 7 and 14 days of treatment and immune organs with lesions were obtained for HE staining to observe the pathological changes.

## 2.4. Study on the diversity of cecum contents microbiota

After dissection of 5 randomly selected test ducks in each group at 14 d after the administration, 2 g of cecum contents were placed in lyophilized tubes and stored at −80°C for the study of intestinal contents flora diversity. The total genomic DNA of the samples was extracted by CTAB/SDS method, and the DNA concentration and purity were detected on 1% agarose gel. Depending on the concentration, DNA was diluted to 1 ng/μL with sterile water, and the 16S rRNA genes of different regions were amplified with specific primers and barcodes. Equal amounts of 1X loading buffer (containing SYB green) were mixed with PCR products, DNA detection was performed on a 2% agarose gel, and the mixed PCR products were purified using Qiagen Gel Extraction Kit. Sequencing libraries were generated using the NEBNext® Ultra™ IIDNA Library Prep Kit (Cat No. E7645). Library quality was assessed by Qubit@2.0 fluorometer (Thermo Science) and Agilent Bioanalyzer 2,100 system. Finally, the library was sequenced on the Illumina NovaSeq platform and a 250 bp paired-end read was generated.

To continue expanding the sequencing volume, the sample size was first predicted and measured by plotting sparsity and species accumulation curves. Based on the results of species annotation, the top 10 species with maximum abundance in each group from taxonomic levels of phylum and genus were selected to generate cumulative bar charts of species relative abundance to visualize species with greater relative abundance at different taxonomic levels and their proportions. Alpha diversity reflects the richness of the sample communities through Chao1, Dominance, Observed_otus, Pielou_e, Shannon, and Simpson. Beta diversity was analyzed by PCA for similarity and similarity in the community structure of different samples. The top 35 genera in terms of abundance were selected and clustered at both species and sample levels based on species annotation and abundance information and plotted as a heat map to facilitate the discovery of the high and low aggregation content of species in each sample. Species abundance data between groups were hypothesis tested using the MetaStat method to obtain *p*-values, species with significant differences between groups were screened based on p-values, and histograms of differential species between groups were plotted. To discover and interpret high-dimensional biomarkers (genes, pathways, and taxonomic units), comparisons were performed using the LEfSe (LDA Effect Size) analysis tool (Segata et al., 2011) to find statistically different Biomarkers between groups based on statistical significance and biological relevance. In addition, KO database-based metabolic function prediction of the colony was performed by PICRUSt2 based on 16S sequencing data.

## 2.5. Data statistical analysis

The raw data of each group was collected during the experiment and analyzed by IBM SPSS Statistics 26 statistical analysis software. The values were analyzed with One-way ANOVA, LSD, and Kruskal-Wallis tests and converted to graphs by GraphPad Prism 8. The analysis results are expressed as "mean ± standard error."

# 3. Results

## 3.1. Effect of Echinacea on growth performance and immune enhancement

The results showed that Echinacea extract significantly improved the slow body weight gain and decreased immune organ index levels

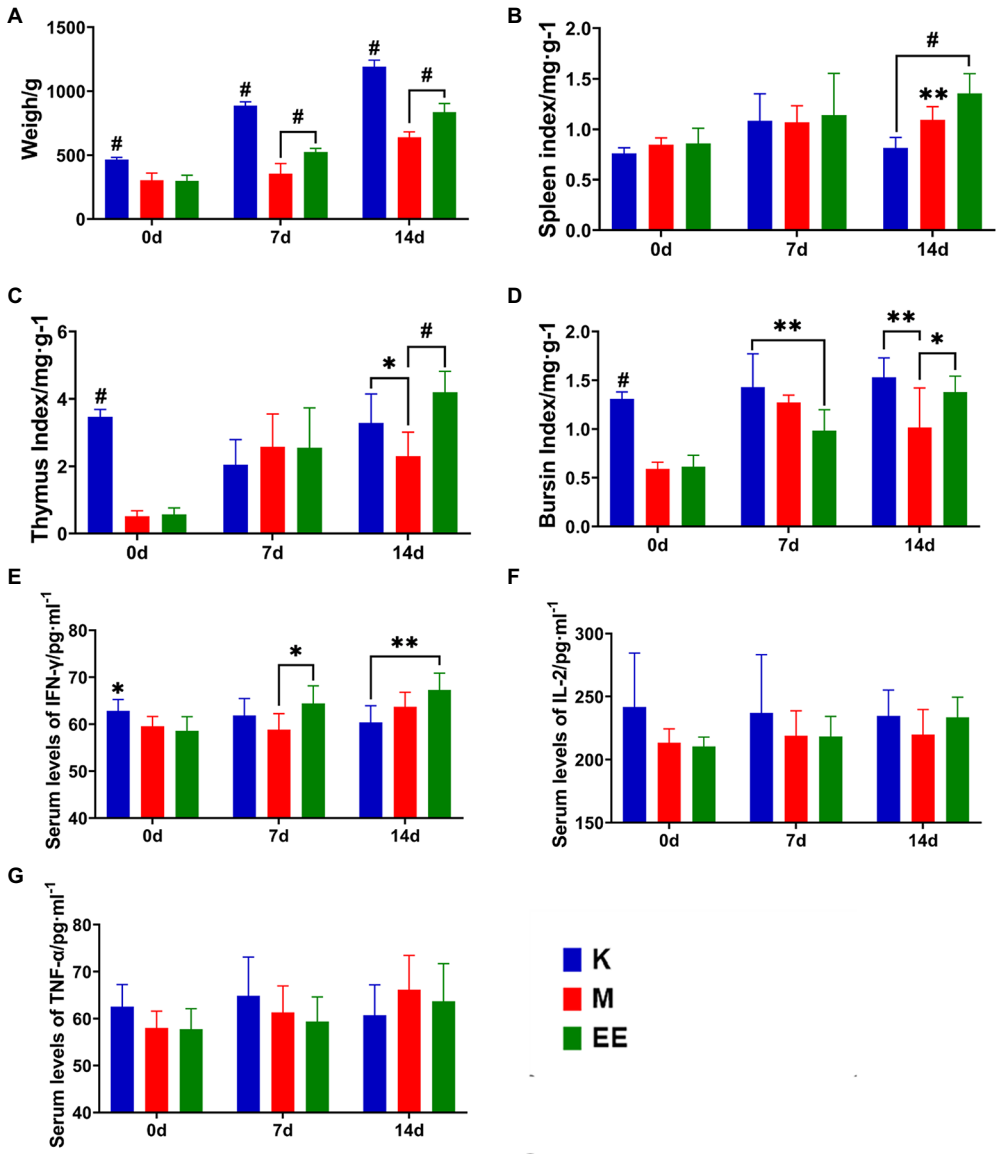


FIGURE 1
Effect of Echinacea on growth performance and immune enhancement. **(A)** Body weight; **(B–D)** Immune organ indices; **(E–G)** Levels of cytokine content in serum. *N*=6, $p<0.05$ (*), $p<0.01$ (**), $p<0.001$ (#).

caused by immunosuppression, and increased the levels of IFN-γ, TNF-α, and IL-2 in the serum of immunosuppressed ducks. The immunosuppressed animal model was established after 7 days of continuous dexamethasone injection. The body weight of animals in the immunosuppressed group was significantly lower compared to the K group ($p<0.001$). Echinacea extract was started in the EE and M groups. At 7 and 14 days, the body weight of ducks in the EE group was significantly higher than in the M group ($p<0.001$). However, there was still a significant difference compared to the K group ($p<0.001$) (Figure 1A). In the comparison of immune organ indices between the groups, the spleen index showed a significant difference between the EE and M groups only at 14 days of the administration, with the EE group being significantly higher than the M group ($p<0.01$) (Figure 1B). While before treatment with Echinacea extract, the thymic and bursal indices showed significant differences between the healthy control group and the immunosuppressed group, immunosuppression significantly reduced the levels of both of these immune organ indices ($p<0.001$). At 14 days of the administration, the EE group showed a significant recovery in the thymus ($p<0.001$) and bursal ($p<0.05$) organ index levels, both higher than the M group (Figures 1C,D). The levels of IFN-γ, TNF-α, and IL-2 in the serum of the EE group showed a tendency to increase during drug administration (Figures 1E–G). IFN-γ showed a significant decrease ($p<0.05$) after immunosuppression. But at 7 days of drug administration, it was significantly higher ($p<0.05$) in the EE group compared with the M group (Figure 1E).

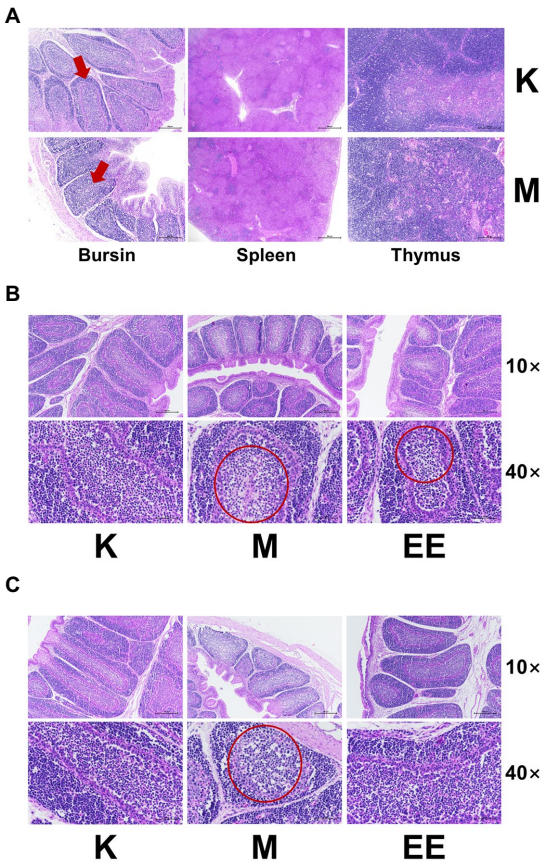


FIGURE 2
Effect of Echinacea on histopathology of immune organs (HE staining). **(A)** Pathological changes of immune organs after 7days of immunosuppression. The area indicated by the red arrow shows a poorly demarcated bursal skin medulla; **(B)** Pathological changes of bursa of each group after 7days of treatment; **(C)** Pathological changes of bursa of each group after 14days of treatment. In the area circled by the red circle, the cells are less aggregated and sparser and the number of lymphocytes is reduced. (*N*=6).

## 3.2. Effect of Echinacea on histopathology of immune organs

After modeling, the cortical and medullary boundaries of the lymph nodules of the bursa phalloides in the model group were indistinct, the epithelial reticular cell layer disappeared, and the cortical and medullary lymphocytes were significantly reduced. In contrast, the spleen and thymus showed no significant abnormalities (Figure 2A). Therefore, after the administration, the bursa was taken for staining at 7 and 14 days, respectively. In the bursa of group K, the lymph nodes were demarcated between the cortex and the medulla, separated by epithelial reticular cells, and there were a large number of lymphocytes in the cortex and medulla. In contrast, lymphocytes were significantly reduced in the M group and slightly reduced in the EE group after 7 days of treatment (Figure 2B). After 14 days, lymphocytes in the cortex and medulla of the bursa of the M group decreased significantly, medullary lymphocytes showed vacuolar degeneration, while the number of lymphocytes in the EE group recovered to healthy levels (Figure 2C).

## 3.3. Regulation of gut flora abundance in immunosuppressed ducks by Echinacea purpurea

The number of species that could be observed leveled off when the sample size reached 19–20, showing that the depth and richness of this sequencing test could already indicate the diversity of species in the sample community. The sequencing results are reliable and can be used for subsequent data analysis.

Among the components of the gut microbial community at the phylum taxonomic level in each group of ducks, *Bacteroidota*, *Firmicutes*, *Desulfobacterota*, *Actinobacteriota*, and *Verrucomicrobiota* were the main dominant microbiotas. The species composition of the K and EE groups was similar, with *Bacteroidota*, *Firmicutes*, and *Verrucomicrobiota* as the main dominant microbiotas. The relative abundance of *Bacteroidota* increased to 49.86% in the EE group, which was markedly higher compared to the K (43.14%) and M (44.46%) groups. The relative abundance of Firmicutes was significantly lower in the EE group (40.68%) compared to the K group (47.19%) and the M group (50.58%). The relative abundance of *Verrucomicrobiota* in the EE group reached 4.55%, more than that of the K group (2.59%) and the M group (0.67%) (Figure 3A). At the genus classification level, *Bacteroides*, *Butyricicoccus*, *Akkermansia*, *Megamonas*, and *Streptococcus* are the main dominant microbiotas. The relative abundance of *Bacteroides* in the EE group (29.88%) is more than that of the K (27.62%) and M (25.51%) groups. The relative abundance of *Megamonas* markedly increased in the M group (16.51%) compared to the K (6.36%) and EE (6.68%) groups. The relative abundance of *Akkermansia* in the EE group reached 4.55%, more than that of the K (2.59%) and M (0.67%) groups. Remarkably, the relative abundance of *Prevotellaceae_UCG-001* in the M group was up to 5.34%, while that of the K group was only 0.25%, and the EE group was 1.36% (Figure 3B).

## 3.4. Effect of Echinacea on the diversity of intestinal flora

None of the α-diversity indices showed significant differences ($p > 0.05$). But the EE group showed a trend of recovery in all indexes compared to the M group. The indices of Chao1, Dominance, and Observed_otus in the M group were lower than those of the K group. In contrast, the indices of the EE group were closer to the K group than the M group. The Shannon, Simpson, and Pielou_e indices increased in group M compared to group K, but those in group EE decreased to a similar level to group K compared to group M (Figure 3C). Analysis of β-diversity using PCA revealed a significant degree of sample separation between the healthy and immunosuppressed groups and a marked effect of

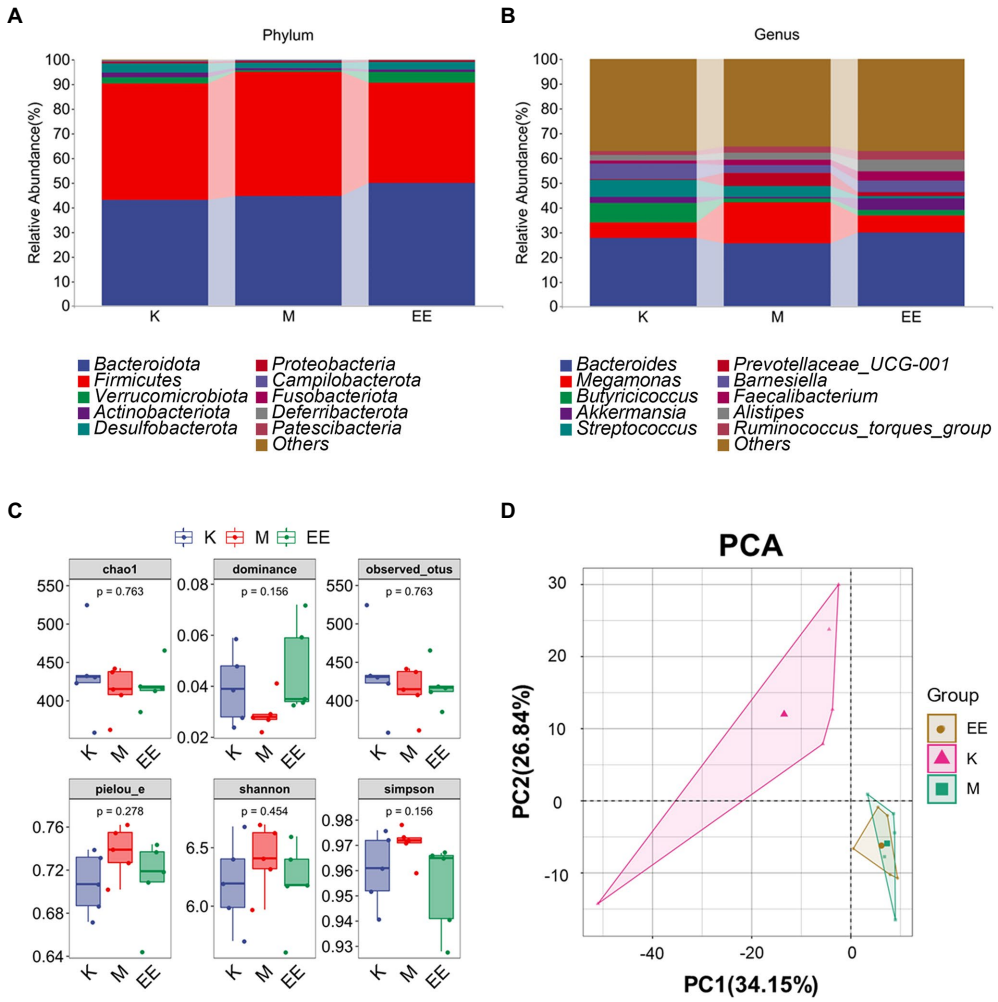


FIGURE 3
Regulation of gut flora abundance in immunosuppressed ducks by Echinacea purpurea. **(A)** Cumulative histogram of the top 10 species in relative abundance at the phylum taxonomic level; **(B)** Cumulative histogram of the top 10 species in relative abundance at the genus taxonomic level; **(C)** Box plot of the alpha diversity index; **(D)** PCA analysis of beta diversity. (*N*=5).

immunosuppression on the gut microbiota. The EE group was more similar to the M group, indicating that no significant changes in the diversity of the gut microbial community were produced after the administration (Figure 3D).

## 3.5. Clustering of the main intestinal flora affected by Echinacea

The top 35 genera in terms of abundance were selected and clustered at both species and sample levels. There were 19 genera belonging to *Firmicutes* and seven genera belonging to *Bacteroidota*. The genera that showed differences in variation due to immunosuppressive effects were mainly in these two groups. It can also be found that the abundance of some genera in the EE group is more convergent to the healthy group compared to the M group. *Enterococcus*, *Megamonas*, and *Fusobacterium* were more abundantly aggregated in the M group, while the genera with higher abundance aggregation in the EE group included *Akkermansia*, *Bacteroides*, and *Alistipes* (Figure 4A).

## 3.6. Analysis of species differences between groups

After 14 days of treatment, it was found by Metastat analysis that *Megamonas* ($p < 0.05$), *Prevotellaceae_UCG_001* ($p < 0.05$), *Ruminococcus_torques_group* ($p < 0.05$), and *Prevotella* ($p < 0.001$) all showed a significant increase in relative abundance, while *Collinsella* ($p < 0.01$), *Muribaculaceae* ($p < 0.05$) showed a significant decrease. The relative abundance of Megamonas, Streptococcus, and Enterococcus was significantly decreased in the EE group compared with the M group ($p < 0.05$). The EE group, in comparison with the K group, significantly increased the

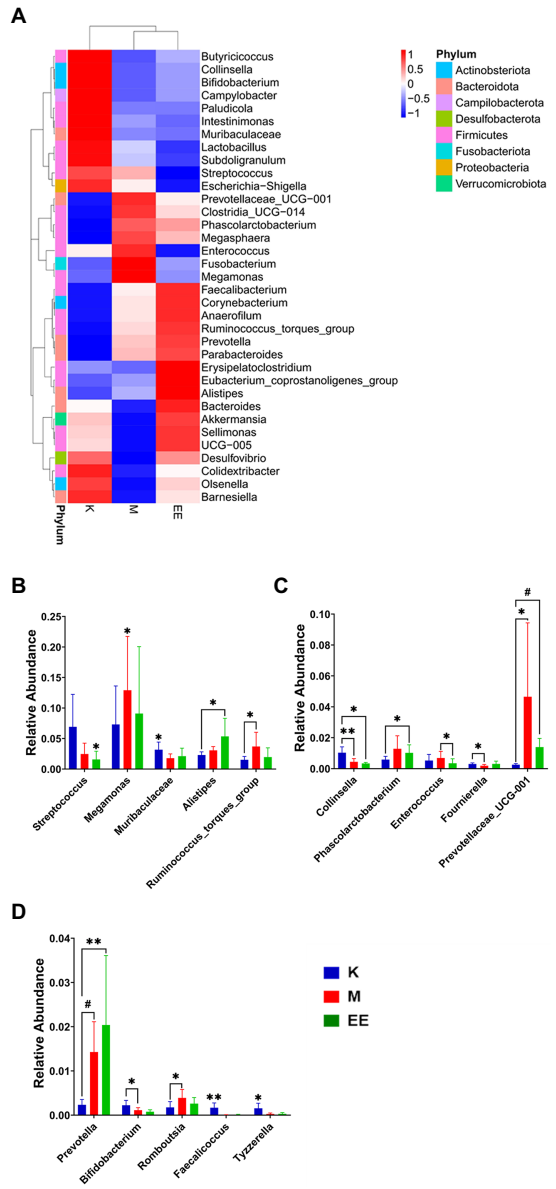


FIGURE 4
Species abundance clustering analysis and analysis of species differences between groups. **(A)** Clusters of species abundance in the top 35 relative abundances at the genus level; **(B–D)** Histograms of species abundance with significant differences between groups (top 15). *N*=5, $p<0.05$ (*), $p<0.01$ (**), $p<0.001$ (#).

relative abundance of *Alistipes* ($p<0.05$), *Prevotellaceae_UCG_001* ($p<0.001$), and *Prevotella* ($p<0.01$). Instead, decreased *Streptococcus*, *Collinsella*, and *Muribaculaceae* in relative abundance ($p<0.05$) (Figures 4B–D). In the Lefse analysis, it was found that the dominant microbiota in the M group was *Prevotellaceae*, *Prevotellaceae_UCG_001*; the K group mainly had *Streptococcaceae*, *Lactobacilliales*, *Butyricoccus*, *Bacilli* as the dominant microbiota; and the dominant microbiota in the EE group was *Mogibacterium_sp_*, *Prevotella* (Figure 5).

## 3.7. Predicting the metabolic function of microbiota affected by Echinacea

Functional predictions based on the KO database showed that among the top 35 metabolic pathways of relevance, the M group had a significantly higher abundance of flora associated with six of these pathways than the K and EE groups, including *K1091*, *K07024*, *K07482*, *K07491*, *K07496*, and *K08303*. Meanwhile the abundance with 15 of these pathways was significantly lower than the other two groups. On the other hand, the EE group had a significantly higher abundance associated with seven of these pathways than the K and M groups, including *K01915*, *K05349*, *K03530*, *K01897*, *K03100*, *K01190*, and *K03169* (Figure 6A). According to the KO database classification of these metabolic pathways, 27.3% of them are related to metabolism, 15.2% to genetic information processing, 12.1% to cellular processes, while organismal systems, human diseases and unclassified each account for 12.1% and environmental information processing for only 9.1% (Figure 6B).

# 4. Discussion

Dexamethasone-induced immunosuppression significantly inhibited the growth performance of ducks. It included a significant slowing of body weight gain, and a marked reduction in the thymus and bursal index ($p<0.001$). In the trial, immunosuppression damaged the normal structure of the bursa of Fasciola and reduced the number of lymphocytes. And this damage was significantly relieved by the administration of Echinacea extract and restored the number of lymphocytes to a healthy level. The above results indicated that Echinacea extract could effectively repair the damage of the bursa of Fasciola, promote lymphocyte proliferation and improve the immune organ index. It was reported in several studies that the immune-enhancing effects of the polysaccharide components of herbal medicine were mainly achieved by significantly increasing the levels of TNF-α, IFN-γ, and IL-2 in serum (Fan et al., 2013; Zhou et al., 2018; Liu et al., 2022; Nam et al., 2022), and Echinacea extract also increased the levels of these three cytokines in the serum in this trial. It is worth considering that there is a link between changes in serum levels of immune-related cytokines and changes in the intestinal flora. Several studies have reported that the flora is involved in host immunity mainly through their metabolites as signaling factors, acting on immune cells and regulating the expression as well as the release of anti-inflammatory or pro-inflammatory factors. For example, butyric acid in SCFAs can inhibit the proliferation of Th1 cells (Guilloteau et al., 2010), the main cytokines secreted by Th1 cells are TNF-α, IFN-γ, and IL-2, so butyric acid can inhibit the secretion of pro-inflammatory factors and play an immunomodulatory role; or lipopolysaccharide in the flora can promote the secretion of pro-inflammatory factors and induce chronic systemic inflammation (Nicholson et al., 2012).

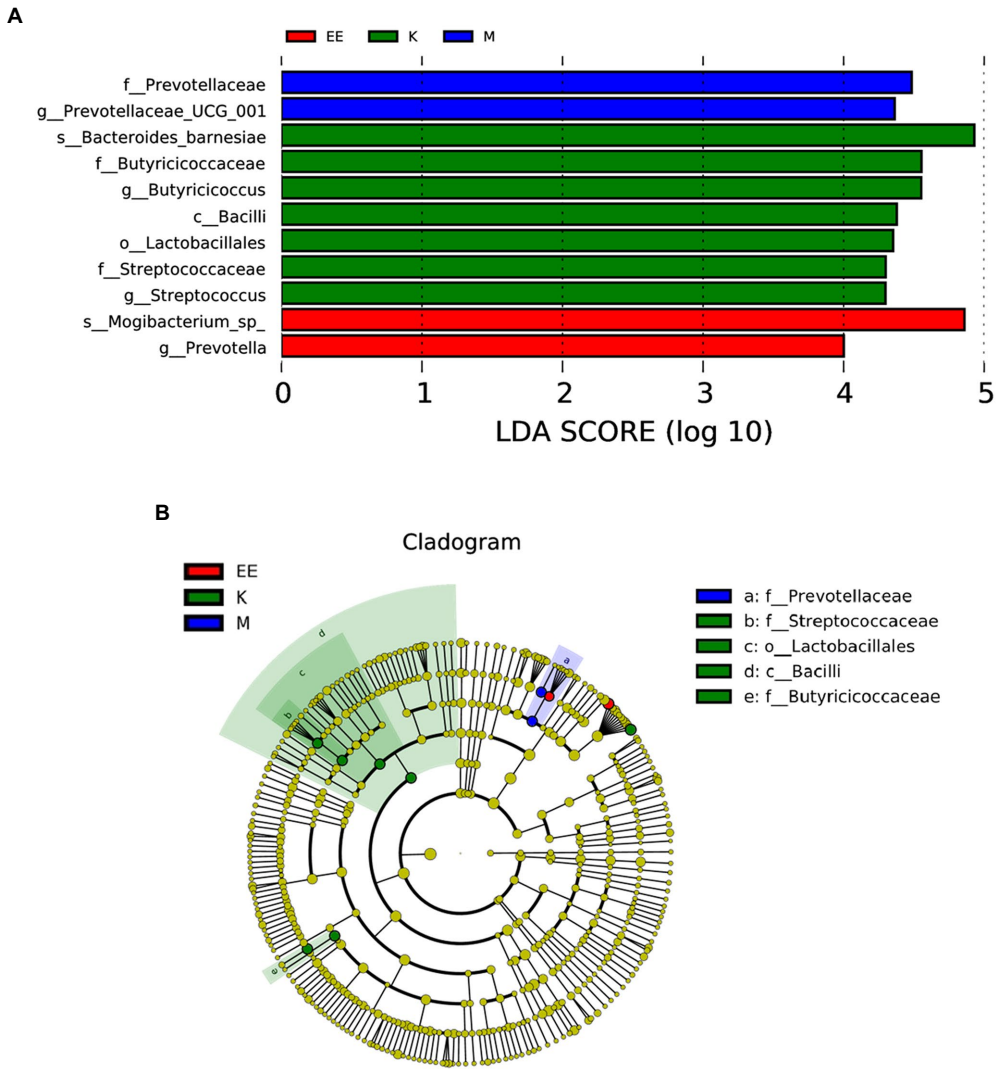


FIGURE 5
Analysis of species differences between groups. **(A)** Histogram of the distribution of LDA values; **(B)** Evolutionary branching plots, *N*=5. Species with LDA scores greater than the set value (set to 4 by default), biomarker with statistical differences between groups, are shown in the histogram of the LDA value distribution. In the evolutionary branching diagram, the circles radiating from inside to outside represent the taxonomic rank from phylum to genus (or species). Each small circle of a different taxonomic level represents a taxon of that level, and the size of the diameter of the small circle is proportional to the relative abundance size.

The intestinal flora, as another organ of the animal body, is not only involved in the digestion and absorption process but also influences the immune process of the animal body by metabolizing and synthesizing essential nutrients needed by the body. The intestinal flora has a crucial role in the development and maturation of the immune system. Lack of colonization of the intestinal flora reduces metabolites associated with the development of the body's immune organs and tissues, thereby inhibiting the development of the body's immune function, which may be defective, as is common in germ-free and neonatal animals (Ennamorati et al., 2020; Yang and Cong, 2021). During colonization, infection training enhances the resistance of the microbiota to infection, while stimulating the host immune system to respond, which can promote the development and maturation of the immune system (Butel et al., 2018; Stacy et al., 2021). The absence of specific intestinal flora may affect the maturation and differentiation of immune cells, such as CD4+ T cells in the spleen (Ostman et al., 2006) and Th17 cells in intestinal lymphoid tissue (Ivanov et al., 2009). Conversely, deletion of immune organs can likewise affect the stability of the gut microbiota, as splenectomy can result in abnormal intestinal flora composition in mice (Wei et al., 2021). Immunosuppression can lead to changes in the intestinal flora, which in turn can cause many problems. In this study, Echinacea purpurea was found to regulate the changes in flora caused by immunosuppression.

The sequencing results revealed a recovery trend in the EE group. Although no significant differences were seen in the alpha-diversity indices ($p > 0.05$), the EE group showed an opposite trend in each index compared to the M group, gradually returning to healthy levels. There were similar reports in the intestine of immunosuppressed mice (Fang et al., 2019; Li et al., 2021).

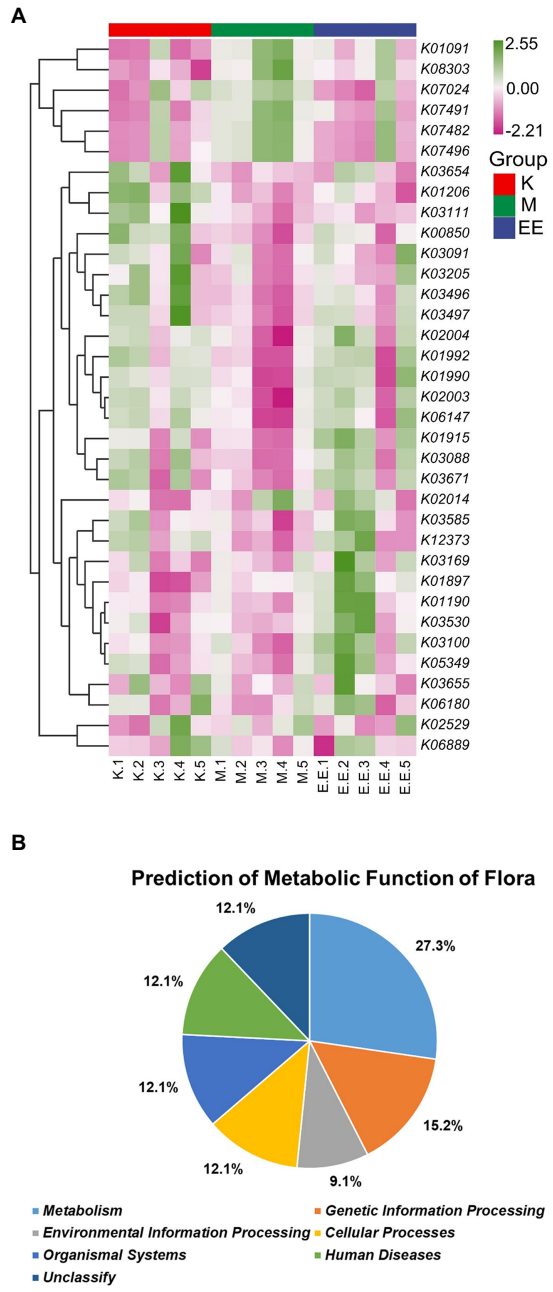


FIGURE 6
Prediction of metabolic function of the microbiota. **(A)** Heat map of the predicted metabolic functions of the flora based on the KO database (top 35). The horizontal coordinate is the sample name and the vertical coordinate is the associated metabolic pathway number, *N*=5; **(B)** Plot of the predicted metabolic functions of the flora as a percentage.

Remarkably, immunosuppression significantly increased the abundance of *Megamonas* and *Prevotellaceae_UCG_001*, while *Akkermansia*, *Alistipes*, and *Butyricicoccus* were significantly reduced. In contrast, Echinacea extract is effective in alleviating these changes in flora and may even increase the abundance of beneficial bacteria to improve the immune deficiency of the body. The relative abundance of *Prevotella*、*Prevotellaceae_UCG_001* was significantly higher in the immunosuppressed group. Both could be potential biomarkers in dexamethasone-induced immunosuppression observed in the Lefse analysis. *Prevotella* is strongly associated with systemic and chronic inflammation. *Prevotella copri* may increase the probability of developing colitis by affecting the structure of the flora when colonized in the mouse intestine (Scher et al., 2013). *Prevotella intestinalis* colonization may affect the metabolic processes of the intestinal flora, exacerbating intestinal inflammation and potentially systemic autoimmunity (Iljazovic et al., 2021). Some studies have reported a positive association between *Prevotella* and HIV-induced intestinal inflammation (Dillon et al., 2016). However, further research is needed to uncover the relationship between *Prevotella* and immunosuppression.

*Megamonas*, together with *Bifidobacterium*, can act as beneficial bacteria to regulate the composition of the gut microbiota to promote the synthesis and secretion of SCFAs (Dillon et al., 2016; Wu et al., 2022). In the immunosuppression model group, its elevated abundance may be more associated with the positive aspects. The decrease in its relative abundance correlates with the activation of abnormal immune responses, such as in the intestine of patients with Crohn's disease (Maldonado-Contreras et al., 2020), immune thrombocytopenia (Yu et al., 2022), or IgA nephropathy (Dong et al., 2020), where its abundance is significantly reduced. It suggests that the relative abundance of *Megamonas* is related to the immune status of the organism. Its abundance increases when the immunity declines, while it decreases significantly with abnormal activation in the immune response.

*Akkermansia* is a genus of beneficial bacteria that has received recent attention in research reports. Its *Akkermansia muciniphila* could enhance the activity of immune cells by being injected intravenously into mice to reduce the tumor burden in mice (Dong et al., 2020; Luo et al., 2021). Its colonization of the intestine increases the expression of genes involved in the immune response, producing IL-8 to participate in the host's mucosal immune regulation. It also produces mucins that positively works on intestinal epithelial cells to maintain the integrity of the intestinal epithelial mucosa (Derrien et al., 2011; Reunanen et al., 2015). Immunosuppression significantly reduced the relative abundance of *Akkermansia* in the gut to only 0.67% in the immunosuppressed model group. Its low abundance may lead to the absence of the functions described above and put the already immune dysregulated hosts at increased risk of disease infection. However, its relative abundance was significantly higher in the EE group supplemented with Echinacea extract, enhancing the protective effect on the intestine and modulating mucosal immune function. It also displays significant anti-inflammatory properties in the intestine, effectively relieving DSS-induced acute colitis (Qu et al., 2021). Echinacea extract may improve intestinal mucosal immune function and restore host immunity by increasing the abundance of *Akkermansia* in the gut of immunosuppressed ducks. It also enhances the immunity by increasing the abundance of *Alistipes*. Because *Alistipes* could bind to *TLR4* and activate the expression of TNF to enhance the immune clearance of tumor cells (Iida et al., 2013). However, there is no definitive evidence for the main components of Echinacea extract that act with the flora.

The gut microbiota interacts with the host primarily through metabolites produced during the metabolism of the flora. The prediction of the metabolic function of the flora revealed that immunosuppression had a significant effect on the metabolism of the flora and involved metabolic pathways associated with some human diseases and organism systems. While Echinacea extract antagonized the effect of immunosuppression on the mycota and increased the abundance of mycota associated with metabolic functions of human diseases and organic systems. The classification based on the KO database revealed that *KO3671* is associated with the immune system. It has a regulatory role not only in plant immune responses (Mata-Perez and Spoel, 2019) but also in mammals，playing a role in the regulation of immune signal release (Kim et al., 2008; Mougiakakos et al., 2011). It mainly through its protection of cells against oxidation and thus reducing immune cell apoptosis positively affects the immune system (Lu and Holmgren, 2012). *Akkermansia*, *Alistipes*, *Butyricoccus*, and *Bacteroides*, whose relative abundance increased in the EE group, were found to have genes corresponding to *KO3671* in the functional prediction. We speculate that the increased abundance of the genus mentioned above may have increased the *Trx* content in the intestine, exerting its enhancing and modulating effects on the immune system. It could be one of the pathways of immune function modulation by Echinacea extract, but more evidence is needed to prove it.

## 5. Conclusion

To sum up, Echinacea extract can significantly alleviate the immunosuppressive effect of dexamethasone on ducks. It mainly contributes by improving the growth performance of immunosuppressed ducks, restoring the function of immune organs, and regulating the level of immune-related cytokines in the serum. 16 s-rRNA sequencing identified *Prevotella* as a potential biomarker for dexamethasone-induced immunosuppression. Echinacea extract may modulate intestinal immune function by increasing the abundance of beneficial bacterial genera such as *Akkermansia* and *Alistipes* in the intestine. The trial provides a possibility for the application of Echinacea in waterfowl and enriches the research on immunosuppression in waterfowl.

## Data availability statement

The datasets presented in this study can be found in online repositories. The names of the repository/repositories and accession number(s) can be found at: https://www.ncbi.nlm.nih.gov/, PRJNA895924.

## Ethics statement

The animal study was reviewed and approved by the Institutional Animal Welfare and Research Ethics Committee of South China Agricultural University, Guangzhou, China.

## Author contributions

RL, CZ, YS, JC, DG, and SL: were responsible for study conception and design. DS: revised the manuscript. RL, CZ, YS, JC, DG, SL, and DS: were involved in the drafting of the manuscript. All authors contributed to the article and approved the submitted version.

## Funding

The study was supported by the General Project of Guangdong Provincial Natural Science Foundation (2021A1515011010), the Key R&D Project of Guangzhou City (202206010189) and the Project of Young Innovative Talents of Guangdong General Universities (2022KQNCX269).

## Conflict of interest

The authors declare that the research was conducted in the absence of any commercial or financial relationships that could be construed as a potential conflict of interest.

## Publisher's note

All claims expressed in this article are solely those of the authors and do not necessarily represent those of their affiliated organizations, or those of the publisher, the editors and the reviewers. Any product that may be evaluated in this article, or claim that may be made by its manufacturer, is not guaranteed or endorsed by the publisher.

## References

Aarland, R. C., Banuelos-Hernandez, A. E., Fragoso-Serrano, M., Sierra-Palacios, E. D., Diaz, D. L. F., Perez-Flores, L. J., et al. (2017). Studies on phytochemical, antioxidant, anti-inflammatory, hypoglycaemic and antiproliferative activities of Echinacea purpurea and Echinacea angustifolia extracts. *Pharm. Biol.* 55, 649–656. doi: 10.1080/13880209.2016.1265989

Blaak, E. E., Canfora, E. E., Theis, S., Frost, G., Groen, A. K., Mithieux, G., et al. (2020). Short chain fatty acids in human gut and metabolic health. *Benef. Microb.* 11, 411–455. doi: 10.3920/BM2020.0057

Block, K. I., and Mead, M. N. (2003). Immune system effects of echinacea, ginseng, and astragalus: a review. *Integr. Cancer Ther.* 2, 247–267. doi: 10.1177/1534735403256419

Butel, M. J., Waligora-Dupriet, A. J., and Wydau-Dematteis, S. (2018). The developing gut microbiota and its consequences for health. *J. Dev. Orig. Health Dis.* 9, 590–597. doi: 10.1017/S2040174418000119

Choi, J. H., Kim, G. B., and Cha, C. J. (2014). Spatial heterogeneity and stability of bacterial community in the gastrointestinal tracts of broiler chickens. *Poult. Sci.* 93, 1942–1950. doi: 10.3382/ps.2014-03974

Correa-Oliveira, R., Fachi, J. L., Vieira, A., Sato, F. T., and Vinolo, M. A. (2016). Regulation of immune cell function by short-chain fatty acids. *Clin. Transl. Immunol.* 5:e73. doi: 10.1038/cti.2016.17

Crouch, E., Reinoso-Perez, M. T., Vanderstichel, R. V., Dhondt, K. V., Dhondt, A. A., Otero, J., et al. (2022). The effect of dexamethasone on hematologic profiles, hemosporidian infection, and splenic histology in house finches (Haemorhous Mexicanus). *J. Wildl. Dis.* 58, 512–523. doi: 10.7589/JWD-D-21-00129

Derrien, M., Van Baarlen, P., Hooiveld, G., Norin, E., Muller, M., and de Vos, W. M. (2011). Modulation of mucosal immune response, tolerance, and proliferation in mice colonized by the mucin-degrader *Akkermansia muciniphila*. *Front. Microbiol.* 2:166. doi: 10.3389/fmicb.2011.00166

Dhama, K., Kumar, N., Saminathan, M., Tiwari, R., Karthik, K., Kumar, M. A., et al. (2017). Duck virus enteritis (duck plague) - a comprehensive update. *Vet. Q.* 37, 57–80. doi: 10.1080/01652176.2017.1298885

Dillon, S. M., Lee, E. J., Kotter, C. V., Austin, G. L., Gianella, S., Siewe, B., et al. (2016). Gut dendritic cell activation links an altered colonic microbiome to mucosal and systemic T-cell activation in untreated HIV-1 infection. *Mucos. Immunol.* 9, 24–37. doi: 10.1038/mi.2015.33

Dong, R., Bai, M., Zhao, J., Wang, D., Ning, X., and Sun, S. (2020). A comparative study of the gut microbiota associated with immunoglobulin a nephropathy and membranous nephropathy. *Front. Cell. Infect. Microbiol.* 10:557368. doi: 10.3389/fcimb.2020.557368

Ennamorati, M., Vasudevan, C., Clerkin, K., Halvorsen, S., Verma, S., Ibrahim, S., et al. (2020). Intestinal microbes influence development of thymic lymphocytes in early life. *Proc. Natl. Acad. Sci. U. S. A.* 117, 2570–2578. doi: 10.1073/pnas.1915047117

Fan, Y., Lu, Y., Wang, D., Liu, J., Song, X., Zhang, W., et al. (2013). Effect of epimedium polysaccharide-propolis flavone immunopotentiator on immunosuppression induced by cyclophosphamide in chickens. *Cell. Immunol.* 281, 37–43. doi: 10.1016/j.cellimm.2013.01.008

Fang, H., Meng, F., Piao, F., Jin, B., Li, M., and Li, W. (2019). Effect of taurine on intestinal microbiota and immune cells in Peyer's patches of immunosuppressive mice. *Adv. Exp. Med. Biol.* 1155, 13–24. doi: 10.1007/978-981-13-8023-5_2

Ferreira, C. M., Vieira, A. T., Vinolo, M. A., Oliveira, F. A., Curi, R., and Martins, F. S. (2014). The central role of the gut microbiota in chronic inflammatory diseases. *J Immunol Res* 2014:689492. doi: 10.1155/2014/689492

Guilloteau, P., Martin, L., Eeckhaut, V., Ducatelle, R., Zabielski, R., and Van Immerseel, F. (2010). From the gut to the peripheral tissues: the multiple effects of butyrate. *Nutr. Res. Rev.* 23, 366–384. doi: 10.1017/S0954422410000247

Hansen, J., Gulati, A., and Sartor, R. B. (2010). The role of mucosal immunity and host genetics in defining intestinal commensal bacteria. *Curr. Opin. Gastroenterol.* 26, 564–571. doi: 10.1097/MOG.0b013e32833f1195

Harada, K., Muramatsu, M., Suzuki, S., Tamura, Y., Sawada, T., and Takahashi, T. (2011). Evaluation on the pathogenicity of Erysipelothrix tonsillarum for pigs by immunosuppression with cyclophosphamide or dexamethasone. *Res. Vet. Sci.* 90, 20–22. doi: 10.1016/j.rvsc.2010.05.009

Hong, Y. T., Kang, M., and Jang, H. K. (2018). Pathogenesis of duck circovirus genotype 1 in experimentally infected Pekin ducks. *Poult. Sci.* 97, 3050–3057. doi: 10.3382/ps/pey177

Hundakova, A., Leva, L., Toman, M., and Knotek, Z. (2022). A ferret model of immunosuppression induced with dexamethasone. *Vet. Immunol. Immunopathol.* 243:110362. doi: 10.1016/j.vetimm.2021.110362

Iida, N., Dzutsev, A., Stewart, C. A., Smith, L., Bouladoux, N., Weingarten, R. A., et al. (2013). Commensal bacteria control cancer response to therapy by modulating the tumor microenvironment. *Science* 342, 967–970. doi: 10.1126/science.1240527

Iljazovic, A., Roy, U., Galvez, E., Lesker, T. R., Zhao, B., Gronow, A., et al. (2021). Perturbation of the gut microbiome by Prevotella spp. enhances host susceptibility to mucosal inflammation. *Mucos. Immunol.* 14, 113–124. doi: 10.1038/s41385-020-0296-4

Ivanov, I. I., Atarashi, K., Manel, N., Brodie, E. L., Shima, T., Karaoz, U., et al. (2009). Induction of intestinal Th17 cells by segmented filamentous bacteria. *Cells* 139, 485–498. doi: 10.1016/j.cell.2009.09.033

Jeklova, E., Leva, L., Jaglic, Z., and Faldyna, M. (2008). Dexamethasone-induced immunosuppression: a rabbit model. *Vet. Immunol. Immunopathol.* 122, 231–240. doi: 10.1016/j.vetimm.2007.11.011

Kamada, N., Seo, S. U., Chen, G. Y., and Nunez, G. (2013). Role of the gut microbiota in immunity and inflammatory disease. *Nat. Rev. Immunol.* 13, 321–335. doi: 10.1038/nri3430

Kim, S. H., Oh, J., Choi, J. Y., Jang, J. Y., Kang, M. W., and Lee, C. E. (2008). Identification of human thioredoxin as a novel IFN-gamma-induced factor: mechanism of induction and its role in cytokine production. *BMC Immunol.* 9:64. doi: 10.1186/1471-2172-9-64

Li, Y., Liu, H., Qi, H., Tang, W., Zhang, C., Liu, Z., et al. (2021). Probiotic fermentation of Ganoderma lucidum fruiting body extracts promoted its immunostimulatory activity in mice with dexamethasone-induced immunosuppression. *Biomed. Pharmacother.* 141:111909. doi: 10.1016/j.biopha.2021.111909

Liu, C., Cao, M., Yang, N., Reid-Adam, J., Tversky, J., Zhan, J., et al. (2022). Time-dependent dual beneficial modulation of interferon-gamma, interleukin 5, and Treg cytokines in asthma patient peripheral blood mononuclear cells by ganoderic acid B. *Phytother. Res.* 36, 1231–1240. doi: 10.1002/ptr.7266

Liu, M., Devlin, J. C., Hu, J., Volkova, A., Battaglia, T. W., Ho, M., et al. (2021). Microbial genetic and transcriptional contributions to oxalate degradation by the gut microbiota in health and disease. *elife* 10:10. doi: 10.7554/eLife.63642

Liu, F., Yin, J., Du, M., Yan, P., Xu, J., Zhu, X., et al. (2009). Heat-stress-induced damage to porcine small intestinal epithelium associated with downregulation of epithelial growth factor signaling. *J. Anim. Sci.* 87, 1941–1949. doi: 10.2527/jas.2008-1624

Lo, D. Y., Lee, W. M., Chien, M. S., Lin, C. C., and Lee, W. C. (2005). Effects of dexamethasone on peripheral blood mononuclear cell phenotype in weanling piglets. *Comp. Immunol. Microbiol. Infect. Dis.* 28, 251–258. doi: 10.1016/j.cimid.2005.03.001

Lu, J., and Holmgren, A. (2012). Thioredoxin system in cell death progression. *Antioxid. Redox Signal.* 17, 1738–1747. doi: 10.1089/ars.2012.4650

Luo, Z. W., Xia, K., Liu, Y. W., Liu, J. H., Rao, S. S., Hu, X. K., et al. (2021). Extracellular vesicles from *Akkermansia muciniphila* elicit antitumor immunity against prostate cancer via modulation of CD8(+) T cells and macrophages. *Int. J. Nanomed.* 16, 2949–2963. doi: 10.2147/IJN.S304515

Maldonado-Contreras, A., Ferrer, L., Cawley, C., Crain, S., Bhattarai, S., Toscano, J., et al. (2020). Dysbiosis in a canine model of human fistulizing Crohn's disease. *Gut Microb.* 12:1785246. doi: 10.1080/19490976.2020.1785246

Mata-Perez, C., and Spoel, S. H. (2019). Thioredoxin-mediated redox signalling in plant immunity. *Plant Sci.* 279, 27–33. doi: 10.1016/j.plantsci.2018.05.001

Mougiakakos, D., Johansson, C. C., Jitschin, R., Bottcher, M., and Kiessling, R. (2011). Increased thioredoxin-1 production in human naturally occurring regulatory T cells confers enhanced tolerance to oxidative stress. *Blood* 117, 857–861. doi: 10.1182/blood-2010-09-307041

Nam, J. H., Choi, J., Monmai, C., Rod-In, W., Jang, A. Y., You, S., et al. (2022). Immune-enhancing effects of crude polysaccharides from Korean ginseng berries on spleens of mice with cyclophosphamide-induced immunosuppression. *J. Microbiol. Biotechnol.* 32, 256–262. doi: 10.4014/jmb.2110.10021

Nicholson, J. K., Holmes, E., Kinross, J., Burcelin, R., Gibson, G., Jia, W., et al. (2012). Host-gut microbiota metabolic interactions. *Science* 336, 1262–1267. doi: 10.1126/science.1223813

Ostman, S., Rask, C., Wold, A. E., Hultkrantz, S., and Telemo, E. (2006). Impaired regulatory T cell function in germ-free mice. *Eur. J. Immunol.* 36, 2336–2346. doi: 10.1002/eji.200535244

Parada, V. D., De la Fuente, M. K., Landskron, G., Gonzalez, M. J., Quera, R., Dijkstra, G., et al. (2019). Short chain fatty acids (SCFAs)-mediated gut epithelial and immune regulation and its relevance for inflammatory bowel diseases. *Front. Immunol.* 10:277. doi: 10.3389/fimmu.2019.00277

Qu, S., Fan, L., Qi, Y., Xu, C., Hu, Y., Chen, S., et al. (2021). *Akkermansia muciniphila* alleviates dextran sulfate sodium (DSS)-induced acute colitis by NLRP3 activation. *Microbiol. Spectr.* 9:e73021. doi: 10.1128/Spectrum.00730-21

Quinteiro-Filho, W. M., Rodrigues, M. V., Ribeiro, A., Ferraz-de-Paula, V., Pinheiro, M. L., Sa, L. R., et al. (2012). Acute heat stress impairs performance parameters and induces mild intestinal enteritis in broiler chickens: role of acute hypothalamic-pituitary-adrenal axis activation. *J. Anim. Sci.* 90, 1986–1994. doi: 10.2527/jas.2011-3949

Randolph, R. K., Gellenbeck, K., Stonebrook, K., Brovelli, E., Qian, Y., Bankaitis-Davis, D., et al. (2003). Regulation of human immune gene expression as influenced by a commercial blended Echinacea product: preliminary studies. *Exp. Biol. Med. (Maywood)* 228, 1051–1056. doi: 10.1177/153537020322800910

Reunanen, J., Kainulainen, V., Huuskonen, L., Ottman, N., Belzer, C., Huhtinen, H., et al. (2015). *Akkermansia muciniphila* adheres to enterocytes and strengthens the integrity of the epithelial cell layer. *Appl. Environ. Microbiol.* 81, 3655–3662. doi: 10.1128/AEM.04050-14

Scher, J. U., Sczesnak, A., Longman, R. S., Segata, N., Ubeda, C., Bielski, C., et al. (2013). Expansion of intestinal *Prevotella copri* correlates with enhanced susceptibility to arthritis. *elife* 2:e1202. doi: 10.7554/eLife.01202

Segata, N., Izard, J., Waldron, L., Gevers, D., Miropolsky, L., Garrett, W. S., et al. (2011). Metagenomic biomarker discovery and explanation. *Genome Biol.* 12:R60. doi: 10.1186/gb-2011-12-6-r60

Sharifi-Rad, M., Mnayer, D., Morais-Braga, M., Carneiro, J., Bezerra, C. F., Coutinho, H., et al. (2018). Echinacea plants as antioxidant and antibacterial agents: from traditional medicine to biotechnological applications. *Phytother. Res.* 32, 1653–1663. doi: 10.1002/ptr.6101

Srinivasan, S., Hoffman, N. G., Morgan, M. T., Matsen, F. A., Fiedler, T. L., Hall, R. W., et al. (2012). Bacterial communities in women with bacterial vaginosis: high resolution phylogenetic analyses reveal relationships of microbiota to clinical criteria. *PLoS One* 7:e37818. doi: 10.1371/journal.pone.0037818

Stacy, A., Andrade-Oliveira, V., McCulloch, J. A., Hild, B., Oh, J. H., Perez-Chaparro, P. J., et al. (2021). Infection trains the host for microbiota-enhanced resistance to pathogens. *Cells* 184, 615–627.e17. doi: 10.1016/j.cell.2020.12.011

Trompette, A., Gollwitzer, E. S., Yadava, K., Sichelstiel, A. K., Sprenger, N., Ngom-Bru, C., et al. (2014). Gut microbiota metabolism of dietary fiber influences allergic airway disease and hematopoiesis. *Nat. Med.* 20, 159–166. doi: 10.1038/nm.3444

Wagenaar, C. A., van de Put, M., Bisschops, M., Walrabenstein, W., de Jonge, C. S., Herrema, H., et al. (2021). The effect of dietary interventions on chronic inflammatory diseases in relation to the microbiome: a systematic review. *Nutrients* 13:3208. doi: 10.3390/nu13093208

Wang, H., Wang, Y., Gao, B., Zhang, S., Diao, Y., and Tang, Y. (2020). Evidence of vertical transmission of novel duck orthoreovirus in ducks. *Vet. Microbiol.* 251:108861. doi: 10.1016/j.vetmic.2020.108861

Wei, Y., Chang, L., Ishima, T., Wan, X., Ma, L., Wuyun, G., et al. (2021). Abnormalities of the composition of the gut microbiota and short-chain fatty acids in mice after splenectomy. *Brain Behav. Immun. Health* 11:100198. doi: 10.1016/j.bbih.2021.100198

Wu, D. T., Yuan, Q., Feng, K. L., Zhang, J., Gan, R. Y., Zou, L., et al. (2022). Fecal fermentation characteristics of rheum tanguticum polysaccharide and its effect on the modulation of gut microbial composition. *Chin. Med.* 17:79. doi: 10.1186/s13020-022-00631-6

Yamashiro, Y. (2017). Gut microbiota in health and disease. *Ann. Nutr. Metab.* 71, 242–246. doi: 10.1159/000481627

Yang, W., and Cong, Y. (2021). Gut microbiota-derived metabolites in the regulation of host immune responses and immune-related inflammatory diseases. *Cell. Mol. Immunol.* 18, 866–877. doi: 10.1038/s41423-021-00661-4

Yu, X., Zheng, Q., He, Y., Yu, D., Chang, G., Chen, C., et al. (2022). Associations of gut microbiota and fatty metabolism with immune thrombocytopenia. *Front. Med.* 9:810612. doi: 10.3389/fmed.2022.810612

Zhai, Z., Liu, Y., Wu, L., Senchina, D. S., Wurtele, E. S., Murphy, P. A., et al. (2007). Enhancement of innate and adaptive immune functions by multiple Echinacea species. *J. Med. Food* 10, 423–434. doi: 10.1089/jmf.2006.257

Zhou, X., Liu, Z., Long, T., Zhou, L., and Bao, Y. (2018). Immunomodulatory effects of herbal formula of astragalus polysaccharide (APS) and polysaccharopeptide (PSP) in mice with lung cancer. *Int. J. Biol. Macromol.* 106, 596–601. doi: 10.1016/j.ijbiomac.2017.08.054

frontiers | Frontiers in Microbiology

TYPE Original Research
PUBLISHED 09 January 2023
DOI 10.3389/fmicb.2022.1050352



OPEN ACCESS

EDITED BY
Yung-Fu Chang,
Cornell University, United States

REVIEWED BY
Imran Muhammad,
Quaid-i-Azam University, Pakistan
Nisha Kannan,
Cornell University,
United States

*CORRESPONDENCE
Yun Sun
✉ syun@163.com

SPECIALTY SECTION
This article was submitted to Microorganisms in Vertebrate Digestive Systems, a section of the journal Frontiers in Microbiology

RECEIVED 21 September 2022
ACCEPTED 21 December 2022
PUBLISHED 09 January 2023

CITATION
Wang H, Zhou C, Gu S and Sun Y (2023) Surrogate fostering of mice prevents prenatal estradiol-induced insulin resistance *via* modulation of the microbiota-gut-brain axis. *Front. Microbiol.* 13:1050352. doi: 10.3389/fmicb.2022.1050352



# Surrogate fostering of mice prevents prenatal estradiol-induced insulin resistance *via* modulation of the microbiota-gut-brain axis

Huihui Wang[1,2,3], Chengliang Zhou[4,5], Shuping Gu[6] and Yun Sun[1,2,3]*

[1]Center for Reproductive Medicine, Renji Hospital, School of Medicine, Shanghai Jiao Tong University, Shanghai, China, [2]Shanghai Key Laboratory for Assisted Reproduction and Reproductive Genetics, Shanghai, China, [3]Animal Laboratory, Renji Hospital, School of Medicine, Shanghai Jiao Tong University, Shanghai, China, [4]International Peace Maternity and Child Health Hospital, School of Medicine, Shanghai Jiao Tong University, Shanghai, China, [5]Shanghai Key Laboratory of Embryo Original Diseases, Shanghai, China, [6]Department of Science and Technology Research, Shanghai Model Organisms, Shanghai, China

**Introduction:** Prenatal and early postnatal development are known to influence future health. We previously reported that prenatal high estradiol (HE) exposure induces insulin resistance in male mice by disrupting hypothalamus development. Because a foster dam can modify a pup's gut microbiota and affect its health later in life, we explored whether surrogate fostering could also influence glucose metabolism in HE offspring and examined mechanisms that might be involved.

**Methods:** We performed a surrogate fostering experiment in mice and examined the relationship between the metabolic markers associated to insulin resistance and the composition of the gut microbiota.

**Results:** HE pups raised by HE foster dams (HE-HE) developed insulin resistance, but HE pups fostered by negative control dams (NC-HE) did not. The gut microbiota composition of HE-HE mice differed from that of NC mice raised by NC foster dams (NC-NC), whereas the composition in NC-HE mice was similar to that of NC-NC mice. Compared with NC-NC mice, HE-HE mice had decreased levels of fecal short-chain fatty acids and serum intestinal hormones, increased food intake, and increased hypothalamic neuropeptide Y expression. In contrast, none of these indices differed between NC-HE and NC-NC mice. Spearman correlation analysis revealed a significant correlation between the altered gut microbiota composition and the insulin resistance-related metabolic indicators, indicating involvement of the microbiota-gut-brain axis.

**Discussion:** Our findings suggest that alterations in the early growth environment may prevent fetal-programmed glucose metabolic disorder *via* modulation of the microbiota-gut-brain axis. These findings offer direction for development of translational solutions for adult diseases associated with aberrant microbial communities in early life.

KEYWORDS

**prenatal exposure, estradiol, surrogate fostering, insulin resistance, microbiota-gut-brain axis**

# Introduction

Perinatal development exerts life-long effects on health and disease (Bateson et al., 2004). This observation has provided important clues for the etiological study and prevention of chronic disease, and has contributed to an increased emphasis on prenatal and postnatal care worldwide. With a rising rate in infertility, assisted reproductive technology (ART) has been adopted widely and has been predicted to contribute an extra 400 million (3.5%) people to the global population by 2,100 (Faddy et al., 2018). The potential health effects of ART on the resulting offspring have received increasing attention. We previously reported that glucose metabolism is impaired in male offspring from fresh embryo transfer with supraphysiologic maternal estradiol during early pregnancies generated by ovulation induction (Wang et al., 2018). This maternal hormone-induced metabolic disorder has been attributed to an intrauterine programming effect on hypothalamus development (Wang et al., 2018, 2021). In the current study, we sought to develop a more comprehensive understanding of the underlying mechanisms and to consider feasible approaches to prevention.

Glucose homeostasis is under the control of cross-talk between multiple organs, and the microbiota-gut-brain axis has emerged as a novel mechanism that is gaining attention (Mayer et al., 2015; Grasset and Burcelin, 2019). In this regulatory axis, microbial metabolites stimulate intestinal endocrine cells to produce a series of peptides. These peptides either directly enter the blood circulation or activate immune responses and vagus nerve *via* the enteric nervous system, ultimately affecting hypothalamic neuronal activity to modify metabolic functions (Coll and Yeo, 2013; Mayer et al., 2015). The past decade has seen a proliferation of studies implicating the microbiota-gut-brain axis in conditions such as obesity, diabetes, autism, and neurodegenerative diseases, indicating its significance in chronic disease and life-long health (Cryan et al., 2019). Thus, it is possible that this regulatory axis involves in the insulin resistance that develops after prenatal estradiol exposure.

The gut microbiota is the largest microecosystem of higher organisms, and has a complex and dynamic symbiotic relationship with the host (Heintz-Buschart and Wilmes, 2018). The gut microbiota colonizes prenatally (Walker et al., 2017; Younge et al., 2019) and its composition is shaped by genetic, nutritional, and environmental factors before and after birth (Gomaa, 2020). Alteration of the fostering environment after birth can thus be expected to influence the gut microbiota. Cross-fostering studies indicate that the nursing dam can permanently change the microbiota of foster pups from infancy (Daft et al., 2015; Treichel et al., 2019), and that this may affect health and disease later in life.

Short-chain fatty acids (SCFAs) are the most abundant microbiota-derived metabolites in the gut, mainly including acetate, propionate, and butyrate (Koh et al., 2016). They are involved in glucose metabolism through multiple mechanisms (Canfora et al., 2015; Kim et al., 2018). In the microbiota-gut-brain axis, SCFAs activate intestinal L cells to promote release of peptide YY (PYY) and glucagon-like peptide 1 (GLP-1), which are transported to the hypothalamus and reduce appetite, food intake, and weight gain (Kim et al., 2018; Kjaergaard et al., 2019). SCFAs are thus important for regulating glucose homeostasis.

Here, we examined whether the gut microbiota composition and the microbiota-gut-brain axis play a role in prenatal estradiol-induced adult hypothalamic insulin resistance (Wang et al., 2018) by conducting a surrogate foster experiment. This study will advance our understanding of prenatally derived glucose metabolism disorders and provide fresh insights into early intervention approaches.

# Materials and methods

## Animal model

We employed a previously described mouse model of prenatal high estradiol (HE) exposure (Wang et al., 2018). Briefly, 8-week-old pregnant C57BL/6 mice received 100 μg/kg/d estradiol valerate (Sigma) by gavage from E5.5 to E11.5 in the HE group, or an equal volume of solvent (corn oil) in the negative control (NC) group. Only male pups were included in the analysis (Wang et al., 2018). Newborn male mice were fostered by non-birth mothers who had given birth in the past 48 h and were ready to nurse, together with their biological offspring. The combinations of nursing mothers and foster pups were as follows: NC nursing mother with NC foster pup (NC-NC), HE nursing mother with HE foster pup (HE-HE), and NC nursing mother with HE foster pups (NC-HE). The number of foster pups and biological pups for each dam was 2: 2, and the foster pups in each given dam were littermates. Fostered pups were weaned at the age of 3 weeks and housed individually until the end of the experiment at 24 weeks. All mice were provided with the same sterilized food and wood chip bedding, and all operations were performed on a clean bench.

## Glucose and insulin tolerance tests

Intraperitoneal glucose tolerance tests (GTTs) and insulin tolerance tests (ITTs) were performed at 3 and 8 weeks after birth as described previously (Wang et al., 2018). Mice were fasted overnight for 16 h before being injected intraperitoneally with glucose at 2 g/kg body weight for the GTT, and were fasted for 6 h before being injected intraperitoneally with insulin at 1 U/kg body weight for the ITT. Glucose levels in tail blood were measured using an automatic glucometer (Roche) at 0, 30, 60, and 120 min after glucose or insulin injection. The area under the curve (AUC) was calculated to measure glucose and insulin tolerance.

## Food intake

The daily intake of each mouse was determined as described previously (Wang et al., 2018) as the difference

between the weight of food given and the weight remaining after 24 h. Daily intake was monitored for 1 week and the average was calculated.

## Enzyme-linked immunosorbent assay

Mice were anaesthetized with isoflurane and blood was collected by removing the eyeball. Serum levels of insulin, GLP-1, PYY, and cholecystokinin (CCK) were analyzed using ELISA kits from Crystal Chem (insulin) and Cusabio (GLP-1, PYY, and CCK) according to the manufacturer's instructions. In brief, serum samples and standards were incubated in the microtiter plate wells, followed by incubation with conjugate solution, substrate solution, and stop solution. The optical density values were measured at 450 nm using a microplate reader. A standard curve is constructed to determine the concentrations of target protein.

## Tissue immunofluorescence

Mice were transcardially perfused with 4% paraformaldehyde under anesthesia. Brains were removed and fixed in 4% paraformaldehyde for 4 h and then infiltrated with 20 to 30% sucrose. Brain sections (20 μm) were made using a freezing microtome (Leica), blocked with 5% bovine serum albumin/0.3% Triton X-100 for 1 h at room temperature, and incubated with primary antibodies overnight at 4°C. Sections were reacted with secondary antibodies at room temperature for 2 h and counterstained with 4′,6-diamidino-2-phenylindole. Primary antibodies were rabbit anti–neuropeptide Y (NPY) (1: 800, Cell Signaling Technology, catalog no. 11976) and rabbit anti-proopiomelanocortin (POMC) (1: 500, Abcam, catalog no. ab254257). The secondary antibody was anti-rabbit Alexa Fluor 594 (1: 1000, Abcam, catalog no. ab150080). NPY-and POMC-positive cells were counted in five serial sections from each mouse using ImageJ software (National Institutes of Health; Arena et al., 2017).

## Quantitative real-time polymerase chain reaction

Mice were euthanized by decapitation, brains were quickly removed, and hypothalami were dissected and homogenized in TRIzol (Invitrogen) on ice. RNA extraction and qPCR were performed to detect the expression of *Npy* and *Pomc* as previously described (Wang et al., 2021). The primers used are listed in Table 1, and β-actin was used as an endogenous control. Relative expression was determined using the $2^{-\Delta\Delta CT}$ method.

## Microbiota community analysis

Fresh feces of offspring were collected with sterile equipment after stimulating the perianal area. Vaginal lavage fluid of pregnant mice was collected by flushing the vagina with 20 μl sterile phosphate-buffered saline using a sterile pipette. We performed 16S rRNA sequencing to analyze the microbiota composition. Total DNA of fecal and vaginal lavage samples was extracted using the QIAamp Rapid DNA Mini kit (Qiagen), and a sequencing library was constructed from amplicons targeting the V3 and V4 regions of the 16S ribosomal RNA gene using primers 338F (5′-ACTCCTACGGGAGGCAGCAG-3′) and 806R (5′-GGACTACHVGGGTWTCTAAT-3′). Paired-end sequencing was performed on the Illumina MiSeq platform, and raw data were filtered by Trimmomatic and FLASH software. All clean reads were clustered into operational taxonomic units using Ribosomal Database Project (RDP) Classifier (v. 2.11) at 97% sequence similarity. Taxonomic assignment of operational taxonomic units was performed using the RDP database (Cole et al., 2014). Chao 1 and Shannon indices were calculated using QIIME 2 (version 2020.2) (Caporaso et al., 2010), and principal coordinates analysis (PCoA) was conducted based on the weighted UniFrac distance. PICRUST2 was used to predict the functional composition of bacterial genera based on the Kyoto Encyclopedia of Genes and Genomes (KEGG) database (Douglas et al., 2020).

## SCFA analysis

SCFAs were measured by liquid chromatography–tandem mass spectrometry (LC–MS/MS) through a commercial laboratory (Lumingbio, Shanghai, China). Briefly, fecal and serum samples were homogenized and ultrasound-extracted in 50% (v/v) acetonitrile/water containing an isotopic internal standard. After centrifugation, supernatants were derivatized with 200 mM 3-nitrophenylhydrazine and 120 mM ethylcarbodiimide hydrochloride-6% pyridine for 30 min at 40°C. Reaction mixtures were analyzed on an AB ExionLC/AB Sciex Qtrap 6500+ LC–MS/MS system.

TABLE 1 Primers used for qPCR.

| Gene | Primer sequence |
|---|---|
| *β-actin* | Forward 5′-GTCCCTCACCCTCCCAAAAG-3′ |
| | Reverse 5′-GCTGCCTCAACACCTCAACCC-3′ |
| *Npy* | Forward 5′-ATGCTAGGTAACAAGCGAATGG-3′ |
| | Reverse 5′-TGTCGCAGAGCGGAGTAGTAT-3′ |
| *Pomc* | Forward 5′-ATGCCGAGATTCTGCTACAGT-3′ |
| | Reverse 5′-TCCAGCGAGAGGTCGAGTTT-3′ |

## Statistical analysis

A one-way analysis of variance (ANOVA) with Tukey *post hoc* test was used for comparisons among three groups, and an unpaired Student's *t*-test was used for comparisons between two groups using the Statistical Package for Sciences Software, v. 21.0 (IBM). Data are presented as mean ± standard error of the mean (SEM). Spearman correlation analysis was performed and plotted using R software. $p < 0.05$ was considered statistically significant.

# Results

## Surrogate fostering prevents insulin resistance in mice exposed prenatally to high estradiol

To induce the mouse model of prenatal HE exposure (Wang et al., 2018), pregnant 8-week-old C57BL/6 mice received gavage of estradiol valerate in corn oil (HE) or corn oil alone (negative control or NC). We compared male HE pups fostered by another HE dam (HE-HE) to male HE pups fostered by an NC dam (HE-NC) and male NC pups fostered by another NC dam (NC-NC) (Figure 1A).

To minimize the influence of handling on the odor of fostered pups and thus avoid cub eating, we monitored pup body weight from weaning at 3 weeks rather than from birth. Consistent with our previous study (Wang et al., 2018), the weight of HE-HE male mice exceeded that of the NC-NC group beginning at 20 weeks; in contrast, no significant difference was observed between the NC-HE and NC-NC groups (Figure 1B). Based on our previous observation that male HE mice present insulin resistance at 24 weeks (Wang et al., 2018), we examined glucose metabolism in the three foster groups at this age. The AUC for both GTT and ITT was higher in the HE-HE group, with no significant difference between the NC-HE and NC-NC groups (Figures 1C,D). We also compared fasting glucose, fasting insulin, and homeostasis model assessment for insulin resistance (HOMA-IR) scores at 24 weeks. No differences in fasting glucose were observed among the three groups (Figure 1E). On the other hand, fasting insulin and HOMA-IR scores were increased in HE-HE mice, with no difference between the NC-HE and NC-NC groups (Figures 1F,G). These observations indicated that HE pups fostered by NC dams no longer presented insulin resistance in later life as those fostered by HE dams did.

## Surrogate fostering modulates the composition of gut microbiota in male HE mice

Because the nursing dam has been shown to induce lasting alterations in the microbiota of foster pups (Daft et al., 2015; Treichel et al., 2019), we sought to investigate whether the prevention of insulin resistance in NC-HE mice could be attributed to a correction of a microflora disorder. We performed 16S rRNA sequencing to analyze the microbiota composition of the intestinal contents in the three groups at 3 and 24 weeks. Chao 1 and Shannon indices were used as measures of α diversity, and PCoA plots were used for β diversity. At both 3 and 24 weeks, HE-HE mice had decreased α diversity, with no significant difference between the NC-NC and NC-HE groups (Figures 2A,B, H, I). The HE-HE clusters in the PCoA plots were clearly separate from the NC-NC and NC-HE clusters, which were overlapped (Figures 2C, J), indicating that there was no significant difference between NC-NC and NC-HE. The heatmap of the top 50 differentiated taxa with the highest genus level at both 3 and 24 weeks demonstrated that the microbiota community composition in HE-HE mice was distinct from that of the other two groups, and that the NC-HE group was closer to the NC-NC group (Figures 2D, K). Phylum-level analysis revealed that the taxonomic distribution of the HE-HE group differed markedly from that of the NC-NC and NC-HE groups (Figures 2E, L), with a significantly higher abundance of *Firmicutes* and lower abundance of *Bacteroidetes* (Figures 2F, M), leading to an increased ratio of *Firmicutes*/*Bacteroidetes* (F/B) (Figures 2G, N). The NC-NC and NC-HE samples had no significant difference in phylum distribution or F/B ratio. These results indicate that HE exposure leads to a change in gut microbiota composition prior to weaning that is sustained at least until the observed age of insulin resistance, and that surrogate fostering by an NC dam prevents this change in gut microbiota.

## Surrogate fostering restores fecal SCFA and intestinal hormone levels in male HE mice

To further investigate how surrogate fostering affects metabolism, we measured gut microbiota metabolites in feces at 24 weeks using LC–MS/MS. Acetic acid, butyric acid, and propionic acid concentrations all decreased significantly in the HE-HE group and were restored in the NC-HE group (Figure 3A). Other SCFAs were not significantly changed. In addition, as downstream molecules of SCFAs in blood circulation, we assessed the levels of serum intestinal hormones GLP-1, PYY, and CCK by ELSIA. GLP-1 and PYY were decreased in HE-HE mice and were restored in NC-HE mice (Figure 3B). CCK levels did not differ among the three groups.

## Surrogate fostering attenuates increased food intake and hypothalamic NPY in male HE mice

Prenatal HE exposure increases both food intake and hypothalamic NPY expression, which contribute to weight gain and insulin resistance (Wang et al., 2018), so we examined these

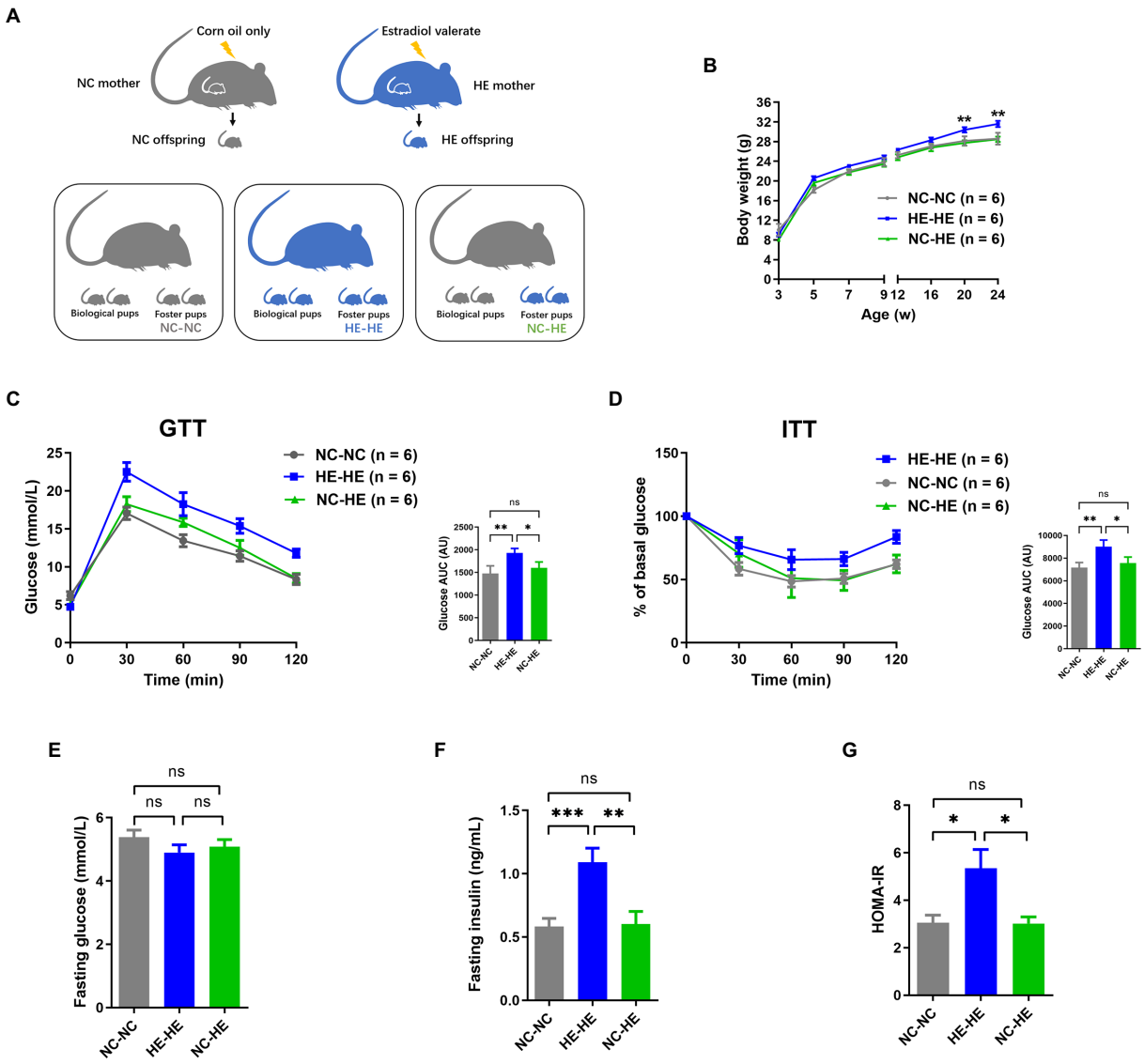


FIGURE 1
Body weight and glucose metabolism assessments of NC-NC, HE-HE, and NC-HE mice from the surrogate fostering mouse model. **(A)** Schematic of method used to generate the model. **(B)** Body weight from 3 to 24weeks after birth. **(C)** GTT, **(D)** ITT, **(E)** fasting glucose, **(F)** fasting insulin, and **(G)** HOMA-IR scores at 24weeks after birth. In **(C,D)**, left shows raw data and right shows AUC in arbitrary units (AU). Error bars represent SEM. Significance determined by one-way ANOVA. *$p$<0.05; **$p$<0.01; ***$p$<0.001; ns, not significant.

parameters in fostered mice. Food intake in HE-HE mice began to increase at 8 weeks, significantly exceeded that of NC-NC and NC-HE mice at 20 weeks, but there was no a difference in food intake between NC-NC and NC-HE mice (Figure 4A). In all three groups, food intake increased with body weight (Figure 1B). Hypothalamic NPY (orexigenic) and POMC (anorexigenic) were examined because they play significant roles in stimulating and suppressing appetite, respectively. Results of qPCR revealed significantly increased expression of *Npy* mRNA in HE-HE mice at 24 weeks, but no difference between NC-HE and NC-NC mice (Figure 4B). *Pomc* mRNA expression did not differ among the three groups (Figure 4B). Immunostaining revealed a significant increase in NPY-positive cells in the arcuate paraventricular nuclei of HE-HE hypothalami, but no difference between NC-HE and NC-NC hypothalami (Figures 4C,D). The number of POMC-positive cells was similar among all three groups (Figures 4E,F).

## Correction of insulin resistance by surrogate fostering involves the microbiota-gut-brain axis

We next assessed the association between the changes in gut microbiota composition and the metabolic alterations observed at 24 weeks. Spearman correlation analysis was performed between the top 50 enriched genera and the significantly

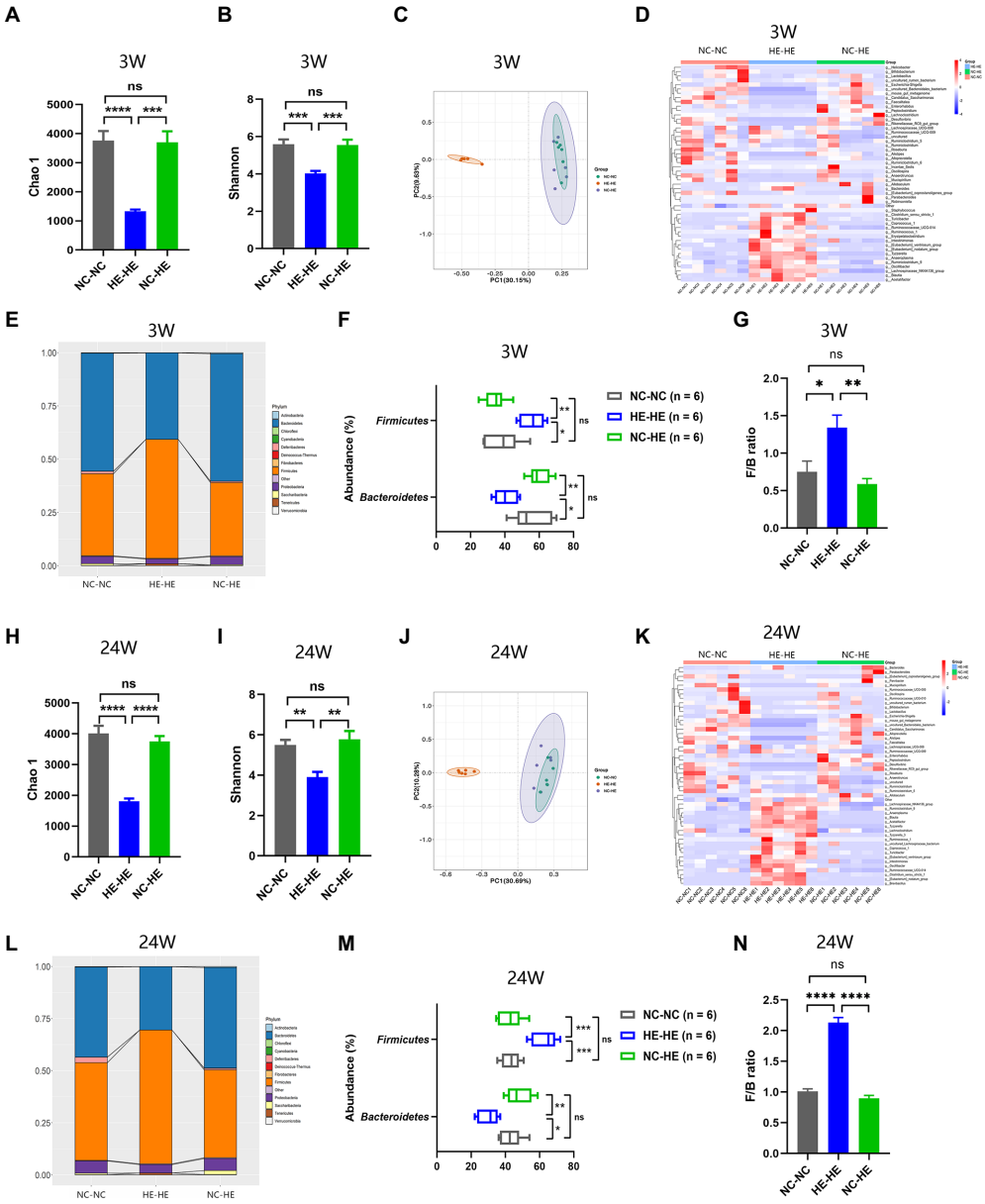


FIGURE 2
Gut microbiota composition analysis in 3-week-old **(A–G)** and 24-week-old **(H–N)** NC-NC, HE-HE, and NC-HE mice. **(A,H)** Chao 1 index, **(B,I)** Shannon index, and **(C,J)** PCoA plots of gut microbiota. **(D,K)** Heatmap of top 50 differentiated genera. **(E,L)** Phylum distribution. **(F,M)** Abundance of *Firmicutes* and *Bacteroidetes*. **(G,N)** Relative *Firmicutes*/*Bacteroidetes (F/B)* ratio. Error bars represent SEM. Significance determined by one-way ANOVA. **p*<0.05; ***p*<0.01; ****p*<0.001; *****p*<0.0001; ns, not significant.

different metabolic indices among the three groups. For metabolic changes, we included acetic acid, butyric acid, propionic acid, GLP-1, and PYY as beneficial indices, and GTT AUC, ITT AUC, fasting insulin, HOMA-IR score, food intake, and body weight as adverse indices. In Figure 5A, correlation index values are presented in a heatmap with asterisks to indicate a significance of $p<0.05$. The majority of genera showed opposite correlations between beneficial and adverse indices, and 22 of 50 presented a significant correlation with all metabolic indices.

Finally, we used PICRUSt2 software online[1] to predict the functional composition of these 22 genera based on the KEGG database. The results indicate that metabolism was the most abundant pathway (level 1), accounting for 41–47% of the total relative abundance (Figure 5B). At level 2, the main contributors to metabolism were carbohydrate metabolism (9.1–9.6%), amino acid metabolism (8.6–9.5%) and energy metabolism (4.5–6.4%)

1 https://www.omicstudio.cn/analysis

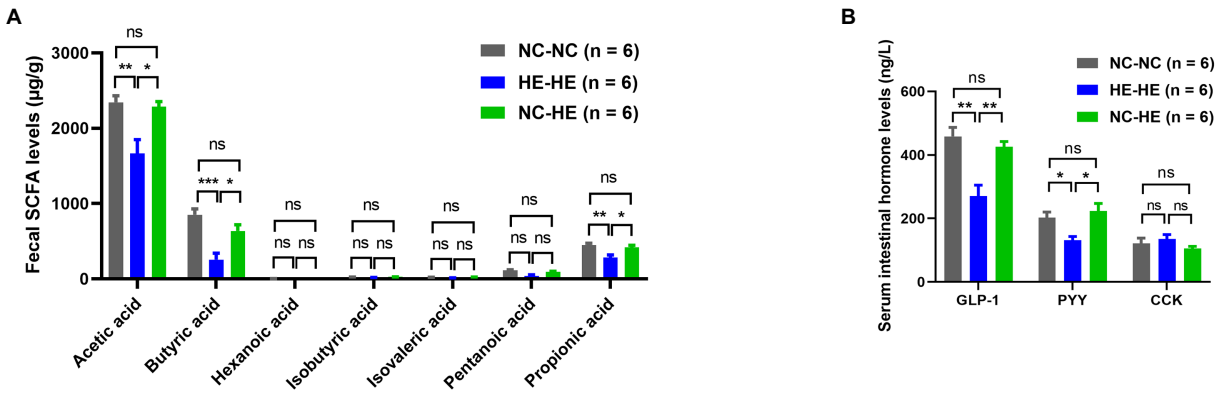


FIGURE 3
Fecal SCFA **(A)** and serum intestinal hormone **(B)** analysis in 24-week-old NC-NC, HE-HE, and NC-HE mice. Error bars represent SEM. Significance determined by one-way ANOVA. *$p$<0.05; **$p$<0.01; ***$p$<0.001; ns, not significant.

(Figure 5C). Therefore, the altered gut microbiota composition resulting from surrogate fostering correlated significantly with the correction of insulin resistance, fecal SCFAs, serum intestinal hormones, and hypothalamic NPY. These factors constitute a microbiota-gut-brain axis that exerted a remodeling effect on prenatal HE-induced glucose metabolic disorder (Figure 6).

## Discussion

Prenatal and postnatal development are critical in the etiology of many chronic diseases. An adverse intrauterine environment contributes to the risk of pathologic conditions such as metabolic syndrome, cardiovascular diseases, and behavioral or cognitive dysfunctions, leading to impaired quality of life and shortened life span (Drever et al., 2010; Rinaudo and Wang, 2012; Reynolds et al., 2019). As ART is increasingly adopted worldwide, involving conditions of abnormal prenatal hormone exposure, monitoring the life-long health of the resulting offspring and exploring interventions for proven adverse outcomes will have undeniable benefits for global health.

Supraphysiologic maternal estradiol induced glucose and insulin intolerance in male rather than female human offspring, and this sex-specific effect was confirmed in a mouse model (Wang et al., 2018). Therefore, as a continuation and extension of this previously published research, our current study continues to focus on male pups. We hypothesize that this gender disparity is caused by male offspring's susceptibility to prenatal high estradiol exposure, albeit the precise mechanism needs to be studied further.

We demonstrated here that prenatal high estradiol exposure disrupted the gut microbiota composition in mice, and that these changes were closely related to changes in metabolic function. It is not clear whether maternal estradiol affects the offspring's gut microbiota directly in the uterus or indirectly after birth. In the current literature, there is no consistent evidence of bacterial communities in mouse fetal tissue (Theis et al., 2020), and cultivatable bacteria with low abundance have been detected in the mouse fetal intestine during mid-gestation but not late gestation (Younge et al., 2019). This suggests that estradiol exposure may not have a direct effect on the microbiota *in utero*, and also that the fetal microbiota is less likely than the postnatal microbiota to affect later health. Since we also discovered that high maternal estradiol modulates hypothalamic neurogenesis and induces hypothalamic insulin resistance in offspring, it is reasonable to speculate that bidirectional brain-gut communication may play a role in changing the gut microbiota in HE-HE mice after birth (Martin et al., 2018), but further investigation is required to elucidate the specific mechanism(s) involved.

Early development is highly vulnerable to environmental challenges, but mounting evidence suggests that favorable conditions can revert the detrimental outcomes. Postnatal antibiotic treatments, diet, and environmental exposures can modulate the infant's microbiome (Tamburini et al., 2016). As a natural source of microbes, the rearing environment plays a crucial role in bacterial colonization in newborns. Cohabitation is known to increase bacterial exchange (Flores et al., 2014), and family members have more similar microbiota than unrelated individuals (Song et al., 2013). Therefore, the idea of dam-to-pup microbiome transfer in the surrogate fostering experiment is valid and feasible.

Because fostering by a nursing mother most certainly induces stress in pups, we designed the experiment so that pups in all groups are raised by foster mothers. The effect of stress on the microbiota is insignificant compared with the effect of the nursing dam itself (Treichel et al., 2019). We compared the vaginal microbiota in HE and NC mothers before delivery at E18.5. The genus heatmap presented a similar microbiota composition (Supplementary Figure S1), ruling out the possibility that the altered gut microbiome in the HE offspring originated from the maternal vagina. This finding supports our previous result that an increased risk of insulin resistance

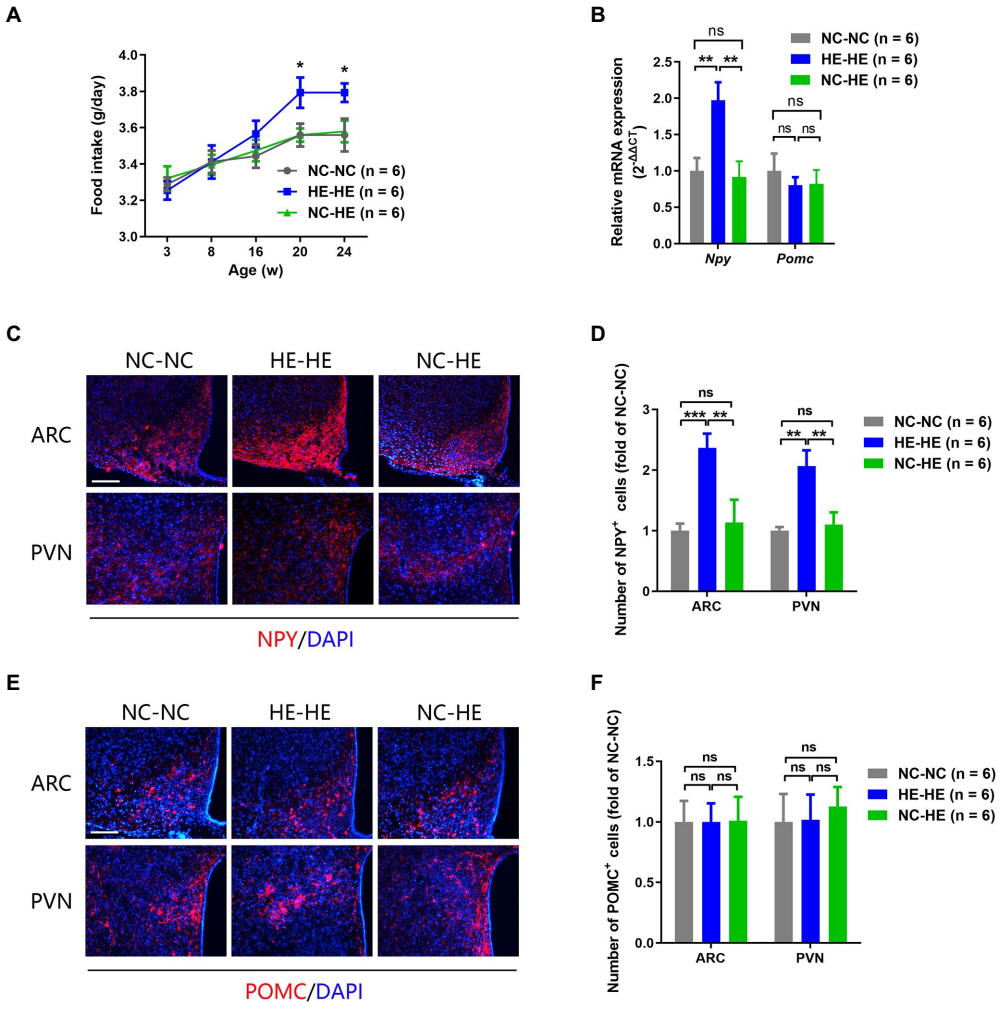


FIGURE 4
Food intake and hypothalamic neuropeptide expression in NC-NC, HE-HE, and NC-HE mice. **(A)** Daily food intake at 3–24weeks. **(B)** qPCR of hypothalamic *Npy* and *Pomc* at 24weeks of age. **(C,E)** Representative images of NPY and POMC immunolabeling in the arcuate nucleus (ARC) and paraventricular nucleus (PVN). Scale bars: 100μm. **(D,F)** Quantification of NYP-and POMC-positive cells in the ARC and PVN. Error bars represent SEM. Significance determined by one-way ANOVA. *$p$<0.05; **$p$<0.01; ***$p$<0.001; ns, not significant.

developed in male newborns and children of fresh embryo transfer (exposed to high maternal estradiol) born both by cesarean delivery and by vaginal delivery (Wang et al., 2018). Based on these observations, we speculate that the different microbiota transferred from dam to pup in our experiment is mainly attributable to a direct transfer through breast milk, or exposure to skin, saliva, or feces of the nursing mother or the co-reared biological pups. Further studies are needed to address this question. Likewise, human studies have verified that the bacteria are vertically transferred from mother to infant by breast feeding (Pannaraj et al., 2017; Wang S. et al., 2020), they can also be determined by older siblings in the home (Christensen et al., 2022). Other perinatal conditions like type of feeding, lifestyle, and environmental exposure can also modulate the development and maturation of the infant gut microbiota in human children (Derrien et al., 2019). These evidences support the supposed way of microbiota transfer in our experiment discussed above.

We found that HE-HE mice had a distinctly different fecal microbiota composition at weaning and in adulthood. This was observed as changes in α diversity, β diversity, and taxonomic distribution. The reduced microbial diversity and elevated F/B ratio in HE-HE pups was consistent with the insulin resistance phenotype (Pascale et al., 2019). The 3-week and 24-week genus heatmaps shared decreased abundances of *Alistipes* and *Alloprevotella* and increased abundances of *Anaerotruncus, Oscillibacter, Blautia, Allobaculum, Acetatifactor, Turicibacter, Tyzzerella,* and *Intestinimonas* in HE-HE feces (Figures 2D, K). These changes were reversed when HE pups were fostered by NC dams. According to published studies, a drop in *Alloprevotella* (Wang J. et al., 2020; Wu et al., 2021; Zhang et al., 2021; Zhao et al., 2021; Hao et al., 2022; Liu et al., 2022) and an increase in *Blautia*

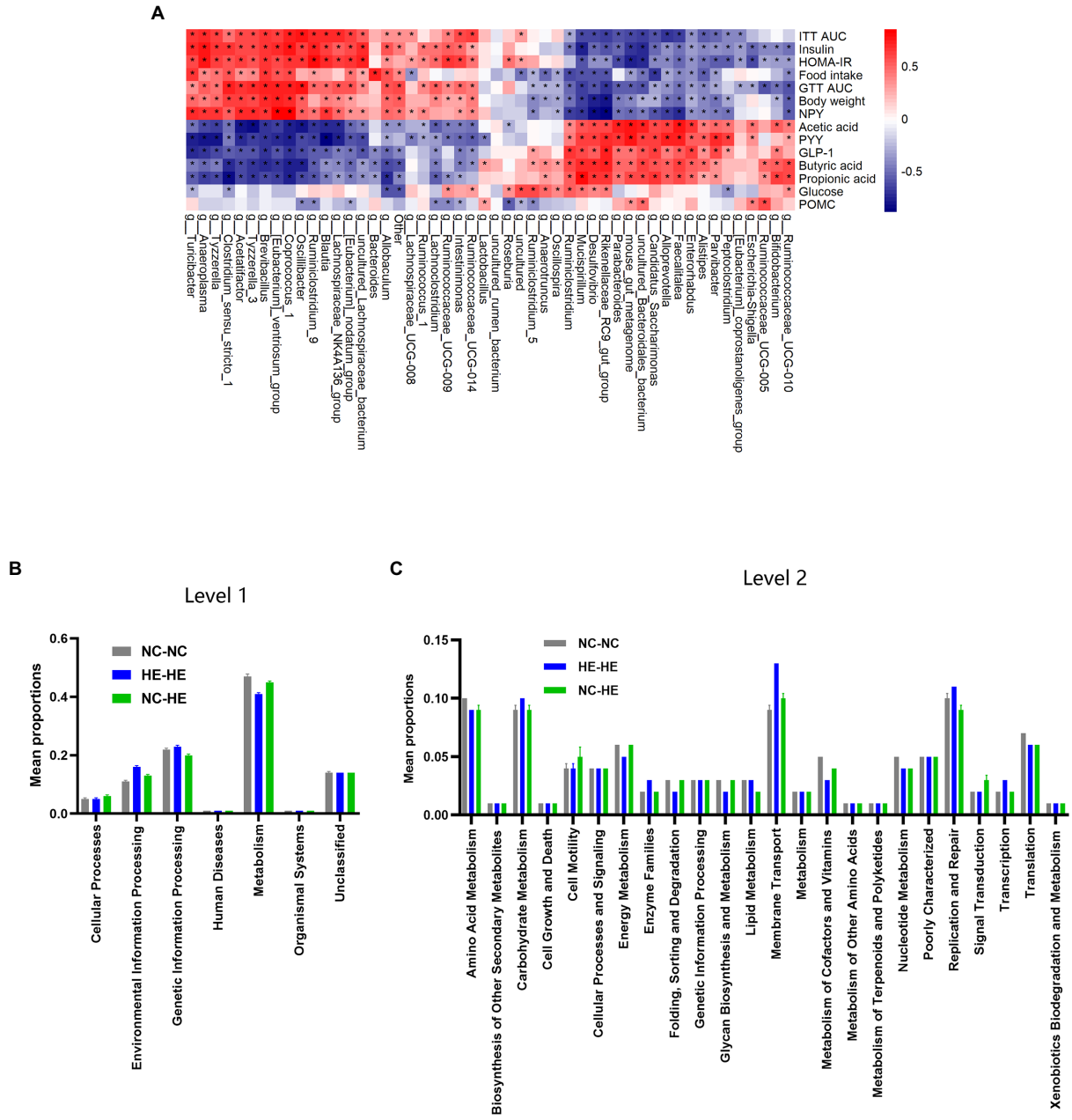


FIGURE 5
Correlation analysis between gut bacterial genera and metabolic indices. **(A)** Heatmap of Spearman correlation analysis between the top 50 differentiated genera and metabolic indices. The degree of correlation is shown by a gradient from red (positive correlation) to blue (negative correlation); asterisks indicate $p<0.05$. **(B,C)** KEGG pathway prediction of genera at levels 1 **(B)** and 2 **(C)** by PICRUSt2 analysis.

(Zhao et al., 2021; Bao et al., 2022) and *Tyzzerella* (Li et al., 2022) are found in animal models of in insulin resistance or glucose intolerance. On the other hand, antidiabetic medications and bioactive compounds modulate the gut microbial community of diabetic mouse model, characterized by increased *Alistipes* (Hu et al., 2019; Jeong et al., 2021; Li et al., 2021; Wu R. et al., 2022) and decreased *Anaerotruncus* (Yong et al., 2022), *Oscillibacter* (Lin et al., 2022; Wang et al., 2022), *Allobaculum* (Jia et al., 2017; Shen et al., 2021; Xu et al., 2021; Ma et al., 2022), *Acetatifactor* (Wu Y. et al., 2022) and *Turicibacter* (Zhao et al., 2021). These findings coincide with the correlation between microbiota and metabolic phenotypes in our study. However, other studies claim *Alistipes* positively correlates with glucose intolerance (Han et al., 2020; Li et al., 2022), while *Allobaculum* (Li et al., 2017; Wang et al., 2017), *Acetatifactor* (Zhao et al., 2022) and *Intestinimonas* (Cai et al., 2020; Ma et al., 2022) are beneficial genera in glucose metabolism. It should be noted that a recent study warned about the inconsistency of microbe-disease associations across a large

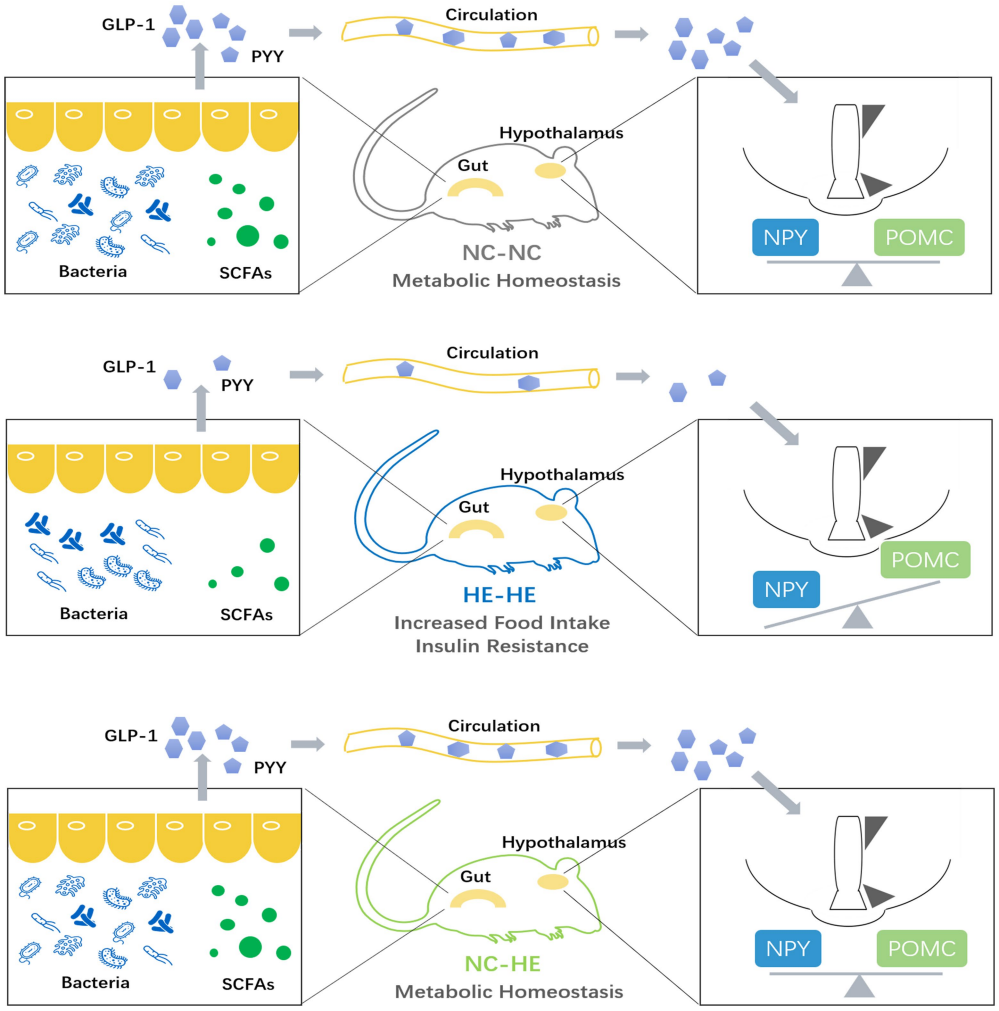


FIGURE 6
Model illustrating the role of the microbiota-gut-brain axis in the prevention of prenatal high estradiol-induced insulin resistance by surrogate fostering.

number of public cohorts and individuals (Tierney et al., 2022). Therefore, our study should be valued for its demonstration of an insulin resistance correction *via* modulation of the overall microbiota community rather than as an etiologic mechanism involving any specific bacterial genus or genera.

Gut-derived SCFAs are microbiota-produced fermentation products. They exert beneficial properties including improving insulin sensitivity, inhibiting white adipose tissue accumulation, and suppressing inflammation (Bolognini et al., 2021). Because over 95% of SCFAs produced in the gut are absorbed by the host (den Besten et al., 2013), the decreased fecal SCFAs observed in HE-HE mice could be attributed to either decreased production or increased absorption. We therefore checked blood levels of acetic acid, butyric acid, and propionic acid and found that they were also decreased in HE-HE mice (Supplementary Figure S2), indicating a reduced total production. This could be associated with the reduced diversity of gut microbes (Martin-Gallausiaux et al., 2021) and the decreased abundance of SCFA-producers like *Alistipes* (Parker et al., 2020) and *Alloprevotella* (Chen et al., 2020) as we described above.

The hypothalamic arcuate nucleus–paraventricular nucleus feeding network releases NPY and POMC, playing a major role in feeding regulation and hypothalamus-centered glucoregulatory system (Parker and Bloom, 2012). We found that hypothalamic NPY was elevated in HE-HE mice and restored in NC-HE mice, while the POMC levels were unaffected by the foster dam. This indicates that the metabolic effect of the nursing dam was exerted through inhibition of orexigenic neurons rather than activation of anorexigenic neurons. Gut microbes produce other neuroactive substances such as folate, serotonin, dopamine, and γ-aminobutyric acid (Asano et al., 2012). The hypothalamus regulates feeding behavior by integrating these interoceptive signals from gut microbes (Moura-Assis et al., 2021) *via* various mechanisms that may involve neurotransmission, neurogenesis, and neuroinflammation (Cryan et al., 2019). Future investigations can examine whether these regulatory mechanisms are also

involved in estradiol-induced insulin resistance and its recovery by surrogate fostering.

In our correlation analysis between microbiota and metabolic indices, 5 of the 11 bacterial genera correlated with beneficial metabolic indices belonged to *Bacteroidetes*, and 10 out of the 11 bacterial genera correlated with adverse metabolic indices belonged to *Firmicutes*. PICRUSt2 analysis revealed metabolic pathways as the most enriched function among these 22 genera, and more specifically carbohydrate, amino acid, and energy metabolism. Carbohydrate metabolism includes active carbon-related metabolic pathways and organic substance biotransformation (Wang P. et al., 2020); amino acid metabolism reflects the role of amino acids as energy sources for microbial growth (Lopez-Gonzalez et al., 2015); and energy metabolism is closely related to glucose homeostasis and energy expenditure in the host (Cani et al., 2019). Thus, these functional predictions provide further evidence for the effect of the dam-to-pup transfer of the microbiome. Although the precise effect of these bacterial genera on host metabolism changes in our study has yet to be determined, microbiota analysis combined with metabolomic and proteomic profiling is likely to reveal a more comprehensive microbiota-gut-brain regulatory network.

Taken together, our observations suggest that altering the early growth environment may be a novel prevention and treatment strategy for regulating the gut microbiota, preventing insulin resistance, and correcting other metabolic disorders resulting from intrauterine hormone exposure. These insights may shed light on potential interventions for children prenatally exposed to high estradiol levels. For example, early environmental modifications such as more frequent contact with children without prenatal high estradiol exposure may improve glucose metabolism in their later life. Such hypotheses will require validation by cohort studies. Overall, our research presents a microbiota-gut-brain regulation axis in prenatal estradiol-induced insulin resistance and offers direction for development of translational solutions for adult diseases associated with aberrant microbial communities in early life.

## Conclusion

Our experiments demonstrate that insulin resistance in male mice prenatally exposed to high estradiol can be prevented by surrogate fostering from birth, and that this effect is mediated by a microbiota-gut-brain modulation axis. This study reveals the crucial importance of the postnatal rearing environment in adult health, and sheds new light on possibilities for early prevention of developmentally mediated glucose metabolism disorder.

## Data availability statement

The datasets presented in this study can be found in online repositories. The names of the repository/repositories and accession number(s) can be found at: https://www.ncbi.nlm.nih.gov/bioproject/PRJNA862308.

## Ethics statement

The animal study was reviewed and approved by the Institutional Animal Care and Use Committee of Shanghai Jiao Tong University.

## Author contributions

HW and YS conceived and designed the experiments. HW, CZ, and SG performed the experiments, collected and analyzed the data, and drafted the manuscript. YS revised the final manuscript. All authors reviewed and approved the final version prior to submission.

## Funding

This work was supported by the National Key R&D Program of China (2019YFA0802604), the National Natural Science Foundation of China (81901552 and 82130046), and the Innovative Research Team of High-Level Local Universities in Shanghai (SHSMU-ZLCX20210200 and SSMU-ZLCX20180401).

## Conflict of interest

The authors declare that the research was conducted in the absence of any commercial or financial relationships that could be construed as a potential conflict of interest.

## Publisher's note



## Supplementary material

The Supplementary material for this article can be found online at: https://www.frontiersin.org/articles/10.3389/fmicb.2022.1050352/full#supplementary-material

SUPPLEMENTARY FIGURE S1
Vaginal microbiota analysis in pregnant E18.5 HE and NC mice. **(A,B)** Chao 1 and Shannon indices ($n$=3). **(C)** Heatmap of top 30 enriched genera. Error bars represent SEM. Significance determined by Student's $t$-test. ns, not significant.

SUPPLEMENTARY FIGURE S2
Serum SCFA concentration in 24-week-old NC-NC, HE-HE, and NC-HE mice. Error bars represent SEM. Significance determined by one-way ANOVA. **$p$<0.01; ***$p$<0.001; ****$p$<0.0001; ns, not significant.

# References

Arena, E. T., Rueden, C. T., Hiner, M. C., Wang, S., Yuan, M., and Eliceiri, K. W. (2017). Quantitating the cell: turning images into numbers with ImageJ. *Wiley Interdiscip. Rev. Dev. Biol.* 6:e260. doi: 10.1002/wdev.260

Asano, Y., Hiramoto, T., Nishino, R., Aiba, Y., Kimura, T., Yoshihara, K., et al. (2012). Critical role of gut microbiota in the production of biologically active, free catecholamines in the gut lumen of mice. *Am. J. Physiol. Gastrointest. Liver Physiol.* 303, G1288–G1295. doi: 10.1152/ajpgi.00341.2012

Bao, M., Hou, K., Xin, C., Zeng, D., Cheng, C., Zhao, H., et al. (2022). Portulaca oleracea L. extract alleviated type 2 diabetes via modulating the gut microbiota and serum branched-chain amino acid metabolism. *Mol. Nutr. Food Res.* 66:e2101030:e2101030. doi: 10.1002/mnfr.202101030

Bateson, P., Barker, D., Clutton-Brock, T., Deb, D., D'Udine, B., Foley, R. A., et al. (2004). Developmental plasticity and human health. *Nature* 430, 419–421. doi: 10.1038/nature02725

Bolognini, D., Dedeo, D., and Milligan, G. (2021). Metabolic and inflammatory functions of short-chain fatty acid receptors. *Curr. Opin. Endocr. Metab. Res.* 16, 1–9. doi: 10.1016/j.coemr.2020.06.005

Cai, W., Xu, J., Li, G., Liu, T., Guo, X., Wang, H., et al. (2020). Ethanol extract of propolis prevents high-fat diet-induced insulin resistance and obesity in association with modulation of gut microbiota in mice. *Food Res. Int.* 130:108939. doi: 10.1016/j.foodres.2019.108939

Canfora, E. E., Jocken, J. W., and Blaak, E. E. (2015). Short-chain fatty acids in control of body weight and insulin sensitivity. *Nat. Rev. Endocrinol.* 11, 577–591. doi: 10.1038/nrendo.2015.128

Cani, P. D., Van Hul, M., Lefort, C., Depommier, C., Rastelli, M., and Everard, A. (2019). Microbial regulation of organismal energy homeostasis. *Nat. Metab.* 1, 34–46. doi: 10.1038/s42255-018-0017-4

Caporaso, J. G., Kuczynski, J., Stombaugh, J., Bittinger, K., Bushman, F. D., Costello, E. K., et al. (2010). QIIME allows analysis of high-throughput community sequencing data. *Nat. Methods* 7, 335–336. doi: 10.1038/nmeth.f.303

Chen, H., Zhang, F., Zhang, J., Zhang, X., Guo, Y., and Yao, Q. (2020). A holistic view of berberine inhibiting intestinal carcinogenesis in conventional mice based on microbiome-metabolomics analysis. *Front. Immunol.* 11:588079. doi: 10.3389/fimmu.2020.588079

Christensen, E. D., Hjelmso, M. H., Thorsen, J., Shah, S., Redgwell, T., Poulsen, C. E., et al. (2022). The developing airway and gut microbiota in early life is influenced by age of older siblings. *Microbiome* 10:106. doi: 10.1186/s40168-022-01305-z

Cole, J. R., Wang, Q., Fish, J. A., Chai, B., McGarrell, D. M., Sun, Y., et al. (2014). Ribosomal database project: data and tools for high throughput rRNA analysis. *Nucleic Acids Res.* 42, D633–D642. doi: 10.1093/nar/gkt1244

Coll, A. P., and Yeo, G. S. (2013). The hypothalamus and metabolism: integrating signals to control energy and glucose homeostasis. *Curr. Opin. Pharmacol.* 13, 970–976. doi: 10.1016/j.coph.2013.09.010

Cryan, J. F., O'Riordan, K. J., Cowan, C. S. M., Sandhu, K. V., Bastiaanssen, T. F. S., Boehme, M., et al. (2019). The microbiota-gut-brain axis. *Physiol. Rev.* 99, 1877–2013. doi: 10.1152/physrev.00018.2018

Daft, J. G., Ptacek, T., Kumar, R., Morrow, C., and Lorenz, R. G. (2015). Cross-fostering immediately after birth induces a permanent microbiota shift that is shaped by the nursing mother. *Microbiome* 3:17. doi: 10.1186/s40168-015-0080-y

den Besten, G., van Eunen, K., Groen, A. K., Venema, K., Reijngoud, D. J., and Bakker, B. M. (2013). The role of short-chain fatty acids in the interplay between diet, gut microbiota, and host energy metabolism. *J. Lipid Res.* 54, 2325–2340. doi: 10.1194/jlr.R036012

Derrien, M., Alvarez, A. S., and de Vos, W. M. (2019). The gut microbiota in the first decade of life. *Trends Microbiol.* 27, 997–1010. doi: 10.1016/j.tim.2019.08.001

Douglas, G. M., Maffei, V. J., Zaneveld, J. R., Yurgel, S. N., Brown, J. R., Taylor, C. M., et al. (2020). PICRUSt2 for prediction of metagenome functions. *Nat. Biotechnol.* 38, 685–688. doi: 10.1038/s41587-020-0548-6

Drever, N., Saade, G. R., and Bytautiene, E. (2010). Fetal programming: early-life modulations that affect adult outcomes. *Curr. Allergy Asthma Rep.* 10, 453–459. doi: 10.1007/s11882-010-0136-9

Faddy, M. J., Gosden, M. D., and Gosden, R. G. (2018). A demographic projection of the contribution of assisted reproductive technologies to world population growth. *Reprod. Biomed. Online* 36, 455–458. doi: 10.1016/j.rbmo.2018.01.006

Flores, G. E., Caporaso, J. G., Henley, J. B., Rideout, J. R., Domogala, D., Chase, J., et al. (2014). Temporal variability is a personalized feature of the human microbiome. *Genome Biol.* 15:531. doi: 10.1186/s13059-014-0531-y

Gomaa, E. Z. (2020). Human gut microbiota/microbiome in health and diseases: a review. *Antonie Van Leeuwenhoek* 113, 2019–2040. doi: 10.1007/s10482-020-01474-7

Grasset, E., and Burcelin, R. (2019). The gut microbiota to the brain axis in the metabolic control. *Rev. Endocr. Metab. Disord.* 20, 427–438. doi: 10.1007/s11154-019-09511-1

Han, L., Zhao, L. H., Zhang, M. L., Li, H. T., Gao, Z. Z., Zheng, X. J., et al. (2020). A novel antidiabetic monomers combination alleviates insulin resistance through bacteria-cometabolism-inflammation responses. *Front. Microbiol.* 11:173. doi: 10.3389/fmicb.2020.00173

Hao, J., Zhang, Y., Wu, T., Liu, R., Sui, W., Zhu, J., et al. (2022). The antidiabetic effects of *Bifidobacterium longum* subsp. longum BL21 through regulating gut microbiota structure in type 2 diabetic mice. *Food Funct.* 13, 9947–9958. doi: 10.1039/d2fo01109c

Heintz-Buschart, A., and Wilmes, P. (2018). Human gut microbiome: function matters. *Trends Microbiol.* 26, 563–574. doi: 10.1016/j.tim.2017.11.002

Hu, T. G., Wen, P., Shen, W. Z., Liu, F., Li, Q., Li, E. N., et al. (2019). Effect of 1-deoxynojirimycin isolated from mulberry leaves on glucose metabolism and gut microbiota in a streptozotocin-induced diabetic mouse model. *J. Nat. Prod.* 82, 2189–2200. doi: 10.1021/acs.jnatprod.9b00205

Jeong, Y. J., Park, H. Y., Nam, H. K., and Lee, K. W. (2021). Fermented maillard reaction products by *Lactobacillus gasseri* 4M13 alters the intestinal microbiota and improves dysfunction in type 2 diabetic mice with colitis. *Pharmaceuticals* 14:299. doi: 10.3390/ph14040299

Jia, L., Li, D., Feng, N., Shamoon, M., Sun, Z., Ding, L., et al. (2017). Anti-diabetic effects of *Clostridium butyricum* CGMCC0313.1 through promoting the growth of gut butyrate-producing bacteria in type 2 diabetic mice. *Sci. Rep.* 7:7046. doi: 10.1038/s41598-017-07335-0

Kim, Y. A., Keogh, J. B., and Clifton, P. M. (2018). Probiotics, prebiotics, synbiotics and insulin sensitivity. *Nutr. Res. Rev.* 31, 35–51. doi: 10.1017/S095442241700018X

Kjaergaard, M., Salinas, C. B. G., Rehfeld, J. F., Secher, A., Raun, K., and Wulff, B. S. (2019). PYY(3-36) and exendin-4 reduce food intake and activate neuronal circuits in a synergistic manner in mice. *Neuropeptides* 73, 89–95. doi: 10.1016/j.npep.2018.11.004

Koh, A., De Vadder, F., Kovatcheva-Datchary, P., and Backhed, F. (2016). From dietary fiber to host physiology: short-chain fatty acids as key bacterial metabolites. *Cells* 165, 1332–1345. doi: 10.1016/j.cell.2016.05.041

Li, C. H., Wang, C. T., Lin, Y. J., Kuo, H. Y., Wu, J. S., Hong, T. C., et al. (2022). Long-term consumption of the sugar substitute sorbitol alters gut microbiome and induces glucose intolerance in mice. *Life Sci.* 305:120770. doi: 10.1016/j.lfs.2022.120770

Li, X., Wang, E., Yin, B., Fang, D., Chen, P., Wang, G., et al. (2017). Effects of *Lactobacillus casei* CCFM419 on insulin resistance and gut microbiota in type 2 diabetic mice. *Benef. Microbes* 8, 421–432. doi: 10.3920/BM2016.0167

Li, S., You, J., Wang, Z., Liu, Y., Wang, B., Du, M., et al. (2021). Curcumin alleviates high-fat diet-induced hepatic steatosis and obesity in association with modulation of gut microbiota in mice. *Food Res. Int.* 143:110270. doi: 10.1016/j.foodres.2021.110270

Lin, J., Wen, J., Xiao, N., Cai, Y. T., Xiao, J., Dai, W., et al. (2022). Anti-diabetic and gut microbiota modulation effects of sacha inchi (*Plukenetia volubilis* L.) leaf extract in streptozotocin-induced type 1 diabetic mice. *J. Sci. Food Agric.* 102, 4304–4312. doi: 10.1002/jsfa.11782

Liu, M., Huang, B., Wang, L., Lu, Q., and Liu, R. (2022). Peanut skin procyanidins ameliorate insulin resistance via modulation of gut microbiota and gut barrier in type 2 diabetic mice. *J. Sci. Food Agric.* 102, 5935–5947. doi: 10.1002/jsfa.11945

Lopez-Gonzalez, J. A., Suarez-Estrella, F., Vargas-Garcia, M. C., Lopez, M. J., Jurado, M. M., and Moreno, J. (2015). Dynamics of bacterial microbiota during

lignocellulosic waste composting: studies upon its structure, functionality and biodiversity. *Bioresour. Technol.* 175, 406–416. doi: 10.1016/j.biortech.2014.10.123

Ma, Q., Zhai, R., Xie, X., Chen, T., Zhang, Z., Liu, H., et al. (2022). Hypoglycemic effects of *Lycium barbarum* polysaccharide in type 2 diabetes mellitus mice via modulating gut microbiota. *Front. Nutr.* 9:916271. doi: 10.3389/fnut.2022.916271

Martin, C. R., Osadchiy, V., Kalani, A., and Mayer, E. A. (2018). The brain-gut-microbiome Axis. *Cell. Mol. Gastroenterol. Hepatol.* 6, 133–148. doi: 10.1016/j.jcmgh.2018.04.003

Martin-Gallausiaux, C., Marinelli, L., Blottiere, H. M., Larraufie, P., and Lapaque, N. (2021). SCFA: mechanisms and functional importance in the gut. *Proc. Nutr. Soc.* 80, 37–49. doi: 10.1017/S0029665120006916

Mayer, E. A., Tillisch, K., and Gupta, A. (2015). Gut/brain axis and the microbiota. *J. Clin. Invest.* 125, 926–938. doi: 10.1172/JCI76304

Moura-Assis, A., Friedman, J. M., and Velloso, L. A. (2021). Gut-to-brain signals in feeding control. *Am. J. Physiol. Endocrinol. Metab.* 320, E326–E332. doi: 10.1152/ajpendo.00388.2020

Pannaraj, P. S., Li, F., Cerini, C., Bender, J. M., Yang, S., Rollie, A., et al. (2017). Association between breast milk bacterial communities and establishment and development of the infant gut microbiome. *JAMA Pediatr.* 171, 647–654. doi: 10.1001/jamapediatrics.2017.0378

Parker, J. A., and Bloom, S. R. (2012). Hypothalamic neuropeptides and the regulation of appetite. *Neuropharmacology* 63, 18–30. doi: 10.1016/j.neuropharm.2012.02.004

Parker, B. J., Wearsch, P. A., Veloo, A. C. M., and Rodriguez-Palacios, A. (2020). The genus alistipes: gut bacteria with emerging implications to inflammation, cancer, and mental health. *Front. Immunol.* 11:906. doi: 10.3389/fimmu.2020.00906

Pascale, A., Marchesi, N., Govoni, S., Coppola, A., and Gazzaruso, C. (2019). The role of gut microbiota in obesity, diabetes mellitus, and effect of metformin: new insights into old diseases. *Curr. Opin. Pharmacol.* 49, 1–5. doi: 10.1016/j.coph.2019.03.011

Reynolds, L. P., Borowicz, P. P., Caton, J. S., Crouse, M. S., Dahlen, C. R., and Ward, A. K. (2019). Developmental programming of fetal growth and development. *Vet. Clin. North Am. Food Anim. Pract.* 35, 229–247. doi: 10.1016/j.cvfa.2019.02.006

Rinaudo, P., and Wang, E. (2012). Fetal programming and metabolic syndrome. *Annu. Rev. Physiol.* 74, 107–130. doi: 10.1146/annurev-physiol-020911-153245

Shen, D., Lu, Y., Tian, S., Ma, S., Sun, J., Hu, Q., et al. (2021). Effects of L-arabinose by hypoglycemic and modulating gut microbiome in a high-fat diet-and streptozotocin-induced mouse model of type 2 diabetes mellitus. *J. Food Biochem.* 45:e13991. doi: 10.1111/jfbc.13991

Song, S. J., Lauber, C., Costello, E. K., Lozupone, C. A., Humphrey, G., Berg-Lyons, D., et al. (2013). Cohabiting family members share microbiota with one another and with their dogs. *eLife* 2:e00458. doi: 10.7554/eLife.00458

Tamburini, S., Shen, N., Wu, H. C., and Clemente, J. C. (2016). The microbiome in early life: implications for health outcomes. *Nat. Med.* 22, 713–722. doi: 10.1038/nm.4142

Theis, K. R., Romero, R., Greenberg, J. M., Winters, A. D., Garcia-Flores, V., Motomura, K., et al. (2020). No consistent evidence for microbiota in murine placental and fetal tissues. *mSphere* 5, 5:e00933-19. doi: 10.1128/mSphere.00933-19

Tierney, B. T., Tan, Y., Yang, Z., Shui, B., Walker, M. J., Kent, B. M., et al. (2022). Systematically assessing microbiome-disease associations identifies drivers of inconsistency in metagenomic research. *PLoS Biol.* 20:e3001556. doi: 10.1371/journal.pbio.3001556

Treichel, N. S., Prevorsek, Z., Mrak, V., Kostric, M., Vestergaard, G., Foesel, B., et al. (2019). Effect of the nursing mother on the gut microbiome of the offspring during early mouse development. *Microb. Ecol.* 78, 517–527. doi: 10.1007/s00248-019-01317-7

Walker, R. W., Clemente, J. C., Peter, I., and Loos, R. J. F. (2017). The prenatal gut microbiome: are we colonized with bacteria in utero? *Pediatr. Obes.* 12, 3–17. doi: 10.1111/ijpo.12217

Wang, J., He, Y., Yu, D., Jin, L., Gong, X., and Zhang, B. (2020). Perilla oil regulates intestinal microbiota and alleviates insulin resistance through the PI3K/AKT signaling pathway in type-2 diabetic KKAy mice. *Food Chem. Toxicol.* 135:110965. doi: 10.1016/j.fct.2019.110965

Wang, G., Li, X., Zhao, J., Zhang, H., and Chen, W. (2017). Correction: *Lactobacillus casei* CCFM419 attenuates type 2 diabetes via a gut microbiota dependent mechanism. *Food Funct.* 8:3814. doi: 10.1039/c7fo90032e

Wang, P., Qiao, Z., Li, X., Su, Y., and Xie, B. (2020). Functional characteristic of microbial communities in large-scale biotreatment systems of food waste. *Sci. Total Environ.* 746:141086. doi: 10.1016/j.scitotenv.2020.141086

Wang, S., Ryan, C. A., Boyaval, P., Dempsey, E. M., Ross, R. P., and Stanton, C. (2020). Maternal vertical transmission affecting early-life microbiota development. *Trends Microbiol.* 28, 28–45. doi: 10.1016/j.tim.2019.07.010

Wang, R., Zhang, L., Zhang, Q., Zhang, J., Liu, S., Li, C., et al. (2022). Glycolipid metabolism and metagenomic analysis of the therapeutic effect of a phenolics-rich extract from noni fruit on type 2 diabetic mice. *J. Agric. Food Chem.* 70, 2876–2888. doi: 10.1021/acs.jafc.1c07441

Wang, H., Zhou, C., Hou, M., Huang, H., and Sun, Y. (2021). Neurogenesis potential evaluation and transcriptome analysis of fetal hypothalamic neural stem/progenitor cells with prenatal high estradiol exposure. *Front. Genet.* 12:677935. doi: 10.3389/fgene.2021.677935

Wang, H. H., Zhou, C. L., Lv, M., Yang, Q., Li, J. X., Hou, M., et al. (2018). Prenatal high estradiol exposure induces sex-specific and dietarily reversible insulin resistance through decreased hypothalamic INSR. *Endocrinology* 159, 465–476. doi: 10.1210/en.2017-03017

Wu, Y., Dong, L., Song, Y., Wu, Y., Zhang, Y., and Wang, S. (2022). Preventive effects of polysaccharides from *Physalis alkekengi* L. on dietary advanced glycation end product-induced insulin resistance in mice associated with the modulation of gut microbiota. *Int. J. Biol. Macromol.* 204, 204–214. doi: 10.1016/j.ijbiomac.2022.01.152

Wu, T., Zhang, Y., Li, W., Zhao, Y., Long, H., Muhindo, E. M., et al. (2021). *Lactobacillus rhamnosus* LRa05 ameliorate hyperglycemia through a regulating glucagon-mediated signaling pathway and gut microbiota in type 2 diabetic mice. *J. Agric. Food Chem.* 69, 8797–8806. doi: 10.1021/acs.jafc.1c02925

Wu, R., Zhou, L., Chen, Y., Ding, X., Liu, Y., Tong, B., et al. (2022). Sesquiterpene glycoside isolated from loquat leaf targets gut microbiota to prevent type 2 diabetes mellitus in db/db mice. *Food Funct.* 13, 1519–1534. doi: 10.1039/d1fo03646g

Xu, N., Zhou, Y., Lu, X., and Chang, Y. (2021). *Auricularia auricula-judae* (Bull.) polysaccharides improve type 2 diabetes in HFD/STZ-induced mice by regulating the AKT/AMPK signaling pathways and the gut microbiota. *J. Food Sci.* 86, 5479–5494. doi: 10.1111/1750-3841.15963

Yong, Z., Ruiqi, W., Yanan, Y., Ning, M., Zhi, Z., Yinfeng, T., et al. (2022). Laurolitsine ameliorates type 2 diabetes by regulating the hepatic LKB1-AMPK pathway and gut microbiota. *Phytomedicine* 106:154423. doi: 10.1016/j.phymed.2022.154423

Younge, N., McCann, J. R., Ballard, J., Plunkett, C., Akhtar, S., Araujo-Perez, F., et al. (2019). Fetal exposure to the maternal microbiota in humans and mice. *JCI Insight* 4:e127806. doi: 10.1172/jci.insight.127806

Zhang, Y., Wu, T., Li, W., Zhao, Y., Long, H., Liu, R., et al. (2021). *Lactobacillus casei* LC89 exerts antidiabetic effects through regulating hepatic glucagon response and gut microbiota in type 2 diabetic mice. *Food Funct.* 12, 8288–8299. doi: 10.1039/d1fo00882j

Zhao, Q., Fu, Y., Zhang, F., Wang, C., Yang, X., Bai, S., et al. (2022). Heat-treated adzuki bean protein hydrolysates reduce obesity in mice fed a high-fat diet via remodeling gut microbiota and improving metabolic function. *Mol. Nutr. Food Res.* 66:e2100907. doi: 10.1002/mnfr.202100907

Zhao, Q., Hou, D., Fu, Y., Xue, Y., Guan, X., and Shen, Q. (2021). Adzuki bean alleviates obesity and insulin resistance induced by a high-fat diet and modulates gut microbiota in mice. *Nutrients* 13:3240. doi: 10.3390/nu13093240

frontiers | Frontiers in Microbiology

TYPE Original Research
PUBLISHED 12 January 2023
DOI 10.3389/fmicb.2022.1050474



OPEN ACCESS

EDITED BY
Hui Zhang,
South China Agricultural University, China

REVIEWED BY
Canaan Whitfield-Cargile,
Texas A&M University, United States
Eva Skrivanova,
Czech University of Life Sciences Prague, Czechia
Houqiang Luo,
Wenzhou Vocational College of Science and Technology, China

*CORRESPONDENCE
Carla Giuditta Vecchiato
✉ carla.vecchiato2@unibo.it

†These authors share last authorship

SPECIALTY SECTION
This article was submitted to Microorganisms in Vertebrate Digestive Systems, a section of the journal Frontiers in Microbiology

RECEIVED 21 September 2022
ACCEPTED 19 December 2022
PUBLISHED 12 January 2023

CITATION
Vecchiato CG, Golinelli S, Pinna C, Pilla R, Suchodolski JS, Tvarijonaviciute A, Rubio CP, Dorato E, Delsante C, Stefanelli C, Pagani E, Fracassi F and Biagi G (2023) Fecal microbiota and inflammatory and antioxidant status of obese and lean dogs, and the effect of caloric restriction.
*Front. Microbiol.* 13:1050474.
doi: 10.3389/fmicb.2022.1050474



# Fecal microbiota and inflammatory and antioxidant status of obese and lean dogs, and the effect of caloric restriction

Carla Giuditta Vecchiato[1]*, Stefania Golinelli[1], Carlo Pinna[1], Rachel Pilla[2], Jan S. Suchodolski[2], Asta Tvarijonaviciute[3], Camila Peres Rubio[4], Elisa Dorato[1], Costanza Delsante[1], Claudio Stefanelli[5], Elena Pagani[6], Federico Fracassi[1†] and Giacomo Biagi[1†]

[1]Department of Veterinary Medical Sciences, University of Bologna, Bologna, Italy, [2]Gastrointestinal Laboratory, Texas A&M University, College Station, TX, United States, [3]Interdisciplinary Laboratory of Clinical Analysis, Interlab-UMU, Regional Campus of International Excellence 'Campus Mare Nostrum', University of Murcia, Murcia, Spain, [4]Department of Animal and Food Science, School of Veterinary Science, Autonomous University of Barcelona, Barcelona, Spain, [5]Dipartimento di Scienze per la Qualità della Vita, University of Bologna, Rimini, Italy, [6]Monge & C. S.p.A., Monasterolo di Savigliano, Italy

**Introduction:** Obesity is the most common nutritional disease in dogs, and is generally managed by caloric restriction. Gut microbiota alteration could represent a predisposing factor for obesity development, which has been associated with a low-grade inflammatory condition and an impaired antioxidant status. Besides, weight loss has been shown to influence the gut microbiota composition and reduce the inflammatory response and oxidative stress.

**Method:** However, these insights in canine obesity have not been fully elucidated. The aim of this study was to assess the differences in serum and inflammatory parameters, antioxidant status, fecal microbiota and bacterial metabolites in 16 obese and 15 lean client-owned dogs and how these parameters in obese may be influenced by caloric restriction. First, for 30days, all dogs received a high-protein, high-fiber diet in amounts to maintain their body weight; later, obese dogs were fed for 180days the same diet in restricted amounts to promote weight loss.

**Results:** Before the introduction of the experimental diet (T0), small differences in fecal microbial populations were detected between obese and lean dogs, but bacterial diversity and main bacterial metabolites did not differ. The fecal Dysbiosis Index (DI) was within the reference range (< 0) in most of dogs of both groups. Compared to lean dogs, obese dogs showed higher serum concentrations of acute-phase proteins, total thyroxine (TT4), and antioxidant capacity. Compared to T0, dietary treatment affected the fecal microbiota of obese dogs, decreasing the abundance of Firmicutes and increasing *Bacteroides* spp. However, these changes did not significantly affect the DI. The caloric restriction failed to exert significative changes on a large scale on bacterial populations. Consequently, the DI, bacterial diversity indices

and metabolites were unaffected in obese dogs. Caloric restriction was not associated with a reduction of inflammatory markers or an improvement of the antioxidant status, while an increase of TT4 has been observed.

**Discussion:** In summary, the present results underline that canine obesity is associated with chronic inflammation. This study highlights that changes on fecal microbiota of obese dogs induced by the characteristics of the diet should be differentiated from those that are the consequence of the reduced energy intake.

KEYWORDS

**canine obesity, fecal microbiota, 16S ribosomal (r)RNA gene, oxidative damage, serum antioxidant capacity, oxidative stress, thyroid homeostasis**

# 1. Introduction

Canine obesity is a growing global health problem, with data of prevalence ranging between 20% and 40% all over the world (Mao et al., 2013; Montoya-Alonso et al., 2017; Porsani et al., 2020).

Obesity results from a prolonged imbalance of energy intake and expenditure, but it is now understood that the etiology of canine obesity represents a complex interaction of genetics, diet, metabolism, and physical activity levels (Chandler et al., 2017). In addition, the composition and function of the gut microbiota may act as a contributing factor through a variety of proposed mechanisms, including the production of bacterial metabolites that may lead to an increase in dietary energy harvest (Turnbaugh et al., 2006) and promote regulation of adipogenesis and inflammatory adipokines release (Arora et al., 2011). Moreover, in humans, obesity is associated with low-grade systemic inflammation (Das, 2001; Cohen et al., 2021) and weight loss has been shown to reverse this condition (Forsythe et al., 2008), while controversial results have been obtained in dogs (German et al., 2009; Tvarijonaviciute et al., 2012a,c). In addition, recent researches in humans indicate that disturbances in pro-oxidant and anti-oxidant balance play a critical role in the pathogenesis of obesity and may lead to chronic inflammation of the adipose tissue (Marseglia et al., 2015; Sánchez-Rodríguez and Mendoza-Núñez, 2019). To date, the assessment of antioxidant status in canine diseases is still in its early stage (Bastien et al., 2015; Rubio et al., 2016, 2017a; Bosco et al., 2018).

Among the variety of predisposing factors that may have a role in the development of obesity in dogs, owner and lifestyle factors might contribute, since dogs share the same environments with their owners (Lund et al., 2006; Courcier et al., 2010; Muñoz-Prieto et al., 2018; Banton et al., 2022). Studies involving client-owned dogs might be, therefore, more representative of the overall target population (German et al., 2015).

Diet plays a role in regulating the composition and metabolic output of the canine gut microbiota, which adapts to the available nutrients by modulating microbial composition and function (Pilla and Suchodolski, 2021). For that reason, therapeutic approaches throughout gut microbiota regulation in preventing obesity and supporting weight loss in dogs are of interest (Kałużna-Czaplińska et al., 2017; Huang et al., 2020).

In previous studies that have investigated the role of canine obesity and weight loss on gut microbiota, it was challenging to distinguish the effects driven by the experimental diets from those caused by decreased calorie intake, because diet and caloric restriction were usually introduced at the same time (Kieler et al., 2017; Bermudez Sanchez et al., 2020). Caloric restriction represents the main therapeutic strategy for achieving weight loss, and the latter may influence the inflammatory and antioxidant status of obese dogs. However, it remains unclear if the decreased nutrient load consequent to caloric restriction might affect the gut microbiota.

In this study, we first aimed to compare fecal microbiota, fecal bacterial metabolome, and inflammatory and antioxidant status in lean and obese client-owned dogs receiving the same diet with no caloric restriction. Then, we evaluated the changes induced by a weight loss program on these parameters in the obese group.

# 2. Materials and methods

## 2.1. Animals and study design

Sixteen overweight or obese (OB) client-owned dogs (Body Condition Score ≥ 7, according to a 9-point body condition scale chart (Laflamme, 1997)) were prospectively enrolled between July 2019 and September 2020 at the Veterinary Teaching Hospital of the University of Bologna (Italy) for a two-phase study. Additionally, 15 clinically healthy adult private-owned dogs, with a BCS of 4–5/9, were involved in the trial as the lean (CTRL) group for the first phase of the study. To ensure that all dogs were healthy before enrolment, complete patient history was obtained, and a physical examination was performed. Furthermore, all dogs had not received any medicaments, such as antibiotics, that could have an impact on the gut microbiota for at least 90 days before being enrolled in the study. The study protocol was approved by the Scientific Ethics Committee of the University of Bologna.

Body weight (BW) of dogs was measured by electronic weigh scales (KERN & Sohn GmbH 3.0). During the first 30 days (phase 1 of the study), OB and CTRL dogs were fed a dry dog extruded

dietetic feed intended for the reduction of excessive body weight (VetSolution Obesity Canine, Monge & C. S.p.a., Monasterolo di Savigliano, Italy, nutrients composition and ingredients are listed in Table 1). During phase 1, the diet was fed in such amounts to maintain the initial body weight of dogs. The maintenance energy requirement (MER) of each dog was calculated using the following equation proposed by FEDIAF (2021) for adult dogs:

$$\mathrm{MER}\left(\mathrm{kcal}/\mathrm{day}\right) = 110 \times \mathrm{BW}\left(\mathrm{kg}\right)^{0.75}$$

where BW is the actual body weight.

For all dogs, the MER was adjusted according to dogs' habitual energy intake that was estimated based on the information provided by owners. Dogs received only the experimental diet, and any additional foodstuffs (e.g., table scrapes and/or treats) were avoided.

At the end of phase 1 (T30), lean CTRL dogs left the study, while OB dogs moved into phase 2, the weight loss treatment (T30-T210), which lasted 180 days.

During phase 2, OB dogs received the same experimental diet, but a caloric restriction was applied. Individual daily energy amounts were calculated based on the target body weight (TBW) according to the equation proposed by German et al. (2007) that considers both sex and neuter status. The TBW was calculated based on BCS, by estimating that each point above 5 (on the scale of 1 to 9) correlates with about a 10% increase in bodyweight (Laflamme, 2006). The expected rate of weight loss was between 0.5 and 2.0% of starting BW per week (German et al., 2007); the BW and BCS of each dog were assessed every 2 weeks and the dietary plan was adjusted if the weight loss was <0.5% of starting BW per week, reducing the daily ration according to the dog size, by 5 grams (<20 kg BW) or 10 grams (>20 kg BW), as proposed by German et al. (2007).

TABLE 1 Nutrient composition of the experimental diet used in the study (VetSolution Obesity Canine, Monge & C. S.p.a., Monasterolo di Savigliano, Italy).

| | AF[a] | DM[b] | Mcal (ME)[c] |
|---|---|---|---|
| Moisture | 5.25 | / | / |
| CP | 35.0 | 36.9 | 109 |
| EE | 9.34 | 9.86 | 29 |
| Starch | 20.4 | 21.5 | 63.2 |
| Ash | 8.54 | 9.02 | 26.5 |
| TDF | 17.3 | 18.3 | 53.8 |
| Soluble fiber | 3.65 | 3.85 | 11.3 |
| Insoluble fiber | 13.7 | 14.4 | 42.5 |

[a]Nutrients expressed as g/100 g as fed (AF).
[b]Nutrients expressed as g/100 g dry matter (DM).
[c]Nutrients expressed as g/1,000 kcal metabolizable energy (ME) calculated according to NRC-National Research Council (2006).

CP: crude protein; EE: ether extract; TDF: total dietary fiber. Composition: dried chicken meat (20%), tapioca, dried fish (anchovy), pea fiber, potatoes, dried eggs, salmon oil, dried duck meat, brewers' yeast, plantago seed (1%), minerals, xylooligosaccharides (0.4%), products and by-products from processing fresh fruits and vegetables (melon juice concentrate—Cucumis melo cantalupensis—source of superoxidedismutase (SOD 0.005%), milk protein powder.

## 2.2. Sampling collection

During phase 1, fecal samples were collected from each dog at baseline (T0) and after 30 days of dietary treatment (T30). During phase 2, fecal samples from OB dogs were collected after 120 and 210 days of caloric reduction (T120 and T210, respectively). Fecal samples were collected by dog owners after spontaneous defecation and immediately transferred to the laboratory, where they were frozen and kept at −80°C until being processed.

Additionally, a single venous blood sample was collected at T30 from CTRL and OB dogs, and at T120 and T210 from OB animals.

## 2.3. Laboratory analysis

### 2.3.1. Fecal samples

#### 2.3.1.1. Chemical analysis

The pH was determined after diluting the fecal samples with deionized water at 1:10 (w/v), using a laboratory pH meter (SevenMulti, Mettler Toledo, Greinfesee, Switzerland; accuracy ±0.01), while fecal ammonia was determined using an enzymatic colorimetric test (Urea/BUN-Color; BioSystems S.A., Barcelona, Spain).

The VFA were measured by gas chromatography, according to the method described by Pinna et al. (2021). Biogenic amines were determined by HPLC separation and fluorimetry quantification according to Stefanelli et al. (1986).

#### 2.3.1.2. Real-time quantitative PCR

An aliquot of 100 mg of feces was extracted for DNA with a commercially available kit following manufacturer instructions (PowerSoil® DNA Isolation Kit, MOBIO Laboratories, Inc., Carlsbad, CA, USA). Quantitative PCR was performed using universal bacteria primers for specific bacterial groups: *Blautia* spp., *Clostridium hiranonis*, *Escherichia coli*, *Faecalibacterium* spp., *Fusobacterium* spp., *Streptococcus* spp., and *Turicibacter* spp., according to a previously described method (Garcia-Mazcorro et al., 2012b). Extracted DNA was quantified, and quality checked, with NanoDrop 2000 spectrophotometer (Thermo Scientific, USA).

Results are expressed as the abundance of DNA for each bacterial group, and logarithms of relative DNA copy number were used to calculate the degree of dysbiosis [DI, AlShawaqfeh et al., 2017)] in feces of lean and obese dogs.

#### 2.3.1.3. 16S rRNA gene sequencing

The V4 region of the 16S rRNA gene was sequenced at Mr. Dna Laboratory (Molecular Research LP, Mr. DNA, Shallowater, TX) using primers 515F [5′-GTGYCAGCMGCCGCGGTAA, Parada et al., 2016] to 806RB [5′-GGACTACNVGGGTWTCTAAT, Apprill et al., 2015]. Briefly, amplification was performed under the following conditions: 95°C for 5 min, followed by 30 cycles of 95°C for 30 s, 53°C for 40 s and 72°C for 1 min, after which a final elongation step at 72°C for 10 min. After amplification, PCR products were checked in 2% agarose gel to determine the success of amplification and the relative intensity of bands. Samples were multiplexed using unique dual indices and pooled together in equal proportions based on their molecular weight and DNA concentrations. Pooled samples were purified using calibrated Ampure XP beads. Then the pooled and purified PCR product was used to prepare an Illumina DNA library. Sequencing was performed at on a MiSeq following the manufacturer's guidelines. Sequences of the 16S rRNA genes were processed using Quantitative Insights Into Microbial Ecology 2 [QIIME 2, v 2018.6, Bolyen et al., 2019]. The raw sequences were uploaded to NCBI Sequence Read Archive under accession number PRJNA822358. The sequence data was demultiplexed, and an amplicon sequence variant (ASV) table was created using DADA2 (Callahan et al., 2016). Prior to downstream analysis, sequences assigned as chloroplast, mitochondria, and low abundance OTUs, containing less than 0.01% of the total reads in the dataset were removed. Samples were rarefied to 4,990 sequences per sample, based on the lowest read depth, to normalize sequencing depth across all samples. Alpha diversity was evaluated with Chao 1, Shannon diversity, and observed species. Beta diversity was evaluated by weighted an unweighted UniFrac distance matrices and visualized using PCoA (Principal Coordinate Analysis) plots.

### 2.3.2. Blood samples

Blood samples were collected after 15 h of fasting, at T30 in CTRL and OB dogs and then at T120 and T210 in OB dogs, to assess a complete blood cell count (CBC) and serum biochemistry profile. The CBC was performed with an automated hematology analyzer (ADVIA 2120, Siemens Healthcare Diagnostics, Tarrytown NY, USA), while chemistry parameters were carried out on an automated chemistry analyzer (AU480, Beckman Coulter/Olympus, Brea, California, USA). Blood samples for the determination of all the biochemistry variables were collected in serum separating tubes. Coagulated blood samples were centrifuged for 10 min at 3,000 *g*; the serum was immediately transferred to plastic tubes, stored at 4°C and analyzed the same day, or stored at −80°C and thawed immediately before analysis. Blood samples for the determination of CBC and chemistry parameters were analyzed the same day of the sampling in all dogs. Inflammatory markers such as C-reactive protein (CRP) and haptoglobin (Hp) were assayed afterward on stored frozen samples obtained from CTRL dogs at T30 and OB dogs at T30 and T210. The CRP concentration was determined by an immunoturbidimetric assay (Beckman Coulter OSR6147, Beckman Coulter Inc., Brea, California) previously validated in dogs (Gentilini et al., 2005). The Hp concentration was determined using an immunoturbidimetric method that had previously been validated for dogs (Mastrorilli et al., 2007). Total T4 was measured using a chemiluminescent enzyme immunoassay (Immulite 2000, Siemens Healthcare) validated for dogs (Singh et al., 1997).

#### 2.3.2.1. Antioxidant capacity

Analyses were performed on stored frozen serum samples obtained from CTRL dogs at T30 and OB dogs at T30 and T210. Cupric reducing antioxidant capacity (CUPRAC), ferric reducing ability of plasma (FRAP), trolox equivalent antioxidant capacity (TEAC) using acidic medium (TEACA), and the TEAC using the horseradish peroxidase (TEACH) were measured to determine the total antioxidant capacity (TAC) of the samples as previously described in dogs (Rubio et al., 2017b). Total serum thiol was measured according the method described by Jocelyn (1987). The serum enzymes butyrylcholinesterase (BChE) and paraoxonase type 1 (PON1) were analyzed as previously described in serum of dogs (Tvarijonaviciute et al., 2012b). All analyses were performed using the autoanalyzer Olympus AU400 (Olympus Diagnostica GmbH, Ennis, Ireland).

#### 2.3.2.2. Oxidant biomarkers

Analyses were performed on stored frozen serum samples obtained from CTRL dogs at T30 and OB dogs at T30 and T210. Thiobarbituric acid reactive substances (TBARS) were measured as described by Buege and Aust (1978) by using a microplate reader (Powerwave XS, Biotek instruments, Carson City, NV). Reactive oxygen species (ROS) levels were assessed by luminol-mediated chemiluminescence assay (Vong et al., 2014). The resulting chemiluminescence was measured using a microplate reader (Victor 21,420 Multilabel Counter; PerkinElmer, Finland) and results were expressed in counts per second (cps). Ferrous oxidation-xylenol orange (FOX) was measured according to the colorimetric method described by Arab and Steghens (2004) and was performed using the Olympus AU400 Automatic Chemistry Analyser.

## 2.4. Statistical analysis

The D'Agostino and Pearson omnibus normality test was used to assess the normality of the data with parametric distribution. All values are presented in the text as the group mean ± SD for normally distributed data and the median (range) if they were not normally distributed.

A 2-way ANOVA was applied to determine the significance of the changes in fecal pH, fecal chemical parameters, microbial communities, and alpha-diversity indices, both temporal within-group (effect induced by dietary treatment during phase 1 of the study) and between-groups (OB vs. CTRL). If indicated, data were logarithmic transformed before statistical analysis with ANOVA.

To evaluate the influence of caloric restriction (phase 2) on fecal chemical parameters, microbial communities, and alpha-diversity indices among the sample collection time points, a repeated measures ANOVA or the non-parametric analog (Friedman test) were used, following the distribution of data. For all multiple testing, $p$-value was adjusted to $q$-value using Benjamini-Hochberg false-discovery rate correction (FDR) and significance was set at $q < 0.05$.

Multivariate analysis was performed on the unweighted UniFrac distance matrixes using ANOSIM (Analysis of Similarity) test within PRIMER 7 software (PRIMER-E Ltd., Luton, UK) to analyze differences in microbial communities.

To determine differences in blood parameters between OB and CTRL, and before and after caloric restriction in OB dogs, unpaired t-test or the Mann–Whitney test, as well as paired t-test or Wilcoxon matched-pairs were used as appropriate. Pearson correlation coefficient was used to assess the relationship between antioxidant capacity and inflammatory markers.

For all statistical analyses, significance was set at $p < 0.05$.

Statistical analyses were conducted using GraphPad Prism version 9.2 (GraphPad Software, San Diego, CA, USA), except for the ANOSIM test that was performed with PRIMER 6 software package (PRIMER-E Ltd., Luton, UK).

# 3. Results

## 3.1. Phase 1—Fecal metabolites and microbiota, and serum analytes in CTRL and OB dogs

### 3.1.1. Animals

In total, 16 private-owned adult OB dogs and 15 private-owned adult healthy lean dogs were applied. Full details of the baseline characteristics (T0) of CTRL and OB dogs, are given in Supplementary Table 1. No statistical differences were detected between CTRL and OB dogs regarding baseline characteristics (signalments) and body weight. The median age of OB dogs was 66 months (20 to 111 months); 10 dogs were male (5 were neutered and 5 were intact) and 6 were female (4 were neutered and 2 were intact). The median age of CTRL dogs was 72 months (14 to 116 months); 10 dogs were male (6 were neutered and 4 were intact) and 5 were neutered females. All dogs were of different breed and size. At T0, median body weight (BW) of OB dogs was 27.5 kg (4.73 to 64.10 kg) and BCS was 8 (7 to 9), while median BW of CTRL dogs was 24.7 kg (7.85 to 45.8 kg) and BCS was 5 (4 to 5). Median energy allocation, expressed as kcal of ME per $kg^{0.75}$ TBW, was 103 (87 to 186) and 99 (70 to 187) for OB and CTRL dogs, respectively.

### 3.1.2. Fecal metabolites and microbiota

Both CTRL and OB groups did not show any significant changes in fecal pH, ammonia and VFA (Table 2) in response to a short-term (30 days) dietary treatment with a diet intended for weight loss, given at a daily amount calculated to provide the energy to maintain their body weight, to avoid any potential effect deriving from caloric restriction. Among biogenic amines (Table 2), spermine fecal concentration was markedly decreased by diet within the CTRL group (T30: 104 nmol/g vs. T0: 297 nmol/g, $q < 0.001$). Moreover, compared with CTRL, fecal spermine was higher in OB dogs ($p = 0.005$) both before (OB T0: 360 nmol/g vs. CTRL T0: 297 nmol/g, $q < 0.001$) and after dietary treatment (OB T30: 251 nmol/g vs. CTRL T30: 104 nmol/g, $q = 0.002$); within OB, instead, the fecal concentrations of biogenic amines were not modified by the dietary treatment (Table 2).

The Shannon, Chao1 and observed operational taxonomic units (OTUs) indices were used to quantify fecal microbiota alpha diversity evenness and richness between OB and CTRL dogs in response to the dietary treatment, without detecting significant differences ($p > 0.05$, Table 3).

Unweighted UniFrac analysis of similarities showed that there not were differences between OB and CTRL dogs at T0 (OB vs. CTRL, $p = 0.070$ and $R = 0.076$, Figure 1), nor after dietary treatment (T30: OB vs. CTRL, $p = 0.166$ and $R = 0.028$, Figure 1A). The dietary treatment, in fact, failed to affect the β-diversity within microbial communities of each group (OB T0 vs. T30, $p = 0.108$ and $R = 0.045$; CTRL T0 vs. T30, $p = 0.062$ and $R = 0.084$, Figure 1A). In the same way, the DI (Figure 1B) did not differ between groups. In OB dogs, in fact, the bacterial abundances were mostly within the reference intervals established for healthy dogs (Supplementary Table 2).

At phyla level, five different phyla were identified as the most abundant in OB and CTRL fecal samples, with no differences between groups ($q > 0.05$, Figure 2). Firmicutes were predominant in OB and CTRL both before and after dietary treatment (range 41–99% and 37–96% for OB and CTRL, respectively), followed by Bacteroidetes (range 0–38% and 0–33% for OB and CTRL, respectively) and Fusobacteria (range 0–29% for both OB and CTRL). In OB dogs, the median abundance of Firmicutes decreased at T30 (T0: 86% vs. T30: 59%, $q = 0.010$, Figure 3A), while dietary treatment did not affect the bacterial populations of healthy dogs.

Differences in terms of bacterial phylum, class, order, family, genera and species between OB and CTRL dogs are available in Supplementary File 1, while significative results are presented in Figure 3; within the phylum Firmicutes, relative abundance of the family Erysipelotrichaceae differed between OB and CTRL (Figure 3B) before dietary treatment started (OB: 3.31% vs. CTRL: 8.56%, $q < 0.001$); moreover, abundance of Erysipelotrichaceae in CTRL dogs was reduced by dietary treatment (T0: 8.56% vs. T30: 5.10%, $q = 0.001$). The same was observed for the genus *Eubacterium* (Figure 3C: OB: 0.12% vs. CTRL: 0.96%, $q = 0.039$ and CTRL T0: 0.96% vs. T30: 0.84%, $q = 0.048$), with *E. biforme* being the most represented species of this genus (Figure 3D: OB T0: 0% vs. CTRL T0: 0.96%, $q = 0.008$ and CTRL T0: 0.96% vs. T30: 0.60%, $q = 0.034$). Abundance of the genus *Bacteroides* (family Bacteroidaceae, phylum Bacteroidetes, Figure 3F) increased in OB in response to the dietary treatment (T0: 2.60% vs. T30: 13.3%, $q = 0.029$, Figure 3F).

TABLE 2 Fecal pH values and concentrations of ammonia (μmol/g), volatile fatty acids (μmol/g) and biogenic amines (nmol/g) in feces of obese (*n*=16) and lean dogs (*n*=15) fed the same experimental diet, without caloric reduction, for 30days (phase 1 of the study).

| | OB | | CTRL | | | ANOVA *p*-value | | |
|---|---|---|---|---|---|---|---|---|
| | T0 | T30 | T0 | T30 | SEM | Group | Diet | Group × Diet |
| pH | 6.82 | 6.79 | 6.89 | 6.77 | 0.044 | 0.794 | 0.425 | 0.618 |
| Ammonia | 29.8 | 33.5 | 35.0 | 38.0 | 1.333 | 0.060 | 0.134 | 0.977 |
| Acetic a. | 55.7 | 61.3 | 66.4 | 73.5 | 2.543 | 0.024 | 0.205 | 0.888 |
| Propionic a. | 30.9 | 27.2 | 40.3 | 36.0 | 1.905 | 0.017 | 0.280 | 0.935 |
| Isobutyric a. | 1.73 | 1.80 | 1.71 | 1.72 | 0.119 | 0.660 | 0.577 | 0.654 |
| *n*-Butyric a. | 10.4 | 10.4 | 11.9 | 13.3 | 0.512 | 0.030 | 0.490 | 0.512 |
| Isovaleric a. | 2.54 | 2.37 | 2.27 | 1.99 | 0.166 | 0.610 | 0.714 | 0.692 |
| Total VFA | 102 | 103 | 123 | 126 | 4.323 | 0.011 | 0.742 | 0.908 |
| Putrescine | 1,078 | 1,010 | 798 | 1,087 | 123 | 0.514 | 0.107 | 0.113 |
| Cadaverine | 834 | 785 | 443 | 602 | 201 | 0.147 | 0.010 | 0.746 |
| Spermidine | 560 | 432 | 456 | 385 | 47.21 | 0.177 | 0.859 | 0.668 |
| Spermine | 360[a] | 251[a] | 297[a] | 104[b] | 39.24 | 0.005 | <0.001 | 0.245 |

OB: obese dogs; CTRL: lean dogs; SEM: standard error of the mean; VFA: volatile fatty acids. Means with different superscripts are significantly different in multiple comparisons with FDR adjustment.

TABLE 3 Alpha-diversity indices of fecal microbiota of obese (*n*=16) and lean dogs (*n*=15) fed the same experimental diet, without caloric reduction, for 30days (phase 1 of the study).

| | OB | | CTRL | | | ANOVA *p*-value | | |
|---|---|---|---|---|---|---|---|---|
| | T0 | T30 | T0 | T30 | SEM | Group | Diet | Group X diet |
| No. of observed OTUs | 134 | 159 | 142 | 148 | 7.161 | 0.888 | 0.129 | 0.358 |
| Chao1 | 136 | 162 | 143 | 150 | 7.439 | 0.831 | 0.126 | 0.376 |
| Shannon Index | 6.45 | 6.77 | 6.62 | 6.65 | 0.085 | 0.826 | 0.140 | 0.238 |

OB: obese dogs; CTRL: lean dogs; OTUs: operational taxonomic units; SEM: standard error of the mean.

### 3.1.3. Serum analytes

Among serum biochemical parameters collected in both groups at T30 (Table 4; Supplementary Table 3), total protein ($p = 0.033$), C-reactive protein (CRP, $p = 0.007$), Hp ($p = 0.003$), Trolox equivalent antioxidant capacity (TEACH, $p = 0.037$), and Thiol ($p = 0.013$) were higher in OB than in CTRL dogs, while the opposite was true for phosphate ($p = 0.008$). However, all phosphate values were within the normal range. Moreover, OB tended to have higher total thyroxine (TT4) than CTRL ($p = 0.07$).

The Pearson correlation test revealed that, in OB dogs, serum Hp concentrations negatively correlated with the following antioxidant capacity biomarkers (Table 5): TEACH ($r = -0.55$; $p = 0.029$), TEACA ($r = -0.59$; $p = 0.017$), Thiol ($r = -0.52$; $p = 0.039$). There was instead no correlation between CRP and antioxidant capacity biomarkers in OB.

## 3.2. Phase 2—Fecal metabolites and microbiota, and serum analytes in OB dogs

### 3.2.1. Weight loss outcomes

Full details of weight loss outcomes of OB dogs are given in Table 6. All dogs lost weight, and 3 out of 16 reached their target weight. The median overall percentage of weight loss was 12.9% (7.3% to 22.3%) of starting body weight (SBW) and, in detail, BW changed by a median of-9% from T30 to T120 (−3.5% to −12.4%) and −6% from T120 to T210 (+0.6% to −11.4%). The median overall rate of weight loss, expressed as a percentage of SBW lost per week, was 0.53% (0.3% to 0.9%), and the rate of weight loss changed by a median of 0.74% from T30 to T120 (0.3% to 1%), to a median of 0.49% from T120 to T210 (−0.06% to 1%). The median overall energy intake,

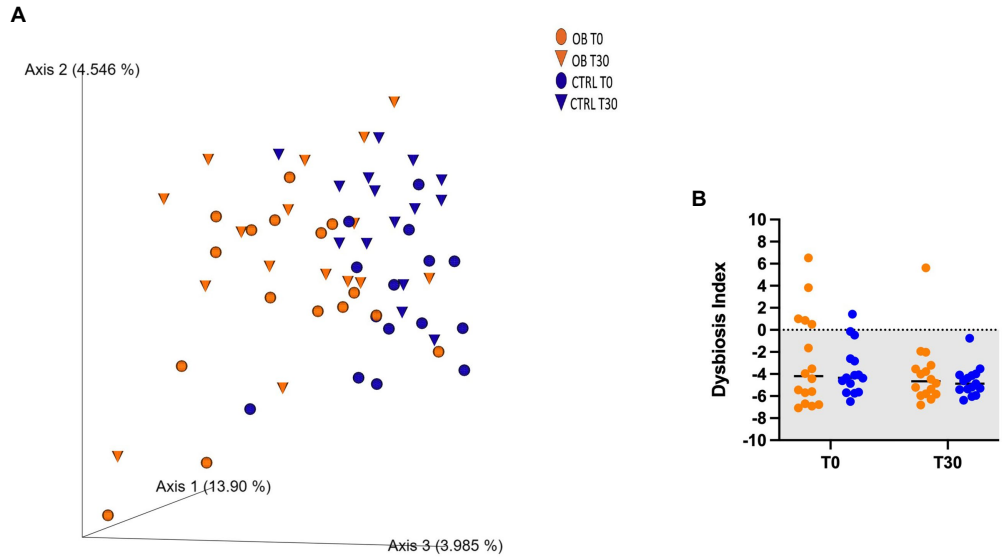


FIGURE 1
**(A)** PCoA plot based on the unweighted UniFrac distance metric of the fecal microbiota of obese (OB, orange, dot=T0; triangle=T30) and lean dogs (CTRL, blue, dot=T0, triangle=T30; **B**) qPCR-based fecal Dysbiosis Index of obese and lean dogs at trial start (T0) and after (T30) dietary treatment. Negative values (the grey area) are indicative of a healthy microbiota, while values between 0 and 2 are considered equivocal.

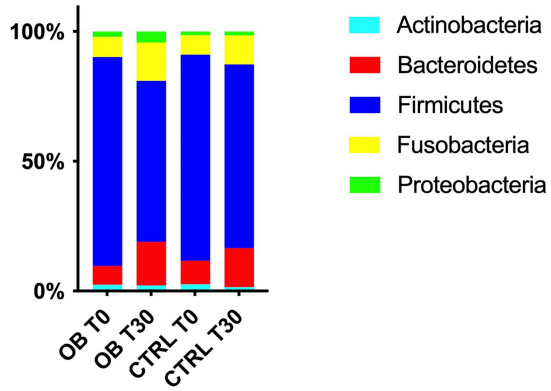


FIGURE 2
Relative abundances of the 5 most abundant phyla in fecal samples of obese and lean dogs at trial start (T0) and after (T30) dietary treatment. In obese dogs, the median abundance of Firmicutes decreased after dietary treatment (T0: 86% vs. T30: 59%, $q$=0.010), while a tendency to an increase was observed for Bacteroidetes and Fusobacteria (T0: 4.5% vs. T30: 19%, $q$=0.065 and T0: 4.4% vs. T30: 15%, $q$=0.054 for Bacteroidetes and Fusobacteria, respectively).

expressed as kcal of ME per kg$^{0.75}$ TBW, during caloric restriction was 69 (55 to 101).

### 3.2.2. Fecal metabolites and microbiota

Fecal pH, ammonia, VFA, and biogenic amines were not affected by caloric restriction ($p$>0.05, Table 7).

Similarly, alpha-and beta-diversity indices, as well as selected bacterial populations detected by qPCR were not influenced by caloric restriction (Table 8; Figure 4A; Supplementary Table 4, respectively). Also, DI was not affected by caloric restriction in OB dogs (Figure 4B).

Among the five most abundant bacterial phyla recovered in OB dogs in Phase 1, only Actinobacteria showed a shift in their community composition during caloric restriction (Figure 5): in particular, the median abundance of Actinobacteria was lower at T120 than as at T30 (0.7% vs. 1.4%, range: 0–2.1 vs. 0–7.2, $q$>0.05) and then significantly increased at T210 compared with T120 (median: 1.9% vs. 0.7% range: 0.3–6.2 vs. 0–2.1, $q$=0.014).

Differences in terms of bacterial class, order, family, genera and species in OB dogs during caloric restriction, are available in Supplementary File 1, while significative results are presented in Figure 6. At the family level (Figure 6A), fecal microbiota composition of OB dogs was characterized by an increase of the family Coriobacteriaceae after the second half of the caloric restriction period (T120: 0.73% vs. T210: 1.66%, $q$=0.018), even if their bacterial abundance at T210 was not different from the one observed at T30 (T30: 1.39% vs. T210: 1.66%, $p$>0.05). The same trend was observed at genus and species levels for the genus *Collinsella* (T120: 0.62% vs. T210: 1.20%, $q$=0.014, Figure 6B) and in particular for *C. stercoris* (T120: 0.62% vs. T210: 1.17%, $q$=0.008, Figure 6C). The relative abundance of the family Clostridiaceae increased significantly after caloric restriction (T210: 23% vs. T30: 20%, $q$=0.04, Figure 6D), while the abundance of the genus *Bacteroides* instead decreased after the second half of the weight loss period (T120: 13% vs. T210: 8.9%, $q$=0.032, Figure 6E).

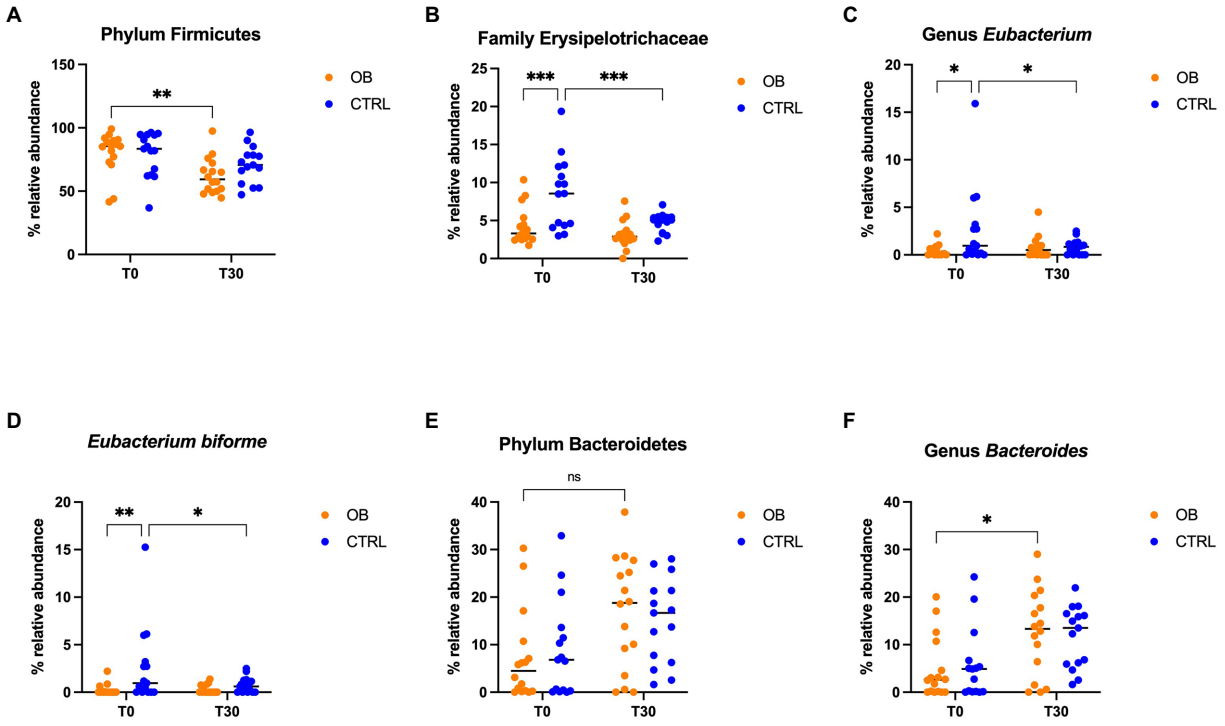


FIGURE 3
Relative abundance of selective bacterial populations: **(A)** phylum Firmicutes, **(B)** family Erysipelotrichaceae, **(C)** genus *Eubacterium*, **(D)** species *Eubacterium biforme*, **(E)** phylum Bacteroidetes, **(F)** genus Bacteroides, in fecal samples of obese and lean dogs before (T0) and after (T30) dietary treatment. Significance level: *$q$<0.05, **$q$<0.01, ***$q$<0.001, ns indicate $p$-values that did not pass FDR correction ($q$=0.08, $p$<0.05).

### 3.2.3. Serum analytes

All serum biochemical parameters are presented in Supplementary Table 5, and significant changes found in OB dogs during caloric reduction are showed in Figure 7. Compared with T30, a decrease of creatinine ($p$ < 0.0001, Figure 7A) and an increase of TT4 serum concentrations ($p$ = 0.007, Figure 7B) were observed at T120 and T210. At T120 serum total protein and gamma-glutamyl transferase (GGT) concentrations decreased ($p$ < 0.0001, Figure 7C) and increased ($p$ = 0.007, Figure 7D), respectively, while at T210 it returned to values similar to those observed at T30.

Caloric restriction did not result in any changes in inflammatory and oxidative status biomarkers (Table 4); moreover, there was no correlation between biomarkers of antioxidant capacity (TEACH, TEACA and Thiol) and inflammatory markers (CRP and Hp; Table 5).

## 4. Discussion

Obesity is the most commonly occurring metabolic disease in dogs, causing severe concurrent clinical conditions, such as functional (Mosing et al., 2013; Tropf et al., 2017) and metabolic disorders (Tvarijonaviciute et al., 2012c), and thus decreasing quality of life and longevity (Kealy et al., 2002; Courcier et al., 2010; German et al., 2012).

When it comes to an excess of body fat in dogs, the protracted imbalance between food intake and energy expenditure must be considered (Courcier et al., 2010), as well as factors related to changes in eating behavior and voluntary physical activity, such as neutering and ageing (Courcier et al., 2010; Kawauchi et al., 2017; Suarez et al., 2022). Such factors might have affected energy expenditure in client-owned OB dogs in this study, which had different age and neuter status. The energy intake assessed in OB dogs, before applying the caloric restriction, showed values similar to what has been considered as appropriate for adult dogs with 1–3 h/day activity level (FEDIAF, 2021). However, the daily activity level of OB dogs was not assessed in the present study.

### 4.1. Thyroid function and serum biochemical profile

Excess body fat is also related to endocrine and inflammatory profile changes in dogs with insulin resistance, modification of adipokine patterns, and lipid metabolism changes being reported (Antonio Brunetto et al., 2011; Clark and Hoenig, 2016). In this study, we observed significant differences in TT4 and acute phase proteins (CRP and Hp) concentrations between a population of 16 client-owned obese and 15 lean dogs.

10.3389/fmicb.2022.1050474

TABLE 4 Serum concentrations of acute phase proteins (CRP and Hp), inflammatory and oxidative stress biomarkers (median [range]) in obese (*n*=16) and lean (*n*=15) dogs fed the same experimental diet, without caloric restriction, for 30days (phase 1 of the study), and in the same obese dogs after 180days of caloric restriction (phase 2 of the study).

| Parameter | CTRL T30 | OB T30 | OB T210 |
|---|---|---|---|
| CRP (mg/dl) | 0.91 [0.80–2.4] | 1.1 [0.8–2.7] | 0.96 [0.74–4.5] |
| RI [0–0.85] | | | |
| *p*-value | **0.007** | | 0.242 |
| Hp (mg/dl) | 30 [1–125] | 85 [16–197] | 74 [3–157] |
| RI [20–140] | | | |
| *p*-value | **0.003** | | 0.395 |
| PON1 (IU/L) | 3.63 [2.62–4.08] | 3.66 [2.40–4.40] | 3.66 [2.74–4.60] |
| *p*-value | 0.310 | | 0.941 |
| CUPRAC (mmol/L) | 0.44 [0.37–0.63] | 0.48 [0.36–0.62] | 0.52 [0.34–0.61] |
| *p*-value | 0.079 | | 0.785 |
| FRAP (mmol/L) | 0.44 [0.30–0.63] | 0.48 [0.31–0.61] | 0.49 [0.33–0.64] |
| *p*-value | 0.271 | | 0.972 |
| TEACH (mmol/L) | 0.65 [0.57–0.85] | 0.73 [0.54–0.81] | 0.71 [0.54–0.82] |
| *p*-value | **0.037** | | 0.374 |
| TEACA (mmol/L) | 0.29 [0.22–0.43] | 0.29 [0.22–0.37] | 0.29 [0.22–0.38] |
| *p*-value | 0.955 | | 0.531 |
| Thiol (μmol/L) | 180 [108–273] | 251 [110–384] | 215 [93–366] |
| *p*-value | **0.013** | | 0.343 |
| BChE (U/mL) | 5.00 [3.30–8.40] | 5.10 [3.60–8.50] | 5.55 [3.80–8.30] |
| *p*-value | 0.942 | | 0.626 |
| TBARS (μmol/L) | 1.83 [1.2–3.1] | 2.19 [0.92–3.24] | 2.79 [1.13–4.30] |
| *p*-value | 0.126 | | 0.201 |
| FOX (μmol/L) | 52.04 [22.68–101] | 51.96 [23.9–89.1] | 55.58 [23.7–74.5] |
| *p*-value | 0.646 | | 0.506 |
| ROS (cps) | 1,510 [828–2,368] | 1,476 [1108–2052] | 1,630 [994–2,314] |
| *p*-value | 0.481 | | 0.133 |

OB: obese dogs; CTRL: lean dogs. BChE: butyrylcholinesterase; CRP: c-reactive protein; CUPRAC: cupric reducing antioxidant capacity; FOX: ferrous oxidation-xylenol orange; FRAP: ferric reducing ability; Hp: haptoglobin; PON1: paraoxonase 1; ROS: reactive oxygen species; TBARS: thiobarbituric acid reactive substances; TEACA, TEACH: trolox equivalent antioxidant capacity. *p*-value quoted are for parametric or not parametric tests comparing CTRL and OB T210 with OB T30. Data in bold highlight statistical significance.

TABLE 5 Coefficients of correlation between serum biomarkers of antioxidant capacity (TEACH, TEACA and Thiol) and serum inflammatory markers (CRP and Hp) in obese dogs (*n*=16) before (T30) and after (T210) caloric restriction (phase 2 of the study).

| | CRP (mg/dl) | | Hp (mg/dl) | |
|---|---|---|---|---|
| | *r* | *p* | *r* | *p* |
| TEACH (mmol/L) T30 | −0.119 | 0.661 | −0.546 | **0.029** |
| T210 | 0.144 | 0.595 | 0.024 | 0.930 |
| TEACA (mmol/L) T30 | 0.069 | 0.798 | −0.588 | **0.017** |
| T210 | 0.153 | 0.570 | 0.278 | 0.297 |
| Thiol (μmol/L) T30 | −0.460 | 0.073 | −0.520 | **0.039** |
| T210 | −0.252 | 0.346 | −0.311 | 0.242 |

CRP: c-reactive protein; Hp: haptoglobin; TEACA, TEACH: trolox equivalent antioxidant capacity. Data in bold highlight statistical significance.

Thyroid hormones are among the main factors involved in the regulation of energy expenditure (Reinehr, 2010; Mullur et al., 2014) and thyroid dysfunctions are responsible of significant changes in body weight in dogs, with hypothyroidism being usually associated with weight gain, reduced thermogenesis and metabolic rate (Scott-Moncrieff, 2015a,b). Although thyroid function is usually normal in obese dogs, they are frequently tested for hypothyroidism before starting a weight-loss protocol. Differences in thyroid function have been previously evaluated in obese and lean dogs showing that obese dogs have higher total triiodothyronine (TT3) and TT4 serum concentrations than lean animals, even if without clinical importance (Daminet et al., 2003). In accordance with these findings, in the present study, TT4 concentrations of OB dogs before caloric restriction tended to be higher than in CTRL animals, but remained within the normality

TABLE 6 Weight loss outcomes of obese dogs (*n*=16) before (T30), after 3months (T120), and at the end (T210) of caloric restriction (phase 2 of the study).

| Parameter | T30 | T120 | T210 | Overall |
|---|---|---|---|---|
| Body weight (kg) | 27.5 [4.6–63.7] | 25.4 [4.10–58] | 23.4 [3.6–58.7] | |
| BCS[a] | 8 [7–9] | 7 [6–9] | 7 [4–8] | |
| Weight loss (%)[b] | | 9.0 [3.5–12.4] | 6.0 [−0.6–11.4] | 12.9 [7.3–22.3] |
| Target body weight reached, *n*. OB (%OB) | | 3 (19%) | | |
| Rate of weight loss[c] | | 0.74 [0.3–1.0] | 0.49 [−0.06–1.0] | 0.53 [0.3–0.9] |
| Daily energy intake[d] | 72 [64–105] | 69 [57–102] | 64 [41–95] | 69 [55–101] |

All data, except for the number of dogs that reached the target body weight, are expressed as median [range].
[a]BCS based on 9 point scale (Laflamme, 1997).
[b]Expressed as the percentage of starting body weight. Positive values indicate a net loss, negative value indicate a net gain.
[c]Expressed as the percentage of starting body weight lost per week.
[d]Expressed as kcal of ME per $kg^{0.75}$ of target body weight.

TABLE 7 Fecal pH values and concentrations of ammonia (μmol/g), volatile fatty acids (μmol/g) and biogenic amines (nmol/g) in feces of obese dogs (*n*=16) before (T30), after 90days (T120) and at the end (T210) of caloric restriction (phase 2 of the study).

| | T30 | T120 | T210 | Pooled SEM | *p*-value |
|---|---|---|---|---|---|
| pH | 6.79 | 6.78 | 6.79 | 0.067 | 0.988 |
| Ammonia | 33.5 | 37.0 | 30.8 | 2.406 | 0.135 |
| Acetic a. | 61.3 | 56.9 | 60.8 | 3.503 | 0.624 |
| Propionic a. | 27.2 | 24.7 | 34.1 | 2.472 | 0.031 |
| Isobutyric a. | 1.80 | 1.47 | 1.76 | 0.165 | 0.509 |
| *n*-Butyric a. | 10.4 | 10.3 | 11.4 | 0.719 | 0.504 |
| Isovaleric a. | 2.37 | 2.08 | 2.48 | 0.263 | 0.820 |
| Total VFA | 104 | 95.5 | 111 | 5.568 | 0.176 |
| Putrescine | 1,010 | 1,134 | 1,163 | 123 | 0.306 |
| Cadaverine | 785 | 598 | 551 | 99.6 | 0.378 |
| Spermidine | 432 | 452 | 456 | 40.7 | 0.804 |
| Spermine | 251 | 237 | 269 | 32.7 | 0.965 |

SEM: standard error of the mean; VFA: volatile fatty acids.

TABLE 8 Alpha-diversity indices of fecal microbiota of obese dogs (*n*=16) before (T30), after 90days (T120), and at the end (T210) of caloric restriction (phase 2 of the study).

| | T30 | T120 | T210 | Pooled SEM | *p*-value |
|---|---|---|---|---|---|
| No. of observed OTUs | 159 | 155 | 150 | 7.556 | 0.719 |
| Chao1 | 162 | 157 | 155 | 7.807 | 0.811 |
| Shannon Index | 6.77 | 6.71 | 6.68 | 0.081 | 0.739 |

OTUs: operational taxonomic units; SEM: standard error of the mean.

range. During two previous studies (Daminet et al., 2003; Diez et al., 2004), a decrease of free thyroxine (fT4) and TT3 was observed in Beagle dogs following a weight loss program, leading authors to suppose that thyroid homeostasis of dogs may be affected by energy restriction. Similarly, fasting and weight loss have been associated with a decrease of thyroid hormone levels in humans, probably as a result of the decline of circulating leptin (Kok et al., 2005; Reinehr, 2010). In contrast with these findings, in the present study, TT4 serum concentrations unexpectedly significantly increased during caloric restriction, albeit remaining within the range of normality. In humans, the interaction between total calories and carbohydrate intake on thyroid hormone response has been previously investigated. An increase of TT4 was also reported in humans consuming a low-carbohydrates diet, resulting in a decrease of fat mass and an increase in lean mass (Volek et al., 2002). A previous study reported a decrease TT3 and no change in TT4 in response to reduced carbohydrate intake (Mathieson et al., 1986). The significant increase in TT4 observed by Volek et al. (2002) and in the present study, may represent an increase in the biologically active hormone available to cells. However, this speculation should be made with caution since, as in the previously cited study, TT3, free T3, or free T4 were not investigated in the present study.

In the present study, serum concentrations of creatinine decreased during caloric restriction, in accordance with what was previously observed in Beagle dogs during a 17-weeks weight loss study, where only a reduction of body fat with no loss of lean mass was confirmed (Salas-Mani et al., 2018). Serum creatinine concentration is used as a marker of muscle mass in dogs, beyond kidney function, with higher concentration being measured in dogs with great muscle mass, such as sighthound dogs, while lower concentrations are seen in small dogs (Braun et al., 2003; Middleton et al., 2017). In the present study, we did not assess changes in body composition by dual-energy X-ray absorptiometry (DEXA), so that some degree of lean mass loss cannot be completely ruled out. However, considering the slow rate of weight loss that we recorded, and according to what has been observed by other authors (German et al., 2015; German, 2016), it is unlikely that, in this study, obese dogs experienced a significant loss of lean mass during caloric restriction.

In line with our results, obese dogs can show higher serum total protein concentrations than lean dogs (Piantedosi et al., 2016; Radakovich et al., 2017), as a result of decreased serum water fraction, antigenic stimulation, or increased protein catabolism associated to their larger body mass (Radakovich et al., 2017). However, in the present study, we did not observe any differences in the serum concentrations of urea, a biochemical marker of muscle and protein catabolism (Gunst et al., 2013), in OB and CTRL dogs.

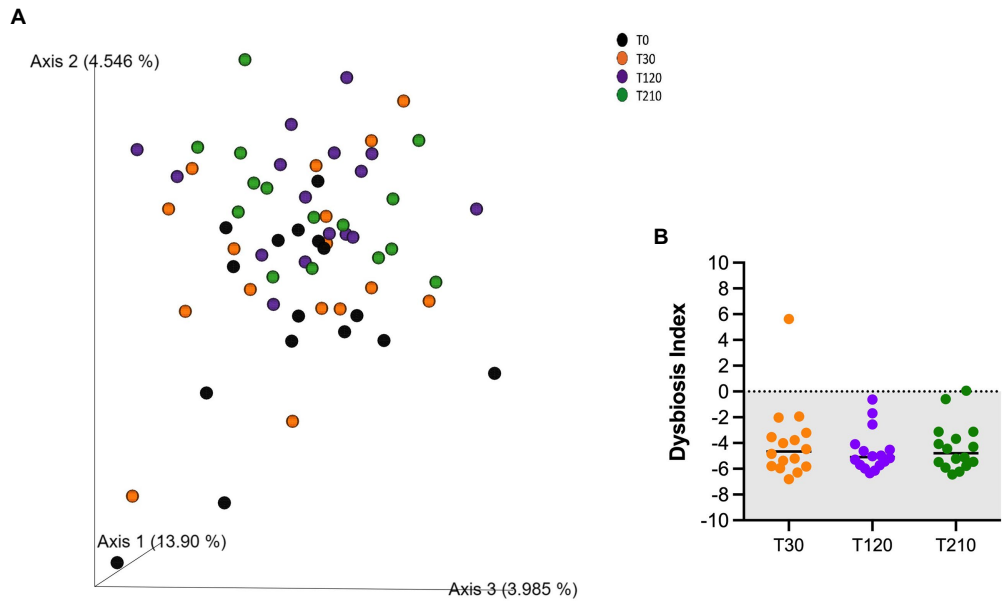


FIGURE 4
**(A)** PCoA plot based on the unweighted UniFrac distance metric of the fecal microbiota of obese dogs. Differences before (T30) and after 90 and 180days of caloric restriction were not observed ($p$>0.05). **(B)** qPCR-based fecal Dysbiosis Index of obese dogs before (T30), after 90days (T120) and at the end (T210) of caloric restriction. Negative values (the grey area) are indicative of a health microbiota, while values between 0 and 2 are considered equivocal.

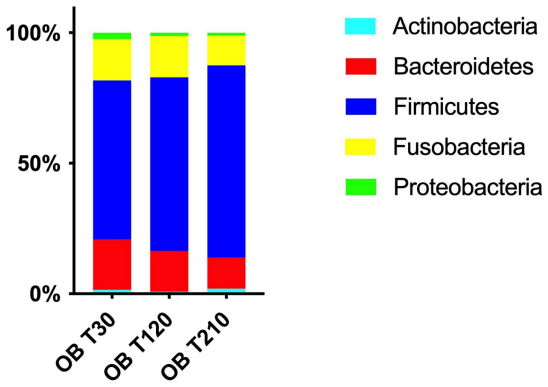


FIGURE 5
Relative abundances of the 5 most abundant phyla in fecal samples of obese dogs before (T30), after 90days (T120) and at the end (T210) of caloric restriction; the median abundance of Actinobacteria numerically decrease at T120 compared with T30 ($q$>0.05) and then significantly increased at T210 compared with T120 (1.9% vs. 0.7%, $q$=0.014). Moreover, a tendency to a decrease was observed between T30 vs. T120 and T120 vs. T210 for Bacteroidetes (T30: 19% vs. T120: 14% and T120: 14% vs. T210: 13%, $q$=0.051) and between T30 vs. T120 for Proteobacteria (T30: 2.4% vs. T120: 1.1%, $q$=0.051).

## 4.2. Inflammatory status and antioxidant response

Progress in human obesity indicates that adipose tissue plays a major role concerning metabolism and inflammation, and it is involved in the release of inflammatory cytokines influencing systemic inflammatory processes (Wozniak et al., 2009; Stolarczyk, 2017). Advances in canine obesity is still in its early stage; however, a decrease of inflammatory markers, such as CRP and Hp, has been observed after weight loss in previous studies, suggesting that also dogs may suffer from a compelling association between low-grade inflammatory state and obesity (German et al., 2009; Ricci et al., 2011; Wakshlag et al., 2011). Interestingly, experimentally induced overfeeding in laboratory dogs failed to stimulate an increase of inflammatory markers (Tvarijonaviciute et al., 2011; Van de Velde et al., 2013; Moinard et al., 2020). To date, only two studies have explored differences in systemic concentrations of pro-inflammatory markers and cytokines in obese and lean dogs, with a lack of evidence of clear differences (Veiga et al., 2008; Piantedosi et al., 2016). In the present study, we observed higher serum concentrations of acute-phase proteins (CRP and Hp) in obese dogs compared to lean subjects and these findings seem to be in accordance with what has been previously observed in some human studies (Das, 2001; Stępień et al., 2014; Cohen et al., 2021), suggesting that also obese dogs may suffer from a subclinical inflammatory state. However, serum concentrations of pro-inflammatory markers were not affected by caloric restriction in this study, and this finding was in agreement with previous reports in dogs, regardless of the type of obesity, short-term experimentally induced or long-term spontaneous disease (Tvarijonaviciute et al., 2012c; Bastien et al., 2015). This finding may indicate that canine obese-related inflammatory condition is not responsive to changes in energy balance, despite the fact that the degree of weight loss that

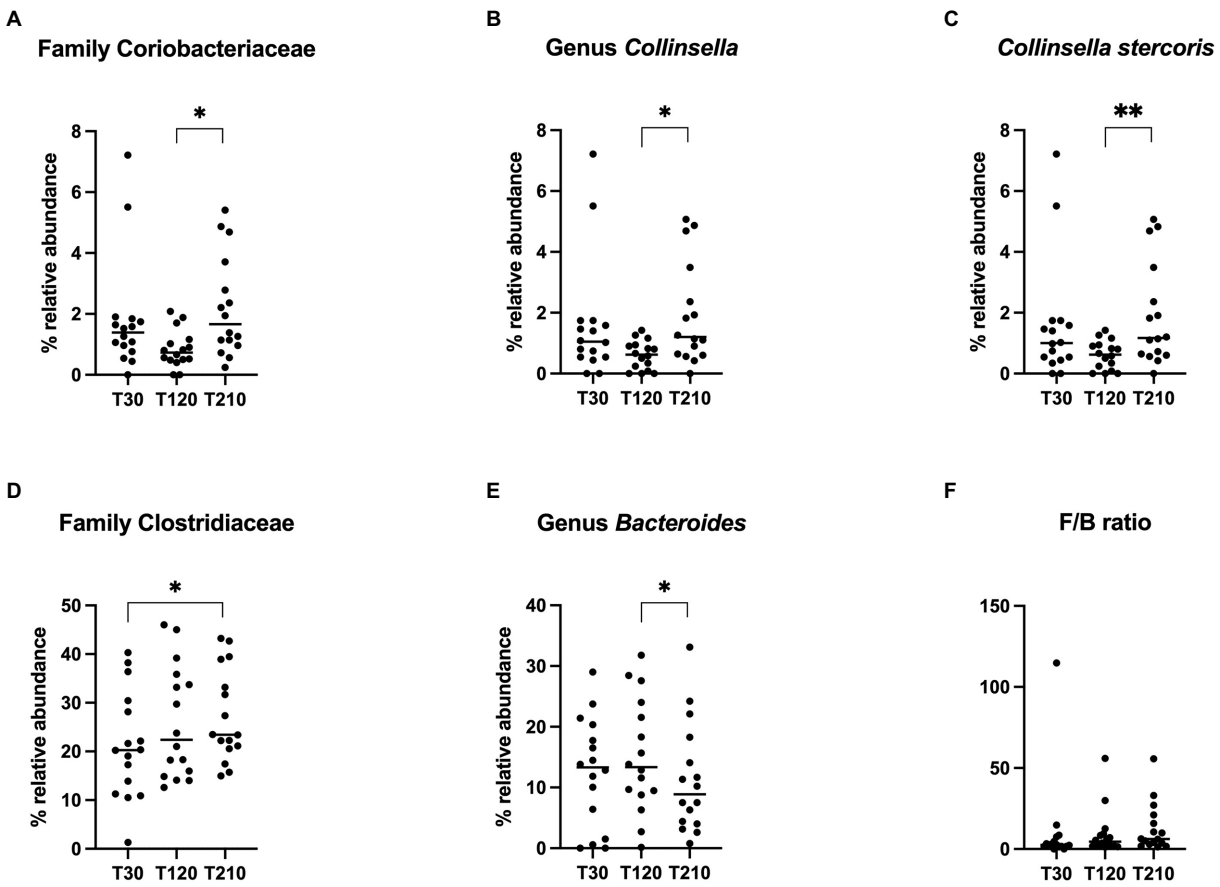


FIGURE 6
Relative abundance of selective bacterial populations: **(A)** family Coriobacteriaceae, **(B)** genus *Collinsella*, **(C)** species *Collinsella stercoris*, **(D)** family Clostridiaceae, **(E)** genus *Bacteroides*, **(F)** Firmicutes/Bacteroidetes ratio, in fecal samples of obese dogs before (T30), after 90days (T120) and at the end (T210) of caloric restriction. Significance level: *$q$<0.05, **$q$<0.01.

we observed was in line with the weight loss degrees that are known to improve inflammatory condition in obese humans (Forsythe et al., 2008). Butyrylcholinesterase (BChE) is an enzyme secreted by the liver under the stimulation of free fatty acids flux originating from adipose tissue (Cucuianu et al., 2002), and it is recognized as a robust marker to predict the development and prognosis of low-grade systemic inflammatory conditions, such as obesity, in humans (Das, 2012). In our study, BChE did not differ between obese and lean dogs and was not affected by caloric restriction, in contrast with previous research in canine obesity; in fact, higher BChE activity was assessed in dogs with obesity-related metabolic dysfunction and in those where obesity was induced (Tvarijonaviciute et al., 2010, 2019); moreover, a significant decrease of this enzyme was observed in dogs that experienced rapid, short-term weight loss (Tvarijonaviciute et al., 2013). Contrary to previous findings, however, our study was not conducted in experimental conditions, and the use of antiparasitic collars were not investigated. In fact, some antiparasitic treatments act as acetylcholinesterase inhibitors, and could therefore have affected the levels of BChE in our dogs (Birdane et al., 2022).

Obesity has also been associated with oxidative stress, as a result of an imbalance between oxidant and antioxidant molecules (Sánchez-Rodríguez and Mendoza-Núñez, 2019); moreover, the oxidant components may increase the risk for systemic low-grade chronic inflammation, which may be related to obesity-associated metabolic disorders (Trayhurn, 2005; Donath and Shoelson, 2011; Lumeng and Saltiel, 2011). Interestingly, in our study, OB dogs showed higher markers of total antioxidant capacity (TAC), such as TEACH and Thiol, than lean dogs. A possible interpretation for this finding might be a compensatory system carried out by obese dogs to restore homeostatic balance by enhancing endogenous antioxidants levels, as previously described in obese humans, where a positive correlation between CRP and TAC was observed (Petelin et al., 2017). Interestingly, we observed that TEACH and Thiol were inversely correlated with Hp in obese dogs before the caloric restriction, suggesting that a high degree of low-grade inflammation may result in the partial loss of antioxidant capacity. Nonetheless, the association between antioxidant status and canine obesity remains intriguing and warrants further research.

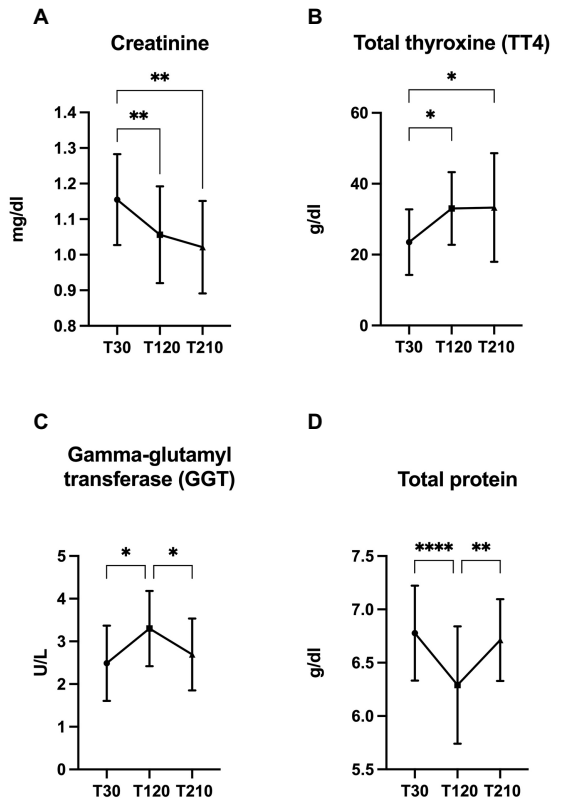


FIGURE 7
Significant changes in the concentration of selected serum metabolites. **(A)** creatinine, **(B)** total protein, **(C)** gamma-glutamyl transferase (GGT), and **(D)** total thyroxine (TT4) in obese dogs ($n$=16) before (T30), after 90days (T120), and at the end (T210) of caloric restriction. Significance level: *$q$<0.5, **$q$<0.01, ****$q$<0.0001.

## 4.3. Fecal bacterial metabolome and microbiota

It is currently well defined that the use of a low-energy, high-protein, high-fiber diet is the most effective strategy to favor weight loss in dogs, reducing voluntary food intake, minimizing muscle loss and attenuating signals of hunger (Blanchard et al., 2004; Laflamme and Hannah, 2005; Weber et al., 2007). The dietary intervention not only helps dogs to lose weight appropriately, but may also impact the gut microbiota and the connection existing between this complex ecosystem and the host; in fact, modulation of the macronutrient content of the diet may affect the intestinal bacteria which in turn may influence the host in many ways, mainly through the release of metabolites that have been acknowledged as beneficial for the host gastrointestinal tract and beyond it.

Among gut microbial metabolites, VFA (mainly acetate, propionate, and butyrate) are produced by anaerobic bacteria in the colon and distal small intestine through the fermentation of resistant starch, dietary fiber, and other low-digestible polysaccharides (Alexander et al., 2019; Ma et al., 2021). In our study, fecal VFA concentrations did not differ between obese and lean dogs and were not affected by dietary treatment. To the best of the author's knowledge, this is the first study in which fecal VFA concentrations from obese and lean dogs have been compared, while studies in mice and humans have shown higher fecal VFA concentrations among obese than lean individuals (Ley et al., 2006; Schwiertz et al., 2010).

It has to be remembered that different fecal sample collection, preservation, and processing methods may all be significant sources of variation in the quantification VFA in feces (Sowah et al., 2019), and likewise, the rapid absorption rate of VFA by the intestinal mucosa affect their fecal concentrations (Swanson et al., 2002). Nevertheless, the potentially higher production and turnover of VFA in obese mice could be related to differences in microbiota composition and function, with an increased potential for energy harvest among obese (Turnbaugh et al., 2006). The fecal VFA concentrations have been found to be reduced in obese humans after weight loss (Duncan et al., 2007), or unchanged (Damms-Machado et al., 2015); lower VFA fecal concentrations in obese humans during weight-loss may be related to the lower production in response to the lower carbohydrate intake, decreased energy harvest or increased mucosal absorption (Sowah et al., 2019). In line with the reported findings in humans, in a study with obese dogs (Kieler et al., 2017), acetic and propionic acid fecal concentrations were found to be lower in a small group of dogs with fast weight loss rate compared to those with slow weight loss rate.

Biogenic amines include gut microbial metabolites such as cadaverine, putrescine, spermidine, and spermine, and are putrefactive compounds produced by intestinal bacteria from the fermentation of undigested amino acids; biogenic amines are required for cells growth and differentiation, and for the synthesis of DNA, RNA, and proteins (Delzenne et al., 2000). Also, biogenic amines have been correlated in humans with increased fecal odor and increased incidence of colon cancer (Johnson, 1977). In this study, fecal biogenic amines of OB and CTRL dogs were determined, and fecal spermine concentration resulted decreased in CTRL after dietary treatment; it has been previously reported that fecal biogenic amines concentrations may be linked to fecal microbiota (Matsumoto and Benno, 2007). In line with our results, other studies have shown that the diet can impact the fecal biogenic amines concentrations in dogs, as fiber addition decreased fecal proteolysis and biogenic amines production (Jackson and Jewell, 2019), while biogenic amines increased in feces of working dogs fed a grain-free high-protein petfood (Chiofalo et al., 2019). The increase in dietary fiber intake is, therefore, the most likely explanation for the reduction of fecal spermine concentration observed in this study in CTRL dogs after dietary treatment, and, even though not significant, a decrease in fecal spermine concentration was also observed in OB dogs fed the same diet. The effects of spermine on host health remain controversial so far; in fact, spermine seems to possess significative physiological activity and toxicity in mice, being strictly controlled by both colonic microbiota and colonocytes (Matsumoto et al.,

2012), but it has also been seen that administration of exogenous spermine inhibited the activation of an inflammatory interleukin in mice, acting as inflammasome inhibitor (Levy et al., 2015). Results from studies conducted with mouse models suggest that biogenic amines metabolism could be dysregulated in the presence of obesity and other metabolic disorders, with the result of impaired glucose regulation, and lipid and energy homeostasis (Ramos-Molina et al., 2019). To date, this is the first study evaluating fecal biogenic amines in obese dogs, and even though their concentrations were affected by neither nutrition status nor caloric restriction, further research is warranted in order to clarify the effects and influence of microbial metabolites in canine obesity.

Studies on the composition of the gut microbiota have provided evidence of existing differences in the bacterial taxa found in lean and obese dogs, with sometimes controversial results (Handl et al., 2013; Park et al., 2015; Forster et al., 2018). At the phylum level, Bacteroidetes (range of abundance 12–38%) together with Firmicutes (14%–48%) and Fusobacteria (7%–44%) co-dominate the core bacterial community both in healthy and obese dogs (Middelbos et al., 2010; Suchodolski, 2011; Herstad et al., 2017; Salas-Mani et al., 2018). In this study, Firmicutes were the dominant phylum in obese as well as in lean dogs, as previously reported in a study involving pet dogs (Handl et al., 2013). However, when obesity was induced in dogs, the proportion of Proteobacteria was increased and Firmicutes were decreased, with the result of Proteobacteria being the dominant phylum in the obese animals (Park et al., 2015). In the present study, we did not observe any difference in the proportions of the major phyla between obese and lean dogs; conversely, inconsistently with our results, two previous researches showed that Actinobacteria were more abundant in obese than in lean pet dogs (Handl et al., 2013; Forster et al., 2018).

In obesity studies involving humans, mice and dogs, differences detected in Bacteroidetes and Firmicutes abundances are widely used as metric of impaired intestinal homeostasis, and an increased Firmicutes/Bacteroidetes (F/B) ratio is usually associated with obesity in mice (Ley et al., 2005) and humans (Ley et al., 2006; Kasai et al., 2015; Koliada et al., 2017). However, other studies revealed no significant differences in the F/B ratio between lean and obese humans (Ismail et al., 2011; Hu et al., 2015) or even opposite findings (Schwiertz et al., 2010; Vaiserman et al., 2020), so that it can be supposed that differences in other phyla, host age and sex, as well as environmental and genetic factors may also affect the F/B ratio (Stojanov et al., 2020; Vaiserman et al., 2020).

In this study, the dietary treatment had a significant impact on the fecal microbiota composition of OB dogs, mainly within the predominant phyla Firmicutes and Bacteroidetes. For instance, the fecal abundance of *Bacteroides* spp. increased, and Firmicutes decreased, in obese in response to the diet fed at maintenance requirement, while no difference was seen between obese and lean dogs; this finding appears to be in agreement with what was observed in a previous study that aimed to evaluate the effects of diets dissimilar in macronutrient composition on dogs of diverse body conditions, finding no differences in bacterial abundances among groups (Li et al., 2017).

The genus *Bacteroides* consists of bile-tolerant microorganisms associated with the consumption of diets rich in protein and fat in humans and dogs (De Filippo et al., 2010; Wu et al., 2011; Salas-Mani et al., 2018), although *Bacteroides* in the latter species are more selective for protein-rich substrates, as a reduction in the fecal abundance of *Bacteroides* occurred in response to the increase of dietary fat in dogs fed high-fat diets (>30% on a dry matter basis; Kilburn et al., 2020). In line with our results, *Bacteroides* were significantly increased in the feces of six healthy dogs fed for 21 days a weight loss diet (Mori et al., 2019) that had a macronutrient profile (carbohydrate, fat and protein content) comparable to the diet that was used in the present study (with the exception of the total dietary fiber content, 28% in the study by Mori et al. vs. 17% in our study, as fed).

*Bacteroides* has been negatively correlated with energy intake and adiposity in humans and dogs (Yatsunenko et al., 2012; Kovatcheva-Datchary and Arora, 2013; Bermudez Sanchez et al., 2020) and the administration of *B. uniformis* CECT7771 was able to reduce weight gain and serum triglycerides and cholesterol concentrations in mice fed high-fat diets (Gauffin Cano et al., 2012).

In this study, Firmicutes, which include species known to metabolize dietary plant polysaccharides and produce VFA (Pilla and Suchodolski, 2021), significantly decreased in the feces of OB dogs after dietary treatment. Consistently with our results, in a previous study (Mori et al., 2019), the proportion of Firmicutes as well as F/B ratio in feces of healthy dogs were lower when animals were fed a weight loss diet than when they received diets proposed for other diseases. Similar findings were observed in obese humans after weight reduction, where a lower F/B ratio was defined as restitution to "lean phenotype" (Ley et al., 2006; Clemente et al., 2012). In our study, the F/B ratio was not significantly affected, but the dietary treatment induced a shift of bacterial taxa considered of key significance in relation to obesity, such as those belonging to the phylum Firmicutes as well as to the family *Bacteroides*. These findings may suggest that feeding a high-protein, high-fiber diet may play a role in the modulation of fecal microbiota in canine obesity. Conversely, in the present study, Firmicutes and Bacteroidetes were not affected by diet in lean dogs. It has been seen that the composition of intestinal microbiota in healthy dogs can be unaffected (Bresciani et al., 2018) or be effectively modified (Mori et al., 2019) by short-term dietary interventions. The effectiveness of persistent changes in the intestinal microbiota induced by dietary interventions has been associated, in recent studies, to prolonged experimental set-ups, as well as to the shift to diets that were extremely different in terms of macronutrients composition (Mori et al., 2019; Allaway et al., 2020). However, obese dogs do not seem to show a clear state of intestinal dysbiosis: in fact, in the present study, the DI of obese dogs remained within the established reference interval for healthy dogs both before and after caloric restriction, in accordance with results previously reported by other authors (Bermudez Sanchez et al., 2020; Phungviwatnikul et al., 2022). Similarly, a relative abundance of microbial populations, as well as diversity of the microbial

community, did not differ between OB and CTRL, in accordance with results from a previous study involving a number of lean and obese colony dogs similar to ours (Handl et al., 2013); on the contrary, other authors have recently reported lower microbial diversity in obese dogs in comparison to lean dogs; in particular, the results described by Park et al. (2015) derived from a lower number of dogs compared to ours, while in the study by Forster et al. (2018) 66 animals, among obese and lean dogs, have been evaluated.

The 16S rRNA gene profiling revealed that OB dogs had a lower abundance of Erysipelotrichi, Erysipelotrichales, Erysipelotrichaceae, *Eubacterium* and *E. biforme* (data not shown for class and order), compared with CTRL dogs. The same findings were observed in a previous study which enrolled pet dogs and compared microbial abundances in obese and normal weight dogs (Forster et al., 2018). Hence, Erysipelotrichaceae and *Eubacterium* spp. abundance seem to be negatively correlated with obesity in dogs, while a positive correlation has been described in humans, where high levels of *E. dolichum* have been associated to increased visceral fat mass (Pallister et al., 2017; Pinart et al., 2022). *Eubacterium* spp., one of the core genera of the human gut microbiota, belongs to Firmicutes and consists of bacterial taxa that have been shown to be involved in carbohydrate metabolism and degradation of dietary fiber; in fact, increased levels of *Eubacterium* spp. are associated with the production of organic acids, from carbohydrates or peptone, including butyric, acetic and formic acids (Louis and Flint, 2017; Mukherjee et al., 2020). In a study by Forster et al. (2018), obese dogs were characterized by a lower abundance of *Eubacterium* spp. and *E. biforme* and reduced concentrations of VFA. In fact, the abundance of *Eubacterium* spp. and other butyrate-producing bacteria in the gut is strongly correlated with VFA concentrations, and the ingestion of dietary fibers has been seen to increase VFA concentrations and abundance of *Eubacterium* spp. (Duncan et al., 2007). However, in the current study, fecal VFA concentrations were not affected, suggesting that the relationship between the fecal abundance of *Eubacterium* spp. and VFA concentrations in obese dogs needs further investigation. In a study with elderly humans, the abundance of *Eubacterium* spp. was negatively correlated with CRP (Ghosh et al., 2020); in accordance with this finding, in the present study, at T0, CTRL dogs showed higher abundance of *Eubacterium* spp. and lower concentrations of inflammatory markers (CRP and Hp), compared with OB.

Erysipelotrichaceae consists of a bacterial family that has been identified in the fecal microbiota of healthy dogs (Garcia-Mazcorro et al., 2012a; Gagné et al., 2013; Panasevich et al., 2014). Interestingly, members of this family have been shown to change in abundance in response to changes in dietary macronutrient composition; in a study performed with dogs fed either kibbles or a raw-meat based diet, Erysipelotrichaceae were positively correlated with dietary fat content and markers linked to carbohydrate fermentation (such as VFA) on one hand, and negatively correlated with crude protein content of the diet on the other (Bermingham et al., 2017); moreover, Erysipelotrichaceae seem to be affected neither by type of protein nor by fat sources (Panasevich et al., 2014). One possible explanation for the decrease in Erysipelotrichaceae abundance that we observed in lean dogs after the dietary treatment may therefore be associated with the high protein content of the weight loss diet. Similarly, low levels of *Eubacterium* spp. have been associated with increased protein, fat, and fructose intake in humans and the consumption of sugar-rich diets in mice (Duncan et al., 2007; Mahowald et al., 2009; Wu et al., 2011; Jones et al., 2019).

An expected result of weight reduction in humans is an increase in the diversity of bacterial communities. However, conflicting results have been obtained depending on the method by which the weight loss was achieved (Damms-Machado et al., 2015; Remely et al., 2015). In a previous study, a reduction of Bacteroidetes abundance was observed in human patients that underwent obesity surgery, while, on the contrary, an increase of this phylum was seen secondary to treatment with a low-calorie diet (Damms-Machado et al., 2015). Other studies found no alteration of Bacteroidetes after weight reduction, challenging the reversibility of reduced Bacteroidetes abundance in obese humans (Remely et al., 2015; Frost et al., 2019).

In the present study, the caloric restriction did not have a significant impact on bacterial diversity and this finding is consistent with the results from a previous research, in which the fecal microbiota of 6 obese Beagle dogs was not affected by a 17-weeks weight loss program (Schauf et al., 2018). Conversely, in a recent study, 20 obese pet dogs showed an increase in bacterial diversity when they reached their ideal body weight; in the same study, bacterial diversity was not improved in a small group of dogs with less effective weight loss (Bermudez Sanchez et al., 2020). In the study by Bermudez Sanchez et al. (2020), the phylum Bacteroidetes significantly increased after weight loss in dogs, and this increase was driven mainly by *Bacteroides* spp.; conversely, in the present study, a decrease in the fecal abundance of this genus was observed after 180 days of caloric restriction. However, in the study by Bermudez Sanchez et al. (2020), dogs were followed until they reached the ideal weight (mean duration = 330 days), whereas our study lasted 180 days and only 3 dogs out of 16 had reached their ideal weight at the end of the trial.

*Collinsella* spp. belong to the Actinobacteria phylum and have been described as fiber degraders and $H_2$ consumers, resulting in the production of mainly lactate and acetate. *Collinsella* spp. and *C. aerofaciens* have been proposed as biomarkers of obesity in humans, as they are positively associated with body mass index and insulin resistance (Companys et al., 2021); moreover, it has been seen that abundance of *Collinsella* spp. in humans was significantly reduced during a weight loss program (Frost et al., 2019; Martínez-Cuesta et al., 2021). In the present study, abundance of *Collinsella* spp. and *C. stercoris* numerically decreased after 90 days of caloric restriction and then significantly increased at the end of the study compared with the previous time point. According to our findings, several human studies have previously shown that changes in the diversity and composition of the gut microbiome rapidly occur during dietary intervention (e.g., caloric reduction) or obesity surgery; nevertheless, these changes are only partially sustained over time, tending toward a

regression to baseline, irrespective of the weight loss achieved (Simões et al., 2014; Heinsen et al., 2017; Frost et al., 2019; Shen et al., 2019). On the contrary, in this study, the family Clostridiaceae was consistently associated with weight loss, increasing its abundance at the end of the study compared with trial start. To date, results on Clostridiaceae abundance in obese dogs are not univocal, and the degree of caloric reduction may represent an important factor; in fact, in previous studies with obese dogs, the genus *Clostridium* showed a decrease after a weight loss program (Salas-Mani et al., 2018; Bermudez Sanchez et al., 2020), in line with what had been observed in humans (Nadal et al., 2009). On the contrary, in other studies with dogs, the use of a high-protein weight-loss diet, fed without any caloric restriction, increased Clostridiaceae (Zentek et al., 2004; Li et al., 2017; Mori et al., 2019), suggesting that Clostridiaceae may be stimulated by dietary protein, rather than by dietary fiber, as previously reported (Panasevich et al., 2013). Our results seem to suggest that the increase in Clostriadaceae was caused by caloric restriction, rather than by the diet, because no changes in their abundance were observed during the first phase of the study.

The study has some limitations. The use of private-owned animals, rather than research dogs introduced variables, both dogs and owners related. Factors affecting populations variability included signalment and different environmental conditions. In addition, the small study populations might not be able to show some significant differences between compared groups. However, results from the present study are plausibly more representative of the overall canine population. A second limitation was related to ethical limitations: in fact, given the requirement for sedation, DEXA scanning cannot be performed in obese dogs, therefore the changes of lean mass or fat mass, before and after the weight loss, were not assessed. Finally, it should be also noted that fT4 was not measured neither the use of antiparasitic collars were investigated in obese dogs, therefore only careful conclusions have been formed regarding thyroid homeostasis and BChE activity in obese dogs.

## 5. Conclusion

The present study has provided evidence that obese dogs suffer from a subclinical inflammatory state, characterized by higher levels of some inflammatory markers and a concomitant higher total antioxidant capacity. However, caloric restriction did not influence the inflammatory status of obese dogs.

The fecal microbiota of obese and lean dogs did not display big differences and neither bacterial diversity nor metabolites (VFA and polyamines) were influenced by dogs' nutritional status.

Caloric restriction resulted in a few changes in the abundance of some bacterial populations but failed to affect bacterial diversity, DI, and metabolites in obese dogs. However, the decrease of *Bacteroides* spp. and the increase of Clostriadiaceae family, were the only changes consistently associated with caloric restriction and weight loss throughout the study.

This study has provided insights into the involvement of the intestinal microbiota, inflammatory and antioxidant status as well as thyroid homeostasis in canine obesity. Further research is warranted to better clarify the influence of these factors on canine obesity, since the mechanism of these connections is somewhat far from being conclusive.

## Data availability statement

The datasets presented in this study can be found in online repositories. The names of the repository/repositories and accession number(s) can be found at: NCBI Sequence Read Archive under accession number PRJNA822358.

## Ethics statement

The animal study was reviewed and approved by Animal Welfare Committee of the University of Bologna (number 96551/2019). Written informed consent was obtained from the owners for the participation of their animals in this study.

## Author contributions

FF and GB conceived and designed the study. CV, SG, and ED carried out the clinical study and collected all data. CV, CP, RP, AT, CR, ED, CD, and CS carried out laboratory work. CV and RP performed statistical analyses. CV wrote the original draft with assistance and feedback from SG, CP, RP, JS, AT, CR, CS, EP, FF, and GB. All authors contributed to the article and approved the submitted version.

## Funding

This study received funding from Monge & C. S.p.A., Monasterolo di Savigliano, Italy (grant number 0018554/2019).

## Acknowledgments

Results were presented, in part, at the 2022 Congress of the European Society of Veterinary and Comparative Nutrition, Basel, Switzerland.

## Conflict of interest

EP is an employee of Monge & C S.p.A, Monasterolo di Savigliano, Italy. JS and RP were employed of the GI Lab at Texas A&M University, which provides the dysbiosis index on a fee for service basis.

The remaining authors declare that the research was conducted in the absence of any commercial or financial relationships that could be construed as a potential conflict of interest.

The authors declare that this study received funding from Monge & C S.p.A. The funder had the following involvement in the study: assistance during manuscript preparation.

The reviewer CWC declared a shared affiliation with the authors RP, JS to the handling editor at the time of review.

## Publisher's note



## Supplementary material

The Supplementary material for this article can be found online at: https://www.frontiersin.org/articles/10.3389/fmicb.2022.1050474/full#supplementary-material

## References

Allaway, D., Haydock, R., Lonsdale, Z. N., Deusch, O. D., O'Flynn, C., and Hughes, K. R. (2020). Rapid reconstitution of the fecal microbiome after extended diet-induced changes indicates a stable gut microbiome in healthy adult dogs. *Appl. Environ. Microbiol.* 86:e00562-20. doi: 10.1128/AEM.00562-20

Alexander, C., Swanson, K. S., Fahey, G. C., and Garleb, K. A. (2019). Perspective: physiologic importance of short-chain fatty acids from nondigestible carbohydrate fermentation. *Adv. Nutr.* 10, 576–589. doi: 10.1093/advances/nmz004

AlShawaqfeh, M. K., Wajid, B., Minamoto, Y., Markel, M., Lidbury, J. A., Steiner, J. M., et al. (2017). A dysbiosis index to assess microbial changes in fecal samples of dogs with chronic inflammatory enteropathy. *FEMS Microbiol. Ecol.* 93, 1–8. doi: 10.1093/femsec/fix136

Antonio Brunetto, M., César Sá, F., Prudente Nogueira, S., de Oliveira Sampaio Gomes, M., Gullo Pinarel, A., Toloi Jeremias, J., et al. (2011). The intravenous glucose tolerance and postprandial glucose tests may present different responses in the evaluation of obese dogs. *Br. J. Nutr.* 106, S194–S197. doi: 10.1017/s0007114511000870

Apprill, A., Mcnally, S., Parsons, R., and Weber, L. (2015). Minor revision to V4 region SSU rRNA 806R gene primer greatly increases detection of SAR11 bacterioplankton. *Aquat. Microb. Ecol.* 75, 129–137. doi: 10.3354/ame01753

Arab, K., and Steghens, J. P. (2004). Plasma lipid hydroperoxides measurement by an automated xylenol orange method. *Anal. Biochem.* 325, 158–163. doi: 10.1016/j.ab.2003.10.022

Arora, T., Sharma, R., and Frost, G. (2011). Propionate. Anti-obesity and satiety enhancing factor? *Appetite* 56, 511–515. doi: 10.1016/j.appet.2011.01.016

Banton, S., von Massow, M., Pezzali, J. G., Verbrugghe, A., and Shoveller, A. K. (2022). Jog with your dog: dog owner exercise routines predict dog exercise routines and perception of ideal body weight. *PLoS One* 17:e0272299. doi: 10.1371/journal.pone.0272299

Bastien, B. C., Patil, A., and Satyaraj, E. (2015). The impact of weight loss on circulating cytokines in beagle dogs. *Vet. Immunol. Immunopathol.* 163, 174–182. doi: 10.1016/j.vetimm.2014.12.003

Bermingham, E. N., Maclean, P., Thomas, D. G., Cave, N. J., and Young, W. (2017). Key bacterial families (Clostridiaceae, Erysipelotrichaceae and Bacteroidaceae) are related to the digestion of protein and energy in dogs. *Peer J.* 5:e3019. doi: 10.7717/peerj.3019

Bermudez Sanchez, S., Pilla, R., Sarawichitr, B., Gramenzi, A., Marsilio, F., Steiner, J. M., et al. (2020). Fecal microbiota in client-owned obese dogs changes after weight loss with a high-fiber-high-protein diet. *Peer J.* 8:e9706. doi: 10.7717/peerj.9706

Birdane, Y. O., Avci, G., Birdane, F. M., Turkmen, R., Atik, O., and Atik, H. (2022). The protective effects of erdosteine on subacute diazinon-induced oxidative stress and inflammation in rats. *Environ. Sci. Pollut. Res.* 29, 21537–21546. doi: 10.1007/s11356-021-17398-2

Blanchard, G., Nguyen, P., Gayet, C., Leriche, I., Siliart, B., and Paragon, B. M. (2004). Rapid weight loss with a high-protein low-energy diet allows the recovery of ideal body composition and insulin sensitivity in obese dogs. *J. Nutr.* 134, 2148–2150. doi: 10.1093/jn/134.8.2148s

Bolyen, E., Rideout, J. R., Dillon, M. R., Bokulich, N. A., Abnet, C. C., Al-Ghalith, G. A., et al. (2019). Reproducible, interactive, scalable and extensible microbiome data science using QIIME 2. *Nat. Biotechnol.* 37, 852–857. doi: 10.1038/s41587-019-0209-9

Bosco, A. M., Almeida, B. F. M., Valadares, T. C., Baptistiolli, L., Hoffmann, D. J., Pereira, A. A. F., et al. (2018). Preactivation of neutrophils and systemic oxidative stress in dogs with hyperleptinemia. *Vet. Immunol. Immunopathol.* 202, 18–24. doi: 10.1016/j.vetimm.2018.06.005

Braun, J. P., Lefebvre, H. P., and Watson, A. D. J. (2003). Creatinine in the dog: a review. *Vet. Clin. Pathol.* 32, 162–179. doi: 10.1111/j.1939-165X.2003.tb00332.x

Bresciani, F., Minamoto, Y., Suchodolski, J. S., Galiazzo, G., Vecchiato, C. G., Pinna, C., et al. (2018). Effect of an extruded animal protein-free diet on fecal microbiota of dogs with food-responsive enteropathy. *J. Vet. Intern. Med.* 32, 1903–1910. doi: 10.1111/jvim.15227

Buege, J. A., and Aust, S. D. (1978). Microsomal lipid peroxidation. *Methods Enzymol.* 52, 302–310. doi: 10.1016/s0076-6879(78)52032-6

Callahan, B. J., McMurdie, P. J., Rosen, M. J., Han, A. W., Johnson, A. J. A., and Holmes, S. P. (2016). DADA2: high-resolution sample inference from Illumina amplicon data. *Nat. Methods* 13, 581–583. doi: 10.1038/nmeth.3869

Chandler, M., Cunningham, S., Lund, E. M., Khanna, C., Naramore, R., Patel, A., et al. (2017). Obesity and associated comorbidities in people and companion animals: a one health perspective. *J. Comp. Pathol.* 156, 296–309. doi: 10.1016/j.jcpa.2017.03.006

Chiofalo, B., De Vita, G., Lo Presti, V., Cucinotta, S., Gaglio, G., Leone, F., et al. (2019). Grain free diets for utility dogs during training work: evaluation of the nutrient digestibility and faecal characteristics. *Anim. Nutr.* 5, 297–306. doi: 10.1016/j.aninu.2019.05.001

Clark, M., and Hoenig, M. (2016). Metabolic effects of obesity and its interaction with endocrine diseases. *Vet. Clin. North Am. Small Anim. Pract.* 46, 797–815. doi: 10.1016/j.cvsm.2016.04.004

Clemente, J. C., Ursell, L. K., Parfrey, L. W., and Knight, R. (2012). The impact of the gut microbiota on human health: an integrative view. *Cells* 148, 1258–1270. doi: 10.1016/j.cell.2012.01.035

Cohen, E., Margalit, I., Shochat, T., Goldberg, E., and Krause, I. (2021). Markers of chronic inflammation in overweight and obese individuals and the role of gender: a cross-sectional study of a large cohort. *J. Inflamm. Res.* 14, 567–573. doi: 10.2147/JIR.S294368

Companys, J., Gosalbes, M. J., Pla-Pagà, L., Calderón-Pérez, L., Llauradó, E., Pedret, A., et al. (2021). Gut microbiota profile and its association with clinical variables and dietary intake in overweight/obese and lean subjects: a cross-sectional study. *Nutrients* 13:2032. doi: 10.3390/nu13062032

Courcier, E. A., Thomson, R. M., Mellor, D. J., and Yam, P. S. (2010). An epidemiological study of environmental factors associated with canine obesity. *J. Small Anim. Pract.* 51, 362–367. doi: 10.1111/j.1748-5827.2010.00933.x

Cucuianu, M., Nistor, T., Hâncu, N., Orbai, P., Muscurel, C., and Stoian, I. (2002). Serum cholinesterase activity correlates with serum insulin, C-peptide and free fatty acids levels in patients with type 2 diabetes. *Rom. J. Intern. Med.* 40, 43–51.

Daminet, S., Jeusette, I., Duchateau, L., Diez, M., Van De Maele, I., and De Rick, A. (2003). Evaluation of thyroid function in obese dogs and in dogs undergoing a weight loss protocol. *J. Vet. Med. Ser. A Physiol. Pathol. Clin. Med.* 50, 213–218. doi: 10.1046/j.1439-0442.2003.00534.x

Damms-Machado, A., Mitra, S., Schollenberger, A. E., Kramer, K. M., Meile, T., Königsrainer, A., et al. (2015). Effects of surgical and dietary weight loss therapy for obesity on gut microbiota composition and nutrient absorption. *Biomed. Res. Int.* 2015:806248, 1–12. doi: 10.1155/2015/806248

Das, U. N. (2001). Is obesity an inflammatory condition? *Nutrition* 17, 953–966. doi: 10.1016/S0899-9007(01)00672-4

Das, U. N. (2012). Acetylcholinesterase and butyrylcholinesterase as markers of low-grade systemic inflammation. *Ann. Hepatol.* 11, 409–411. doi: 10.1016/s1665-2681(19)30940-8

De Filippo, C., Cavalieri, D., Di Paola, M., Ramazzotti, M., Poullet, J. B., Massart, S., et al. (2010). Impact of diet in shaping gut microbiota revealed by a

comparative study in children from Europe and rural Africa. *Proc. Natl. Acad. Sci. U. S. A.* 107, 14691–14696. doi: 10.1073/pnas.1005963107

Delzenne, N. M., Kok, N., Deloyer, P., and Dandrifosse, G. (2000). Dietary fructans modulate polyamine concentration in the cecum of rats. *J. Nutr.* 130, 2456–2460. doi: 10.1093/jn/130.10.2456

Diez, M., Michaux, C., Jeusette, I., Baldwin, P., Istasse, L., and Biourge, V. (2004). Evolution of blood parameters during weight loss in experimental obese beagle dogs. *J. Anim. Physiol. Anim. Nutr. (Berl).* 88, 166–171. doi: 10.1111/j.1439-0396.2003.00474.x

Donath, M. Y., and Shoelson, S. E. (2011). Type 2 diabetes as an inflammatory disease. *Nat. Rev. Immunol.* 11, 98–107. doi: 10.1038/nri2925

Duncan, S. H., Belenguer, A., Holtrop, G., Johnstone, A. M., Flint, H. J., and Lobley, G. E. (2007). Reduced dietary intake of carbohydrates by obese subjects results in decreased concentrations of butyrate and butyrate-producing bacteria in feces. *Appl. Environ. Microbiol.* 73, 1073–1078. doi: 10.1128/AEM.02340-06

FEDIAF (2021). The European Pet Food Industry Federation. "Nutritional guidelines for complete and complementary pet food for cats and dogs".

Forster, G. M., Stockman, J., Noyes, N., Heuberger, A. L., Broeckling, C. D., Bantle, C. M., et al. (2018). A comparative study of serum biochemistry, Metabolome and microbiome parameters of clinically healthy, Normal weight, overweight, and obese companion dogs. *Top. Companion Anim. Med.* 33, 126–135. doi: 10.1053/j.tcam.2018.08.003

Forsythe, L. K., Wallace, J. M. W., and Livingstone, M. B. E. (2008). Obesity and inflammation: the effects of weight loss. *Nutr. Res. Rev.* 21, 117–133. doi: 10.1017/S0954422408138732

Frost, F., Storck, L. J., Kacprowski, T., Gärtner, S., Rühlemann, M., Bang, C., et al. (2019). A structured weight loss program increases gut microbiota phylogenetic diversity and reduces levels of Collinsella in obese type 2 diabetics: a pilot study. *PLoS One* 14, 1–14. doi: 10.1371/journal.pone.0219489

Gagné, J. W., Wakshlag, J. J., Simpson, K. W., Dowd, S. E., Latchman, S., Brown, D. A., et al. (2013). Effects of a synbiotic on fecal quality, short-chain fatty acid concentrations, and the microbiome of healthy sled dogs. *BMC Vet. Res.* 9:246. doi: 10.1186/1746-6148-9-246

Garcia-Mazcorro, J. F., Dowd, S. E., Poulsen, J., Steiner, J. M., and Suchodolski, J. S. (2012a). Abundance and short-term temporal variability of fecal microbiota in healthy dogs. *Microbiology* 1, 340–347. doi: 10.1002/mbo3.36

Garcia-Mazcorro, J. F., Suchodolski, J. S., Jones, K. R., Clark-Price, S. C., Dowd, S. E., Minamoto, Y., et al. (2012b). Effect of the proton pump inhibitor omeprazole on the gastrointestinal bacterial microbiota of healthy dogs. *FEMS Microbiol. Ecol.* 80, 624–636. doi: 10.1111/j.1574-6941.2012.01331.x

Gauffin Cano, P., Santacruz, A., Moya, Á., and Sanz, Y. (2012). Bacteroides uniformis CECT 7771 ameliorates metabolic and immunological dysfunction in mice with high-fat-diet induced obesity. *PLoS One* 7:e41079. doi: 10.1371/journal.pone.0041079

Gentilini, F., Mancini, D., Dondi, F., Ingrà, L., Turba, M. E., Forni, M., et al.. (2005). Validation of a human immunoturbidimetric assay for measuring canine C-reactive protein [Conference presentation]. *15th ECVIM-CA Congress, Glasgow, Scotland*.

German, A. J. (2016). Outcomes of weight management in obese pet dogs: what can we do better? *Proc. Nutr. Soc.* 75, 398–404. doi: 10.1017/S0029665116000185

German, A. J., Hervera, M., Hunter, L., Holden, S. L., Morris, P. J., Biourge, V., et al. (2009). Improvement in insulin resistance and reduction in plasma inflammatory adipokines after weight loss in obese dogs. *Domest. Anim. Endocrinol.* 37, 214–226. doi: 10.1016/j.domaniend.2009.07.001

German, A. J., Holden, S. L., Bissot, T., Hackett, R. M., and Biourge, V. C. (2007). Dietary energy restriction and successful weight loss in obese client-owned dogs. *J. Vet. Intern. Med.* 21, 1174–1180. doi: 10.1892/06-280.1

German, A. J., Holden, S. L., Wiseman-Orr, M. L., Reid, J., Nolan, A. M., Biourge, V., et al. (2012). Quality of life is reduced in obese dogs but improves after successful weight loss. *Vet. J.* 192, 428–434. doi: 10.1016/j.tvjl.2011.09.015

German, A. J., Titcomb, J. M., Holden, S. L., Queau, Y., Morris, P. J., and Biourge, V. (2015). Cohort study of the success of controlled weight loss programs for obese dogs. *J. Vet. Intern. Med.* 29, 1547–1555. doi: 10.1111/jvim.13629

Ghosh, T. S., Rampelli, S., Jeffery, I. B., Santoro, A., Neto, M., Capri, M., et al. (2020). Mediterranean diet intervention alters the gut microbiome in older people reducing frailty and improving health status: the NU-AGE 1-year dietary intervention across five European countries. *Gut* 69, 1218–1228. doi: 10.1136/gutjnl-2019-319654

Gunst, J., Vanhorebeek, I., Casaer, M. P., Hermans, G., Wouters, P. J., Dubois, J., et al. (2013). Impact of early parenteral nutrition on metabolism and kidney injury. *J. Am. Soc. Nephrol.* 24, 995–1005. doi: 10.1681/ASN.2012070732

Handl, S., German, A. J., Holden, S. L., Dowd, S. E., Steiner, J. M., Heilmann, R. M., et al. (2013). Faecal microbiota in lean and obese dogs. *FEMS Microbiol. Ecol.* 84, 332–343. doi: 10.1111/1574-6941.12067

Heinsen, F. A., Fangmann, D., Müller, N., Schulte, D. M., Rühlemann, M. C., Türk, K., et al. (2017). Beneficial effects of a dietary weight loss intervention on human gut microbiome diversity and metabolism are not sustained during weight maintenance. *Obes. Facts* 9, 379–391. doi: 10.1159/000449506

Herstad, K. M. V., Gajardo, K., Bakke, A. M., Moe, L., Ludvigsen, J., Rudi, K., et al. (2017). A diet change from dry food to beef induces reversible changes on the faecal microbiota in healthy, adult client-owned dogs. *BMC Vet. Res.* 13, 147–113. doi: 10.1186/s12917-017-1073-9

Hu, H. J., Park, S. G., Jang, H. B., Choi, M. G., Park, K. H., Kang, J. H., et al. (2015). Obesity alters the microbial community profile in Korean adolescents. *PLoS One* 10, 1–14. doi: 10.1371/journal.pone.0134333

Huang, Z., Pan, Z., Yang, R., Bi, Y., and Xiong, X. (2020). The canine gastrointestinal microbiota: early studies and research frontiers. *Gut Microbes* 11, 635–654. doi: 10.1080/19490976.2019.1704142

Ismail, N. A., Ragab, S. H., ElBaky, A. A., Shoeib, A. R. S., Alhosary, Y., and Fekry, D. (2011). Frequency of Firmicutes and Bacteroidetes in gut microbiota in obese and normal weight Egyptian children and adults. *Arch. Med. Sci.* 3, 501–507. doi: 10.5114/aoms.2011.23418

Jackson, M. I., and Jewell, D. E. (2019). Balance of saccharolysis and proteolysis underpins improvements in stool quality induced by adding a fiber bundle containing bound polyphenols to either hydrolyzed meat or grain-rich foods. *Gut Microbes* 10, 298–320. doi: 10.1080/19490976.2018.1526580

Jocelyn, P. C. (1987). Spectrophotometric assay of thiols. *Methods Enzymol.* 143, 44–67. doi: 10.1016/0076-6879(87)43013-9

Johnson, K. A. (1977). The production of secondary amines by the human gut bacteria and its possible relevance to carcinogenesis. *Med. Lab. Sci.* 34, 131–143.

Jones, R. B., Alderete, T. L., Kim, J. S., Millstein, J., Gilliland, F. D., and Goran, M. I. (2019). High intake of dietary fructose in overweight/obese teenagers associated with depletion of Eubacterium and streptococcus in gut microbiome. *Gut Microbes* 10, 712–719. doi: 10.1080/19490976.2019.1592420

Kałużna-Czaplińska, J., Gątarek, P., Chartrand, M. S., Dadar, M., and Bjørklund, G. (2017). Is there a relationship between intestinal microbiota, dietary compounds, and obesity? *Trends Food Sci. Technol.* 70, 105–113. doi: 10.1016/j.tifs.2017.10.010

Kasai, C., Sugimoto, K., Moritani, I., Tanaka, J., Oya, Y., Inoue, H., et al. (2015). Comparison of the gut microbiota composition between obese and non-obese individuals in a Japanese population, as analyzed by terminal restriction fragment length polymorphism and next-generation sequencing. *BMC Gastroenterol.* 15, 1–10. doi: 10.1186/s12876-015-0330-2

Kawauchi, I. M., Jeremias, J. T., Takeara, P., de Souza, D. F., de Carvalho Balieiro, J. C., Pfrimer, K., et al. (2017). Effect of dietary protein intake on the body composition and metabolic parameters of neutered dogs. *J. Nutr. Sci.* 6, 1–5. doi: 10.1017/jns.2017.41

Kealy, R. D., Lawler, D. F., Ballam, J. M., Mantz, S. L., Biery, D. N., Greeley, E. H., et al. (2002). Effects of diet restriction on life span and age-related changes in dogs. *J. Am. Vet. Med. Assoc.* 220, 1315–1320. doi: 10.2460/javma.2002.220.1315

Kieler, I. N., Kamal, S. S., Vitger, A. D., Nielsen, D. S., Lauridsen, C., and Bjornvad, C. R. (2017). Gut microbiota composition may relate to weight loss rate in obese pet dogs. *Vet. Med. Sci.* 3, 252–262. doi: 10.1002/vms3.80

Kilburn, L. R., Koester, L. R., Schmitz-Esser, S., Serão, N. V. L., and Rossoni Serão, M. C. (2020). High-fat diets led to OTU-level shifts in fecal samples of healthy adult dogs. *Front. Microbiol.* 11, 1–13. doi: 10.3389/fmicb.2020.564160

Kok, P., Roelfsema, F., Langendonk, J. G., Frölich, M., Burggraaf, J., Meinders, A. E., et al. (2005). High circulating thyrotropin levels in obese women are reduced after body weight loss induced by caloric restriction. *J. Clin. Endocrinol. Metab.* 90, 4659–4663. doi: 10.1210/jc.2005-0920

Koliada, A., Syzenko, G., Moseiko, V., Budovska, L., Puchkov, K., Perederiy, V., et al. (2017). Association between body mass index and Firmicutes/Bacteroidetes ratio in an adult Ukrainian population. *BMC Microbiol.* 17, 4–9. doi: 10.1186/s12866-017-1027-1

Kovatcheva-Datchary, P., and Arora, T. (2013). Nutrition, the gut microbiome and the metabolic syndrome. *Best Pract. Res. Clin. Gastroenterol.* 27, 59–72. doi: 10.1016/j.bpg.2013.03.017

Laflamme, D. P. (1997). Development and validation of a body condition score system for dogs. *Canine Pract.* 22, 10–15.

Laflamme, D. P. (2006). Understanding and managing obesity in dogs and cats. *Vet. Clin. North Am. Small Anim. Pract.* 36, 1283–1295. doi: 10.1016/j.cvsm.2006.08.005

Laflamme, D. P., and Hannah, S. S. (2005). Increased dietary protein promotes fat loss and reduces loss of lean body mass during weight loss in cats. *Int. J. Appl. Res. Vet. Med.* 3, 62–68.

Levy, M., Thaiss, C. A., Zeevi, D., Dohnalová, L., Zilberman-Schapira, G., Mahdi, J. A., et al. (2015). Microbiota-modulated metabolites shape the intestinal microenvironment by regulating NLRP6 Inflammasome signaling. *Cells* 163, 1428–1443. doi: 10.1016/j.cell.2015.10.048

Ley, E. R., Turnbaugh, P. J., Klein, S., and Gordon, J. I. (2006). Human gut microbes associated with obesity. *Nature* 444, 1022–1023. doi: 10.1016/s0084-3741(08)70094-5

Ley, R. E., Bäckhed, F., Turnbaugh, P., Lozupone, C. A., Knight, R. D., and Gordon, J. I. (2005). Obesity alters gut microbial ecology. *Proc. Natl. Acad. Sci. U. S. A.* 102, 11070–11075. doi: 10.1073/pnas.0504978102

Li, Q., Lauber, C. L., Czarnecki-Maulden, G., Pan, Y., and Hannah, S. S. (2017). Effects of the dietary protein and carbohydrate ratio on gut microbiomes in dogs of different body conditions. *MBio* 8:e01703-16. doi: 10.1128/mBio.01703-16

Louis, P., and Flint, H. J. (2017). Formation of propionate and butyrate by the human colonic microbiota. *Environ. Microbiol.* 19, 29–41. doi: 10.1111/1462-2920.13589

Lumeng, C. N., and Saltiel, A. R. (2011). Inflammatory links between obesity and metabolic disease. *J. Clin. Invest.* 121, 2111–2117. doi: 10.1172/JCI57132

Lund, E. M., Armstrong, P. J., Kirk, C. A., and Klausner, J. S. (2006). Prevalence and risk factors for obesity. *Int. J. Appl. Res. Vet. Med.* 4, 1–6.

Ma, J., Piao, X., Mahfuz, S., Long, S., and Wang, J. (2021). The interaction among gut microbes, the intestinal barrier and short chain fatty acids. *Anim. Nutr.* 11, 159–174. doi: 10.1016/j.aninu.2021.09.012

Mahowald, M. A., Rey, F. E., Seedorf, H., Turnbaugh, P. J., Fulton, R. S., Wollam, A., et al. (2009). Characterizing a model human gut microbiota composed of members of its two dominant bacterial phyla. *Proc. Natl. Acad. Sci. U. S. A.* 106, 5859–5864. doi: 10.1073/pnas.0901529106

Mao, J., Xia, Z., Chen, J., and Yu, J. (2013). Prevalence and risk factors for canine obesity surveyed in veterinary practices in Beijing, China. *Prev. Vet. Med.* 112, 438–442. doi: 10.1016/j.prevetmed.2013.08.012

Marseglia, L., Manti, S., D'Angelo, G., Nicotera, A., Parisi, E., Di Rosa, G., et al. (2015). Oxidative stress in obesity: a critical component in human diseases. *Int. J. Mol. Sci.* 16, 378–400. doi: 10.3390/ijms16010378

Martínez-Cuesta, M. C., del Campo, R., Garriga-García, M., Peláez, C., and Requena, T. (2021). Taxonomic characterization and short-chain fatty acids production of the obese microbiota. *Front. Cell. Infect. Microbiol.* 11, 1–12. doi: 10.3389/fcimb.2021.598093

Mastrorilli, C., Dondi, F., Agnoli, C., Turba, M. E., Vezzali, E., and Gentilini, F. (2007). Clinicopathologic features and outcome predictors of Leptospira interrogans Australis serogroup infection in dogs: a retrospective study of 20 cases (2001-2004). *J. Vet. Intern. Med.* 21, 3–10. doi: 10.1111/j.1939-1676.2007.tb02921.x

Mathieson, R. A., Walberg, J. L., Gwazdauskas, F. C., Hinkle, D. E., and Gregg, J. M. (1986). The effect of varying carbohydrate content of a very-low-caloric diet on resting metabolic rate and thyroid hormones. *Metabolism* 35, 394–398. doi: 10.1016/0026-0495(86)90126-5

Matsumoto, M., and Benno, Y. (2007). The relationship between microbiota and polyamine concentration in the human intestine: a pilot study. *Microbiol. Immunol.* 51, 25–35. doi: 10.1111/j.1348-0421.2007.tb03887.x

Matsumoto, M., Kibe, R., Ooga, T., Aiba, Y., Kurihara, S., Sawaki, E., et al. (2012). Impact of intestinal microbiota on intestinal luminal metabolome. *Sci. Rep.* 2, 1–10. doi: 10.1038/srep00233

Middelbos, I. S., Boler, B. M. V., Qu, A., White, B. A., Swanson, K. S., and Fahey, G. C. (2010). Phylogenetic characterization of fecal microbial communities of dogs fed diets with or without supplemental dietary fiber using 454 pyrosequencing. *PLoS One* 5:e9768. doi: 10.1371/journal.pone.0009768

Middleton, R. P., Lacroix, S., Scott-Boyer, M. P., Dordevic, N., Kennedy, A. D., Slusky, A. R., et al. (2017). Metabolic differences between dogs of different body sizes. *J. Nutr. Metab.* 2017:4535710. doi: 10.1155/2017/4535710

Moinard, A., Payen, C., Ouguerram, K., André, A., Hernandez, J., Drut, A., et al. (2020). Effects of high-fat diet at two energetic levels on fecal microbiota, colonic barrier, and metabolic parameters in dogs. *Front. Vet. Sci.* 7:566282. doi: 10.3389/fvets.2020.566282

Montoya-Alonso, J. A., Bautista-Castaño, I., Peña, C., Suárez, L., Juste, M. C., and Tvarijonaviciute, A. (2017). Prevalence of canine obesity, obesity-related metabolic dysfunction, and relationship with owner obesity in an obesogenic region of Spain. *Front. Vet. Sci.* 4:59. doi: 10.3389/fvets.2017.00059

Mori, A., Goto, A., Kibe, R., Oda, H., Kataoka, Y., and Sako, T. (2019). Comparison of the effects of four commercially available prescription diet regimens on the fecal microbiome in healthy dogs. *J. Vet. Med. Sci.* 81, 1783–1790. doi: 10.1292/jvms.19-0055

Mosing, M., German, A. J., Holden, S. L., MacFarlane, P., Biourge, V., Morris, P. J., et al. (2013). Oxygenation and ventilation characteristics in obese sedated dogs before and after weight loss: a clinical trial. *Vet. J.* 198, 367–371. doi: 10.1016/j.tvjl.2013.08.008

Mukherjee, A., Lordan, C., Ross, R. P., and Cotter, P. D. (2020). Gut microbes from the phylogenetically diverse genus Eubacterium and their various contributions to gut health. *Gut Microbes* 12:1802866. doi: 10.1080/19490976.2020.1802866

Mullur, R., Liu, Y. Y., and Brent, G. A. (2014). Thyroid hormone regulation of metabolism. *Physiol. Rev.* 94, 355–382. doi: 10.1152/physrev.00030.2013

Muñoz-Prieto, A., Nielsen, L. R., Dąbrowski, R., Bjørnvad, C. R., Söder, J., Lamy, E., et al. (2018). European dog owner perceptions of obesity and factors associated with human and canine obesity. *Sci. Rep.* 8, 1–10. doi: 10.1038/s41598-018-31532-0

Nadal, I., Santacruz, A., Marcos, A., Warnberg, J., Garagorri, M., Moreno, L. A., et al. (2009). Shifts in clostridia, bacteroides and immunoglobulin-coating fecal bacteria associated with weight loss in obese adolescents. *Int. J. Obes.* 33, 758–767. doi: 10.1038/ijo.2008.260

NRC-National Research Council (2006). "Energy" in *Nutrient Requirements of Dogs and Cats* (Washington, DC: National Academies Press), 28–48.

Pallister, T., Jackson, M. A., Martin, T. C., Glastonbury, C. A., Jennings, A., Beaumont, M., et al. (2017). Untangling the relationship between diet and visceral fat mass through blood metabolomics and gut microbiome profiling. *Int. J. Obes.* 41, 1106–1113. doi: 10.1038/ijo.2017.70

Panasevich, M. R., Kerr, K. R., Dilger, R. N., Fahey, G. C., Guérin-Deremaux, L., Lynch, G. L., et al. (2014). Modulation of the faecal microbiome of healthy adult dogs by inclusion of potato fibre in the diet. *Br. J. Nutr.* 113, 125–133. doi: 10.1017/S0007114514003274

Panasevich, M. R., Rossoni Serao, M. C., de Godoy, M. R. C., Swanson, K. S., Guérin-Deremaux, L., Lynch, G. L., et al. (2013). Potato fiber as a dietary fiber source in dog foods. *J. Anim. Sci.* 91, 5344–5352. doi: 10.2527/jas.2013-6842

Parada, A. E., Needham, D. M., and Fuhrman, J. A. (2016). Every base matters: assessing small subunit rRNA primers for marine microbiomes with mock communities, time series and global field samples. *Environ. Microbiol.* 18, 1403–1414. doi: 10.1111/1462-2920.13023

Park, H. J., Lee, S. E., Kim, H. B., Isaacson, R. E., Seo, K. W., and Song, K. H. (2015). Association of Obesity with serum Leptin, Adiponectin, and serotonin and gut microflora in beagle dogs. *J. Vet. Intern. Med.* 29, 43–50. doi: 10.1111/jvim.12455

Petelin, A., Tedeschi, P., Maietti, A., Jurdana, M., Brandolini, V., and Pražnikar, Z. J. (2017). Total serum antioxidant capacity in healthy Normal weight and asymptomatic overweight adults. *Exp. Clin. Endocrinol. Diabetes* 125, 470–477. doi: 10.1055/s-0043-107783

Phungviwatnikul, T., Lee, A. H., Belchik, S. E., Suchodolski, J. S., and Swanson, K. S. (2022). Weight loss and high-protein, high-fiber diet consumption impact blood metabolite profiles, body composition, voluntary physical activity, fecal microbiota, and fecal metabolites of adult dogs. *J. Anim. Sci.* 100:skab379. doi: 10.1093/jas/skab379

Piantedosi, D., Di Loria, A., Guccione, J., De Rosa, A., Fabbri, S., Cortese, L., et al. (2016). Serum biochemistry profile, inflammatory cytokines, adipokines and cardiovascular findings in obese dogs. *Vet. J.* 216, 72–78. doi: 10.1016/j.tvjl.2016.07.002

Pilla, R., and Suchodolski, J. S. (2021). The gut microbiome of dogs and cats, and the influence of diet. *Vet. Clin. North Am. Small Anim. Pract.* 51, 605–621. doi: 10.1016/j.cvsm.2021.01.002

Pinart, M., Schlicht, K., Laudes, M., Bouwman, J., Forslund, S. K., Pischon, T., et al. (2022). Gut microbiome composition in obese and non-obese persons: a systematic review and meta-analysis. *Nutrients* 14, 1–41. doi: 10.3390/nu14010012

Pinna, C., Vecchiato, C. G., Delsante, C., Grandi, M., and Biagi, G. (2021). On the variability of microbial populations and bacterial metabolites within the canine stool. An in-depth analysis. *Animals* 11:225. doi: 10.3390/ani11010225

Porsani, M. Y. H., Teixeira, F. A., Oliveira, V. V., Pedrinelli, V., Dias, R. A., German, A. J., et al. (2020). Prevalence of canine obesity in the city of São Paulo, Brazil. *Sci. Rep.* 10:14082. doi: 10.1038/s41598-020-70937-8

Radakovich, L. B., Truelove, M. P., Pannone, S. C., Olver, C. S., and Santangelo, K. S. (2017). Clinically healthy overweight and obese dogs differ from lean controls in select CBC and serum biochemistry values. *Vet. Clin. Pathol.* 46, 221–226. doi: 10.1111/vcp.12468

Ramos-Molina, B., Queipo-Ortuño, M. I., Lambertos, A., Tinahones, F. J., and Peñafiel, R. (2019). Dietary and Gut Microbiota Polyamines in Obesity- and Age-Related Diseases. *Front. Nutr.* 6:24. doi: 10.3389/fnut.2019.00024

Reinehr, T. (2010). Obesity and thyroid function. *Mol. Cell. Endocrinol.* 316, 165–171. doi: 10.1016/j.mce.2009.06.005

Remely, M., Tesar, I., Hippe, B., Gnauer, S., Rust, P., and Haslberger, A. G. (2015). Gut microbiota composition correlates with changes in body fat content due to weight loss. *Benef. Microbes* 6, 431–439. doi: 10.3920/BM2014.0104

Ricci, R., Jeusette, I., Godeau, J. M., Contiero, B., and Diez, M. (2011). Effect of short-chain fructooligosaccharide-enriched energy-restricted diet on weight loss and serum haptoglobin concentration in beagle dogs. *Br. J. Nutr.* 106, 120–123. doi: 10.1017/s0007114511004107

Rubio, C. P., Martínez-Subiela, S., Hernández-Ruiz, J., Tvarijonaviciute, A., Cerón, J. J., and Allenspach, K. (2017a). Serum biomarkers of oxidative stress in dogs with idiopathic inflammatory bowel disease. *Vet. J.* 221, 56–61. doi: 10.1016/j.tvjl.2017.02.003

Rubio, C. P., Martinez-Subiela, S., Tvarijonaviciute, A., Hernández-Ruiz, J., Pardo-Marin, L., Segarra, S., et al. (2016). Changes in serum biomarkers of oxidative stress after treatment for canine leishmaniosis in sick dogs. *Comp. Immunol. Microbiol. Infect. Dis.* 49, 51–57. doi: 10.1016/j.cimid.2016.09.003

Rubio, C. P., Yilmaz, Z., Martínez-Subiela, S., Kocaturk, M., Hernández-Ruiz, J., Yalcin, E., et al. (2017b). Serum antioxidant capacity and oxidative damage in clinical and subclinical canine ehrlichiosis. *Res. Vet. Sci.* 115, 301–306. doi: 10.1016/j.rvsc.2017.06.004

Salas-Mani, A., Jeusette, I., Castillo, I., Manuelian, C. L., Lionnet, C., Iraculis, N., et al. (2018). Fecal microbiota composition changes after a BW loss diet in beagle dogs. *J. Anim. Sci.* 96, 3102–3111. doi: 10.1093/jas/sky193

Sánchez-Rodríguez, M. A., and Mendoza-Núñez, V. M. (2019). Oxidative stress indexes for diagnosis of health or disease in humans. *Oxidative Med. Cell. Longev.* 2019, 1–32. doi: 10.1155/2019/4128152

Schauf, S., de la Fuente, G., Newbold, C. J., Salas-Mani, A., Torre, C., Abecia, L., et al. (2018). Effect of dietary fat to starch content on fecal microbiota composition and activity in dogs. *J. Anim. Sci.* 96, 3684–3698. doi: 10.1093/jas/sky264

Schwiertz, A., Taras, D., Schäfer, K., Beijer, S., Bos, N. A., Donus, C., et al. (2010). Microbiota and SCFA in lean and overweight healthy subjects. *Obesity* 18, 190–195. doi: 10.1038/oby.2009.167

Scott-Moncrieff, J. (2015a). "Feline hyperthyroidism," in *Canine and feline endocrinology*, eds. E. C. Feldman, R. Nelson and C. Reusch, and J. Scott-Moncrieff. St. Louis, MO: Elsevier Saunders, 136–195.

Scott-Moncrieff, J. (2015b). "Hypothyoridism" in *Canine and Feline Endocrinology*. eds. E. C. Feldman, R. Nelson, C. Reusch and J. Scott-Moncrieff (St. Louis, MO: Elsevier Saunders), 77–135.

Shen, N., Caixàs, A., Ahlers, M., Patel, K., Gao, Z., Dutia, R., et al. (2019). Longitudinal changes of microbiome composition and microbial metabolomics after surgical weight loss in individuals with obesity. *Surg. Obes. Relat. Dis.* 15, 1367–1373. doi: 10.1016/j.soard.2019.05.038

Simões, C. D., Maukonen, J., Scott, K. P., Virtanen, K. A., Pietiläinen, K. H., and Saarela, M. (2014). Impact of a very low-energy diet on the fecal microbiota of obese individuals. *Eur. J. Nutr.* 53, 1421–1429. doi: 10.1007/s00394-013-0645-0

Singh, A. K., Jiang, Y., White, T., and Spassova, D. (1997). Validation of nonradioactive chemiluminescent immunoassay methods for the analysis of thyroxine and cortisol in blood samples obtained from dogs, cats, and horses. *J. Vet. Diagn. Investig.* 9, 261–268. doi: 10.1177/104063879700900307

Sowah, S. A., Riedl, L., Damms-Machado, A., Johnson, T. S., Schübel, R., Graf, M., et al. (2019). Effects of weight-loss interventions on short-chain fatty acid concentrations in blood and feces of adults: a systematic review. *Adv. Nutr.* 10, 673–684. doi: 10.1093/advances/nmy125

Stefanelli, C., Carati, D., and Rossoni, C. (1986). Separation of N1-and N8-acetylspermidine isomers by reversed-phase column liquid chromatography after derivatization with dansyl chloride. *J. Chromatogr.* 375, 49–55.

Stępień, M., Stępień, A., Wlazeł, R. N., Paradowski, M., Banach, M., and Rysz, J. (2014). Obesity indices and inflammatory markers in obese non-diabetic normo- and hypertensive patients: a comparative pilot study. *Lipids Health Dis.* 13, 10–13. doi: 10.1186/1476-511X-13-29

Stojanov, S., Berlec, A., and Štrukelj, B. (2020). The influence of probiotics on the firmicutes/bacteroidetes ratio in the treatment of obesity and inflammatory bowel disease. *Microorganisms* 8, 1–16. doi: 10.3390/microorganisms8111715

Stolarczyk, E. (2017). Adipose tissue inflammation in obesity: a metabolic or immune response? *Curr. Opin. Pharmacol.* 37, 35–40. doi: 10.1016/j.coph.2017.08.006

Suarez, L., Bautista-Castaño, I., Peña Romera, C., Montoya-Alonso, J. A., and Corbera, J. A. (2022). Is dog owner obesity a risk factor for canine obesity? A "one-health" study on human–animal interaction in a region with a high prevalence of obesity. *Vet. Sci.* 9:243. doi: 10.3390/vetsci9050243

Suchodolski, J. S. (2011). Intestinal microbiota of dogs and cats: a bigger world than we thought. *Vet. Clin. North Am. Small Anim. Pract.* 41, 261–272. doi: 10.1016/j.cvsm.2010.12.006

Swanson, K. S., Grieshop, C. M., Flickinger, E. A., Bauer, L. L., Healy, H. P., Dawson, K. A., et al. (2002). Supplemental fructooligosaccharides and mannanoligosaccharides influence immune function, ileal and total tract nutrient digestibilities, microbial populations and concentrations of protein catabolites in the large bowel of dogs. *J. Nutr.* 132, 980–989. doi: 10.1093/jn/132.5.980

Trayhurn, P. (2005). Adipose tissue in obesity - an inflammatory issue. *Endocrinology* 146, 1003–1005. doi: 10.1210/en.2004-1597

Tropf, M., Nelson, O. L., Lee, P. M., and Weng, H. Y. (2017). Cardiac and metabolic variables in obese dogs. *J. Vet. Intern. Med.* 31, 1000–1007. doi: 10.1111/jvim.14775

Turnbaugh, P. J., Ley, R. E., Mahowald, M. A., Magrini, V., Mardis, E. R., and Gordon, J. I. (2006). An obesity-associated gut microbiome with increased capacity for energy harvest. *Nature* 444, 1027–1031. doi: 10.1038/nature05414

Tvarijonaviciute, A., Barić-Rafaj, R., Horvatic, A., Muñoz-Prieto, A., Guillemin, N., Lamy, E., et al. (2019). Identification of changes in serum analytes and possible metabolic pathways associated with canine obesity-related metabolic dysfunction. *Vet. J.* 244, 51–59. doi: 10.1016/j.tvjl.2018.12.006

Tvarijonaviciute, A., Ceron, J. J., Holden, S. L., Cuthbertson, D. J., Biourge, V., Morris, P. J., et al. (2012a). Obesity-related metabolic dysfunction in dogs: a comparison with human metabolic syndrome. *BMC Vet. Res.* 8:147. doi: 10.1186/1746-6148-8-147

Tvarijonaviciute, A., Ceron, J. J., and Tecles, F. (2013). Acetylcholinesterase and butyrylcholinesterase activities in obese beagle dogs before and after weight loss. *Vet. Clin. Pathol.* 42, 207–211. doi: 10.1111/vcp.12032

Tvarijonaviciute, A., Kocaturk, M., Cansev, M., Tecles, F., Ceron, J. J., and Yilmaz, Z. (2012b). Serum butyrylcholinesterase and paraoxonase 1 in a canine model of endotoxemia: effects of choline administration. *Res. Vet. Sci.* 93, 668–674. doi: 10.1016/j.rvsc.2011.09.010

Tvarijonaviciute, A., Martinez, S., Gutierrez, A., Ceron, J. J., and Tecles, F. (2011). Serum acute phase proteins concentrations in dogs during experimentally short-term induced overweight. A preliminary study. *Res. Vet. Sci.* 90, 31–34. doi: 10.1016/j.rvsc.2010.05.008

Tvarijonaviciute, A., Tecles, F., and Ceron, J. J. (2010). Relationship between serum butyrylcholinesterase and obesity in dogs: a preliminary report. *Vet. J.* 186, 197–200. doi: 10.1016/j.tvjl.2009.07.030

Tvarijonaviciute, A., Tecles, F., Martínez-Subiela, S., and Cerón, J. J. (2012c). Effect of weight loss on inflammatory biomarkers in obese dogs. *Vet. J.* 193, 570–572. doi: 10.1016/j.tvjl.2012.02.015

Vaiserman, A., Romanenko, M., Piven, L., Moseiko, V., Lushchak, O., Kryzhanovska, N., et al. (2020). Differences in the gut Firmicutes to Bacteroidetes ratio across age groups in healthy Ukrainian population. *BMC Microbiol.* 20, 1–8. doi: 10.1186/s12866-020-01903-7

Van de Velde, H., Janssens, G. P. J., Rochus, K., Duchateau, L., Scharek-Tedin, L., Zentek, J., et al. (2013). Proliferation capacity of T-lymphocytes is affected transiently after a long-term weight gain in beagle dogs. *Vet. Immunol. Immunopathol.* 152, 237–244. doi: 10.1016/j.vetimm.2012.12.011

Veiga, A. P. M., Price, C. A., De Oliveira, S. T., dos Santos, A. P., Campos, R., Barbosa, P. R., et al. (2008). Association of canine obesity with reduced serum levels of C-reactive protein. *J. Vet. Diagn. Investig.* 20, 224–228. doi: 10.1177/104063870802000214

Volek, J. S., Sharman, M. J., Love, D. M., Avery, N. G., Gómez, A. L., Scheett, T. P., et al. (2002). Body composition and hormonal responses to a carbohydrate-restricted diet. *Metabolism* 51, 864–870. doi: 10.1053/meta.2002.32037

Vong, L., Lorentz, R. J., Assa, A., Glogauer, M., and Sherman, P. M. (2014). Probiotic *Lactobacillus rhamnosus* inhibits the formation of neutrophil extracellular traps. *J. Immunol.* 192, 1870–1877. doi: 10.4049/jimmunol.1302286

Wakshlag, J. J., Struble, A. M., Levine, C. B., Bushey, J. J., Laflamme, D. P., and Long, G. M. (2011). The effects of weight loss on adipokines and markers of inflammation in dogs. *Br. J. Nutr.* 106, 11–14. doi: 10.1017/s0007114511000560

Weber, M., Bissot, T., Servet, E., Sergheraert, R., Biourge, V., and German, A. J. (2007). A high-protein, high-fiber diet designed for weight loss improves satiety in dogs. *J. Vet. Intern. Med.* 21, 1203–1208. doi: 10.1892/07-016.1

Wozniak, S. E., Gee, L. L., Wachtel, M. S., and Frezza, E. E. (2009). Adipose tissue: the new endocrine organ? A review article. *Dig. Dis. Sci.* 54, 1847–1856. doi: 10.1007/s10620-008-0585-3

Wu, G. D., Chen, J., Hoffmann, C., Bittinger, K., Chen, Y. Y., Keilbaugh, S. A., et al. (2011). Linking long-term dietary patterns with gut microbial enterotypes. *Science* 334, 105–108. doi: 10.1126/science.1208344

Yatsunenko, T., Rey, F. E., Manary, M. J., Trehan, I., Dominguez-Bello, M. G., Contreras, M., et al. (2012). Human gut microbiome viewed across age and geography. *Nature* 486, 222–227. doi: 10.1038/nature11053

Zentek, J., Fricke, S., Hewicker-Trautwein, M., Ehinger, B., Amtsberg, G., and Baums, C. (2004). Dietary protein source and manufacturing processes affect macronutrient digestibility, fecal consistency, and presence of fecal Clostridium perfringens in adult dogs. *J. Nutr.* 134, 2158S–2161S. doi: 10.1093/jn/134.8.2158S

frontiers | Frontiers in Microbiology

TYPE Original Research
PUBLISHED 13 January 2023
DOI 10.3389/fmicb.2022.1082835



OPEN ACCESS

EDITED BY
Mujeeb Ur Rehman,
Livestock and Dairy Development Department, Pakistan

REVIEWED BY
Yuwei Wang,
Shaanxi University of Chinese Medicine, China
Walaa K. Mousa,
Mansoura University, Egypt
Yubo Wang,
Capital Medical University, China

*CORRESPONDENCE
Congqing Jiang
wb002554@whu.edu.cn
Rui Gui
guiruitmmu@163.com

†These authors have contributed equally to this work

SPECIALTY SECTION
This article was submitted to Microorganisms in Vertebrate Digestive Systems, a section of the journal Frontiers in Microbiology

RECEIVED 28 October 2022
ACCEPTED 28 December 2022
PUBLISHED 13 January 2023

CITATION
Hong Y, Chen B, Zhai X, Qian Q, Gui R and Jiang C (2023) Integrated analysis of the gut microbiome and metabolome in a mouse model of inflammation-induced colorectal tumors.
*Front. Microbiol.* 13:1082835.
doi: 10.3389/fmicb.2022.1082835



# Integrated analysis of the gut microbiome and metabolome in a mouse model of inflammation-induced colorectal tumors

Yuntian Hong[1,2,3†], Baoxiang Chen[1,2,3†], Xiang Zhai[1,2,3†], Qun Qian[1,2,3], Rui Gui[4*] and Congqing Jiang[1,2,3*]

[1]Department of Colorectal and Anal Surgery, Zhongnan Hospital of Wuhan University, Wuhan, China, [2]Clinical Center of Intestinal and Colorectal Diseases of Hubei Province, Wuhan, China, [3]Key Laboratory of Intestinal and Colorectal Diseases of Hubei Province, Wuhan, China, [4]Department of Infectious Diseases, Southwest Hospital, Third Military Medical University (Army Medical University), Chongqing, China

Colorectal cancer (CRC) is a common malignancy worldwide, and the gut microbiota and metabolites play an important role in its initiation and progression. In this study, we constructed a mouse model of inflammation-induced colorectal tumors, with fixed doses of azoxymethane/dextran sulfate sodium (AOM/DSS). We found that colorectal tumors only formed in some mice treated with certain concentrations of AOM/DSS (tumor group), whereas other mice did not develop tumors (non-tumor group). 16S rDNA amplicon sequencing and liquid chromatography-mass spectrometry (LC-MS)/MS analyses were performed to investigate the microbes and metabolites in the fecal samples. As a result, 1189 operational taxonomic units (OTUs) were obtained from the fecal samples, and the non-tumor group had a relatively higher OTU richness and diversity. Moreover, 53 different microbes were identified at the phylum and genus levels, including *Proteobacteria*, *Cyanobacteria*, and *Prevotella*. Furthermore, four bacterial taxa were obviously enriched in the non-tumor group, according to linear discriminant analysis scores ($\log_{10}$) > 4. The untargeted metabolomics analysis revealed significant differences between the fecal samples and metabolic phenotypes. Further, the heatmaps and volcano plots revealed 53 and 19 dysregulated metabolites between the groups, in positive and negative ion modes, respectively. Styrene degradation and amino sugar-nucleotide sugar metabolism pathways were significantly different in positive and negative ion modes, respectively. Moreover, a correlation analysis between the metabolome and microbiome was further conducted, which revealed the key microbiota and metabolites. In conclusion, we successfully established a tumor model using a certain dose of AOM/DSS and identified the differential intestinal microbiota and characteristic metabolites that might modulate tumorigenesis, thereby providing new concepts for the prevention and treatment of CRC.

KEYWORDS

**colorectal tumor, AOM, DSS, microbiota, metabolite, analysis**

# Introduction

Colorectal cancer (CRC) is one of the most common malignancies and a major cause of cancer-related deaths worldwide (Siegel et al., 2020; Sung et al., 2021). In the past 20 years, CRC incidence and mortality have gradually increased, and this disease has tended to affect younger people, especially in China, Japan, and other eastern countries (Dekker et al., 2019; Siegel et al., 2020; Akimoto et al., 2021). To some extent, this could be related to the westernization of diets and lifestyles. Western diets rich in red meat, processed meat, sugar, and refined carbohydrates can increase the risk of colitis-related tumors by changing the intestinal microenvironment, damaging intestinal DNA, and inducing inflammation (Vernia et al., 2021; Arima et al., 2022). However, some intestinal probiotics and beneficial metabolites can effectively antagonize carcinogenesis (Hradicka et al., 2020; Matson et al., 2021). In this context, the role of intestinal microecology changes in CRC initiation and progression is worthy of further exploration.

The inflammation–cancer transformation tumor model, induced with azoxymethane/dextran sulfate sodium (AOM/DSS), is an effective tool to study the mechanisms underlying colorectal tumorigenesis in an inflammatory environment. This animal model, established based on a combination of a mutagen and inflammatory agent, can simulate the entire process of mucosa inflammation-associated tumor formation (Neufert et al., 2007; Angelou et al., 2018). The induced neoplasms in this model mostly occur in the distal colon and first appear in the form of polyps, similar to CRC establishment in humans (Snider et al., 2016). Hence, it can reflect the progression from colitis to carcinoma in humans. However, with respect to AOM/DSS-induced tumorigenesis in mice, we found that with a certain dose, colorectal tumors are successfully induced in some animals, whereas no neoplasm-like changes occur in the others. We speculated that the intestinal microecology of those mice without tumor lesions might have a preventative effect on AOM/DSS-induced carcinogenesis. Therefore, in the current study, 16S rDNA amplicon sequencing and liquid chromatography-mass spectrometry (LC-MS)/MS analyses were used to explore the intestinal flora and metabolites of mice with or without tumors after AOM-DSS treatment, which might help us to further understand the initiation and development of enteritis-related CRC and provide new ideas for the prevention and treatment of CRC from the perspective of the intestinal microecology.

# Materials and methods

## Animals and treatment

Animal experimentation was approved by the Animal Committee of the Chinese Academy of Sciences Institutional Laboratory [WIVA042020003]. In total, 70 female C57BL/6 mice (6-weeks-old, 20–24 g) were used in this study. AOM was purchased from Sigma-Aldrich (No. A5486, USA), and DSS was purchased from MP Biomedicals (No. 160110, CA). The animal experiments were conducted in two stages.

In the first stage, 35 mice were randomly divided into seven groups ($n = 5$) and treated with AOM/DSS at different concentrations as follows: Group A, 10 mg/kg AOM, 2% DSS; Group B, 10 mg/kg AOM, 1% DSS; Group C, 10 mg/kg AOM, 0.5% DSS; Group D, 10 mg/kg AOM, 0.25% DSS; Group E, 7.69 (10/1.3) mg/kg AOM, 2% DSS; Group F, 5.92 ($10/1.3^2$) mg/kg AOM, 2% DSS; Group G, 4.55 ($10/1.3^3$) mg/kg AOM, 2% DSS. The mice were intraperitoneally injected with AOM on the first day. Then, 1 week later, the mice were treated with DSS solution for 1 week, followed by 2 weeks of normal drinking water, for three cycles. All mice were euthanized until 14 weeks. The animal modeling process is shown in **Figure 1A**.

In the second stage, 35 mice were randomly divided into an experimental group ($n = 30$) and control group ($n = 5$). Here, we hypothesized that DSS at a certain dose might result in tumors in 50% of mice, without tumors in the other 50% of mice. The expected dose of DSS was calculated as 0.5359% according to the method in a previous study (Sanchez et al., 2018). Mice in the experimental group were treated with 10 mg/kg AOM and 0.5359% DSS in drinking water, based on the aforementioned procedure. Meanwhile, mice in the control group were maintained under standard conditions for 14 weeks. Finally, the colon tissues and fecal samples of all mice were collected for further investigation.

## 16S rDNA amplicon sequencing

The fecal genomic DNA was extracted using a Stool DNA Kit (Qiagen, Germany) according to the manufacturer's experimental steps. After determining the DNA integrity and concentration, the qualifying DNA samples were used for amplification. Specific primers were designed for the 16S rRNA V3–V4 region (F: 5′-CCTACGGGAGGCAGCAG-3′; R: 5′-GGACTACHVGGGTATCTAAT-3′). PCR amplification was performed using High-Fidelity PCR Master Mix with GC Buffer (New England Biolabs, USA). Then, the PCR products were separated using 2% agarose gel electrophoresis and magnetic beads and purified with a Gel Extraction Kit (Qiagen, Germany). The amplicon libraries were constructed using a TruSeq® DNA PCR-Free Sample Preparation Kit (Illumina, USA), then quantified with a Qubit and qPCR, and finally sequenced on a NovaSeq6000 (Illumina, USA) platform. The effective tags were analyzed and obtained with the assistance of Novogene Biotechnology (Guangzhou, China). Operational taxonomic units (OTUs) were clustered based on tags of more than 97% identity using the Uparse v7.0.1001 method. Further analyses, including alpha and beta diversity, were subsequently performed.

## Untargeted metabolomics analysis

Untargeted metabolomics were investigated via LC-MS/MS analyses. Fecal samples (100 mg) were placed in Eppendorf tubes and quickly treated with liquid nitrogen. Then, the samples were resuspended well with 80% methanol and 0.1% formic acid. After incubation for 5 min in an ice bath, the mixture was centrifuged at 15,000 × *g* and 4°C for 20 min. The supernatants were transferred and diluted with LC-MS grade water with methanol at a final concentration of 53%. Following another centrifugation step at 15,000 × *g* and 4°C for 15 min, the resulting supernatants were collected for subsequent experiments.

LC-MS/MS analyses were performed using the Vanquish UHPLC system and Orbitrap Q Exactive™HF-X mass spectrometer (Thermo Fisher Scientific, Germany) provided by Novogene (Beijing,

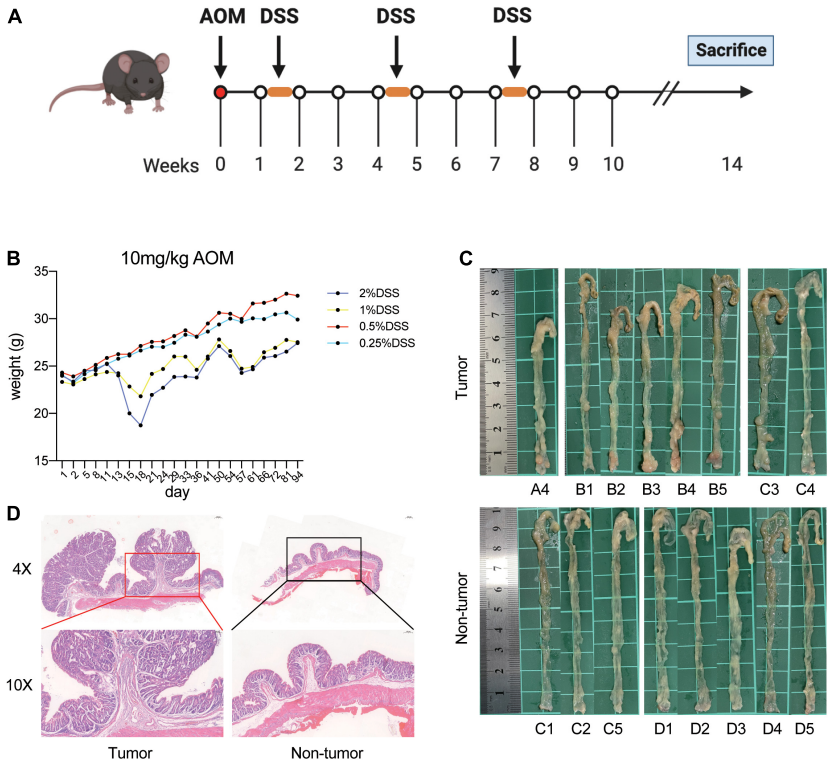


FIGURE 1
Establishment of AOM/DSS-induced mice models. **(A)** Flow chart of the mice treated with AOM/DSS. **(B)** Weight of mice in each group during AOM/DSS treatment. **(C)** Macroscopic view of colon. **(D)** Representative hematoxylin and eosin stain of the distal colon with tumor and no tumor.

China). The samples were injected into a Hypesil Gold column (2.1 mm × 100 mm, 1.9 μm), and the flow rate was 0.2 ml/min. Eluent A was 0.1% formic acid in water, and eluent B was methanol for the positive polarity mode, whereas for the negative polarity mode, eluent A was 5 mmol/L ammonium acetate in water, pH 9.0, and eluent B was methanol. The solvent gradient was set as follows: 1.5 min, 2% B; 12 min, 2–100% B; 14 min, 100% B; 14.1 min, 98% B; 17 min, 2% B. A QExactiveTMHF-X mass spectrometer was used with the source conditions as follows: sheath gas flow rate of 40 Arb, aux gas flow rate of 10 Arb, spray voltage of 3.2 kV, capillary temperature of 320°C. The raw data files were generated based on UHPLC-MS/MS and processed using Compound Discoverer 3.1 (Thermo Fisher, USA).

## Statistical analysis

Qiime software (Version 1.9.1) was used to calculate Observed-OTU, Chao1, Shannon, and Simpson indices. Differences in alpha diversity indices among groups were analyzed based on the rarefaction curve and rank abundance curve. A Wilcox test was used for alpha diversity and beta diversity analyses. ANOSIM analysis was performed to test for differences in the microbial communities among groups. Raw data of LC-MS/MS were analyzed using Compound Discoverer 3.1. The differences in metabolic patterns among different groups were revealed based on partial least squares discrimination analysis (PLS-DA). To study phenotypic changes that might be caused by changes in the host microbial community structure, correlation analyses between the microbiome and metabolome were performed based on Pearson's correlation analysis, correlation network diagram analysis, and correlation Sankey diagram analysis. $P < 0.05$ was considered statistically significant.

# Results

## Generation of AOM/DSS-induced tumor mouse models

First, the mice were treated with AOM/DSS at different concentrations. After the initiation of tumorigenesis for 14 weeks, the mice were euthanized and investigated. We observed that mice in the group administered 1 and 2% DSS lost significantly more weight than those in the other two groups (Figure 1B). Moreover, the nodular tumors were macroscopically visible in the distal colon of mice in different groups (Figure 1C). In addition, the mice had obvious tumors in group A and B, whereas group D had no tumors (Table 1 and Figures 1C, D). However, the mice treated with 2% DSS and different concentrations of AOM had poor survival outcomes (Table 1). Therefore, we selected DSS as a variable factor to establish the target mouse models.

Here, we hypothesized that DSS at a specific dose would cause 50% of mice in a test population to develop tumors, and the theoretical dose was 0.5359% based on the results of groups A–D. Next, the mice in the experimental group ($n = 30$) were treated with 10 mg/kg AOM and 0.5359% DSS, and a negative control group of mice ($n = 5$) was also used in parallel. Fourteen weeks later, the mice were euthanized and investigated. As a result, 12 mice had

10.3389/fmicb.2022.1082835

TABLE 1 Incidence of tumor in mice treated with different doses of AOM/DSS.

| Group ($n$ = 5) | Application | | Survival | With tumor | Incidence (%) |
|---|---|---|---|---|---|
| | AOM (mg/kg) | DSS (%) | | | |
| A | 10 | 2 | 1 | 1 | 100 |
| B | 10 | 1 | 5 | 5 | 100 |
| C | 10 | 0.5 | 5 | 2 | 40 |
| D | 10 | 0.25 | 5 | 0 | 0 |
| E | 7.69 | 2 | 2 | 2 | 100 |
| F | 5.92 | 2 | 3 | 2 | 66.67 |
| G | 4.55 | 2 | 2 | 1 | 50 |

tumors and 18 mice had no tumors in the experimental group. Then, we randomly selected the nine mice with tumors (tumor group), nine mice with no tumors (non-tumor group), and five control mice (control group) for further experiments and analysis.

## Alterations to the gut microbiomes in different groups

To explore whether tumorigenesis is related to the gut microbiome, 16S rRNA sequencing was performed to identify gut microbiota profiles. In total, 1,189 OTUs were obtained among the three groups, comprising 828 in the control group, 797 in the tumor group, and 883 in the non-tumor group (**Figure 2A**). Moreover, a relative increase in bacterial richness was found in the non-tumor group, as revealed based on the rarefaction curve, compared with that in the other two groups (**Figure 2B**). In addition, the rank abundance curve yielded similar results (**Figure 2C**). To investigate bacterial diversity, we analyzed the alpha diversity indices and observed that there were statistically significant differences in the observed species, Shannon, Simpson, and Chao1 indices among different groups (**Figures 2D–G**). The principal component analysis showed that there were three separations of gut microbiota distributions among the three groups (**Figure 2H**). Non-metric multi-dimensional scaling analysis also revealed different distributions of microbial communities among the three groups (**Figure 2I**).

## Identification of differential bacteria among different groups

The gut microbial community structures at the phylum and genus levels in the three groups were analyzed, and the top 10 differences are presented in **Figures 3A, B**. The differences in the microbial distribution among the groups were determined through ANOSIM analysis (**Supplementary Figures 1A–C**). Next, the differential component proportions of microbes in each group were revealed based on the heatmaps (**Figures 3C, D**). In addition, at the phylum level, we observed that the Cyanobacteria, Proteobacteria, and Fusobacteriota were significantly enriched in the non-tumor group compared to abundances in the tumor groups, and Verrucomicrobiota was more abundant in controls (**Supplementary Figures 1D–F**). At the genus level, *Prevotella*, *Alloprevotella*, *Neisseria*, and *Akkermansia* exhibited marked differences among the groups (**Supplementary Figures 1G–I**).

To further determine the specific gut microflora associated with colorectal tumorigenesis, linear discriminant analysis effect size was performed among the three groups. The branching maps containing six levels, from phylum to species, reveled the signature microbiota. We found that the family Prevotellaceae and class Gammaproteobacteria may have a great effect in the non-tumor group, whereas the families Pseudomonadaceae and Akkermansiaceae, orders Pseudomonadales and Verrucomicrobiales, and class Verrucomicrobiae might play important roles in the control group (**Figure 3E**). Moreover, based on linear discriminant analysis scores ($\log_{10}$) > 4, the histogram showed that four bacterial taxa, including Proteobacteria, Gammaproteobacteria, Prevotellaceae, and Prevotella, were enriched in the non-tumor group, two bacterial taxa were enriched in the tumor group, and 10 bacterial taxa were enriched in the control group (**Figure 3F**).

## Changes in fecal metabolites among different groups

To identify the signature metabolites from fecal samples among the groups, we performed untargeted LC-MS/MS-based metabolomics. The PLS-DA showed significant differences between the fecal samples and metabolic phenotypes of different groups in both positive and negative ion modes (**Figures 4A, B**). In total, 1,112 and 554 metabolites were found to be changed in the tumor group, non-tumor group, and control group, in positive and negative ion modes, respectively (**Supplementary Table 1**). The differences in metabolites among the three groups are shown in **Figure 4C**. Further, we focused on the differences between the tumor group and non-tumor group. The heatmaps revealed the metabolite differences across each sample within the two groups (**Figure 4D**). The volcano plots also showed the significant upregulated or downregulated metabolites in the tumor group compared with levels in the non-tumor group (**Figure 4E**). Briefly, in positive ion mode, levels of 31 and 22 fecal metabolites were up- and downregulated, respectively, in the non-tumor group, with statistically significant differences compared to those in the tumor group. Meanwhile, in negative ion mode, levels of 10 and nine fecal metabolites were significantly up and downregulated, respectively, in the non-tumor group, with statistically significant differences compared to those in the tumor group. The structures of these metabolites were diverse, with many of the metabolites being either directly generated or modulated by the gut bacteria, including homogentisic acid, 3-methyladenine, and 2'-deoxyguanosine (downregulated in positive ion mode); nicotinic acid mononucleotide, N-acetyl-L-leucine, and linoleoyl ethanolamide (upregulated in positive ion mode); glycoursodeoxycholic acid, 2'-deoxyuridine, and pentadecanoic acid (downregulated in negative ion mode); and hydrocinnamic acid, oxoadipic acid, and 3-methyladipic acid (upregulated in negative ion mode). Moreover, Kyoto Encyclopedia of Genes and Genomes (KEGG) pathway analysis was used to identify the enriched pathways associated with differential metabolites in the two groups, and the top 20 most enriched pathways are listed in **Figure 4F**. Among them, styrene degradation and amino sugar-nucleotide sugar metabolism, were significantly altered in positive and negative ion modes, respectively.

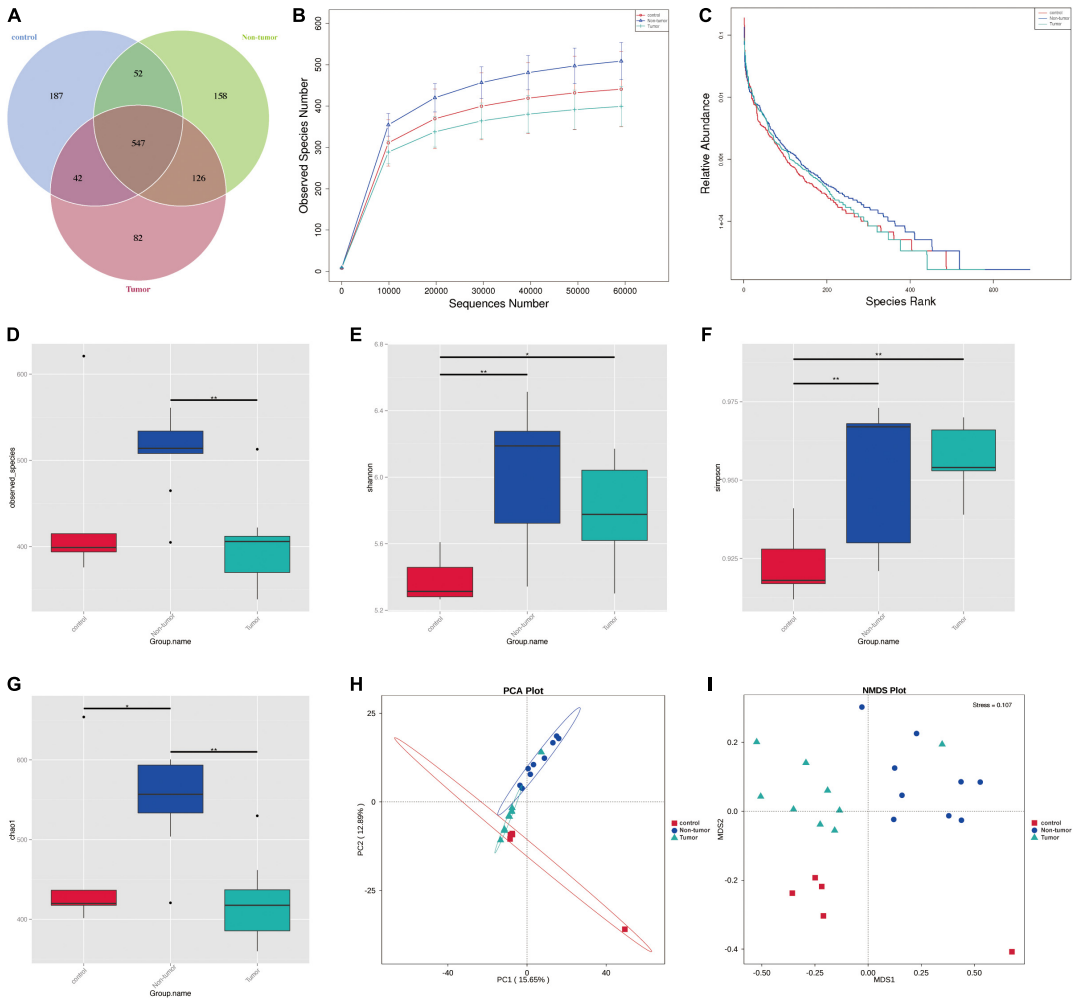


FIGURE 2
The diversity of the microbial communities in three groups. **(A)** Venn diagram shows the compositions of OTUs. **(B)** Rarefaction curve. **(C)** Rank abundance curve. **(D–G)** Alpha diversity index analysis (ACE, Shannon, Simpson, and Chao1). **(H)** Principal component analysis; **(I)** NMDS analysis. $*p < 0.05$, $**p < 0.01$.

## Correlation analysis between the gut microbiota and metabolites

To investigate the association between differential microbiota and metabolites in fecal samples, we conducted correlation analysis based on top 10 different bacteria at the genus level and top 20 different metabolites between the tumor group and non-tumor group. As shown in Figures 5A, B, the correlation heatmaps revealed the association between metabolites and microbiota, based on Pearson correlation coefficient analysis, in positive and negative ion methods. To further reveal the key bacterial flora and metabolites, we generated correlation network diagrams and observed that the connections were multiple and consanguineous (Figures 5C, D). Moreover, the correlation Sankey chart analysis also visually demonstrated the association between the gut microbiota and metabolites (Figures 5E, F). Notably, in positive ion mode, we observed that D-α-tocopherol was significantly negatively correlated with most microbiota, including *Actinobacillus*, *Capnocytophaga*, F0058, *Lautropia*, and *Peptostreptococcus*. Similarly, N1-(5-methylisoxazol-3-yl)-2-tetrahydro-1H-pyrrol-1-ylacetamide also exhibited negative correlations with most microbes. Meanwhile, 1,2-di(3,4-dimethoxyphenyl)diaz-1-ene, 3-methyl-5-oxo-5-(4-toluidino)pentanoic acid, oxymatrine, pantothenic acid, progesterone, and styrene showed positive correlations with the vast majority of microbe–metabolite pairs. In negative ion mode, the results showed highly negative associations for several microbe–metabolite pairs, such as *Actinobacillus*/L-methionine sulfone, *Capnocytophaga*/L-methionine sulfone, and *Parasutterella*/2'-deoxyuridine. However, *Lautropia*/glycoursodeoxycholic acid, *Capnocytophaga*/glycoursodeoxycholic acid, *Lautropia*/4-hydroxyisoleucine, and F0058/LPG 15:0, among others exhibited opposite relationships. Taken together, these results revealed significant correlations with respect to key microbe–metabolite pairs in the tumor and non-tumor groups, suggesting their potential roles in modulating tumorigenesis.

# Discussion

The AOM/DSS-induced mouse model is a common experimental tumor model to develop colitis-associated colon cancer. Specifically, it can mimic the non-hereditary features of CRC in terms of the

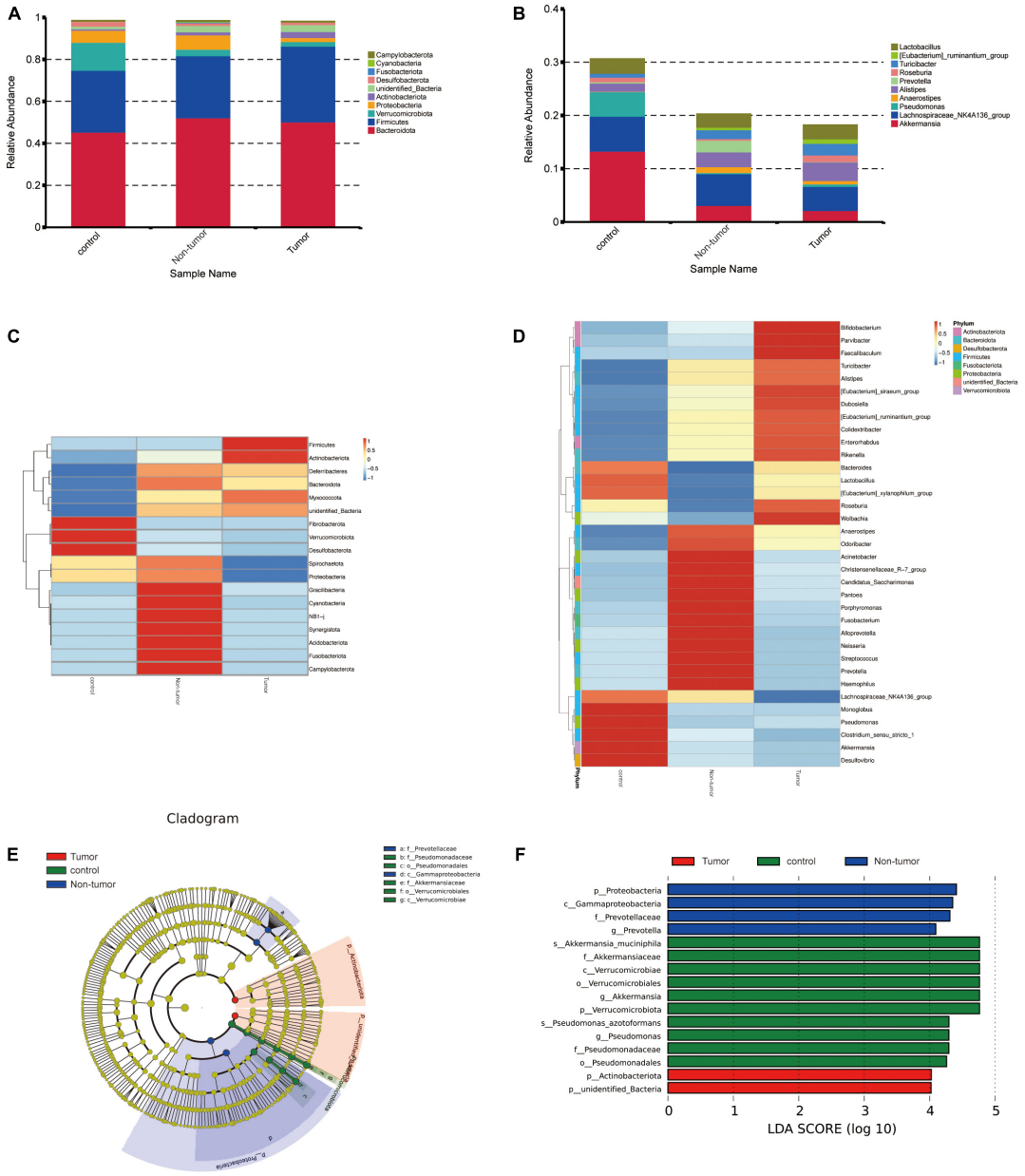


FIGURE 3
Identification of the differential bacteria from the three groups. **(A,B)** Component proportion of bacteria at the phylum **(A)** and genus **(B)** level in different groups. **(C,D)** Heat maps to identify different fecal microbiota at the phylum **(C)** and genus **(D)** level in the different groups. **(E)** The cladogram to show specific differential bacteria in the three groups. **(F)** LEfSe indicating the different bacterial taxa.

normal epithelium/adenoma/carcinoma progression (Neufert et al., 2007; Dekker et al., 2019). Further, it is an essential tool to investigate the underlying mechanisms of CRC initiation and progression, but it is also a valuable and effective model for the evaluation of novel therapeutic options. For example, Wei et al. elucidated the role and molecular mechanism of NDRG2 in tumor development using AOM/DSS mice (Wei et al., 2020). Moreover, Gobert revealed the protective function of spermine oxidase in colon inflammation and tumorigenesis (Gobert et al., 2022).

In previous studies, researchers have devoted time to finding the optimal conditions of AOM and DSS utilization to induce tumor development, including the doses of AOM and/or DSS (Bissahoyo et al., 2005; Suzuki et al., 2005; Neufert et al., 2007; Angelou et al., 2018). Interestingly, we observed that when mice were administrated various concentrations of AOM/DSS, different tumor burdens were noted. Compared to those in the 5 mg/kg AOM group, the percentage of tumor-bearing mice, tumor multiplicity, and size were significantly increased in the 10 mg/kg AOM group, whereas 20 mg/kg AOM resulted in acute toxicity (Bissahoyo et al., 2005). Moreover, in another study, Suzuki administered 10 mg/kg AOM to the mice, followed by DSS solution at levels of 0.1, 0.25, 0.5, 1, and 2%. The incidences of neoplasms were 0, 0, 20, 100, and 100% for each group, respectively (Suzuki et al., 2005). To some extent, the tumor-promoting ability of AOM/DSS might thus be dose-dependent. Therefore, we hypothesize that there is a certain dose of these chemical agents that could lead to a 50% possibility of tumor development.

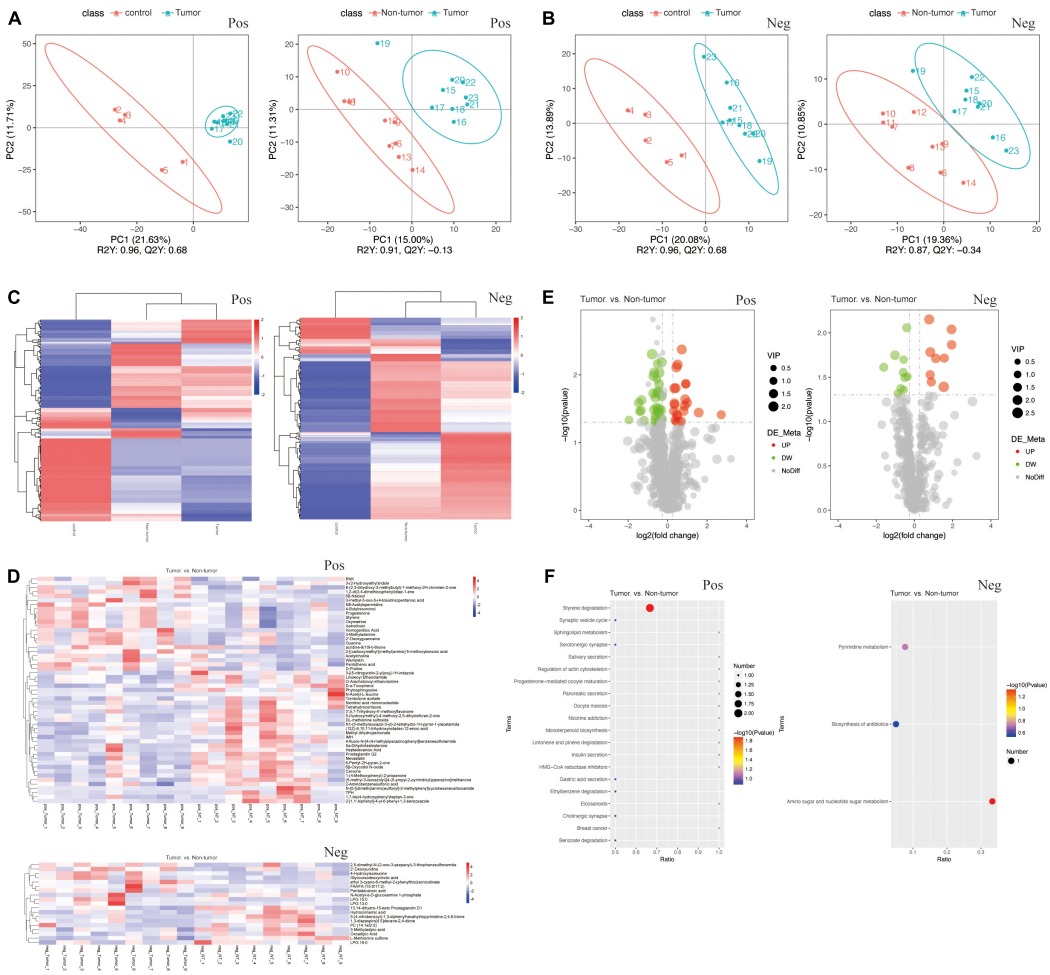

FIGURE 4
Changes of the fecal metabolites in the groups. **(A,B)** PLS-DA of fecal samples between tumor group and control group **(A)**, between tumor group and non-tumor group **(B)**, by the positive and negative ion methods. **(C)** Heat maps of different fecal metabolites among three groups. **(D)** Heat maps of different metabolites in each fecal samples between tumor group and non-tumor group. **(E)** Volcano Plots indicating the variation of fecal metabolites between the two groups. **(F)** KEGG pathway analysis of metabolism between the two groups.

In our study, we generated the mouse models with multiple combinations of AOM and DSS doses, as presented in **Table 1**. As a result, we found increasing incidences of tumors in the mice treated with DSS, from 0.25 to 2% (the dose of AOM was 10 mg/kg). Among these concentrations, 1 and 2% DSS resulted in a tumor incidence of 100%, whereas 0.5 and 0.25% DSS induced lower incidences, specifically less than 50%. However, 2% DSS treatment led to poor survival outcomes in the groups. Thus, we set the AOM dose at 10 mg/kg and the targeted dose of DSS at 0.5359% for the following animal experiment ($n$ = 30), which was thought to be associated with a theoretical 50% probability of tumor initiation. Finally, in the experimental group, 12 mice developed tumors and 18 mice had no tumors. We next sought to determine what factors contribute to this phenomenon.

With the continuous progress of high-throughput sequencing and bioinformatics, studies on the human intestinal flora have been further developed. Numerous studies have indicated that genetic and environmental factors play important roles in carcinogenesis (Song et al., 2015; Yang et al., 2019). CRC occurs directly in the gut and is therefore closely related to changes in the intestinal microecology. Accumulating evidence demonstrates that dysbiosis of the intestinal flora could modulate the progression, development, and treatment of CRC (Louis et al., 2014; Feng et al., 2015; Fong et al., 2020; Huang et al., 2020, 2022). For example, a recent study showed that CRC patients have gut microbiome imbalances, which were characterized by an increase in the abundance of cancer-related bacteria, such as pks + *Escherichia coli*, enterotoxigenic *Bacteroides fragilis*, and *Fusobacterium nucleatum*, whereas the abundance of beneficial bacteria such as *Roseburia*, *Clostridium*, and *Bifidobacterium* were found to be decreased (Janney et al., 2020). Similarly, in the current study, the abundances of *Colidextribacter* and *Bacteroides* were increased in the tumor group, suggesting that these harmful bacteria might participate in the process of colorectal tumorigenesis. Interestingly, although the abundance of the beneficial bacteria *Clostridium* increased in the tumor group, other probiotics commonly believed to play a role in CRC, such as *Bifidobacterium* and *Roseburia*, did not show a decrease in abundance in the tumor group, indicating that changes in the composition of gut microbes during inflammation-mediated colorectal tumorigenesis might be different from those occurring with conventional CRC. These so-called "abnormal" intestinal flora changes deserve further study and discussion, in the context of the AOM/DSS-mediated inflammation

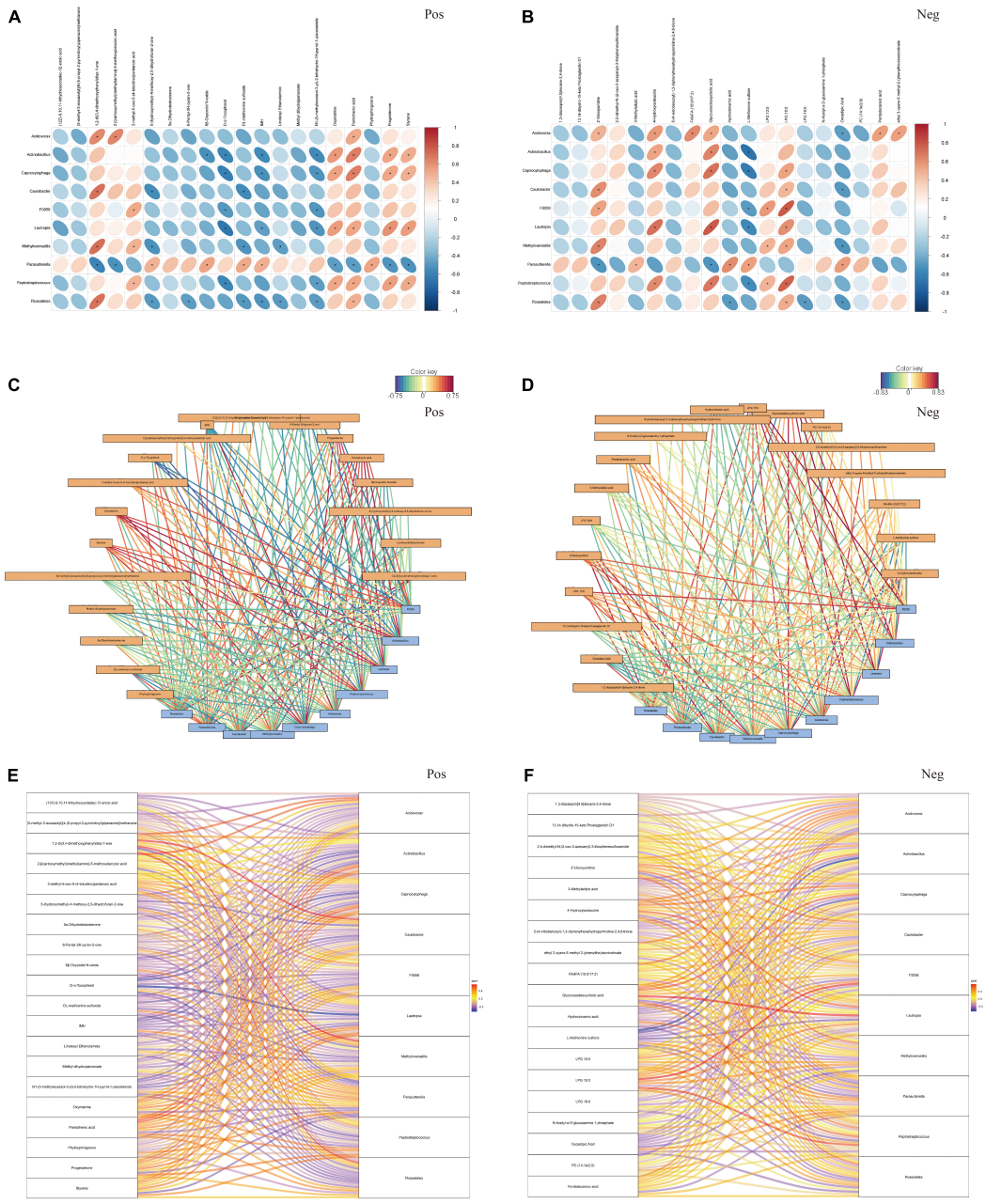


FIGURE 5
The association analysis between top 10 differential fecal microbiota at genus level and top 20 differential metabolites. **(A,B)** Pearson correlation coefficient analysis. **(C,D)** Correlation network diagram analysis. **(E,F)** Correlation Sankey diagram analysis, by the positive and negative ion methods, separately. Red represented that the microbiota was positively correlated with metabolites, and bule represented that the microbiota was negatively correlated with metabolites. *$P < 0.05$.

tumor animal model. Moreover, at the phylum level, we observed that a variety of microbes, such as Proteobacteria and Cyanobacteria, were significantly increased in the non-tumor group compared to the abundance in the tumor group. Proteobacteria, as a source of natural products, provides unappreciated potential to discover and develop novel bioactive molecules with antibiotic and anticancer effects (Buijs et al., 2019). Cyanobacteria and its metabolites also have favorable potential as anticancer drugs (Mondal et al., 2020).

Metabolomics can clearly reflect the functional changes in the gut microbiota under specific conditions through the detection of metabolites, which might provide clues to reveal the relationship between the gut microbiota and the occurrence and development of diseases (Han et al., 2021; Krautkramer et al., 2021; Bauermeister et al., 2022). Our metabolomic analysis showed that 72 metabolites in the non-tumor group were significantly changed, compared with levels in the tumor group. Among them, tetrahydrocortisone, O-arachidonoyl ethanolamine, and D-α-tocopherol were enriched in the non-tumor group. These metabolites and their analogs have some anti-inflammatory properties. For example, as an endogenous cannabinoid, O-arachidonoyl ethanolamine has been proven to be an endogenous inhibitor of cytochrome P450 cyclooxygenase, with anti-inflammatory effects (Carnevale et al., 2018). Moreover, tetrahydrocortisone is a metabolic product of hydrocortisone, and its enrichment indicates that the glucocorticoid anti-inflammatory

pathway might be active (Wang et al., 2018; Sagmeister et al., 2019). D-α-Tocopherol can play an anti-inflammatory role by reducing the release of proinflammatory cytokines (such as interleukin-1 β, interleukin-6, and tumor necrosis factor α) and chemokines (such as interleukin-8) and reducing the adhesion of monocytes to the endothelium. The KEGG pathway analysis showed that some pathways, such as styrene degradation and amino sugar-nucleotide sugar metabolism, were significantly enriched between the groups. Interestingly, environmental nanoparticles, especially polystyrene nanoparticles, are a potential risk for intestinal injury. It has been reported that PNP exposure can induce cytotoxic and genotoxic effects on cells by inducing oxidative stress related to nuclear damage (Vecchiotti et al., 2021). Homogentisic acid is a metabolite annotated to the styrene degradation pathway, and it has been proven to be cytotoxic for various cell lines (Jurič et al., 2022). However, whether it can participate in CRC is worth further exploring.

It is known that the gut microbiome can regulate metabolic homeostasis, and we further conducted correlation analysis of the gut microbiome and metabolome. Notably, in our findings, D-α-tocopherol, an anti-inflammatory factor enriched in the non-tumor group, was significantly negatively correlated with several microbes, such as *Actinobacillus*, *Capnocytophaga*, and *Lautropia*. A previous study revealed that *Actinobacillus* had the higher degree of centrality across the progression of precancerous lesions of gastric cancer, and *Acinetobacter* might contribute to the occurrence of intraepithelial neoplasia (Liu et al., 2021). *Capnocytophaga*, an oral bacterium, was also found to be highly present in oral squamous cell carcinoma tissues and exert tumor-promoting effects on oral cancer (Zhu et al., 2022). Moreover, Li et al. (2020) revealed that *Lautropia* was enriched in hepatitis patients and might participate in the progression of liver cancer. Therefore, in the future, more experiments should be performed to validate the effect of the identified microbiota and metabolites on CRC progression and treatment.

It should be noted that, whether the changes in the gut microbiota could affect disease development or the occurrence of disease may cause an imbalance in the intestinal flora, as well as the mechanism underlying such phenotypes, need to be further elucidated. Moreover, although some differential microbiota and metabolites were identified in the animal models, their antitumor effects in animal models and in humans have not been further demonstrated. Despite this, our study investigated the intestinal microecology of colorectal tumors using an AOM/DSS mouse model, with a specific concentration used for treatment. We demonstrated the differentially abundant microbiota and metabolites in the gut and identified the potential key relationships between them. These findings might provide guidance to elucidate the mechanism underlying the pathogenesis of inflammation-mediated colorectal tumors.

## Conclusion

In this study, we successfully generated an AOM/DSS mouse model, based on a certain dose that could influence the development of CRC. Using this model, 16S sequencing and LC-MS/MS analyses were performed to identify and explore the differential gut microbiota and metabolites that might be associated with tumorigenesis. This could ultimately provide a new direction for the prevention and treatment of CRC.

## Data availability statement

The raw data supporting the conclusions of this article will be made available by the authors, without undue reservation.

## Ethics statement

This animal study was reviewed and approved by Animal Committee of Chinese Academy of Sciences Institutional Laboratory (WIVA042020003).

## Author contributions

CQJ and RG conceived and designed experiments. YTH, RG, and BXC performed the experiments. YTH, BXC, XZ, and QQ interpreted the results of experiments. YTH wrote the manuscript. All authors reviewed and approved the final manuscript.

## Funding

This research was supported by Engineering construction project of improving diagnosis and treatment ability of difficult diseases (oncology) (ZLYNXM202012), Wu Jieping Medical Research Foundation (320.6750.2021-11-8), and Joint Foundation of Health Commission of Hubei Province (znpy2019086).

## Acknowledgments

We thank Jinwen Yin, for the tremendous support in the past years.

## Conflict of interest

The authors declare that the research was conducted in the absence of any commercial or financial relationships that could be construed as a potential conflict of interest.

## Publisher's note



## Supplementary material

The Supplementary Material for this article can be found online at: https://www.frontiersin.org/articles/10.3389/fmicb.2022.1082835/full#supplementary-material

# References


Akimoto, N., Ugai, T., Zhong, R., Hamada, T., Fujiyoshi, K., Giannakis, M., et al. (2021). Rising incidence of early-onset colorectal cancer - a call to action. *Nat. Rev. Clin. Oncol.* 18, 230–243. doi: 10.1038/s41571-020-00445-1

Angelou, A., Andreatos, N., Antoniou, E., Zacharioudaki, A., Theodoropoulos, G., Damaskos, C., et al. (2018). A novel modification of the AOM/DSS model for inducing intestinal adenomas in mice. *Anticancer Res.* 38, 3467–3470. doi: 10.21873/anticanres.12616

Arima, K., Zhong, R., Ugai, T., Zhao, M., Haruki, K., Akimoto, N., et al. (2022). Western-style diet, pks island-carrying *escherichia coli*, and colorectal cancer: Analyses from two large prospective cohort studies. *Gastroenterology* 163, 862–874. doi: 10.1053/j.gastro.2022.06.054

Bauermeister, A., Mannochio-Russo, H., Costa-Lotufo, L. V., Jarmusch, A. K., and Dorrestein, P. C. (2022). Mass spectrometry-based metabolomics in microbiome investigations. *Nat. Rev. Microbiol.* 20, 143–160.

Bissahoyo, A., Pearsall, R. S., Hanlon, K., Amann, V., Hicks, D., Godfrey, V. L., et al. (2005). Azoxymethane is a genetic background-dependent colorectal tumor initiator and promoter in mice: Effects of dose, route, and diet. *Toxicol. Sci.* 88, 340–345. doi: 10.1093/toxsci/kfi313

Buijs, Y., Bech, P. K., Vazquez-Albacete, D., Bentzon-Tilia, M., Sonnenschein, E. C., Gram, L., et al. (2019). Marine *Proteobacteria* as a source of natural products: Advances in molecular tools and strategies. *Nat. Prod. Rep.* 36, 1333–1350. doi: 10.1039/c9np00020h

Carnevale, L. N., Arango, A. S., Arnold, W. R., Tajkhorshid, E., and Das, A. (2018). Endocannabinoid virodhamine is an endogenous inhibitor of human cardiovascular CYP2J2 epoxygenase. *Biochemistry* 57, 6489–6499. doi: 10.1021/acs.biochem.8b00691

Dekker, E., Tanis, P. J., Vleugels, J. L., Kasi, P. M., and Wallace, M. B. (2019). Colorectal cancer. *Lancet* 394, 1467–1480.

Feng, Q., Liang, S., Jia, H., Stadlmayr, A., Tang, L., Lan, Z., et al. (2015). Gut microbiome development along the colorectal adenoma-carcinoma sequence. *Nat. Commun.* 6:6528.

Fong, W., Li, Q., and Yu, J. (2020). Gut microbiota modulation: A novel strategy for prevention and treatment of colorectal cancer. *Oncogene* 39, 4925–4943.

Gobert, A. P., Latour, Y., Asim, M., Barry, D., Allaman, M., Finley, J., et al. (2022). Protective role of spermidine in colitis and colon carcinogenesis. *Gastroenterology* 162, 813–827.

Han, S., Treuren, W. V., Fischer, C. R., Merrill, B. D., DeFelice, B. C., Sanchez, J. M., et al. (2021). A metabolomics pipeline for the mechanistic interrogation of the gut microbiome. *Nature* 595, 415–420.

Hradicka, P., Beal, J., Kassayova, M., Foey, A., and Demeckova, V. (2020). A novel lactic acid bacteria mixture: Macrophage-targeted prophylactic intervention in colorectal cancer management. *Microorganisms* 8:387. doi: 10.3390/microorganisms8030387

Huang, J., Jiang, Z., Wang, Y., Fan, X., Cai, J., Yao, X., et al. (2020). Modulation of gut microbiota to overcome resistance to immune checkpoint blockade in cancer immunotherapy. *Curr. Opin. Pharmacol.* 54, 1–10.

Huang, J., Liu, D., Wang, Y., Liu, L., Li, J., Yuan, J., et al. (2022). Ginseng polysaccharides alter the gut microbiota and kynurenine/tryptophan ratio, potentiating the antitumour effect of antiprogrammed cell death 1/programmed cell death ligand 1 (anti-PD-1/PD-L1) immunotherapy. *Gut* 71, 734–745. doi: 10.1136/gutjnl-2020-321031

Janney, A., Powrie, F., and Mann, E. H. (2020). Host-microbiota maladaptation in colorectal cancer. *Nature* 585, 509–517. doi: 10.1038/s41586-020-2729-3

Jurič, A., Huđek Turković A, Brčić Karačonji I., Prđun, S., Bubalo, D., and Durgo, K. (2022). Cytotoxic activity of strawberry tree (*Arbutus unedo* L.) honey, its extract, and homogentisic acid on CAL 27, HepG2, and Caco-2 cell lines. *Arh. Hig. Rada Toksikol.* 73, 158–168. doi: 10.2478/aiht-2022-73-3653

Krautkramer, K. A., Fan, J., and Bäckhed, F. (2021). Gut microbial metabolites as multi-kingdom intermediates. *Nat. Rev. Microbiol.* 19, 77–94. doi: 10.1038/s41579-020-0438-4

Li, D., Xi, W., Zhang, Z., Ren, L., Deng, C., Chen, J., et al. (2020). Oral microbial community analysis of the patients in the progression of liver cancer. *Microb. Pathog.* 149:104479. doi: 10.1016/j.micpath.2020.104479

Liu, D., Chen, S., Gou, Y., Yu, W., Zhou, H., Zhang, R., et al. (2021). Gastrointestinal microbiota changes in patients with gastric precancerous lesions. *Front. Cell Infect. Microbiol.* 11:749207. doi: 10.3389/fcimb.2021.749207

Louis, P., Hold, G. L., and Flint, H. J. (2014). The gut microbiota, bacterial metabolites and colorectal cancer. *Nat. Rev. Microbiol.* 12, 661–672.

Matson, V., Chervin, C. S., and Gajewski, T. F. (2021). Cancer and the microbiome-influence of the commensal microbiota on cancer, immune responses, and immunotherapy. *Gastroenterology* 160, 600–613. doi: 10.1053/j.gastro.2020.11.041

Mondal, A., Bose, S., Banerjee, S., Patra, J., Malik, J., Mandal, S., et al. (2020). Marine cyanobacteria and microalgae metabolites-a rich source of potential anticancer drugs. *Mar. Drugs* 18:476. doi: 10.3390/md18090476

Neufert, C., Becker, C., and Neurath, M. F. (2007). An inducible mouse model of colon carcinogenesis for the analysis of sporadic and inflammation-driven tumor progression. *Nat. Protoc.* 2, 1998–2004. doi: 10.1038/nprot.2007.279

Sagmeister, M. S., Taylor, A. E., Fenton, A., Wall, N. A., Chanouzas, D., Nightingale, P. G., et al. (2019). Glucocorticoid activation by 11β-hydroxysteroid dehydrogenase enzymes in relation to inflammation and glycaemic control in chronic kidney disease: A cross-sectional study. *Clin. Endocrinol.*90, 241–249. doi: 10.1111/cen.13889

Sanchez, K. K., Chen, G., Schieber, A., Redford, S., Shokhirev, M., Leblanc, M., et al. (2018). Cooperative metabolic adaptations in the host can favor asymptomatic infection and select for attenuated virulence in an enteric pathogen. *Cell* 175, 146–158. doi: 10.1016/j.cell.2018.07.016

Siegel, R. L., Miller, K. D., Sauer, A. G., Fedewa, S. A., Butterly, L. F., Anderson, J. C., et al. (2020). Colorectal cancer statistics, 2020. *CA Cancer J. Clin.* 70, 145–164.

Snider, A. J., Bialkowska, A. B., Ghaleb, A. M., Yang, V. W., Obeid, L. M., and Hannun, Y. A. (2016). Murine model for colitis-associated cancer of the colon. *Methods Mol. Biol.* 1438, 245–254.

Song, M., Garrett, W. S., and Chan, A. T. (2015). Nutrients, foods, and colorectal cancer prevention. *Gastroenterology* 148, 1244–1260.

Sung, H., Ferlay, J., Siegel, R. L., Laversanne, M., Soerjomataram, I., Jemal, A., et al. (2021). Global cancer statistics 2020: GLOBOCAN estimates of incidence and mortality worldwide for 36 cancers in 185 countries. *CA Cancer J. Clin.* 71, 209–249.

Suzuki, R., Kohno, H., Sugie, S., and Tanaka, T. (2005). Dose-dependent promoting effect of dextran sodium sulfate on mouse colon carcinogenesis initiated with azoxymethane. *Histol. Histopathol.* 20, 483–492.

Vecchiotti, G., Colafarina, S., Aloisi, M., Zarivi, O., Carlo, P. D., and Poma, A. (2021). Genotoxicity and oxidative stress induction by polystyrene nanoparticles in the colorectal cancer cell line HCT116. *PLoS One* 16:e0255120. doi: 10.1371/journal.pone.0255120

Vernia, F., Longo, S., Stefanelli, G., Viscido, A., and Latella, G. (2021). Dietary factors modulating colorectal carcinogenesis. *Nutrients* 13:143.

Wang, Y., Fujioka, N., and Xing, C. (2018). Quantitative profiling of cortisol metabolites in human urine by high-resolution accurate-mass MS. *Bioanalysis* 10, 2015–2026. doi: 10.4155/bio-2018-0182

Wei, M., Ma, Y., Shen, L., Xu, Y., Liu, L., Bu, X., et al. (2020). NDRG2 regulates adherens junction integrity to restrict colitis and tumourigenesis. *EBioMedicine* 61:103068. doi: 10.1016/j.ebiom.2020.103068

Yang, Y., Misra, B. B., Liang, L., Bi, D., Weng, W., Wu, W., et al. (2019). Integrated microbiome and metabolome analysis reveals a novel interplay between commensal bacteria and metabolites in colorectal cancer. *Theranostics* 9, 4101–4114. doi: 10.7150/thno.35186

Zhu, W., Shen, W., Wang, J., Wang, J., Wang, J., Zhang, J., et al. (2022). *Capnocytophaga gingivalis* is a potential tumor promotor in oral cancer. *Oral Dis.* doi: 10.1111/odi.14376 [Epub ahead of print].

frontiers | Frontiers in Microbiology

TYPE Original Research
PUBLISHED 16 February 2023
DOI 10.3389/fmicb.2023.1113730



OPEN ACCESS

EDITED BY
Tang Zhaoxin,
South China Agricultural University,
China

REVIEWED BY
Zeeshan Ahmad Bhutta,
Chungbuk National University,
Republic of Korea
Ambreen Ashar,
North Carolina State University,
United States
Liwei Guo,
Yangtze University,
China

*CORRESPONDENCE
Mingjin Wang
✉ wangmj1967@163.com
Jinping Ma
✉ wudaoyi123321@163.com

SPECIALTY SECTION
This article was submitted to Microorganisms in Vertebrate Digestive Systems, a section of the journal Frontiers in Microbiology

RECEIVED 01 December 2022
ACCEPTED 23 January 2023
PUBLISHED 16 February 2023

CITATION
Wang L, Wu D, Zhang Y, Li K, Wang M and Ma J (2023) Dynamic distribution of gut microbiota in cattle at different breeds and health states.
*Front. Microbiol.* 14:1113730.
doi: 10.3389/fmicb.2023.1113730



# Dynamic distribution of gut microbiota in cattle at different breeds and health states

Lei Wang[1,2], Daoyi Wu[1], Yu Zhang[2], Kun Li[3], Mingjin Wang[1]* and Jinping Ma[1]*

[1]Bijie Institute of Animal Husbandry and Veterinary Science, Bijie, China, [2]College of Veterinary Medicine, Huazhong Agricultural University, Wuhan, China, [3]College of Veterinary Medicine, Institute of Traditional Chinese Veterinary Medicine, Nanjing Agricultural University, Nanjing, China

Weining cattle is a precious species with high tolerance to cold, disease, and stress, and accounts for a large proportion of agricultural economic output in Guizhou, China. However, there are gaps in information about the intestinal flora of Weining cattle. In this study, high-throughput sequencing were employed to analyze the intestinal flora of Weining cattle (WN), Angus cattle (An), and diarrheal Angus cattle (DA), and explore the potential bacteria associated with diarrhea. We collected 18 fecal samples from Weining, Guizhou, including Weining cattle, Healthy Angus, and Diarrheal Angus. The results of intestinal microbiota analysis showed there were no significant differences in intestinal flora diversity and richness among groups ($p>0.05$). The abundance of beneficial bacteria (*Lachnospiraceae*, *Rikenellaceae*, *Coprostanoligenes*, and *Cyanobacteria*) in Weining cattle were significantly higher than in Angus cattle ($p<0.05$). The potential pathogens including *Anaerosporobacter* and *Campylobacteria* were enriched in the DA group. Furthermore, the abundance of *Lachnospiraceae* was very high in the WN group ($p<0.05$), which might explain why Weining cattle are less prone to diarrhea. This is the first report on the intestinal flora of Weining cattle, furthering understanding of the relationship between intestinal flora and health.

KEYWORDS

**Weining cattle, Angus cattle, diarrhea, gut microbiota, 16S**

## Introduction

Weining is located in southwest China at an average altitude of 2,200 meters. It is a large livestock county where cattle raising is the main economic income of farmers. In 2021, the stock of cattle in Weining was 153,600, accounting for 6.5% of the local agricultural output, with the most farmed species being Weining cattle and Angus cattle. The Weining cattle are an ancient ruminant with hypoxia tolerance, anti-oxidant action, and disease resistance, and have become the symbol of Weining Guizhou. They resemble ordinary cows with short horns and yellow hair, but also have many characteristics of their own. Due to the nutritious quality of their meat, their strength, and their docility, Weining play a significant role in local farming and prosperity. In addition, the incidence of intestinal diseases is fairly low compared to other types of cattle, one of the most important reasons for local people keeping Weining cattle.

The normal intestine harbors over 100 trillion microorganisms including bacteria (98%), fungi (0.1%), viruses, protists, archaea, and these microbial communities (Liu J. et al., 2019; Li et al., 2021). The gut microbiota colonizing the intestinal tract forms a symbiotic relationship with the host and plays a vital role in maintaining nutrient intake, immune regulation, and intestinal barrier integrity. In addition, the gut microbiome is believed to be a biochemical transformation that exerts beneficial

substances such as antimicrobial peptides, vitamins, and enzymes. Increasing evidence suggests that the diversity and composition of the gut microbiome have been linked to species and health, with species being the primary cause of the gut microbiota, followed by health status. However, to date, knowledge of the gut microbiota characteristics of Weining and Angus cattle is limited.

As is well known, diarrhea occurs in all animals, especially in newborns, and causes death in about half of the ruminants (Li et al., 2018; Bu et al., 2020). Calf mortality due to diarrhea remains very high in most countries, e.g., 17% in Germany and 5% in the United States (Urie et al., 2018; Eibl et al., 2021). Several studies have also indicated that intestinal microbial dysbiosis drives the development of diarrhea (Han et al., 2017; Shao et al., 2020). Healthy and balanced intestinal flora reduce the risk of diarrhea (Huang et al., 2019; Zuo et al., 2021). Previous studies have shown that intestinal bacteria in some ruminants alternate between dominant and weak populations with diarrheal symptoms (Yang et al., 2017). Thus, there may be some unavoidable links between the alteration of intestinal microbial communities and diarrhea. In the last few years, we have found that other types of cattle like Angus were more susceptible to diarrhea in Weining China. The mortality rate of other types of cattle was 9%, whereas in Weining cattle it was 3%. However, so far, there is little information about the relationship between diarrhea and gut microbiota in Angus cattle.

Regarding this phenomenon, we speculated about whether the low incidence of diarrhea in Weining cattle was related to intestinal flora. Possible reasons are that the Weining cattle's ancestors lived in relative isolation after entering the mountains and developed individual gut flora. However, the characteristics of gut microbiota in Weining cattle remain unclear. Here we seek to investigate and compare the composition and variability of gut bacteria in Weining cattle (WN), healthy Angus cattle (An), and diarrheal Angus cattle (DA). In addition, although there have been recent studies on gut microbiota and diarrhea, very few studies have been conducted on Angus cattle, and our study aims to better understand how gut microbes affect organismal health, exploring potential pathogenic microbes. Meanwhile, we aimed to explore the potential bacteria associated with disease resistance. These findings will aid in the future development of dietary interventions that may resolve or prevent enteric and diarrheal diseases in ruminants.

# Materials and methods

## Sample acquisition

Samples were taken between June and August 2022 in Weining China, the peak period for diarrhea incidence in cattle. In total, 18 individual fresh fecal samples were taken from 6 Weining cattle, 6 healthy Angus cattle, and 6 diarrheal cattle. All the cattle were a half-year-old and had lived in the same conditions. Prior to sampling, all specimens are tested by a professional veterinarian to assess their health, and the samples collected are immediately placed in liquid nitrogen fixation and transported back to the laboratory in dry ice as soon as possible.

## 16S rRNA gene amplicon sequencing

DNA was extracted from 200 mg of feces using the QIAamp DNA Mini Kit (QIAGEN, Hilden, Germany). A fragment from the V3-V4 hypervariable region of the bacterial 16S rRNA gene was amplified using the linker primer 338F (ACTCCTACGGGAGGCAGCA) and the reverse primer 806R (GGACTACHVGGGTWTCTAAT). PCR reactions contained: 1 μL forward index primer (10 mM), 1 μL reverse index primer (10 mm), 1 μL 10 ng/μL DNA template, and 17 μL mixPfx AccuPrime master (Invitrogen, United States). The reaction conditions are as follows: initial denaturation at 95°C for 5 min, followed by 30 cycles of denaturation at 95°C for 30 s, annealing at 55°C for 30 s, and extension at 72°C for 1 min, and final elongation for 5 min at 72°C. The PCR amplification was performed in duplicate under the same conditions to ensure the accuracy of the results. In addition, we constructed the quality libraries with a single peak and concentration of more than 2 nM using a bioanalyzer (Agilent Technologies, United States) and quantitative PCR (qPCR). At last, the qualified library was sequenced on the Hiseq6000 platform (Illumina, United States), targeting the sequences with paired-end reads (Wang et al., 2022).

## Sequencing analysis

Quality screening of raw data generated by high-throughput sequencing using QIIME software (Qiime1.9.1). Questionable sequences such as short sequences (<200 bp), mismatched primers, and chimeras were removed. The resulting eligible sequences were segmented and clustered by OTU based on 97% similarity. The αlpha diversity indices of gut diversity were calculated based on the relative abundance distribution of OTUs in each sample. Meanwhile, βeta diversity indices were used to dissect the differences and similarities of the major components of the gut flora. Additionally, sparsity curves were generated for each sample to assess the sequencing depth. The data were statistically analyzed using GraphPad Prism (version 9.0c). Data are expressed as Mean ± SD, and $p < 0.05$ was considered statistically significant.

# Results

## Data acquisition and analysis

In the 16S rDNA high-throughput sequencing, 18 stool samples yielded a total of 1,441,028 raw sequences, of which the AN (healthy Angus), DA (Diarrheal Angus), and WN (Weining cattle) groups contained 480,043, 480,101, and 480,884 sequences, respectively (Table 1). The quality of the raw data was assessed and a total of 1,434,904 qualified sequences were obtained (An: 479260, DA: 479311, WN: 480104). Both the sparsity curve and the rank abundance curve showed a saturation trend, indicating that the depth and uniformity of sequencing could meet the requirements of the subsequent analysis (Figures 1A–C). The qualified sequences were clustered into 2,736 OTUs based on 97% nucleic acid sequence similarity, with the number of OTUs per sample ranging from 495 to 806 (Figures 1D,E). There were 841 shared OTUs in AN, DA, and WN groups and unique OTUs in each group were 232, 241, and 503, respectively.

## Comparative analysis of gut microbial diversity

Alpha analysis was applied to discover the difference in intestinal microbial community richness and diversity. The averages of the

TABLE 1 The bacterial sequence information of each sample.

| Sample | Raw reads | Clean reads | Denoised reads | Merged reads | Effective reads | Effective (%) |
|---|---|---|---|---|---|---|
| An1 | 79,844 | 79,710 | 78,547 | 77,107 | 75,534 | 94.60% |
| An2 | 80,227 | 80,092 | 78,702 | 76,813 | 74,138 | 92.41% |
| An3 | 80,084 | 79,951 | 78,474 | 76,635 | 73,689 | 92.01% |
| An4 | 79,887 | 79,762 | 78,207 | 76,281 | 73,983 | 92.60% |
| An5 | 79,992 | 79,859 | 78,254 | 76,310 | 73,514 | 91.90% |
| An6 | 80,009 | 79,886 | 78,258 | 76,096 | 73,004 | 91.24% |
| DA1 | 80,230 | 80,100 | 78,572 | 76,355 | 73,208 | 91.25% |
| DA2 | 80,006 | 79,883 | 78,242 | 76,220 | 73,661 | 92.06% |
| DA3 | 80,116 | 79,980 | 78,366 | 76,194 | 73,243 | 91.42% |
| DA4 | 79,964 | 79,838 | 78,183 | 76,047 | 73,275 | 91.63% |
| DA5 | 79,968 | 79,837 | 78,214 | 75,943 | 73,470 | 91.87% |
| DA6 | 79,817 | 79,673 | 78,018 | 75,990 | 73,220 | 91.73% |
| WN1 | 80,221 | 80,084 | 78,432 | 76,051 | 73,622 | 91.77% |
| WN2 | 80,392 | 80,275 | 78,467 | 76,369 | 73,978 | 92.02% |
| WN3 | 80,091 | 79,977 | 78,176 | 75,869 | 73,714 | 92.03% |
| WN4 | 80,093 | 79,944 | 78,037 | 75,843 | 73,387 | 91.62% |
| WN5 | 79,942 | 79,823 | 78,093 | 75,738 | 72,924 | 91.22% |
| WN6 | 80,145 | 80,001 | 78,411 | 76,347 | 74,313 | 92.72% |

Shannon index were 8.64, 8.79, and 8.96 in the WN, An, and DA groups ($p < 0.05$). Moreover, there were no significant differences in the Chao1 (An = 714.67, DA = 772.67, WN = 657.25), Simpson (An = 0.99, DA = 0.99, WN = 0.99), and ACE (An = 714.40, DA = 772.78, WN = 657.29) index, indicating that the diversity of intestinal flora in groups WN, An and DA were not significantly different (Figures 2A–D). PCoA was applied to dissect the gut microbial variability and similarity among intergroup and intragroup individuals. The results of PCoA and NMDS showed that the samples from An and DA were clustered together and separated from the WN group, indicating that the intestinal flora composition of Weining cattle was different from Angus cattle, and the intestinal microbiota community diversity index was slightly affected by diarrhea in the An and DA groups (Figures 2E,F).

## Analysis of gut microbial community

The relative proportions of different levels of sample-dominated flora were detected by microbial taxon assignment. At the phyla level, a total of 12 phyla were detected from all samples, ranging from 8 to 11 per sample. *Firmicutes* (63.89, 64.87, and 67.80%), *Bacteroidota* (32.42, 31.42, and 26.86%), *Desulfobacterota* (0.93, 0.93, and 1.52%) were the most abundant in the An, DA, and WN groups under phyla level, occupying more than 90% of all bacteria composition (Figure 3A). *Proteobacteria* (0.63, 0.50, and 1.22%), *Cyanobacteria* (0.38, 0.61, and 1.01%), *Fibrobacterota* (0.04, 0.13, and 0.23%), *Spirochaetota* (0.02, 0.12, and 0.09%), *Patescibacteria* (0.90, 0.49, and 0.57%), *Verrucomicrobiota* (0.55, 0.54, and 0.56%), and *Campylobacterota* (0.19, 0.32, and 0.01%) were observed with a lower abundance in the An, DA, and WN groups.

Among the genus identified, the *Lachnospiraceae* (12.23%) was notably enriched in the WT group, closely followed by UCG_005 (10.38), unclassified_UCG_010 (0.73%), *Rikenellaceae_RC9_gut_group* (0.55%), *unclassified_[Eubacterium]_coprostanoligenes_group* (6.8%), *Alistipes* (3.0%) and *Monoglobus* (4.3%). The results showed a very high proportion of beneficial bacteria in the Weining cattle.

In addition, the *Rikenellaceae_*RC9 (6.2 and 6.3%), UCG_005 (11.79 and 10.55%), *Lachnospiraceae* (6.29 and 4.82%), *unclassified_[Eubacterium]_coprostanoligenes_group* (5.57 and 5.56%), *Prevotellaceae_UCG_003* (4.74 and 4.86%), *Monoglobus* (3.12 and 3.09%), and *unclassified_Oscillospiraceae* (3.23 and 2.98%) were the main bacterial genus in An and DA groups (Figure 3B). The data indicated that most of the bacteria that are beneficial for health are significantly higher in the An group than in the DA group. The heatmap showed higher intra-group similarity and greater inter-group variability, revealing differences in gut microbiota composition between the An, DA, and WN groups (Figure 3C).

Metastatic analysis was performed to explore differences in gut microbiota between the WN, An, and DA groups. A comparison of the An and DA groups showed a significant decline in the abundances of 7 genus (*unclassified_rumen_bacterium_YS2*, *unclassified_[Clostridium]_methylpentosum_group*, *unclassified_Butyricicoccaceae*, *uncultured_Ruminococcaceae_bacterium*, *unclassified_Peptostreptococcaceae*, *Anaerosporobacter,* and *unclassified_Oscillospirales*) as well as a significant increase in the abundances of 3 genus (*Defluviitaleaceae_UCG_011*, *Dorea,* and *UCG_009*; Figure 4). At the phyla level, the An group showed dramatically higher abundances of *Campylobacterota* and *Bacteroidota*, whereas the WN group enriched for *Cyanobacteria* and *Elusimicrobiota*. Compared with the An group, the gut microbiota in the WN group showed a distinct decrease in the relative abundances of *Prevotellaceae_UCG_003*, *unclassified_Clostridia_vadinBB60_group*, *Campylobacter*, *Faecalibacterium*, *Erysipelotrichaceae_UCG_009*, *UCG_004*, *unclassified_Paludibacteraceae*, *Candidatus_Soleaferrea*, *unclassified_gir_aah93h0*, *unclassified_UCG_010*, *Saccharofermentans*, *unclassified_Erysipelatoclostridiaceae*, *Parabacteroides*, *NK4A214_group*, *unclassified_Rikenellaceae*, *Dorea*, *unclassified_Oscillospiraceae*, *EMP_G18*, *dgA_11_gut_group*, *unclassified_Barnesiellaceae*, *Parasutterella*,

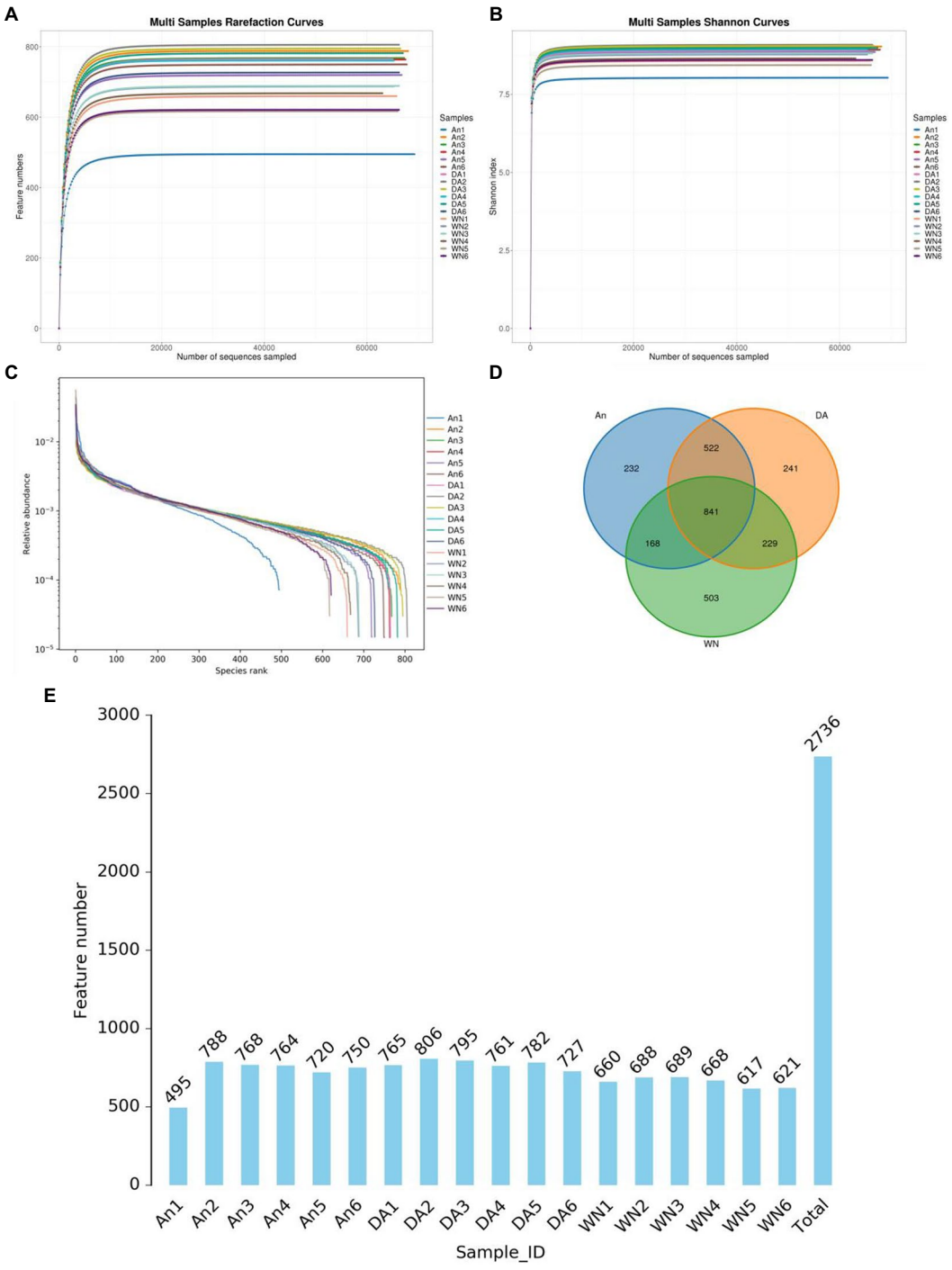


FIGURE 1
Feasibility analysis and OTUs distribution of amplicon sequencing. **(A,B)** Rarefaction curves. **(C)** rank abundance curves. **(D)** Venn diagram. **(E)** The numbers OTUs in each sample.

*Anaerofustis*, *Romboutsia*, *Papillibacter*, *uncultured_compost_bacterium*, *UCG_005*, *unclassified_Bacteroidales_RF16_group* and *Blautia*, whereas *Anaerosporobacter*, *unclassified_Lachnospiraceae*, *Lachnospiraceae_UCG_001*, *Ruminobacter*, *unclassified_Gastranaerophilales*, *unclassified_Hydrogenoanaerobacterium*, *unclassified_[Eubacterium]_coprostanoligenes_group*, *uncultured_rumen_bacterium*, *uncultured_Clostridium_sp.*, *Peptococcus*, *Frisingicoccus*, *unclassified_Oscillospirales*, *Anaerovorax*, *Caproiciproducens*, *uncultured_Alphaproteobacteria_bacterium*, *[Eubacterium]_ruminantium_group*, *Ruminococcus*, *Paludicola*, *unclassified_Clostridia_UCG_014*, *unclassified_Muribaculaceae*, and *Monoglobus* increased significantly (Figure 5). Moreover, the cladogram was generated by applying LefSe to further investigate variability in bacterial taxa composition. In addition to the significantly different bacteria mentioned above, we observed that several bacteria such as *Campylobacteria* and *Anaerosporobacter* were reached in the DA group, whereas beneficial bacteria such as *Lachnospiraceae* were significantly overrepresented in the WN group (Figure 6).

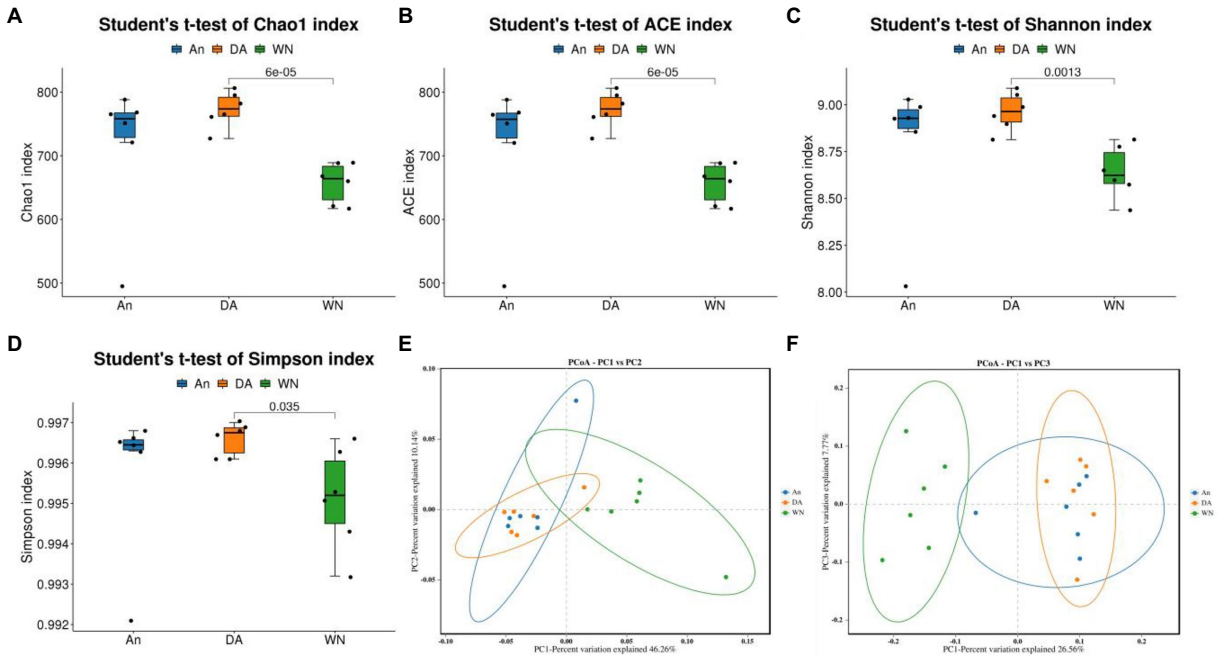


FIGURE 2
Changes of gut microbial diversity associated with species and diarrhea. **(A–D)** Chao1, ACE, Shannon, and Simpson indices. **(E,F)** PCoA plots based on the weighted and unweighted UniFrac distance.

## Correlation network analysis

*Prevotellaceae_UCG_003* was positively associated with *unclassified_UCG_010*. *Ruminobacter* was negatively related to *dgA_11_gut_group*, *uncultured_Ruminococcaceae_bacterium*, *unclassified_UCG_010*, *UCG_009*, *NK4A214_group*, *unclassified_Clostridia_vadinBB60_group*, *Prevotellaceae_UCG_003* but positively associated with *unclassified_Lachnospiraceae, UCG_002* and *Monoglobus* (Figure 7).

# Discussion

Diarrhea is the most common disease in calves and severely affects the animal's growth and development. According to previous reports, the economic damage caused by diarrhea is enormous and difficult to control (Fischer et al., 2016; Lorenz et al., 2021). Studies indicated that the etiology of bovine diarrhea is multifactorial, with pathogens and management factors (housing, feeding, and sanitary conditions) playing an important role (Bendali et al., 1999). A study in diarrheal calves in Belgium estimated the prevalence of *E. coliRotavirus*, *Coronavirus,* and *C. parvum* at 4, 20, 8, and 31%, respectively. In a recent Swiss study on diarrheal calves, the prevalence of these *Enteropathogens* remained at high levels. Moreover, diarrhea inevitably accompanies intestinal damage, suggesting that the intestinal microbiota may be altered (Xia et al., 2018; Zhai et al., 2019). As the habitat of intestinal flora, the gastrointestinal tract is more susceptible to various diseases such as inflammatory bowel disease and diarrhea due to the influence of intestinal flora (Liu C. S. et al., 2019; Yue et al., 2019; Zhang et al., 2022). In addition, although the gut microbiota inhabits the gut, significant changes in the gut microbiota may also lead to the development of other diseases such as liver disease, diabetes, and obesity, etc. (Guo et al., 2022; Ye et al., 2022). More importantly, significant changes in gut microbiota also affect gut permeability, which may lead to a leaky gut and increased rates of pathogenic bacterial infection (Yue et al., 2020; Xu et al., 2021). Therefore, the characterization of gut microbiota is crucial for the prevention, control, and diagnosis of diarrhea (Bjorkman et al., 2003; Singh et al., 2015).

Gut microbial diversity and richness constantly decrease under the influence of diarrhea (Zhang L. et al., 2020; Cui et al., 2021; Ren et al., 2022). In our study, we found no significant difference in gut microbiota diversity and richness between the An group and DA group, the lack of difference is most likely due to an increase in pathogenic bacteria due to diarrhea and a decrease in beneficial bacteria in the DA group. In Han's report, there was no significant difference in gut microbial diversity between healthy and diarrheal yaks, which was consistent with our findings (Han et al., 2017). Similarly, He's results are also similar to ours: diarrhea does not significantly alter the diversity and richness of gut microbiota in pigs (He et al., 2020). Although the diversity and richness of intestinal microbiota did not change significantly, the composition of bacteria did. *Anaerosporbacter* were rich in the DA group but were not detected in the An group. *Anaerosporbacter* is likely to be associated with the occurrence of colorectal cancer. In Yu's study, the results manifested that the *Anaerosporbacter* were abundant in the colorectal cancer group compared to the healthy group (Yu et al., 2017). *Campylobacter* is recognized as the most common cause of bacterial enteritis (Liu et al., 2018). Among bacterial infections reported in recent years, *Campylobacter* spp. predominated. In Singh's report, *Campylobacter* usually causes asymptomatic infections, diarrhea, and hemorrhagic colitis (Singh et al., 2015; Shin et al., 2021). Interestingly, the aforementioned potentially pathogenic bacteria exhibited a significant relative abundance in the DA group compared to the An group. *Candidatus Soleaferrea* secretes homeostatic protective properties and has anti-inflammatory effects (Zhang et al., 2015), there was no significant difference in the proportion of *Candidatus Soleaferrea* in the

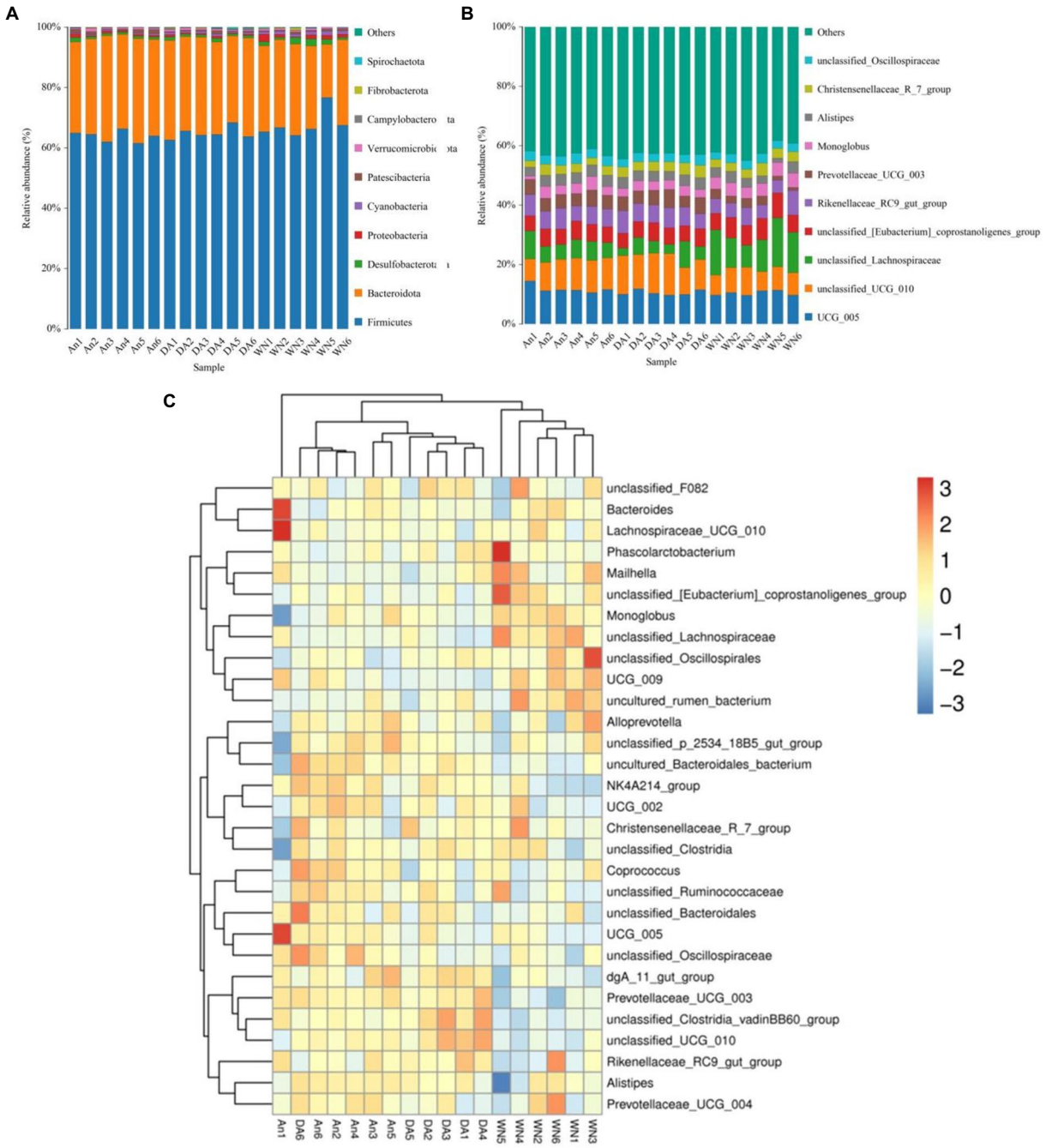


FIGURE 3
Changes of gut microbial composition associated with species and diarrhea. **(A,B)** Composition and the relative ratio of preponderant bacteria at the phylum and genus levels. **(C)** Heatmap of the 50 most abundant bacterial genera.

An and DA groups. Conversely, the beneficial bacteria including *Dorea*, *Muribaculaceae, UCG-009,* and *Monoglobus* were significantly lower in the DA group compared with healthy Angus cattle. *Monoglobus* is a beneficial bacteria that modulates the metabolism (Kim et al., 2019). Unique among known human gut flora, *Monoglobus* plays an active role in pectin degradation and sugar utilization (Kim et al., 2019). *Muribaculaceae* can produce propionate, which is closely related to gut health. Related studies have reported that *Muribaculaceae* are closely related to acarbose consumption (Smith et al., 2021). In addition, *Dorea* and *UCG-009* are capable of regulating health and absorbing nutrients. In the current study, the gut microbiota of Angus cattle with diarrhea was significantly altered, implying an imbalance in gut homeostasis. Our study showed that gut microbiota dysbiosis is an important factor driving the development of diarrhea. At the same time, the findings shed light on potential pathogens including *Anaerosporbacter* and *Campylobacter*, which cause diarrhea in Angus cattle.

It is well known that gut microbiota are an important indicator for evaluating gut function and homeostasis (Xia et al., 2018; Duan et al., 2020; Reese et al., 2021). However, the diversity of gut microbiota is easily affected by various factors such as species, age, and various diseases (Ding et al., 2019; Wu et al., 2020, 2022). Species are the most important factor affecting gut microbiota (Yang et al., 2018; Huang et al.,

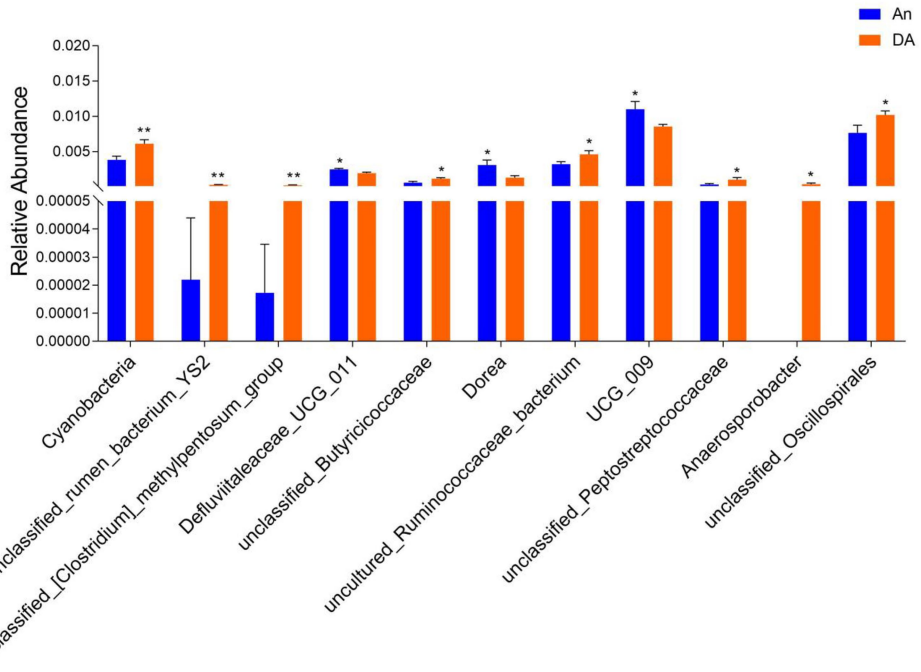


FIGURE 4
Statistical analysis of differential bacteria between An and DA groups at the phylum and genus levels.

2020; Zhong et al., 2021). Animals of various species need to evolve different intestinal flora structures to adapt to their habitats, and diet characteristics, etc. (Liu et al., 2021, 2022). For example, herbivores have a higher intestinal flora structure to digest cellulose and realize energy conversion (Dong et al., 2020; Yang et al., 2022). In addition, different breeds of sheep and chickens also have different intestinal flora structures (Rettedal et al., 2019; Qin et al., 2020). Captive horses, for example, have lower gut microbiota composition and lower numbers of pathogenic bacteria than wild donkeys (Zhou et al., 2022). In addition, compared with cattle living in plain areas, yaks need to evolve a more diverse intestinal flora structure to adapt to the high-altitude hypoxic environment of the Qinghai-Tibet Plateau (Fu et al., 2021; Wang et al., 2021). Intestinal flora are executors of intestinal function and the supervisor of intestinal health, so changes in intestinal flora also affect the health of the host (Yin et al., 2019; Zhang P. et al., 2020; Chen et al., 2022).

Weining cattle are a native breed in Guizhou, while Angus cattle are an exotic breed introduced to Weining in the last 10 years. Weining cattle and Angus cattle are currently the main breeds in Weining Guizhou, occupying more than 90% of the local cattle industry. In the past 3 years, the incidence of diarrhea was less than 3% in Weining cattle. However, the rate of diarrhea in other breeds of cattle was significantly higher than 5%. Previous studies have demonstrated that the gut microbiome is correlated with species and health. In some studies, greater quantities of *Firmicutes* were found in the WN group compared to the An groups. Previous research has reported that *Firmicutes* are closely related to the health of gut microbiota (Eckburg et al., 2005), which contribute to maintaining gut microbiota balance, regulating the gut environment, and inhibiting pathogens (Sun et al., 2016). In addition, *Lachnospiraceae*, *Rikenellaceae,* and *Coprostanoligenes* were the most dominant genus in the WN group. *Lachnospiraceae* is closely linked to host health by producing

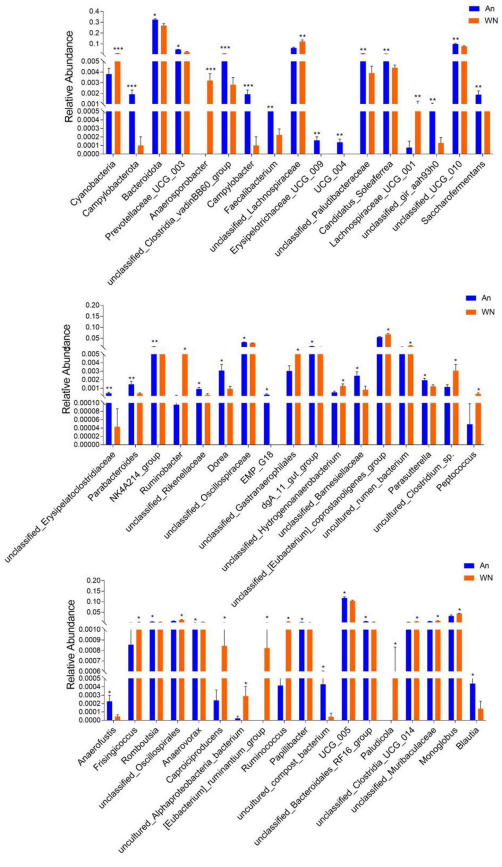


FIGURE 5
Statistical analysis of differential bacteria between An and WN groups at the phylum and genus levels.

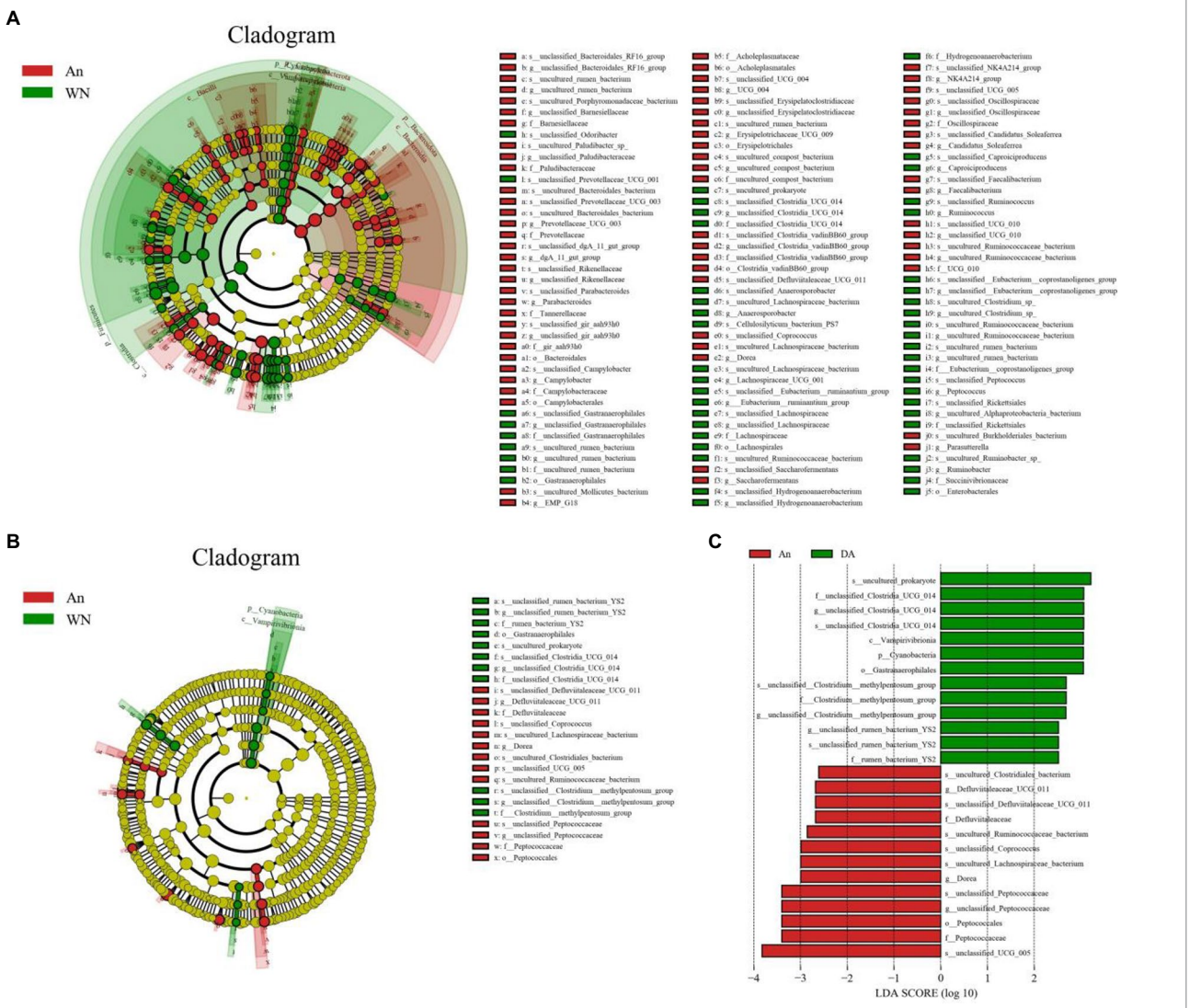


FIGURE 6
LEfSe integrated with LDA scores recognized differentially abundant taxon related to species and diarrhea. **(A,B)** Cladogram shows the phylogenetic distribution of differential taxon. **(C)** LDA scores >2 are considered significant.

short-chain fatty acids, converting primary to secondary bile acids, and inhibiting intestinal pathogens (Sorbara et al., 2020). The *Rikenellaceae* and *Coprostanoligenes* were regarded as a beneficial bacterium in modulating health and serum dyslipidemia (Tavella et al., 2021). *Rikenellaceae* plays an essential role in maintaining intestinal mucosal immunity, Previous studies have demonstrated that HIV infection is distinctly involved with the loss of *Rikenellaceae* (Dubourg et al., 2017). Similarly, in Teresa Tavella's research, *Rikenellaceae* could significantly reduce visceral adipose tissue and help maintain a healthier metabolic profile, which proved that adequate *Rikenellaceae* could improve the body's health and metabolism (Backhed et al., 2015; Dubin et al., 2016). Meanwhile, Wei et al. (2021) reported that *Coprostanoligenes* have the ability to modulate serum dyslipidemia. *Overall,* the highest abundance of beneficial bacteria was present in the WN group compared to the An and DA groups. In particular, the *Lachnospiraceae* are over-represented in Weining cattle, showing significantly higher abundances compared to Angus cattle. Interestingly, the *Muribaculaceae*, which plays an important role in anti-inflammatory action was also enriched in the WN group. Conversely, the potential pathogens including *Alistipes* and *Campylobacteria* were lower present in the WN group compared to the An group. Overall, the greater abundance and diversity of beneficial bacteria indicated the potential of Weining cattle for diarrhea prevention and health modulation. The data revealed that a good gut microbiome structure improves the body's disease resistance and health status. In addition, Weining cattle have great potential as an isolated source of probiotics.

## Conclusion

This study characterized the gut microbiota diversity and composition in Weining cattle and Angus cattle. The WN group had a greater abundance of beneficial bacteria and a lower abundance of potential pathogens. While there was no significant difference between healthy Angus and diarrheal Angus, there was a significant change in the type and proportion of bacteria. The potential pathogens including *Anaerosporbacter* and *Campylobacter* were higher in diarrheal cattle, conversely, the beneficial bacteria including *Dorea*, *Muribaculaceae,*

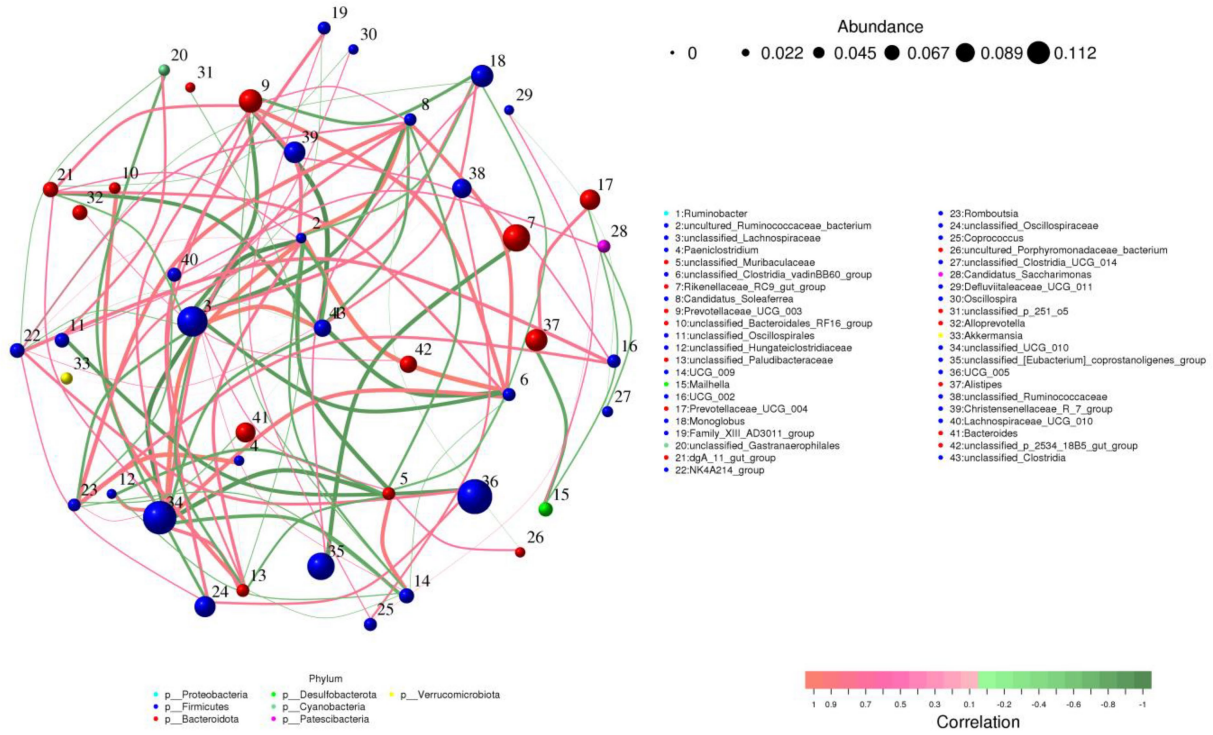


FIGURE 7
Correlation network analysis of gut microbiota. Positive and negative correlations are indicated by red and green lines, respectively.

*UCG-009*, and *Monoglobus* were significantly lower compared to healthy cattle. This is the first report of gut microbiota in Weining cattle and broadens the knowledge of gut microbiota. Our results convey the message that diarrhea not only directly modifies the diversity and abundance of gut microbiota but also indirectly affects some functional bacteria. In addition, this study revealed potentially pathogenic bacteria and provided basic data for the subsequent treatment of diarrhea in Angus cattle.

## Data availability statement

The datasets presented in this study can be found in online repositories. The names of the repository/repositories and accession number(s) can be found at: https://www.ncbi.nlm.nih.gov/, PRJNA931445.

## Ethics statement

The study was conducted under the guidance and approval of the Animal Welfare and Ethics Committee of Huazhong Agricultural University.

## Author contributions

LW, JM, and MW provided the research idea. DW, JM, and MW contributed reagents, materials, and analysis tools. LW wrote the manuscript. KL and YZ revised the manuscript. All authors participated in writing and reviewing the manuscript, contributed to the article and approved the submitted version.

## Funding

The study was supported by Research and Demonstration of Key Technology for Nutritional Control and Efficient Utilization of Roughage for Weining Cattle [Guizhou Science (2021) General project No. 153], the Weining Cattle Breeding Base of Weining County, Guizhou Province, and the Sixth Batch of Talent Base Project of Guizhou Province [Guizhou people Hair Collar (2018) No. 3].

## Conflict of interest

The authors declare that the research was conducted in the absence of any commercial or financial relationships that could be construed as a potential conflict of interest.

## Publisher's note



## Supplementary material

The Supplementary material for this article can be found online at: https://www.frontiersin.org/articles/10.3389/fmicb.2023.1113730/full#supplementary-material

# References


Backhed, F., Roswall, J., Peng, Y., Feng, Q., Jia, H., Kovatcheva-Datchary, P., et al. (2015). Dynamics and stabilization of the human gut microbiome during the first year of life. *Cell Host Microbe* 17, 690–703. doi: 10.1016/j.chom.2015.04.004

Bendali, F., Bichet, H., Schelcher, F., and Sanaa, M. (1999). Pattern of diarrhoea in newborn beef calves in south-West France. *Vet. Res.* 30, 61–74. PMID: 10081113

Bjorkman, C., Svensson, C., Christensson, B., and de Verdier, K. (2003). Cryptosporidium parvum and giardia intestinalis in calf diarrhoea in Sweden. *Acta Vet. Scand.* 44, 145–152. doi: 10.1186/1751-0147-44-145

Bu, D., Zhang, X., Ma, L., Park, T., Wang, L., Wang, M., et al. (2020). Repeated inoculation of young calves with rumen microbiota does not significantly modulate the rumen prokaryotic microbiota consistently but decreases diarrhea. *Front. Microbiol.* 11:1403. doi: 10.3389/fmicb.2020.01403

Chen, A. S., Liu, D. H., Hou, H. N., Yao, J. N., Xiao, S. C., Ma, X. R., et al. (2022). Dietary pattern interfered with the impacts of pesticide exposure by regulating the bioavailability and gut microbiota. *Sci. Total Environ.* 858:159936. doi: 10.1016/j.scitotenv.2022.159936

Cui, M., Wang, Y., Elango, J., Wu, J., Liu, K., and Jin, Y. (2021). Cereus sinensis polysaccharide alleviates antibiotic-associated diarrhea based on modulating the gut microbiota in c57bl/6 mice. *Front. Nutr.* 8:751992. doi: 10.3389/fnut.2021.751992

Ding, J., An, X. L., Lassen, S. B., Wang, H. T., Zhu, D., and Ke, X. (2019). Heavy metal-induced co-selection of antibiotic resistance genes in the gut microbiota of collembolans. *Sci. Total Environ.* 683, 210–215. doi: 10.1016/j.scitotenv.2019.05.302

Dong, H., Liu, B., Li, A., Iqbal, M., Mehmood, K., Jamil, T., et al. (2020). Microbiome analysis reveals the attenuation effect of lactobacillus from yaks on diarrhea via modulation of gut microbiota. *Front. Cell. Infect. Microbiol.* 10:610781. doi: 10.3389/fcimb.2020.610781

Duan, H., Yu, L. L., Tian, F. W., Zhai, Q. X., Fan, L. P., and Chen, W. (2020). Gut microbiota: a target for heavy metal toxicity and a probiotic protective strategy. *Sci. Total Environ.* 742:140429. doi: 10.1016/j.scitotenv.2020.140429

Dubin, K., Callahan, M. K., Ren, B., Khanin, R., Viale, A., Ling, L., et al. (2016). Intestinal microbiome analyses identify melanoma patients at risk for checkpoint-blockade-induced colitis. *Nat. Commun.* 7:10391. doi: 10.1038/ncomms10391

Dubourg, G., Surenaud, M., Levy, Y., Hue, S., and Raoult, D. (2017). Microbiome of hiv-infected people. *Microb. Pathog.* 106, 85–93. doi: 10.1016/j.micpath.2016.05.015

Eckburg, P. B., Bik, E. M., Bernstein, C. N., Purdom, E., Dethlefsen, L., Sargent, M., et al. (2005). Diversity of the human intestinal microbial flora. *Science* 308, 1635–1638. doi: 10.1126/science.1110591

Eibl, C., Bexiga, R., Viora, L., Guyot, H., Felix, J., Wilms, J., et al. (2021). The antibiotic treatment of calf diarrhea in four european countries: a survey. *Antibiotics (Basel)* 10:910. doi: 10.3390/antibiotics10080910

Fischer, S., Bauerfeind, R., Czerny, C. P., and Neumann, S. (2016). Serum interleukin-6 as a prognostic marker in neonatal calf diarrhea. *J. Dairy Sci.* 99, 6563–6571. doi: 10.3168/jds.2015-10740

Fu, H., Zhang, L., Fan, C., Liu, C., Li, W., Cheng, Q., et al. (2021). Environment and host species identity shape gut microbiota diversity in sympatric herbivorous mammals. *Microb. Biotechnol.* 14, 1300–1315. doi: 10.1111/1751-7915.13687

Guo, Z., Pan, J., Zhu, H., and Chen, Z. Y. (2022). Metabolites of gut microbiota and possible implication in development of diabetes mellitus. *J. Agric. Food Chem.* 70, 5945–5960. doi: 10.1021/acs.jafc.1c07851

Han, Z., Li, K., Shahzad, M., Zhang, H., Luo, H., Qiu, G., et al. (2017). Analysis of the intestinal microbial community in healthy and diarrheal perinatal yaks by high-throughput sequencing. *Microb. Pathog.* 111, 60–70. doi: 10.1016/j.micpath.2017.08.025

He, K., Yan, W., Sun, C., Liu, J., Bai, R., Wang, T., et al. (2020). Alterations in the diversity and composition of gut microbiota in weaned piglets infected with balantioides coli. *Vet. Parasitol.* 288:109298. doi: 10.1016/j.vetpar.2020.109298

Huang, A., Cai, R., Wang, Q., Shi, L., Li, C., and Yan, H. (2019). Dynamic change of gut microbiota during porcine epidemic diarrhea virus infection in suckling piglets. *Front. Microbiol.* 10:322. doi: 10.3389/fmicb.2019.00322

Huang, S. M., Wu, Z. H., Li, T. T., Liu, C., Han, D. D., Tao, S. Y., et al. (2020). Perturbation of the lipid metabolism and intestinal inflammation in growing pigs with low birth weight is associated with the alterations of gut microbiota. *Sci. Total Environ.* 719:137382. doi: 10.1016/j.scitotenv.2020.137382

Kim, C. C., Healey, G. R., Kelly, W. J., Patchett, M. L., Jordens, Z., Tannock, G. W., et al. (2019). Genomic insights from monoglobus pectinilyticus: a pectin-degrading specialist bacterium in the human colon. *ISME J.* 13, 1437–1456. doi: 10.1038/s41396-019-0363-6

Li, A., Liu, B., Li, F., He, Y., Wang, L., Fakhar-e-Alam Kulyar, M., et al. (2021). Integrated bacterial and fungal diversity analysis reveals the gut microbial alterations in diarrheic giraffes. *Front. Microbiol.* 12:712092. doi: 10.3389/fmicb.2021.712092

Li, K., Mehmood, K., Zhang, H., Jiang, X., Shahzad, M., Dong, X., et al. (2018). Characterization of fungus microbial diversity in healthy and diarrheal yaks in gannan region of Tibet autonomous prefecture. *Acta Trop.* 182, 14–26. doi: 10.1016/j.actatropica.2018.02.017

Liu, C. S., Liang, X., Wei, X. H., Jin, Z., Chen, F. L., Tang, Q. F., et al. (2019). Gegen qinlian decoction treats diarrhea in piglets by modulating gut microbiota and short-chain fatty acids. *Front. Microbiol.* 10:825. doi: 10.3389/fmicb.2019.00825

Liu, F., Ma, R., Wang, Y., and Zhang, L. (2018). The clinical importance of *campylobacter* concisus and other human hosted *campylobacter* species. *Front. Cell. Infect. Microbiol.* 8:243. doi: 10.3389/fcimb.2018.00243

Liu, J., Wang, H. W., Lin, L., Miao, C. Y., Zhang, Y., and Zhou, B. H. (2019). Intestinal barrier damage involved in intestinal microflora changes in fluoride-induced mice. *Chemosphere* 234, 409–418. doi: 10.1016/j.chemosphere.2019.06.080

Liu, W., Wang, Q., Song, J., Xin, J., Zhang, S., Lei, Y., et al. (2021). Comparison of gut microbiota of yaks from different geographical regions. *Front. Microbiol.* 12:666940. doi: 10.3389/fmicb.2021.666940

Liu, J., Wang, X., Zhang, W., Kulyar, M. F., Ullah, K., Han, Z., et al. (2022). Comparative analysis of gut microbiota in healthy and diarrheic yaks. *Microb. Cell Factories* 21:111. doi: 10.1186/s12934-022-01836-y

Lorenz, I., Huber, R., and Trefz, F. M. (2021). A high plane of nutrition is associated with a lower risk for neonatal calf diarrhea on bavarian dairy farms. *Animals (Basel)* 11:3251. doi: 10.3390/ani11113251

Qin, W., Song, P., Lin, G., Huang, Y., Wang, L., Zhou, X., et al. (2020). Gut microbiota plasticity influences the adaptability of wild and domestic animals in co-inhabited areas. *Front. Microbiol.* 11:125. doi: 10.3389/fmicb.2020.00125

Reese, A. T., Chadaideh, K. S., Diggins, C. E., Schell, L. D., Beckel, M., Callahan, P., et al. (2021). Effects of domestication on the gut microbiota parallel those of human industrialization. *elife* 10:60197. doi: 10.7554/eLife.60197

Ren, S., Wang, C., Chen, A., Lv, W., and Gao, R. (2022). The probiotic *Lactobacillus paracasei* ameliorates diarrhea cause by escherichia coli o (8) via gut microbiota modulation (1). *Front. Nutr.* 9:878808. doi: 10.3389/fnut.2022.878808

Rettedal, E. A., Altermann, E., Roy, N. C., and Dalziel, J. E. (2019). The effects of unfermented and fermented cow and sheep milk on the gut microbiota. *Front. Microbiol.* 10:458. doi: 10.3389/fmicb.2019.00458

Shao, H., Zhang, C., Xiao, N., and Tan, Z. (2020). Gut microbiota characteristics in mice with antibiotic-associated diarrhea. *BMC Microbiol.* 20:313. doi: 10.1186/s12866-020-01999-x

Shin, J., Noh, J. R., Choe, D., Lee, N., Song, Y., Cho, S., et al. (2021). Ageing and rejuvenation models reveal changes in key microbial communities associated with healthy ageing. *Microbiome* 9:240. doi: 10.1186/s40168-021-01189-5

Singh, P., Teal, T. K., Marsh, T. L., Tiedje, J. M., Mosci, R., Jernigan, K., et al. (2015). Intestinal microbial communities associated with acute enteric infections and disease recovery. *Microbiome* 3:45. doi: 10.1186/s40168-015-0109-2

Smith, B. J., Miller, R. A., and Schmidt, T. M. (2021). Muribaculaceae genomes assembled from metagenomes suggest genetic drivers of differential response to acarbose treatment in mice. *Msphere* 6:e85121. doi: 10.1128/msphere.00851-21

Sorbara, M. T., Littmann, E. R., Fontana, E., Moody, T. U., Kohout, C. E., Gjonbalaj, M., et al. (2020). Functional and genomic variation between human-derived isolates of lachnospiraceae reveals inter-and intra-species diversity. *Cell Host Microbe* 28, 134–146.e4. doi: 10.1016/j.chom.2020.05.005

Sun, B., Wang, X., Bernstein, S., Huffman, M. A., Xia, D. P., Gu, Z., et al. (2016). Marked variation between winter and spring gut microbiota in free-ranging tibetan macaques (*macaca thibetana*). *Sci. Rep.* 6:26035. doi: 10.1038/srep26035

Tavella, T., Rampelli, S., Guidarelli, G., Bazzocchi, A., Gasperini, C., Pujos-Guillot, E., et al. (2021). Elevated gut microbiome abundance of christensenellaceae, porphyromonadaceae and rikenellaceae is associated with reduced visceral adipose tissue and healthier metabolic profile in italian elderly. *Gut Microbes* 13, 1–19. doi: 10.1080/19490976.2021.1880221

Urie, N. J., Lombard, J. E., Shivley, C. B., Kopral, C. A., Adams, A. E., Earleywine, T. J., et al. (2018). Preweaned heifer management on us dairy operations: part i. descriptive characteristics of preweaned heifer raising practices. *J. Dairy Sci.* 101, 9168–9184. doi: 10.3168/jds.2017-14010

Wang, Y. P., An, M., Zhang, Z., Zhang, W. Q., Kulyar, M., Iqbal, M., et al. (2022). Effects of milk replacer-based lactobacillus on growth and gut development of yaks' calves: a gut microbiome and metabolic study. *Microbiol. Spectrum.* 10:e0115522. doi: 10.1128/spectrum.01155-22

Wang, Y., Fu, Y., He, Y., Kulyar, M. F., Iqbal, M., Li, K., et al. (2021). Longitudinal characterization of the gut bacterial and fungal communities in yaks. *J Fungi (Basel)* 7:559. doi: 10.3390/jof7070559

Wei, W., Jiang, W., Tian, Z., Wu, H., Ning, H., Yan, G., et al. (2021). Fecal g. *streptococcus* and g. *Eubacterium_coprostanoligenes*_group combined with sphingosine to modulate the serum dyslipidemia in high-fat diet mice. *Clin. Nutr.* 40, 4234–4245. doi: 10.1016/j.clnu.2021.01.031

Wu, N., Wang, X. B., Xu, X. Y., Cai, R. J., and Xie, S. Y. (2020). Effects of heavy metals on the bioaccumulation, excretion and gut microbiome of black soldier fly larvae (*hermetia illucens*). *Ecotoxicol. Environ. Saf.* 192:110323. doi: 10.1016/j.ecoenv.2020.110323

Wu, H. F., Zheng, L., Tan, M. T., Li, Y. N., Xu, J. S., Yan, S., et al. (2022). Cd exposure-triggered susceptibility to *Bacillus thuringiensis* in lymantria dispar involves in gut microbiota dysbiosis and hemolymph metabolic disorder. *Ecotoxicol. Environ. Saf.* 241:113763. doi: 10.1016/j.ecoenv.2022.113763

Xia, J., Jin, C., Pan, Z., Sun, L., Fu, Z., and Jin, Y. (2018). Chronic exposure to low concentrations of lead induces metabolic disorder and dysbiosis of the gut microbiota in mice. *Sci. Total Environ.* 631-632, 439–448. doi: 10.1016/j.scitotenv.2018.03.053

Xu, B., Qin, W., Xu, Y., Yang, W., Chen, Y., Huang, J., et al. (2021). Dietary quercetin supplementation attenuates diarrhea and intestinal damage by regulating gut microbiota in weanling piglets. *Oxidative Med. Cell. Longev.* 2021:6221012. doi: 10.1155/2021/6221012

Yang, X., Fan, X., Jiang, H., Zhang, Q., Basangwangdui, , Zhang, Q., et al. (2022). Simulated seasonal diets alter yak rumen microbiota structure and metabolic function. *Front. Microbiol.* 13:1006285. doi: 10.3389/fmicb.2022.1006285

Yang, Q., Huang, X., Zhao, S., Sun, W., Yan, Z., Wang, P., et al. (2017). Structure and function of the fecal microbiota in diarrheic neonatal piglets. *Front. Microbiol.* 8:502. doi: 10.3389/fmicb.2017.00502

Yang, H., Xiang, Y., Robinson, K., Wang, J. J., Zhang, G. L., Zhao, J., et al. (2018). Gut microbiota is a major contributor to adiposity in pigs. *Front. Microbiol.* 9:3045. doi: 10.3389/fmicb.2018.03045

Ye, J., Wu, Z., Zhao, Y., Zhang, S., Liu, W., and Su, Y. (2022). Role of gut microbiota in the pathogenesis and treatment of diabetes mullites: advanced research-based review. *Front. Microbiol.* 13:1029890. doi: 10.3389/fmicb.2022.1029890

Yin, N., Gao, R., Knowles, B., Wang, J., Wang, P., Sun, G., et al. (2019). Formation of silver nanoparticles by human gut microbiota. *Sci. Total Environ.* 651, 1489–1494. doi: 10.1016/j.scitotenv.2018.09.312

Yu, T., Guo, F., Yu, Y., Sun, T., Ma, D., Han, J., et al. (2017). *Fusobacterium nucleatum* promotes chemoresistance to colorectal cancer by modulating autophagy. *Cells* 170, 548–563.e16. doi: 10.1016/j.cell.2017.07.008

Yue, Y., He, Z., Zhou, Y., Ross, R. P., Stanton, C., Zhao, J., et al. (2020). *Lactobacillus plantarum* relieves diarrhea caused by enterotoxin-producing escherichia coli through inflammation modulation and gut microbiota regulation. *Food Funct.* 11, 10362–10374. doi: 10.1039/d0fo02670k

Yue, S. J., Liu, J., Wang, W. X., Wang, A. T., Yang, X. Y., Guan, H. S., et al. (2019). Berberine treatment-emergent mild diarrhea associated with gut microbiota dysbiosis. *Biomed. Pharmacother.* 116:109002. doi: 10.1016/j.biopha.2019.109002

Zhai, Q., Wang, J., Cen, S., Zhao, J., Zhang, H., Tian, F., et al. (2019). Modulation of the gut microbiota by a galactooligosaccharide protects against heavy metal lead accumulation in mice. *Food Funct.* 10, 3768–3781. doi: 10.1039/c9fo00587k

Zhang, L., Gu, X., Wang, J., Liao, S., Duan, Y., Li, H., et al. (2020). Effects of dietary isomaltooligosaccharide levels on the gut microbiota, immune function of sows, and the diarrhea rate of their offspring. *Front. Microbiol.* 11:588986. doi: 10.3389/fmicb.2020.588986

Zhang, Y. J., Li, S., Gan, R. Y., Zhou, T., Xu, D. P., and Li, H. B. (2015). Impacts of gut bacteria on human health and diseases. *Int. J. Mol. Sci.* 16, 7493–7519. doi: 10.3390/ijms16047493

Zhang, Y., Liu, H., Yue, Z., Tan, P., Sun, M., Ji, L., et al. (2022). *Wickerhamomyces anomalus* relieves weaning diarrhea via improving gut microbiota and redox homeostasis using a piglet model. *Food Funct.* 13, 11223–11235. doi: 10.1039/d2fo01861f

Zhang, P., Lu, G., Liu, J., Yan, Z., and Wang, Y. (2020). Toxicological responses of carassius auratus induced by benzophenone-3 exposure and the association with alteration of gut microbiota. *Sci. Total Environ.* 747:141255. doi: 10.1016/j.scitotenv.2020.141255

Zhong, Y., Cao, J., Deng, Z., Ma, Y., Liu, J., and Wang, H. (2021). Effect of fiber and fecal microbiota transplantation donor on recipient mice gut microbiota. *Front. Microbiol.* 12:757372. doi: 10.3389/fmicb.2021.757372

Zhou, Z., Tang, L., Yan, L., Jia, H., Xiong, Y., Shang, J., et al. (2022). Wild and captive environments drive the convergence of gut microbiota and impact health in threatened equids. *Front. Microbiol.* 13:832410. doi: 10.3389/fmicb.2022.832410

Zuo, Q. L., Cai, X., Zheng, X. Y., Chen, D. S., Li, M., Liu, Z. Q., et al. (2021). Influences of xylitol consumption at different dosages on intestinal tissues and gut microbiota in rats. *J. Agric. Food Chem.* 69, 12002–12011. doi: 10.1021/acs.jafc.1c03720

# Frontiers in Microbiology

**Explores the habitable world and the potential of microbial life**

The largest and most cited microbiology journal which advances our understanding of the role microbes play in addressing global challenges such as healthcare, food security, and climate change.

---

## Discover the latest Research Topics

See more →


**Frontiers**

Avenue du Tribunal-Fédéral 34
1005 Lausanne, Switzerland
frontiersin.org

**Contact us**

+41 (0)21 510 17 00
frontiersin.org/about/contact